SPIE
Connecting minds. Advancing light.

2012 Remote Sensing

Conference: 24–27 September 2012
www.spie.org/rs

2012 Security+ Defence

Conference: 24–27 September 2012
Exhibition: 25–26 September 2012
www.spie.org/sd

Technical Abstracts

Location
Edinburgh International Conference Centre
Edinburgh, United Kingdom

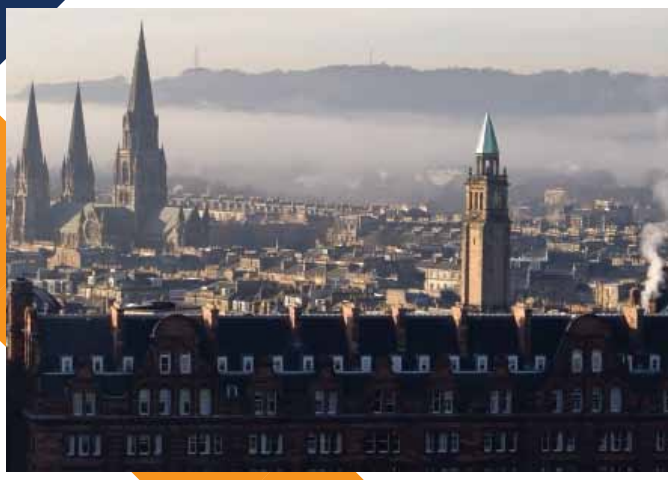

SPIE Remote Sensing

SPIE Security+Defence

Karin Stein
Fraunhofer-IOSB Institute of Optronics, System Technologies and Image Exploitation, Germany
2012 Symposium Chair

David H. Titterton
Defence Science and Technology Lab., United Kingdom
2012 Symposium Chair

Charles R. Bostater
Marine-Environmental Optics Lab & Remote Sensing Center, Florida Institute of Technology, United States
2012 Symposium Co-Chair

Reinhard Ebert
Fraunhofer IOSB, Germany
2012 Symposium Co-Chair

Co-Sponsoring Organisations

SELEX GALILEO
A Finmeccanica Company

THALES

Delivered with the support of Scottish Enterprise

SCOTTISH DEVELOPMENT INTERNATIONAL

Scottish Enterprise

Cooperating Organisations

EARSC

IOP Institute of Physics
Instrument Science and Technology Group

SCOTTISH OPTOELECTRONICS ASSOCIATION

[dstl]

REMOTE SENSING AND PHOTOGRAMMETRY SOCIETY

Knowledge Transfer Network
Electronics, Sensors Photonics

SPIE would like to express its deepest appreciation to the symposium chairs, conference chairs, Programme committees, and session chairs who have so generously given of their time and advice to make this symposium possible. The symposium, like our other conferences and activities, would not be possible without the dedicated contribution of our participants and members.

This Programme is based on commitments received up to the time of publication and is subject to change without notice.

Contents

SPIE Remote Sensing

SPIE Security+Defence

Conference 8531: Remote Sensing for Agriculture, Ecosystems, and Hydrology

Monday - Wednesday 24–26 September 2012 • Part of Proceedings of SPIE Vol. 8531
Remote Sensing for Agriculture, Ecosystems, and Hydrology XIV

8531-1, Session 1

Comparing results of a remote sensing driven interception-infiltration

model for regional to global applications with ECMWF data

Markus Tum, Erik Borg, Deutsches Zentrum für Luft- und Raumfahrt e.V. (Germany)

We present a remote sensing based modelling approach to simulate the one dimensional water transport in the vadose zone of unsaturated soils on a daily basis, which can be used for regional to global applications. To calculate the hydraulic conductivity our model is driven by van Genuchten parameters, which we estimated using the ISRIC-WISE Harmonized Global Soil Profile Dataset Ver. 3.1 and the Rosetta programme. All needed parameters were calculated for 26 global main soil types and 102 soils of second order. All soil types are based on the original, global FAO 1974 soil classification. Soil depth and the layering of one to six layers were independently defined for each soil. Interception by vegetation is also considered by using Leaf Area Index (LAI) time series from SPOT-VEGETATION. Precipitation is based on daily time series from the European Centre for Medium-Range Weather Forecasts (ECMWF). For our area of interest - Germany we compared our model output with soil moisture data from the ECMWF, because it is based on the same precipitation dataset. We found a good agreement for the general characteristics of our modelled plant available soil water with this dataset, especially for soils which are close to the standard characteristics of the ECMWF. Disagreements were found for shallow soils and soils under stagnant moisture, which are not considered in the ECMWF model scheme, but can be distinguished with our approach. Our proposed approach to combine established models to describe interception and the one-dimensional vertical water transport with time-series of remote sensing data intends to contribute to the realistic parameterization of the soil water budged. This is especially needed for the global and regional assessment of e.g. net primary productivity which can be calculated with vegetation models.

8531-2, Session 1

Comparison of leaf area index derived by statistical relationships and inverse radiation transport modeling using RapidEye data in the European alpine upland

Sarah Asam, Julius-Maximilians-Univ. Würzburg (Germany); Doris Klein, Deutsches Zentrum für Luft- und Raumfahrt e.V. (Germany); Stefan Dech, Deutsches Zentrum für Luft- und Raumfahrt e.V. (Germany) and Julius-Maximilians-Univ. Würzburg (Germany)

The Leaf Area Index (LAI) is a key parameter of vegetation structure and a relevant input parameter for flux modeling of energy and matter in the biosphere. It is provided by global operational products in a coarse spatial resolution (1 km) such as the MODIS LAI product. However, in a heterogeneous landscape with a small-scale land use pattern such as the alpine upland in Bavaria, global products are less suited. Additionally, the highly dynamic and owner dependent mowing and pasturing practices in grasslands result in a high temporal and spatial heterogeneity. Thus, the newly available high spatial resolution (5 m) RapidEye data are tested for their applicability for deriving LAI in grassland. Thereby, also the potential of RapidEye's new red edge channel is investigated. As LAI derivation methods, the empirical-statistical approach based on regression functions with vegetation indices as well as radiation transfer modeling are used. First, established indices (Normalized Difference Vegetation Index, Renormalized Difference Vegetation Index, Soil-Adjusted Vegetation Index) as well as new indices substituting the red band information with RapidEye's red edge band (Normalized Difference Vegetation Index NDVIrededge, Rededge Ratio Index 1, Rededge Ratio Index 2) are calculated for four scenes from beginning of May, end of May, June and September 2011. The correlations of these indices with in situ LAI data, which are collected during the contemporaneous weeks in the River Ammer catchment, are analyzed. The in situ LAI was measured with the LI-COR LAI2000 Plant Canopy Analyzer. From the resulting statistical relationships individual regression equations are derived. The coefficients of determination (R2) of the regressions vary between indices, with results suggesting that the red edge indices outperform the traditional indices. In the physical modeling approach, the RapidEye reflectances are used as input data to an inverted radiation transfer model. The coupled PROSPECT+SAILh model (PROSAIL) is parameterized with leaf optical and canopy properties collected in the field over the vegetation periods of 2011 and 2012. Regarding the inversion, look up tables are applied. While the radiation transfer model inversion has been reported to be the superior method in other studies, specific calibration and underdetermination issues are expected. Thus, the comparison of the results obtained by the radiation modeling for all time steps to those achieved with the empirical-statistical method reveals valuable information about the quality and constraints of these algorithms in order to give an estimate on the uncertainties associated with modeling.

8531-3, Session 1

Contribution of radar images for grassland management identification

Pauline Dusseux, Xing Gong, Univ. Rennes 2 (France) and LIAMA (China); Thomas Corpetti, LIAMA (China); Laurence Hubert-Moy, Samuel Corgne, Univ. Rennes 2 (France)

This paper is concerned with the identification of grassland management using both optical and radar data. In that context, grazing, mowing and a mix of these two managements are commonly used by the farmers on grassland fields. These practices and their intensity of use have different environmental impact. Thus, the objectives of this study are, firstly, to identify grassland management practices using a time series of optical and radar imagery at high spatial resolution and, secondly, to evaluate the contribution of radar data to improve identification of farming practices on grasslands. Because of cloud coverage and revisit frequency of satellite, the number of available optical data is limited during the vegetation period. Thus, radar data can be considered as an ideal complement. The present study is based on the use of SPOT, Landsat and RADARSAT-2 data, acquired in 2010 during the growing period. After pre-processing computation, several vegetation indices, bio- physical variables, backscattering coefficients and polarimetric discriminators were computed on the data set. Furthermore, based on a statistic test taking into account the separability between variables, only some variables, identified as the most discriminating, were used to classify grassland fields. To take into account the temporal variation of variables, temporal indexes as first and second order derivatives were used. Classification process was based on training samples resulting from field campaigns and computed according six methods: Decision Trees, K-Nearest Neighbor, Neural Networks, Support Vector Machines, the Naive Bayes Classifier and Linear Discriminant Analysis. Results show that combined use of optical and radar remote sensing data is more efficient for grassland management identification.

8531-4, Session 2

Overview of USAID-World Bank-NASA collaboration to address water management issues in the MENA region *(Invited Paper)*

Shahid Habib, NASA Goddard Space Flight Ctr. (United States)

The World Bank, USAID and NASA have recently established a joint project to study multiple issues pertaining to water related applications in the Middle East North Africa (MENA) region. The main concentration of the project is on utilization of remote sensing data and hydrological

models to address crop irrigation and mapping, flood mapping and forecasting, evapotranspiration and drought problems prevalent in this large geographic area. Additional emphases are placed on understanding the climate impact on these areas as well. Per IPCC 2007 report, by the end of this century MENA region is projected to experience an increase of 3°C to 5°C rise in mean temperatures and a 20% decline in precipitation. This poses a serious problem for this geographic zone especially when majority of the hydrological consumption is for the agriculture sector and the remaining amount is for domestic consumption. The remote sensing data from space is one of the best ways to study such complex issues and further feed into the decision support systems. NASA's fleet of Earth Observing satellites offer a great vantage point from space to look at the globe and provide vital signs necessary to maintain healthy and sustainable ecosystem. These observations generate multiple products such as soil moisture, global precipitation, aerosols, cloud cover, normalized difference vegetation index, land cover/use, ocean altimetry, ocean salinity, sea surface winds, sea surface temperature, ozone and atmospheric gasses, ice and snow measurements, and many more. All of the data products, models and research results are distributed via the Internet freely through out the world. This project will utilize several NASA models such as global Land Data Assimilation System (LDAS) to generate hydrological states and fluxes in near real time. These LDAS products will then be further compared with other NASA satellite observations (MODIS, VIIRS, TRMM, etc.) and other discrete models to compare and optimize evapotranspiration, soil moisture and crop irrigation, drought assessment and water balance. The floods being a critical disaster in many of the MENA countries, NASA's global flood mapping and modeling framework (CREST) will be customized for country specific needs and delivered to the remote sensing organizations for their future use. Finally, capacity building is a critical part of this project and NASA will assist in this effort as well.

8531-5, Session 2

Evaluating several satellite precipitation estimates and global ground-based dataset on Sicily (Italy)

Francesco Lo Conti, Univ. degli Studi di Palermo (Italy); Kuo-Lin Hsu, University of California, Irvine (United States); Leonardo V. Noto, Univ. degli Studi di Palermo (Italy); Soroosh Sorooshian, University of California, Irvine (United States)

The developing of satellite-based precipitation retrieval systems, presents great potentialities for several applications ranging from weather and meteorological applications to hydrological modelling. Evaluating performances for these estimates is essential in order to understand their real capabilities and suitability related to each application.

In this study an evaluation analysis of satellite precipitation retrieval systems has been carried out for the area of Sicily (Italy). The high density rain gauges has been used to evaluate selected satellite precipitation products. Sicily has an area of 26,000 km2 and the gauge density of the network considered in this study is about 250 km2/gauge. It is an island in the Mediterranean sea with a particular climatology and morphology, which is considered as an interesting test site for satellite precipitation products on the European mid-latitude area. Three satellite products (CMORPH, PERSIANN, TMPA-RT) along with two adjusted products (TMPA and PERSIANN Adjusted) have been selected for the evaluation. Evaluation and comparisons between selected products is performed with reference to the data provided by the gauge network of Sicily and using statistical and visualization tools.

Results show that bias is considerable for all satellite products and climatic considerations are reported to address this issue along with an overall analysis of the PMW retrieval algorithm performance. Moreover bias issues are observed for the adjusted products even though it is reduced respect to only-satellite products. In order to understand this result, the ground-based precipitation dataset used by adjusted products (GPCC dataset), has been examined and weaknesses arising from spatial sampling of precipitation process have been identified for the study area. Therefore possible issues deriving from using global ground-based datasets for local scales are pointed out from this application.

8531-6, Session 2

An integrated information system for the acquisition, management and sharing of environmental data aimed to decision making

Goffredo La Loggia, Elisa Arnone, Giuseppe Ciraolo, Antonino Maltese, Leonardo Valerio Noto, Univ. degli Studi di Palermo (Italy); Umberto Pernice, TeRN - Technological District of the Basilicata (Italy)

This paper reports the first results of the Project SESAMO - SistEma informativo integrato per l'acquisizione, geStione e condivisione di dati AMbientali per il supportO alle decisioni (Integrated Information System for the acquisition, management and sharing of environmental data aimed to decision making), funded by the Regional Sicilian Government within the "Linea di intervento 4.1.1.1 - POR FESR Sicilia 2007-2013".

The main aim of the project is to provide monitoring services for decision support, integrating data from different environmental monitoring systems (including WSN). From a technological viewpoint an ICT platform based on a service-oriented architecture (SOA) will be developed: in this way it will be possible to coordinate a wide variety of data acquisition systems, based on heterogeneous technologies and communication protocols, providing different monitoring services.

The implementation and validation of the SESAMO platform involves three specific domains: 1) Urban water losses; 2) Early warning system for rainfall-induced landslides; 3) Precision irrigation planning.

Services in the first domain are enabled by a low cost sensors network collecting and transmitting data, in order to allow the pipeline network managers to analyse pressure, velocity and discharge data for reducing water losses in an urban contest.

Services in the second domain are enabled by a prototypal early warning system able to identify in near-real time high-risk zones of rainfall-induced landslides. These services include three macro-components: the first allows deriving susceptibility maps of landslides vocation, which identify the hot-spots areas, on the basis of static variables characterizing the territory; the second will integrate rainfall data obtained by rainfall radar and forecast models to monitor and take into account actual rainfall; the third will incorporate hydrological and slope stability models to forecast landslides probability of hot-spot area using rainfall data from second component and measurements from the WSN monitoring system (humidity, temperature, etc..). Some of the variables monitored in real time (e.g. terrain displacements, terrain acceleration) will be also used as indicators of a near oncoming risk.

Services in the third domain are aimed to optimize irrigation planning of vineyards depending on plant water stress. Irrigation planning is nowadays based on field measurements of pre-dawn leaf water potential, that give a fragmentary framework of the vineyard water stress, both in time and in space. Moreover measurements of quality is related to the ability of the agronomist to interpret the plant response also in uncomfortable situations (such as in night time). Data interpretation should take into account environmental forcing due to solar radiation, air temperature and humidity, wind speed and direction, air carbon dioxide concentration, etc.. Irrigation planning could be based on evapotranspiration maps derived using remote or proximity sensing techniques. Within this framework a relationship between leaf water potential and actual evapotranspiration has been implemented and calibrated on some cultivars. Maps of both leaf water potential and actual evapotranspiration will be released in near-real time to the farmers through the SESAMO platform to allow the irrigation planning as function of the actual plants water stress.

The paper reports the first results of the latter two domains of services detailing the remote sensing applications for rainfall monitoring and precision irrigation planning.

8531-7, Session 2

Possibility of use of surface water resource in an arsenic contaminated region, Prubasthali I and II Block, Burdwan, West Bengal: a GIS approach

Biplab Biswas, The Univ. of Burdwan (India)

Arsenic values in groundwater above the maximum permissible limit of 0.05 mg/l (Indian standards) have been reported from Bhagirathi-Hooghly flood plain regions of West Bengal. The present study at Purbasthali I and II block in Burdwan district, West Bengal, is located in active the flood plain. Many flood plain features are mapped using conventional topographical maps and updated by satellite images. Lots of shallow depth (<10 metre) tube wells were set up in the recent past to meet the domestic and agricultural water need. The tube wells are still providing water for domestic and irrigation purposes. But unfortunately most of the tube wells' water is arsenic contaminated. It has been studied that the higher amount of arsenic content tube wells (>0.50mg) are located around the major flood plain features like ox-bow lakes. Using Buffer analysis in GIS, it has been studied the majority of the villages are located around these features. These features are capable of holding lots of water and can supply water for the villagers at least for drinking purpose. Arsenic of surface water is harmless and it can be suggested that the villagers can use surface water, with proper purification for their daily uses. If the remaining less than 50 per cent population are interested to walk for an average distance of 250 meters, will get a big pond or lake for the much needed arsenic free water. The villagers must be provided purified alternative safe drinking water from surface water bodies.

8531-94, Session 2

Combined X- and L-band PSI analyses for assessment of land subsidence in Jakarta

Fifamè N. Koudogbo, Javier Duro, Alain Arnaud, Altamira Information (Spain); Philippe Bally, ESA European Space Research Institute (Italy); Hasanuddin Z. Abidin, Institut Teknologi Bandung (Indonesia); Heri Andreas, Institute of Technology Bandung (Indonesia)

Jakarta is the capital city of Indonesia with a population of about 9 million people, inhabiting an area of about 660 Km2 along the coast of the Java Sea. The subsidence due to groundwater extraction, increased development, natural consolidation of soil and tectonics in Jakarta has been known since the early part of the 20th century [1]. Evidence of land subsidence exists through monitoring with GPS, level surveys, preliminary InSAR investigations and cracking of buildings.

Studies conservatively estimate land subsidence in Jakarta occurring at an average rate of 5 cm per year, and in some areas, over 1 meter was already observed. If land subsidence continues at this rate, by 2010, critical areas particularly in north and west Jakarta could have subsided by 500 cm. Recent studies of land subsidence found that while typical subsidence rates were 7.5-10cm a year, in localized areas of north Jakarta subsidence in the range 15-25 cm a year was occurring, which if sustained, would result in them sinking to 4 to 5 meters below sea level by 2025. Land subsidence will require major interventions, including increased pumping, dikes and most likely introducing major infrastructure investment for sea defence [1].

With the increasing prevalence of Earth Observation (EO), the World Bank and the European Space Agency (ESA) have set up a partnership that aims at highlighting the potential of EO information to support the monitoring and management of World Bank projects. It in this framework that was defined the EOWorld projects [2]. Altamira Information, company specialized in ground motion monitoring, was in charge of one of those projects, focusing on the assessment of land subsidence in Jakarta.

The area of interest (AOI) considered extends over about 1300 km2; it covers the Agglomeration of Jakarta but also the suburban district of Cikarang, located in the Benkasi district.

The technical solution proposed by Altamira is based on the combination of both VHR X-band data for high density of measurement points and L-band to detect strong motion, which is optimal for a densely constructed area with strong ground motion. The processing was performed with the PSI processing chain developed by Altamira and qualified in the framework of the GSE ESA project Terrafirma called Stable Points Network interferometric Process [3].

In order to cover the extended AOI, two adjacent frames of COSMO-SkyMed data have been required. The frames have been processed separately, and techniques of mosaicking has been developed in order to derive uniform and calibrated information on terrain deformation affecting the AOI.

ALOS and COSMO-SkyMed measurement maps show a good agreement. Common subsidence patterns have been highlighted. The better temporal distribution of measurements achieved with the high revisit rate of the COSMO-SkyMed mission (acquisition each 16 days) allows to better assess changes of trend of the subsidence (acceleration and slowdown). This fast revisit time also allows fast motion to be monitored.

In this paper the technical solution proposed by Altamira is presented and the results discussed.

[1] Z. H. Abidin, H. Andreas, M. Gamal, I. Gumilar, M. Napitupulu, Y. Fukuda, T. Deguchi, Y. Maruyama and E. Riawan. Land subsidence characteristics of the Jakarta basin (Indonesia) and its relation with groundwater extraction and sea level rise. in IAH selected papers 16, Groundwater Response to Changing Climate, eds. M. Taniguchi and I.P. Holman, CRC Press, 113-130, 2010

[2] http://siteresources.worldbank.org/INTURBANDEVELOPMENT/Resources/336387-1278006228953/EOworld_Progress_Report.pdf

[3] N. Adam, A. Parizziet M. Crosetto. Practical Persistent Scatterer Processing Validation in the Course of the Terrafirma Project. Journal of Applied Geophysics, vol. 69, pp.59-65, 2009

8531-8, Session 3

RapidEye water quality support service for the environmental agency in Brandenburg, Germany

Sandra Reigber, RapidEye AG (Germany)

In 2000, the EU parliament made the framework decision that all member countries need to analyse and evaluate the water quality of lakes with a surface area greater than 50 ha. With more than 10.000 lakes Brandenburg has more water bodies than any other state in Germany. Less than 250 of them have to be analysed regarding to the EU water directive. An entire overview of the water quality of all lakes in Brandenburg is therefore not given. At the same time, such an overview is not achievable with conventional sampling techniques due to logistic and financial reasons. Alternatively, remote sensing based analysis methods can be effectively used for this task.

The RapidEye constellation of five identical earth observation satellites is capable of collecting over 4 million km? of 5 m resolution imagery every day. This, combined with the existence of the RedEdge band, makes RapidEye well suited for a large-scale lake water monitoring. This paper presents the results of a feasibility study with the objective to monitor the trophic state of all Brandenburgian lakes with a surface area greater than 10 ha (828 lakes).

In order to determine the trophic state of the lakes, the chlorophyll-a content and the Secchi depth were estimated from RapidEye remote sensing data. Regarding to the EU water framework directive, chlorophyll-a (chl-a) is an indicator of the biological quality of a lake. The Secchi depth (SD) is a parameter for the transparency of a lake. According to the European and national water directives both parameters have to be determined at least four times a year.

In 2009, RapidEye was able to generate six satellite image coverages of Brandenburg throughout the bio-productive season of the lakes. Coverages were done: once in spring (March-April), four times during the summer season (May-September) and once in autumn (October-November). Because of the enormous amount of satellite images (more than 1000 RapidEye tiles), all data were automatically atmospherically corrected using the atmospheric correction tool ATCOR. Simultaneous to the RapidEye data recording, in-situ data were acquired at several reference lakes. Using these data, chlorophyll-a and Secchi depth algorithms were developed and applied to all RapidEye satellite images. As a result of this study, seasonal maps of chlorophyll-a concentration and Secchi depth were generated for every analysed lake. Additionally, lake minimum, maximum, mean and median values of chlorophyll-a and Secchi depth were estimated for further analyses.

In a last step all results were evaluated based on a set of validation data. These data were acquired in the course of the regular water sampling activities of the Ministry of Environment, Health and Consumer Protection in Brandenburg. The provided validation data were taken within a minimum of five days before or after an image acquisition.

First validation results show that the user requirements of the Ministry can be achieved for most of the lakes in this study. Additionally, a detailed error analysis was carried out and will be also described in this paper.

8531-9, Session 3

Monitoring a river channel network at Salar de Uyuni using Landsat ETM+ images

Seyed Enayat Hosseini Aria, Rick Donselaar, Roderik Lindenbergh, Roderik Koenders, Jiaguang Li, Anneleen Oyen, Technische Univ. Delft (Netherlands)

In this paper the potential of Landsat ETM+ images to detect the temporal and spatial changes of river channels at the terminus of a fluvial system in the Uyuni closed drainage basin in the south west of Bolivia has been investigated. Rivers in semi-arid areas experience downstream reduction of water volume and consequently decrease of fluvial channel size. There is increasing evidence that these dryland rivers terminate as a stream breaks its natural or artificial bank and deposit sediment on the floodplain (crevasse splay). Abandonment of old river channels and creation of the new ones results in a complex pattern over time.

Salar de Uyuni in the basin center is the world's largest salt pan with an area of ca. 12,500 km2, with drainage area about 5000 km2 (Fig.1). Daily precipitation records between 1995-2010 from the local weather stations were used to find out highly precipitation events. Rainfall is concentrated in the austral summer months December-March, and characterized by short, 24-48 hour periods of torrential rain. We have also collected field work information in terms of sedimentology and terrestrial measurements which were used to interpret the images more precisely, and producing quantitative results.

The useful available Landsat ETM+ images for this region (WRS-2, Path 233, Row 074) are from July 1999 till April 2003, as after May 2003, the Landsat-7 scan-line corrector failed, so the ETM+ is losing approximately 22% of the data due to the increased scan gap. On average, there are about five complete images in each year, where still some images are affected by clouds. In this research, the focus is on detecting new crevasses splays and changes in meanders (winding bends of a river) which formed after intensive precipitation. In addition, identification of areas affecting salinization and degradation for the identified 4-year period were also studied. Image processing techniques such as best band selection for semi-arid areas, stretching, band ratioing, and data fusion were applied to enhance change detection and interpretation.

The first ETM+ image analysis results show changes in river morphology, and allow to identify new crevasses splays and changes in channel locations. It was also observed that the reflectance of abandoned channels increased after several consecutive weeks of high precipitation(Fig. 2.). It seems that those channels became reactivated, while their water transported sediments in suspension which caused a rapid growth in the reflectance in visible bands. Salt identification using Landsat spectral-band analysis is easiest at end of the dry season (Fig. 3.), as salt dissolve during the rainy season. Furthermore, salt detection is hampered in multispectral images by increasing moisture, because of the lower spectral response. Outcrop observations confirm that a salt crust formed in the upper part of the soil in the dry period. The study shows that Landsat ETM+ images in combination field work data have good potential to identify temporal and spatial changes in river morphology, more specifically the variation in channel locations and crevasse splay growth.

8531-10, Session 3

An object-based method for mapping ephemeral river areas from WorldView-2 satellite data

Benedetto Figorito, CNR-ISSIA (Italy); Eufemia Tarantino, Gabriella Balacco, Umberto Fratino, Politecnico di Bari (Italy)

Karst landscapes are generally not dominated by surface runoff. The "Murge" karstic area in Apulia (Southern Italy) shows a well-developed drainage-network, formed by a dense dendritic pattern in the headwater zone ("Murge Alte") which evolves into regularly spaced, incised valleys moving towards the coastal area ("Murge Basse"). These valleys are locally named "lame", and show subvertical rocky flanks and a flat bottom. Valleys cutting the Murge area act as water channels only during and immediately after heavy rainfall, and can be classified as episodic (ephemeral) rivers.

In the last years, the important hydraulic function of the lame has been heavily altered, so that these sites, which were originally drainage lines only, became pasture or agricultural land and later areas of intensive quarrying and urbanisation. These alterations have increasingly transformed, disturbed, and partially or totally destroyed the karst landscape causing modification of the surficial and underground drainage, and deterioration in the quality of groundwater. Moreover, floods, once a rare phenomenon, are becoming frequent in Apulia, especially along its Ionian side. As consequence, a high level of attention must always be given to the protection of the territory in order to avoid high risk situations. Once hydraulic operations are carried out, they must be maintained and monitored in terms of land use and vegetation dynamics in order to continue their efficiency which cannot be put to risk by poor territorial planning.

Classification is a widely studied issue in remote sensing image processing. The common application ranges from land use analysis to change detection. Among the classes of interest, urban areas, farmland, forest, and river/lake areas are traditionally selected. The observation of water body from remote sensing images, is of particular importance during these recent years for two main reasons: there is an important need to assess existing water resource and, because of the increasing water scarcity and related problems, timely information of water increase may help to develop some strategy to restrict flood calamities.

Recently available Worldview-2 high-resolution imagery (WV-2) with nine spectral bands and very high resolutions (spectral and radiometric) affords the opportunity to bring forth new knowledge regarding the on-going debate of whether object-oriented or spectral-based classification approaches are more accurate.

In this work object-oriented and spectral-based methods for land cover mapping and water-body delineation of an ephemeral river area along the Ionian side of Apulia were implemented. Results were compared with analogous spatial resolution data, i. e. based on historical true color orthophoto, to determine temporal transformations along the investigated study area. The object-oriented and spectral-based approaches were evaluated to estimate impact based upon classification accuracy.

8531-11, Session 4

Small-scale albedo-temperature relationship contrast with large-scale relations in Alaskan acidic tussock tundra

Hella E. Ahrends, Univ. of Cologne (Germany); Steven Oberbauer, Florida International Univ. (United States); Werner Eugster, ETH Zürich (Switzerland)

Arctic tundra vegetation is characterized by an extreme heterogeneity at a small spatial scale. Small differences in microtopography and moisture conditions cause different types of ecosystems. Different ecosystems are expected to respond differently to climate change. These differences are therefore critical for extrapolating plot measurements to larger spatical scales (e.g. the resolution of aircraft and satellite imagery) and for correctly representing arctic ecosystems in climate models. A detailed knowledge and understanding of soil-vegetation-atmosphere feedback mechanisms at different spatial scales is needed. However, the short growing season and harsh environmental conditions strongly limit the frequency and spatial cover of spectral and thermal measurements. Here we aim at presenting our results from the analyses of data simultaneously measured by a mobile multi-sensor platform. We show the need for such observations for an improved understanding of complex feedback-mechanisms in the tundra.

In the framework of the International Tundra Experiment (ITEX) Arctic Observation Network (AON) we aim to establish the infrastructure for automated multi-sensor observations of tundra vegetation across a topographic transect in the Arctic. During growing seasons 2010 and 2011 first measurements were performed at two sites located in the acidic tussock tundra in northern Alaska. The measurement set-up is moved along a transect that can be spanned by a cable and covers an area of approximately 50 m length and 2 m width. The sensor trolley was equipped with state-of-the-art instruments for recording the distance to vegetation canopy (SR50a Sonic Distance, Campbell Scientific), up- and downwelling short- and longwave radiation (CNR4 net radiometer, Kipp & Zonen), air temperature and surface temperature (SI-111 IR radiometer, Apogee Instruments Inc.) and spectral reflection (Jaz Combo-2, Ocean Optics; GreenSeeker

RT100 (505), NTech). The spectral and thermal properties of the surface were measured at a height of approximately 0.8-1.2 m over local ground level. The transects reflect the typical small-scale transitions from dry, shrub and lichen-dominated tundra surfaces to wet, hummocky and tussock-dominated tundra over which traditional large-scale approaches need to integrate. The data were aggregated to distance increments of 45 cm along the transects and standardized (mean-centered) to account for observation date-specific offsets in measurements that were related to specific light and weather conditions but not to the local vegetation surface.

A relative increase in the albedo of 0.01 (1%) was related to an increase in radiometric surface temperatures of 0.1 to 1 K, which is the inverse of the generally accepted surface temperature-albedo relationship observed at larger spatial scales. We explain this finding with cooling effects of the albedo-influencing surface wetness which primarily results from moss and soil evaporation. This cooling effect dominates over other more general heating effects that can be expected over surfaces with lower albedo under absence or near-absence of evaporation. Our findings are also supported by NDVI measurements. These locally inverted temperature-albedo feedbacks need to be considered in climate models that resolve Arctic environments with a high abundance of moss covers. Our results show that frequent observations of different tundra ecosystems from multi-sensor platforms can provide data critical for the interpretation of large scale data from aircraft or satellite platforms and for understanding the land-atmosphere-interactions for the Arctic and the global system.

8531-12, Session 4

A sequential Bayesian procedure for integrating heterogeneous remotely sensed data for irrigation management

Paolo Addesso, Roberto Conte, Maurizio Longo, Rocco Restaino, Gemine Vivone, Univ. degli Studi di Salerno (Italy)

Continuous and detailed tracking of physical properties variations is crucial in many agricultural applications of remote sensing. In irrigation management the crop water requirements are evaluated through a balance equation that quantifies the water exchange between land surface and atmosphere. In this case a crucial parameter is constituted by the radiometric surface temperature [Rivas04] that can be estimated by using near and thermal infrared data.

However the desirable conjunction of high spatial and temporal resolutions results in conflicting requirements for any real sensor. Accordingly a research effort is nowadays devoted to integrate data at high acquisition rate with data provided by sensors with small pixel sizes. Hence the objective of the present work is to design a procedure for sequential estimation of relevant physical quantities by taking advantage of such heterogeneous information sources.

The exploitation of heterogeneous data is commonly approached from two different points of view. The first aims to construct a fictitious dataset that satisfies the application specifications (data-level fusion). Valuable results have been achieved with this methodology in the field of multispectral image enhancement through panchromatic images, the so-called pansharpening process [Alparone07]. The complementary approach focuses on the combination of higher level characteristics (feature-level fusion) and now represents the most effective method for segmentation of remotely sensed images [Tarabalka10].

However the optimality of the existing methods is surely debatable, being they often derived from pragmatic approaches. On the other side the Bayesian framework offers a powerful statistical tool for dealing with random quantities and, very interestingly, with uncertain data. In this paper we exploit this opportunity by formalizing the fusion of data collected from different sensors within the FInite Set Statistics (FISST) framework [Goodman97]. In particular we model the available images as Ambiguously Generated Ambiguous (AGA) measurements [Mahler07] in which the typical randomness due to statistical variations of the observations is combined with the vagueness determined by the pixel size.

The described approach is here applied to derive a Bayesian sequential method that profits from multitemporal multisource data in order to improve estimation of radiometric surface temperature that is essential for agricultural resource management. The performances are evaluated by comparing the predicted values with a high spatial resolution ground truth.

References

[Alparone07] L. Alparone, L. Wald, J. Chanussot, C. Thomas, P. Gamba, and L.M. Bruce, “Comparison of pansharpening algorithms: Outcome of the 2006 GRS-S data-fusion contest,” IEEE Trans. Geosci. Remote Sens., vol. 45, no. 10, pp. 3012-3021, Oct 2007.

[Goodman97] I. Goodman, R. Mahler and H. Nguyen, Mathematics of Data Fusion, Kluwer Academic Publishers, 1997.

[Mahler07] R.P.S. Mahler, Statistical Multisource-Multitarget Information Fusion, Artech House, 2007.

[Rivas04] R. Rivas V. Caselles, “A simplified equation to estimate spatial reference evaporation from remote sensing-based surface temperature and local meteorological data, Remote Sens. Environ., vol. 93, pp. 68-76, Oct 2004.

[Tarabalka10] Y. Tarabalka, M. Fauvel, J. Chanussot, and J. Benediktsson, “SVM- and MRF-based method for accurate classification of hyperspectral images,” IEEE Geosci. and Remote Sens. Letters, vol. 7, no. 4, pp. 736-740, Oct 2010.

8531-13, Session 4

Frost monitoring of fruit tree with satellite data

Jinlong Fan, Mingwei Zhang, China Meteorological Administration (China)

The orchards are developing very fast in the northern China in recent years with the increasing demands on fruits in China. In most part of the northern China, the risk of frost damage to the fruit tree in early spring is very high under the background of the global warming. The main reason is that the tolerance to low temperature is decreasing when the leaf is extending, the fruit tree is blooming, and the small green fruit is forming. In some year, the grow season comes earlier than it does in the normal year due to the warm weather in earlier spring and the risk will be higher in this case. The frost damage happens when the cold atmosphere around zero degree flows over the area. According to the reports, frost event in spring happens almost every year in some area in northern China. In bad cases, late frosts in spring can be devastating to all fruit.

In the past 10 year, more than 5 severe frost events have happened in Ninxia Region, northwest China, in April and May and caused no harvest. So frost damage to fruit trees is a significant concern. Lots of attentions have been given to monitoring, evaluating, and protecting the frost. Two orchards in Ninxing, Taole and Jiaozishan orchards were selected as the study areas. The apple, pear are major trees in the orchards. The frost events have been recorded in the orchards since 2000. 5 severe events in April 8 and May 3, 2004, May 13, 2006, May 12, 2007, April 12, 2010 are chosen as the case study. The MODIS data and FY data are used to monitoring the events in combination with minimum air temperature recorded at the weather station. FY is the short name of the Chinese meteorological satellite- FengYun, meaning wind and cloud in English. FY-3 is the second general polar orbiting Chinese meteorological satellite. 11 sensors are onboard FY-3A, launched in May 2008, and FY-3B, launched in November 2010. MERSI onboard FY-3 is similar with the MODIS. The surface temperature is retrieved from the MODIS data and FY data during the events. A remote sensing model for the identification of the frost freeze is developed referring to the meteorological frost model. Finally the paper presents the methodology of monitoring frost with satellite data. The monitoring information will be expected to help the fruit farmers to cope with the damage and loss.

8531-14, Session 5

A comparison of two coupling methods for improving a sugarcane model’s yield estimation

Julien Morel, Jean-François Martiné, Agnès Bégué, Pierre Todoroff, CIRAD (France); Michel Petit, Institut de Recherche pour le Développement (France)

Coupling remote sensing data with crop model has been shown improving accuracy of model’s yield estimation.

MOSICAS model simulates with a great accuracy sugarcane yield in controlled conditions plot, based on different variables, including interception efficiency index (i). In this study, we compared two different coupling approaches between this model and remote

sensing acquired interception efficiency index data.

Study area was located in Reunion Island (Indian Ocean). Six agricultural plots with surfaces ranging from 8.1 to 25.6 hectares were studied from October 2011 to April 2012 in southern part of the island. Nine repetitions were made for each of these plots, in order to overcome spatial heterogeneities. Three pluviometers were dispatched over our study area, gathering daily data. Weekly ground measurements were made using an Accupar LP80 coupled with external sensor, collecting a total of 39 values of interception efficiency index. Normalized Difference Vegetation Index values were computed using four Spot 4 and three Spot 5 “Top of Canopy” images acquired over the same period. A linear relationship between i and NDVI has then be computed, showing significant accuracy (R? = 0.8934). New values of i have then been calculated with this relationship using Spot 4 and Spot 5 images acquired from January 2011 to October 2011 (NDVI2011). A logistic regression has then been applied on NDVI2011 to compute NDVI values at daily time step. Acquired data have been used to compute i at daily time step for each plots’ growth period. Growth simulations for every studied plot have been made using MOSICAS sugarcane model. Three types of simulations have been made. The first one consisted in a standard simulation where the only input data are daily precipitations, daily temperatures and daily global radiations. The second type has been made using the forcing coupling method, where MOSICAS computed values of i have been replaced by NDVI computed i for each available satellite image. The third type finally consisted in using the assimilation coupling method, where all MOSICAS simulated i have been replaced by NDVI computed i.

Preliminary results showed interesting prospects. For a field measured yield of 96 tons of sugarcane per hectare, MOSICAS computed a yield of 143 tons per hectare, while MOSICAS coupling with i using assimilation method computed a yield of 128 ton per hectare. Forcing method did not show notable improvement in yield prediction, as we had a lack of satellite images for the last half part of the simulation, preventing us from computing i values for this period.

8531-16, Session 5

Land cover change estimation for protected areas in Sub-Saharan Africa

Zoltan Szantoi, Dario Simonetti, Andreas Brink, European Commission Joint Research Ctr. (Italy)

The European Union supports conservation efforts as well as Protected Area’s management in the African continent, especially in Sub-Saharan Africa. However, access to up to date information regarding the status, threats and value of these areas are lacking. Thus, a semi-automated processing chain to detect land cover change for protected areas and their surroundings is being developed by the Joint Research Centre of the European Commission. The Global Forest Resource Monitoring (TREES3) project based on systematic sampling of medium resolution imagery showed that many of the protected areas are disturbed and their surrounding zones are changing rapidly. Thus, the aim of this study was to detect, map and quantify these changes in selected protected areas across Sub-Saharan Africa and to estimate the tree cover loss and degradation of the natural landscape, using medium resolution imagery (Landsat and UK-DMC 2) and object based classification with spectral library. The imagery was collected for the years of 1990 - 2000 - 2010. The pre-processing steps of the imagery involved radiometric calibration, cloud and cloud shadow masking, topographic correction using Shuttle Radar Topographic Mission’s digital elevation data (90m), de-hazing, mosaicing and radiometric normalization. Six different land cover classes were mapped for the protected areas as well as for their 20 km buffer zone using the object based classification method. The classes were based on the recent TREES3 project of the European Commission’s Joint Research Centre’s Land Cover Classification System, which included (1) tree cover, (2) tree mosaic, (3) other wooded land, (4) other vegetation cover, (5) bare or artificial and (6) water. In this paper we are focusing mainly on the explanation of the pre-processing steps of the semi-automated method, which was developed to work in a semi-automatic way over different type of ecoregions. However, the detected land cover dynamics are also presented as change detection maps for the study areas, while quantitative results reveal information on tree loss, deforestation, fragmentation or in some cases revegetation during the investigated period. The changes are then discussed within the framework of tropical deforestation, agricultural intensification and urbanization.

8531-17, Session 5

Water productivity assessment by using MODIS images and agrometeorological data in the Petrolina municipality, Brazil

Antônio Heriberto C. Teixeira, Embrapa Semiárido (Brazil); Morris Sherer-Warren, Agência Nacional de Águas (Brazil); Fernando B. T. Hernandez, Univ. Estadual Paulista (Brazil); Hélio L. Lopes, Univ. Federal do Vale do São Francisco (Brazil)

The municipality of Petrolina, located in the semi-arid region of Brazil, is highlighted as an important growing region, with the commercial agriculture being the main activity. The areas with fruit crops are expanding creating a boost for the rural economy; however the irrigated areas have cleared natural vegetation inducing a loss of biodiversity. The contrast between these two systems becomes apparent when analysing the regional biomass production (BIO). Two models were coupled to assess BIO. Monteith´s equation was applied for estimating the absorbed photosynthetically active radiation (APAR), while the Teixeira’s algorithm was used to retrieve the latent heat flux (λE) that together with net radiation (Rn) acquired with the Slob equation, included the effect of land moisture on BIO by the energy partitioning. As the agricultural drainage can adversely affect the water quality, the water productivity (WP) was analysed by the ratio of BIO by ET along the years, considering the irrigated and rain fed areas, being this classification done by a threshold value for the surface resistance to the water fluxes (rs). The bands 1, 2, 31 and 32 from 25 MODIS images together with 10 agro-meteorological stations were used, covering the period of 2010 to 2011, with field calibrations and interpolations. Energy balance measurements in irrigated crops and natural vegetation, during 2002 and 2004, were used to develop equations for surface albedo (α0), using the bands 1 and 2, and for surface temperature (T0), using the split windows technique with the bands 31 and 32. The basic input remote sensing parameters were NDVI, α0 and T0 for the regional scale ET and rs acquirements. The highest BIO values occur after the rainy period in April, around 2100 kg ha-1 month-1 for irrigated crops and 1550 kg ha-1 month-1 for natural vegetation. Maximum mean values for ET and WP, 67 mm month-1 and 2.9 kg m-3, respectively, happened also during this month. As the rains keep the soil moisture uniform this time of the year, the differences between irrigated crops are the lowest ones. The highest incremental values of BIO, ET and WP, as a result of the irrigated crops introduction, are from August to October, outside the rainy period, when the sun is around the zenith position, average totals of precipitation around 5 mm month-1 and high atmosphere demand, with reference evapotranspiration (ET0) rates from 170 to 195 mm month-1. More uniformity on the water variables studied along the year occurs in natural vegetation, evidenced by the lower standard deviation when comparing to irrigated crops, where due to the different cultural and irrigation managements the differences in WP values are more than the double of those for natural vegetation during the driest period of the year. The models applied with MODIS images at the municipality level are considered to be suitable for water productivity analyses and for quantifying the effects of increasing irrigated areas over natural vegetation on regional water consumption in situations of quick changing land use pattern, as in the case of Petrolina municipality.

8531-18, Session 6

Hyperspectral imaging: do information content, land cover classification, sensitivity analysis and inverse modeling of spectral reflectance lead to the same set of optimal spectral bands? *(Invited Paper)*

Massimo Menenti, A. Mousivand, Seyed Enayat Hosseini Aria, Ben Gorte, Technische Univ. Delft (Netherlands)

Terrestrial targets are characterized by heterogeneity at all scales and the observed spectral radiance across the 0.4 m - 2.4 m spectral region is determined by a complex combination of target geometry and bio-geophysical and chemical composition of target elements. The assumption underlying the quest for the continuous and reliable provision of hyper-spectral data from space is that exhaustive coverage and high spectral resolution sampling of reflected radiance is necessary to characterize such terrestrial targets. Literature provides conflicting evidence to this regard and we argue

that to a significant extent this is due to the fundamentally different requirements of four different applications of hyper - spectral image data:

- identification of independent spectral features;

- classification of land cover;

- understand the relation of spectral radiance with the properties of observed targets;

- retrieval of target properties by inversion of spectro - directional radiometric data

Theoretically the information content of a spectral sample is measurable by entropy which shows the amount of disorder, or unpredictability in the sample. If a spectral band is assumed as an independent sample, we can measure the information content of it, which is affected by several factors. Basically, the more heterogeneous the spectral radiance in a spectral band is, the higher the information content.. Therefore, radiometric resolution, width of bands (spectral resolution), etc. can influence on heterogeneity of a band which leads to changes in its information content. We have determined the optimal set of bands for very different scenes by using two different approaches: a) minimizing the correlation of selected bands; b) maximizing the amount of mutual information. In a spectral point of view, the spectral bands which can reconstruct full reflectance spectrum precisely can immensely useful to improve pattern recognitions issues.

The classification of land cover builds upon the separability, reliability and accuracy of class characterization using spectral attributes. Different band combinations are needed to assign various classes correctly, i.e. a unique band set may not be ideal for all applications. We identified different optimal sets for water, vegetation and 'mineral' sites, but these sets are not necessarily the same needed to distinguish *between* water, vegetation and 'mineral' objects.

The relation of spectral radiance with target has been investigated by a detailed analysis of the sensitivity of spectral radiance to the properties of observed targets. This has been done by using a model of radiative transfer in the soil-vegetation system and developing a new method to perform sensitivity analysis.. With this approach, in spite of looking for high variance among various spectral bands, we have identified the spectral bands most sensitive to specific target properties.

Retrieval by inverse modeling of spectro-radiometric image data has been widely employed to extract bio-geophysical information (such as LAI) from vegetated areas. When the objective is to estimate a certain vegetation property, the optimal band selection with focus on the content of the data is not applicable and efficient anymore. In this sense, a precise knowledge about which spectral bands are most sensitive to which parameter is an asset.

8531-20, Session 6

Assessing irrigated cropland dynamics in central Asia between 2001 and 2010 based on MODIS time series

Christopher Conrad, Fabian Loew, Moritz Rudloff, Gunther Schorcht, Julius-Maximilians-Univ. Würzburg (Germany)

Despite the transformation processes initiated after independence from the Soviet Union in 1991, most Central Asian countries heavily rely on high productivity in the agricultural sector. But the decline of the 8 Million ha of irrigated land caused by water uncertainties, declining irrigation and drainage infrastructure, and several other factors is recurrently reported to be continuing in the entire Aral Sea Basin. Spatially explicit information, for instance received from remote sensing based analyses, can be beneficial for regional assessments of trends in cropland development or for identifying options for improvements of land and water management in this region.

The proposed presentation focuses on assessment of irrigated cropland dynamics in Central Asia during the past decade by analyzing MODIS time series. Extend of cropland, cropping intensity (number of cropping seasons per year), and spatio-temporal cropping patters (monoculture and rotation systems) are assessed based on phenological profiles extracted from 8day MODIS products at a spatial resolution of 250m. Four MODIS tiles were processed to cover entire Central Asia. The quality assessment science data sets of the selected MODIS products indicated a high data quality throughout the year, which obviously occurs due to excellent atmospheric conditions and the dry continental climate in the lowlands of Central Asia. Decision trees generated from cropping calendars (expert knowledge) and automated algorithms (random forest) have been applied and compared. Time series of vegetation indices were calculated and temporally segmented for feature generation. Descriptive statistics of temporal segmentation accounts for variability of management, water availability, temperature development influencing sowing dates and other crop phenological steps. For training (only random forest) and validation, existing high resolution (Landsat and RapidEye) crop maps of Khorezm, the Fergana Valley (both in Uzbekistan), the Kashka Darya region (Tajikistan and Uzbekistan) and the Kyzyl-Orda region in Kazakhstan were utilized. Multiple seasons (e.g. winter wheat followed by a summer crop) were extracted by counting the peaks of each time series at pixel level and crop rotations were assessed by statistical comparison of two subsequent years (auto-correlation and cross-correlation).

Accuracy assessment returned acceptable results, even though in some regions degraded but vegetated land can hardly be distinguished from crops such as cotton under drought conditions - irrespectively if knowledge-based decision trees or automated classifiers were applied. The results show high dynamics of cropland extends in both dimensions, spatial and temporal. Especially water scarce years such as 2000, 2001, or 2008, show low to zero productivity at the fringes of the irrigation systems in the river catchments of Amu Darya and Syr Darya. Altogether, MODIS time series of croplands allow for regional assessments of cropping conditions in irrigation systems and the situation of water deficit indicated by unused downstream locations of the irrigation systems. Based on MODIS like data long-term observations at regional scale can be established not only in Central Asia, but also in other arid environments, where irrigation agriculture is essential for rural income generation and food security.

8531-21, Session 6

Caveats in calculating crop specific pixel purity for agricultural monitoring using MODIS time series

Gregory Duveiller, European Commission Joint Research Ctr. (Italy)

Monitoring agriculture at regional to global scales with remote sensing requires the use of sensors that can provide information over large geographic extends with a high revisit frequency. Current sensors satisfying these criteria have, at best, a spatial resolution of the same order of magnitude as the field sizes in most agricultural landscapes. Landscape fragmentation combined with crop rotation practices further complicates the task of obtaining adequate crop specific time series of remotely-sensed observations. As a consequence, a coarser signal describing the general cropland is used, limiting the potential of remote sensing technology.

Research has demonstrated that crop specific monitoring is possible with coarse spatial resolution such as MODIS (approximately 250 m at nadir) if a selection purer time series is used. To do so, a mask of the target crop is necessary at fine spatial resolution in order to calculate the crop specific pixel purity at the coarser spatial resolution. This pixel purity represents the relative contribution of the surface of interest, in this case the surface covered by the target crop, to the signal detected by the remote sensing instrument. A straightforward way to compute pixel purity is to calculate the area of the target crop that falls in the coarse spatial resolution grid. However, the observation footprint is generally much larger than the squared projection of the pixel. Furthermore, the relative contribution within this footprint is not homogeneous and depends on the spatial response of the sensor. These effects are particularly important for MODIS which has a triangular point spread function and which scans the Earth with high view zenith angles, heavily distorting the observation footprint.

This study analyses the consequences of calculating crop specific pixel purity using a model of the MODIS spatial response with respect to basing it only on the percentage of surface falling in the squared grid in which the product is delivered. The MODIS spatial response model is constructed taking into account different components of its point spread function (PSF): the detector PSD, the image motion PSD and the optical PSF. Since the result is anisotropic, the model must further be adjusted according to the angle between the north-south direction and the ground track of the satellite, the latter varying with latitude. Using this model on a given case study, differences in pixel purity can range between -10 to 15%, depending on the correspondence between the grid and the fields and on the absolute value of pixel purity that is considered. The spatial response is also different depending on whether the MODIS sensor is on-board of the Terra (descending) or Aqua (ascending) platform, and the repercussion on the calculation is also explored. The effect of high view zenith

angles on the purity calculation is also quantified with respect to the spatial response at nadir. Finally, the consequences of underestimating the spatial response when calculating pixel purity is illustrated by analysing the effect on the quality of daily MODIS time series.

8531-22, Session 6

Plant optical properties for chlorophyll assessment

Rumiana Kancheva, Georgi Georgiev, Denitsa Borisova, Space Research and Technology Institute (Bulgaria)

Remote sensing techniques acquire increasing importance in vegetation phytodiagnostics. Visible and near infrared multispectral data have proved abilities in vegetation monitoring. This wavelength region reveals significant sensitivity to plant pigment content. The optical signatures of leaves are mostly defined by the composition of photosynthetic pigments and their stress-induced changes, and as such provide valuable information about the physiological status of plants. The information is carried by the specific spectral behaviour of healthy plants and plants subjected to short-term or long-term stress impacts. Chlorophyll content is a prime bioindicator of plant condition being responsible for light absorption and the photosynthetic processes. In our study, optical multispectral data have been used to reveal the performance of different spectral signatures in chlorophyll estimation. Reflectance factors, vegetation indices, red edge shift, fluorescence parameters, and chromaticity features, have been related in a statistical manner to plant chlorophyll in order to examine the statistical significance of plant spectral response to chlorophyll variations. High correlation have been found permitting quantitative dependences to be established and used for plant diagnosis. Empirical relationships between plant spectral properties and chlorophyll concentration have been established that allow chlorophyll estimation and plant condition assessment in terms of chlorophyll variation to be performed by using diverse spectral indicators.

8531-23, Session 7

Sources of uncertainty for eddy covariance measurements over heterogeneous surfaces in a semi-arid region: impact to remote sensing *(Invited Paper)*

John H. Prueger, Agricultural Research Service (United States); Lawrence E. Hipps, Utah State Univ. (United States); Joe G. Alfieri, Agricultural Research Service (United States); Christopher M. U. Neale, Utah State Univ. (United States); William P. Kustas, U.S. Dept. of Agriculture (United States); Jerry L. Hatfield, Agricultural Research Service (United States)

Surface measurements of land-atmosphere exchange processes, such as the turbulent transport of heat and moisture, provide critical “ground truth” data for the evaluation of remote sensing-based products and models. Eddy covariance measurements of turbulent fluxes of water heat and momentum are routinely used in complex remote sensing experiments and are considered the most physically based approach for such measurements. Regardless, there is uncertainty associated with eddy covariance measurements of surface fluxes due to both the limitations of the sensors and the theoretical assumptions underlying the various measurement techniques. Additional sources of uncertainty can be found in the spatiotemporal variations of both the atmospheric conditions and the surface properties within the source area of the measurements. This is particularly true for remote sensing scenes captured over complex landscapes where limited fetch and patchwork-like surface characteristics are problematic for many surface measurement techniques. However, all of these potential sources of uncertainty can significantly impact comparisons of remotely sensed and surface data depending on the complexity of the landscape and the resolution of the data. We present and discuss potential sources of eddy covariance measurements and present results from a remote sensing study in Bushland, Texas under complex or extreme conditions such as heterogeneous terrain and strong advection.

8531-24, Session 7

Basin-scale evapotranspiration assessment based on vegetation coefficients derived from thermal remote sensing

Ana Andreu, Instituto de Investigación y Formación Agraria y Pesquera (Spain); Cristina Aguilar, Maria Jose Polo, Grupo de Dinámica Fluvial e Hidrología (Spain) and Instituto Interuniversitario de Investigacion del Sistema Tierra en Andalucia (Spain); Elisabeth Carpintero, Grupo de Dinámica Fluvial e Hidrología (Spain); M. Patrocinio Gonzalez-Dugo, Instituto de Investigación y Formación Agraria y Pesquera (Spain)

Evapotranspiration (ET) is a critical variable in hydrological modelling at watershed scale, whose actual regime is forced by the atmospheric conditions and limited by the available water in the soil profile. An accurate estimation is required to assess water managers in the short, medium, and long term, especially in arid and semiarid environments. However, ET is difficult to measure in many situations, especially when medium-large scales are considered, and crops and natural vegetation coexist. Currently, the integration of remotely sensed data into evapotranspiration models has broaden their area of application at basin or regional scales, providing us with a better representation of vegetation heterogeneity, and accounting for the local meteorological conditions to some extent.

A simple and operative method for calculating actual evapotranspiration is based on the use of crop coefficients (Kc). This approach has been traditionally used by the agricultural community for irrigation management and scheduling. Crop coefficients relate the ET of a given crop to the ET of a reference vegetated surface, computing it as the product of a reference evapotranspiration, ETo, as an index of climatic demand, and a Kc that integrates the effects of an specific crop characteristics (Doorenbos and Pruitt, 1992). A few attempts have recently extended this methodology to natural ecosystems (Descheemaeker et al. 2011, Glenn et al., 2011). This methodological revisit is key to address basin-scale applications, especially in Mediterranean environments with complex cropping patterns and mosaics made up of both crops and natural vegetation. This work presents a methodology to estimate ET at basin scale, by combining meteorological and remotely sensed data in a surface energy balance approach to model crop and natural vegetation coefficients.

The study area is the Guadalfeo river basin in southern Spain. Seven Landsat 5 TM images acquired between 2003 and 2005 were processed after applying geometrical, atmospheric, and topographical corrections, to provide the required input data. The available meteorological data were spatially interpolated (Herrero et al., 2007). Reference evapotranspiration surfaces were generated applying FAO56-PM (Allen et al., 1998) equation, as detailed in Aguilar and Polo (2011). ET was estimated by using a two source energy balance model (TSM, Norman et al., 1995, Kustas and Norman, 1999), which computes separately fluxes coming from the soil and the vegetation. Areas in the basin where the application of the model was not appropriated, such as water bodies, snow or urban, were masked before the application. Crop and vegetation coefficients were obtained as the ratio between ET and ETo.

ETo, ET, and Kc maps were analyzed in terms of each vegetation type and development. Natural ecosystems in the area are primarily composed by oak trees, Mediterranean shrubs, and high mountain grasslands, while agricultural areas include olive and almond groves, subtropical trees, and some irrigated field crops. The resulting coefficients ranged between 0.1 and 1.5, and their values were directly related to vegetation ground cover. Relationships based on these coefficient are proposed to monitor the water use by vegetation on a regular basis and using only optical remote sensors, with higher frequency and spatial resolution than thermal sensors.

8531-25, Session 7

Evapotranspiration monitoring in a vineyard using satellite-based thermal remote sensing

Maria Pat. González-Dugo, Instituto de Investigación y Formación Agraria y Pesquera (Spain); José González-Piqueras, Isidro Campos, Instituto de Desarrollo Regional de la Univ. de Castilla-La Mancha (Spain); Ana Andreu, Instituto de

Investigación y Formación Agraria y Pesquera (Spain); Claudio Balbontín, Alfonso Calera, Instituto de Desarrollo Regional de la Univ. de Castilla-La Mancha (Spain)

Irrigation is an essential management practice to guarantee crop production in arid and semiarid areas. Timely and accurate information about the water balance components, especially the evapotranspiration (ET) of the crops, would help to improve the irrigation scheduling and systems, contributing to save water. Satellite-based land surface temperature can be input in energy balance models providing accurate estimations of actual evapotranspiration and crop water stress. These variables are of great interest in vineyards, where the management of water stress is important for both maximizing water productivity and increasing fruit quality. However, the scarce vegetation ground cover of this crop, exhibiting a large fraction of bare soil, a remarkable three-dimensional structure and a strong stoma control difficult the application of satellite-based models.

A two-source energy balance model (TSM, Norman et al., 1995, Kustas and Norman, 1999) has been applied over a drip-irrigated vineyard in Central Spain using a series of Landsat-5 and 7 images acquired during the spring and summer of 2007. The thermal band images were corrected for atmospheric and surface emissivity effects using the atmospheric radiative transfer model MODTRAN, obtaining at-surface radiometric temperatures (TR). The same model was used to correct the shortwave bands for atmospheric transmittance, estimating at-surface reflectance values. Surface energy balance approaches the partition of available energy using the TR to constrain the sensible heat flux, computing ET as a residual to the energy balance. The TSM is based on the separation of surface fluxes between the soil and canopy components and it is appropriate for low canopy covered areas (Timmermans et al. 2007).

Flux estimations from the model are compared with semi-hourly and daily values obtained by an eddy covariance flux tower installed in the same location during the experiment. In order to compare the observed fluxes with the model output, which assumes the energy conservation principle, closure in the measurements was forced using the residual-LE method. It is analysed the ability of the two-source model to estimate ET under the low vegetation cover and semiarid conditions of the experiment. It is also reported model performance in the separation of the beneficial (transpiration) and non-beneficial (evaporation from the soil) fractions, key information to improve water productivity.

8531-26, Session 7

An integrated approach for high spatial resolution mapping of water and carbon fluxes using multi-sensor satellite data

Carmelo Cammalleri, Martha C. Anderson, Agricultural Research Service (United States); Rasmus Houborg, European Commission Joint Research Ctr. (Italy); Feng Gao, William P. Kustas, Mitchell Schull, Agricultural Research Service (United States)

In the last years, modeling of surface processes, such as water and carbon balances, vegetation growth and energy budget, seems to be focused on integrated approaches that combine aspects of hydrology, biology and meteorology into unified analyses. In this context, remotely sensed data often have a core role due to the cross-cutting impact of this novel source of spatially distributed information on all these research areas. However, several applications, such as drought monitoring, yield forecasting and crop management, require spatially detailed products at sub-field scales, which can be obtained only with support of adequately fine resolution remote sensing data (< 100 m). In particular, observations in the visible to the near infrared (VIS/NIR) spectral region can be used to derive biophysical and biochemical properties of the vegetation such as leaf area index and leaf chlorophyll. Complementarily, the thermal infrared (TIR) signal provides valuable information about land surface temperature status, which in turn represents an accurate proxy indicator of the sub-surface moisture status by means of surface energy budget analysis. Additionally, the strong link between crop water stress and stomatal closure allows inference of crop carbon assimilation using the same tools. In this work, an integrated approach is proposed to model both carbon and water budgets at field scale by means of a joint use of a thermal-based Two Source Energy Budget (TSEB) model and an analytical, Light-Use-Efficiency (LUE) based model of canopy resistance. This modeling framework allows integration of information retrieved by both high and coarse resolution satellites by means of a data fusion procedure.

A set of Landsat and MODIS images are used to investigate the suitability of this approach, and the modeled fluxes are compared with observations made by several flux towers in terms of both water and carbon fluxes.

8531-27, Session 7

Application of Landsat images for quantifying the energy balance under conditions of fast land use changes in the semi-arid region of Brazil

Antônio Heriberto C. Teixeira, Embrapa Semiárido (Brazil); Fernando Braz T. Hernandez, Univ. Estadual Paulista (Brazil); Hélio L. Lopes, Univ. Federal do Vale do São Francisco (Brazil)

In the Nilo Coelho irrigation scheme, Brazil, the natural vegetation has been progressively replaced by irrigated agriculture, being important the quantification of the effects on the energy exchanges between the vegetated surfaces and the low atmosphere. Landsat images and agro-meteorological stations from 1989 to 2011, involving conditions outside the rainy periods, were used together, for modelling the large scale energy balance components. Surface albedo (α0), NDVI and surface temperature (T0) were the basic remote sensing parameters necessary for using together with reference evapotranspiration data (ET0), to acquire the latent heat flux (λE) and surface resistance to evapotranspiration (rs) at the large scale. The daily net radiation (Rn) was retrieved from α0, air temperature (Ta) and transmissivity (τsw) throughout the slob equation, allowing the quantification of the sensible heat flux (H) by residual in the energy balance, assuming a zero value for the soil heat flux (G) at this time scale. With a threshold value for rs, it was possible to separate the irrigated crops from natural vegetation ("caatinga") for evaluation the long term behaviour of the vegetation variables and the daily energy partition, giving an idea of the irrigated areas increments along the years. There was no distinction of α0 values between "caatinga" and irrigated crops, however, for T0, the average values were lower under irrigation conditions and the differences between the two kind of vegetation increases with time by a rate of 0.4 K yr-1. On the other hand, the mean NDVI values for irrigated crops were higher than those for natural vegetation and the differences increased at a rate of 0.02 per year. Considering all period and only the irrigated areas, the averaged fractions of Rn partitioned as H and λE, were 44 and 60%, respectively. Taking into account the mixed vegetation, the fraction used as H increased to 69%, while that as λE decreased to 32%. Although there were some evidences of raises and declines of these fractions along the years, depending on the environmental conditions, it was observed an increase of the energy used in the evapotranspiration process inside irrigated areas from 46% in 1989 to 73% in 2011, with a mean rate of 2.3% per year. Heat advection from the dry to irrigated lands was also observed, with the energy fluxes sometimes exceeding Rn till 27% more. Evaluating only the areas with absence of irrigation, the fraction of Rn used as H and λE were more constant, averaging, respectively, 95 and 5%. The biggest rates of the first flux from the natural vegetation is the reason of the additional energy to increase λE from irrigated crops. The ratio λE/Rn was well correlated with the changes in size of the irrigated areas along the years, being evidenced an increase from 20 to 61% inside a total perimeter of 41,000 ha, presenting an average rate of 4 % per year. The tools and models tested in this research, can subsidize water allocation, when aiming improvements on water productivity in the future, avoiding conflicts among different irrigation users.

8531-28, Session 7

Mapping evapotranspiration on vineyards: a comparison between Penman-Monteith and energy balance approaches for operational purposes *(Invited Paper)*

Giuseppe Ciraolo, Fulvio Capodici, Univ. degli Studi di Palermo (Italy); Guido D'Urso, Univ. degli Studi di Napoli Federico II (Italy); Goffredo La Loggia, Antonino Maltese, Univ. degli Studi di Palermo (Italy)

Estimation of evapotranspiration in Sicilian vineyard, is an emerging issue since these agricultural systems are more and more converted

from rainfed to irrigated conditions, with significant impacts on the management of the scarce water resources of the region. The choice of the most appropriate methodology for assessing water use in these systems is still an issue of debating, due to the complexity of canopy and root systems and for their high spatial fragmentation.

In vineyards, quality and quantity of the final product are dependent on the controlled stress conditions to be set trough irrigation. This paper reports an application of the well-known Penman-Monteith approach, applied in a distributed way, using high resolution remote sensing data to map the potential evapotranspiration (ETp). In 2008 a series of airborne multispectral images were acquired on “Tenute Rapitalà”, a wine farm located in the northwest of Sicily. Five airborne remote sensing scenes were collected using a SKY ARROW 351 650 TC/TCNS aircraft, at a height of nearly 1000 m a.g.l.. The acquisitions were performed encompassing a whole phenological period, period between June and September 2008 (approximately every three weeks). The platform had on board a multi-spectral camera with 3 spectral bands at green (G, 530-570 nm), red (R, 650-690 nm) and near infrared (NIR, 767-832 nm) wavelengths, and a thermal camera with a broad band in the range 7.5-13 μm. The nominal pixel resolution was approximately 0.7 m for VIS/NIR acquisitions, and 1.7 m for the thermal-IR data.

Field data were acquired simultaneously to airborne acquisitions. These data include spectral reflectances in VIS-NIR-MID, leaf area index (LAI), soil moisture at different depths (both in row and below plants). Moreover, meteo variables were measured by a standard weather-station whereas fluxes were measured by means of an Eddy correlation tower located within the field.

The VIS-NIR bands were atmospherically corrected and calibrated in order to calculate albedo, NDVI and LAI, that represented the distributed inputs of the Penman-Monteith algorithm.

Moreover a sensitivity analysis has been carried out on input parameters (such as albedo). A sensitivity was carried out to highlight the variability of outputs (such as ETp) on the accuracy in the parameters assessment obtainable using high spatial resolution airborne images. The comparison between ETp and actual evapotranspiration (ETa) evaluated using an energy balance approach, allows assessing whether a simplified approach, not taking into account the radiative temperature of the soil-vegetation system, is suitable for operational purposes.

Scale effects have been also investigated by means of an artificial degradation of images spatial resolution.

8531-29, Session 7

Calibration of soil hydraulic parameter into a distributed hydrological model using satellite data of land surface temperature

Chiara Corbari, Marco Mancini, Politecnico di Milano (Italy)

Calibration and validation of distributed models at basin scale generally refer to external variables, which are integrated catchment model outputs, and usually depend on the comparison between simulated and observed discharges at the available rivers cross sections, which are usually very few. However distributed models allow an internal validation due to their intrinsic structure, so that internal processes and variables of the model can be controlled in each cell of the domain. In particular this work investigates the potentiality to control evapotranspiration and its spatial and temporal variability through the detection of land surface temperature (LST) from satellite remote sensing.

This study proposes a methodology for the calibration of distributed hydrological models at basin scale using remote sensing data of land surface temperature.

The distributed energy water balance model, Flash-flood Event-based Spatially-distributed rainfall-runoff Transformation - Energy Water Balance model (FEST-EWB) will be calibrated in the Upper Po river basin (Italy) closed at the river cross section of Ponte della Becca with a total catchment area of about 38000 km2.

The model algorithm solves the system of energy and mass balances in term of the representative pixel equilibrium temperature (RET) that governs the fluxes of energy and mass over the basin domain. This equilibrium surface temperature, which is a critical model state variable, is comparable to the land surface temperature (LST) from satellite. So a pixel to pixel semi-automatic calibration procedure of soil and vegetation parameter is presented through the comparison between the model internal state variable RET and the remotely observed LST. A similar calibration procedure will also be applied performing the traditional calibration using only discharge measurements for different sub-basins of the Upper Po river basin.

130 diurnal and nocturne LST MODIS products are compared with FEST-EWB land surface temperature over the 4 years of simulation from 2000 to 2003 where meteorological and hydrological ground data are available.

In this abstract the internal validation of FEST-EWB model is presented showing the feasibility of using land surface temperature retrieved from remote sensing data at different spatial and temporal resolutions as a control of mass balance accuracy into a distributed hydrological model in each pixel of the domain. For the specific test case of the Upper Po River it has been shown that relative and absolute errors on simulated land surface temperature significantly improve from the simulation with the literature values of soil and vegetation parameters to that using the modified parameters after the calibration process. In fact relative goes from values between 15.8 % and 26.2 % to values between 1.9 % and 7.8 %. The traditional calibration procedure based on a “trial and error” approach between observed and simulated discharges has also been tested, leading to different values of soil and vegetation parameters which are characterized by different values of soil hydraulic parameters for each sub-basin of the Upper Po river basin.

8531-30, Session 8

Flood mapping of Yialias River catchment area in Cyprus using ALOS PALSAR radar images

Dimitrios D Alexakis, Diofantos G Hadjimitsis, Athos Agapiou, Kyriacos Themistocleous, Cyprus Univ. of Technology (Cyprus); Adrianos Retalis, National Observatory of Athens (Greece); Silas Michaelides, Meteorological Service of Cyprus (Cyprus); Stelios Pashiardis, Filippos Tymvios, Cyprus Meteorological Service (Cyprus)

The increases of flood inundation events occurring in different regions all over the world have enhanced the need for effective flood risk management. Floods are among the most frequent and costly natural disasters in terms of human and economic loss and are considered to be a weather-related natural disaster. Many methods exist to provide qualitative estimations of the risk level of flood susceptibility mapping within a watershed. However, earth observation techniques such as satellite remote sensing can contribute toward a more efficient flood risk mapping according to EU Directives of 2007/60.

This study strives to highlight the potential of flood inundation monitoring and mapping in a catchment area in Cyprus (Yialias river) with the use of radar satellite images. Due to the lack of satellite data acquired during dates that flood inundation events took place, the research team selected specific images acquired during dates that severe precipitation events were recorded from the rain gauge station network of Cyprus Meteorological Service in the specific study area. The relationship between soil moisture and precipitation was thoroughly studied and linear regression models were developed to predict future flood inundation events. Specifically, the application of fully polarimetric (ALOS PALSAR) and dual polarimetric (ERS - 2) Synthetic Aperture Radar (SAR) data acquired over different dates for soil moisture mapping is presented. The PALSAR (Phased Array type L-band Synthetic Aperture Radar) sensor carried by the ALOS (Advanced Land Observing Satellite) have quadruple polarizations (HH, VV, HV, VH). The amount of returned radiation (as backscatter echoes) that dictates the brightness of the image depends on factors such as the roughness, size of the target relative to the signal’s wavelength, volumetric and diffused scattering. The variation in soil moisture pattern during different precipitation events is presented through soil moisture maps obtained from ALOS PALSAR and ERS2 data acquired during different dates with different precipitation rates. Soil moisture variation is clearly seen through soil moisture maps and the developed regression models are used to simulate future inundation events. The results indicated the considerable potential of radar satellite images in soil moisture and flood mapping in catchments areas of Mediterranean region.

The project is supported by the Cyprus Research Promotion Foundation.

8531-31, Session 8

Critical analysis of the thermal inertia approach to map soil water content under sparse vegetation and changeable sky conditions

Antonino Maltese, Fulvio Capodici, Univ. degli Studi di Palermo (Italy); Chiara Corbari, Politecnico di Milano (Italy); Giuseppe Ciraolo, Goffredo La Loggia, Univ. degli Studi di Palermo (Italy); José A. Sobrino, Univ. de València (Spain)

The paper reports a critical analysis of the thermal inertia method to map surface soil water content on bare and sparsely vegetated soils by means of remotely sensed data. The study area is an experimental area located in Barrax (Spain). Field data were acquired within the Barrax 2011. AHS airborne images including VIS/NIR and TIR bands were acquired both day and night time by the INTA (Instituto Nacional de Técnica Aeroespacial) between the 11th and 13rd of June 2011. Images cover a corn pivot surrounded by bare soil. A set of in situ data have been collected previously and simultaneously to overpasses. To validate remotely sensed estimations a preliminary proximity sensing set up has been arranged, measuring spectra and surface temperatures on transects by means of ASD hand-held spectroradiometer and an Everest Interscience radiometric thermometer respectively. These data were collected on two transects: the first one on bare soil and the second from bare to sparsely vegetated soil; soil water content in both transects ranged approximately between field and saturation value. Furthermore thermal inertia was measured using a KD2Pro probe, and surface water content of soil was measured using FDR and TDR probes. This ground dataset was used: 1) to verify if the thermal inertia method can be applied to map water content also on soil covered by sparse vegetation, and 2) to quantify a correction factor of the downwelling shortwave radiation taking into account sky cloudiness effects on thermal inertia.

The experiment tests both Xue and Cracknell approximation to retrieve the thermal inertia from a dumped value of the phase difference and the three-temperature approach of Sobrino to estimate the phase difference spatial distribution.

Both methods were then applied to the remotely sensed airborne images collected during the following days, in order to obtain the spatial distribution of the surface soil moisture on bare soils and sparse vegetation coverage.

Results verify that the thermal inertia method can be applied on sparsely vegetated soil characterized by a fractional cover was up to ~0.25 (maximum value within this experiment); a lumped value of the phase difference allows a good estimate of the thermal inertia, whereas the comparison with the three-temperature approach didn't give conclusive responses because ground radiometric temperatures were not acquired in optimal conditions. Results also show that clear sky only during the remote sensing acquisitions is not sufficient to apply the thermal inertia method due to the adopted boundary conditions. A corrective coefficient taking into account the actual sky cloudiness throughout the day allows accurate estimates of the spatial distribution of the thermal inertia (r2 ~ 0.9) and soil water content (r2 ~ 0.7).

8531-32, Session 8

From SAR-based flood mapping to water level data assimilation into hydraulic model

Laura Giustarini, Patrick Matgen, Renaud Hostache, Jacques Dostert, Ctr. de Recherche Public - Gabriel Lippmann (Luxembourg)

The main objective of this work is to propose a fully automatic processing chain that employs SAR images for retrieving water stage information to be assimilated into a hydraulic forecasting model. This chain is composed of three steps: flood extent delineation, water stage retrieval and data assimilation of stage information into a hydraulic model.

The flood-mapping step is addressed with a fully automatic algorithm, based on image statistics and applicable to all existing SAR datasets. Combining radiometric thresholding, region growing and change detection it enables the automated, objective and reliable flood extent extraction from SAR images. Uncertainty on the flood extent map is represented with an ensemble of flood extent maps, obtained following a bootstrap methodology.

Water stage observations are then retrieved intersecting the flood shoreline of a flood extent map with the floodplain topography. The ensemble of flood extent maps allow extracting multiple water levels at any river cross section of the hydraulic model, taking into account the uncertainty associated with the flood-mapping step.

Finally, data assimilation concerns the integration of uncertain observations, i.e. SAR-derived water stages, with uncertain hydraulic model simulations.

The proposed processing chain was applied to two case studies. The January 2011 flood event on the Sure River (Luxembourg) was observed by 5 satellite images: 1 RadarSat-2 image, shortly after the peak flow, and 4 images during the receding limb, 2 COSMO-SkyMed images and 2 ENVISAT WSM images. The second case study refers to the Po River (Italy): 1 ENVISAT WSM image is available close to the peak flow for the event of June 2008.

The results show that with the assimilation of SAR-derived water stages, significant improvements can be achieved in the forecasting performance of the hydraulic model. The flood-mapping algorithm, with its characteristics of full automatization and computational efficiency, satisfies operational flood management requirements.

8531-34, Session 8

Neural network ensembles: combining multiple models for downscaling of soil moisture

Soo See Chai, Kok Luong Goh, Univ. Malaysia Sarawak (Malaysia); Geoff West, Curtin University of Technology (Australia); Naranyan Kulathuramaiyer, Univ. Malaysia Sarawak (Malaysia)

Derivation of soil moisture by passive microwave remote sensing has proven to be possible. However, passive microwave derived soil moisture is at coarse resolution (~40 kilometers). It is desirable to downscale the soil moisture to finer resolutions, especially 1 to 5 kilometers. Neural network ensembles are known to be able to effectively improve the generalization of a neural network system by combing a set of neural network classifiers whose error distributions are diverse.

In this paper, ensemble neural network method is used to downscale soil moisture content from low resolution L-band passive microwave observation from 20km to 2km. The brightness temperature observations used in this study have been collected during the month-long NAFE field campaign held in November 2005. The study area is situated at the northern part of the Goulburn River catchment, located in a semiarid area of south-eastern Australia. Soil moisture data for the 40km?40km study area was derived at 1km nominal resolution from the L-band airborne data using the L-MEB (L-band Microwave Emission of the Biosphere) model [1]. The MODIS/Aqua Surface Reflectance Daily L2G Global 250 m and MODIS/Aqua Land Surface Temperature and Emissivity Daily L3 Global 1km products were also used in this work. Three dates : 7th Nov, 14th Nov and 21st Nov 2005 where full coverage of L-band passive microwave observations of the study area was obtained, were used as the training and testing of the ensemble models in this study. The study area was getting wetter for these three days. The study area is gridded into a few 20km?20km area in order to generate enough data for training the neural network models.

The proposed ensemble neural networks model consists of a number of backpropagation neural networks that are trained using the same data from one single date (7th Nov 2005) to downscale the soil moisture from 20km to 2km resolution for the other two dates (14th and 21st Nov). Each neural network unit will focus on downscaling a particular area of 2kmx2km area on the 20km resolution area. The ensemble neural network is constructed in two steps: 1. Design the individual neural networks. This is done by training the neural networks on different training sets to generate a group of networks which are error uncorrelated directly. In order to obtain the different training sets, 11 sub-grid of 20km?20km were used. 2. Combining the output. This is done by simple averaging.

The average Root Mean Square (RMSE) error was 2.41%v/v on 14 Nov 2005 and 2.24%v/v on 21st Nov 2005. A strong correlation of around 0.9 was obtained for both dates. The encouraging results showed that ensemble neural networks could be used as a data driven model for downscaling of soil moisture data from 20km to 2km. Moreover, from the results, it is believed that by using individual neural network model, the spatial heterogeneity characteristics could be

captured by the ensemble models. This is shown with the ability of the trained model to downscale the soil moisture at two different dates.

Reference:

[1] Panciera, R., Effect of Land Surface Heterogeneity on Satellite near-Surface Soil Moisture Observations in Dept. of Civil and Environmental Engineering. 2009, The University of Melbourne: Melbourne.

8531-35, Session 9

Estimation of high density wetland biomass: combining regression model with vegetation index developed from Worldview-2 imagery

Elhadi E. Adam, Onisimo Mutanga, Univ. of KwaZulu-Natal (South Africa)

The high biomass accumulation in wetland vegetation plays a vital role in the ecological, economic and hydrological functions of wetland systems in tropical Africa. Therefore, accurate estimates of wetland biomass are critical for an efficient wetland monitoring and management system. However, most tropical wetlands are characterized by high density biomass, especially during rainfall seasons, a challenging variable to estimate using remote sensing. Recent field spectroscopy experiments have shown that narrow band vegetation indices computed from the red edge and the NIR shoulder can improve the estimation of biomass in such situations. However, the wide scale unavailability of high spectral resolution satellite sensors with red edge bands has not seen the up-scaling of these techniques to spaceborne remote sensing of high density biomass. This paper explored the possibility of estimate biomass in a densely vegetated wetland area using normalized difference vegetation index (NDVI) computed from WorldView-2 imagery, which contains a red edge band centred at 725 nm. Predicting biomass on an independent test data set using the random forest algorithm and 3 NDVIs computed from the red edge and NIR bands yielded a root mean square error of prediction (RMSEP) of 0.441kg/m2 (12.9 % of observed mean biomass) as compared to the stepwise multiple linear regression that produced an RMSEP of 0.5465 kg/m2 (15.9 % of observed mean biomass). The results demonstrate the utility of WorldView-2 imagery and random forest regression in estimating and ultimately mapping vegetation biomass at high density - a previously challenging task with broad band satellite sensors

8531-37, Session 9

Changes in satellite-derived vegetation growth trend in China from 2002 to 2010

Juan Gu, Lanzhou Univ. (China); Xin Li, Chunlin Huang, Cold and Arid Regions Environmental and Engineering Research Institute (China)

Net primary production (NPP) is the production of organic compounds from atmospheric or aquatic carbon dioxide, principally through the process of photosynthesis. Climate changes of this magnitude are expected to affect the NPP of the world's land ecosystems. In this study, we used a light-use efficiency model and linear regression model to describe and analyze the spatial and temporal patterns of terrestrial net primary productivity (NPP) in China during 2002-2010. First, we used the reconstructed 16-day 0.05°MODIS NDVI product (MOD13C1), 0.05°gridded GLDAS (Global Land Data Assimilation System) meteorological data and land use map to estimate the NPP in China. The spatial variability of NPP was analyzed during all periods, growing seasons and different seasons, respectively. Based on regression analysis method, we quantified the trend of NPP change in China during 2002-2010. Our results indicate: (1) The NPP estimation based on remote sensing data is more reasonable for regional scale study. Specially, the reconstructed time-series MODIS NDVI data has been applied and improved the accuracy of NPP estimation by removing the noise. Estimation shows that the total annual terrestrial NPP is about 3.78 Gt C/a in China during 2002-2010, the spring terrestrial NPP is about 0.64Gt C/a, the autumn terrestrial NPP is about 1.59Gt C/a, and the summer terrestrial NPP is about 0.81Gt C/a. (2) The fundamental spatial pattern of annual NPP in China was characterized by high NPP levels distributed in the southeast and low NPP levels in the northwest which was likely due to difference of major climatic factors along latitude. In all vegetation types, the maximum annual NPP was observed on evergreen broadleaf. The high level NPP was distributed in the south part of Hainan province, the southwest part of Yunnan province, and the southeast part of Qinghai-Tibet Plateau. The significant seasonal change feature was shown in all vegetation types in which the change amplitude of evergreen vegetation is the highest, and the desert is the lowest. (3) The whole forest ecosystems occupied the largest part of NPP in China (40.32%), then the farmland (24.30%), followed by grassland (10.32%). The desert occupied the lowest part of NPP in China (0.66%). (4) The variation of NPP was slight in China during 2002-2010. The NPP was increasing in northwest China but decreasing in northeast China and southeast China. Most part of China change significantly around 2004 or 2006 due to climate change, which include the north part of Xinjiang, the east part of Inner Mongolia and the southeast part of Qinghai Tibet Plateau. (5) As a whole, the NPP in growing season showed an increasing trend during 2002-2010. 26.6% of the total area was increasing and 21% was decreasing. In spring, 14.5% of the total area was increasing and 10.4% was decreasing. In summer, 19.5% of the total area was increasing and 17.1% was decreasing. In autumn, 21.4% of the total area was increasing and 19.6% was decreasing.

8531-38, Session 9

Analysis of vegetation time-space dynamics and its effect factor in northwestern China

Mingwei Zhang, Jinlong Fan, China Meteorological Administration (China); Hui Deng, Chinese Academy of Agricultural Sciences (China); Yanling Qiu, China Meteorological Administration (China)

The vegetation's variation is very sensitive to climatic change and Human activates in Northwestern China. The vegetation distribution in Northwest of China since 1981 to 2003 is assessed with Normalized Difference Vegetation Index (NDVI) data. The vegetation season change is in accord with change of surface energy. And the vegetation distribution in Northwest China is related to rainfall. The value of drought index is in accord with the change of NDVI in Northwest China. More rainfall in spring or summer resulted in the increase of NDVI in Shanxi, Inner Mongolia, Ganshu, Ningxia, and Qinghai. But the NDVI in arid region, such as Xingjiang, has been little influenced by rainfall. The conclusion is that The NDVI is control by rainfall in semi-arid region in northwest China.

8531-39, Session 10

Terrestrial photography as an alternative to satellite images to study snow cover evolution at hillslope scale

Rafael Pimentel, Fluvial Dynamics and Hydrological Research Group. (Spain) and Interuniversitary Institute for Research on the Earth System in Andalucia. University of Granada (Spain); Javier Herrero, Fluvial Dynamics and Hydrological Research Group (Spain) and Interuniveristary Institure for the Research Earth System in Andalucia. University of Granada. (Spain); María José Polo, Fluvial Dynamics and Hydrological Research Group (Spain) and Interuniversitary institue for Research on the Earth System in Andalucia. University of Cordoba (Spain)

The water present in the snowpack is a basic component in the hydrological cycle in mountainous areas. In Mediterranean regions, where the water shortage is a serious and recurrent problem, it is essential to know the behaviour and evolution of this layer. Their climate conditions strongly enhance the spatiotemporal variability of the snow distribution, which increases its difficulty in being measured and monitored. Satellite remote sensing is widely used to find out the evolution of the snow cover extension at medium-large scales. But these techniques pose some constraints if snow is heterogeneously distributed, as they do not correctly represent the physical processes that occur on a smaller scale than the satellite image resolutions (e.g., NOAA, daily images with 1x1 km cell size ; MODIS, daily images with 250x250m cell size ; Landsat, 15-day images with 30x30m cell size), such as quick melting of snow on sunny and warm days, which may change snow cover substantially in a few days, or the persistence of snow patches from 10 to 1 m during many weeks in early summer. In such cases, terrestrial photographs, whose resolution can be more easily adapted to the required resolution for these study cases, are an economic and also efficient alternative.

This work presents a methodology for the georeferencing and automatic detection of snow in terrestrial photography, as an alternative to the use of satellite images for the study of the snow cover evolution in small areas. This technique is based on basic principles of graphics design and mainly needs a digital elevation model (DEM) to reference the images, and to produce snow masks that show the snow-covered pixels in the photographed area. The temporal resolution of these masks ranges from 1 to 2 days, and their spatial resolution is given by the DEM used (10x10 m in this study). This methodology has been evaluated during the snowmelt period in the spring of 2009 at a study site in Sierra Nevada Natural Park (Southern Spain). The region studied covers an area of 3 km? with altitudes ranging from 1500 to 3500 m.a.s.l.. The resulting snow maps have been compared with the results available for that period obtained from the analyses of four Landsat images (Herrero et al., 2011).

The results show that the use of Landsat generally overestimated the extension of the snow cover in this area. This overestimation is greater at the beginning of the snowmelt period (2.85 km? covered by snow identified by Landsat vs 2.45 km? registered in the terrestrial photographs), when the initial patches of free-of-snow soil cannot be detected by the Landsat resolution. Snow patches in the late melting season are detected but also overestimated (0.40 km? of snow in Landsat vs 0.35 km? in terrestrial photograph) because patch size is normally under Landsat resolution. This technique greatly improves the quality of the measurements of the snow cover evolution and provides us with a deeper insight of the seasonal variability exhibited by the snow processes in semiarid climates, which results in a sounder knowledge of the dynamics of such processes and their better further modelling at the watershed scale. In this case, the biased misclassification of snow-covered pixels from the use of satellite images can lead to substantial deviations in the estimation of the total snow cover.

8531-40, Session 10

Estimation of snow-pack characteristics by means of polarimetric SAR data

Antonio Reppucci, Xavier Banque, Starlab (Spain); Carlos Lopez-Martinez, Univ. Politec. de Catalunya (Spain); Yu Zhan, Alberto Alonso, Univ. Politec. de Catalunya (Spain)

Monitoring of snow cover is fundamental in hydrological applications. Information about spatial and temporal variability of snow parameters is needed for the modelling and forecasting of snow involved phenomena such as melt runoff, avalanche prediction and water resources forecasting. Thanks to their night/day capabilities and weather conditions independence active microwave remote sensing instruments represent a valuable tool in the enhancement of snow monitoring.

The study presented here summarize the results of the research work conducted in the frame of EOSWAN project, targeting the feasibility of snow monitoring with C-band fully polarimetric SAR data over mountainous regions. In particular the research carried out has been focused to check the sensitivity of fully polarimetric C-band satellite SAR data to dry snow and to the volume of snow-pack. The choice of C-band frequency and mountainous region test site aims to the development of a snow monitoring tool, which would target seasonal snow in northern hemisphere countries, due to snow's main role in the water management, and which would be guaranteed in continuity by future's ESA's Sentinel-1 and CSA Radarsat Constellation.

The monitored area chosen for the study is located in an alpine environment in the Catalan Pyrenees. Three different RADARSAT-2 data set were acquired in Fine Quad Pol configuration, providing fully polarimetric information (HH,HV,VH and VV) with a pixel spatial resolution of around 8 meter. The SAR acquisitions were supported with simultaneous ground measurements campaigns, consisting of snow measurements of depth and density, as well as a general assessment of the snow status carried out by a snow expert who was present in both campaigns.

Preliminary results obtained from the statistical analysis of the different polarimetric channels over the area of study suggest the possibility of defining a a new polarimetric parameter that would be sensitive to dry snow presence. Such type of classifier would allow the development of a methodology for the identification of the presence of snow, and its status concerning liquid water content (dry or wet snow).The effect of the terrain slope on the orientation angle of the polarization has been taken in account and corrected. The X-Bragg surface scattering has been used to model surface backscattering of the test site in order to more accurately define a model for the snow-pack polarimetric backscattering at C-band that can be used to infer snow geo-physical parameters.

Main outcome of this study is the definition of a new polarimetric parameter sensitive to snow presence, able to distinguish between dry, wet and non snow cover, allowing a quantitative remote sensing with C-band polarimetric space-borne SAR. The importance of developing application based on remote sensed data will be discussed.

8531-41, Session 10

Thermal remote sensing of snow cover to identify the extent of geothermal areas in Yellowstone National Park

Christopher M. U. Neale, Saravanan Sivarajan, Ashish Masih, Utah State Univ. (United States); Cheryl Jaworowski, Henry Heasler, U.S. National Park Service (United States)

High resolution airborne multispectral and thermal infrared imagery (1-meter pixel resolution) was acquired over several geothermal areas in Yellowstone National Park both in September of 2011 and in early March, during the winter of 2012, when snow cover was still present in most of the Park. The multitemporal imagery was used to identify the extent of the geothermal areas, as snow accumulation is absent in hot geothermal areas. The presence or absence of snow depends on the geothermal heat flow generated at the surface as well as antecedent snow precipitation and temperature conditions. The paper describes the image processing and analysis methodology and examines heat flow thresholds and conditions that result in the presence or absence of snow cover.

8531-42, Session 10

Assimilation of MODIS snow cover fraction for improving snow variables estimation in west China

Chunlin Huang, Cold and Arid Regions Environmental and Engineering Research Institute (China)

Snow cover plays an important role in energy and water cycles by modifying turbulent and radiative exchange between the ground and atmosphere. In climatological, hydrological, and numerical modeling studies, spatially continuous and temporally consistent snow cover data is very useful for examining associations with the climate system at various temporal scales. Various snow cover products are currently produced through optical remote sensing sensors such as Geostationary Operational Environmental Satellites (GOES), Advanced Very High Resolution Radiometer (AVHRR), and Moderate-Resolution Imaging Spectrometer (MODIS). However, these snow cover data are easy to be contaminated by cloud, which results in spatially and temporally discontinuous snow cover data. Additionally, Land surface models or snow models also can propagate snow variables (such as snow cover, snow density, snow depth, snow temperature, and snow water equivalence) evolution in time and space, but accuracies of the modeled snow variables depend on model physics, model parameters and atmospheric forcing data.

In this work, we try to assimilate daily 0.05° MODIS snow cover data (MOD10C1) into land surface model based on Ensemble Kalman filter (EnKF) algorithm to produce spatially continuous and temporally consistent snow variables in West China. The candidate of land surface model is Common Land Model (CoLM). The 3-houly atmospheric forcing data were drawn from the Global Land Data Assimilation System (GLDAS) forcing database at 0.25° resolution (Rodell et al., 2004). Then the forcing data are convert to hourly 0.05° using the method proposed by Liston and Elder (2006). Our assimilation experiment is conducted in January, 2003. The preliminary results are very promising and show that distributions of snow variables (such as snow cover, snow depth, and SWE) are more reasonable and reliable after assimilating MODIS snow cover data.

8531-33, Session PS

Soil moisture retrieval by active/passive microwave remote sensing data

Shengli Wu, Lijuan Yang, CMA National Satellite Meteorological Ctr. (China)

This study develops a new algorithm for estimating bare surface soil moisture using combined active / passive microwave remote sensing on the basis of TRMM (Tropical Rainfall Measuring Mission). Tropical Rainfall Measurement Mission was jointly launched by NASA and NASDA in 1997, whose main task was to observe the precipitation of the area in 40 ° N-40 ° S. It was equipped with active microwave radar sensors (PR) and passive sensor microwave imager (TMI). To accurately estimate bare surface soil moisture, precipitation radar (PR) and microwave imager (TMI) are simultaneously used for observation. According to the frequency and incident angle setting of PR and TMI, we first need to establish a database which includes a large range of surface conditions; and then we use Advanced Integral Equation Model (AIEM) to calculate the backscattering coefficient and emissivity. Meanwhile, under the accuracy of resolution, we use a simplified theoretical model (GO model) and the semi-empirical physical model (Qp Model) to redescribe the process of scattering and radiation. There are quite a lot of parameters effecting backscattering coefficient and emissivity, including soil moisture, surface root mean square height, correlation length, and the correlation function etc. Radar backscattering is strongly affected by the surface roughness, which includes the surface root mean square roughness height, surface correlation length and the correlation function we use. And emissivity is differently affected by the root mean square slope under different polarizations. In general, emissivity decreases with the root mean square slope increases in V polarization, and increases with the root mean square slope increases in H polarization.

For the GO model, we found that the backscattering coefficient is only related to the root mean square slope and soil moisture when the incident angle is fixed. And for Qp Model, through the analysis, we found that there is a quite good relationship between Qpparameter and root mean square slope. So here, root mean square slope is a parameter that both models shared. Because of its big influence to backscattering and emissivity, we need to throw it out during the process of the combination of GO model and Qp model. The result we obtain from the combined model is the Fresnel reflection coefficient in the normal direction gama(0). It has a good relationship with the soil dielectric constant. In Dobson Model, there is a detailed description about Fresnel reflection coefficient and soil moisture. With the help of Dobson model and gama(0) that we have obtained, we can get the soil moisture that we want.

The backscattering coefficient and emissivity data used in combined model is from TRMM/PR, TMI; with this data, we can obtain gama(0); further, we get the soil moisture by the relationship of the two parameters-- gama(0) and soil moisture. To validate the accuracy of the retrieval soil moisture, there is an experiment conducted in Tibet.

The soil moisture data which is used to validate the retrieval algorithm is from GAME-Tibet IOP98 Soil Moisture and Temperature Measuring System (SMTMS). There are 9 observing sites in SMTMS to validate soil moisture. Meanwhile, we use the SMTMS soil moisture data obtained by Time Domain Reflectometer (TDR) to do the validation. And the result shows the comparison of retrieval and measured results is very good.

Through the analysis, we can see that the retrieval and measured results in D66 is nearly close; and in MS3608, the measured result is a little higher than retrieval result; in MS3637, the retrieval result is a little higher than measured result.

According to the analysis of the simulation results, we found that this combined active and passive approach to retrieve the soil moisture improves the retrieval accuracy.

8531-44, Session PS

The Leaf Area Index(LAI) monitoring and retrieval based on MODIS-NDVI

Hong-Wei Zhang, Key Lab. of Agrometeorological Safeguard and Applied Technique (China) and Xinxiang Meteorological Bureau (China); Huai-Liang Chen, Key Lab. of Agrometeorological Safeguard and Applied Technique (China); Guan-Hui Zhou, Xinxiang Meteorological Bureau (China)

The Real-time retrieval of land surface variables from satellite monitoring is the fastest method to grasp the land surface changes, and provide necessary technology support for dynamic monitoring of crops. The proposed method in this paper, which based on the data of MODIS-NDVI, can promote the retrieval accuracy of LAI, This method is simple and practical, and has overcome many cumbersome operation in calculating of the mechanism& semi-mechanism model which need a large number of parameters. So, it is suit for the dynamic retrieval of LAI.

Extract the spectra data from MODIS and converts them to NDVI, compared with the leaf area index (LAI) in si-to observation. The results showed there is no significant correlation between LAI and NDVI.

But when the NDVI & LAI was accumulated separately from the period of turning green to maturity, the correlation between them get promoted and significant correlation could be display as below:

There, Y is the Accumulated LAI (ƩLAI), and X is the Accumulated NDVI (ƩNDVI). The relation between ƩLAI &ƩNDVI can be showed as below.

Based on the relationship between ƩNDVI&ƩLAI, then the validation could be tested.

Take the advantage of MODIS-NDVI in 2008-2010, the ƩLAI is retrievable, and the results showed the accuracy was satisfied.

8531-45, Session PS

Assessing the extent of conservation tillage across agricultural landscapes

Craig S. T. Daughtry, Peter C. Beeson, Sushil Milak, Bakhyt Akhmedov, Ali M. Sadeghi, E. Raymond Hunt Jr., Mark D. Tomer, Agricultural Research Service (United States)

Crop residue (or plant litter) on the soil surface can decrease soil erosion and runoff, improve soil quality, and reduce the amounts of nutrients and pesticides that reach streams and rivers. Quantification of crop residue cover is required to evaluate the effectiveness of conservation tillage practices as well as the extent of biofuel harvesting. For agricultural fields, the line-point transect method is the standard technique for measuring crop residue cover; however, it is not well suited for assessing cover over large areas in a timely manner.

Remote sensing approaches for assessing soil tillage intensity and crop residue cover have traditionally used broadband multispectral sensors, such as Landsat Thematic Mapper (TM). Within these broad bands, crop residue can be brighter or darker than soils depending on soil type, crop type, moisture content, and residue age, making it difficult to distinguish crop residues from soils. With hyperspectral reflectance data, relatively narrow absorption features, centered near 2100 and 2300 nm, can be detected that are associated with cellulose and lignin concentrations. Although these features are not readily discernible in the spectra of green vegetation, they are evident in reflectance spectra of dry non-photosynthetic vegetation, including crop residues. Reflectance spectra of dry soils also lack these absorption features but may have additional absorption features associated with minerals.

Our objectives are (1) to assess crop residue cover and soil tillage intensity using remotely sensed data, and (2) to examine effects of crop management decisions on soil and water quality. We started with the fundamental spectral properties of crop residues and soils, extended the results to fields and watersheds, and finally simulated the effects of biofuel harvesting on soil erosion and soil C.

Reflectance spectra of corn, soybean, and wheat residues and a wide range of soils were acquired in the laboratory with a spectroradiometer. Additional spectra were acquired in situ from production fields in five test sites in Maryland, Indiana, and Iowa. Airborne and satellite hyperspectral images were also acquired shortly after planting for each test site. The cellulose absorption index (CAI), which measured the relative intensity of the absorption feature near 2100 nm, was calculated using three 10-nm bands centered at 2030, 2100, and 2210 nm.

For each data set, crop residue cover was linearly related to CAI. Three useful categories of soil tillage intensity based on crop residue cover were defined: intensive tillage has <15% residue cover; reduced tillage has 15-30% residue cover; and conservation tillage has >30% residue cover. Classification accuracy was 66-82% for all scenes. Crop and soil management scenarios, including crop residue removal for biofuel, were evaluated using field and watershed-scale models. These simulations demonstrated the levels of crop residue removal that are sustainable vary with soil type, tillage management practices,

and climatic conditions. Different rates of crop residue removal may be required for different areas of the same field. Robust decision support systems required suites of models to adequately address all agronomic, environmental, and economic issues.

8531-47, Session PS

Mixed pixel clumping index: definition, methodology, analysis and product generation

Qingmiao Ma, Jing Li, Institute of Remote Sensing Applications (China); Qiang Liu, Beijing Normal Univ. (China); Qinghuo Liu, Institute of Remote Sensing Applications (China)

Clumping index (CI), is a key vegetation structure parameter to describe the foliage clumping in canopy quantitatively. It is defined as the ratio of effective leaf area index (LAI) and true LAI. It plays an important role in improving the modeling of the carbon cycle, simulations of canopy-level photosynthesis and LAI retrieval from satellite data. In previous studies, the effect of foliage clumping is generally considered at the canopy and below canopy scale in pure pixel. However, for a mixed pixel with low resolution, the spatial inhomogeneity inside the pixel makes the clumping characteristic of the pixel totally different with the pure pixel. It is necessary to redefine the clumping index for the mixed pixel, and make research its estimation method.

The definition of Mixed-pixel clumping index (MPCI), which represents cluster effect in pixel scale, was first proposed in this paper. Then a new method to calculate MPCI based on Nilson's gap frequency equation was presented. Sensitivity analysis showed that the MPCI calculated by the proposed equation, is sensitive to the heterogeneity degree of vegetation type, fractional vegetation cover inside the mixed pixel. Then the proposed method was compared with the two main methods used to estimate the clumping index of mixed pixel now, the method used in GLOBECARBON, and the method based on NDHD, by VALERI dataset and the model simulation. At last the MPCI map with 1km resolution over China in June, 2010 was generated using HJ-1A/B CCD images.

8531-48, Session PS

Vegetation index retrieval by coupling optical and SAR images

Fulvio Capodici, Univ. degli Studi di Napoli Federico II (Italy); Giuseppe Ciraolo, Univ. degli Studi di Palermo (Italy); Guido D'Urso, Univ. degli Studi di Napoli Federico II (Italy); Goffredo La Loggia, Antonino Maltese, Univ. degli Studi di Palermo (Italy)

The monitoring of spatial and temporal variability of land surface parameters through vegetation indices (VIs) are important issues in the management of land and water resources, with significant impact on the sustainability of modern agriculture and environmental protection (e.g. flooding).

Algorithms based on optical data give accurate products, however temporal cloud cover often dramatically reduces resolution of these outputs. The lunch of new SAR missions such as COSMO-Skymed opened new avenues within the field of Synthetic Aperture Radar (SAR) applied to agro-hydrological applications. Indeed, these satellites may represent a suitable source of data for operational uses especially due to their high spatial and temporal resolutions (15 m Single Look in PingPong acquisition mode, best revisit time with 4 satellites: at equator 4 images per day; at 40° latitude, every 7 hours on average). Although X band is not optimal for agricultural and hydrological applications reliable continuous assessment of the vegetation indices VIs can be achieved combing optical and SAR images. To this aim an algorithm coupling VI derived from optical DEIMOS images (VIopt) and backscattering σ0HV (PingPong in HV polarization) was implemented and validated.

A correlation analysis between σ0 and VIs measurements taken simultaneously to Cosmo-SkyMed acquisitions in several plots in the Sele plain has been performed. The correlation analysis was based on the following parameters: incidence angle, spatial resolution and polarization mode. Results have shown that the crossed HV bascattering, σ0HV, acquired with high angles (i.e. with a beam off nadir angle > 40°) produced the best correlation between variations of VI and σ0HV (ΔVI and Δσ0HV). The correlation of ΔVI vs. Δσ0HV is always verified in time (temporal stability). Based on this experimental evidences a model to infer the VISAR at the t+1 once known the VIopt at a reference time, t and Δσ0HV between times t+1 and t was implemented and verified.

The study is carried out over the SELE plain (south-east of Campania, Italy) mainly characterized by herbaceous crops. Five couples of COSMO-Skymed and optical DEIMOS images have been acquired from August to September 2011. These data have been collected within the COSMOLAND project (Use of COSMO-SkyMed SAR data for LAND cover classification and surface parameters retrieval over agricultural sites) funded by the Italian Space Agency (ASI). Results confirm that VISAR obtained using the combined model is a satisfactory surrogate of the VIopt.

8531-49, Session PS

A local post-retrieval tool for satellite precipitation estimates

Francesco Lo Conti, Antonia Incontrera, Leonardo V. Noto, Univ. degli Studi di Palermo (Italy)

As illustrated by several literature case studies spread around different geographic locations, satellite precipitation estimates, obtained by means of consolidated algorithms, often result being considerably biased. Moreover observed bias is related to geographic location since particular features such as latitude, presence of coastal areas and climatological and weather regime, affects performances. Bias adjusted products are available that make use of global ground-based precipitation estimates, but still these dataset show a relevant bias level.

In this study a procedure to bias-adjust satellite precipitation estimates has been developed for the local area of Sicily (Italy) based on rain gauge network data. Considering that the latency time of satellite precipitation estimates is nowadays very short and close to that of satellite data availability, it has been investigated the possibility of designing a procedure that able to apply the bias reduction to satellite estimates without timely corresponding rain gauge network data. Therefore, in order to obtain a tool that make available a first precipitation map estimate, the emphasis has been put on data readiness instead of achieving the best correction result.

The adopted algorithm uses a Bayesian formulation to link satellite and spatially interpolated rain gauge network data.

The developed procedure demonstrate to be able to improve the overall bias performances of examined satellite precipitation data. It is expected that such an approach increases its suitability as the developing of satellite estimates algorithms leads to improvements on identifying precipitation occurrences.

8531-50, Session PS

NDVI sensitivity to the hydrological regime in semiarid mountainous environments

Pedro J. Gómez-Giráldez, Cristina Aguilar, María José Polo, Grupo de Dinámica Fluvial e Hidrología (Spain)

Mediterranean basins are characterized by a seasonal rainfall climate, with periods of strong water stress for vegetation in the dry season and hyper annual variability, alternating wet and dry years. Furthermore, there is a common occurrence of torrential rain events that, unlike moderate rain events, do not contribute to maintaining soil moisture available for the canopy. On the other hand, the presence of steep slopes and different soil types in mountain areas determines a great spatial variability in hydrological behaviour. Thus, the different kinds of vegetation covers are based on different bioclimatic levels, conditioned by gradients of temperature, precipitation, soil structure and composition, time of exposure to direct sunlight, etc. This is especially significant when there is snow.

In the Sierra de los Filabres, south-western Spain, the altitudinal range is of between 300 and 2186 meters in an area of approximately 1500 hectares. Currently, there are vast plantations of pine, with areas of Holm oak and scrub appearing at lower levels. Despite the arid nature of the area, the presence of snow allows water availability for vegetation during the early summer, and this occurrence marks the interannual variability of water stress.

This work shows the sensitivity of NDVI as an indicator of the global hydrological regime of the year,. In order to do this, the annual

water balance in the area was simulated during the period 2001 to 2010 from a physically distributed hydrological model suitable for semiarid mountains (WiMMed) and calibrated, and NDVI was obtained from Landsat TM images taken at the end of the dry season in order to evaluate the cumulative effect of the hydrological regime of the year in the canopy. The analyzed sample consisted of 1000 points randomly distributed over the pine cover and the influence of different hydrological processes related to water balance in the soil on the NDVI value was analyzed at each point. Hydrological variables were selected a priori according to their influence on the cover state (precipitation, precipitation as snow, evaporation, snowmelt, infiltration, etc) and correlated with NDVI at different time scales. Pearson correlation matrices were obtained and Principal Components Analyses were performed for each year, which allowed the identification of the variables with the highest incidence in the cover state. The results showed that, at the end of the hydrological year, the NDVI is particularly sensitive to the regime of annual variables related to snow dynamics, especially snowmelt. These relationships were quantified, with the best fit being obtained between NDVI and the dimensionless index snowmelt divided by precipitation (with R2 around 0.7). In this way, the relationship was established between the cover state at the end of the hydrological year and its hydrological regime. The relations obtained could, in the future, be a tool for estimating hydrological variables from satellite data in data-poor situations conditioned by steep slopes and a difficult access to these kinds of areas.

8531-51, Session PS

Monitoring of ice caps over Himalaya region using MODIS data

In-hwan Kim, Kyung-Soo Han, Kyoung-Jin Pi, Chang-Suk Lee, Min-Ji Lee, Pukyong National Univ. (Korea, Republic of)

Monitoring the extent of ice caps in the Himalaya region is significant to understand climate change. On the regional scale, the remote sensing data for mapping snow cover is useful, especially Moderate Resolution Imaging Spectroradiometer (MODIS) snow cover products, with 500 m spatial and daily and 8-daily temporal resolution, can provide extensive regional snow cover mapping and monitoring of ice caps. In this study, we present the result of ice caps monitoring during 3-months (August to October) period extending from 2001 to 2011. Seasonal changes of the snow cover area considering elevation of snow pixels are analyzed. The steps are based on spatial and temporal information of snow covered pixels - combining data from MODIS and USGS Digital Elevation Model (DEM); adjustment spatial filtering; temporal filtering based on snow line from MODIS snow products; analysis of inter-annual change from ice caps region. The results show inter-annual variability of maximum snow extent and ice caps duration over the last decade. The snow line goes up lower than 5000m and the ice caps areas were found significant decline in Himalaya region during the last decade.

8531-52, Session PS

Exploring vegetation photosynthetic light-use efficiency using hyperspectral data

Liangyun Liu, Quanjun Jiao, Dailiang Peng, Ctr. for Earth Observation and Digital Earth (China)

Photosynthetic light-use efficiency (LUE) is an important indicator of plant photosynthesis and a key parameter for remote sensing-based models to monitor vegetation productivity. In principle, chlorophyll fluorescence combined with non-photochemical quenching (NPQ) is an expression of the balance between light harvesting (absorption) and light utilization in the photosynthetic process.

In the more natural state of continuous illumination by sunlight, photosynthetic chlorophyll fluoresces continuously, adding a weak signal to the spectral reflectance (solar-induced fluorescence). The chlorophyll fluorescence emission can be separated from the observed reflected spectrum. Furthermore, when light exceeds the amount that can be used for photosynthesis, the redundant energy will be diverted from the chlorophyll pigments to the pigments of the xanthophyll reaction, as part of a process known as non-photochemical quenching (NPQ). Dynamic changes in the xanthophyll cycle are accompanied by a reflectance change in a narrow region of the visible spectrum centred at 531 nm. A normalized difference reflectance index based on two bands of 531nm and 570 nm is expressed as the photochemical reflectance index (PRI), which has been found to be sensitive to changes in the xanthophyll cycle of NPQ.

The aim of this study was to examine the above principle using solar-induced ChlF and PRI derived from the canopy reflectance spectrum. Four independent experiments were carried out on summer maize (C4 plant) on 5 July 2008, and winter wheat (C3 plant) on 18 April 2008, 16 April 2010 and 13 May 2010 by synchronously measuring daily canopy radiance spectra and photosynthetic LUE.

The complementary relation between fluorescence and photochemical yield makes it possible to monitor photosynthesis using fluorescence. LUE-ChlF models were developed for ChlF at 688 nm (R2 = 0.72) and 760 nm (R2 = 0.59) based on the experiment data from 13 May 2010 at the Guantao flux site. The LUE-ChlF models were validated by three independent experiments, and the results show the feasibility of the use of ChlF at 688 nm to estimate photosynthetic LUE. However, the LUE-ChlF relationship can be weakened by different species, canopy density and environmental conditions.

As an easy, rapid, non-intrusive method, PRI also provides an instantaneous assessment of dynamic photosynthetic LUE. The significant negative relation between non-photochemical quenching (NPQ) and PRI was confirmed. Although there was a significantly positive relation between LUE and PRI for all four independent experiments, the PRI-LUE relation was evidently weakened by the canopy and environmental conditions. The PRI difference (PRI) from the minimum reference PRI around noontime could greatly eliminate the interference factors. The LUE-PRI model was developed based on the experiment data from 13 May 2010 at the Guantao flux site (with an R2 value of 0.85), and validated by the other three independent experiments. Therefore, we proposed a potential method to evaluate plant photosynthetic status by two-temporal PRI remote sensing data, one acquisition at morning, another at noon.

8531-53, Session PS

Spectrally-based quantification of plant heavy metal-induced stress

Rumiana Kancheva, Space Research and Technologies Institute (Bulgaria) and Bulgarian Academy of Sciences (Bulgaria); Georgi Georgiev, Space Research and Technologies Institute (Bulgaria); Denitsa Borisova, Institute for Space Research and Technologies (Bulgaria)

Recent developments in environmental studies are greatly related to worldwide ecological problems associated with anthropogenic impacts on the biosphere. Pollution is an undesirable product of human activity. Industry, agriculture, forestry, and transportation all generate substances and by-products that are considered pollutants. These activities have been direct causes of pollution and have contributed a significant impact on the environmental quality. Contaminated land is a continuing concern because of the potential risks to human health and vegetation resources. Remote sensing technologies are an effective tool in numerous ecology-related investigations aimed at ecosystems preservation, biodiversity conservation and other problems of global importance. In agriculture, remote sensing is widely used for assessing plant growth, health condition, and detection of stress situations. Agricultural lands are subjected to enormous pressure, and their monitoring and assessment have become an important ecological issue. Heavy metals constitute a group of environmentally hazardous substances whose deposition in soils and uptake by species affect soil fertility, and plant development and productivity. The spreading acceptance of the concept of precision agriculture running generates much interest in the early detection of crop growth stress. The implementation of modern remote sensing techniques is one of the basic assumptions of this concept. In agricultural monitoring, the analysis of multispectral data has proven capabilities for crop condition assessment and yield prediction.

This paper is devoted to the study of crop response to heavy metal contamination. A prime goal of the investigation is to assess the ability and the predictive power of various spectral indicators to detect and quantify plant heavy metal-induced stress. Spring barley, pea and alfalfa plots have been subjected to Ni and Cd pollution. Crop performance under varying stress conditions (heavy metal concentration in the soil) has been evaluated in terms of growth variables and yield. Multispectral data acquired at different phenological stages has been statistically related to plant variables and the pollution amounts in order to derive empirical relationships quantifying the stress impact. Soil acidity and different types of

nitrogen fertilizers applied have been examined as additional factors influencing crop performance under heavy metal pollution. Significant correlations have been found between the stress factors, plant growth variables (biomass, canopy cover, leaf area index, pigments and yield), and spectral features (reflectance, absorbtion and transmittance properties, vegetation indices). Statistically meaningful relationships have been established between the heavy metal concentration in the soil and plant stress responses, thus providing a quantitative dimension of the stress impact.

8531-56, Session PS

Testing automatic procedures to map rice area and detect phenological crop information exploiting time series analysis of remote sensed MODIS data

Giacinto Manfron, Alberto Crema, Mirco Boschetti, Istituto per il Rilevamento Elettromagnetico dell'Ambiente (Italy); Roberto Confalonieri, Univ. degli Studi di Milano (Italy)

Rice crop is one of the most important agricultural activities in the world. 153 MHa are cultivated every year providing more than 670 Mton of paddy rice (FAO-STAT, 2010). Among other cereals, rice is mainly cultivated for self-consumption and it is the staple food for people living in developing countries. In Asia alone, almost 90% of the world's rice is produced employing more than 200 million farmers. Information on crop condition throughout space and time, is a very important issue for helping rice farming and stabilize commodity price. Moreover, up-to-date crop status information during on-going season result very important to support food security initiatives in developing countries. In particular, remote sensing contribution can be very important because satellite images provide a continuous agro-ecosystem monitoring tool which allows to retrieve spatial distribution information on large scale.

The present work is framed in this research field and wants to evaluate reliability of automatic image processing methods for the identification of rice cultivated areas and their status assessment. A method developed for Asian tropical areas (Xiao et al, 2005) have been studied and implemented to test its performance on Mediterranean temperate area. The study area covers the main rice crop districts in Italy, France and Spain (about 84% of the total European production, IRRI-STAT, 2009). The "Corine Land Cover (2006)" thematic cartography (1:100.000 scale) available for all Europe and a second more precise referring thematic cartography at 1:10.000 scale were used as a reference to evaluate the method outputs.

Rice mapping and monitoring was conducted using MODIS MOD09A1 products for the period 2002-2011, that provides reflectance images in 7 spectral bands with 8-days temporal resolution and 500m spatial resolution. The temporal analysis of Vegetation Indices (VIs), derived by MODIS data, allowed to produce rice cultivated area maps; different improvements of the Xiao's method were evaluated comparing the accuracy of the different mapping results. Finally, a new approach based on temporal series analysis has been tested on the Northern Italy rice district. This new approach allowed us to interpret the seasonal dynamics (flooding, growing period, heading, maturity) derived by VIs temporal series analysis.

This work highlighted that the original algorithm developed for tropical area does not well perform in the study area as revealed by the strong presence of commission errors. The error analysis reveals that the method is not flexible when applied to another geographic condition. Specific alternative solutions were necessary to adapt the original algorithm to Mediterranean conditions with a reduction of false positive detection of 25%. On the contrary the new method resulted to be the more robust solution because the rice crop map produced shows few commission error (< 13%) without introducing external information. This should guarantee flexibility and robustness when applied in alternative agricultural conditions.

In conclusion, our study confirmed that satellite monitoring offers a reliable solution to study large-scale rice cultivations and, given some adjustment to existing algorithms and implementation of more flexible solutions, can retrieve spatially and temporally distributed information on the cropping system, over different agro-ecosystems.

8531-57, Session PS

Feasibility study and optimization of image tasking in the context of the European Union CAP CwRS

Blanka Vajsova, Pär Johan Åstrand, European Commission Joint Research Ctr. (Italy); Axel Oddone, e-GEOS S.p.A (Italy); George Ellis, European Space Imaging (EUSI) (Germany)

CwRS (Control with Remote Sensing) is a control method foreseen by the CAP (Common Agricultural Policy) which is used to check if agriculture area-based subsidies are correctly granted to EU farmers. A series of Very High Resolution (VHR) and High Resolution (HR) satellite sensors participate in the acquisition program. Imagery is collected in specific multi-temporal, short time-windows, and used for parcel area determination, for crop identification and for control of measures of Good Agricultural and Environmental Conditions (GAECS).

JRC image acquisition Team has been appointed as a referent for the management of the CwRS image acquisition campaign and the purchase of satellite images on behalf of the Directorate-General for Agriculture and Rural Development for the EU MS. JRC manages specific Framework Contracts with all relevant Image Providers.

This presentation, speech, will focus in particular on the management of the VHR campaign.

Whereas in 2003 Campaign 37 VHR zones with overall area 12.500 km? were checked by CwRS technique in 2011 Campaign 426 VHR control zones were acquired covering an overall area of 242.000 km?, with a total expenditure of 7.1 M euro. The steady increase of using CwRS method is pointed out together with the increasing requirements on the imagery (better elevation angle, resolution, radiometry..). Due to this huge increase of the controlled area and the number of zones it has been essential to develop a solid image acquisition approach that guarantees a successful acquisition Campaign.

One of the crucial features requested by EU MS is window length, usually quite short (3-4 weeks). A feasibility analysis for all zones is therefore done before each VHR Campaign starts in order to ensure a maximal statistical success rate. The presentation will describe the complexity of the technical and competitive feasibility taking into account parameters like satellite characteristics (revisit capacity, number of passes), zone size, zone shape, zone latitude, elevation angle, acquisition window, priority level, cloud cover, statistical weather forecasting and other competitive conflicting tasking requests. The final result of such analysis is a probability of the zone acquisition within the defined acquisition window expressed in a percentage value. The goal is to achieve reliable and optimal results that lead to the best possible allocation of the control zones among the VHR optical sensors participating in the CwRS programme.

To increase the efficiency of the image acquisition a real local tasking can be compared to a tasking performed through a so-called virtual station. Both approaches allow integrating last minute information into the imaging plan and yield for instance better cloud cover results. Illustrative examples will be presented.

The JRC Image acquisition team (*) closely cooperate with Image providers as well as with the Member State Administrations and private companies working in the field of remote sensing in order to optimize the methodology of the image acquisition process chain. To this end HR and VHR specifications are established and agreed upon in the execution of the CwRS.

(*) http://cidportal.jrc.ec.europa.eu/home/image-acquisition/

8531-58, Session PS

Crop classification at subfield level using RapidEye time series and graph theory algorithms

Gunther Schorcht, Fabian Löw, Sebastian Fritsch, Christopher Conrad, Julius-Maximilians-Univ. Würzburg (Germany)

Sustainable and economical use of irrigation water is crucial to irrigated agriculture, especially in the arid and semi-arid regions of the Amu Darya delta in Central Asia, where water is a scarce and valuable resource. The state controlled crop cultivation on large fields, a leftover of the Soviet Union era, encourages local farmers to subdivide their fields in order to cultivate additional crops to optimize benefits under

the given restrictions. Furthermore, the region faced several severe drought conditions with water shortages over the past years, forcing the farmers to abandon parts of or complete fields. The knowledge of detailed and up-to-date cropping patterns at subfield level supports therefore a sustainable land and water management and is important for water managers in charge of regional water supply.

The presented study explores small scale cropping patterns within given field boundaries in order to update given land use information at field level and to further improve the water management options. Time series of vegetation indices of bi-monthly Rapid Eye satellite data were calculated and algorithms from graph theory were utilized to segment the given field boundaries into small scale field units. The graph algorithms solve the Max Flow Min Cut problem on imagery and are widely used in medical departments where large images need to be processed with the help of expert knowledge. The adaptation and automation of the algorithms to process time series of vegetation indices gained in an accountable and stand-alone segmentation of fields covering different vegetation types. A random forest classification was subsequently performed in order to examine the possible different crop types in the fields. More than 120 features extracted from the resulting subfield segments were used in the classification process. Post classification procedures involving expert knowledge eventually improves the classification results.

The approach enhances existing crop type classifications at field level, allowing for more detailed knowledge of crop diversification. Accuracy assessments indicate that the segmentation performs more robust in agricultural environments compared to existing segmentation algorithms. The classification performed with an accuracy of more than 88%. The promising results are not only usable to indicate cropping patterns, but also to examine abandoned parts of fields. The information is especially useful in times of water scarcity where fields have to leave out short-dated of the irrigation plan. The whole approach is widely automated and easy to adapt for further regions including other climatology zones. Altogether, time series of Rapid Eye satellite data with both high spatial and temporal resolution, allow for regional assessment of crop diversification at subfield level and the situation of crop water demand, highly valuable information for food security in the region.

8531-59, Session PS

Hyperspectral remote sensing applications for monitoring and stress detection in cultural plants: viral infections in tobacco plants

Dora D. Krezhova, Space Research and Technology Institute (Bulgaria); Nikolai M. Petrov, Svetla Maneva, Plant Protection Institute (Bulgaria)

Remote sensing techniques are changing very fast and newer and advanced techniques are being introduced. Hyperspectral remote sensing is one of techniques providing worth for various studies like environment, agriculture, geology, etc. It is an efficient technology for monitoring of agricultural land use and plant condition monitoring for different purposes. Green plants all have unique spectral features, mainly because of the chlorophyll and carotenoid, and other pigments and water content can together constitute the spectral feature of a plant. Chlorophyll fluorescence results from the primary reactions of photosynthesis and during the last decade it finds widening application as a means for revelation of stress and diseases. Spectral reflectance and chlorophyll fluorescence are functions of tissue optical properties and biological status of the plants.

Two remote sensing techniques (hyperspectral reflectance and chlorophyll fluorescence) were applied to reveal the presence of viral infections in tobacco plants (Nicotiana tabacum L.), cultivars Plovdiv and Rustica. Greenhouse studies were carried out with these two Bulgarian cultivars known as most widespread and with different sensitivity to viral infections. At growth stage 4-6 expanded leaf 30 plants of cultivar Plovdiv were inoculated with Potato virus Y (PVY). The leaves from 30 plants, cultivar Rustica, were inoculated with Tomato spotted wilt virus (TSWV). These two viruses are worldwide distributed and cause significant yield losses in many economically important crops.

Spectral reflectance and chlorophyll fluorescence measurements were performed by a portable fibre-optics spectrometer in the visible and near-infrared spectral ranges (450-850 nm and 600-900 nm), respectively. For both cultivars the spectral measurements were carried out on the 1st and 7th days after the inoculation. As control plants healthy untreated tobacco plants were used. The concentration of the viruses was assessed by serological analyses via the Double antibody sandwich enzyme-linked immunosorbent assay (DAS-ELISA) technique. Specific differences of the reflectance spectra within the green (520-580 nm), red (640-680 nm), red edge (690-720 nm) and near infrared (720-780 nm) spectral ranges were observed for infected leaves. The predominated differences between fluorescence spectra of control and infected leaves were appeared in the forefronts. The statistical significance of the differences was analysed by means of Student's t-criterion. Several vegetation indices: Simple ratio (SR), Red edge (RE) and Renormalized difference vegetation indices (RDVI), were computed at different wavelengths for each set of spectral data and the comparative analysis were performed. The results show the efficiency and sensitivity of spectral reflectance and chlorophyll fluorescence for revelation of stress and diseases as well as for early diagnosis of symptoms in plants at different stages of infections.

8531-61, Session PS

Spatialization of instantaneous and daily mean net radiation and soil heat flux in the territory of Itaparica, northeast Brazil

Helio L. Lopes, Bernardo B da Silva, Univ. Federal de Pernambuco (Brazil); Antônio H. Teixeira, Embrapa Semiárido (Brazil); Luciano J. Accioly, Embrapa Solos / UEP Recife (Brazil)

Knowledge of agro-meteorological processes on the basis of land use and land cover are important for sustainable development. Satellite imagery can help water resources management and their conservation while minimizing environmental impacts. We used MODIS images of 2008 in a mixed agro-ecosystem of native vegetation and irrigated crops located in a semi-arid region in Northeast Brazil, aiming to classify different land uses and land covers. It was observed that there is a range of biophysical values within types of land cover and especially between classes of land use and land cover of caatinga ecosystem. We visited the area in 2008 in order to georreference several classes, taking GPS coordinates in the middle of irrigated canopies to avoid spurious pixels when applying descriptive statistics to each classe. The modeling of the equations was performed in software for image processing (Spring 5.1) in spatial language for geoprocessing of spatial variables. The biophysical parameters analyzed were soil heat flux and Instantaneous, maximum and daily mean net radiation. Areas of dense Caatinga showed mean values of soil heat flux (Go) of 124.9 W m-2, while those with erosion incidence, present average value of 132.6 W m-2. For irrigated field, it was found mean Go values of 103.8, 98.6 and 113.9 W m-2, for banana, coconut and papaya crops respectively. In relation to instantaneous net radiation (Rn), dense caatinga presented mean value of 626.1 Wm-2, while sparse disturbed Caatinga had mean of 575.2 W m-2. Irrigated areas present Rn of 658.1, 647.4 and 617.9 W m-2 respectively for banana, coconut and papaya crops. When applying sinusoidal model to spatialize maximum (Rnmax) and daily mean net radiation (Rnmean) it were found values of 655.2 and 417.1 W m-2 respectively, while sparse disturbed caatinga showed Rnmax of 596.8 W m-2 and Rnmean of 379.9 W m-2. Considering irrigated crops Rnmax was 676.9, 677.4 and 646.6 W m-2, and Rnmean was of 430.9, 431.3 and 411.6 W m-2 respectively for banana, coconut and papaya crops. It was concluded that the sinusoidal model to quantify the maximum and daily mean net-radiation can be used on the basis of each class of soil use and soil cover, however, there is a need of comparison with field data for the model validation in both caatinga ecosystem and irrigated crops at the daily time scale. No downscaling method was applied and spatial resolution of pixels must be considered in local scale field to get more accurate results. In the future, as a function of agro-meteorological data and land use and land cover, can be generated imagery of biophysical parameters using geostatistics and thematic maps involving natural vegetation and irrigated areas.

8531-62, Session PS

Validation of AMSR-E soil moisture products in Xilinhot grassland

Shengli Wu, Jie Chen, CMA National Satellite Meteorological Ctr. (China)

Soil moisture is a primary product of Advanced Microwave Scanning Radiometer for EOS (AMSR-E) which onboard Aqua satellite. AMSR-E soil moisture product provides us global soil moisture dataset from

2002 to present. It is known to all that validation is a big problem in the use of satellite remote sensing soil moisture product. The instantaneous field of view (IFOV) of different channel of AMSR-E ranges from 10 km to 50 km. For the lower frequency which is more sensitive to soil moisture, IFOV is larger. This means that a single point of AMSR-E soil moisture product contain average soil moisture of hundreds of km2 land surface. The traditional soil moisture measurement only gives us a single point soil moisture measurement result which is not equal to large area soil moisture.

In this paper, we present an experiment to validate the soil moisture product of AMSR-E. The experiment was carried out from July 15, 2008 to September 30, 2008. 9. The location of the experiment is in Xilinhot grassland, Neimeng province, China. During the former period, we put 9 soil moisture and temperature measurement systems (ECH2O) in an area of about 3kmx3km. We selected this area because it's a very typical area in the Xilinhot grassland, which contain most land cover types and terrain types in the grassland. For each point, 5 layers of soil moisture and temperature were measured by ECH2O. The 5 layers are 2cm, 5cm, 10cm, 20cm and 50cm respectively. Considering the penetration depth of AMSR-E, 2cm measurements were used to do the validation. The location of the 9 ECH2O is very dispersive and the elevations of them are very different. Measurement result shows that the main factor that affects the soil moisture distribution is elevation. In grassland, soil moisture in higher place is always smaller than that of lower place. Which means a single soil moisture measurement is not suit for the soil moisture used purpose.

Precipitation measurement was also done in this area during the experiment period. Result shows that the precipitation is more effective to the top layers soil moisture than the bottom layers. In our sites, only 2cm and 5cm layers are affected by the precipitation. Other layer didn't change much during the whole period.

The average soil moisture measurement result in this area during the experiment is 11.8cm3/cm3, while the soil moisture product of AMSR-E in this area shows that the average soil moisture during this period is 13.3cm3/cm3. The RMSE of them is 3.7cm3/cm3.

Result show that AMSR-E soil moisture product has a good accuracy in the grassland of north China.

8531-63, Session PS

Integration of drought monitoring with remote sensing into the global drought information system

Jinlong Fan, Mingwei Zhang, China Meteorological Administration (China)

Drought occurs everywhere in the world and one of the costliest natural hazards. Its annual economic impact has been estimated globally in the hundreds of billions of dollars. In terms of the definition of drought types, there are meteorological drought, hydrological drought, agricultural drought and social and economic drought. Difference indices have been developed and used to depict those droughts. In general, the weather station data is often applied to calculate the indices. However, the remote sensing data is also attracted the attention from the research community. Among those four types of droughts, agricultural drought is more benefited from the remote sensing monitoring. According to the survey, varieties of drought monitoring system with remote sensing at regional, national or local level are existing but the integration with the drought system based on the weather station data, in particular at the global level is still weak.

Recognizing the importance of global drought monitoring with the international collaboration, the Group on Earth Observations (GEO) has advocated implementing a Global Drought Early Warning System (GDEWS) since 2007 but little was accomplished. However, the GEO Global Agricultural Monitoring Initiative, GEO-GLAM proposed by GEO agricultural Community of practice, was recognized by the G20 agricultural ministers and will be help enhance agriculture production estimated through the use of Earth observations to further reduce market volatility for the world major crops and make sure the global food security. It should be noted that it will be essential to develop the linkage between the GEO-GLAM and GDEWS.

The capability for a component of drought monitoring with remote sensing is there in place from the global agriculture community of practice. The MODIS data has been used to globally track the distribution of crop failures due to droughts. A global NDVI time-series database is produced in USA at a spatial resolution of 250 meters with a 16-day compositing period. And a web interface allows crop analysts to query data by pre-defined sub-regions, interactive regional sub setting, and by implementing crop/water masks to plot VI graphs over the growing seasons to assess crop conditions and anomalies, monitor current conditions through VI images, view VI anomalies spatially to compare current conditions to previous years, or historical mean and plot histograms of current and historical VI data. NDVI Anomaly (AVI) for June 26 to July11, 2010 computed as a difference between NDVI and NDVI averaged over all reference years (2000 - 2009) may be depicting the drought impacts on the crop growth. In China, the Chinese meteorological satellite is also ready to monitoring drought globally. FY is the short name of the Chinese meteorological satellite- FengYun, meaning wind and cloud in English. FY-3 is the second general polar orbiting Chinese meteorological satellite. 11 sensors are onboard FY-3A, launched in May 2008, and FY-3B, launched in November 2010. MERSI onboard FY-3 is similar with the MODIS and helpful to monitor the occurrence, development of drought at different scales. Joint Research Centre (JRC) of European Commission (EC) issues periodical bulletin on agricultural conditions under MARS project which uses vegetation index, thermal based evapotranspiration and microwave based indicators. Agricultural Division of Statistics, Canada issues weekly crop condition reports based on NOAA AVHRR based NDVI along with agro meteorological statistics. National Remote Sensing Agency, Department of Space issues biweekly drought bulletin and monthly reports at smaller administrative units for India under National Agricultural Drought Assessment and Monitoring System (NADAMS) which uses NOAA AVHRR and IRS WiFS based NDVI with ground based weather reports. Similar program is followed in many countries world-wide.

Drought monitoring mechanism exists in most of the countries based on ground based information on drought related parameters such as rainfall, weather, crop condition and water availability, etc. Earth observations from satellite are highly complementary to those collected by in-situ systems. Satellites are often necessary for the provision of synoptic, wide-area coverage and frequent information required for spatial monitoring of drought conditions. The informed information of drought is helpful for governmental officials and formers to in advance prepare for coping with the likely coming drought. The global efforts should be in place to promote the global drought information system with a remote sensing drought component.

8531-64, Session PS

Estimation of cotton canopy water content by hyperspectral band combinations

Qiuxiang Yi, Anming Bao, Qiang Wang, Xinjiang Institute of Ecology and Geography (China)

Biomass is one of the key biophysical variables of interest in vegetation studies (both cultivated and natural vegetation). Biomass can either be defined in terms of fresh matter weight or as dry matter weight. In addition, the canopy water content, being the difference between fresh and dry weight, is of interest in many applications. Canopy water content (CWC) is important for mapping and monitoring the condition of the terrestrial ecosystem, for instance detecting locations of environmental stresses, detecting wildfire potential, or improving soil moisture retrievals. Remote sensing offers an important opportunity for quantitative assessment of vegetation properties at different scales. Together with other parameters, vegetation water content is an important property that can be investigated by using remotely sensed data. With the development of hyperspectral remote sensing technique, direct detection approaches of vegetation water content have been proposed and further used to evaluate crop drought condition.

For quantifying the water content, at the leaf level use is often made of the leaf water content in terms of the so-called equivalent water thickness (EWT), defined as quantity of water per unit leaf area in g cm -2. At the canopy level, the canopy equivalent water thickness (EWTcanopy, cm) can be defined as the leaf water content per unit area of ground surface, and it allows scaling of leaf water content at canopy level by multiplying canopy LAI with the EWT. Another parameter for canopy water content is vegetation water content (VWC, kg m-2), which is defined as the quantities of water per unit ground area. Quite a number of different have been developed for the estimation of vegetation water content, such as the normalized difference infrared index (NDII), the water index (WI) and so on. The results obtained in these studies indicate that the knowledge of connection between the investigated variable and the spectral data can improve the performance of the vegetation indices. Further improve in indices is possible through different band combinaitons. To date, however, relationships between cotton canopy water content and the narrow band type of vegetation index and the normalized difference type of vegetation index involving all possible two-band

combinations of 2150 bands (from 350 nm to 2500 nm) have not been well investigated.

The objective of the present investigation was to (i) exploit the relationships between water content (EWTcanopy, VWC) and all possible two-band combinations indices; (ii) identify the best combinations of narrow wavebands for EWTcanopy and VWC estimation; (iii) evaluate the predictive power of the three types of hyperspectral reflectance, i.e. single narrow band reflectance, the published water indices for water content estimation and the new band combination index. The study should further our understanding of the relationships between hyperspectral indices and cotton canopy water content.

8531-65, Session PS

Estimating canopy water content of wetland vegetation using hyperspectral and multispectral remote sensing data

Yonghua Sun, Xiaojuan Li, Huili Gong, Capital Normal University (China); Ruiliang Pu, University of South Florida (United States)

Currently one of the main scientific issues is to understand and quantify the impact of global climate change on the earth system. One of the challenges is to understand the role of terrestrial ecosystems and the changes they may undergo. The water cycle is one of their most important characteristics. Wetlands, which are described as a “storage area of natural genes” and the “kidney of the Earth”, play an important role in water cycle. Water and vegetation is the key characteristics of wetland. In this respect, the canopy water content represents the health condition of vegetation and wetland itself. In this paper, we focus on innovative approaches for retrieving canopy water content from optical remote sensing data-multispectral and hyperspectral data.

Therefore, in this study, we selected Honghe National Nature Reserve (HNNR) (47°42’18”-47°52’N, 133°34’38”-133°46’29”E), which is a miniature of wetlands in the Sanjiang Plain, Northeast China as the study area. Field spectrum data, Landsat-5 TM images and ground truth data was used to estimate canopy water content of wetland vegetation. The analysis methods include three-edge parameters, narrow band vegetation indexes, absorption indexes from hyperspectral data and different vegetation indexes from multispectral data.

1. Canopy water content estimated model based on three-edge parameters (Table2, Fig.1, and Table3)

The correlation between the indexes ((SDr-SDb)/(SDr+SDb), SDr/SDb) and canopy water content reach to a very significant test level.

2. Canopy water content estimated model based on narrow band vegetation index (Fig.2 and Table4)

Narrow band vegetation index (NDVI) is a normalized difference index between any two hyperspectral bands. In this study, 39340 ( ) (spectral resolution =5nm) NDVIs were built. According to correlation analysis, NDVI based on reflectance of 970nm and 900nm has the maximum correlation with canopy water content.

3. Canopy water content estimated model based on general vegetation index (Table5, Fig.3 and Table 6)

Based on previous literatures, 14 vegetation indexes(PVIHYP, ATSAVI, DSWI, LWVI1, LWVI2, MSI, NDII, NDWI, PRI, RVIHYP, RVSI, SIWSI, SRWI, WI)were used for estimating canopy water content(Detailed definition of the VIs were listed in Table 5).Finally, WI which was built by R900/R970 has the maximum correlation and was selected to build estimated model.

4. Canopy water content estimated model based on absorption features (Fig.4 and Table 7)

The article selected the absorption features around the 970nm and 1200nm, such as absorption depth, absorption width and absorption area. Absorption depth of 1200nm has the maximum correlation and was selected to build estimated model.

5. Canopy water content estimated model based on TM image

The article extracted 11 VIs from Landsat5 TM image. According to correlation analysis with survey data, NDII((TM4-TM5) /(TM4+TM5)) was selected to build the estimated model. Based on the model, distribution map of canopy water content in HNNR was generated.

8531-66, Session PS

Soil moisture monitoring over a semiarid region using Envisat ASAR data

Atef A Amriche, Ecole Nationale Superieure Agronomique d’Alger (Algeria); Mokhtar Guerfi, Ecole Nationale Supérieure des Sciences de la Mer et de l’Aménagement du Littoral (Algeria)

Soil moisture plays a critical role in seed germination and plant growth. It’s also a key parameter for irrigation scheduling and crop yield prediction. The use of remote sensing for the retrieval and mapping of soil moisture offers interesting spatial and temporal resolutions, thus allowing a precise study at a regional scale.

In this paper, a simple approach for mapping near-surface soil moisture from Envisat ASAR data was developed. Four high-resolution images covering a semiarid zone in North East Algeria were acquired with the same sensor configuration (mode, polarization, swath... etc). We performed the pretreatment using the Basic Envisat SAR Toolbox of the European Space Agency. Then, we extracted the backscattering coefficient $\sigma 0$ (dB) from the filtered and calibrated images. On the other hand, five training sites with different physical properties and vegetation cover were selected for monitoring soil moisture. The field campaigns were conducted concomitantly with the images acquisitions, to measure soil water content in the top five centimeters using the gravimetric method. The analysis of the radar backscattering coefficient frequency histograms helps explaining its temporal variability and determining the main factors affecting it at each site. Furthermore, the study of linear regressions associated to the change detection approach allowed the expression of the backscattering coefficient as a function of volumetric soil moisture ($\sigma 0 = a*mv + b$). The coefficients “a” and “b” of the equation slightly differ from one site to another and also from one season to the next. This difference is mainly due to the effects of surface roughness and vegetation biomass variation. Our study confirms a good agreement between the volumetric near-surface soil moisture and the radar backscattering coefficient for all the test fields (r values range from 0.62 to 0.86). The comparison between measured and estimated soil moisture proves the accuracy of the inversion method used here with a mean error of less than 5%. At the end, high resolution maps of soil moisture distribution were obtained from the acquired radar images.

8531-67, Session PS

A re-examination of perpendicular drought indices over central and southwest Asia

Alireza Shahabfar, Maximilian Reinwand, Christopher Conrad, Gunther Schorcht, Julius-Maximilians-Univ. Würzburg (Germany)

Drought monitoring models and products assist decision makers in drought planning, preparation, and mitigation, all of which can play a role in reducing drought impacts. Therefore, in this study, the performance of newly developed remote sensing-based drought indices, the perpendicular drought index (PDI) and modified perpendicular drought index (MPDI), are further explored for regional drought monitoring to construct a drought early warning system over different climatological zones in agricultural regions located in Central and South Western Asia. The study area covers regions from moderate and wet climatological zones with dense vegetation coverage to semi-arid and arid climatological conditions with moderate to poor vegetation coverage. This area characterized by a high portion of rural population has faced several severe drought conditions in recent years. The spatio-temporal patterns of surface drought derived by PDI and MPDI from MODerate Resolution Imaging Spectroradiometer (MODIS) data in 8-day time steps are compared against field-measured precipitation and regional meteorological conditions. Results indicate that there are significant negative correlations between the PDI, the MPDI and precipitation. The results confirm previous studies which has been analyzing the PDI and the MPDI over some study points in Iran. In this research, however, implementation of higher resolution data (MOD09Q1) in both spatial (250 m) and temporal (8-days) dimensions revealed a greater agreement between the drought information extracted by the MPDI, PDI and field meteorological measurements. It is recommended that MPDI could be used in fully to partially vegetation covered regions and PDI could be applied for bare and poor vegetation covered soil applications. Due to its structure, it does not require calculation of additional information such as the fraction of vegetation which may

contain some uncertainties. The applied perpendicular indices could be used as a drought early warning system over case study region and other regions with arid and semi-arid climatological conditions.

8531-68, Session PS

Wheat yield response to water deficit index using remote sensing

Mohammed A. El-Shirbeny, Ayman F. Abou Hadid, Sayed M. Arafat, National Authority for Remote Sensing and Space Sciences (Egypt); Abd-Elghany M. El-Gindy, Ain Shams Univ. (Egypt)

The climate in Egypt is Dry Arid According to Köppen Climate Classification System, where precipitation is less than 50% of potential evapotranspiration, Annual average temperature is over 18°C. Limited water resources and scarcity of water in Egypt is the main challenge for agricultural horizontal expanding policies and strategies. El-Salhia project is located at the South Western of Ismaillia city and to the East southern of El-Kassaseen city. Normalized Difference Vegetation Index (NDVI) and Land Surface Temperature (LST) were extracted from Landsat and NOAA/AVHRR satellite data. Water Deficit Index (WDI) uses both Land Surface Temperature (LST) minus air temperature (Tair) and vegetation index to estimate the relative water status. Yield response factor (ky) derived from relationship between relative yield decrease and relative evapotranspiration deficit. The relative Evapotranspiration deficit replaced by WDI. The relation between WDI and yearly average wheat yield was linear and R2 was 0.79. Air temperature affected by LST so the relation between Tair and LST was done and R2 was 0.74. GIS technique used to produce WDI, NDVI and LST maps. The main objective of the paper is using remote sensing to study sensitivity of wheat yield to Water Deficit.

8531-69, Session PS

Remote sensing and mapping of vegetation community patches at Gudong Oil Field, China: a comparative use of SPOT 5 and ALOS data

Qingsheng Liu, Dan Huang, Gaohuan Liu, Chong Huang, Institute of Geographic Sciences and Natural Resources Research, CAS (China)

It is extremely common and objective fact that the vegetation was damaged and subsided by Shengli Oil Field development in the Yellow River Delta (YRD). But few reports were focused on the extending phenomenon of vegetation caused by oil field development. In fact, the extending phenomenon of vegetation community caused by seismic exploration has been found in the many areas of YRD. From the ecological role, such extension of vegetation caused by oil field development is beneficial to the ecological restoration and protection and re-vegetation of YRD. This vegetation extension, obviating the need for additional funds, is necessary to lucubrate, and look for the countermeasures which make it change from spontaneous state into artificial coordinating for maximum extension in the suitable areas, which will help to better coordinate the contradiction between the oil field development and the wetland ecosystem protection. In order to facilitate the monitoring of vegetation extension and quantify the mechanism of vegetation patch succession, there is a clear need for accurate and economical of detecting the different structures of vegetation patches. In this paper, we are interested in comparing the efficacy for vegetation community patch detection between high spatial resolution SPOT 5 and ALOS data. Firstly we performed the geometric rectification to the image with 27 ground control points collected by the Differential GPS (DGPS) within the image range. Then ALOS data were registered according to SPOT 5 image after geometric rectification. In order to produce a multispectral image with 2.5 m spatial resolution, we used the pan sharpening technique in PCI software for the fusion of ALOS 2.5 m panchromatic band and 10 m visible and near infrared bands. SPOT 2.5m simulated real color data was from SPOT Image Company. Finally, the subset of the fusion-ready SPOT 5 and ALOS image are used in this paper. Firstly, two images were transformed from RGB into HSV color space by using the RGB2HSV function in MATLAB software. Then Wiener filter (3?3) was used to remove the noise of the S component images after image enhancement. Secondly, canny edge detector was used to find the edges of the images. Thirdly, traced the exterior edges of targets and label the targets using BWBOUNDARIES function in MATLAB software. Then the centroid coordinates of the targets are calculated and saved. Finally, the row and column coordinates and the actual and theoretical areas of targets were calculated and saved. When the ratio between the actual and theoretical area of the target was greater than 0.3 and less than 1.2, the vegetation patches were detected very well. At the same Ground Spatial Distance (2.5m), SPOT 5 yielded greater vegetation patch detection accuracy (91.2%) than ALOS (89.3%). This likely was a consequence: 1) image definition of SPOT 5 is better than ALOS data; 2) the separability of vegetation patches in 2005 is greater than that of 2008. The experiments implemented in the study area show that high spatial resolution satellite images are effective and sufficient to identify the circular or elliptic vegetation patches.

8531-70, Session PS

Analysis of regional vegetation changes with medium and high resolution imagery

Javier Marcello, Francisco Eugenio, IOCAG - Univ. de Las Palmas de Gran Canaria (Spain); Anabella Medina, Univ. de Las Palmas de Gran Canaria (Spain)

The singular characteristics of the Canarian archipelago (Spain) have allowed the development of a unique biological richness. Not surprisingly, 42% of its territory is protected to preserve biodiversity and the natural environment of these islands. In particular, almost 20% of the total area is occupied by forests. In consequence, the monitoring of vegetated regions plays an important role for regional administrations which aim to develop the corresponding policies for the conservation of such ecosystems.

Many vegetation indices have been developed to study green areas from satellite images. They involve combinations of spectral channels, namely the red and near-infrared bands, merged in such a way that they strengthen the spectral contribution of green vegetation, minimizing the disturbing influence of soil background, irradiance, solar position, atmospheric attenuation, etc. In any case, influences due to the atmosphere, the relief, the terrain, the topography and the anisotropy of land covers must be corrected when performing regional studies.

The Normalized Difference Vegetation Index (NDVI) is a common index applied for vegetation studies. It is important to emphasize that NDVI is sensor-dependent, since its value depends, not only on the net sensor system gain in the channels used, but also on the specific bandwidth and location. Furthermore, this index changes depending on the land use, the season, the hydric situation and the climate of the area. So, a fixed threshold cannot be set, even for the same sensor or season, to properly segment vegetation areas. In this context, a robust methodology has been developed to ensure a reliable estimation of changes using the same sensor in multiple dates or different sensors. To that respect, different strategies were assessed to properly map green areas. A supervised procedure was finally considered consisting on the selection of different regions (barren land, urban, water and vegetation) within each image. That way, we can precisely map each cover with its associated NDVI values and, in consequence, obtain the optimal threshold to properly segment vegetation.

We have developed a C++ tool to perform regional analysis of vegetation changes in the Canary Islands using data from different sensors. In particular, all cloud free Landsat images from 1984 to 2011 were processed; Deimos and SPOT scenes were also considered and, finally, higher resolution Ikonos, Geoeye and Quickbird were selected to conduct precise studies in specific areas.

The complete methodology incorporates all the required pre-processing (radiometric calibration, atmospheric, topographic and BRDF correction) for each sensor and it can compute several indices (NDVI, RVI, EVI, SAVI, OSAVI, ARVI, etc.). Pansharpening techniques have been added and change detection image processing techniques have also been included. Ground data, provided by the Canary Island Government, from particular locations was used to validate the overall methodology.

In summary, a complex but robust tool for regional vegetation analysis has been developed and applied to monitor the vegetation health of the Canary Islands using imagery from medium and high resolution sensors. In general, the vigor of forests and remaining vegetation covers is optimal. A detailed study was also conducted to analyze the impacts of a very severe fire happening in 2007, which affected more than 30.000 hectares. The analysis demonstrates that most of the burned areas have recovered in 2011.

8531-71, Session PS

Climate changes and their impacts on Romanian mountain forests

Maria A. Zoran, National Institute of Research and Development for Optoelectronics (Romania); Liviu-Florin Zoran, Polytechnical Univ. of Bucharest (Romania); Adrian I. Dida, Ministry of Agriculture and Rural Development (Romania); Mariana Rodica Dida, Univ. of Medicine and Pharmacy of Craiova (Romania)

During last years, due to anthropogenic and climatic changes, most mountain areas in Romania are experiencing environmental degradation. As in mountain areas, climate changes rapidly with height over relatively short horizontal distances, mountain forests represent unique areas for the detection of climatic change and the assessment of climate-related impacts. Forest systems are all sensitive to climatic factors and extreme events and are likely to have different vulnerability thresholds according to the species, the amplitude, and the rate of climatic stressors. As a result of global climate change, there is growing evidence that some of the most severe weather events could become more frequent in Romania over the next 50 to 100 years. Effects of climate extremes on forests can have both short-term and long-term implications for standing biomass, tree health and species composition. Multispectral, multiresolution and multitemporal satellite imagery is used to classify and map various forest and spatio-temporal land-cover changes. In mountain forests, the more frequent occurrence of climatic changes may accelerate the replacement of sensitive tree species and reduce carbon stocks, and the projected slight increase in the frequency of extreme storms by the end of the century could increase the risk of windthrow. Mountain forest landscape pattern and the biogeophysical variables (NDVI, EVI, FPAR) controlling observed patterns can be addressed using time series remote sensing satellite imagery. The specific aim of this paper was to: 1) quantify the changes and rates of change between 1990 and 2011 in vegetative composition across a forest landscape in Romanian Carpathians on Prahova Valley using Landsat TM and ETM, IKONOS, MODIS images; 2) examine the changes in landscape structure in relation with climatic changes and extreme events; 3) assess the climate risks and their potential impact on Romanian mountain forests; 4) investigate and discuss the spatio-temporal changes observed in the landscape composition, pattern and structure o in the context of forest management activities and other disturbances.

To evaluate the impacts of the management practice on biophysical properties of the mountain forest system, a set of biophysical variables were estimated from Landsat TM and ETM+ and MODIS data. The data included vegetation indices, surface broadband albedos. To study climatic and anthropogenic impacts, several classifications of forest vegetation over tested area have been done. Image pairs of the same vegetation index, for subsequent years, were subtracted producing continuous maps indicating areas of change. Statistical analysis was carried out to see if there is a correlation between the two sets of output. The analysis of different classifications over selected test area have shown mountain forest changes due to high levels of atmospheric pollution mainly close of main road traffic and some local industries, air masses dynamics at local and regional level as well as due to deforestation for land-use conversion, insect and disease epidemics. The preservation and enhancement of mountain forest vegetation cover in natural, semi-natural forestry ecosystems is an essential factor in sustaining environmental health and averting natural hazards. In order to decrease the risk for socio-economic impacts, long-term adaptive strategies in modern forest research seem necessary.

8531-72, Session PS

Laser-induced fluorescence monitoring of Chinese Longjing Tea

Liang Mei, Zhejiang Univ. (China); Zuguang Guan, ALOMAR Observatory (Norway); Gabriel Somesfalean, Sune Svanberg, Lund Univ. (Sweden)

Laser-induced fluorescence (LIF) of green plant leaves excited by ultraviolet radiation can reveal significant information about the plant. The fluorescence spectrum contains two fundamental parts, one is the blue-green fluorescence (BGF), and the other part is due to the fluorescence of chlorophyll which has two peaks in the red region (RF) and far red region (FRF), i.e., around 685 nm and 735 nm, respectively. Since chlorophyll also reabsorbs the red fluorescence around 685 nm, the intensity ratio between FRF and RF has been utilized as a means to analyze the chlorophyll concentration [1]. Extensive efforts have been devoted to identify the types, growth and nutrient conditions of plants by analyzing the relationship between BGF, RF and FRF remotely.

Recently, the LIF technique was also applied to identify the quality and type of Chinese jasmine tea and oolong tea [2] in laboratory measurements, where a chemometric method based on singular value decomposition (SVD) and linear discriminant analysis (LDA) was utilized to analyze the fluorescence spectra of dried tea leaves. Encouraged by the good prediction results for tea qualities and classification using LIF, we now present remote fluorescence measurements on Chinese Longjing tea plants, and apply the chemometric method to evaluate the quality of Longjing tea leaves.

The mobile lidar system of the Atomic Physics Division, Lund University, Sweden, was shipped to Zhejiang University, Hangzhou, China for different types of lidar work. A tea bush and some fresh branches were brought from different tea villages around Hangzhou. The remote fluorescence spectra of the green tea bush and fresh tea branches were investigated in the Zijingang Campus of Zhejiang University, where the experiments were performed with the samples at 50-m distance from the lidar system. The experimental results show that the chlorophyll fluorescence is varying for the different kinds of tea samples. In order to draw conclusions for the exact chlorophyll content of the tea branches from different tea villages, more samples are needed. By using a more representative sample averaging, e.g., a footprint of around 1 meter in diameter as measured, e.g., from a helicopter, assessments might be more quantitative.

Several dried Longjing tea samples with different qualities, were also measured and evaluated by the chemometric method. However, the predicted results of Longjing tea samples do not show any correlation with the tea quality evaluated by the tea expert, which suggests that the tea quality of the Longjing tea has no obvious relationship with fluorescence spectra excited by 355 nm - their fluorescence spectra are almost identical. A compact hand-held system based on light emitting diodes (LED) might be constructed to evaluate the tea quality, whereby the use of multiple excitation wavelengths is suggested in further studies. Thus information related to the wavelength-dependent light penetration through the wax layer and the related effectiveness of excitation of the underlying chlorophyll can also be explored.

REFERENCES

1. A. A. Gitelson, C. Buschmann, and H. K. Lichtenthaler, 1998: “Leaf chlorophyll fluorescence corrected for re-absorption by means of absorption and reflectance measurements,” Journal of plant physiology 152, pp 283-296.

2. Liang Mei, Patrik Lundin, Mikkel Brydegaard, Shuying Gong, Desong Tang, Gabriel Somesfalean, Sailing He, and Sune Svanberg, 2012: “Tea classification and quality assessment using laser induced fluorescence and chemometric evaluation,” Applied Optics 51, pp 803-811.

8531-73, Session PS

Study of vegetation index selection and changing detection thresholds in land cover change detection assessment using change vector analysis

Duy Ba Nguyen, Tran Thi H. Giang, Hanoi Univ. of Mining and Geology (Viet Nam); Tong Si Son, Space Technology Institute (Viet Nam)

In recent years, Vietnamese rapidly developing economy has led to speedy changes in land cover.

The study of changing detection of land cover plays an important role in making the strategy of the managers. There are two main approaches in changing detection research by using remote sensing and GIS: post- classication change detection analysis approach and pre-classication changing spectral determination approach. Each has their own dierent advantages and dis- advantages. The second one is further divided into: Image Dierencing, Multi-date Principal Component Analysis (MPCA); Change Vector Analysis (CVA). In this study, researchers introduce CVA method. This method is based on two important index to show the primary feature of land cover, such as: vegetation index (NDVI-) and barren land index (-BI). Ability to apply methods of CVA has been mentioned in the studies [1, 2, 3, and 4]. However, in these studies did not mention the NDVI index selection and changing detection threshold in changing detection assessment? This paper proposes application to solve these two problems.

8531-74, Session PS

Mapping aquatic vegetation through remote sensing data: a comparison of different Vegetation Indices performances

Paolo Villa, Istituto di Scienza e Tecnologie dell'Informazione "A.Faedo" (Italy) and Istituto per il Rilevamento Elettromagnetico dell'Ambiente (Italy); Mariano Bresciani, Istituto per il Rilevamento Elettromagnetico dell'Ambiente (Italy); Federica Braga, Istituto di Scienze Marine (Italy); Rossano Bolpagni, Univ. delgi Studi di Parma (Italy)

Aquatic vegetation, including helophytes and macrophytes, is a crucial component of transitional environments and coastal ecosystems, from a naturalistic and economic point of view. This target is well suited to be subject of remote sensing analysis, because of the advantages synoptic view have on traditional in situ survey. In particular, studying and mapping aquatic vegetation through remote sensing (especially in its optical reflectance properties) is a powerful and effective way to monitor vegetation status, growth and bio-physical parameters and good monitoring capabilities in this field are ensured by the use of Vegetation Indices (VIs).

This work aims at running a brief comparison of different VIs in mapping aquatic vegetation over 3 distinct study areas and wetlands ecosystems, by employing multi-spectral and multi-sensor dataset ranging from aerial to satellite data, with varying spatial (1-30 meter) and spectral resolution (5 nm-100 nm), in order to evaluate the best performing ones.

Study areas and dataset exploited are briefly introduced in the following list: (a) Southern portion of Lake Garda, Northern Italy: AISA and MIVIS hyperspectral data, GeoEye and WorldView-2 multispectral data (2-4 meter resolution); (b) Lakes of Mantua, Northern Italy: APEX and Proba-1 CHRIS hyperspectral data (3-15 meter resolution); and (c) Venice Lagoon, North-eastern Italy: EO-1 Hyperion hyperspectral data and Landsat5 TM multispectral data (30 meter resolution).

A set of four different VIs were subject of comparison for each of the scene of the multi-sensor dataset covering the 3 study areas. The remote sensing dataset was pre-processed for deriving atmospherically corrected ground reflectance values, and pre-processed data were used as input for VIs derivation. Three of the VIs utilized are well known in literature: Normalized Difference Vegetation Index (NDVI), Enhanced Vegetation Index (EVI), and Red Green Ratio Index (RGRI); the remaining index, instead is being introduced and tested here, and has been called Normalized Difference Water Vegetation Index (NDWVI). NDWVI follows the common and broadly tested normalized differencing approach and comes as an adaptation of the common NDVI specifically targeted at aquatic vegetation, where the vegetation background is usually composed of water instead that of soil.

From VIs results over the dataset, performances in terms of both wetland vegetation mapping capabilities and vegetation features separability were assessed, also with the use of ancillary field and laboratory spectral information. Best performances were shown by different indices depending on the study area and dataset utilized, with EVI generally over-performing NDVI, and NDWVI showing good to very good results especially in terms of vegetation features separability, which makes it a useful tool for integration with the other VIs in wetland vegetation mapping. RGRI instead, exploits vegetation spectral characteristics, linked to leaf pigments, different from vegetation vigour and biomass (linked to NDVI, EVI and NDWVI), thus demonstrating its usefulness in vegetation monitoring analysis. We can draw the conclusion that all the four VIs tested - and the novel NDWVI in particular - are carrying useful information about wetland vegetation, and their integrated use can be envisaged in order to effectively map aquatic vegetation from remote sensing.

8531-75, Session PS

Fuzzy logic for marine coastal zone land cover changes assessment

Liviu-Florin V. I. Zoran, Polytechnical Univ. of Bucharest (Romania); Maria A. Zoran, National Institute of Research and Development for Optoelectronics (Romania)

The Romanian Black Sea coastal zone as an integrating part of European coastal zone has geomorphic and metabolic characteristics similar to those of other coastal areas (Baltic Sea, Mediterranean Sea, and the European Atlantic coast including the North Sea), and during last century suffered severe changes due to anthropogenic and natural factors. Black Sea, draining most of North-Eastern Europe through a number of major rivers, can be taken as the ultimate representative of an environmentally-stressed enclosed sea. Among large marine water bodies, the Black Sea has a significantly high ratio of drainage basin to water basin area, accompanied by a high population density in the catchments area itself. As a consequence, it is subject to a considerable anthropogenic impact on Black Sea ecosystem. Satellite imagery offers great potential for marine coastal areas mapping and spatio-temporal dynamics assessment. Due to climate and anthropogenic-induced changes on coastal zone morphology as well as on stocks of plankton and fish, climate-sea interactions and their response on marine ecosystems have recently been focus of considerable attention. Fuzzy theory applied for the analysis of coastal areas changes, for which each pixel on the map is assigned a membership grade in all classes, represent reasonable alternatives to traditional fixed classifications. Fuzzy classifications and mixture/subpixel models provide information on variations in spectral signature between pixels and not on differences in the on-the-ground content of mapped land cover. The coastal zone units are recognized on a ground truth map of an area using Landsat Thematic Mapper (TM) and Enhanced Thematic Mapper (ETM) as well as IKONOS and Quickbird imagery for North-Western Black Sea coastal zone, Romania, over 1990-2011 period. The application of fuzzy logic for quantifying magnitudes of land cover changes is highly appealing because of its capability to deal with uncertainties such as in the case when one cannot accurately identify a threshold value to separate areas of change from areas of no-change. Anthropogenic eutrophication and coastal erosion affects the Romanian North-Western Black Sea to various extents. As an indication of land use/cover change, the extension of the road network and the intensive process of urbanization over urban areas were registered between 1990 and 2011. Also the change in the position of the coastline in Constantza area is examined and linked to the urban expansion in order to determine if the changes are mainly human induced or natural. A distinction is made between landfill/sedimentation processes on the one hand and dredging/erosion processes on the other. The impact of fluvial discharges (both a direct effect due to the sediment load and an indirect one induced on the planktonic flora by the associated nutrient load) was evaluated from the comparison of inshore and offshore optical characteristics appearing in the remote sensing data. The analysis of an ever longer time series of satellite data, and the derivation of bio-optical algorithms with sounder statistical foundations will allow the exploration of such features in more detail, and in particular the definition of their evolution in both the spatial and temporal domains.

8531-76, Session PS

Planktothrix rubescens in freshwater reservoirs: remote sensing potentiality for mapping phycocyanin concentration

Antonino Maltese, Fulvio Capodici, Giuseppe Ciraolo, Goffredo La Loggia, Univ. degli Studi di Palermo (Italy); Antonio Granata, Agenzia Regionale per la Protezione dell'Ambiente Siciliana (Italy)

P. rubescens is sadly famous for producing microcystins (MC), which are powerful hepatotoxins. Recently (2006) P. rubescens has been found in the Pozzillo, Nicoletti, Ancipa, Prizzi and Garcia reservoirs. This paper compares the optical properties of the water of an infested reservoir and those of a clear water reservoir. Furthermore it compares empirical methods based single reflectance ratio and semi-empirical methods based on two nested ratios, highlighting whether the former fail to accurately evaluate the phycocyanin concentration.

Field campaigns were carried out in February/March 2008 to quantify the diffuse attenuation coefficient, by measuring underwater downwelling irradiance at different depths as well as water spectral reflectance. The possibility of detecting P. rubescens using its spectral characteristics through diachronic remote sensing techniques was investigated. During periods of low shortwave irradiance such as winter, when light weakly penetrates water columns and the water cools, P. rubescens filaments float up to the surface, forming red-colored blooms. Water samples were collected for both phytoplankton counting and biovolume estimation and for the analysis of microcystins. Meteorological measurements highlighted the low temperatures (< 2° C) for this region, which occurred between two frosts in December 2007 and February 2008, with a contemporaneous reduction in the incident total solar radiation that probably triggered P.

rubescens to float up to the water surface in the infested lake.

Underwater spectral irradiances and in-air upwelling spectral radiances were acquired in February/March 2007 in order to characterize the extinction optical properties of the lake infested by the red algae and the un-infested lake. The results showed that optical properties are significantly altered when P. rubescens infests lake water. Comparison between the reflectance spectrum of water dominated by P. rubescens and the spectrum of the reference lake water showed higher reflectance in the former case.

However, even if Landsat ETM+ images have an appropriate spatial resolution for monitoring Sicilian reservoirs, that are characterized by an average extension of few kilometers; these images cannot be used to distinguish the contribute of chlorophyll from that of cyanobacteria and the characterizing pigment (the phycocianin - PC) at early stage formation of cyanobacterial blooms, and their concentration cannot be assessed accurately. When cyanobacteria dominate, the PC absorption is identified by a rising of spectral reflectance in red and near infrared spectral ranges.

Even if MODIS has appropriate spectral bands at a spatial resolution of 1 km that, however, it is not spatially suitable for lakes monitoring; A time series of at a spatial resolution of MODIS images with a spatial resolution of 250 m have been processed and compared to in situ density, and total concentration of microcystins. The retrieved empirical equations tend to overestimate the actual values for low (and absent) surface filaments.

A short time series of MERIS images were also processed using a nested band ratio algorithm using 620, 665, 709 and 779 nm bands. The semi-empirical algorithm allows distinguish both contributes of cyanobacteria and chlorophyll also when the former does not dominate the water emerging spectral radiance. However, also MERIS images are characterized by too low spatial resolution for operational applications (300 m).

8531-77, Session PS

Investigation of the difference between thermal infrared canopy temperature and microwave effective canopy temperature over homogeneous corn canopy

Jing Liu, Institute of Remote Sensing Applications (China) and Graduate School of Chinese Academy of Sciences (China); Qinhuo Liu, Institute of Remote Sensing Applications (China); Hongzhang Ma, China Univ. of Petroleum (China); Le Yang, Institute of Remote Sensing Applications (China); Jingjing Peng, Institute of Remote Sensing Applications (China) and Graduate School of Chinese Academy of Sciences (China)

Land surface temperature (LST) plays a very important role in the energy balance of the Earth surface. It is an essential input variable of land hydrological model, numerical weather or climate prediction pattern and inversion of soil moisture. Many achievements have been presented for retrieving LST from thermal infrared satellite sensor data. The accuracy of retrieval results can reach 1K or less, but thermal infrared remote sensing is so strictly influenced by cloud that it is incapable in cloudy weather. By contrast, microwave remote sensing is influenced slightly by cloud and atmosphere, and it is also multi-polarized, so passive microwave remote sensing holds a unique advantage in retrieving LST. Nowadays, the combination of infrared temperature and microwave temperature is a trend in the application of LST. However, thermal infrared temperature and microwave temperature have different physical significances and values. For vegetation land, Microwave temperature data contains the canopy temperature information of different layers within the penetration depth through the vegetation and the soil, which helps get more soil information. So we designate the microwave temperature as microwave effective temperature. Thermal infrared temperature is the surface skin temperature that contains the observed vegetation information and the observed soil information. When the temperature of the foliage component is unequal to that of the soil component, thermal infrared canopy temperature and microwave canopy temperature have different values. It is necessary to accomplish the conversion between thermal infrared canopy temperature and microwave effective canopy temperature before the combination of them in research.

In this study, the homogeneous canopy is the leaf-dominated crown layer ignoring the effect of branches. Two layers with different temperature, the canopy layer and the soil layer, are considered. The leaves with random distribution in azimuth angles are regarded as effective dielectric circle-disc scatters assuming average sizes. It is assumed that the foliage component temperature and the soil component temperature at thermal infrared band and microwave band are the same. MESCAM model based on matrix doubling method has been modified by getting rid of the effects of the main and secondary stems. So the modified MESCAM model can be used for the scene constructed in this paper. The effect of multiple scattering at L and C band has been studied by comparing the results of tao-omiga model with that of the modified MESCAM model. It can be concluded that the effect of multiple scattering at L band can be neglected, but at C band the effect of multiple scattering needs to be considered. Transmissivity, emissivity and single scattering albedo of the vegetation at L band are computed by the modified MESCAM model. The soil emissivity is computed by IEM model. Then we adopted tao-omiga model to compute the canopy brightness temperature at L band and a simple geometric-optical model basing on gap probabilities to compute the canopy brightness temperature at thermal infrared band in the same scene. The difference between the foliage component temperature and the soil component temperature varies diurnally. There are three cases, including the foliage component temperature TC is approximately equal to the soil component temperature TS before sunrise, then TC starts to become greater than TS, and after that TS starts to be greater than TC. The relationship and the difference between thermal infrared physical canopy temperature and L band effective canopy temperature with different soil moisture have been analyzed as the change of LAI (leaf area index) in these three situations when the observation angle is zero. When TC is lower than TS, as the increase of LAI, thermal infrared canopy temperature decreases as a form of exponent and the contribution of the soil decreases, but L band canopy effective temperature decreases as a form of approximate linearity and the contribution of the soil decreases. As the increase of soil moisture, the changing rate of L band canopy effective temperature increases and the contribution of the vegetation is greater, becoming more sensitive to the change of LAI. When TC is higher than TS, the changing trend is reverse. The relationship between thermal infrared canopy temperature and L band canopy effective temperature with different soil moisture as the change of LAI (leaf area index) is nonlinear. It is a base of further exploring the cooperative inversion combining infrared with passive microwave.

8531-78, Session PS

Application of thermal infrared images in crop field studies of land-atmosphere interactions

Hella E. Ahrends, Susanne Crewell, Univ. of Cologne (Germany); Anke Schickling, Uwe Rascher, Forschungszentrum Jülich GmbH (Germany)

Land surface temperatures (LST) are an indicator of climate change, and an important variable in the energy balance of ecosystems. Therefore, they are critical factors in models quantifying land surface-atmosphere interactions (e.g., Reichle et al. 2010). In vegetated ecosystems canopy temperatures are an indicator for transpiration and canopy stomatal conductance (Jones 2004). However, there are complex interactions between canopy temperatures, ambient conditions and surface properties. Thus far these interactions are poorly understood, and have thus mainly been studied under standardized conditions and at the leaf scale. Larger scale field studies rely on standardized measure with sufficient spatial coverage. Such data are only available in the form of remotely sensed thermal infrared or microwave radiation data. With known surface emissivity these data can be used to calculate radiometric surface skin temperatures. Satellites provide global cover of radiometric LST and emissivities. However, there is a considerable amount of uncertainty due to narrow spectral bandwidths, atmospheric influences and the temporal and spatial variability of land surface emissivities (Li et al. 2007). Furthermore, the temporal resolution of satellite LST products is limited. Ground-based observations on the other hand have limited spatial cover. The differences in the air temperature at different measurement heights are frequently used as a proxy for surface temperatures. Infrared radiometers provide spatially integrated skin temperatures at the plot scale. However, they assume a constant emissivity of the observed surface which is often unrealistic. Recently thermal cameras operating at higher temporal and spatial resolution are becoming more cost-effective and applicable for thermography studies under field conditions. Image processing techniques allow for pixelwise correction of emissivities. In our study we aim at discussing the suitability of IR images for observing canopy surface-atmosphere interactions under highly variable ambient conditions. We will present results on possible synergies between thermal, hyperspectral and

stereoscopic observation techniques.

A thermal camera (FLIRA315, 60Hz, 7.5-13µm) is installed at an agricultural research site located in the Rur catchment, West Germany (Tansregio 32 project; www.tr32.de). The camera automatically captures diurnal and nocturnal infrared images of a 1m x 1m area covered by winter wheat at a temporal resolution of 10 minutes during the growing season (April-September) of 2012. Thermocouples are used for validating the observations and for separating changes in emissivity and the skin temperature. We use data from an eddy covariance station and from a near-by meteorological observation center (JOYCE) to characterize meteorological conditions. Time lapse camera images are applied for the identification of surface components. We relate radiometric temperatures to continuous measurements of spectral vegetation indices and sun-induced chlorophyll fluorescence as a proxy for the canopy photosynthetic activity (Meroni et al.2009). We also collate biweekly data on spatio-temporal changes in the canopy structure using a stereoscopic camera set up (Biskup et al., 2007). Based on these data sets we model the spatial variability of stomatal conductance (Blonquist et al. 2009). We will quantify spatio-temporal variations in plant adaptation strategies to environmental conditions. We present results on synergies between sensor techniques and discuss uncertainties of thermography studies under field conditions. We hypothesize that the combined information from thermal and stereoscopic images is needed for the interpretation and understanding of vegetation indices and sun-induced fluorescence. Such ground based studies on the thermal response of vegetation canopies under field conditions provide data sets urgently needed for the validation and understanding of data from aircraft campaigns and from recent and next generation satellite sensors (Jin & Dickinson 2010).

8531-79, Session PS

Thermal pollution assessment in nuclear power plant environment by satellite remote sensing data

Maria A Zoran, Roxana S. Savastru, Dan M. Savastru, Sorin I. Miclos, Marina N. Tautan, Laurentiu V. Baschir, National Institute of Research and Development for Optoelectronics (Romania)

The main environmental issues affecting the broad acceptability of NPP (Nuclear Power Plant) are the emission of radioactive materials, the generation of radioactive and heat waste, and the potential for nuclear accidents. Satellite remote sensing is an important tool for spatio-temporal analysis and surveillance of environment, thermal heat waste of waters being a major concern in many coastal ecosystems involving nuclear power plants, as sharp changes in water temperature can significantly affect the distribution and physiology of aquatic biota and contribute to global warming. The thermal plume signature in the NPP hydrological system in TIR (Thermal Infrared) spectral bands of Landsat TM and ETM TIR band 6 as well as MODIS TIR bands time series satellite have been used for WST (Water Surface Temperature) detection, mapping and monitoring. As a test case the methodology was applied for NPP Cernavoda, Romania during period of 1990-2011 years. At the present time in Romania there is one operational Nuclear Power Plant (NPP), located at Cernavoda, in Constanta county, South-Eastern part of the country. The plant was designed to comprise five CANDU 700 MWe units. NPPC Unit 1 started operation in 1996, Unit 2 in 2007. There are under construction NPP Cernavoda Unit 3 and 4. Cernavoda NPP Units 3 and 4 will each have 720 MW gross electrical capacities. Radioactive emissions are low under normal conditions of function, but the main radioactive waste products, in gaseous and liquid status, are associated with tritium and carbon-14 emissions that can, in time, accumulate in the trophic chain and finally in humans. Together with colder water, emissions of heavy tritiated water (HTO) arrive in the Danube River. Thermal discharge from two nuclear reactors cooling is dissipated as waste heat in Danube-Black -Sea Channel and Danube River. If during the winter thermal plume is localized to an area of a few km of NPP, the temperature difference between the plume and non-plume areas being about 1.5°C, during summer and fall, is a larger thermal plume up to 5-6 km far along Danube Black Sea Channel, the temperature change being of about 1.0°C.

During summer, the stratified waters confine the warm thermal plume in the upper few meters of the water column. The discharge of the warm water further increases the surface water temperature, which enhances stratification. Variation of surface water temperature in the thermal plume was also analyzed. The strong seasonal difference in the thermal plume is related to vertical mixing of the water column in winter and to stratification in summer. Thermal effluent from the Cernavoda nuclear power plant disperses mainly on the Danube - Black Sea Channel surface around the outlet due to its higher water temperature than the ambient coastal water, and affects the biota around the power plant. Therefore the quantitative prediction of the dispersion of thermal effluent from the power plant is very important for the successful environmental assessment and management associated with the construction of new UNIT 3 and UNIT 4 reactors for power plant, planned to be operational around 2015 year.

8531-80, Session PS

Climatic driving forces in inter-annual variation of global FPAR

Dailiang Peng, Liangyun Liu, Ctr. for Earth Observation and Digital Earth (China); Xiaohua Yang, Space Weather Center, Meteorological and Hydrographic Department (China); Bin Zhou, Hangzhou Normal Univ. (China)

Fraction of Absorbed Photosynthetically Active Radiation (FPAR) characterizes vegetation canopy functioning and its energy absorption capacity, and all factors related to vegetation cover and plant growth change, plant photosynthesis, will contribute to the anomalous variation of FPAR. In this paper, we focus on the analysis of climatic driving forces in inter-annual variation of global FPAR from 1982 to 2006. Advanced Very High Resolution Radiometer (AVHRR) Global Inventory Modeling and Mapping Studies (GIMMS) Normalized Difference Vegetation Index (NDVI) from 1982 to 2006 was used to estimate FPAR at the global scale, by the method of FPAR-Simple Ratio Vegetation Index (SR) relationship. We examined the correlation between inter-annual variation of FPAR and temperature, precipitation derived from Global Historical Climatology Network (GHCN-Monthly), during the periods of March-May (MAM), June-August (JJA), September-November (SON), December-February (DJF) over from 1982 to 2006, to analyze the climate driving effect of FPAR inter-annual change. Results showed that: A similar spatial pattern of the significant correlation between FPAR and temperature is observed during MAM, SON, and DJF with the significance levels of 95% ($P < 0.05$) or less over the world. There are some stations in the regions between 30° N and 60° N and around 30° S in South America, where the annual FPAR variation showed a significant positive correlation with temperature at the 99% or 95% level ($P < 0.01$ or $P < 0.05$) during MAM, SON, and DJF, as well as in Europe during MAM and SON period. A negative correlation for more stations was observed during JJA, especially for the area in Europe and Japan. A slight different correlation pattern was observed between FPAR and precipitation, there were many stations showed a significant positive correlation with precipitation at the level of 99% or 95% ($P < 0.01$ or $P < 0.05$). Such as the tropical rainfall forest of Africa and Amazon during the dry season of JJA and SON; South Africa in MAM and SON; south part of the South America, prairies in North America, some stations in Eurasia and Austria in all periods except DJF. It was found that in South Africa the impact of precipitation on annual FPAR change was stronger in MAM and SON than in JJA and DJF. However, precipitation had a negative correlation with annual FPAR variation in MAM and SON periods in Eurasia. Theoretically, the temperature and precipitation influence time series variation (accurately seasonal variation) of FPAR by heat energy and plant water stress, and then affect plant phenology and growth directly. Whereas, for the inter-annual change of FPAR, except for global climate change, another primary driving force is land cover change, such as deforestation, afforestation, fire disaster, urban expansion, and so on, those are involved in land cover change, and cause the FPAR annual variation. In addition, land cover change could disturb the correlation of FPAR annual variation with climate change.

8531-81, Session PS

One method for HJ-1-A HSI and CCD data fusion

Wencheng Xiong, Ministry of Environmental Protection (China)

The paper tried the data fusion for Hyper Spectral Imager (HSI) and CCD data of HJ-1-A which was developed by China independently, choosing Honghe wetland as the study area.

The traditional fusion methods considered less about the spectral characteristics and the waveform changes of the fusion images of hyperspectral image and high-resolution image. As for waveform distortion of fusion image, Tong Qingxi (2005) proposed a model

of spatial fusion based spectral reversion (SFSR). Gary D R (2000) also proposed a fusion method for the high spectral and high spatial resolution data based on spectral decomposition. These methods not only improved the image spatial resolution, but also maintain the waveform of the original high spectral data as much as possible. However, these methods are not suitable for the fusion of HIS and CCD of HJ-1-A since they are designed for high spatial resolution panchromatic and hyperspectral data. In this paper, we took full advantage of 4-band CCD information and synchronism of HIS and CCD to enhance the spatial resolution of hyperspectral data and minimize the spectral distortion of hyperspectral data.

8531-82, Session PS

Evaluation of Heliosat-? method of deriving solar irradiation from FY-2 images in China

Mingwei Zhang, Jian Liu, Jinlong Fan, China Meteorological Administration (China); Hui Deng, Chinese Academy of Agricultural Sciences (China)

Solar irradiation is a way to characterize the climate of particular region, and used in tourism and agriculture. The Heliosat-Ⅱ method of deriving solar irradiation from FY-2C geostationary satellite images was evaluated for China. The results clear show that the FY-2 data can be used for mapping surface solar irradiation over China. The FY-2C data is useful for where the measured solar irradiation is not available.

8531-83, Session PS

The use of remotely sensed environmental data in the study of asthma disease

Diogo Ayres-Sampaio, Ana C. Teodoro, Alberto Freitas, Neftali Sillero, Univ. do Porto (Portugal)

Asthma is a chronic inflammatory disorder of the airway that affects people of all ages throughout the world. The chronic inflammation is associated with airway hyperresponsiveness that leads to recurrent episodes of wheezing, breathlessness, chest tightness, and coughing, particularly at night or in the early morning. It is estimated that 300 million individuals are affected by asthma, which, when uncontrolled, can place severe limits on daily life and sometimes can be fatal. The expression of this disease can be influenced by some environmental factors such as allergens, air pollution or climate conditions. In previous epidemiological studies, remote sensing data have been used for modelling the spatial and temporal distribution of environment related diseases.

The main objective of this work is to relate some environmental variables, retrieved from satellite observations, with asthma public hospitals admissions in Mainland Portugal, between 2000 and 2010. We considered data from the Moderate Resolution Imaging Spectroradiometer (MODIS) on board NASA's Terra and Aqua satellites to retrieve the environmental variables. Air temperature profile (ATP), total columnar water vapour (TCWV), and surface pressure (SP) data, were extracted from the daily Atmospheric Profile product (MOD07_L2/MYD07_L2). ATP and SP were used to estimate the near-surface air temperature (TAIR), by an interpolating procedure, and TCWV to estimate the near-surface dew point temperature (DP), based on ground-stations measurements. Then the relative humidity (RH) was estimated using these parameters. We also used daily Aerosol Optical Thickness (AOT) data at 470 nm (MOD04_L2/MYD04_L2) to calculate monthly estimations of concentrations of PM10, based on in-situ measurements, the Normalized Difference Vegetation Index (NDVI) product (MOD13A3), and the Burned Area product (MCD45A1).

Several ecological niche models (ENM) were applied (e.g., Maxent, ENFA, and GARP) in order to relate the environmental variables with asthma. According to Sillero (2011), the theory behind these models is based on the ecological niche concept, a central theme in ecology and evolutionary biology understood the niche as a subdivision of the habitat containing the environmental conditions that enable individuals of a species to survive and reproduce, based on broad-scale variables (climate) that are not affected by species density. The selection of the models was constrained by the fact that asthma admissions is a presence-only variable. In addition, we followed other statistical approaches, often used with public health data. Methods like the chi-square test, analysis of variance (ANOVA) or logistic regression were used, considering the sex and the age-group of the asthma patients (defined based on previous works).

Our results suggests that NDVI and PM10 have a strong relation with Asthma. An increase in NDVI values is accompanied by higher concentrations of pollens in the air, because pollens are plant's form of reproduction. This leads to an increase in the expression of asthma (e.g., in Spring).

Sillero, N. (2011). What does ecological modelling model? A proposed classification of ecological niche models based on their underlying methods. Ecological Modelling, Vol. 222, 1343-1346.

8531-84, Session PS

Millimeter-wave and laser system for environmental monitoring

Yaroslav V. Savenko, Fedir Repa, National Technical Univ. of Ukraine (Ukraine)

Millimeter wave and laser system for environmental monitoring investigates properties of biological objects of environment in millimeter and optical range both in active and passive mode of scanning. Using these data it is possible to provide an environment monitoring in real-time. Combination of millimeter range measuring system and optical range measuring system allows produce more informative data about biological object and provide more effective scanning program. Effectiveness of monitoring system and monitoring process are provided by high informative data about object and effective scanning program, which are provided by combination of millimeter and optical ranges specialties. It is also possible to use the monitoring system for medical, ecological and agricultural applications as well. In addition to the monitoring it is possible to provide treatment technologies by millimeter and laser radiation for correction of own properties of biological objects for medical, ecological and agricultural purposes. Creating of millimeter wave and laser system for environmental monitoring had been divided on the following stages: creating of model for scanning system; development of millimeter and optical range measuring system;; simulation and experimental researches of millimeter and optical scanning system; investigation of requirements for special type monitoring system and development the program for real-time monitoring a special kind of object, for example: river, ocean and other water environment, crops and other agricultures. Investigation of real-time monitoring system in millimeter and optical ranges consists of modeling of object for monitoring, modeling of monitoring process, computer researches, development of monitoring system and possible application.

8531-85, Session PS

Remote monitoring of road conditions during winter with NIR filter wheel system and a microwave radar

Sumanth Kumar Pavuluri, Univ. of Glasgow (United Kingdom) and Heriot -Watt Univ. (United Kingdom); Alistair Gorman, Andy Harvey, Univ. of Glasgow (United Kingdom); Colin Irvine, Findlay Irvine Ltd. (United Kingdom)

Automated road-surface condition monitoring is important for optimal maintenance of safe operating conditions. Simple spectral reflectivity measurements in the near infrared (NIR) (1.1-1.7μm wavelength) and texture measurements based on back reflection of a laser beam are able to provide characterisation of cover on road surfaces by water, frost, snow and ice. A near-infrared filter wheel system has been developed for remote sensing and monitoring of road surfaces. It is anticipated that apart from the above road-cover conditions the system can be able to classify the different ice conditions such as white ice, black ice and slush ice.

The system automatically records the spectra associated with the backscattering of light from the road surface. The differentiation of the spectra and thereby the differentiation of road cover conditions is implemented using a spectral angle mapping. Road-surface temperature is monitored by the use of an infrared pyrometer and the temperature is used as a parameter in the classifying algorithm. In addition, the system can log automatically the snapshots of the road surface along with the temperature of the road surface. Two sets of data are recorded in order to verify the applicability of the system in order to accurately classify the above road cover condition. For the first set, samples are prepared of ice on concrete and tarmac slabs with the thickness of ice in the range of 1mm to 10 mm. Spectra associated with melting of these samples is recorded and then

classified using the spectral angle mapper. The second set of data is recorded outdoors with the spectra obtained from a piece of Tarmac for a period of 3 months. The data is than analysed and classified again with the Spectral angle mapper. The results obtained with these two sets of data will be presented at the conference.

Radar backscatter varies with ice types as a result of differences in both internal properties (salinity and subsequent dielectric properties and density etc) and surface properties (roughness, snow cover, distribution of water etc). Salinity of ice and ice thickness will be investigated with frequency modulated continuous wave (FMCW) radar in the C band using the microwave reflectometry principle. The radar system will be at a distance of 5 meters from the road surface. The FMCW system is configured to identify the desired reflected measurement signal by identifying the first and second states and their different durations and intensities in the desired reflected measurement signal. This acquired data outputted is interfaced to a numerical analysis software package and is plotted and processed. The results obtained with the two sets of data using the FMCW radar as outlined above will be presented.

8531-86, Session PS

Monitoring for “Agri-Environmental Measures Effectiveness”, case study: Guadalquivir, Spain

Hakki Emrah Erdogan, European Commission Joint Research Ctr. (Italy)

The policies integration process between agriculture and environment in Europe fosters the development of agricultural practices that preserve the environment and safeguard the countryside.Various EU directives and programmes, such as the Rural Development Programme, the Water Framework Directive and others, set strategic guidelines for the Common Monitoring and Evaluation Framework by defining objectives and indicators to evaluate the progress and achievement in environmental protection measures. The AgriEnvironment Core Information Service (AgriEnv CIS) contribute to the improvement of the timely and accurate monitoring of agricultural land use state and its changes at European, national and regional levels by providing common methodologies and indicators to monitor the impact of the programmes and their measures. This study describes the background, the materials and the methods use as well as the definition, context, policy drivers, approaches and preliminary results for the elaboration of an agri-environmental indicator named “agri-environmental measures effectiveness” in the framework of the GMES-Geoland2 project.

8531-87, Session PS

Implementation of a General Linear Model using LiDAR derived explanatory variables: a case study in Scotland

Silvia S. Flaherty, Univ. of Edinburgh (United Kingdom); Peter W. W. Lurz, Consultant (Germany); Genevieve Patenaude, Univ. of Edinburgh (United Kingdom)

The importance of forest structural parameters for red squirrels habitat mapping was investigated in this study. A General Linear Model (GLM) was used to relate forest structural parameters to red squirrel feeding behaviour in two forests of Scotland: Aberfoyle and Abernethy. Results show that mean canopy closure, mean tree height and total number of trees are significant predictors of number of cones stripped by squirrels at the plot level and explain 43% of the variance in number of cones, which is assumed to be an indicator of habitat preferences by red squirrel. However, this analysis is restricted to a few sample plots due to limited availability of structural data along with cost-efficient data collection methods. The use of remote sensing -in particular Light Detection and Ranging (LiDAR) - enables cost efficient forest structure assessment at large scales and can be used to retrieve these three variables that relate to red squirrel feeding behaviour: canopy cover, tree height and number of trees. The objectives of this study are 1) implementing the GLM using LiDAR derived explanatory variables in order to estimate habitat quality over the whole study area; 2) classify the results in order to generate a map with three levels of habitat suitability for red squirrels: low, medium and height 3) assess the usefulness of LiDAR remote sensing for habitat management for red squirrels.

8531-88, Session PS

Using spectroscopy and satellite imagery to assess the total iron content of soils in the Judean Desert (Israel)

Thomas Jarmer, University of Osnabrück (Germany)

Especially the semi-arid ecosystems provide important land resources for adapted land use and livestock farming. But the pressure on arid and semi-arid areas resulting from climatic variability, climate change, demands of increasing stocking rates and population development was probably never as high as nowadays. In semi-arid and arid environments the total iron content in soils developed on carbonatic bedrock material is a major soil development indicator. High total iron concentrations often indicate more developed soils while low contents point to weakly developed or degraded soils. Since the spatial distribution of soil total iron is a valuable indicator for monitoring soil condition status, it is necessary to develop a remote sensing based approach for spectral determination of total iron content.

Consequently, the aim of this study is the spatial assessment of the total iron content of soils. Soil samples have been collected and analysed for total iron along a hypsometric rainfall gradient in the Judean Desert (Israel) covering semi-arid, arid and hyper-arid regions. Mean annual rainfall in the investigated area decreases on a distance of only 33 km from 620 mm in the west to about 100 mm in the east. All test sites are located on limestone bedrock and soils mainly vary according to the amount of rainfall.

Additional to soil chemical laboratory analysis the spectral reflectance of the soil samples has been measured in the range of 0.35 and 2.5 µm. These reflectance measurements have been convex-hull-normalised to derive individual absorption features and the continuous spectra were used to calculate colour parameters according to the Commission Internationale de l´Eclairage (CIE) colour scheme. Subsequently, derived parameters of the convex hull normalised iron absorption band in the near infrared around 0.9 µm and the CIE-chromaticity coordinates were tested for their significance to predict the total iron content. Accordingly, a method for spectral detection of total iron content was generated based on statistical analysis which allows the prediction of the soils total iron content of the investigated soils with a cross-validated r? above 0.8.

Spatial analysis of the total iron content of soils based on low spectral resolution Landsat imagery required a modification of the established model. Since CIE-chromaticity coordinates were found to be well suitable parameters for predicting the total iron content of soils under laboratory conditions, the reflectance values of the Landsat bands were transformed into CIE-chromaticity coordinates. Subsequently, the CIE-based model approach was adapted to a Landsat image with low vegetation cover from July 1998 in order to predict spatial distribution of the soils total iron content for the investigated region.

Concentrations obtained from the satellite image are in accordance with the concentration range of the chemical analysis. The predicted soil total iron concentrations reflect the geographic conditions and show a dependence on the annual rainfall amount. A general trend to decreasing concentrations of total iron can be stated with increasing aridity. Furthermore, local conditions are well reflected by the predicted concentrations. In addition, the limitations of the introduced approach will be discussed.

8531-89, Session PS

A validation of the GLASS albedo product with tower-based pyranometer measurements and Landsat-TM images

Lizhao Wang, Beijing Normal Univ. (China) and State Key Lab. of Remote Sensing Science (China); Qiang Liu, State Key Lab. of Remote Sensing Science (China) and Beijing Normal Univ. (China) and Institute of Remote Sensing Applications (China)

Land surface albedo is a key parameter in energy balance and global change studies. Recently, Chinese scientists have generated the GLASS (Global Land Surface Satellite) remote sensing data products which are long time series of global land surface parameters including leaf area index, broadband albedo, broadband emissivity, incident shortwave radiation, and photosynthetically active radiation. The GLASS albedo product provides daily black-sky and white-sky albedo at shortwave region in 1-kilometer resolution from 2000 to 2010. The GLASS albedo product is retrieved from MODIS directional reflectance

data with the Angular Bin (AB) algorithm, which is an empirical method based on a training BRDF database. It is able to retrieve the albedo only relying on a single observation. It is potential to reflect the rapid changes of land surface. But the quality of this product has not yet been systematically evaluated, and a global analysis across different continents is needed. In order to validate the product, globally distributed FLUXNET measurements, corresponding TM images and GLASS albedo images are compared in this work.

Albedo can be computed as the ratio of downward and upward global radiation measured by the pyranometer on the flux tower. To reduce the random noise, the ground-truth albedo is calculated as the hourly average of albedo measurements around the local noon.

Several sites are selected from FLUXNET as the validation sites. Table 1 lists the name, location and land cover type of these sites. Landsat TM/ETM+ images of these sites within the corresponding periods have been obtained from NASA/USGS data portal (http://glovis.usgs.gov). TM image has been processed for radiant calibration, atmosphere correction and fine geometric calibration. The albedo of TM images is retrieved by a direct-estimation algorithm named angular bin (AB) which is also the main inversion algorithm of GLASS albedo (Liu et al., 2011;Qu et al., 2012).

¡¡¡¡ The time-series GLASS albedos of the pixels nearing the above sites are extracted for the validation. The clear-sky diffuse ratio at local noon is necessary for the computing of actual albedo. The diffuse ratio r_d is calculated from the following formula,

r_d=0.122+0.85e^(-4.8?Ì_0)

¡¡¡¡ where ?Ì_0 is the cosine of the zenith angle (Stokes and Schwartz, 1994). The actual albedo can be expressed in the form of (Lucht et al., 2002),

?Á= ?Á_bs*(1-r_d)+ ?Á_ws*r_d

¡¡¡¡ where ?Á is the actual albedo, ?Á_bs and ?Á_ws is black-sky albedo and white-sky albedo respectively. The TM actual albedo is calculated in the same way.

In this study, there are two procedures, which show the accuracy of GLASS albedo at different scales. The first is comparing the ground-truth albedo and the corresponding TM albedo directly. Then, the average TM albedo of 33¡Á33 pixels with the FLUXNET sites as the center is compared with the GLASS albedo. Secondly, considering the possibility of misregistration, the albedo of these two satellites at coarser scale was compared, that is, the average GLASS albedo of an area containing 3¡Á3 pixels was compared with the corresponding average TM albedo.

In order to acknowledge the accuracy of GLASS albedo with various land cover types, 8 sites distributed across four continents were selected in the validation. Until now, all the necessary data has been collected and in process. The validation at 3 sites of them has been done, which shows that the absolute error between surface observations and TM albedo is less than 5%, as well as that between TM upscaled albedo and GLASS albedo.

8531-91, Session PS

Mapping salinity stress in sugarcane fields with hyperspecteral satellite imagery

Saeid Hamzeh, Shahid Chamran Univ. of Ahvaz (Iran, Islamic Republic of); Abd Ali Naseri, shahid chamran university of ahvaz (Iran, Islamic Republic of); Seyed Kazem Alavi Panah, University of Tehran (Iran, Islamic Republic of); Barat Mojaradi, Iran Univ. of Science and Technology (Iran, Islamic Republic of); Harm Bartholomeus, Martin Herold, wageningen university (Netherlands)

With an area of more than 70,000 ha sugarcane farming and its by-products are the major agricultural activities in the Khuzestan province, in the southwest of Iran. Soil salinity is the main factor negatively affecting the sugarcane yield in this area. Therefore, mapping and identification of soil salinity is the most important issue to improve management of large scale crop production in this area. Besides labour intensive fieldwork, remote sensing is the most suitable technique to assess soil salinity for larger areas. This study was carried to investigate the capability of Hyperion spaceborne hyperspecteral data for mapping the salinity stress in the sugarcane fields and determine the best method to classify soil salinity into 3 classes (low, moderate and high salinity). For this purpose the capability of different classification methods like support Vector Machine (SVM), Spectral Angle Mapper (SAM), Binary Encoding (BE), Minimum Distance (MD) and Maximum Likelihood (ML) in conjunction with the different band combinations (all bands, principle component analysis (PCA), Vegetation Indices) as an input data was performed. Results indicated that best method for classification is SVM classifier when we use all bands or PCA(1-5) as an input data for classification with an overall accuracy and kappa coefficient of 78.7% and 0.68 respectively.

8531-92, Session PS

Using hyperspectral remote sensing data for the assessment of topsoil organic carbon from agricultural soils

Bastian Siegmann, Thomas Jarmer, Univ. Osnabrück (Germany); Thomas Selige, Technische Univ. München (Germany); Holger Lilienthal, Nicole Richter, Julius Kühn-Institut (Germany); Bernhard Höfle, Ruprecht-Karls-Univ. Heidelberg (Germany)

The assessment and mapping of soil organic carbon is very important in order to develop strategies to mitigate global warming. Soil can store more than twice as much carbon compared to vegetation or atmosphere. So improving carbon storage as soil organic matter by the adoption of land-use and land management practices is an option to reduce the carbon dioxide content in the atmosphere.

Spectral reflectance of soils is affected by varying combinations of mineral components, organic matter and soil moisture. Many studies demonstrated the relationship between soil properties, like grain size distribution, soil moisture, iron oxides, carbonate content and organic matter and its resulting spectral reflectance. Most of the studies were performed under controlled laboratory conditions to derive soil properties and the corresponding spectral data. Applications under field conditions are limited to relatively small test sites. On the contrary airborne and spaceborne hyperspectral imagery data have a great potential to derive soil parameters at a larger scale. In this study the potential of hyperspectral imagery for the spatial assessment of soil organic carbon from agricultural soils is investigated.

During a field campaign in May 2011 soil samples were collected on an agricultural field northwest of Koethen (Saxony-Anhalt, Germany) and the organic carbon content of the samples was determined in laboratory afterwards. At the same time image data of the test site was acquired by the hyperspectral airborne scanner AISA-DUAL (450-2500 nm). For parameter prediction, an empirical model based on partial least squares (PLS) regression was developed from AISA-DUAL image spectra extracted at the geographic location of the soil samples and the analytical laboratory results. Subsequently, the PLSR-model has been applied to the AISA-DUAL image data to cover the whole field.

The derived soil organic carbon concentrations obtained from the AISA-DUAL data are consistent to the chemical analysis from laboratory. The developed PLSR-model has a high coefficient of determination (r2cv=0.75) and the predicted soil organic carbon values reflect the spatial distribution of the investigated field. The results clearly indicate the high potential of the presented method to perform a fast and reliable spatial assessment of soil organic carbon from hyperspectral imagery. The developed screening tool is a suitable alternative to chemical analyses in laboratory, which are commonly cost- and time intensive. Furthermore, increasing benefit is expected with the availability of new hyperspectral remote sensing satellites, like the German hyperspectral System EnMAP, which will be launched in 2015.

8531-93, Session PS

Integration of optical and SAR remotely sensed data for monitoring wildfires in Mediterranean forests (stand-by oral presentation)

Ramin Azar, Politecnico di Milano (Italy) and Istituto per il Rilevamento Elettromagnetico dell'Ambiente (France); Daniela Stroppiana, Mirco Boschetti, Antonio Pepe, Luca Paglia, Riccardo Lanari, Pietro Alessandro Brivio, Istituto per il Rilevamento Elettromagnetico dell'Ambiente (Italy)

Large wildfires in forests of southern European countries such as Portugal, Spain, Greece, France and Italy are one key ecological disturbance of the Mediterranean environment. The assessment of

the burned area perimeters is the first and most important parameter for wildfire monitoring and the basis for post-fire estimates of burn severity and vegetation re-growth. Optical data have been largely used for burned area mapping and literature provides an extensive reference for the typical spectral signal of burns and the methodologies applied to extract burn perimeters. However, due to cloud coverage and weather conditions it is not always possible to have enough coverage of forested areas by optical remote sensing. Moreover, unburned targets, such as cloud and topographic shadows and water, might have a spectral signal similar to burned areas and can be misclassified as burns. Due to the limitations of optical remote sensing, SAR data has gained interested by scientists for monitoring natural resources including wildfires. SAR data due to capability of penetrating clouds and evaluating the moisture of scene by different backscatters could be used for wildfire imagery. In particular, medium resolution Landsat TM/ETM+ images are suitable for systematic monitoring of burns in the Mediterranean ecosystem since, with the exception of very severe events, burned areas are of medium/small size. Our study focuses on a study site in southern Italy (Salento region) where Landsat TM/ETM+ images have been downloaded from the USGS Glovis web site (http://glovis.usgs.gov/). These images are provided as level 1T corrected (systematic radiometric and geometric accuracy based on ground control points and Digital Elevation Model (DEM)). We applied post processing consisting in calibration of Digital Numbers (DN) to at-sensor radiance and atmospheric correction using the 6S code. Besides optical data, SAR acquisitions have been collected over the study area and processed to extract backscatter signals. SAR products have subsequently been properly geocoded and used for monitoring post-fire areas. A method for mapping wildfires based on Fuzzy Logic and vegetation indices has been developed; it integrates positive and negative evidence of burn derived from both optical and radar data for classifying burned and unburned areas. The method had been previously tested with Landsat TM/ETM+ images for mapping burned areas in southern Europe and gave satisfactory results. In this work we integrate radar data into this methodological framework to provide additional information on the condition of the surface (burned/unburned) aiming at exploiting the synergy between different remote sensing techniques. Hence, burned area maps have been produced by multisource classifications of SAR and optical remote sensing data; the results have been verified against perimeters derived by visual interpretation and discussed also as a function of the land cover type as derived from the CORINE Land Cover 2000 map. Results show that radar data can contribute to overcome limitations of optical data although further testing is foreseen in the future for evaluating the robustness of the proposed approach with respect to different environmental conditions.

8531-95, Session PS

Assessment of soil degradation in the northern part of the Nile Delta, Egypt using remote sensing and GIS techniques

Alaa H. El Nahry, National Authority for Remote Sensing and Space Sciences (Egypt)

The present work aims at monitoring soil degradation process within the last two decades in the northern part of the Nile Delta. The investigated area lies between longitudes 31° 00- & 31° 15- E and latitudes 31° 00’ & 31° 37’ N., covering an area of about 161760 feddans. Detecting soil degradation and recognizing its various types is a necessity to take the practical measures for combating it as well as conserving and keeping the agricultural soil healthy. Land degradation was assessed by adopting new approach through the integration of GLASOD/FAO approach and Remote Sensing / GIS techniques. The main types of human induced soil degradation that observed in the studied area are salinity, alkalinity (sodicity), compaction and water logging. On the other hand water erosion because of sea rise is assessed. The obtained data showed that, areas that were affected by compaction increment have been spatially enlarged by 40.9 % and those affected by compaction decrease have been spatially reduced by 22.6 % of the total area ,meanwhile areas that have been unchanged were estimated by 36.5% of the total area. The areas that were affected by water logging increase have been spatially enlarged by 52.2 % and those affected by water logging decrease have been spatially reduced by 10.1 % of the total area, meanwhile the areas which have been unchanged were represented by 37.7 % of the total area. Areas that were affected by salinity increase have been spatially enlarged by 31.4 % of the total area and those affected by salinity decrease have been reduced by 43.3 % of the total area. An area represented by 25.2 % of the total area has been unchanged. Alkalinization (sodicity) was expressed by the exchangeable sodium percentage (ESP).Areas that were affected by sodicity increase have been spatially enlarged by 33.7 %, meanwhile those affected by sodicity decrease have been spatially reduced by 33.6 % of the total area. An area represented by 32.6 % of the total area has been unchanged. Multi-dates satellite data from Landsat TM & ETM+ images dated 1983 and 2003 were used to detect the changes of shoreline during the last two decades. The obtained results showed that, the eroded areas were determined by 547.4 feddans , meanwhile the accreted areas were detected by 476.5 feddans during the twenty years period.

Conference 8532: Remote Sensing of the Ocean, Sea Ice, Coastal Waters, and Large Water Regions 2012

Wednesday - Thursday 26–27 September 2012 • Part of Proceedings of SPIE Vol. 8532 Remote Sensing of the Ocean, Sea Ice, Coastal Waters, and Large Water Regions 2012

8532-1, Session 1

SYSIPHE: the new-generation airborne remote sensing system *(Invited Paper)*

Laurent Rousset-Rouviere, Christophe Coudrain, Sophie Fabre, Nicolas Guerineau, Jean-Paul Bruyant, ONERA (France); Ivar Baarstad, Trond Løke, Andrei Fridman, Soeren Blaaberg, Norsk Elektro Optikk AS (Norway)

The SYSIPHE system is the state of the art airborne hyperspectral imaging system developed in European cooperation.

With a unique wide spectral range and a fine spatial resolution, its aim is to validate and quantify the information potential of hyperspectral imaging in military, security and environment applications.

The first section of the paper recalls the objectives of the project. The second one describes the sensors, their implementation onboard the platform and the data processing chain. The last section gives illustrations on the work in progress.

8532-3, Session 1

CARVE-FTS Observations of Arctic CO2, CH4, and CO: overview of the instrument

Fabien Dupont, François Tanguay, Gaetan P. Perron, Manyuan Li, ABB Analytical Measurement (Canada); Charles E. Miller, Steven J. Dinardo, Jet Propulsion Lab. (United States)

CARVE-FTS is a near-IR Fourier-Transform Spectrometer (FTS) used for the Carbon in Arctic Reservoirs Vulnerability Experiment (CARVE). CARVE is a 5-year mission of intensive aircraft campaigns in the Alaskan Arctic selected as part of NASA's Earth Ventures program (EV-1). The CARVE-FTS has been designed, manufactured and tested by ABB Inc. The objective of the CARVE-FTS is to provide integrated column measurements of carbon dioxide (CO2), methane (CH4), and carbon monoxide (CO). The system is inspired from the TSUKUBA-FTS built and delivered by ABB for the Japanese Aerospace Exploration Agency (JAXA). JAXA uses the instrument for preparation, calibration and validation within the space-based observations GOSAT program. The spectral coverage made by CARVE-FTS also overlaps OCO-2 bands. The instrument thus provides opportunities for synergy among airborne remote sensing community.

The instrument is a Michelson based FTS with three spectral bands. Field of view is about 9°.That corresponds to a footprint of 157 feet at an altitude of 1,000 feet. The light modulator is a Michelson single pass type interferometer with high aperture and high spectral resolution. It provides infrared spectra from 12,900 cm-1 to 13,200 cm-1, from 5,800 cm-1 to 6,400 cm-1, and from 4,200 cm-1 to 4,900 cm-1. This instrument is also able to measure the scene flux with S and P polarization simultaneously using monopixel detectors. The instrument thus has six channels. The instrument is fixed to a damping platform and is installed in an aircraft. It delivers continuous data for flight campaign over Alaskan Arctic. A visible camera provides synchronized images of the scene. The instrument weight is about 300 lbs for an envelope that is less than 10 cubic feet. CARVE-FTS data is combined to two other instruments part of the CARVE mission to deliver accurate total atmospheric columns of CO2, CH4, and CO.

Critical features of the instrument for columns retrieval are the Signal to Noise Ratio (SNR), and Instrument Line Shape (ILS). The instrument has been optimized to deliver high SNR and narrow symmetrical ILS. High optical aperture combined with fine tuned electronics for each detector lead to optimized performances in each band. SNR higher than 100 is reached for each band and we measured ILS full width half maximum as low as 0.26 cm-1 at 6,566 cm-1. We present the instrument design, its specification and test results obtained in our laboratory at ABB.

8532-4, Session 1

Development of advanced miniaturized Dyson imaging spectrometer for Mars rover and small aircrafts

Shen-En Qian, Michael Maszkiewicz, Allan Hollinger, Canadian Space Agency (Canada); Eric Martin, Canadia Space Agency (Canada); Jean-Pierre Ardouin, Alexander Jouan, Defence Research and Development Canada, Valcartier (Canada)

Under its Exploration Core Program, the Canadian Space Agency (CSA) has funded its industry and completed a concept study for Hyperspectral and Luminescence Observer (HALO). The study was for possible inclusion on the proposed ESA-NASA-led Mars Sample Return Network (MSR-NET). The HALO consists of two instruments: an orbital imaging spectrometer and a landed fluorescence spectrometer. Both of them target at understanding geological process on Mars and the MSR-NET. The HALO spectrometer concept builds on lessons learned from previous Mars mission and research project conducted as part of a previous concept study - CHIMERA (Canadian Hyperspectral Imager for Mars Exploration and Resource Assessment). The orbital imaging spectrometer is based on CSA's heritage from imaging spectrometer design for Hyperspectral Environment and Resource Observer (HERO) mission.

A unique Dyson optical design of the spectrometer was selected after the trade-off study. This design consists of a single Dyson block, one concave grating, one slit and one dichroic beam splitter. The spectral range is split into two by the dichroic beam splitter, which is attached to the exit surface of the Dyson block, then focuses on the separated detectors. The VNIR (from 380 nm to 1250 nm) works in -2nd order, while SWIR (from 940 nm to 2510 nm) works in -1st order. The preliminary results show that the requirements have been achieved. The detailed results of the optical design of the Dyson spectrometer will be described.

Defence Research and Development Canada (DRDC) is also interested in compact hyperspectral imaging sensor operating in the solar reflective spectral region from 0.4 to 2.5 µm to be deployed on a small aircraft. The CSA and DRDC recently teamed up to jointly design, build and test an advanced airborne miniaturized imaging spectrometers that meet both the CSA and DRDC needs. For this work, a Dyson design was selected due to its compactness, high optical output and low distortion and this new project will benefit from the HALO concept study discussed in this paper.

8532-9, Session 1

On the use of SAR interferometry to aid navigation of UAV

Davide O. Nitti, GAP S.r.l. (Italy); Fabio Bovenga, Research National Council of Italy (Italy); Alberto Morea, Univ. degli Studi di Bari (Italy); Fabio M. Rana, Consiglio Nazionale delle Ricerche (Italy); Luciano Guerriero, GAP S.r.l. (Italy); Mario Greco, Gianpaolo Pinelli, IDS Ingegneria Dei Sistemi (Italy)

This study is devoted to explore the potentials of SAR Interferometry (InSAR) to aid Unmanned Aerial Vehicles (UAV) navigation. The basic idea is to infer both position and attitude of an aerial platform by inspecting the InSAR phase derived by a real time SAR interferometer mounted onboard the platform.

In the assumption of bistatic acquisitions (absence of both temporal decorrelation and atmospheric contribution), high resolution data and short wavelengths (no volume decorrelation), the interferometric coherence is expected to be quite high except for the noise related to the processing (autofocusing and coregistration) as well as to the thermal noise of the device. Different configurations were explored and, in general, very favorable conditions for successfully phase unwrapping are expected. Also the geometrical decorrelation is expected to be extremely low as usual in case of real time airborne interferometry except for areas affected by strong SAR distortions. This allows us to derive from InSAR acquisitions an InSAR phase field

which is representative of the terrain elevation. A preliminary concept schema of the InSAR-based georeferencing procedure can be designed by taking advantage from these considerations.

By using both approximated position and attitude values of the platform as well as a reference digital terrain model (DTM) from a database available onboard, it is possible to generate a synthetic InSAR phase model to be compared w.r.t. that derived by SAR observations. The geometrical transformation needed to match these two terrain models depends on the difference between position and attitude values derived by the instruments available on board and their actual values. Hence, this matching provides a feedback to be used for adjusting position and attitude.

In order to assess the reliability of the proposed approach, we evaluated the interferometric sensitivity to changes in position and attitude. This analysis defines the limits of applicability of the InSAR-based approach and provides indications and requirements on geometric and radiometric parameters.

Concerning the sensitivity of the interferometric phase w.r.t. changes in position and attitude of the aircraft, our analysis pointed out that it is poorly correlated with the terrain height. This means that no fringe pattern is expected by beating the actual and the simulated interferometric phase fields. So, the phase variation doesn't seem to be a useful figure to correct position and attitude. In general, its sensitivity to position and attitude increases as aircraft altitude, baseline and look values increase.

On the contrary, the exploration of SAR coordinates variation due to changes in position and attitude of the aircraft appears to be more effective. In this case, the sensitivity increases with aircraft altitude while its behavior w.r.t. the look angle is quite variable. This result suggests that, for the matching algorithm, it seems more promising to explore the difference in range and azimuth location between the real and simulated interferometric phase profiles, instead of looking at the phase differences.

8532-2, Session 2

Remote sensing spectrometric system for emergency response onboard of unmanned helicopter

Doyno Petkov, Hristo Nikolov, Denitsa Borisova, Space Research and Technology Institute (Bulgaria)

The goal of the project is the working out of a multichannel spectrometric system in the visible and near infrared bands of the electromagnetic spectrum for remote sensing with the following purposes: recognition of main land covers (soils, natural and agricultural vegetation, water areas); state assessment of the studied objects.

The multichannel spectrometric system is designed to measure the reflected by ground objects solar radiation in the visible and near infrared range of the electromagnetic spectrum on board of a remotely-controlled airborne platform (helicopter). The measurements will be performed in a main working regime - nadir, helicopter velocity - up to 20 km/h, height - up to 1000 m (optimal 200 m), flight duration - up to 30 min.

Components of the system are: multichannel spectrometer; digital camera (optional); data control on-board system; on-board power supply device; fitting elements for installation on board; ground-based computing system for storage and processing of spectrometric data.

Technical specifications of the spectrometric system are: spectral VIS-NIR range (450-900) nm; number of spectral channels 128-64; channel location even; spectral resolution (3-10) nm; spatial resolution (1-25) m2; CCD line elements 2048; dynamic range of the system 4 x 104 and per scan 2000:1; exposure time (3-60) ms; measurement flight duration (10-30) min.

Thematic selection of the spectral bands as well as number, width and location of the spectral channels is oriented to the vegetation and soil reflected spectral characteristics. The reflected by vegetation solar radiation has a specific spectral distribution. In the visible (VIS) spectral band (400-710) nm vegetation optical properties depend mainly on plant pigment content and concentration. A reflectance maximum is observed at 550 nm, i.e. in the green region where the absorption of the incident radiation is relatively low. Plant senescence or stress factors inhibiting chlorophyll synthesis or causing chlorophyll destruction decrease the amount of the absorbed solar radiation in the red spectral band at 670 nm where the zone of vegetation minimum reflection is located. This leads to higher reflectance values in this spectral band. In the near infrared region (NIR) of the spectrum (710-1300) nm the vegetation reflectance ability increases, a steep slope being observed in the wavelength range (700-760) nm. Reflectance variation in the NIR band depends on plant structural parameters and can be used for vegetation classification and state assessment. The soils have a reflectance increase in the VIS-NIR spectral range. The reflectance behavior is a function of various soil parameters such as mineral composition, organic matter content, surface moisture and roughness.

Main tasks are investigation of the relationships between the reflectance and biophysical features of the studied objects; development and validation of spectral-biophysical models for estimation of land cover parameters; soil state assessment - type, moisture content, surface texture; vegetation state assessment - type, phonological and growth parameters, detection of stress situations and emergency response.

8532-5, Session 2

In with the new, out with the old? auto-extraction for remote sensing archaeology *(Invited Paper)*

Dave C Cowley, RCAHMS (United Kingdom)

This paper explores the implications for aerial photographic interpretation and the use of airborne laser scanning data of changing practice stimulated by innovations in technology and software. The impact on interpretative processes of a rapid and universal adoption of digital photography and a GIS-based working environmental are examined, deconstructing aspects of practice and discussing potentially unintended consequences of change. The challenges of developing new approaches to complex and extensive datasets is discussed with specific reference to airborne laser scanning, identifying the need for reflexive analysis of approaches and the important synergies between auto-extraction techniques and knowledge-based experience.

8532-6, Session 2

Change detection of trees in urban areas using multi-temporal airborne lidar point clouds

Wen Xiao, Faculty of Geo-Information Science and Earth Observation (ITC), University of Twente (Netherlands) and IGN, MATIS; Université Paris-Est (France); Sudan Xu, Sander Oude Elberink, George Vosselman, Faculty of Geo-Information Science and Earth Observation (ITC), University of Twente (Netherlands)

Changes in vegetation are of great interest since they play crucial roles in ecosystem monitoring, where remotely-sensed data has been proven extremely profitable. They have mainly been detected by conventional remote sensing technologies. As a relatively new technology, light detection and ranging (lidar) provides a promising way of detecting changes of vegetation in three dimensions (3D). Vegetation changes in forestry at plot level, such as biomass or average height, have been studied. However, no research has used lidar to detect tree changes in urban areas. This study aims at the detection of changes in trees in 3D with a high level of automation.

Three datasets covering a part of Rotterdam, The Netherlands, are available. Two were obtained in 2008 (March and November) and the third in April 2010. Point density of the data in March of 2008 is around 10-15 points per square meter (pts/m2), while the other two are about 30-50 pts/m2.

The datasets were already classified into several classes including high vegetation (trees). This study focused on semi-automatically detecting and quantifying the changes in trees. Because lidar points are unstructured, a connected components algorithm was applied first to group the points of a tree together. Since a few non-tree points were misclassified, the attributes of components, e.g., component size, height span, minimum height, reflectance, were utilised to differentiate tree components from others. Points from neighbouring trees might be clustered together, so a point based local maxima algorithm was implemented to distinguish single tree from multiple tree components. After that, parameters of trees were derived through two independent ways: a point based method using 3D alpha shapes and convex hulls; and a model based method which fits a Pollock

tree model to the data. Parameters, i.e., area and volume, of single tree components were derived from both the Pollock model and the convex hull. Parameters of multiple tree components were computed through 3D alpha shapes, which were also used to thin and unify the datasets. Then the changes were detected by comparing the parameters of corresponding tree components which were matched by a tree to tree matching algorithm using the overlapping of bounding boxes and point to point distances.

The results were visualized and statistically analysed. The correctness and completeness of the removal of non-tree components was assessed resulting in overall quality of 94%. The difference of parameters and the difference of changes derived from point based and model based methods were both lower than 10%. The comparison of these two methods illustrates the consistency and stability of the parameters. The detected changes show the potential to monitor the growth and pruning of trees.

8532-7, Session 2

Airborne remote sensing in littoral zones for subsurface feature detection

Charles R. Bostater Jr., Florida Institute of Technology (United States)

Surface and subsurface feature detection in littoral zones and near coastal waters is described. The purpose of this paper is to describe an approach for integrating multiple sensing systems for low altitude imaging for subsurface feature detection in coastal waters and littoral zones. The sensor acquisition and imaging processes include capturing real time data streams from multiple sensors using (a) failsafe data storage techniques, followed by (2) post processing of pushbroom imagery using IMU and DGPS data streams using Kalman filtering and smoothing algorithms in order to take into account the yaw, pitch and roll dominant platform motions. Steps involved with georeferencing imagery is discussed as well an examples of georeferenced image mosaics of image types, including synthetic imagery derived using resolution enhancement data fusion techniques. The system of instruments includes 5 different imaging systems, 2 different point measuring spectrographs for instrument cross calibration, IMU and DGPS sensors. Upwelling and downwelling radiance and irradiance sensors are utilized as well. The calibrations of the systems are described which include the use of spectral calibration spheres, calibration targets, spectral line sources, and film scanning calibration targets. The final imagery products are described in term their utility as well as the limitations of the data and sensor systems.

8532-8, Session 2

Architecture and methods for UAV-based heterogeneous sensor network applications

Pedro Antonio, TEKEVER EMEA (Portugal); Davide Caputo, Alessandro Gandelli, Francesco Grimaccia, Marco Mussetta, Politecnico di Milano (Italy)

Nowadays wireless sensor netwoks (WSN) employ miniaturized devices which integrate sensing, processing, and communication capabilities.

In this paper an innovative mobile platform for heterogeneous sensor networks is presented, combined with adaptive methods to optimize the communication architecture for novel potential applications in multimedia and entertainment.

In fact, in the near future, WSN data collection could be performed by UAV platforms which can be a sink for ground sensors layer, acting essentially as a mobile gateway.

In order to maximize the system performances and the network lifespan, the authors propose a recently developed hybrid technique based on evolutionary algorithms.

This procedure is here applied to optimize the communication energy consumption in WSN by selecting the optimal multi-hop routing schemes, with a suitable hybridization of different routing criteria.

The proposed approach can be potentially extended and applied to ongoing research projects focused on UAV-based sensing with WSN augmentation and real-time processing for immersive media experiences.

In particular, in this paper we propose a communication-efficient solution to manage data distribution modeling in a complex multi-platform sensor system supported by a clustered structure of the network.

When the amount of sensor nodes goes to hundreds and they are no more fixed in the space, the centralized approach must be reviewed.

The authors here proposed an evolutionary technique to optimize the WSN lifetime considering to extend the same approach to heterogeneous networks with mobile nodes adopting a multi-hop routing scheme.

The use of such advanced bio-inspired computing techniques appears to be useful in this context especially in optimizing the network energy distribution.

The key idea of this algorithm is to address all computational costs to the base station, in order to apply the optimization in run-time, without affecting the power consumption of the sensor nodes.

In particular, the obtained behavior reflects the ability of the optimization technique in optimizing the routes from several nodes to the base station under an energy saving point of view, in order to preserve the network functionality and to avoid premature death of the most solicited nodes.

Final results also suggest further improvements for the proposed technique to be extended to ubiquitous and cooperative networks for real life applications as suggested by ongoing research activities reported in this work.

8532-10, Session 3

Examination of coastal and inland water quality characteristics based on spectral signature analyses

Christiana Papoutsa, Diofantos G. Hadjimitsis, Cyprus Univ. of Technology (Cyprus)

Remote sensing is a valuable tool for monitoring water quality parameters in inland and coastal water bodies. It involves analyses of the variations in magnitude and spectral quality of the water-leaving radiation to derive quantitative and qualitative information on the type and concentrations of the substances present in the water. The main goal of this research is to examine the optical properties of different water bodies such as coastal water; oligotrophic and eutrophic inland water by observing their spectral signatures. Spectral profiles of sampling points, which correspond to water bodies with different water quality characteristics, are extracted and analyzed. Field spectroscopy is a very important tool giving critical information for the comprehension of spectral signatures of different water bodies. It enables us to identify and classify the at-satellite water reflectance and therefore improve or develop new algorithms and methodology to determine water quality parameters using remotely sensed data. Field spectroradiometric data were obtained for inland water in Asprokremmos Dam, Paphos District/Cyprus and in Karla Lake, Volos District/Greece and for coastal water in Zugi-Vasilikos-Old Harbour, Limassol District/Cyprus.

8532-11, Session 3

Raman spectral analysis for remote measurement of water temperature

Christopher P. Artlett, Helen M. Pask, Macquarie Univ. (Australia)

Measurement of the physical and chemical properties of bodies of water is of importance in fields including oceanography, climate change research and marine engineering. In particular, parameters such as temperature and salinity cannot be profiled rapidly in three dimensions with the direct measurement methods currently available. A practical technique for rapid, sub-surface, depth-resolved temperature measurement would complement the currently available technologies.

Active optical remote sensing has the potential to fulfil these criteria. Optical techniques are well suited to sensing of water properties to depths in the tens of metres due to the low absorption of water for blue-green wavelengths[1,2]. By employing integrated intensity measurements over relatively narrow spectral bands (~5-10 nm) rapid collection of data can be achieved.

The measurement of water Raman scattering in particular has the potential to acquire water temperature and salinity data

simultaneously. Multiple groups have conducted work in this area in the past[3-6], though in general such studies have been limited purely to laboratory investigations, measurements at a single depth near the water surface, or approximate temperature readings over the accessible portion of the water column.

Raman scattering of water exhibits a spectral response to temperature change[7,8]. This temperature dependence is observed in a weak, broad emission band from 2900 - 3900 cm-1, which consists of overlapping vibrational transitions resulting from symmetric and antisymmetric stretching vibrations of both free and lattice bonded OH groups[9]. As water temperature increases the intensities of these transitions are altered around isoskedastic (sometimes misnamed isosbestic) points in the spectra.

In order to measure water temperature, one or more spectral parameters which exhibit repeatable temperature dependence are required. The ratio of unpolarised intensity of a pair of spectral channels around the isoskedastic point in the OH band provides a simple parameter which varies linearly with temperature. The depolarisation ratio of the OH stretching band can be employed (i.e. the ratio of perpendicular to parallel polarised scattering intensity) [10], which has the advantage of requiring signal acquisition over a single spectral band to produce a measurement, effectively eliminating differential attenuation as a concern6. These two parameters can be used independently to measure water temperature, although each can suffer from various forms of interference which can negatively impact measurement accuracy. To compensate for these issues, a linear combination of several parameters may be employed, which is anticipated to improve both the precision and robustness of temperature measurement to chemical and physical changes within the sampled volume.

In this work, characterisation of the behaviour of water Raman scattering with temperature variation is conducted. Careful analysis of spectral measurements is applied, to quantify the sensitivity of Raman spectral changes and calibration parameters to temperature variation. Multiple water samples from different locations around Sydney, both fresh and salt water, are analysed and the effect of water quality on this behaviour is examined. We demonstrate laboratory-based temperature measurement through the combination of multiple parameters drawn from water Raman spectra, and describe the development and characterisation of a prototype ranged sensing system based on these studies.

1. Pope, R. M. and Fry, E. S., “Absorption spectrum (380-700 nm) of pure water. II. Integrating cavity measurements”, Appl. Opt. 36 (33), 8710 (1997).

2. Smith, R. C. and Baker, K. S., “Optical properties of the clearest natural waters (200-800 nm)”, Appl. Opt. 20 (2), 177 (1981).

3. Breschi, B., Cecchi, G., Pantani, L. et al., “Measurement of Water Column Temperature by Raman Scattering”, EARSeL ADVANCES IN REMOTE SENSING Vol. 1, 131, (1992).

4. Burikov, S., Churina, I., Dolenko, S. et al., “New approaches to determination of temperature and salinity of seawater by laser Raman spectroscopy”, EARSeL eProceedings 3 (3), 298 (2004).

5. James, J. E., Lin, C. S. and Hooper, W. P., “Simulation of Laser-Induced Light Emissions from Water and Extraction of Raman Signal”, J. Atmos. Oceanic Technol. 16 (3), 394 (1999).

6. Leonard, D., Caputo, B. and Hoge, F., “Remote sensing of subsurface water temperature by Raman scattering”, Appl. Opt. 18 (11), 1732 (1979).

7. Walrafen, G., “Raman spectral studies of the effects of temperature on water structure”, J. Chem. Phys. 47, 114 (1967).

8. Walrafen, G., Hokmabadi, M. and Yang, W., “Raman isosbestic points from liquid water”, J. Chem. Phys. 85, 6964 (1986).

9. Tominaga, Y., Fujiwara, A. and Amo, Y., “Dynamical structure of water by Raman spectroscopy”, Fluid Phase Equilib. 144 (1-2), 323 (1998).

10. Cunningham, K. and Lyons, P. A., “Depolarization ratio studies on liquid water”, J. Chem. Phys. 59 (4), 2132 (1973).

8532-12, Session 3

Hyperspectral derivatives analysis for intertidal habitat mapping

Natascha M. Oppelt, Florian Schulze, Christian-Albrechts-Univ. zu Kiel (Germany); Inka Bartsch, Alfred-Wegener-Institut für Polar- und Meeresforschung (Germany)

Analysis of coastal marine algae communities enables to adequately estimate the state of coastal marine environment and provides evidence for environmental changes. Hyperspectral remote sensing provides a tool for mapping macroalgal habitats if the algal communities are spectrally resolvable. We compared the performance of a new easy-to-use approach with two conventional classification approaches to determine the distribution of macroalgae communities in the rocky intertidal zone of Heligoland (Germany) using airborne hyperspectral (AISAeagle) data. The results of supervised approaches (maximum likelihood classifier and spectral angle mapping) are compared with an approach combining k-Means classification of derivative measures. We identified regions of different slopes between main pigment absorption features of macroalgae and classified the resulting slope bands. The maximum likelihood classifier gained best results (Cohan’s kappa = 0.81), but the new approach turned out as time effective possibility to identify the dominating macroalgae species with sufficient accuracy (Cohan’s kappa = 0.77), even in the heterogeneous and patchy coverage of the study area.

8532-14, Session 3

Resolution enhancement optimizations for data fusion of multiple satellite and airborne sensor data of the water surface

Charles R. Bostater Jr., Florida Institute of Technology (United States)

In this paper optimization and testing of a data fusion methodology is presented. The technique is applied to multispectral and hyperspectral imagery of the water surface, nearby coastal land vegetation as well coastal urbanized areas. The techniques described utilize precision georeferencing methods used in GIS analysis, nearest neighborhood and linear remapping of multi-resolution spatial and spectral imagery. The optimization procedures in the identification of “feature areas” in order to build multiple “SVD” singular value decomposition models, and optimized selection of synthetic image models using non-parametric K-S test techniques. The methodology utilized utilizes discrete cosine and inverse cosine 2D filtering, 2D Butterworth filtering and optimization of the Butterworth cutoff and order coefficients. The final optimized images are then tested using stratified random sampling of pixels for K-S tests in order to select optimal models and coefficients based upon spectral signature difference minimization between observed and synthetic hyperspectral signatures. The optimization techniques, methods to describe the data fusion process errors and differences (spatially and spectrally) are presented. It is shown that the resolution enhancement methodology is most sensitive to (a) the pixels used in the SVD model building process and (b) the Butterworth cutoff frequency selected.

8532-15, Session 4

Investigation Into the Use of Satellite Remote Sensing Data Products as Part of a Multi-Modal Marine Environmental Monitoring Network

Edel O’Connor, Alan F. Smeaton, Noel E. O’Connor, Fiona Regan, Dublin City Univ. (Ireland)

Water quality monitoring is an important part of monitoring our natural environment and includes monitoring the quality of both coastal and inland marine locations. For many years water managers relied on field measurements for coastal monitoring and water quality evaluation which involves costly, time-intensive sampling and collection. This type of sampling is too limited on temporal and spatial scales to adequately monitor the quality of water bodies on a long-term basis and to capture dynamic marine events, which is essential for increased knowledge and proactive decision making. In recent years, the introduction of sophisticated sensor technology and wireless sensor networks have provided an opportunity for real-time remote monitoring of marine and freshwater environments at greater temporal and spatial scales.

The last ten years have seen the emergence of a variety of initiatives from very simple WSN deployments to highly complex coastal observation systems which make physical, chemical and biological measurements. However the current state of the art in this technology still poses many challenges for environmental monitoring applications. In general sensing devices to be deployed in a marine environment are subject to harsh conditions, possible failure or inaccurate data, require

a lot of power for operation, and are very costly. Although a network of in-situ sensors can provide detailed information on a specific region, they are effectively single point sensors monitoring one specific point of a vast region and there is often limited redundancy due to budgetary constraints.

In our research we are investigating how in-situ sensor networks can be complemented by the numerous satellite data streams available through the many available platforms orbiting the earth and also the subsequent reprocessing of that data into combined data products available through services such a MyOcean as part of GMES. Despite the numerous benefits associated with the use of satellite remote sensing data products, there are a number of limitations with their use in coastal zones.

In our research we investigate the availability of satellite remote sensing data that can enhance the use of the in-situ sensor nodes in an operational multi-modal sensor network enabling better decision making and providing a form of redundancy in the network. The objectives of this work thus require near real-time cooperation between the two sensor streams. The site and the in-situ data sources of interest here are Galway Bay and data from the SmartBay environmental monitoring buoys deployed as part of the national SmartOcean initiative. We investigate a variety of SST and chlorophyll satellite data products and their potential use as a complementary sensing modality to the SmartBay sensors for a smarter more intelligent network. This also involves an analysis of consistency between data readings from the in-situ sensors and a variety of satellite data products, determining the most suitable products for use in Galway Bay.

8532-16, Session 4

Mapping Arctic sea ice by fusing MODIS and AMSR-E data

Yi Luo, Environment Canada (Canada)

Mapping, tracking and forecasting Arctic sea ice is becoming increasingly important due to expanding human activities and significant regional environment changes as the impact of global climate change. The advancements in remote sensing technologies have now provided large volumes of data from various sensors to the scientific and operational communities. It has become critical to fully exploit the data from different sensors and to efficiently automate data processing and produce useful products. The Canadian Ice Service (CIS) intends to develop and operationally implement automation and data fusion algorithms to take advantage of various data sets. Among them MODIS and AMSR-E data have their specific advantages and limitations in terms of sea ice observation. MODIS includes multiple visible and infrared bands and can easily distinguish between sea ice and open water. It also has higher spatial resolution and much wider image swath and then more frequent revisit. However, the presence of cloud or haze can block the surface radiance. AMSR-E passively measures the Earth microwave radiation at multiple bands with dual polarization modes. It is very good at mapping ice concentration and classifying ice types and has no cloud impact, but its spatial resolution is relatively coarse. In this study, fusion is not only made on image basis but also on physical basis. A correlation model between visible/infrared reflectance from MODIS and brightness temperature from AMSR-E will be built based on selected training data, then a high resolution ice concentration product can be derived using MODIS data only. The preliminary results show the new product can offer detailed ice information, especially along coast area or around small islands. It can also offer thin ice information to which the microwave sensor is not sensitive. Another good thing is the total Arctic ice cover area calculated based on this product is more accurate than those based on coarser resolution data. This is very important in improving estimation of minimum ice extent of each year. Generally, fusing MODIS and AMSR-E data can take advantage of the benefits of each dataset in an efficient manner. It is able to optimally present important sea ice features such as ice concentration, ice edge and ice type. The new product is useful to operations for ice analysis and ice modeling. This practice can be also a preparatory stage for data from new sensors such as Suomi NPP/VIIRS and AMSR-2.

8532-17, Session 4

Accuracy assessment of water column correction based on bio-physical parameters for case 2 waters

Tina Geisler, Natascha M. Oppelt, Christian-Albrechts-Univ. zu Kiel (Germany); Thomas Heege, EOMAP GmbH & Co. KG (Germany)

Numerous approaches characterising the radiation field of a water column have been developed and correction attempts for remote sensing data have been applied successfully. Algorithms published by Gordon, Davies-Colley, Gitelson, Mobley, Lee and many others describe the complex interaction of bio-physical parameters with down- and upwelling radiation in a water body and form the basis for water column correction. In coastal regions bio-physical parameters continuously vary in time and space, even during recording of the remote sensing data. Additional factors such as bottom reflection, varying water depth and effects on the water surface (e.g. sun glint, waves, whitecaps) aggravate a correct parameterization of water column correction models. Applying these models, their sensitivity to the quality and accuracy of input parameters is of special interest. In this paper we discuss the sensitivity of the complex water column correction model MIP2 (modular inversion program) to a non-accurate adjustment of specific bio-physical parameters, i.e. SPM (suspended matters) and CHL (chlorophyll) for coastal 2 waters.

The study region is located on the rocky shores of the island Helgoland (Germany). Strong currents, varying sediment loads originating from the Elbe river and the rugged bottom morphology create complex flow patterns of the water bodies. The heterogeneous water body results in varying and spatially uncorrelated concentrations of the bio-physical parameters which further aggravate accurate parameter adjustment. In August 2010, an airborne flight campaign was conducted using the hyperspectral AISA eagle sensor. AISA eagle is an airborne pushbroom scanner covering the spectral range between 400 nm and 900 nm with a nominal spectral resolution of 2 nm. During analysis, special focus is set on areas with varying water characteristics such as vegetated bedrock, shallow sandy spots and deep water areas. Simultaneously to image acquisition, in situ measurements of bio-physical parameters SPM, CHL, Y (yellow substance), Zsd (visual depth) were carried out and analysed in the laboratory; RAMSES underwater light field measurements were taken for calibration and validation purposes.

Water column correction is performed using MIPs sub-module WATCOR. The pixel based sub-module applies an iterative fitting algorithm to calculate the subsurface reflectance by adjusting modelled and measured parameters according to Nelder and Mead´s downhill simplex method. We tested the sensitivity of WATCOR to variations of CHL and SPM concentrations. Analyses are accomplished at specific areas with varying optical properties of the water body; resulting WATCOR variations are analysed statistically and the resulting model sensitivity is discussed.

8532-18, Session 4

Algal fluorescence in coastal waters: impact and potential for retrieval from measurements of the underwater degree of polarization

Samir Ahmed, Alberto Tonnizo, Amir Ibrahim, Alex Gilerson, Barry M. Gross, Fred Moshary, The City College of New York (United States)

Algorithms for retrieving inherent optical properties (IOPs) in coastal waters from remote sensing of water leaving reflectance spectra, and particularly retrievals of concentrations of phytoplankton and chlorophyll a, [Chl], its optically active component, are increasingly focused on analysis of spectral features in the red and near infrared (NIR) spectral bands, since the simple blue - green ratio approach, valid in open oceans, fails when strongly scattering inorganic particles and colored dissolved organic matter (CDOM) are present. NIR spectra can however be significantly impacted by overlapping chlorophyll a fluorescence, and considerable progress has been made to quantify its contribution, and hence achieve more accurate [Chl] retrievals. Recently, because of useful additional information that can be obtained on IOPs, refractive indices and size distributions of water constituents, when compared with that obtained from

standard reflectance data, we have been studying the hyperspectral polarization characteristics of the underwater scattered light, using a comprehensive approach and our recently developed Stokes vector polarimeter to fully measure the Stokes parameters. In these studies, information on the state of the water constituents can be obtained through analysis of the spectral and geometrical angular dependences of the polarized light components, and in particular the characteristics of non - algal particles (NAP), which are the primary source of underwater polarized elastic scattering, can be retrieved. In contrast, elastic scattering by phytoplankton cells has very weak polarization effects, since the real part of planktonic refractive index is very close to the real part of the refractive index of water. In addition to weak elastic scattering, phytoplankton cells also exhibit considerable inelastic scattering due to chlorophyll a fluorescence in the NIR around 685 nm which is unpolarized. The unpolarized nature of fluorescence has been the subject of previous preliminary studies by us, seeking to distinguish its contribution from that of spectrally overlapping elastic reflectance. Field measurements in coastal waters, with our polarimeter, permit more accurate and comprehensive measurements of the underwater polarized field, whose changes are mainly due to NAP scattering, and the very pronounced depolarization impact of the phytoplankton chlorophyll a fluorescence on the NIR polarized spectrum. Multiangular hyperspectral measurements of the underwater polarization light field, combined with those of IOPs collected in eutrophic waters of Chesapeake/Virginia and New York Harbor/Hudson River areas, showed that chlorophyll a fluorescence markedly impacts (reduces) the underwater degree of polarization (DOP) in the 650 - 700 nm spectral region. By noting the unpolarized nature of algal fluorescence and the partially polarized properties of elastic scattering, we are able to separate the chlorophyll a fluorescence signal from the total reflectance. The analysis is based on comparisons of experimental measurements with vector/scalar radiative transfer computations using measured IOPs as inputs. Relationships between change in observed DOP and fluorescence contributions are examined, and the possibility of using DOP measurements for underwater fluorescence retrieval is evaluated for different scattering geometries.

8532-19, Session 4

Development of optical remote sensing technique for monitoring of water basins

Victor I Titov, Victor Bakhanov, Stanislav Ermakov, Ivan Kapustin, Alexander Luchinin, Irina Sergievskaja, Emma Zuikova, Institute of Applied Physics (Russian Federation)

The energy spectra of short waves are obtained in real time by spectral analysis of sea surface image with spectral analyzer operating under no coherent light. That analyzer has some advantages: absence of intermediate registration of sea surface image, instant Fourier transformation of image, absence of influence of motion aberration of image, great dynamical range of spectra (there is only one photo diode in analyzer), recording and monitoring spectra in real time. But previous measurements of spectra had relative characters. The technique for retrieval of absolute value of wave spectra is proposed. Preliminary model of two dimensional spectra of gravity - capillary waves for various winds derived from spectra of sea surface images is presented.

The spectral-kinematics characteristics of long energy waves are determined from optical RTI images (range-time-intensity images) constructed from optical profiles of sea surface. It is possible to form RTI images with range from some hundreds meters to kilometers depending on spatial resolution needed. The original device for recoding of RTI images using the linear array of CCD-photodiodes is created.

The principles of retrieval of spectral-kinematics characteristics of surface waves from RTI images are developed and method for formation of RTI images permitted to remove influence of ships roll is proposed. The method for retrieval long wave's field including swells and waves caused by local wind by optical RTI images derived from the ship is presented.

The high-speed optical system based on linear array of CCD photodiodes for registration RTI images of capillary waves using artificial illumination is created. The data on free and bounded capillary waves, surface wave's breaking derived with this system is presented.

One from directions of our work is investigation of oil slicks by optical technique.

The optical features of oil slicks derived in laboratory and natural conditions, variations of wave spectra in oil slicks are presented.

The complex of optical devices may be used from shore, ship or aerial platform for monitoring of water basins in real time.

This work was supported by the grant RFBR 11-05-97045, 11-05-97027, 11-05-97022, 11-05-00384, 10-05-00101, 11-05-97029 and 11-05-00295.

8532-20, Session 4

Data fusion of significant wave height from HY-2A and other satellite altimeters

Jingsong Yang, The Second Institute of Oceanography, SOA (China)

The HY-2A satellite (launched on Aug. 16th, 2011) is a marine remote sensing satellite developed by China. It includes a dual-frequency altimeter in Ku and C-bands. Data fusion of significant wave height (SWH) from HY-2A altimeter and other satellite altimeters (Jason-1/2 and Envisat) is used to analyze the characteristics of SWH in China Seas and their adjacent waters. Data fusion methods such as inverse distance to a power method, Kriging method and successive correction method are studied in this paper. Some results show that (1) there is little difference between the merged results from different fusion methods in case the altimeter data are not sparse; (2) data from at least three satellites are needed in the fusion processes; (3) in winter SWH in Bohai Sea is usually less than 1.5m, SWH in northern Yellow Sea is usually about 1.5m, SWH in central and southern Yellow Sea is even as large as 2.5m, SWH in East China Sea is usually between 2 and 3m, SWH in South China Sea is relatively large and even reaches 3.5m, and SWH in the Open Ocean east of Luzon Strait is usually larger than 2.5m. Comparisons show that the results are reasonable and HY-2A altimetry data work well with other satellite altimetry data.

8532-29, Session PS

Bifurcation and application advantages of generalized logistic equations on time scales

Wen Hu, Nanjing Changjiang Electronics Group Co., Ltd. (China); Yong Li, Nanjing Univ. of Aeronautics and Astronautics (China)

The theory of dynamic equations on time scales has received much attention as unification and extension of the theories of the differential and difference equations. Some basic mathematical problems of dynamic equations on time scales are researched, which include stability condition of equilibrium and sufficient conditions for oscillation (nonoscillation) of the solutions of different classes of dynamic equations on time scales. On the other hand, the applications of dynamic equations on time scales are of great interest. However, to the best of the author's knowledge, few authors have analyzed the bifurcation of dynamic equations on time scales as well as the advantages of applying dynamic equations on time scales in radar waveform design.

Based on the above discussion, in this paper, we investigate the bifurcation and the potential application advantages of the generalized Logistic equations on time scales and thus provides a foundation for future advanced application in engineering.

We investigate the effect of variation of time scale by bifurcation diagram and then analyze the expanded parameters spaces. The main tools used are fixed-point stability theorem, bifurcation diagram, and Lyapunov exponents. The result of bifurcation diagram display novel dynamical features including multiple period doubling bifurcation and multiple transcritical bifurcation. Moreover, the chaotic regions of parameters space of the generalized Logistic equations are expanded on time scales. The expansion of the chaotic regions generally means larger available waveform space providing potential advantages in application of chaos-based MIMO radar waveform design.

In the justification of this paper, the symmetry of parameters is obviously shown, which halving the available parameters space. Fortunately, the dimension of parameters space and chaotic regions can be expanded by increasing the period of time scales. Asymmetrical large chaotic regions can be found in higher dimensional parameters space, which shows an almost continuous chaotic region given a special set of parameters.

The existence of unknown multiple period doubling bifurcation route to chaos, multiple transcritical bifurcation, bistability, and co-existence

of chaotic orbit and periodic orbit, which are demonstrated in the generalized Logistic equations on generalized time scales.

By exploiting the generalized Logistic equations, we generate a set of waveforms that are nearly orthogonal. The transmit signals are generated by the frequent modulation for low peak to average power ratio. By using cross-ambiguity function and fast Fourier transform, the nearly orthogonal waveforms from chaotic systems are shown to possess many desirable remote sensing properties including a compact spectrum, low range sidelobes. Since each waveform can be represented with a small number of the generalized Logistic equations. A large chaotic regions means a high number of nearly orthogonal chaotic waveforms exist for a given time and bandwidth. Thus the proposed generation procedure can potentially be used to generate a new transmit waveform on each pulse.

8532-30, Session PS

Estimating Qinghai Lake area with BP neural network based on genetic algorithm

Chengfeng Luo, You Haoyan, Chinese Academy of Surveying and Mapping (China); Liu Hui, Qinghai Geomatics Center (China); Liu Zhengjun, ChineseAcademy of Surveying and Mapping (China)

The Qinghai Lake (QL) is located at the northeast edge of the Qinghai-Tibet Plateau, which is one of the most important parts of the plateau. At the same time, QL is the largest saline and inland lake in China. The mean elevation is approximately 3,266 m above sea level, covering an area of 4,200 km2. QL lies the intersectant region among West arid region, East monsoon region and Qinghai-Tibet Plateau. The QL water and the abundant grass vegetation around the QL control and adjust the entironment of the QL watershed. Moreover the QL is a natural barrier which bars the hungriness spreading form West to East. With the integrated affection of the climate change and humanity activity, a series of entironment problems, such as descending water level, declining grass latest decades and severe soil deserting, deteriorate the fish culture resource reducing and wild animal and avifauna inhabit environment. As an important entironment indicator for QL, the area change of QL always can catch people's attention.

With the quick development of the observation technology from Space, remote sensing technique has been becoming the main measure for extracting QL area information. It is easy to identify water body and other matters using middle resolution image, but when it comes to water boundary among the transition region between water body and no water body. Generally water body boundary information was included in mixed pixels for middle resolution image, which make it difficult to identify the accurate water area whenever with automatism method or manual work. This study aims to introduce BP neural network based on genetic algorithm to estimate the water body percentage in the mixed pixels.

With the high resolution image and Gauss mixture model, the posterior probability of the pixel belonging to different classes is calculated. Then the BP and GA models were built with end-members in the pixel. The net was trained with the samples selected, the near best net weights set in the global space can be found by GA, and then BP use grads descends method to search the infinitesimal point in local space until find the best net weights set. Finally the trained net was used to emulate the water percent for boundary mixed pixels.

Using BP neural network based on GA to decompose the end-members in the boundary mixed pixels, the more precision area can be extracted for the mixed pixels. With regard to extracting water body area information automatically using high resolution image or interpreting the boundary to calculate the area, the ways and means mentioned above can improve the work efficiency and precision synchronously, which can be adopted to survey the area change of the QL quickly and continuously.

8532-31, Session PS

The numerical analysis method of depolarizer for broadband imaging spectrometer

Fang Chen, Ming Li, Pengmei Xu, Beijing Institute of Space Mechanics and Electricity (China)

With the wide application of broadband imaging spectrometer in the ocean remote sensor, the depolarizer in front of the optical system must satisfy the high requirement. Based on the character of simple structure and good stability, Lyot depolarizer is widely used in the fiber and grating spectrometer in which the polarization should be controlled strictly. Lyot depolarizer is composed by two crystals with the same wedge angle. The angle of the two optical axis is 45°and the ratio of the thickness is 2:1. Nowadays the design method of Lyot depolarizer based on the coherent condition is mostly used for laser and sensors of narrow band. However, the solution of coherent condition is suitable for narrow band, not for the broadband and high spectral resolution.

To solve this problem, the numerical analysis method has been summarized. According to the theory of matrix optics, the relationship between the residual polarization and the angle and thickness of the depolarizer has been analyzed in the wide wavelength range. The formula is too complicated to get an analysis solver. With the numerical results, as the wedge angle increasing the residual polarization dying oscillates to a stable value. As the crystal thickness increasing the value of residual polarization is oscillating to zero. As a result, increasing the wedge angle and the thickness both could reduce the residual polarization of the depolarizer, but considering the dimension and the resolution of the optical system the wedge angle and the thickness of the depolarizer have restrictions. The wavelength also has effect on the magnitude of the value and the speed of the oscillation. As the wavelength increasing, the magnitude is bigger and the speed is slower. Therefore, the residual polarization of the depolarizer at the longest wavelength is in the range, for the whole band range it also satisfies the requirement. Using the numerical analysis, the design process of Lyot depolarizer used for broadband are summarized as follows:

1. Using the numerical solution the variability of the residual polarization along the wedge angle and thickness are analyzed;

2. According to the requirement of the spectral resolution the wedge angle could be chosen;

3. While the wedge angle is curtained, based on the numerical results the suitable thickness could be solved satisfying the requirement of the residual polarization.

This method can be widely applied to the depolarizer design in imaging spectrometer of broadband which can cover several hundred nanometers and high spectral resolution which is to several nanometers. In this article a Lyot depolarizer has been designed for a broadband imaging spectrometer used in ocean observation. In the wavelength from 400nm to 950nm, the residual polarizations of the depolarizer are less than 2%. This is necessary for the instrument to obtain the accurate radiance data of the target.

8532-32, Session PS

Vertical profiles of beam attenuation coefficients in East China Sea

Qiong Liu, The Second Institute of Oceanography, SOA (China) and Wuhan University (China); Delu Pan, Yan Bai, Xuan Zhang, Lin Zhang, Qiankun Zhu, The Second Institute of Oceanography, SOA (China)

The beam attenuation coefficient have been usually used to characterize distributions and variability of suspended particulate matter(SPM) in marine water. In August 2009 and November-December 2010, the summer and late autumn cruises were conducted in the East China Sea (ECS). Data of the vertical profiles of particulate beam attenuation coefficient at 660nm, Cp(660) and Particulate Organic Carbon(POC) was analyzed to examine patterns and control factors of vertical distributions of particulate matter in ECS. In late autumn, the Cp(660) profiles showed uniform distribution against depth in most of shelf region, and high value of Cp(660) was found in some inshore stations caused by strong resuspension. In summer Cp(660) exhibited weak subsurface maximum phenomenon in outer shelf areas and well vertical mixed in the northern coast areas of ECS. The variability of Cp(660) between summer and autumn were caused by the changes of thermocline distribution in ECS. In the late autumn, water temperature and salinity were characterized as fully vertical mixed, while the strong stratification of water column was observed in summer. The POC profiles showed more complex pattern than Cp(660), most of them characterized with subsurface maximum phenomenon. Apart from the several inshore stations which were influenced mostly by terrestrial input, significant relationships between POC and CP(660) were observed in both late autumn and summer. In late autumn, the rapid mixing of suspended particulate matter accounted for the significant relationships, and in

summer, it resulted from the subsurface chlorophyll maximum which controlled both the Cp(660) and POC vertical profiles in shelf region. The close relationships between POC and Cp(660) also indicate an potential application to retrieve the POC profiles from in situ CP(660) measurements, and to the observation from space.

8532-33, Session PS

Assessment of suspended particulate matter concentration retrieved by Aqua-MODIS and SeaWiFS in the East China Sea

Qianfang Cui, Nanjing Univ. of Science & Technology (China); Delu Pan, Yan Bai, Xianqiang He, Jianyu Chen, The Second Institute of Oceanography, SOA (China)

The East China Sea(ECS) is the 11th largest marginal seas around the world. ECS has widely continental shelf, and has relatively high concentration of suspended particulate matter (TSM) affected by the terrestrial material from the large rivers, including the Changjiang River, and also affected by the resuspension in the winter. Recently, several regional algorithms for the TSM retrieval in the ECS have been proposed, such as the algorithms developed by Zhang et al. (2010) and Han et al. (2006). Due to the variation of the components of TSM, it is significant to study whether existing algorithms are adequate and reliable for the inversion of the concentration of TSM in the ECS for all seasons. Yet, up to now, the validation of the satellite retrieved TSM is still poor because of the lack of the in-situ data and the standard TSM product in the ECS. In the past three years, we have carried out four cruises covering the whole ECS and all seasons, including the spring cruise from May to June 2011, the summer cruise in August 2009, the autumn cruise from November to December 2010, and the winter cruise from December 2009 to January 2010. In this paper, we firstly analyzed the spatial-temporal distribution of the TSM in the ECS. The results showed that there was remarkable seasonal variation with higher concentration in the winter half year and lower concentration in the summer half year. Finally, based on the remote sensing reflectance retrieved by the Aqua-MODIS data, the performance of the four inversion algorithms of TSM were evaluated using the in-situ measured TSM data in the ECS, including the Clark's model in the SeaDAS, Zhang's model, Han's model and Tassan's model.

8532-34, Session PS

A method for retrieving the directional ocean wave spectra from synthetic aperture radar image

Lin Ren, Jingsong Yang, Peng Chen, The Second Institute of Oceanography, SOA (China)

Directional ocean wave spectra can describe the energy distribution of ocean wave and play an important role in oceanography. Synthetic aperture radar (SAR) can measure wave spectra based on a nonlinear mapping relation between the image spectra (or cross spectra) and wave spectra. Due to the complexity of variable estimation and the partial loss of wave in the mapping process, some scientists have been endeavoring to improve the retrieval of wave spectra from SAR. SAR complex image can calculated the cross spectra from two sub-look images brought by multi-look processing. Compared with real image spectra, cross spectra can resolve the 180 degree ambiguity of wave propagation direction.

This paper proposes a parametric method for the retrieval from the SAR complex image, which don't depend on any external information except wind direction. Firstly, the image is divided into sub-looks to calculate cross spectra and averaged in some samples to remove noise. The modulation transfer function (MTF) is calculated including real aperture radar (RAR) MTF and velocity bunching MTF. The former is derived from a CMOD-like empirical model and the azimuth cut-off wave-number in the later by fitting a Gaussian function to the auto-variance function of the cross spectra. Then the wave spectra mapping in the image are retrieved directly from the quasi-linear mapping model simply. These retrieved spectra contain the main wave energy but lose the short wave information, especially in the azimuth direction. In this step, the processing doesn't consider the nonlinear effect and the retrieval have certain deviation with the real one. So the first guess spectra are adopted to compensate the lost. It is constructed by parametric wave model. The corresponding parameters are extracted including the significant wave height (Hs), dominant wave length (L) and direction (D) from the formerly retrieved spectra and wind speed from the SAR image based on CMOD-IFR2 method. The 180 degree ambiguity of D is removed from the imaginary part of cross spectra. Then these parameters are imported into wave model and nonlinear mapping model to match image cross spectra. In the process of matching, the parameters are modified with limits. The wave spectra from the wave model decided by modified parameters, which can match the cross spectra best, be considered as the first guess spectra. Finally, the wave spectra are retrieved iteratively from the first guess spectra like MPI method.

The Envisat ASAR complex image (IMS mode) is used to validate the method. The retrieval is compared with one from Sartool (wave spectra retrieval software) in terms of Hs, L and D. The standard deviation is lower than 0.4 m on Hs, 15 m on L and 10 degree on D. The Hs in this method is higher slightly than the Sartool. Further validation needs other buoy data

8532-35, Session PS

Speckle noise reduction in SAR images ship detection

Ji Yuan, Bin Wu, Yuan Yuan, Qingqing Huang, Jingbo Chen, Institute of Remote Sensing Applications (China); Ren Lin, State Key Laboratory of Satellite Ocean Environment Dynamics,Second Institute of Oceanography (China)

The accuracy of ship detection in Synthetic Aperture Radar (SAR) images have many effects, such as speckle noise, some oceanic phenomena and atmospheric phenomena, including underwater bottom topography, oceanic internal waves, meso-scale ocean circulation, structures of ocean eddies and ocean currents, ocean surface waves, oily slicks, sea surface wind field, atmospheric internal waves and some other ocean surface features. In these effects, speckle noise plays the most important role. When the speckle noise is very strong, ships will be mixed with speckle noise.

At present, there are two types to detect ships in SAR images. One is a direct detection type, detecting ships directly. The other is an indirect detection type. That is, it firstly detects ship wakes, and then seeks ships around wakes. The two types all effect by speckle noise. In order to improve the accuracy of ship detection and get accurate ship and ship wakes parameters, such as ship length, ship width, ship area, the angle of ship wakes and ship outline from SAR images, it is extremely necessary to remove speckle noise in SAR images before data used in various SAR images ship detection.

The use of speckle noise reduction filter depends on the specification for a particular application. We will study these filters in ship detection application. In out study, we firstly summarize some best known filter methods which were used for removing speckle noise in SAR images, such as the mean filter, the median filter, the lee filter, the enhanced lee filter, the kuan filter, the frost filter, the enhanced frost filter, k-mean filter and gamma filter, etc.

Based on above filter methods, we remove speckle noise in SAR images. In addition, several measurement criteria to evaluate and compare the technique merits of some of the well-known adaptive filters were define. These criteria include the measurement of the bias, equivalent number looks, the ability of keeping the edges, etc.

Secondly, a mathematical function known as the wavelet transform and multi-resolution analysis were used to localize an SAR ocean image into different frequency components or useful subbands, and effectively reduce the speckle in the subbands according to the local statistics within the bands. Two approaches were focused, one is application of wavelet shrinkage techniques on the individual subbands according to the local variance within each subbands, and another one is application of a global shrinkage technique based on the lowest threshold of all the subbands.

Finally, the analysis of the statistical results are presented, which demonstrates the advantages and disadvantages of using wavelet shrinkage techniques over standard speckle filters.

8532-36, Session PS

Remote sensing and buoy based effect analysis of typhoon on hypoxia off the Changjiang (Yangtze) Estuary

Jianyu Chen, Xiaobo Ni, Zhihua Mao, Yifan Wang, Lijin Liang, Fang Gong, The Second Institute of Oceanography, SOA (China)

Long-time series data observed by buoys and two cruises before and after Typhoon Muifa (2011), long-time series observation of bottom buoy at 2009, and one cruise before and two cruises after Typhoon Soudelor at 2003 are used in analysis the effecting of typhoon on hypoxia off the Changjiang Estuary. The Ekman pumping velocity during and after Typhoon was calculated. From buoys observation, typhoon passed by cause the water exchange between upper and lower layer. The mixture made the Dissolved Oxygen (DO) level changed to high level in short time. The level of oxygen ascended to 5-6 after the covering of about 30 knots circle of typhoon. The mixture procedure occurred in short time about 1-2 hours. And then the oxygen kept receding if less-wind weather during 10-15 days by observation during Typhoon Muifa and Morakot from buoys. The raise and resume result also has been verified from cruise observations. Typhoon effects hypoxia in many aspects. The level of hypoxia increased from low level to a high level after mixture between upper and lower water. Sea surface temperature (SST) decreased as typhoon passed directly over. The surface chlorophyll-a concentration triggered by the typhoon increased 10 times on average during its five-day stay. The decreased speed of hypoxia level at effected area was larger. The hypoxia level decreased to low level last 10-15 days.

8532-37, Session PS

Radar backscattering from breaking water waves: wave tank study

Stanislav A. Ermakov, Ivan Kapustin, Irina Sergievskaya, Institute of Applied Physics (Russian Federation)

Investigation of physical mechanisms of electromagnetic wave scattering from gravity-capillary waves is very important for correct interpretation of remote sensing observations of oceanic and atmospheric processes imprinting on the sea surface. Marine radars and synthetic aperture radars used for ocean remote sensing operate typically in L-C-X-K-bands, so that short gravity-capillary waves in the centimeter-decimeter wavelength range are mainly responsible for sea surface imaging. Short wind waves are characterized by high steepness values even at comparably low winds, and breaking of short wind waves plays a decisive role when studying radar (and optical) scattering. Previous experiments have revealed some peculiarities of wave breaking process, which can be described as gentle or strong breaking. Gentle breaking of cm-dm-scale gravity-capillary waves of comparably low amplitudes is associated with the generation of so-called parasitic capillary ripples. Longer dm-m-scale waves at large enough amplitudes are usually known as strongly breaking waves, with wave crest overturning with foam and bubble formation. The parasitic ripples generation was investigated in our previous wave tank experiments using optical (laser) gauge, and dependencies of ripples characteristics (steepness and wavelength) of characteristics of carrying cm-dm-scale waves have been studied.

The present study is focused on better understanding of the mechanisms of radar scattering by breaking waves in different wavelength ranges. Wave tank experiments on radar scattering from breaking waves with wavelengths ranged from some cm to about 1 m has been carried out using Ka-band scatterometer (wavelength 0.87 cm). Radar measurements were carried out at incidence angles of about 40-50 degrees, when Bragg scattering mechanism dominates, the wavelength of the ripples responsible for radar backscattering was about 5-6 mm.

Analysis of characteristics of radar signals scattered by breaking cm-dm-scale waves has shown that the radar backscattering is due to parasitic ripples, the radar backscatter is characterized by a threshold dependence on the steepness of breaking basic waves, and the radar Doppler shift is determined by the phase velocity of the basic waves. It is because the parasitic ripples propagate with the same phase velocity as the basic wave, i.e. “frozen” into the basic wave profile.

To achieve strong breaking of longer, meter scale steep waves the dispersive focusing of a frequency modulated wave packet was used. From the analysis of radar Doppler spectra it has been concluded that radar backscattering from strongly breaking m-scale waves is due to free propagating ripples which velocities are different from the phase velocities of m-scale waves. The free waves can be generated by the breaking wave crest, while the parasitic capillary waves bound to the m-scale wave profile are practically absent in this case.

For breaking waves in the intermediate wavelength range (some decimeters) the ripples responsible for radar backscattering is found to be a “mixture” of the free waves and the parasitic ripples.

The obtained results are very important for interpretation of Doppler radar shifts, in particular for correct measurements of marine currents using radar.

This work has been supported by RFBR (projects 11-05-00295, 11-05-97027, 10-05-00101, 11-05-97029).

8532-38, Session PS

The analysis of bloom areas drifted to the northwest caused by three hurricanes in the East China Sea

Dongyang Fu, Delu Pan, The Second Institute of Oceanography, SOA (China)

On the one hand, the Kuroshio is a strong west boundary current along northwest of the Pacific, it infloods into the East China Sea in the northeast of Taiwan and to the north along shelf. Its velocity changes with time and position., and the other hand, Taiwan Warm Current passes through the Taiwan Strait and enters into the East China Sea. And the same time, the strong Yangtze river diluted water in the summer and autumn outpouring into the East China Sea. These 3 strong currents have important effects to the East China Sea such as physical, chemical character, climate, environment and so on.

From summer to autumn, there is about 10 times of hurricane entering into the East China Sea area, and The vast majority of hurricanes passing through the East China Sea are usually straight north or northwest directly, but there are a few hurricanes going forward straightly to west or rotating northeastward even turning back to the south after entering into the East China Sea, such as Nari in 2001, Sinlaku in 2002 and Meari in 2004. In this article, the authors analyzed the 3 times of phytoplankton bloom by these 3 hurricanes which had special paths in the East China Sea with SeaWiFS remote sensing data average fussion and then found: the average growth of chlorophyll a concentration after hurricanes in the East China Sea were remarkable, respectively up to 70%, 40%, 90%. But the central region of the blooms were different to that caused by the hurricane in general directly northward. These central region of the blooms were neither in the central area where the hurricane passed by nor on both sides of the path, but they all located northwest away from the center of the strong winds, about 100km away. However, the bloom areas caused by hurricane Matsa entered into the East China Sea along northwest and landed on Zhejiang in August and Damrey passing through the South China Sea and landed on Hainan in September were consistent with the hurricanes center region. Why did the bloom areas by hurricanes Nari in 2001, Sinlaku in 2002 and Meari in 2004 drift to the northwest, but this phenomenon are not been observed for hurricanes moving directly to the north in this area or in the other sea area. According to the historical data of the Yangtze diluted water and the nutrients in the East China Sea, the preliminary results indicated: these 3 times of bloom water mass did not located in the area where the Yangtze river diluted water reacted on in summer or autumn, so these blooms were not caused by the high nutrients from the Yangtze river diluted water, but most likely due to the strong mixing and upwelling caused algal blooms in the center areas by hurricanes and then pushed jointly by the Kuroshio invasion component westward and the Taiwan Warm Current northward, so the water masses of bloom drifted to the northwest.

8532-39, Session PS

Seasonal and interannual variability of sea surface wind over the China seas and its adjacent ocean from QuikSCAT and ASCAT data during 2000-2011

Xiaoyan Chen, The Second Institute of Oceanography, SOA (China) and Zhejiang Univ. (China); Delu Pan, Xianqiang He, Yan Bai, Yifan Wang, Qiankun Zhu, The Second Institute of Oceanography, SOA (China)

A total of 12 years (2000-2011) of sea surface wind data from QuikSCAT and ASCAT are employed to identify the seasonal and interannual variability over the China Seas and its adjacent ocean. The wind speed and direction, strong wind frequency, monsoon onset and transition time are revealed by statistic analysis. The result shows that (1) the wind speed is highest in winter and lowest in summer in the study area. The southeast of Indo-China Peninsula, Luzon Strait, Taiwan Strait and ocean east of Japan are the regions with the higher wind speed throughout the year, especially more than 12 m/s in winter. (2) The monsoon prevails in the China Seas, southwesterly in summer and northeasterly in winter, while southeast wind also occurs all the

seasons except winter. The northwest wind only occurs north of 27°N in winter. (3)The strong wind more than 10 m/s exceeds 140 days per year in the Taiwan Strait while only 30 days in the Bohai Sea and Yellow Sea. In addition, the Luzon Strait can reach 120 days, second only to the Taiwan Strait. (4) The time of monsoon onset changes from year to year. Generally, the southwest wind in the low latitudes begins in May and ends in September or October, then turns to northwest wind completely which almost have no transition time. For the mid-latitudes, the southwest wind begins in June and ends in August. May and September are the transition time. Then the northeast wind begins to prevail. (5) The trend of sea surface wind speed in the study area is decreasing from 2000 to 2011. The annual mean wind speed is lowest in 2002 during the period of 2000-2011.

8532-40, Session PS

Detecting the red tide based on remote sensing data in optically complex East China Sea

Xiaohui Xu, South China Sea Institute of Oceanology, Chinese Academy of Science (China) and The Second Institute of Oceanography, SOA (China) and University of Chinese Academy of Sciences (China); Delu Pan, Zhihua Mao, Bangyi Tao, Qiong Liu, The Second Institute of Oceanography, SOA (China)

The red tide cause significant ecological and economic damage typically occurs as well as the greatest hazard to human health, such as fish kills and water discoloration; tourism industries have also incurred millions of dollars in lost revenue due to red tide events causing fish kills and water discoloration. East China Sea is the “high incidence” of the red tide disaster in China, the number and the area of red tide was significantly higher than the in other three sea: the Bohai Sea, Yellow Sea and South China Sea. The red tide outbreak in the East China Sea, showing the area of red tide was increase and the regional concentration and toxic and harmful algae increased. Therefore, the study of the mechanism and forecast , prediction and prevention of red tide is a major scientific issues. The remote sensing technology has characteristics of fast, synchronization and can monitor a large area, which is very important for monitor red tide, the remote sensing is one of the most effective means. Ocean color sensors measure the amount of light reflected from the surface of the ocean at specific wavebands, from which the concentration of chlorophyll a, Chl, can be retrieved. But chlorophyll estimates from space can be overestimated when algorithms that do not account for colored dissolved organic matter absorption and bottom reflectance are used, satellite-derived chlorophyll concentrations alone are not suitable for detecting blooms from space. a robust technique capable of distinguishing red tide is required. Therefore this paper selected the East China Sea, the high incidence area of red tide, as the main study area, study the remote sensing extraction algorithm of red tide.

This article systematically analysis the spectral difference and its produce mechanisms in the red tide water bodies and non-red tide water body. From the spectral curves, we can see that the spectral of the red tide water bodies and non-red tide water body exists significant difference, there are two peaks and two valley in red tide water body, instead of non-red tide water body does not exist. The results show that the Rrs555/Rrs488> 1.5 can be well distinguished by the red tide water from the non-red tide water in the East China Sea. From 16 historical red tide events show that using this method can distinguish between red tide and non-red tide water.

8532-41, Session PS

Satellite study of the influence of coastal upwelling on a red tide in the Zhejiang Coastal Waters

Xiulin Lou, Aiqin Shi, Qingmei Xiao, Peng Chen, Lin Ren, The Second Institute of Oceanography, SOA (China)

Upwelling water carries nutrients from deeper layer to surface layer and promotes the growth of planktons. The Zhejiang Coastal Waters in the western East China Sea is the major one of upwelling regions in China seas, and it is also a high frequency area of red tides. In this article, we monitored a red tide dominated by Chaetoceros sp. occurred on July 20 and lasted until August 6 in 2007 in the Zhejiang Coastal Waters with EOS MODIS imagery, the Zhejiang Coastal Upwelling was also observed during this red tide event and the influence of the coastal upwelling on this red tide was analyzed. First, four cloud-free and date-continuous MODIS ocean color (CHL-a) and sea-surface temperature (SST) images were selected and then rectified to a standard transverse Mercator projection in order to monitor the red tide and measure the upwelling in this study. Secondly, according the field observations of chlorophyll concentration of this red tide, pixels with CHL-a value greater than a certain threshold were masked out from ocean color image data and considered as red tide waters so as to obtain spatial information of the red tide. Then based on the temperature characteristics of upwelling, a temperature-threshold approach was employed to measure the physical parameters of the coastal upwelling from the SST images. Since the upwelling water is colder than the surface water that it displaces, the upwelling areas can be easily identified in the SST images with a certain temperature threshold. By applying this threshold method, for an upwelling region, the location, area and temperature can directly be measured from the SST images. Finally, the temporal and spatial distributions of the red tide and the coastal upwelling were analyzed by using temporal-spatial analysis method. The results show that there exists a high degree of correlation in spatial distribution between the coastal upwelling and the red tide. The coastal upwelling has effects on the space cover of the red tide according to their spatial correlation. The coastal upwelling plays a crucial role in the development of the red tide in term of water temperature. The coastal upwelling is an important dynamic factor for the formation of red tides in the Zhejiang Coastal Waters.

8532-42, Session PS

Study on the temporal-spatial change of aerosol on the yellow sea using MODIS products

Hongchun Peng, Huaihai Institute of Technology (China)

This article summarized the temporal-spatial character of aerosol of the Yellow Sea by extracting and analysing AOD (Aerosol Optical Depth) and Angstrom index (α and β) based on the aerosol products data of 2006 we could aquire. It indicated that the AOD of the Yellow Sea and its adjacent sea area decreased from coast to sea waters. The AOD changed obviously with seasonal change, whose values were the highest in Spring, the lowest in Winter. Angstrom index α could reflect the kind of aerosol particles: the size of most aerosol particles was small and it was dominated by small particles emitted by human and dust-like particles in Summer and Autumn. Moreover, it was occupied by sea-salt aerosol in Autumn and Winter. With the increase of the distance to the shore, AOD and Angstrom index β decreased gradually, meanwhile AOD and Angstrom index β in the South of the Yellow Sea were larger than those in the North of the Yellow Sea.

8532-43, Session PS

Study on aerosol changes in the Yellow Sea based on MODIS products

Hongchun Peng, Haiying Li, Huaihai Institute of Technology (China); Chunlin Huang, Cold and Arid Regions Environmental and Engineering Research Institute, (China); Hao Gao, Huaihai Institute of Technology (China)

This study utilized MODIS aerosol data and aerosol data from AERONET which is real-time monitoring data about aerosol in a station in January, April, July and October of 2006, the study area is located in the Yellow Seas. The key of this study was to extract aerosol optical depth and Angstrom (α and β) from MODIS products, and the indexes were combined the data of aerosol distribution from AERONET. With analysis of AOD and Angstrom-α and -β, the spatial-temporal feature of aerosol optical depth and type was obtained, and especially the possible environmental factors that caused the distribution was brought. The AERONET data is selected to validate the precision and accuracy of MODIS data, and point and area data were linked together to improve data precision and enlarge the study range. The data of AOD and Angstrom indexes from AERONET in July was observed in 550 nm, while MODIS data was in 500 nm, so the two set of data must be matched with a certain match equation. The data of MODIS was preprocessed with the correction of geometric and bow-tie effect and clipped with vector data to obtain the appropriate area. The distribution image and curve diagram were produced with AOD and

Angstrom-α and -β. The values of AOD and Angstrom indexes were analyzed correlatively.

This study adopted some indexes such AOD (Aerosol Optical Depth) and Angstrom index (α and β), and analyzed monthly distribution and annual average of aerosol. The result suggested that AOD had significant negative correlation with Angstrom-α (r=-0.7261), and significant positive correlation with Angstrom-β (r=0.9576), and Angstrom-α had significant negative correlation with Angstrom-β (r=-0.8791). AOD and Angstrom-β came up to the maximum in Spring, then in Summer and Winter, and down to the minimum in Fall in the study area, and Angstrom-α was completely opposite. AOD and Angstrom-β had a upward trend from offshore to deep sea area, and from the north to the south of the Yellow Sea, while Angstrom-α had a downward trend. Analysis of Angstrom-α displayed that the offshore was polluted by small particles from anthropic activities, and the main content of aerosol was large particle of sea salt in the deep sea field. The main type of aerosol was consisted of small particle aerosol emitted from anthropic activities in Summer and Fall, and of sea-salt particle in Spring and Winter in the Yellow Sea. Spatially the diameter of aerosol in the north of the sea was bigger than one in the south. This study obtained the general distribution spatially and temporally in the Yellow Sea of China, and especially the fact that the main content of aerosol in the offshore was small particle from anthropic activities was paid attention to.

8532-44, Session PS

A preliminary study on the application of remotely sensed SST in locating evaporation duct height by using Babin's methodology

Muhammad Hasan Al Baig, Institute of Remote Sensing Applications (China)

As an important cause of sudden and special atmospheric stratification at lower boundary layer just above a sea, the evaporation duct has a significant impact to the spread of electromagnetic waves in the atmosphere. So it is of great significance to analyze and forecast evaporation duct based on the actual atmospheric and marine environmental data especially from the military point of view. Rise in Sea Surface Temperature followed by high relative humidity caused change in the refractive index at the lower boundary layer. This change in refractive index created stratification in the boundary layer between sea and atmosphere. Thus led in a trapping of radar signals and other modes of communication by electromagnetic waves. As Numerical Weather Prediction products normally are of low vertical resolution, so as a next-generation mesoscale numerical model, Weather Research and Forecasting Model (WRF) is designed to be a flexible, state-of-the-art atmospheric simulation system which can be applied to simulate the region of evaporation duct occurred in boundary layer. By utilizing its high vertical and horizontal resolution for the simulation of different duct processes over sea, finally the Babin evaporation duct model was used on the output parameters of the surface layer from WRF to retrieve the evaporation duct height. In this study South China Sea was considered as a domain for different years but for the same month of July. Remote sensing data of SST is used in this research along with the reanalysis data. Very clear duct height was calculated at the same area over sea in different time domains. While in the month of April, this evaporation duct height was not observed. Model is processed by using both high resolution SST data and comparatively low resolution data.

Surprisingly, duct height was observed more high in low resolution data as compared to that of high resolution data. This study paves a way for futuristic study of evaporation duct monitoring and forecasting by assimilation of satellite remote sensing data especially through that of Geo-stationary satellites.

8532-45, Session PS

Surface wind speed retrieval from SAR imagery and its contribution to typhoon track forecasting in west Pacific Ocean

Hui Shen, Institute of Oceanology (China)

With the development of climate change and global warming, more and more severe tropical storms, hurricanes and typhoons tend to emerge, leading devastating threat and damage to human lives and social productions. Accurate forecasting of storm track and intensity is of vital importance to help evacuation and hence decrease losses. However, the accuracy of storm forecast heavily depends on the amount of precise measurements under the storm that occurs. Few data were obtained under such strong forced wind in the ocean due to limited measurement methods. In-situ buoys are generally broken under such strong wind. Satellite remote sensing tend to be the candidate for effective storm monitoring in the ocean. Objectives of this presentation are obtaining ocean surface wind speed with fine scale spatial resolution from SAR imagery and studying impact of new wind data on the forecasting of typhoon track and intensities in west Pacific.Based on the valuable Hurricane Watch dataset, a large number of Radarsat-1 images which are captured during various typhoon period in west Pacific, a SAR wind speed retrieval algorithm developed by Shen et al. (GRL, 2006) is applied to get wind speed and direction information from SAR imagery. For super forced typhoon cases (with intensity stronger than category 5 hurricanes), a wind speed ambiguity problem exist in SAR measurements of lower to middle radar incident angles [Shen et al., CJRS 2009]. The ambiguity removal algorithm must be applied in order to derive the true typhoon wind speed [Shen et al., IJRS,2009;]. The final retrieved wind speed is assimilated into meso-scale atmospheric numerical model MM5 using 4D-Var assimilation technique to investigate its impact on improving accuracy of typhoon forecasting. With the assimilation of the new data, the NWP model shows better accuracy on hurricane track forecasting as well as hurricane intensity. The methodology and results suggested the necessity to include SAR measurements on the ocean surface into future operational typhoon forecasting.

8532-46, Session PS

Arabian Sea cyclone: structure analysis using satellite data

Lubna Rafiq, Pakistan Space and Upper Atmosphere Research Commission (Pakistan)

Advances in earth observation technology over the last two decades have resulted in improved forecasting of various hydrometeorological-related disasters. In this study the severe tropical cyclone Gonu (2-7 June, 2007) has been investigated using multi-sensor satellite data sets (i.e. AIRS, METEOSAT, MODIS and QSCAT data) to monitor its overall structure, position, intensity, and motion. A high sea surface temperature and warm core anomalies (at 200 hPa and above) with respect to the pressure minima in the central core were found to have influenced the pattern of development of the tropical cyclone. High relative humidity in the middle troposphere was aligned with temperature minima at 850 hPa and 700 hPa; high winds (above 120 knots) and closed pressure contours were observed during the intensification stage. A contour analysis of outgoing longwave radiation (OLR) provided an explanation for the direction of movement of the cyclone. The translational movement and velocities (ground speed) of the tropical cyclone were calculated using the surface pressure of the cyclone's central core. Statistical analyses revealed a strong correlation between the maximum wind speeds within the cyclone and various atmospheric parameters. We conclude with a discussion of the significance of these findings with regard to cyclone forecasting within the framework of early warning and disaster management

Detailed analyses of various satellite data sets (particularly AIRS data) have enabled us to document the following features of the severe tropical cyclone Gonu that formed over the Arabian Sea in June 2007:

• High sea-surface temperatures were recorded for the northern part of the Arabian Sea prior to, and during, the formation of the cyclone. This provided sufficient fuel for tropical cyclone Gonu to maintain its movement in a north-westerly direction.

• A warm anomaly in the troposphere reaching up to the tropopause could be documented, spatially centred over the pressure minima.for all of the relevant days studied during the lifetime of the cyclone, high relative humidity values in the lower-troposphere were centred over the temperature minima.

• The AIRS data on outgoing longwave radiation (OLR) was found to be very useful for monitoring both structural changes within the cyclone and the direction of movement of the tropical disturbances. The statistical analyses have verified that physical correlations exist between the maximum speed values for a tropical cyclone and various AIRS-derived atmospheric parameters.

Our results serve to emphasize that unravelling the causes of changes in cyclone activity requires not only an understanding of which factors influence their origin and development (i.e. high sea surface temperatures prior to formation), but also an understanding of which

factors influence the direction in which they will track (i.e. high relative humidity, outgoing longwave radiation, air temperature etc.)

The high temporal frequency of remote sensing data provides good potential for real time monitoring of cloud movements, sea surface temperatures, and tropospheric conditions through various meteorological parameters, producing data with multiple applications for early warnings. With these data, for example, the formation and track of a tropical cyclone can be monitored and specific warnings relating to its location, timing, expected intensity, and the expected rainfall, can be issued several hours ahead of the actual impact.

This study provides important insights into the formation and intensification of Arabian Sea tropical cyclones that will be useful for operational analysis and forecasting as well as for designing disaster mitigation measures, and may also play a major role in the development of cyclone warning strategies.

8532-47, Session PS

Acquisition of airborne imagery in support of Deepwater Horizon oil spill recovery assessments

Charles R. Bostater Jr. Jr., Heather Frystacky, Florian A. Levaux, Florida Institute of Technology (United States); Frank E. Muller-Karger, Univ. of South Florida (United States)

Remote sensing imagery was collected from a low flying aircraft along the near coastal waters of the Florida Panhandle and northern Gulf of Mexico and into Barataria Bay, Louisiana, USA, during March 2011 and May 2012. Imagery was acquired from an aircraft that simultaneously collected traditional photogrammetric film imagery, digital video, digital still images, and digital hyperspectral imagery. The original purpose of the project was to collect airborne imagery to support assessment of weathered oil in littoral areas influenced by the Deepwater Horizon oil and gas spill that occurred during the spring and summer of 2010. This paper describes the data acquired and presents information that demonstrates the utility of small spatial scale imagery to detect the presence of weathered oil along littoral areas in the northern Gulf of Mexico. Examples of imagery collected are presented and methods used to plan and acquire the imagery are described. Results show weathered oil in littoral areas after the spill was contained at the source.

8532-48, Session PS

Coastal Zone Mapping and Imaging Lidar (CZMIL): First Flights and System Validation

Viktor I Feygels, Joong Yong Park, Jennifer Aitken, Minsu Kim, Andy Payment, Vinod Ramnath, Optech, Inc. (United States)

CZMIL is an integrated lidar-imagery sensor system and software suite designed for the highly automated generation of physical and environmental information products for mapping the coastal zone.

This paper presents the results of CZMIL system validation in turbid water condition in the Gulf coast of Mississippi and in relatively clear water condition at Florida late spring 2012. The system performance test shows that CZMIL was successfully achieved 7-8m depth in Kd =0.46m-1 (Kd is the diffuse attenuation coefficient) in Mississippi and up to 41m when Kd=0.11m-1 in Florida. With 7 segment array for topographic mode and shallow water zone, CZMIL generated high resolution products with maximum pulse rate of 70 kHz, and with 10 kHz in deep water zone. Diffuse attenuation coefficient, bottom reflectance and other environmental parameters for the whole multi km2 area were estimated, based on fusion of lidar and CASI-1500 hyper spectral camera data.

8532-50, Session PS

Contrast based band selection for optimized weathered oil detection in hyperspectral images

Florian A. Levaux, Charles R. Bostater Jr. Jr., Florida Institute of Technology (United States); Xavier Neyt, Royal Belgian Military Academy (Belgium)

Hyperspectral Imagery offers unique benefits for detection of land and water features due to the information contained in reflectance signatures (Bi-directional Reflectance Distribution Function - BRDF) that directly show relative absorption and backscattering features of targets. Such feature detection can be very useful in shoreline monitoring or surveillance applications, for example to detect weathered oil. However, for a real-time application, processing of hyperspectral data can be an important issue. Band selection is thus important in those applications in order to select only the essential information for the detection. In the present paper, band selection is based upon the optimization of target detection using contrast algorithms. The common definition of the contrast (using only one band out of all possible combinations available within a hyperspectral image) is generalized in order to consider all the possible combinations of wavelength dependent contrasts using hyperspectral images. The inflection (defined here as an approximation of the second derivative) is also used in order to enhance the variations in the reflectance spectra as well as in the contrast spectrums in order to assist in optimal band selection. The results of the selection in term of target detection (false alarm and missed detection) are also compared with a more known method to perform a feature detection, namely the matched filter.

In this paper, imagery is acquired using a pushbroom hyperspectral sensor mounted on the bow of a small vessel. The sensor is mechanically rotated using a optical rotation stage. This opto-mechanical scanning system produces hyperspectral images with pixel sizes on the order of mm to cm scales, depending upon the distance between the sensor and the shoreline being monitored. The motion of the platform during the acquisition induces distortions in the collected HSI imagery. It is therefore necessary to apply a motion correction to the images. In this paper, imagery is corrected for the pitching motion of a vessel, which causes most of the deformation when the vessel is anchored at 2 points (bow and stern) during the acquisition of the image.

8532-21, Session 5

Investigation of fine spatial structure of currents and submesoscale eddies based on satellite radar data and concurrent acoustic measurements

Olga Y. Lavrova, Space Research Institute (Russian Federation); Andrey N. Serebryany, Space Research Institute (Russian Federation) and Andreev Acoustics Institute (Russian Federation); Tatiana Yu Bocharova, Marina I. Mityagina, Space Research Institute (Russian Federation)

Satellite high-resolution radar data from Envisat ASAR, RADARSAT-2 and TerraSAR-X sensors are used for the detection and investigation of fine structure of currents and submesoscale eddies. The fine structure of sea currents is manifested in radar images as quasiperiodic slick strips of a horizontal scale from tens of meters to several kilometers. The strips are typically elongated along the currents apparently indicating their jet character and intermittence. The focus is on filamentary slick bands involved into small scale vortical processes and allowing estimation of spatial characteristics of submesoscale eddies based on their SAR signatures.

Small-scale or submesoscale eddies with diameters of less than Rossby radius of deformation could hardly be investigated by traditional oceanographic means due to spontaneity of their appearance, nonstationarity and short lifetimes. Sources of their generation are still not well known. A large archive of satellite data accumulated during 1999-2011 over different parts of the Black, Baltic and Caspian Seas has been analyzed in order to search, systemize and reveal mechanisms of formation and evolution of small scale eddy structures in these areas. Atmospheric and hydrological fronts and current instability have been found to play a significant role in small-scale eddies generation.

Subsatellite measurement using acoustic Doppler profiler (ADCP) “Rio Grande 600 kHz” have been performed aimed at verification and adjustment of the results obtained based on satellite radar data. Results of experimental work conducted in September-October 2011 on the Black Sea shelf are presented. During the experiment, sections from the shoreline to shelf edge were made in conjunction with radar imaging of the region from Envisat, RADARSAT-2 and TerraSAR-X satellites and optical imaging by Envisat MERIS and Terra/Aqua MODIS sensors. The formation and drift of a near-shore anticyclonic eddy of 20 km in diameter as well as submesoscale eddies of 5-7 km in diameter were observed. The currents induced by those eddies in

the shelf zone were measured. The eddy structures detected by SAR were identified in ADCP current data and their impact through the water depth was traced.

The work was conducted under projects of RFRBR #10-05-00428-a and the Russian Federal Thematic Programme “Scientific and scientific-educational professionals of innovative Russia” for 2009-2013.

8532-22, Session 5

Remote sensing of oil films on the water surface using radar

Stanislav A. Ermakov, Institute of Applied Physics (Russian Federation); Jose da Silva, Univ. do Porto (Portugal); Ivan Kapustin, Irina Sergievskaya, Institute of Applied Physics (Russian Federation)

The problem of remote sensing of films on the sea surface, including detection, discrimination between biogenic and anthropogenic films and oil spill monitoring is very urgent and still far from solution. Very perspective all-weather tools for film remote sensing are microwave radars, in particular satellite synthetic aperture radars (SAR). Film slicks can be clearly seen in radar images of the sea surface due to the effect of depression of wind waves by surface films, this effect is determined by film characteristics and by the sea state. The most efficient approach to the problem solution is field experiments on radar probing of films with known physical parameters and development corresponding theoretical models of slick radar imaging. Particularly valuable are radar measurements of film slicks from boats and/or platforms simultaneous and co-located with SAR observations. Such experiments due to their complexity are quite scarce at the moment.

In this paper results of field experiments on radar imaging of surfactant films using satellite SAR (TerraSAR-X) simultaneous with measurements of radar backscattering from a ship using X-band and Ka-band scatterometers are described and analyzed. The experiments were performed with oleic acid films with pre-measured physical parameters, the surface tension and the film elasticity, in a wide range of wind velocities (up to 10 m/s). Radar contrasts characterizing depression of radar backscatter in slicks have been obtained, and X-band SAR contrasts appeared to be consistent with X-band scatterometer contrasts, while contrasts in Ka-band are found to be normally higher.

Theoretical analysis of radar contrasts for moderate incidence angles has been carried out based on a composite radar imaging model and on a hydrodynamic model of wind wave damping due to films. The radar model takes into account Bragg scattering and specular scattering, the latter is usually negligible compared to the Bragg effect at moderate incidence angles (larger than 30-35 degrees), but is obtained to give noticeable contribution to backscattering at smaller incidence angles particularly for slick areas when cm-scale ripples is strongly depressed by films. Damping of cm-scale ripples was described in the frame of a hydrodynamic model for the spectrum of short wind waves. The hydrodynamic model takes into account wind wave generation described by an empirical expression for the wind wave growth, theoretical formula for wave damping due to viscoelastic films and phenomenological terms describing energy input to the spectrum of cm-scale waves from longer, dm-scale waves. Theoretical calculations of radar contrasts in slicks are in satisfactory agreement with experiment.

Along with the estimation of contrasts, data processing included analysis of frequency spectrum of radar signals and estimation of radar Doppler shifts. An effect of changing of the radar Doppler shifts in slicks has been revealed in the experiments. It is obtained that Ka-band radar Doppler shift increased in the slick areas, while X-band Doppler shift decreased in slicks. A physical explanation of the effect is given based on different contributions of free wind waves and so-called bound waves propagating with different phase velocities to the resulting Doppler shifts. Both radar backscattering depression and the change of radar Doppler shifts can be used for detection/characterization of oil slicks from remote sensing data.

This work was supported by RFBR (projects 11-05-00295, 11-05-97027, 10-05-00101, 11-05-97029).

8532-23, Session 5

Study on wind wave variability by inhomogeneous currents in the closed seas

Victor V. Bakhanov, Nikolai A. Bogatov, Aleksei V. Ermoshkin, Institute of Applied Physics (Russian Federation); Andrei Ivanov, P.P. Shirshov Institute of Oceanology of RAS (Russian Federation); Olga N. Kemarskaya, Victor I. Titov, Institute of Applied Physics (Russian Federation)

Complex experiments were performed in the north-eastern part of the Black Sea in 2007 - 2009 and in the south-eastern part of the White Sea in 2009 - 2011 in the summer period to study variability of the current fields and other characteristics of sea bulk, wind waves, and parameters of the near-surface atmospheric layer. Measurements were carried out from the onboard of the scientific research vessels on move and in drift by optical, radar and acoustic equipment. The heterogeneity of bottom topography in Black Sea had quasi-one-dimensional character (the depth-drop area). Accordingly, the heterogeneity of currents had also quasi-one-dimensional nature. The case of the two-dimensionally heterogeneous relief of the bottom was investigated in White Sea. The peculiarity of this experiment was simultaneous measurements from onboard of vessel synchronously with acquisitions of synthetic aperture radar (SAR) images of the Envisat and TerraSAR-X satellites. Hydrometeorological conditions during observations varied essentially.

We have detected for the case of the quasi-one-dimensionally heterogeneous relief of the bottom a difference between the sea surface roughness above the shelf zone and the roughness at the deep bottom. The character of this difference depends on hydrometeorological conditions and the direction of sounding. Under stationary meteorological conditions, we observed regions of surface roughness attenuation (slicks) on the sea surface, which had the shape of strips with various radar contrasts extended approximately along the flow. We found that the inhomogeneities of the bottom topography can manifest as a change not only in the amplitude of different characteristics, but also in a frequency spectrum. Based on a wavelet-analysis of current-velocity data, we reveal the low-frequency scale of variations over the shelf induced by bottom topography, which, for different reasons, manifests itself in surface heaving and the atmospheric near-water layer.

The changeability of the wind waves above the two-dimensional heterogeneities of the bottom has more complex nature than in the case of the one-dimensionally heterogeneous bottom. In White Sea region with the secluded underwater hill streamlined with powerful currents was selected. Data about the field of current during different phases of tide are received. The special features of the flow of the powerful tidal current (to 1 m/s) around the secluded underwater elevation and the spatial structure of surface anomalies in the field of these two-dimensional- heterogeneous currents are analyzed.

The numerical simulation of the wind wave transformation in the field of two-dimensional- heterogeneous flows is carried out on the basis of kinetic equation for the spectral density of the wave action of surface waves. The qualitative agreement of the calculation results with the experimental data is shown.

This work was supported by the grant RFBR 08-05-00195, 09-05-10033, 10-05-10045, 11-05-10073, and 11-05-01143.

8532-24, Session 5

A method for cross-comparison of scatterometer data using natural distributed targets: application to ERS-1 and ERS-2 data during the tandem mission

Anis El Youncha, Xavier Neyt, Royal Belgian Military Academy (Belgium)

No Abstract Available

8532-25, Session 6

Oil films detection on the sea surface using an optical remote sensing method

Irina Sergievskaya, Stanislav A. Ermakov, Institute of Applied Physics (Russian Federation)

Film detection and identification on the ocean surface is a very important problem because of necessity of discrimination of oil spills cased by oil mining and transportation and film slicks of another origin (natural, biogenic pollution and etc). Manifestations of films in the sea surface optical images is connected with changing of reflected radiance due to strong depression of short gravity-capillary waves by film and due to changing of the reflection coefficient when light is reflected from two boundaries of the film. Variations of the sea surface radiance and possibilities to detect these variations in optical images of the sea surface depend on observation/illumination conditions, optical wavelength, surface waves and film parameters. In some cases low resolution optical systems (averaging over short gravity-capillary waves) are very effective for the film characterization. Contribution of different components: the sun/sky radiance reflected from the sea surface and the sun radiance backscattered from the water volume are analyzed. Marine films of different origin and with different parameters were used to calculate the surface wave spectrum in slick areas. First, natural marine and biogenic films which spread down to monomolecular layers were tested. Wave damping due to monomolecular films can be characterized by the elasticity and the surface tension coefficient. The surface tension coefficient for biogenic film is usually varied in the range from about 40 mN/m to 60 mN/m, while the elasticity ranges from some mN/m to about 30 mN/m or larger. Another tested films were crude oil and oil derivatives films. Wave damping due to oil films depends on more physical parameters, including the oil density, viscosity and elasticity of two film boundaries, etc. The wave damping due to oil films and the value of the radiance reflection coefficient from the sea surface are determined by the oil film thickness, too.

Slicks are assumed to be “visible” if fluctuations of the sea surface radiation become smaller than the variations of the mean radiance of the surface in slicks. The threshold values of the film elasticity (for monomolecular films) and thickness (for oil film with fixed parameters) at which slicks become “visible” on the sea surface are estimated. It was obtained that films with elasticity of some mN/m can be observed if the film area dimensions are comparable or larger than typical wavelengths of wind waves. The principal possibility of the estimation of film parameters is theoretically demonstrated. Experimental verification of the model is presented based on measurements of the sea surface radiance contrast in slicks with known film parameters. The measurements were carried out in field experiments with artificial slicks carried out from an Oceanographic Platform on the Black Sea using optical spectrum analysers and photometers at different sea states and geometry of observations. The experimental results are shown to be in good agreement with the discussed optical model.

This work has been supported by the Russian Foundation of Basic Research (projects 11-05-00295, 11-05-97027, 10-05-00101, 11-05-97029).

8532-26, Session 6

Direct problems of aerospace optical remote sensing of the ocean: Monte Carlo modeling

Boris A. Kargin, Arseny B. Kargin, Sergei M. Prigarin, Institute of Computational Mathematics and Mathematical Geophysics (Russian Federation)

The optical radiation field of the ocean-atmosphere system is formed to a great extent by the influence of the rough ocean surface which reflects and refracts incoming electromagnetic radiation. A typical feature of this influence is caused by the random character of the ocean surface’s wind-generated roughness. Because of this, a precise solution of a vast majority of direct and inverse problems of the ocean-atmosphere system optics is possible only in the statistical approach. The mathematical gist of such problems is in calculating corresponding functionals from the solution of the radiation transfer theory equation, defined on a random field, of which the rough ocean surface is an example. The Monte Carlo method was applied for the first time to calculation of solar radiation transfer in the ocean-atmosphere system, probably, in [1], where to describe the choppy ocean surface the so-called flat “facet” model was implemented, in which the boundary between air and water is a random surface comprising a set of elementary areas the centers of which lie in a single plane and the normals to the areas are distributed according to a certain one-point distribution function. The calculations in [1] utilized a direct modeling process of radiation transfer. The calculations in [1], therefore, were obtained without regard of overshadowing and re-reflection from the surface’s elements. In the paper [2] the optical properties of the rough ocean surface are already considered in a more adequate, spectral model of wind-driven waves, approach of which allows the Monte Carlo method to take into account the effects of overshadowing and re-reflection of radiation from surface elements. In [3] the integral stationary equation of radiation transfer in a medium with a randomly-inhomogeneous refracting boundary is written out and a weight algorithm for the solution of this equation by the Monte Carlo method is proposed. The current paper is dedicated to perfecting practical realization of this algorithm in connection with solving of practical problems of passive and active aerospace ocean probing within the bounds of several special-purpose grants. A numerical model of the optical radiation field of the ocean-atmosphere system is constructed. It is shown that simulation of the field of heights of the irregularities of the sea surface makes it possible to determine more accurately the optical characteristics of the wind-driven waves with an account of the effects of radiation re-reflection and shading by the surface elements. Mean energy of a return signal of an airborne lidar operating at various wavelengths under conditions of the wind-driven sea waves are estimated. It’s dependence on the wind velocity varying in the range 1 <= V <= 10 m/s, on the optical conditions, and on the experimental geometry is studied. The formation of lidar return received from the underwater is shown to be primarily determined by the sea surface state.

1. Plass G.N., Kattawar G.W. Radiative Transfer in an Atmosphere-Ocean System // Appl. Opt. 1969. V. 8, № 2. P. 455-466.

2. Kargin B.A., Prigarin S.M. Simulation of the sea surface roughness and study of its optical properties by the Monte Carlo method // Atmospheric and Oceanic Optics. 1992. V. 5, No.03. P. 186-192.

3. Kargin B.A., Rakimgulov K.B. A weighting Monte Carlo method for modelling the optical radiation field in the ocean-atmosphere system // Russ. J. Numer. Anal. Math. Modelling. 1992. V. 7, № 3. Р. 221-240.

8532-27, Session 6

Complex modulation of airborne lidar light pulse: the effects of rough sea surface and multiple scattering

Alexander G Luchinin, Institute of Applied Physics (Russian Federation)

An ocean airborne lidar design based on a complex modulated illuminating beam and the received echo signal processing is proposed, which involves the extraction of the modulated component and its matched filtering. A model of this lidar taking into account the effect of surface waves and multiple scattering in water is constructed. The lidar limiting longitudinal and transverse resolutions determined by random light refraction on the surface and scattering in water are estimated. The performed calculations enable us to make some conclusions on the advantages, disadvantages, and possible applications of the proposed lidar design.

We have shown that the use of complex modulated illuminating beams with subsequent compression of the received echo signal provides high resolution of lidar on all the three coordinates. This effect is due to an incoherent sum of the components of various scattering ratios at the modulation frequency. Therefore, it is possible to construct an underwater imaging system that uses such a beam and a receiver detecting the variable component and having a higher resolution. This effect is the stronger, the higher the modulating frequency range. At the same time, an increase of the operating range of modulating frequencies reduces the energy potential of lidar. This loss can be partially compensated using a long duration pulse. However, its duration cannot exceed the travel time of the probing signal from lidar to the bottom and back. The optimum range of modulating frequencies can be chosen only on the basis of a more accurate model of modulated beam propagation in scattering media. In particular, this model should give the correct asymptotic behavior at high frequencies, at which, as expected, a scattering medium behaves as a nonscattering medium with the absorption coefficient equal to the sum of the scattering and absorption coefficients.

8532-28, Session 6

Spatial structure of the sea level seasonal cycle within the Gulf of Cadiz

Irene M. Laiz, Begoña Tejedor, Jesús Gómez-Enri, Alazne Aboitiz, Pilar Villares, Univ. de Cádiz (Spain)

Sea level anomaly maps from high-resolution gridded multi-mission altimeter data (AVISO) have been retrieved for the Gulf of Cadiz for the time period 1997-2008, along with maps of Dynamic Atmospheric Correction (DAC), atmospheric pressure at sea level from the European Centre for Medium-Range Weather Forecast (ECMWF) and satellite Sea Surface Temperature (SST) from the 4 km AVHRR Pathfinder Version 5 SST Project. Data were averaged in time to obtain maps of monthly mean time series in order to analyze the seasonal variability of sea level and its main forcing agents along the Gulf of Cadiz. Moreover, a very high resolution climatology (0.05º x 0.05º) for the Gulf of Cadiz provided by the GeoHydrodynamics and Environment Research group of the University of Liège was combined with the SST maps in order to explore the steric contribution on sea level with enough spatial resolution near the coast. While both the inverse barometer correction and the DAC have a similar offshore performance in this region in terms of percentage of explained variance, the former provides better results near the coast. Thus, the AVISO sea level anomaly monthly maps were initially de-corrected using the DAC product and then corrected using the classical inverse barometer method. Atmospheric pressure explained more than 55% of the offshore sea level variance and between 35-45% of the sea level variance within the continental shelf. The amplitude of the pressure-adjusted sea level semiannual signal was considerably reduced, confirming its meteorological origin. Special attention was paid to the steric contribution on the pressure-adjusted sea level. Steric heights were calculated for each of the combined SST-climatology profile locations using either 500m for the open ocean or the maximum depth for coastal waters as the reference level, and used to correct the pressure-adjusted sea level for what we defined as “local steric contribution”. Furthermore, the steric contribution was divided into “basin-wide” “western continental shelf” and “eastern continental shelf” contributions, respectively, by averaging the steric heights over the open ocean (i.e., offshore of 500 m depth), and over the western and eastern continental shelves, correspondingly. While the “basin-wide” steric contribution was used to correct the pressure-adjusted sea level over the whole basin, the “western/eastern shelf” contributions were only used to correct the pressure-adjusted sea level over the corresponding continental shelf. Overall, the “basin-wide” contribution explained a higher percentage of variance than the “local” or the “western/eastern” contributions all over the basin with the exception of the western continental shelf, where the best results were obtained with the “local steric contribution”. After correcting for the best steric contribution, the amplitude of the remaining offshore annual signal is negligible, oscillating between 0.5-1.0 cm (± 1 cm). As for the continental shelves, although the steric contribution reduced the amplitude of the annual signal in 1-2 cm, there are still 2-3 cm (± 0.5-1 cm) unexplained, probably due to local effects related with the shelves dynamics. The combination of SST maps with a very high resolution climatology has proved a valuable tool to explore the steric contribution near the coast.

8532-49, Session 6

Coupling ocean models and satellite derived optical fields to estimate LIDAR penetration and detection performance

Sergio deRada, Sherwin Ladner, Robert A. Arnone, U.S. Naval Research Lab. (United States)

A global-scale climatological assessment of the temporal and spatial relationships between physical and optical ocean layers was previously performed to determine LIDAR efficiency for measuring the 3D Ocean. That effort provided estimates of laser sensor penetration depth (PD) in the global oceans and identified critical coupling between Mixed Layer Depth (MLD) and Optical Depth (OD) based on potential laser power and ensuing attenuation. We make use of a Bio-Physical ocean model configured for the Gulf of Mexico (GOM) along with remotely sensed satellite measurements to examine LIDAR performance in the Gulf of Mexico coastal regions. The 4Km GOM ocean model runs in near-real-time and produces physical and bio-optical fields which are coupled to in-house derived satellite bio-optical products such as the Diffuse Attenuation Coefficient at 490nm (Kd490). PD and MLD are coupled to determine laser power efficiency rates across multiple attenuation lengths. The results illustrate the potential utilization of spaceborne oceanographic LIDAR to penetrate through the water column, elucidating its applicability for a variety of scientific (characterization of the ocean subsurface layers) and applied (target detection) objectives.

Conference 8533: Sensors, Systems, and Next-Generation Satellites

Monday - Thursday 24–27 September 2012 • Part of Proceedings of SPIE Vol. 8533 Sensors, Systems, and Next-Generation Satellites XVI

8533-1, Session 1

Status of ESA Science Earth Observation missions: The Explorers (Invited Paper)

Paolo Bensi, Roland Meynart, European Space Research and Technology Ctr. (Netherlands)

The Earth Explorer missions are the backbone of the European Space Agency Living Planet Programme, providing an important contribution to the global endeavour of understanding the Earth's System, particularly in view of global climate change. The missions are driven by the scientific needs to advance the understanding of how the ocean, atmosphere, cryosphere and Earth's interior processes interact as part of an interconnected system. These research missions, exploiting European excellence in science and technological innovation, pave the way towards new development of future Earth Observation applications.

The presentation provides a summary about the status of the Earth Explorer missions in operation and in their final development stage as well as an overview of the candidate missions competing to become the 7th and 8th Earth Explorer and for which preparatory activities are currently in progress.

[1] European Space Agency (2008) Candidate Earth Explorer Core Missions – Reports for Assessment, ESA SP-1313(5), Mission Science Division, ESA-ESTEC, Noordwijk, The Netherlands, ISSN 0379-6566, 104pp, available at http://www.congrex.nl/09c01/

[2] European Space Agency (2006) The Changing Earth: New scientific challenges for ESA's Living Planet Programme. ESA SP1304, see also http://www.esa.int/esaLP

8533-2, Session 1

Status of ESA Application Earth Observation missions: meteorology and GMES

Roland Meynart, European Space Research and Technology Ctr. (Netherlands)

No Abstract Available

8533-3, Session 2

Japanese Earth observation programs *(Invited Paper)*

Haruhisa Shimoda, Tokai Univ. (Japan)

Five programs, i.e. TRMM, ADEOS2, ASTER, and GOSAT are going on in Japanese Earth Observation programs. PR on TRMM and ASTER on EOS-Terra are operating well except SWI channels of ASTER. ASTER SWI channels have stopped the operation because of a refrigerator failure in 2009. ADEOS2 was failed, but AMSR-E on Aqua was operating until 14, Oct. 2011. AMSR-E has stopped at that time because of the antenna driving mechanism's torque increase. Now, AMSR-E instrument has been on from March 2012 without antenna rotation. SMILES is now on JEM of ISS. SMILES is a sub-millimeter limb sounding instrument using super conducting mixer and measures stratospheric ozone and related compounds. Unfortunately, SMILES stopped its operation on 21, April, 2010. ALOS was launched on 24, Jan., 2006 and stopped on 22, April, 2011 by power anomaly. ALOS carried three instruments, i.e., PRISM, AVNIR-2 and PALSAR. PRISM is a 3 line panchromatic push broom scanner with 2.5m IFOV. AVNIR-2 is a 4 channel multi spectral scanner with 10m IFOV. PALSAR is a full polarimetric active phased array SAR. GOSAT was launched on 23, Jan., 2009. GOSAT carries 2 instruments, i.e. a green house gas sensor (TANSO-FTS) and a cloud/aerosol imager (TANSO-CAI). TANSO-FTS is a Fourier transform spectrometer (FTS) and covers 0.76 to 15 μm region with 0.2 cm-1 resolution. TANSO-CAI is a 5 channel push broom scanner to observe aerosols and clouds. Both sensors are operating well. Next generation satellites will be launched in 2012-2015 timeframe. They are GCOM-W1, GCOM-C1, GPM core satellite, EarthCare, ALOS2 and ALOS3. GCOM-W1 will carry AMSR2. The orbit is A-train and has higher resolution than AMSR-E. GCOM-W1 will be launched on May, 2012. GCOM-C1 will carry SGLI. SGLI has polarization channels. GCOM-C will be launched on 2015. GPM is a joint project with NASA and will carry two instruments. JAXA is developing DPR. DPR has Ka band channel in addition to Ku band channel. GPM will be launched on 2013. Another project is EarthCare. It is a joint project with ESA and JAXA is going to provide CPR with NICT. EarthCare will be launched on 2015. ALOS F/O is composed by 2 satellites like GCOM. One is called ALOS-2 and will carry L-band SAR while the other is called ALOS-3 and will carry optical sensors. ALOS-2 will be launched on 2013.

8533-4, Session 2

Onboard calibration of the ASTER instrument over twelve years

Fumihiro Sakuma, Masakuni Kikuchi, Japan Resources Observation System and Space Utilization Organization (Japan); Hitomi Inada, NEC TOSHIBA Space Systems, Ltd. (Japan); Shigeki Akagi, Mitsubishi Electric Corp. (Japan); Hidehiko Ono, Fujitsu Ltd. (Japan)

The ASTER Instrument is one of the five sensors on the NASA's Terra satellite on orbit since December 1999. ASTER consists of three radiometers, VNIR, SWIR and TIR whose spatial resolutions are 15 m, 30 m and 90 m, respectively. Unfortunately SWIR stopped taking pictures since May 2008 due to the offset rise caused by the cooler temperature rise, but VNIR and TIR are taking Earth pictures of good quality. VNIR and TIR experienced responsivity degradation while SWIR showed little change. Band 1 decreased 30 % in eleven years and most among three VNIR bands. Band 12 (9.1 m) decreased 40 % and most among five TIR bands. There are some discussions of the causes of the responsivity degradation of VNIR and TIR. Possible causes are contamination accretion by silicone outgas, thruster plume and plasma interaction. We marked hydrazine which comes out unburned in the thruster plume during the inclination altitude maneuver (IAM). Hydrazine has the absorption spectra corresponding to the TIR responsivity degradation in the infrared region. We studied the IAM effect on the ASTER by allocating the additional onboard calibration activities just before and after the IAM while the normal onboard calibration activity is operated once in 49 days. This experiment was carried out three times, October 16 (IAM #29) and 19 (IAM #30) in 2011 and February 23 in 2012 (IAM #31). The burn time was 320 seconds for each IAM. As a draft result TIR showed small changes in radiometric calibration coefficients (RCC) while VNIR showed almost no effect. The change of the spectral response was almost independent of the TIR bands. The change in IAM #30 was about two thirds of that of IAM #29.

8533-5, Session 2

The current status of GOSAT and the concept of GOSAT-2

Masakatsu Nakajima, Akihiko Kuze, Hiroshi Suto, Japan Aerospace Exploration Agency (Japan)

GOSAT was launched almost 3 and half years ago, and the calibration and validation activities have been continued.

Based on these cal/val activities, the data processing algorithm have been improved a few times. In April of 2012, the latest version of the level 1B algorithm, version 150 was released and the re-processing of the all data that had been obtained until the release of the latest version had been performed in parallel with the nominal precessing of new data. Until now in addition to the level 1B data,which is the spectrum, the higher level products have been disclosed to public users as well as PIs. The results of the three and half years operation will be summarized in this presentation at first.

GOSAT has accomplished certain results and we have recognized the availability of the GHG observation from space. And it has been

required to expand this mission for real to make it useful for mankind. So Japan's three parties, Ministry of the Environment(MOE), National Institute for Environmental Studies(NIES) and JAXA which have led the GOSAT project have studied the requirements for the greenhouse gases observations from space. And we defined them with a goal of the contribution to the policies on the climate changes such as the decision of the emission reduction targets based on the scientific facts, the monitor of the emission reduction efforts and so on. It is assumed that these goals will be acheved by a few generatios of the GOSAT follow on.

So we have studied that how much level GOSAT-2 should aim to improve the concentration measurement precison and estimation error of the fluxes as the step toward realization of these requirements and have determined the measurement accuracy target of Carbon Dioxide concentrarion as 0.5 ppm at 500km and 2,000km mesh spatial resolution over the land and ocean, respectively and 1 month average.

To acheve this target, GOSAT-2 will continuously adopt the Fourier Transform Spectrometer (FTS) as the instrument to measure the carbon dioxide and methane, and will equip the imager to compensate the FTS data.

To achieve the requirements, the performance of these instruments will be improved, for example the new observation band to measure the carbon monoxide will be added to FTS and the observation band in UV of CAI will adopt the grating spectrometer for the measurement of NO2 and to improve the aerosol retrievals

In addition to these improvements, we will conduct the increase in the number of the effective data by a number of FOVs and reduction of the diameter of FOV.

The diamter of FOV of GOSAT is 10.5km and this large diameter make it easy to be contaminated by the clouds. And it's possible to reduce the influence of the clouds by the small FOV.

Following the presentation of the GOSAT observation results, the requirements for GOSAT-2 and the specification of the satellite and two mission instruments will be shown with the results of the studied concerning the improvements of the mission instruments.

8533-6, Session 2

Status of AMSR2 on GCOM-W1

Marehito Kasahara, Keiji Imaoka, Misako Kachi, Japan Aerospace Exploration Agency (Japan); Hideyuki Fujii, The University of Tokyo (Japan); Kazuhiro Naoki, Takashi Maeda, Norimasa Ito, Keizo Nakagawa, Japan Aerospace Exploration Agency (Japan); Taikan Oki, The Univ. of Tokyo (Japan)

The Global Change Observation Mission (GCOM) consists of two polar orbiting satellite observing systems, GCOM-W (Water) and GCOM-C (Climate), and three generations to achieve global and long-term monitoring of the Earth. GCOM-W1, the first satellite of the GCOM-W series, is scheduled for launch on May 18, 2012. The satellite system is already at the Tanegashima Space Center, from where the satellite will be launched, and all the final preparations are underway. On October 4, 2011, the Advanced Microwave Scanning Radiometer for the Earth Observing System (AMSR-E) halted its observation due to the increase of antenna rotation torque. Although all the efforts are being made to resume the AMSR-E observation, early initiation of the Advanced Microwave Scanning Radiometer-2 (AMSR2) observation is highly desired. Development of the ground segment, including systems for receiving, processing, archiving, and distributing the GCOM-W1 data, is also completed. At-launch retrieval algorithms were also delivered to the ground segment and used for the final testing. These algorithms will be validated and updated through calibration and validation activities. Regarding the validation activity, some of the preparations of validation sites are still underway, such as the installation of the flux tower observing instruments into the Murry-Darling basin in Australia for land parameter validation. Public data release is scheduled one year after launch for geophysical parameters, and more earlier for Level-1 products. Standard products will be available via online, free of charge, from the GCOM-W1 data providing service system. The AMSR-E products are already available from the same system.

8533-7, Session 3

LAND VALIDATION for GCOM-C1/SGLI using UVA *(Invited Paper)*

Yoshiaki Honda, Chiba Univ. (Japan)

Japan Aerospace Exploration Agency (JAXA) is going to launch new Earth observation satellite GCOM-C1 in near future. The core sensor of GCOM-C1, Second Generation Global Imager (SGLI) has a set of along track slant viewing Visible and Near Infrared Radiometer (VNR). These multi-angular views aim to detect the structural information from vegetation canopy, especially forest canopy, for estimating productivity of the vegetation. SGLI Land science team has been developing the algorithm for above ground biomass, canopy roughness index, shadow index, etc.

In this paper, we introduce the ground observation method developed by using Unmanned Aerial Vehicle (UAV) in order to contribute the algorithm development and its validation. Mainly, multi-angular spectral observation method and simple BRF model have been developed for estimating slant view response of forest canopy. The BRF model developed by using multi-angular measurement has been able to obtain structural information from vegetation canopy. In addition, we have conducted some observation campaigns on typical forest in Japan in collaboration with other science team experienced with vegetation phenology and carbon flux measurement. Primary results of these observations are also be demonstrated.

8533-8, Session 3

Status of proto-flight model of the dual-frequency precipitation radar for the global precipitation measurement

Takeshi Miura, Masahiro Kojima, Kinji Furukawa, Yasutoshi Hyakusoku, Takayuki Ishikiri, Hiroki Kai, Japan Aerospace Exploration Agency (Japan); Toshio Iguchi, Hiroshi Hanado, Katsuhiro Nakagawa, National Institute of Information and Communications Technology (Japan)

The Dual-frequency Precipitation Radar (DPR) on the Global Precipitation Measurement (GPM) core satellite is being developed by Japan Aerospace Exploration Agency (JAXA) and National Institute of Information and Communications Technology (NICT). The GPM is a follow-on mission of the Tropical Rainfall Measuring Mission (TRMM). The objectives of the GPM mission are to observe global precipitation more frequently and accurately than TRMM. The frequent precipitation measurement about every three hours will be achieved by some constellation satellites with microwave radiometers (MWRs) or microwave sounders (MWSs), which will be developed by various countries. The accurate measurement of precipitation in mid-high latitudes will be achieved by the DPR. The GPM core satellite is a joint product of National Aeronautics and Space Administration (NASA), JAXA and NICT. NASA is developing the satellite bus and the GPM microwave radiometer (GMI), and JAXA and NICT are developing the DPR. JAXA and NICT are developing the DPR through procurement. The contract for DPR is NEC TOSHIBA Space Systems, Ltd. The configuration of precipitation measurement using an active radar and a passive radiometer is similar to TRMM. The major difference is that DPR is used in GPM instead of the precipitation radar (PR) in TRMM. The inclination of the core satellite is 65 degrees, and the flight altitude is about 407 km. The non-sun-synchronous circular orbit is necessary for measuring the diurnal change of rainfall similarly to TRMM. The DPR consists of two radars, which are Ku-band (13.6 GHz) precipitation radar (KuPR) and Ka-band (35.55 GHz) precipitation radar (KaPR). According to the different detectable dynamic ranges, The KaPR will detect snow and light rain, and the KuPR will detect heavy rain. In an effective dynamic range in both KuPR and KaPR, drop size distribution information and more accurate rainfall estimates will be provided by a dual-frequency algorithm. The proto-flight test for DPR have finished in February 2012. The status of proto-flight model of DPR will be presented.

8533-9, Session 3

ALOS-2 development status and draft acquisition strategy

Shinichi Suzuki, Yukihiro Kankaku, Yuji Osawa, Japan Aerospace Exploration Agency (Japan)

The Advanced Land Observing Satellite-2 (ALOS-2) will succeed to the radar mission of the ALOS "Daichi" which had contributed to cartography, regional observation, disaster monitoring, and resources surveys for more than 5 years until its termination of operation in May 2011.

The state-of-the-art L-band Synthetic Aperture Radar (SAR) called PALSAR-2 onboard ALOS-2 will have enhanced performance in both high resolution (1m * 3m at finest in the Spotlight mode) and wide swath (up to 490km in the ScanSAR wide mode), compared to ALOS / PALSAR. It will allow comprehensive monitoring of disasters such as inundated area caused by Tsunami. Wider bandwidth and shorter revisit time will give better conference for INSAR data analysis such as crustal deformation and deforestation. Also the burst timings between different image acquisitions are synchronized to obtain successful interferometry for the ScanSAR mode.

The SAR antenna consists of 5 panels with total 1,080 radiation elements which are driven by 180 Transmit-Receive-Modules (TRMs) in order to steer and form a beam in both range and azimuth direction. In order to reduce range ambiguities, PALSAR-2 is capable to transmit up or down chirp signal alternatively and has phase modulation with zero or pi as well. The Proto Flight Model of ALOS-2 including PALSAR-2 is under integration and testing at JAXA's Tsukuba Space Center and the system performance such as SAR antenna pattern is being evaluated.

Since more acquisition modes of PALSAR-2 than those of PALSAR may trigger more conflicts among user requests, systematic acquisition strategy is very important to achieve the mission requirements. For example, trade-off studies have been made for INSAR basemap data acquisition through discussion with user groups, and an optimum scenario was proposed to fulfill both requirements for quick response and time-series data acquisition under a same condition (incidence angle, descending/ascending, left/right look). As the ALOS data resulted in a comprehensive and homogeneous global archive, consistent data archives will be requested for ALOS-2 as well.

This paper describes the current development status of ALOS-2 and a draft acquisition strategy for PALSAR-2.

8533-10, Session 3

A conceptual design of PRISM-2 for Advanced Land Observing Satellite-3(ALOS-3)

Hiroko Imai, Haruyoshi Katayama, Masakazu Sagisaka, Yasushi Hatooka, Shinichi Suzuki, Yuji Osawa, Masuo Takahashi, Takeo Tadono, Japan Aerospace Exploration Agency (Japan)

The Advanced Land Observing Satellite (ALOS) "DAICHI" launched in January 2006 was operated successfully on orbit for more than five years. About 6.5 million scenes of images over the Earth acquired by ALOS's three sensors contributed to a variety of fields including cartography, regional observation, disaster monitoring, etc.

The acquired images of the Panchromatic Remote-sensing Instrument for Stereo Mapping (PRISM), one of ALOS's sensors, are very useful for extracting topography, producing and updating a map with 1:25,000 scale. The timely updated geographical information such as topographic maps, land-use and land-cover, and vegetation, is required by users. In addition, the importance of disaster monitoring has been clarified by the last great earthquake and subsequent tsunami in mainly Tohoku region, Japan on March 11, 2011, which caused great damage in huge areas. ALOS's wide coverage could contribute to understanding of the serious damages just after the disaster. The precise images obtained by satellites with wide coverage and high geo-location accuracy will be increasingly important for reconstruction work in recovery phase.

The Japan Aerospace Exploration Agency (JAXA) is planning a satellite system including ALOS-2 and ALOS-3 for the ALOS follow-on program. ALOS-3 will carry the optical sensor named "PRISM-2" and succeed ALOS missions with enhanced capabilities. PRISM-2 will have a capability to collect high resolution (0.8 m) and wide swath (50 km) images with high geo-location accuracy without ground control points by utilizing the precise geo-location determination techniques developed for ALOS. PRISM-2 will acquire stereo pair images with two telescopes for stereo mapping and precise digital surface models (DSMs). These capabilities are ideal for the large scale geographical information including elevation and land cover-map that will be used in many research areas and practical applications including disaster management support.

It is also being considered to carry Hyper-spectral Imager Suite (HISUI), which is developed by the Ministry of Economy, Trade and Industry (METI) of Japan. HISUI is composed of multispectral sensor with four spectral bands in visible and near infrared and hyperspectral sensor in the wavelength region from visible to short infrared. A combination of high resolution stereoscopic images and hyperspectral imagery has a possibility to create new applications.

JAXA has conducted the phase-A study on ALOS-3 spacecraft and mission instruments, and now is working on prototype of the light-weight large mirror for PRISM-2's telescope using off-axis three mirror anastigmatic (TMA) technique, and CCDs for large-format detector array. JAXA is also developing a high-speed, high-capacity data recorder that will realize Gbps data I/O and TByte capacity. In addition, a system utilizing an advantage of the next data relay satellite will enable the transmission of global observation data.

8533-11, Session 3

Effect of temperature on onboard calibration reference material for spectral response functions retrieval of the hyperspectral sensor of HISUI-SWIR spectral case

Kenji Tatsumi, Jun Tanii, Hisashi Harada, Toneo Kawanishi, Fumihiro Sakuma, Japan Space Systems (Japan); Hitomi Inada, Takahiro Kawashima, NEC TOSHIBA Space Systems, Ltd. (Japan); Akira Iwasaki, The Univ. of Tokyo (Japan)

HISUI (Hyperspectral Imager SUIte) is the next Japanese earth observation sensor, which is composed of hyperspectral and multispectral sensors. The hyperspectral sensor is an imaging spectrometer with the VNIR(400-970nm) and the SWIR(900-2500nm) spectral channels. Spatial resolution is 30 m with spatial swath width of 30km. The spectral resolution will be better than 10nm in the VNIR and 12.5nm in the SWIR. The multispectral sensor has four VNIR spectral bands with spatial resolution of 5m and swath width of 90km. HISUI will be installed in ALOS-3 which is an earth observing satellite by JAXA. It will be launched in FY 2015.

Prelaunch calibration of any remote sensing instrument is essential and usually carried out in ground-based satellite test facilities. However, the parameters associated with the instrument radiometric and spectral calibrations might change after launch into space. Such changes are mostly due to mechanical vibrations/shocks, temperature and pressure changes at the moment of launch or due to ageing-driven degradation of the instrument during flight. Typically, shifts in channel wavelengths and broadenings in spectral bandwidth of spectral response functions (SRFs) are likely to occur for hyperspectral sensor due to the distortion in the spectrometer, the optics and the detector assembly. It was pointed out that accuracy of the radiance measured by imaging spectrometers in the solar-reflected spectrum is sensitive to the accuracy of the spectral calibration, so a spectral uncertainty approaching 1% is necessary to suppress the error in measured radiance spectrum.

Several approaches have been developed to deal with the onboard spectral calibration of the hyperspectral sensors. We have studied and reported the onboard wavelength calibration method using the combination of a calibration reference material (NIST:SRM2065) and a tungsten-halogen lamp. The measured data profile on board is compared with pre-flight test data profile. The wavelength shift and broadening of the SRFs are estimated by using the spectrum matching technique.

This paper is concerned with the effect of temperature on the calibration reference material for SRFs retrieval of the hyperspectral sensor. Since the location and intensity of absorption features are sensitive to material temperature, the estimated center wavelength and bandwidth of the SRFs may include the uncertainty. Therefore it is necessary to estimate the deviation of the wavelength and the bandwidth broadening of the SRFs when the material temperature changes. In this paper we describe the simulation model, the

evaluation of the center wavelength shift, bandwidth broadening and the uncertainty of the SRF's retrieval of SWIR spectral channels. We also show some simulation's results.

8533-12, Session 3

EarthCARE/CPR design and verification status

Kazuyuki Okada, Toshiyoshi Kimura, Hirotaka Nakatsuka, Yoshihiro Seki, Gaku Kadosaki, Jun Yamaguchi, Japan Aerospace Exploration Agency (Japan); Nobuhiro Takahashi, Yuichi Ohno, Hiroaki Horie, Kenji Sato, National Institute of Information and Communications Technology (Japan)

The Earth Clouds, Aerosols and Radiation Explorer (EarthCARE) mission is joint mission between Europe and Japan for the launch year of 2015. Mission objective is to improve scientific understanding of cloud-aerosol-radiation interactions that is one of the biggest uncertain factors for numerical climate and weather predictions. The EarthCARE spacecraft equips four instruments such as an ultra violet lidar (ATLID), a cloud profiling radar (CPR), a broadband radiometer (BBR), and a multi-spectral imager (MSI) and perform complete synergy observation to observe aerosols, clouds and their interactions simultaneously from the orbit. Japan aerospace exploration agency (JAXA) is responsible for development of the CPR in this EarthCARE mission and the CPR will be the first space-borne W-band Doppler radar. The CPR is defined with minimum radar sensitivity of -35dBz (6dB better than current space-borne cloud radar, i.e. CloudSat, NASA), radiometric accuracy of 2.7 dB, and Doppler velocity measurement accuracy of 1m/s. These specifications require highly accurate pointing technique in orbit and high power source with large antenna dish. JAXA and National Institute of Information and Communications Technology (NICT) have been jointly developed this CPR to meet these strict requirements so far and then achieved the development such as new CFRP flex-core structure, long life extended interaction klystron, low loss quasi optical feed technique, and so on. Through these development successes, CPR development phase has been progressed to critical design phase with almost completion of engineering model testing. In addition, new ground calibration technique is also being progressed for launch of EarthCARE/CPR. This evaluation method will also be the first use for spacecraft as well as Doppler cloud radar.

This presentation will show the summary of the CPR design and CPR EM testing status, and activity status of development of ground calibration method with a few results of experiment using current space-borne cloud radar.

8533-13, Session 4

NASA Earth Science Flight Program *(Invited Paper)*

Steven P. Neeck, Stephen M. Volz, NASA Headquarters (United States)

Earth is a complex, dynamic system we do not yet fully understand. The Earth system, like the human body, comprises diverse components that interact in complex ways. We need to understand the Earth's atmosphere, lithosphere, hydrosphere, cryosphere, and biosphere as a single connected system. Our planet is changing on all spatial and temporal scales. The purpose of NASA's Earth Science Division (ESD) is to develop a scientific understanding of Earth's system and its response to natural or human-induced changes, and to improve prediction of climate, weather, and natural hazards. A major component of NASA's ESD and residing in its Flight Program is a coordinated series of satellite and airborne missions for long-term global observations of the land surface, biosphere, solid Earth, atmosphere, and oceans. This coordinated approach enables an improved understanding of the Earth as an integrated system. NASA is completing the development and launch of a set of Foundational missions, Decadal Survey missions, and Climate Continuity missions. As a result of the recent launches of the Aquarius/SAC-D and Soumi National National Polar-orbiting Partnership (NPP) satellites, 16 missions are currently operating on-orbit and the Flight Program has three mission in development and a further eight Decadal Survey and Climate Continuity missions under study. Technology development is continuing for a remaining five third tier Decadal Survey mission. Plans are well underway for the selection of the first Earth Venture (EV) low to moderate cost, small to medium-sized full orbital mission. The EV-1 sub-orbital projects continue in implementation. Instruments for orbital missions of opportunity and the second set of EV sub-orbital projects are also being planned. An overview of plans and current status will be presented.

8533-14, Session 4

Global Precipitation Measurement (GPM) L-18

Steven P. Neeck, Ramesh K. Kakar, NASA Headquarters (United States); Ardeshir A. Azarbarzin, Arthur Y. Hou, NASA Goddard Space Flight Ctr. (United States)

The Global Precipitation Measurement (GPM) mission is an international network of satellites that provide the next-generation global space-based observations of rain and snow. Building upon the success of the Tropical Rainfall Measuring Mission (TRMM), the GPM concept centers on the deployment of a Core Observatory carrying an advanced radar / radiometer system to measure precipitation from space and serve as a reference standard to unify precipitation measurements from a constellation of research and operational satellites. Through improved measurements of precipitation globally, the GPM mission will help to advance our understanding of Earth's water and energy cycle, improve forecasting of extreme events that cause natural hazards and disasters, and extend current capabilities in using accurate and timely information of precipitation to directly benefit society. GPM, initiated by NASA and the Japan Aerospace Exploration Agency (JAXA) as a global successor to TRMM, comprises a consortium of international space agencies, including the Centre National d'Études Spatiales (CNES), the Indian Space Research Organisation (ISRO), the National Oceanic and Atmospheric Administration (NOAA), the European Organisation for the Exploitation of Meteorological Satellites (EUMETSAT), and others. The GPM Core Observatory is currently in its system level environmental test program (Phase D) following delivery and integration of the two science instruments, the JAXA Dual-frequency Precipitation Radar (DPR) and the NASA GPM Microwave Imager (GMI). Launch is scheduled for February 2014 from JAXA's Tanegashima Space Center on a H-IIA launch vehicle.

8533-15, Session 4

Surface Water and Ocean Topography (SWOT) Mission

Steven P. Neeck, Eric J. Lindstrom, NASA Headquarters (United States); Parag V. Vaze, Lee-Lueng Fu, Jet Propulsion Lab. (United States)

The Surface Water Ocean Topography (SWOT) mission was recommended in 2007 by the National Research Council's Decadal Survey, "Earth Science and Applications from Space: National Imperatives for the Next Decade and Beyond", for implementation by NASA. The SWOT mission is a partnership between two communities, the physical oceanography and the hydrology, to share high vertical accuracy and high spatial resolution topography data produced by the science payload, principally a Ka-band radar Interferometer (KaRIn). The SWOT payload also includes a precision orbit determination system consisting of GPS and DORIS receivers, a Laser Retro-reflector Assembly (LRA), a Jason-class nadir radar altimeter, and a JASON-class radiometer for tropospheric path delay corrections. The SWOT mission will provide large-scale data sets of ocean sea-surface height resolving scales of 15km and larger, allowing the characterization of ocean mesoscale and submesoscale circulation. The SWOT mission will also provide measurements of water storage changes in terrestrial surface water bodies and will provide estimates of discharge in large (wider than 100m) rivers, globally. The SWOT measurements will provide a key complement to other NASA spaceborne global measurements of the water cycle measurements by directly measuring the surface water (lakes, reservoirs, rivers, and wetlands) component of the water cycle. The SWOT mission is an international partnership between NASA and the Centre National d'Etudes Spatiales (CNES). The Canadian Space Agency (CSA) is also expected to contribute to the mission. SWOT is currently preparing to enter Formulation (Phase A).

8533-16, Session 4

JPSS instrument transition to NASA and development status

Chris W. Brann, NASA Goddard Space Flight Ctr. (United States)

The Joint Polar Satellite System (JPSS) Program is a co-operative program between the National Aeronautics and Space Agency (NASA) and the National Oceanic and Atmospheric Administration (NOAA) to design, develop, and fly the next suite of US civilian polar orbiting environmental sensing instruments. The JPSS Program is a product of the restructuring of the National Polar-orbiting Operational Environmental Satellite System (NPOESS) Program, which occurred in 2010. The JPSS Program will satisfy the requirements for collection of global multi-spectral radiometry and other specialized meteorological, oceanographic, and solar-geophysical data via remote sensing of land, sea, and atmospheric data. This data is necessary for meteorological and global climate observation and tracking.

The first JPSS satellite is scheduled for launch in 2016. Each JPSS Flight Satellite is comprised of five instruments, Advanced Technology Microwave Sounder (ATMS), Cloud and Earth's Radiant Energy System (CERES), Cross-track Infrared Sounder (CrIS), Ozone Mapping and Profiler Suite (OMPS), and Visible/Infrared Imager Radiometer Suite (VIIRS).

The Goddard Space Flight Center (GSFC) is responsible for overall implementation of the JPSS Flight Mission. GSFC has issued contracts to industry for the spacecraft development with Ball Aerospace Technology Corporation (BATC); to Raytheon Space and Airborne Systems (RSAS) for VIIRS; to BATC for OMPS; to Exelis for CrIS; and to Northrop Grumman Electronic Systems (NGES) for ATMS. Langley Research Center (LaRC) is responsible for CERES and has issued a contract to Northrop Grumman Aerospace Systems (NGAS) for CERES. The Kennedy Space Center is responsible for launch services.

The ATMS instrument, a cross-track scanner with 22 channels, providing sounding observations needed to retrieve profiles of atmospheric temperature and moisture for civilian operational weather forecasting as well as continuity of these measurements for climate monitoring purposes. The CrIS instrument, a Fourier transform spectrometer with 1305 spectral channels, produces high-resolution, three-dimensional temperature, pressure, and moisture profiles. VIIRS, a scanning radiometer, collects visible and infrared imagery and radiometric measurements of the land, atmosphere, cryosphere, and oceans. OMPS, an advanced suite of three hyper-spectral instruments, extends the 25-plus year total-ozone and ozone-profile records. CERES is a three-channel radiometer that measures both solar-reflected and Earth-emitted radiation from the top of the atmosphere to the surface. It also determines cloud properties including the amount, height, thickness, particle size, and phase of clouds using simultaneous measurements by other instruments.

The 2010 launch of the Suomi National Polar-orbiting Partnership (NPP) satellite consists of the same five instruments planned for operations with the JPSS program. NPP was initially intended to not only provide valuable science, but also provide critical lessons learned and risk reduction for the follow on instruments. With the transition to NASA, the JPSS instruments have undergone significant review with numerous updates to the designs as well as made significant progress toward delivering a superior capability to the Nation. This paper will discuss the program transition as it relates to the instruments and the associated transition review efforts, key findings, important changes to the instruments for JPSS and their current development status. The VIIRS instrument will be presented separately.

8533-75, Session PS

The Hyperspectral Infrared Imager (HyspIRI) and supporting projects (stand-by oral presentation)

Simon J. Hook, Elizabeth M. Middleton, Robert O. Green, Jet Propulsion Lab. (United States)

In 2004, the National Aeronautics and Space Administration (NASA), the National Oceanic and Atmospheric Administration (NOAA), and the U.S. Geological Survey (USGS) requested the National Research Council (NRC) identify and prioritize the satellite platforms and associated observational capabilities that should be launched and operated over the next decade for Earth observation. The resulting NRC study Earth Science and Applications from Space: National Imperatives for the Next Decade and Beyond, also known as the Earth Science Decadal Survey, (NRC, 2007) recommended launching 15 missions in three time phases. These three time phases are referred to as Tier 1, Tier 2, and Tier 3, respectively. The Hyperspectral Infrared Imager (HyspIRI) mission is one of the Tier 2 missions recommended for launch in the 2013–2016 timeframe.

HyspIRI is a global mission designed to address a critical set of questions on how the surface of the earth and in particular ecosystems, are responding to natural and human-induced changes. It will help us assess the status of biodiversity around the world and the role of different biological communities on land and within inland water bodies. It will provide critical information on wildfires and the emissions from them as volcanic eruptions. The mission will advance our scientific understanding of how the Earth is changing as well as provide valuable societal benefit, in particular, in understanding and tracking dynamic events such as volcanoes and wildfires.

The HyspIRI mission includes two instruments: a visible shortwave infrared (VSWIR) imaging spectrometer operating between 0.38 and 2.5 μm at a spatial scale of 60 m with a swath width of 145 km and a thermal infrared (TIR) multispectral scanner operating between 4 and 12 μm at a spatial scale of 60 m with a swath width of 600 km. The VSWIR and TIR instruments have revisit times of 19 and 5 days, respectively. Several of the other Decadal Survey missions provide complementary measurements for use with HyspIRI data albeit at much coarser spatial scales compared to the local and landscape scales observable with HyspIRI. While the synergy between HyspIRI and other sensors, including those on operational satellites, benefits all missions and would support relevant scientific endeavors, the ability of HyspIRI to achieve its primary mission goals is not dependent on data from these other instruments.

General scientific guidance for the activities associated with HyspIRI is provided by the NASA appointed HyspIRI Science Study Group (SSG). The SSG includes experts from Academia, Government and Industry who will ultimately be end users of the data. The SSG developed a more detailed set of overarching thematic questions that were separated into three groups. The first two groups deal with overarching questions that may be addressed by only one of the two instruments. The third group requires data from both instruments. All three groups may require supporting measurements from other instruments, whether spaceborne, airborne, or ground. The three question groups are referred to as the 1) VSWIR questions (VQ), 2) TIR questions (TQ) and 3) Combined questions (CQ), respectively. Within each of these overarching thematic questions, there are a set of thematic subquestions, and it is these subquestions that provide the necessary detail to understand the measurement requirements.

All HyspIRI data will be available in a timely manner and current plans will allow a subset of the data to be transmitted in near real time. It is expected that the near real time data will be particularly valuable for applications related studies such as monitoring volcanic events or assessing the water needs of crops.

In support of the HyspIRI mission NASA is developing two airborne instruments the Hyperspectral Thermal Emission Spectrometer (HyTES) and the Advanced Visible InfaRared Imaging Spectrometer Next Generation (AVIRIS-NG). HyTES has 256 spectral channels between 7.5 and 12 micrometers with a swath width of 512 pixels and spatial resolutions of a few meters. AVIRIS-NG has a similar number of spectral channels between 0.38 and 2.5 micrometers and similar swath width. In addition to the airborne instruments NASA is also developing the Prototype HyspIRI Thermal Infrared Radiometer (PHyTIR) - a laboratory prototype of the spaceborne TIR system.

In this paper the HyspIRI mission will be described together with recent results from HyTES, AVIRIS-NG and PHyTIR.

8533-18, Session 5

Accomplishments from 9.5 years of AMSR-E observations

Elena S Lobl, The Univ. of Alabama in Huntsville (United States)

Advanced Microwave Scanning Radiometer for the Earth Observing System (AMSR-E) is flying on the NASA's Aqua satellite in the afternoon constellation, also called the "A-train". The instrument was provided by the Japan Aerospace Exploration Agency (JAXA). Aqua was launched May 4 2002.

AMSR-E provided microwave observations from launch until 4 October 2011. The engineering analysis concluded that the instrument stopped scanning due to the aging motor; AMSR-E worked flawlessly

for more than three times its lifetime.

This presentation will summarize the accomplishments of AMSR-E over its lifetime. The products developed from AMSR-E observations are: an ocean suite (sea surface temperature, sea surface winds, integrated cloud liquid water and integrated water vapor), sea ice parameters (sea ice concentration, sea ice drift and snow over sea ice), precipitation (both over ocean and land), soil moisture and snow water equivalent. Near-real-time new products were also produced in the last year of the instrument's life. The Land Atmosphere Near-real-time Capability for EOS (LANCE) provide application users, operational agencies and researchers products for a wide range of purposes, from weather forecasting to monitoring natural hazards. These users often need data much sooner than available through routine science processing and are willing to trade science quality for timely access. LANCE is part of the Earth Observing System Data and Information System (EOSDIS).

Some of the important findings from AMSR-E observations are: the cold wake of a hurricane, which can be used as a prediction tool; sea ice extent which showed the sea ice minimum in 2007. Remote Sensing Systems (RSS) has found that in the wake of a hurricane, the sea is mixed with lower, colder layers, and the surface temperature cools. A second hurricane moving on the same track, will encounter this cool water and collapse. Examples of this phenomena will be presented.

Acknowledgements: Thanks are due to JAXA, US AMSR Science Team, and AMSR-E Science Investigator-led Processing System (SIPS)

8533-19, Session 5

Simulation of the performance and image quality characteristics of the Landsat OLI and TIRS sensors using DIRSIG

John R. Schott, Aaron Gerace, Rochester Institute of Technology (United States); Matthew Montanaro, Sigma Space Corp. (United States)

The Digital Imaging and Remote Sensing (DIRS) Image Generation (DIRSIG) model has been significantly upgraded to support the Landsat Data Continuity Mission (LDCM). The DIRSIG improvements simulate the LDCM Thermal Infrared Sensor (TIRS) and the Orbital Land Imager (OLI) sensor's characteristics in support of the NASA and USGS image quality assessment programs. These improvements allow for simulation of space craft orbits using standard NORAD two line element (TLE) orbital descriptors. Sensor improvements include individual detector element lines of site, relative spectral response (RSR), bias, gain, non linear response, and noise. Using DIRSIG's existing source-target-sensor radiative transfer, atmospheric propagation, scene simulation and thermal models simulated Landsat 8 imagery was generated. These tools were developed to enable assessment of design trades during instrument development and build, and evaluation of expected performance during instrument test as test data is used to refine the modeled instrument performance. Ongoing efforts are aimed at refining predicted performance models, simulating on orbit calibration maneuvers and generation of data to test data processing and analysis algorithms. Initial studies will be reviewed aimed at assessing band-to-band registration artifacts, impact of RSR variation on banding and striping in both OLI and TIRS, use of side slither (90° Yaw) as a potential method to characterize and potentially compensate for non linearity effects and impact of edge shape anomalies on TIRS image quality. Ongoing work aimed at simulating targets to support image based registration of the OLI and TIRS instruments will also be presented.

In general, the use of advanced simulation and modeling tools to support instrument design trades, image quality prediction, on orbit image quality assessment and operational trades will be reviewed. The overall effort is designed to provide simulated imagery incorporating all aspects of the instrument acquisition physics and scene phenomenology in support of acquisition developers, operators, and earth observation scientists.

8533-20, Session 5

Innovative multi-angle imaging spectrometer and analysis approach to remotely quantify ecosystem-atmosphere carbon and water exchange

Forrest G. Hall, NASA Goddard Space Flight Ctr. (United States); Thomas Hilker, Oregon State Univ. (United States); Compton J. Tucker, James C. Smith, Catherine T. Marx, NASA Goddard Space Flight Ctr. (United States)

Accurate estimates of terrestrial photosynthesis been a long sought after goal of the Earth Science community, as understanding vegetation feedback on climate change is key to predicting future climate scenarios and atmospheric CO2 levels. However, forest photosynthetic exchange rates at landscape scales have proven difficult to either measure or estimate from models. Here, we describe a breakthrough multi-angle imaging spectrometer design and analysis approach to quantify forest light use efficiency and vegetation photosynthetic rate across ecosystems, thereby overcoming many of the limitations that are faced by the earth science community today. Together with a new generation ecosystem-atmosphere, carbon and water exchange model our approach allows us to infer net primary production and evapotranspiration at fine spatial scales, globally and continuously. In this paper, we describe the technical design and foundations of this new sensor concept, which is based on recent theoretical and experimental developments and has been extensively validated using tower-based spectrometer measurements and scaled to space using multi-angle imagery from the European CHRIS/PROBA satellite.

To date, our inability to obtain accurate estimates of GPP over land from satellite remote sensing remains the single most important obstacle for quantifying the terrestrial carbon, water and energy budget globally. As a result, improvements in estimates of plant carbon uptake and respiration will be key for improving global carbon models, predicting future climate scenarios, observing hydrological processes as a response to climatological changes at ecosystem level and forecasting of future precipitation rates.

8533-21, Session 6

PCW/PHEOS-WCA: Quasi-geostationary Arctic measurements for weather, climate and air quality from highly eccentric orbits

Richard L Lachance, ABB Analytical Measurement (Canada); Jack C. McConnell, Tom McElroy, York Univ. (Canada); Norm O'Neill, Univ. de Sherbrooke (Canada); Ray Nassar, Environment Canada (Canada); Henry Buijs, ABB Analytical Measurement (Canada); Peyman Rahnama, COM DEV International Ltd. (Canada); Kaley Walker, Univ. of Toronto (Canada); Randall Martin, Dalhousie Univ. (Canada); Chris Sioris, York Univ. (Canada); Louis Garand, Alexander Trichtchenko, Environment Canada (Canada); Martin Bergeron, Canadian Space Agency (Canada)

The PCW (Polar Communications and Weather) mission is a dual satellite mission with each satellite in a highly eccentric orbit with apogee ~ 42,000 km and a period (to be decided) in the 12-24 hour range to deliver continuous communications and meteorological data over the Arctic and environs. For several hours before and after apogee the viewing is quasi-geostationary due to the slow satellite motion. The satellite duo give 24x7 coverage. The operational meteorological instrument is a 21-channel spectral imager with UV, visible, NIR and MIR channels similar to ABI. The PHEOS-WCA (weather, climate and air quality) mission is intended as an atmospheric science complement to the operational PCW mission. The target PHEOS-WCA instrument package considered optimal to meet the full suite of science team objectives consists of FTS and UVS imaging sounders with viewing range of ~4.5° or a FoR ~ 3400x3400 km2 from near apogee. The goal for the spatial resolution at apogee of each imaging sounder is 10?10 km2 or better and the goal for the image repeat time is targeted at ~ 2 hours or better. The FTS has 4 bands than span the MIR and NIR. The MIR bands cover 700-1500 cm-1 and 1800-2700 cm-1 with a spectral resolution of 0.25 cm-1 similar to IASI. They should provide vertical tropospheric profiles of temperature and water vapour in addition to partial columns of other gases of interest for air quality such as O3, CO, HCN, CH3OH, etc and also CO2 and CH4. The two NIR bands cover 5990-6010 cm-1 (0.25 cm-1) and 13060-13168 cm-1 (0.5 cm-1) and target columns of CO2 and CH4 and the O2-A band for surface pressure, aerosol OD and albedo. The UVS is an imaging spectrometer that covers the spectral range of 280 - 650 nm with 0.9 nm resolution with 3 samples and targets the tropospheric column densities of O3 and NO2. It is also planned to obtain tropospheric columns of several other atmospheric

gases as well as the aerosol index. The quasi-stationary viewing will provide the ability to measure the diurnal behavior of atmospheric properties under the satellites and the ability to provide data for weather forecasting and also chemical data assimilation. One of the important goals for PHEMOS-FTS is to measure changes in CO2 and CH4 throughout the day-lit hours over the boreal forest in the NIR near apogee. The imaging design is to be sufficiently flexible so that it can be directed at special events and the FoR reduced to have more rapid spatial coverage. The PHEOS-WCA Phase A study was completed in March 2012and was funded by the Canadian Space Agency (CSA). The outcome of the study was three configurations one of which was compliant with the volume constraints imposed and that met a significant number of science objectives, one which included all features that matched the objectives but with a smaller telescope and a one configuration that met the full suite of science objectives. We will present the outcome of the PHEOS Phase A study.

8533-22, Session 6

Technology development for the meteorological multispectral imager of the Canadian Polar Communications and Weather Mission

Louis M. Moreau, Jacques Giroux, Francois Tanguay, Frederic Girard, Patrick Dubois, ABB Analytical Measurement (Canada)

The Polar Communications and Weather (PCW) mission is proposed by the Canadian Space Agency (CSA), in partnership with Environment Canada, the Department of National Defence and several other Canadian government departments. The objectives of the PCW mission are to offer meteorological observations and telecommunications services for the Canadian North. These capabilities are particularly important because of increasing interest in the Arctic and the desire to maintain Canadian sovereignty in this region. The PCW mission has completed its Phase A in 2011.

The PCW Meteorological Payload is a multi-spectral imager that will provide near-real time weather imagery for the entire circumpolar region with a refresh period of 15 to 30 minutes. Two satellites on a highly elliptical orbit will carry the instrument so as to observe the high latitudes 24 hours per day from a point of view that is almost geostationary. The data from the imager are expected to greatly enhance accuracy of numerical weather prediction models for North America and globally. The mission will also produce useful information on environment and climate in the North.

During Phase A, a certain number of critical technologies were identified. The CSA has initiated an effort to develop some of these so that their Technology Readiness Level (TRL) will be suitable for the follow-on phases of the program. An industrial team lead by ABB has been selected to perform technology development activities for the Meteorological Payload.

The goal of the project is to enhance the TRL of the telescope, the spectral separation optics and the infrared multi-spectral cameras of the PCW Meteorological Payload by fabricating and testing breadboards for these items. We will describe the Meteorological Payload concept and report on the status of the development activities.

The concept and approach will be presented. At the time of the conference, we expect that most of the breadboards will be at or near their critical design. We will also present the mission and the concept for the complete flight instrument. The instrument is in the same class as the Advanced Baseline Imager of GOES-R and the Flexible Combined Imager of MTG.

8533-23, Session 6

Novel pole-sitter mission concepts for continuous polar remote sensing

Matteo Ceriotti, Jeannette Heiligers, Colin R. McInnes, Univ. of Strathclyde (United Kingdom)

Spacecraft in geostationary orbit have demonstrated the significant benefits offered by continuous coverage of the equatorial and temperate zones of the Earth. At higher latitudes, similar services are currently provided by two types of conventional platforms: highly-eccentric, inclined orbits, or low or medium polar orbits. Despite that the spatial resolution offered from these orbits can be high, the temporal resolution is usually low, as it relies on multiple spacecraft polar passes, each one covering a narrow swath of the hemisphere. To overcome this limitation, the pole-sitter spacecraft concept was proposed: it is stationary above one of the poles, aligned with the Earth's rotation axis, in the same way as a GEO spacecraft is stationary above one point on the equator. The pole-sitter would constitute a novel platform for remote sensing and telecommunications with the high-latitude regions of the Earth. As such, it is the only platform that can offer a truly continuous view of one of the poles, enabling real-time imaging over the entire disc. The temporal resolution is clearly high, limited only by the instrument suite and the bandwidth available to download data. In addition, this vantage point offers a hemispheric view of the Earth's poles in a single frame.

The pole-sitter requires a constant thrust for station-keeping, which limits the distance from the Earth to significant values (order of one million km). Nonetheless, the utility of this platform for Earth observation and telecommunications is clear, and applications include polar weather forecasting and atmospheric science, glaciology and ice pack monitoring, ultraviolet imaging for aurora studies, continuous telecommunication links with polar regions, arctic ship routing and support for future high-latitude oil and gas exploration.

This paper proposes two mission scenarios, in which different propulsion technologies are used. The first, which is suitable for a near-term mission, uses a solar electric propulsion (SEP) thruster, while the latter is an advanced hybrid concept, that combines a solar sail with an SEP system. SEP is now a mature propulsion technology which has been used for a number of mission applications.

A full mission design for both propulsion options is presented, including launch (Ariane 5 and Soyuz vehicles are proposed) and optimized operational orbits. An optional transfer from the north pole to south pole and vice-versa is also designed, allowing viewing of both poles in summer.

The paper furthermore focuses on payloads that could be used in such a mission concept. In particular, by using instruments that were designed for past deep space missions, such as the Lagrange point Earth observation satellite DSCOVR (at 1.5 million km from the Earth), it is possible to obtain resolutions up to 10 km/pixel or less in the visible part of the spectrum, which is sufficient for the science applications mentioned above. The mass of these payloads is of the order of 40 kg, and well within the capabilities of the pole-sitter design. A systems design reveals that the SEP-only mission lifetime extends to about 4 years, while the hybrid propulsion technology enables missions of up to 7 years.

8533-24, Session 6

A novel design concept for space-based polar remote sensing

Malcolm Macdonald, Pamela Anderson, Univ. of Strathclyde (United Kingdom); Carl Warren, EADS Astrium Ltd. (United Kingdom)

This paper introduces a novel mission concept based on currently available spacecraft technology, including low-thrust propulsion technology, to provide continuous hemispherical polar remote sensing. The concept offers the potential to reduce the cost of completing the Global Observing System (GOS) whilst also enabling single-platform observations that would otherwise be impossible, simultaneously reducing complexity and deployment and operations costs, while significantly enhancing observation quality.

To date, remote sensing observations are conducted from two types of orbit, low-Earth (LEO), offering high-resolution observations at the expense of large-scale contextual information, and geostationary (GEO), which provides the large-scale contextual information required for meteorological products, offering rapid-scan operations, feature tracking and atmospheric motion vectors. However, space-derived products from GEO platforms are critically limited due to the rapidly decreasing horizontal resolution with increasing latitude; many such data products are not available beyond approximately 55° latitude, by which time the zenith observation angle (ZOA) tends towards 60°.

The limitations of GEO-based observations means that the wealth of climate and meteorological data accessible for the tropics and mid-latitudes is increasingly degraded for latitudes beyond 55°, resulting in a data-deficit over the critical polar regions due to restricted spatio-temporal sampling. To some extent this deficient can be compensated for through the use of composite images, however it has been shown that a 'ring' of missing observations occurs between 50 and 70 degrees.

It has been proposed that a high-inclination Highly Elliptical Orbit be used to counteract the restricted spatio-temporal sampling of the 'traditional' LEO/GEO architecture; such orbits are known as Molniya orbits. However, a spacecraft at apogee on a Molniya orbit observing 'over' the pole to a southern latitude limit of 55 degrees has a peak ZOA approximately 10 degrees higher than when the same location is observed from GEO. Consequently, despite the merits of the Molniya orbit for remote sensing the problem of viewing Polar regions is not fully resolved as no single platform can provide sufficiently hemispheric observations that can be coupled with the near-hemispheric observations obtained from GEO. As a result, polar observations, unlike equatorial observations, will remain dependent upon composite images that will be discontinuous in viewing geometry. To provide continuous observation to the latitudes required, with composite images, three spacecraft on Molniya orbits in three separate orbit planes, requiring three separate spacecraft launches, are required.

The concept introduced herein requires only two spacecraft, in a single orbit plane, to provide continuous visibility with composite images of all regions above 55 degrees latitude with a ZOA of less than 60 degrees. It is also found that a third spacecraft in the same orbit plane enables continuous visibility without the use of composite images, providing observation opportunities of at least equal quality to a GEO platform and from a similar altitude. Critically the use of a single orbit plane significantly reduces the constellation deployment costs. As such, the introduced mission concept offers significant advantages over a Molniya orbit in observation quality, operations cost and complexity, and the cost of deploying and maintaining a complete GOS.

8533-25, Session 6

Invitation to a Forum - Architecting operational 'Next Generation' earth monitoring satellites based on best modeling, existing sensor capabilities, with constellation efficiencies to secure trusted datasets for the next 20 years

Douglas B Helmuth, Lockheed Martin Corp. (United States)

Understanding the earth's climate and collecting requisite signatures over the next 30 years is a shared mandate by many of the world's governments. But there remains a daunting challenge to bridge scientific missions to 'operational' systems that truly support the demands of decision makers, scientific investigators and global users' requirements for trusted data. In this paper we will share an architectural structure that takes advantage of current earth modeling examples including cross-model verification and a first order set of critical climate parameters and metrics; that in turn, are matched up with existing space borne collection capabilities and sensors. The tools used and the frameworks offered are designed to allow collaborative overlays by other stakeholders nominating different critical parameters and their own treaded connections to existing international collection experience. These aggregate design suggestions will be held up to a disciplined review of 'reuse in space systems engineering'; and extended as a potential constellation solutions with incremental and spiral developments - including cost benefits and organizational opportunities. This effort is by design an inclusive 'operational constellation' design forum and panel discussion extension to the three earlier papers.

8533-26, Session 6

Design tradeoffs for a high-resolution, wide-field, pushbroom camera for a small-sat Earth observation mission

Denis P. Naughton, Sierra Imaging Systems (Australia) and Selex Galileo S.p.A. (Italy); Demetrio Labate, Selex Galileo S.p.A (Italy)

Advances in CCD technology, optics manufacturing, spacecraft performance and the availability of low-cost launch vehicles capable of carrying multiple payloads into low-Earth-orbit have led to the deployment of small and agile Earth observation satellites. Small-satellite electro-optical camera systems were initially conceived to fill a product gap by providing lower cost imagery at medium resolution, over a wide area and with repetitive monitoring capabilities that are not achievable with the very-high resolution systems that have traditionally been used for commercial, civil and defence surveillance missions.

As the number of operational small-satellite systems has increased there has been a desire in the imagery user community for improved resolution while maintaining the area coverage capability and revisit schedules that these systems currently provide. However, developing a remote sensing camera with these characteristics is difficult to achieve and in a sense these capabilities are at cross purposes imposing performance tradeoff and design constraints on the optical system, focal plane and spacecraft. For example, several small-satellite cameras currently provide resolution capability of less than or equal to 5 m GSD, but the available swath is only on the order of 20 km.

This paper describes the use of fundamental electro-optical system parameters in the design of a multi-spectral, high-resolution, wide-area coverage, small-satellite camera (HWSC) for an Earth observation mission. The driving requirements for the HWSC are assumed to be a resolution capability specified at GSD < 5 km, a swath equal to ~ 50 km or greater, a revisit schedule at the Equator from 3.5 to 4.5 days, an MTF at Nyquist equal to ~ 0.15 or greater, an SNR equal to ~80 or greater and a radiometric sensitivity NEdeltarho < 1% in all bands which are similar to the Landsat ETM+ VNIR bands.

The fundamental interaction between detector sampling and the image formation properties of the optical system is first examined to size the camera and establish first order performance parameters. An image chain analysis methodology is then used to model and assess the performance of a notional set of multi-spectral cameras in terms of achievable resolution, modulation transfer function (MTF), signal-to-noise ratio (SNR) and radiometric sensitivity based on assumed mission criteria. A comparative analysis of currently operational and planned small-satellite cameras was conducted to develop a refined set of HWSC specifications and coupled with this analysis produced a camera solution set meeting the design goals.

A feasibility analysis was then conducted to create a subset of potentially manufacturable cameras. As a result a prototype camera design based on a Korsch optical form, commercially available CCD-based focal planes, and Selex-Galileo heritage in low-noise, high-speed processing electronics and instrument manufacturing was developed. This design is suitable for a small-satellite camera in terms of estimated performance, mass, volume and power consumption. The results of the trade study and the validation of the HWSC design prototype are presented.

8533-27, Session 7

PERSIST: prototype Earth observing system using image slicer mirrors

David Lee, UK Astronomy Technology Ctr. (United Kingdom); James M. Barlow, The Univ. of Edinburgh (United Kingdom); Andy Vick, Peter Hastings, David Atkinson, Sandi Wilson, Martin Black, UK Astronomy Technology Ctr. (United Kingdom); Paul Palmer, The Univ. of Edinburgh (United Kingdom)

The measurement of the atmospheric concentration of greenhouse gases such as carbon dioxide (CO2) requires the simultaneous observation of a number of wavelength channels. Current and planned CO2 missions typically measure three wavebands using a hyperspectral sensor containing three spectrometers fed by an optical relay system to separate the wavelength channels. The use of one spectrometer per wavelength channel is inefficient in terms of number of detectors required and the mass and volume.

This paper describes the development of alternative solution which uses two key technologies to enable a more compact design; an image slicer mirror placed at the focal plane, and a multiple slit spectrometer operating in multiple diffraction orders. Both of these technologies are in common use in advanced astronomical spectrometers on large telescopes. The imager slicer mirror technology, as used on the James Webb Space Telescope instrument MIRI, enables the spectrometer to be illuminated with three input slits, each at a different wavelength. The spectrometer then disperses the light into multiple diffraction orders, via an echelle grating, to simultaneously capture spectra for three wavelength channels.

The United Kingdom Astronomy Technology Centre, in collaboration with the Department of Geosciences at the University of Edinburgh, has built a prototype system to demonstrate the image slicer and multiple order spectrometer technology. This paper will describe

the design and performance results obtained from PERSIST - the Prototype Earth obseRving System using Image Slicer Technology. The paper will also present a summary of the performance benefits this technology can provide.

8533-28, Session 7

Science capability of the NOAA/NESDIS/ STAR Algorithm and Data Products (ADP) Program: Suomi-NPP Satellite

Laurie A. Rokke, National Oceanic and Atmospheric Administration (United States)

The NOAA/NESDIS/STAR ADP program was established to provide science support for the operational sensors and algorithm products. The polar orbiting Suomi-NPP satellite was launched in October 2011 and is designed to meet the scientific needs for continued satellite remote sensing of the atmospheric column, land and ocean surface properties. The enterprise system developed to calibrate a multi-sensor platform and generate its products is especially well suited to observing detailed interdisciplinary components of the Earth's atmosphere and surface. This presentation will review the current capabilities of the ADP program and summarize early findings of the NOAA Suomi-NPP sensors and operational products.

8533-29, Session 7

Development plan of next generation geostationary ocean color imager

Seongick Cho, Korea Ocean Research & Development Institute (Korea, Republic of); Ki-Beom Ahn, Yonsei Univ. (Korea, Republic of); Eunsong Oh, Yu-Hwan Ahn, Youngje Park, Joo-Hyung Ryu, Korea Ocean Research & Development Institute (Korea, Republic of)

After the successful launch and operation of Geostationary Ocean Color Imager(GOCI), necessity of succession of GOCI mission, ocean environment monitoring with ocean color, is highly increasing into international ocean color remote sensing users as well as domestic users in Korea.

GOCI, the world's first ocean color observation satellite in geostationary orbit, was launched on June 2010. After the successful in-orbit test during 6 months, GOCI nominal operation has been started since 20 April 2011. About one year operation, GOCI has proved its unique capability, hourly-based ocean environment monitoring with shorter GSD(Ground Sampling Distance), by the observation of oil spill in Bohai Sea in China, movement and expansion of green tide in Yellow Sea.

In order to maintain mission continuity of GOCI and to fulfill the national demands to establish Improved National Ocean Observation Network , development of GOCI-II is planned to be started in 2012 and to be launched in 2018 regarding 7-year mission life time of GOCI. The mission and user requirements of GOCI-II are defined by Korea Ocean Research & Development Institute (KORDI) and domestic international GOCI PI(Principal Investigator)s. GOCI-II will be able to monitor the nearly full Earth disk area on 128.2˚E longitude in geostationary orbit, and to acquire the local area(observation region can be freely definable by user) image with 250m spatial resolution(2 times high at the center of reference local area(i.e. current GOCI coverage area). Spectral Bands of GOCI-II consists of 15 spectral bands in visible, NIR(Near Infra-Red), and SWIR(Short Wave IR). These enhanced features will enable the monitoring and research of long-term ocean environment change with better image quality. Additional 7 spectral bands and a dedicated panchromatic band for nighttime observation will be added to improve the accuracy of data products such as chlorophyll concentration, total suspended sediments, dissolved organic matters, enhancement of atmospheric correction, and to have a novel capability such as PFT(Phytoplankton Functional Type) which enables to discriminate harmful or unharmful red tide. GOCI-II has a plan to implement the user-definable local area observation mode to satisfy the user requests such as ocean observation over clear sky without clouds and special ocean event area. It is expected that this new capability will produce more applicable data products about special event area such as typhoon, oil spill, green algae bloom, and etc. GOCI- II will acquire the observation data with 8 times per day as same as temporal resolution of GOCI. Additionally, daily global observation once or twice per day is planned for GOCI-II for the research of long-term climate change in ocean. In order to develop the GOCI-II with the full satisfaction of user requirements, technical feasibility research is inevitable. In this paper, we present the preliminary concept design as a result of GOCI-II technical feasibility to satisfy GOCI-II user requirements and development plan of GOCI-II.

8533-30, Session 7

DubaiSat-2 mission overview

Ali AlSuwaidi, Emirates Institution for Advanced Science and Technology (United Arab Emirates)

The Emirates Institution for Advanced Science and Technology (EIAST) was established on February 2006 as an independent institution by Dubai government. It was founded to inspire scientific innovation and foster technological advancement in the United Arab Emirates through its various space initiatives and programs. DubaiSat-1 satellite mission is the first initiative introduced by EIAST. The satellite was designed and developed by Satrec Initiative (SI) - a pioneer satellite manufacturing company in South Korea, with active participation of EIAST engineers. DubaiSat-1 is a low earth orbital (LEO) remote sensing satellite and it was launched on 29th of July 2009 onboard Dnepr rocket from Baikonur launch site in Kazakhstan. Also, it generates high-resolution optical images with 2.5 m resolution in panchromatic (PAN) and 5 m resolution in red, green, blue and near-infrared bands (MS). DubaiSat-2, the second UAE remote sensing satellite is being developed and manufactured in South Korea. It is a collaborative project between EIAST and SI and it is part of technology transfer program to convey advanced satellites technology to the UAE. It is similar to DubaiSat-1 in term of orbit type and spectral bands, while it is not in resolution and altitude. DubaiSat-2 generates resolution optical images with 1 m in panchromatic (PAN) band and 4 m in Multi-Spectral bands (MS), while its altitude will be between 580 to 600 Km. In additions, this satellite includes new systems and features that were not implemented in DubaiSat-1 such as thruster, stereo and strip images capabilities. The launch of DubaiSat-2 was planned and scheduled for the last quarter of 2012.

8533-31, Session 7

Research of the multispectral camera of ZY-3 satellite

Bin Fan, Xiaohong Zhang, Weijun Cai, Ying Huang, Wenchun Jiao, Beijing Institute of Space Mechanics and Electricity (China)

The multispectral camera mounted on ZY-3 satellite (the first high resolution stereoscopic mapping and resources satellite of China which was successfully launched on January 9, 2012) has been developed in BISME for NASG (National Administration of Surveying, Mapping and Geo-information). This wide field off-axis TMA visible camera can provide 5.8-m ground sampling distance at nadir and 51-km swath from an altitude of 506km. The camera uses 3 TDICCD detectors of 20μm pixel size, which comprise multi-spectral bands in one detector. In the resources imaging modes, the multispectral camera works and delivers as well false color images, and true color ones, using the four channels blue, green, red, and near-infrared.

The multispectral off-axis camera has been developed aiming at a mapping camera. With some significant efforts, the main goals have been reached: low distortion, good optical quality, high radiometric quality, excellent structural and thermal stability, shorter alignment time and lower costs.

By means of technologies such as converging of analog signals, low temperature control of detectors, filtering of powers, optimizing of time order and high precision A/D conversion, the highly compact signal processing circuits were realized and the noises of detectors and circuits were greatly decreased. Thus radiometric quality of the images was obtained.

The 1.75-m focal length,6.0°?0.3° field of view optical system employed the quasi-telecentric in image space as well flat field. Over its whole field of view, the telescope achieved nearly diffraction limited image quality higher than 0.69@25lp/mm (detector Nyquist frequency) modulation transfer function and the relative distortion was less than 0.01%. By optimizing of optical parameters, the telescope allowed wide tolerances and thus the difficulties of the structure and alignment were significantly decreased and the fabrication risk was also reduced.

To guarantee a good image quality and high stabilities of distortion and intrinsic parameters, great stability of the figure and position

of the optical mirrors is necessary. Multi-point spherical hinge supporting structure which has the capability of decoupling of Degrees of Freedom (DOF) was used to support off-axis mirrors. Thermal stresses from the unmatched thermal distribution were filtered while the structure retained a sufficient high stiffness to withstand launch vibrations. Working within 20℃±3℃ temperature range, the focal plane location remains stable and the maximum reduction of the telescope MTF is less than 0.02 without any focal plane adjustment. The titanium main structure of the telescope was designed with the technologies of topology optimization thus a high stiffness-to-weight ratio was realized, and the first frequency of the telescope was higher than 160Hz. The flexible structure was used to mount the telescope on the magnesian frame of the satellite. By distortions of the flexible blades which acted as filtration elements, the stresses coming from expanding and shrinking of the satellite platform during the temperature were filtered thus keeping the stabilities of the optical components and focal plane.

By means of computer-aided alignment technology, the special alignment software was used to predict the necessary shifts of the mirrors. Combined with errors sensitivity matrix analysis, the optical alignment went along more orderly, more quantificational and higher effective. The whole alignment time of the telescope matching with the WFE requirement was completed within two weeks and the alignment quality ratio was larger than 0.92.

On January 11, 2012, the first multispectral raw images down-linked from board which looked clearer and sharper. The radiometric and geometrical quality of the following standard products remains good and stable.

The first part of this paper will focus on the designing, fabricating and alignment of the camera. The second part will outline results of the environmental test and performance test. The verification in orbit will be the third part of the paper.

8533-32, Session 7

An effective unloading opto-structure design of multispectral camera on ZY-3

Cai Weijun, Fan Bin, Fengqin Zhang, Qinglin Li, Wei Xin, Beijing Institute of Space Mechanics and Electricity (China)

The Multi-Spectral Camera is one of main payloads of ZY-3 satellite, which was launched in 2012 in China, and was used to land surveying, resources exploring, and 3D mapping. The Multi-Spectral Camera provides color image for the map. Due to the applying to mapping, the stability of elements of interior orientation becomes more important.

The Multi-Spectral camera applies a three mirror off-axis optical system, so reflectors of the camera are key factors for imaging quality. Under the condition of space, the change of thermal environment will lead to distortion of opt-structure, so the location of the reflectors will change, which affects the imaging quality and the stability of elements of interior orientation. So the first problem for the mechanical design is to insure the stability of reflectors' position throughout alignment, experiments, and launch. In one word, the structure of tree mirror off-axis optical system must have excellent stability; include mechanics and thermal stability.

According to the requirement of optical system, the primary mirror's tilt ≤10", the second mirror's tilt ≤20"and the third mirror's tilt ≤15". If the camera is mounted on the satellite directly, according the results of FME, the reflector's angle will change Significant(exceed 40") when the satellite frame has 5 ℃ temperature variation. The distortion exceeds optical precision and can't insure the imaging quality.

To satisfy the requirement of the opt-structure's stability, an effective unloading structure is designed in this paper. The structure is on the principle of flexible hinge. There are four mounting feet on the Camera. One mounting foot constraints all the six freedoms. Flexible hinges on the other three of mounting feet can release the freedom at the distortion direction, so the camera is quasi statically determinate system on the satellite. Besides the structure has enough stiffness to bear the load of launching.

The flexible structure is finally determinated after FEA analysis and detailed design considering the processing properties, convenience adjustment and stability under installation. The material of the unloading structure is titanium alloy. Every unloading structure contains three hinges and the distance of each two hinges is 20mm. The thickness and highness of the hinges is 1mm and 25mm. The modal analysis results show that first modal frequency of camera is 116HZ. It can satisfy the demand of satellite. Through the thermal analysis, the temperature of the camera is ranged from 18℃ to 22℃, and the temperature of the satellite frame is ranged from 25℃ to 15℃. Relative to the primary mirror, the change of the second and the third mirror's tilt is≤8". In order to verify the result of FEA analysis, a simulated thermal experiments on the whole camera was done. The result shows that the angle of the mirror's tilt is coincidence with FEA analysis. So this flexible hinges can release the thermal-distortion of the satellite on-orbit efficiently. The excellent imaging results on orbit proved the stability of the camera opt-mechanics directly.

This flexible structure can also provide reference for other precision instrument installed to satellite.

8533-33, Session 7

Enhancing the temperature sensitivity of Bragg gratings using different sensor heads

Parne Saidi Reddy, National Institute of Technology, Goa (India); R. L. N. Sai Prasad, National Institute of Technology, Warangal (India); G. R. C. Reddy, National Institute of Technology, Goa (India)

Two methods have been proposed for the enhancement of temperature sensitivity from room temperature to 100 ℃. The first method presents theoretical and experimental results carried out on a simple structure based on bimetallic cantilever to enhance temperature sensitivity of Fiber Bragg Grating (FBG) sensors. Two metals of equal length and width but having different coefficients of thermal expansion (CTE) are bonded with electric-arc welding to form the bimetallic strip and FBG was longitudinally affixed to that metallic strip having larger coefficient of thermal expansion. It was observed that the temperature sensitivity of the proposed FBG sensor has increased 5 times more compared to the bare FBG sensor. In the second method, a novel structure based on bimetallic strips has been designed for enhancing temperature sensitivity of fiber Bragg grating sensors. Two different types of sensor heads have been designed for this implementation. The first sensor head consists of a FBG is fixed between ceramic block one side and a bimetallic strip made up of aluminum and copper on the other. The second sensor head consisting of the FBG is fixed between two bimetallic strips. Theoretical and experimental studies carried out on these proposed sensor heads resulted in an increase in temperature sensitivity of about six times greater than that of bare FBG sensor. Further, the proposed sensors have shown excellent linearity and stability.

8533-76, Session PS

Infrared focal plane detector modules for space applications at AIM

Dominique Hübner, Kai-Uwe Gassmann, Markus Haiml, Luis-Dieter Haas, Stefan Hanna, Andreas Weber, Johann Ziegler, Hans-Peter Nothaft, Richard Thöt, Wolfgang Fick, AIM INFRAROT-MODULE GmbH (Germany)

In this presentation, AIM reports the status of some of its currently ongoing focal plane detector module developments for space applications covering the spectral range from the long-wavelength infrared (LWIR) and very-long-wavelength infrared (VLWIR) to the short-wavelength infrared (SWIR). Both spectroscopy and imaging applications will be addressed. In particular, the integrated detector cooler assemblies for a mid-wavelength infrared (MWIR) push-broom imaging satellite mission, for the German hyperspectral satellite mission EnMAP and dedicated detector modules for LWIR/VLWIR sounding will be elaborated.

8533-35, Session 8

InGaAs sensors inVGA format at 15 µm pitch for space applications

Anne Rouvie, Jean Decobert, Eric Costard, Mauricio Pires, Jean-Luc Reverchon, Alcatel-Thales III-V Lab. (France); Bogdan Arion, Yang Ni, Vincent Noguier, New Imaging Technologies SAS (France)

SWIR image sensors based on InGaAs p-i-n photodiodes arrays present a large interest for remote sensing. This paper presents several modules based on InGaAs photodiodes arrays from III-VLab based on a VGA format of 640 x 512 pixels with a pitch of 15 µm. We give the latest electro-optics performances in terms of dark current and visible extension capabilities useful for spectro-imaging.

InGaAs sensors are prompt to irradiation in space environment. This issue has been studied on our ? VGA based sensor submitted to irradiation tests. We will discuss two different readout circuit approaches to deal with this issue. The traditional approach is based on CTIA readout circuit biased at 0 V. We will analyze its consequence in terms of electrical noise, darks signal and photoresponse non-uniformity. This paper also describes a second opportunity based on a solar cell readout developed by New Imaging Technologies. It results in a single-chip InGaAs SWIR senor with more than 140 dB intrinsic operational dynamic.

8533-36, Session 8

New Sofradir VISIR-SWIR large format detector for next generation space missions

Bruno Fièque, Bertrand Terrier, Philippe Chorier, Nicolas Jamin, Patricia Pidancier, Laurent Baud, SOFRADIR (France)

For now more than 10 years, Sofradir is involved SWIR detector manufacturing, developing and improving its SWIR detectors technology, leading to a mature technology that enables to address most of missions needs in term of performances, but also with respect to hard environmental constraints.

SWIR detection range at Sofradir has been qualified for space applications thanks to various programs already run (APEX or Bepi-Colombo programs) or currently running (Sentinel 2, PRISMA mission). Recently, for PRISMA mission, Sofradir is extending its Visible-Near infra-red technology, called VISIR, to 1000x256 hyperspectral arrays. This technology has the huge advantage to enable detection in both visible range and SWIR detection range (0.4µm up to 2.5µm).

As part of the development of large format infrared detectors, Sofradir has developed Jupiter 1280x1024, 15µm pixel pitch detector in mid 2000s and this detector is available at production level since the end of year 2000s.

Based on the experiences acquired in SWIR and VISIR technologies as well as in the development of large format infrared detectors, since 2011, in the frame of an ESA program (named Next Generation Panchromatic detector), Sofradir is developing a new VISIR 1kx1k detector. This new detectors has a format of 1024x1024 pixels with a 15 µm pixel pitch and it is adapted to spectral range from UV to SWIR domain. This development contains mainly two challenges:

- the extension of the detector sensitivity down to UV spectral range

- the development of a large format ROIC with 15µm pixel pitch adapted to VISIR and SWIR spectral range involving in particular low input fluxes.

In this paper, we will describe the architecture and functionalities of this new detector. The expected performances will be presented as well. Then, first electro-optical characterizations and results will be described. Finally, main applications of this kind of detectors and expected spatial missions will be presented.

8533-37, Session 8

Overview of p-on-n HgCdTe IRFPAs at DEFIR

Laurent R. Mollard, Guillaume Bourgeois, Olivier Gravrand, Nicolas Baier, Gérard Destéfanis, CEA-LETI (France); Alexandre Kerlain, Alain Manissadjian, SOFRADIR (France)

In this paper, we report on results obtained both at CEA/LETI and SOFRADIR on p-on-n HgCdTe Infra-Red Focal Plane Arrays (IR FPAs) from the Short-wave (SW) to the Very-long-wave (VLW) spectral range. For many years, p-on-n arsenic-ion implanted planar technology has been developed and improved within the framework of the joint laboratory DEFIR, a collaborative effort bringing together the expertise of both teams. Compared to n-on-p, p-on-n technology allows for much lower dark current and series resistance by means of long-lifetime minority carriers (hole) and high-mobility majority carriers (electrons). Consequently, p-on-n photodiodes are well-adapted for very large FPAs operating either at high temperature or very low flux. The mid wave (MW) and long wave (LW) spectral ranges have been firstly addressed with TV/4, 30 µm pitch FPAs. Our results showed state-of-the-art detector performances, consistent with “Rule 07”, a relevant indicator of the maturity of photodiode technology. The subsequent development of p-on-n imagers has produced more compact, less energy consuming systems, with a substantial resolution enhancement. In this way, MW and LW TV format with 15 µm pixel pitch have been designed. First results obtained in MW (λc=5.3 µm @80 K) for High Operating Temperature (HOT) applications have showed highly promising Electro-Optical (EO) performances above 130 K.

Space applications are another exciting but challenging domains, and are good candidates for the p-on-n technology. In this way, imagers dedicated to low-flux detection have first been realized as TV/4 FPAs, with 15µm pitch in the SW spectral range (2 µm). Their dark currents are coherent with those found in the literature. Finally, TV/4 arrays, 30 µm pixel pitch, have been manufactured for the very long wave spectral range. For this detection range, the quality of material and reliability of technology are the most critical. The measured dark current fits “Rule 07” well, with homogeneous imagers.

In conclusion, DEFIR team have developed, improved and characterized p-on-n IR FPAs from SW to VLW spectral range. In all spectral ranges, we have demonstrated state-of-the-art results, which highlight the quality of material and viability of technology. That technology, currently industrialized by SOFRADIR, opens new ways for next generation of imagers.

8533-38, Session 8

Very long wave HgCdTe p-on-n FPAs for space applications

Nicolas Baier, Laurent Mollard, Olivier Gravrand, Gérard Destefanis, Guillaume Bourgeois, Jean-Paul Zanatta, CEA-LETI (France); Philippe Chorier, SOFRADIR (France); Laurie Tauzième, Alain Bardoux, Ctr. National d’Études Spatiales (France)

This paper presents recent developments made at CEA-LETI Infrared Laboratory about the fabrication and characterization of planar p-on-n very long-wavelength HgCdTe infrared photodiodes for space applications. This technology has been developed since 2005 in the scope of the DEFIR joint laboratory between CEA-LETI and SOFRADIR. This architecture presents some advantages compared to the n-on-p. It enables to lower dark current and series resistance by means of higher lifetime of minority carriers (holes) and higher mobility of majority carrier (electrons). Thus, this p-on-n technology is well adapted for low flux detection, high operating temperature and large format focal plane arrays.

This technology relies partially on the n-on-p process developed since many years. However, some technical challenges need to be overpassed to manufacture p-on-n photodiodes in this wavelength range with high performances, namely base layer extrinsic n-type doping using Indium and p-type doping using Arsenic. The HgCdTe active layer was grown by liquid-phase epitaxy (LPE) on lattice matched CdZnTe. The n-type doping of this layer was obtained by indium doping during epitaxy. Planar p-on-n photodiodes were made by Arsenic ion implantation. Arsenic was selected as the candidate acceptor impurity for p-type doping. Its activation is provided by post-implanted annealing under Hg overpressure vapour. Moreover, a good control of electrical p-on-n junction is made possible due to low As diffusivity, improving junction quality. This process also benefits from studies on a new ultra-flat LPE process, which dramatically increase focal plane arrays homogeneities (current and responsivity ones). Previous studies have shown very good results on FPAs on short-, mid- and long-wavelength spectral ranges.

Three different sets of detectors have been manufactured, with different aims in terms of cutoff wavelength: 12.5 µm at 77K, 12.5 µm at 40K and 15 µm at 77K. Electro-optical characterizations on these p-on-n photodiodes were made on 384?288 at 25 µm pixel pitch and 320?240 at 30 µm pixel pitch ROICs. Results show excellent current operabilities (over 99.9% at best) and very low dispersion, below 4%. The quantum efficiency is higher than 70% and remains constant on the whole detection spectrum. These photodetectors are shotnoise limited with a measured RMS noise to current shotnoise ratio lower than 1.05. Dark current is very low for every set of detectors, leading to mean figure of merit R0A products comparable to the state of the art and following the “Rule07”. This rule gives a heuristic prediction law of remarkable performances of high end p-on-n detectors and enables the comparison between measured results from different

manufacturer. These results highlight the very good quality of p-on-n technology developed at DEFIR. Measured currents as a function of operating temperature show that dark current is limited by carrier diffusion down to low temperature, pointing out the device high quality material and process. Part of these studies has been funded by French National Space Studies Center (CNES) to evaluate this technology for various space applications.

8533-39, Session 9

Overview of Aqua MODIS 10-year on-orbit calibration and performance *(Invited Paper)*

Xiaoxiong Xiong, NASA Goddard Space Flight Ctr. (United States); Brian Wenny, Sigma Space Corp. (United States); William Barnes, Univ. of Maryland, Baltimore County (United States)

Since launch in May 2002, Aqua MODIS has successfully operated for nearly 10 years, continuously collecting global datasets for scientific studies of key parameters of the earth's land, ocean, and atmospheric properties and their changes over time. The quality of these geophysical parameters relies on the input quality of sensor calibrated radiances. MODIS observations are made in 36 spectral bands with wavelengths ranging from visible (VIS) to long-wave infrared (LWIR). Its reflective solar bands (RSB) are calibrated using data collected from its on-board solar diffuser and regularly scheduled lunar views. The thermal emissive bands (TEB) are calibrated using an on-board blackbody (BB). The changes in the sensor's spectral and spatial characteristics are monitored by an on-board spectroradiometric calibration assembly (SRCA). This paper presents an overview of Aqua MODIS 10-year on-orbit operation and calibration activities, from launch to present, and summarizes its on-orbit radiometric, spectral, and spatial calibration and characterization performance. In addition, it will illustrate and discuss on-orbit changes in sensor characteristics and corrections applied to continuously maintain the sensor level 1B (L1B) data quality, as well as lessons learned that could benefit future calibration efforts.

8533-40, Session 9

Evaluation of Terra and Aqua MODIS thermal emissive band calibration consistency

Brian Wenny, Sigma Space Corp. (United States); Xiaoxiong Xiong, NASA Goddard Space Flight Ctr. (United States); Sriharsha Madhavan, Science Systems and Applications, Inc. (United States)

Terra and Aqua MODIS have operated continuously for more than 12 and 10 years respectively and are key instruments for NASA's Earth Observing System missions. The 16 thermal emissive bands (TEB), covering wavelengths from 3.5 to 14.4 micrometer with a nadir spatial resolution of 1-km are used to regularly generate a variety of atmosphere, ocean and land science products. As the sensors age well past their prime design life of 6 years, understanding the instrument on-orbit performance is necessary to maintain consistency between sensors in the long-term data records. Recurrent observations of Dome C, Antarctica by both Terra and Aqua MODIS over mission lifetime are used to track the calibration consistency and stability of the two sensors. A ground temperature sensor provides a proxy reference measurement useful for determining the relative bias between the two instruments. This technique is most useful for the land surface sensing bands, such as bands 29, 31 and 32, but can be applied to all other TEB to provide a metric to assess long-term trends. A change in the TEB calibration approach for the MODIS Collection 6 reprocessing mitigate a cold scene bias previously observed for retrievals of brightness temperatures well below the on-board blackbody calibrator temperature range (270-315 K). The impact of the Collection 6 calibration changes are illustrated using the Dome C observations.

8533-41, Session 9

Comparison of MODIS and VIIRS onboard Blackbody performance

Xiaoxiong Xiong, Jim Butler, NASA Goddard Space Flight Ctr. (United States)

MODIS has 16 thermal emissive bands (TEBs), covering wavelengths from 3.7 to 14.4 microns. MODIS TEBs are calibrated on-orbit by a v-grooved blackbody (BB) on a scan-by-scan basis. The BB temperatures are measured by a set of 12 thermistors. As expected, the BB temperature uncertainty and stability have direct impact on the quality of TEB calibration and, therefore, the quality of the science products derived from TEB observations. Since launch, Terra and Aqua MODIS have successfully operated for more than 12 and 10 years, respectively. Their on-board BB performance has been satisfactory in meeting the TEB calibration requirements. The first VIIRS, launched on-board the Suomi NPP spacecraft on October 28, 2011, has successfully completed its initial Intensive Calibration and Validation (ICV) phase. VIIRS has 7 thermal emissive bands (TEBs), covering wavelengths from 3.7 to 12.4 microns. Designed with strong MODIS heritage, VIIRS uses a similar BB for its TEB calibration. Like MODIS, VIIRS BB is nominally controlled at a pre-determined temperature (set point). Periodically, a BB Warm-Up and Cool-Down (WUCD) operation is performed, during which the BB temperatures vary from instrument ambient (temperature) to 315K. This paper examines NPP VIIRS BB on-orbit performance. It focuses on its BB temperature scan-to-scan variations at nominally controlled temperature as well as during its WUCD operation and their impact on TEB calibration uncertainty. Comparisons of VIIRS (NPP) and MODIS (Terra and Aqua) BB on-orbit performance and lessons learned for future improvements are also presented in this paper.

8533-42, Session 9

Modeling the detector gain of the Suomi NPP VIIRS reflective solar bands

Ning Lei, Sigma Space Corp. (United States); Jack Xiong, NASA Goddard Space Flight Ctr. (United States); Zhipeng Wang, Sigma Space Corp. (United States); Bruce Guenther, Stellar Solutions (United States); James Gleason, NASA Goddard Space Flight Ctr. (United States)

Right after the opening of the NADIR door of the Visible/Infrared Imager/Radiometer Suite (VIIRS) aboard the Suomi National Polar-orbiting Partnership (NPP), it has been observed that the detector gains of the Near Infrared (NIR) bands have decreased much more than expected, indicating large degradation of the VIIRS sensor optical system. To determine the root cause and to gauge the potential outcome for the degradation, we developed mathematical models based on physical hypothesis on the optical system, especially the Rotating Telescope Assembly Mirror surfaces. Current detector gains are consistent with a model of a four-mirror system, with each mirror having a thin layer of material, generated through solar radiation, absorbing light. The ratios of the absorption coefficients are in good agreement with those from the reflectance measurement of the Telescope Witness Mirror independently carried out as part of the degradation anomaly investigation. In this presentation, we describe in detail the model and discuss the results.

8533-43, Session 9

First results from the Cross-track infrared sounder (CRIS) on NPP

Vladimir V. Zavyalov, Mark P. Esplin, Mark Greenman, Deron Scott, Brandon Graham, Charles Mayor, Lee D. Phillips, Utah State Univ. Research Foundation (United States); Yong Han, National Oceanic and Atmospheric Administration (United States)

The Joint Polar Satellite System (JPSS) mission is a joint effort involving the National Aeronautics and Space Administration (NASA) and National Oceanographic and Atmospheric Administration (NOAA). This satellite system developed earlier as the U.S. National Polar-orbiting Operational Environmental Satellite System (NPOESS) is being developed to monitor global environmental conditions and collect and disseminate data related to weather, atmosphere, oceans, land and near-space environment. The first NPOESS Preparatory Project (NPP) satellite of the JPSS project has been launched on the October 28, 201.

The Cross-track Infrared Sounder (CrIS) is a key component of the larger Cross-track Infrared/Microwave Sounding Suite (CrIMSS), which consists of CrIS and the Advanced Technology Microwave Sounder (ATMS). Together, these instruments provide precise measurements of vertical distributions of temperature, moisture, and pressure within the Earth's atmosphere. CrIS is a sophisticated interferometric sounding sensor which accurately measures upwelling infrared radiance at very high spectral resolution. The science heritage for CrIS was derived from the Atmospheric Infrared Radiation Sounder (AIRS) on the NASA EOS Aqua satellite and Infrared Atmospheric Sounding Interferometer (IASI) on the European MetOp platform. The CrIS system is comprised of a space born instrument and ground based scientific algorithms. The CrIS observations data is delivered to the users in the form of the Raw Data Records (RDRs), Sensor Data Records (SDRs), and Environmental Data Records (EDRs). The level 1B ground segment algorithm transforms raw instrument measurements (RDR product produced by the on-board software) to the geo-located, spectrally and radiometrically calibrated spectra (SDR product). The SDRs are subsequently used by the separate EDR algorithm to retrieve atmospheric temperature, moisture, and pressure profiles forming the EDR product.

This paper describes the first in-flight results of the key parameters of the CrIS SDR product performance including Noise Equivalent differential Noise (NEdN), Radiometric Performance, and Spectral Accuracy. The results reported herein were processed with the latest version of the CrIS SDR algorithm and thus the performance of the entire CrIS system (instrument and SDR algorithm) has been tested and the results are included in this paper. We will provide a comparison to the AIRS and IASI heritage sensors that it builds upon. On-orbit sensor performance will be compared with sensor qualification, characterization, and calibration data obtained during ground thermal-vacuum tests.

8533-44, Session 9

Calibration of VIIRS F1 sensor fire detection band using Lunar observations

Jeff McIntire, Boryana Efremova, Sigma Space Corp. (United States); Xiaoxiong Xiong, NASA Goddard Space Flight Ctr. (United States)

Visible Infrared Imager Radiometer Suite (VIIRS) Fight 1 (F1) sensor includes a fire detection band at roughly 4 microns. This spectral band has two gain states; fire detection occurs in the low gain state above approximately 345 K. The thermal bands normally utilize an on-board blackbody to provide on-orbit calibration. However, as the maximum temperature of this blackbody is 315 K, the low gain state of the 4 micron band cannot be calibrated in the same manner as the rest of the thermal bands. Regular observations of the moon provide an alternative calibration source. The lunar surface temperature has been recently mapped by the DIVINER sensor on the LRO platform. The periodic on-board high gain calibration along with the DIVINER surface temperatures was used to determine the emissivity and solar reflectance of the lunar surface at 4 microns; these factors and the lunar data are then used to fit the low gain calibration coefficients of the 4 micron band. Furthermore, the emissivity of the lunar surface is well known near 8.5 microns due to the Christiansen feature (an emissivity maximum associated with Si-O stretching vibrations) and the solar reflectance is negligible. Thus, the 8.5 micron band is used for relative calibration with the 4 micron band to de-trend any temporal variations. In addition, the remaining thermal bands are analyzed in a similar fashion, with both calculated emissivities and solar reflectances produced.

8533-53, Session PS

Evaluation of a new sensor design technique for satellite navigation

George Dekoulis, Frederick Univ. (Cyprus)

This paper describes the design of a new type of sensor for implementing satellite attitude and heading control. The tri-axial fluxgate sensor type has been flown on unmanned aerial vehicles, missile guidance systems, spinning and non-spinning rockets and spacecrafts, but the new design is exploiting the advantages of a recently developed sensor design methodology. The implementation is using advanced materials in a new optimized configuration, which reduce radically the sensor's and the overall system's power consumption. Among a variety of advanced soft magnetic alloy materials the presented solution exhibits a balanced relationship between the maximum relative permeability and minimum saturation magnetic flux density. The sensor's sensitivity is enhanced and the weight leads to a considerably less massive solution. The low noise spectral density qualifies the sensor for spacecraft navigation.

A new cobalt-based material has been used for this implementation, which assisted in successfully implementing the optimization methodology. Furthermore, exceptional levels of noise performance and minimum error compensation were achieved. Special care is required for handling the sensitive core material. The prototyping results indicate maximum performance in terms of directivity and noise susceptibility for the rectangular structures. Three individually gimbaled optimized sensors have been assembled to provide the heading information. The pitch and roll is provided by winding additional coils to the sensor's configuration that detect the alternating current field generated by the axial components. The pitch, roll and yaw data of the attitude sensor are produced in a process similar to magnetic resolving and are not affected by structural induced magnetic fluctuations.

Similarly, the noise spectrum of the optimized sensor arrangement has been produced by averaging 128 overlapped samples in the range 0-25 Hz. The noise spectral density is 4.35 pT/sqrt Hz at 1 Hz. The RMS noise level is 9.14 pT for the frequency range of 100 mHz - 16 Hz or 10.25 pT up to 50 Hz. The peak-to-peak value is approximately 9.6 pT. Heading misalignments observed are due to the Space Physics induced contents of the Earth's magnetic field. Although minor and in the range of a few nT, they are dealt with by the software error compensation. It is not widely known that spacecraft navigation with magnetic sensors can be corrected without the need for ancillary sensors. Additionally, there are no limitations on the number of revolutions per second for the spinning models. Attitude and heading control has been tested for various maneuvers. Typical errors observed for the pitch, roll and yaw values are presented. Minimum error compensation has been applied to show the limits of deviation. The heading accuracy error is up to 0.013 °/h in the range 0-360°. The pitch is 0.012 °/h for +/-45 ° and 0.017 °/h for +/-90°. The roll is approximately 0.0011 °/h in the range 0-360°. The sensor has exceeded the initial target accuracy goals, although further testing is necessary when updating the hardware and software components.

8533-54, Session PS

Supercontinuum-source-based system for pre-launch calibration of the hyperspectral sensor

Yu Yamaguchi, Yoshiro Yamada, Juntoro Ishii, National Metrology Institute of Japan (Japan)

The first Japanese earth observing hyperspectral/multispectral imager mission, the HISUI (Hyper-spectral Imager SUIte) mission, is currently underway. The HISUI hyperspectral sensor will have 185 bands, 57 of which are in the visible and the near infrared and the remaining 128 in the short wavelength infrared, covering the spectral range from 400 nm to 2.5 μm. In order to guarantee the observed data with its high spatial and wavelength resolution, it is necessary to evaluate the difference of the spectral sensitivity among the detector devices arrayed two-dimensionally and correct spectral and spatial misregistrations and the effect of stray light. Since there are tens of thousands of detectors in the HISUI hyperspectral sensor, they have to be evaluated in parallel by the special technique for the hyperspectral sensor. Hence, the new light-source system which has high radiance with the spatial uniformity and widely tunable wavelength-range is required instead of the conventional lamp system. Here we report the new setup of the supercontinuum (SC)-source-monochromator system and its fundamental performance. Supercontinuum sources are laser sources which emit broadly and continuously over extended spectral range. The white light is generated from pulse lasers through nonlinear optical materials, such as photonic crystal fibers. Recently, commercial SC sources with high power and wide wavelength ranges are available, and then their applications to metrology were reported. We effectively coupled a high-power SC source to a single monochromator and obtained spatial uniformity through a integrating sphere or a relay-optics system. The SC source covers a wavelength range of 450-2400 nm. The total output power is up to 6 W and can be controlled with a resolution of 0.1%. The light exits from a single-mode fiber and is collimated to a Gaussian beam with a diameter of a few millimeter. The beam is focused to micrometer-order size spot at the slit of the monochromator with well-aligned lenses and mirrors. Therefore,

unlike a lamp, both 100% incident efficiency and high wavelength resolution are achieved at the same time. The radiance three or more magnitudes higher than a tungsten halogen lamp was measured with the supercontinuum-source based system. The output power of the system varied periodically within a range of ± 1% at the same wavelength. The spatial uniformity of radiance at the 6 mm integrating-sphere port was within ± 0.1%. Using the system, the relative spectral responsivity, spectral and spatial misregistrations and the stray light of a hyperspectral imager, which is consist of a polychromator and two-dimensional array of CCD, were measured.

8533-55, Session PS

Research and design of measuring methods for parameters of infrared focal plane array

Xu Lina, Beijing Institute of Space Mechanics and Electricity (China)

Infrared Focal Plane Array is the most important photo-electronic device of the infrared imaging system to capture infrared radiation information, which is composed of Infrared Detectors array and Readout circuit array. The device is applied extensively in the military and civil field. It has huge prospect on developing and applying. Parameters of Infrared Focal Plane Array play an important role in infrared imaging. The performance and parameters should be measured after Infrared Detectors array has been selected. Measuring methods for parameters of infrared focal plane arrays are analyzed in this paper. The main parameters of Infrared Detectors array, such as responsivity, detectivity and responsivity non-uniformity, can be measured by electronic hardware platform, which consists of testing circuit, blackbody and data acquisition and processing system. The software is designed by the way of programming in VC++. The testing results of infrared focal plane arrays are in accordance with the technical prescript, having some effects on the estimation of infrared focal plane arrays performance.

8533-57, Session PS

MODIS TEB calibration approaches in collection 6

Brian Wenny, Aisheng Wu, Sigma Space Corp. (United States); Xiaoxiong Xiong, NASA Goddard Space Flight Ctr. (United States); Sriharsha Madhavan, Science Systems and Applications, Inc. (United States); Zhipeng Wang, Na Chen, Yonghong Li, Kwo-fu Chiang, Sigma Space Corp. (United States)

The MODerate Resolution Imaging Spectroradiometer (MODIS) is a heritage sensor functioning from the Terra and Aqua platforms, and has so far collected remotely sensed data for a combined mission time of twenty plus years. The instrument robustness and performance during the lifetime has been very satisfactory, is well calibrated using its on-board calibrators (OBC). The radiometric fidelity of MODIS instrument has ensured the high quality of science products derived from the Level 1B (L1B) imagery. MODIS Thermal Emissive Bands (TEB) are calibrated on-orbit using an on-board blackbody (BB) and through the space-view (SV) port. The MODIS BB is nominally controlled at 290K in Terra and at 285K in Aqua. Periodically, a BB warm-up and cool-down (WUCD) process is implemented, during which the BB temperatures vary from instrument ambient (approximately 272K) to 315K. The calibration coefficients for the 16 TEB bands are characterized using the above mentioned on-board BB operations (i.e. using nominal and WUCD operations). The technical report presented in this paper will focus on the calibration algorithms of the TEB developed for collection 6 (C6) processing, its impact on the Level 1B (L1B) product in comparison to collection 5 (C5), and the methodology for issuing a Look Up Table (LUT) update for L1B processing.

8533-58, Session PS

In-orbit quantitative evaluation methods research of infrared focal plane array detector performance

Yanhua Zhao, Beijing Institute of Space Mechanics and Electricity (China)

Performance index of the infrared FPA (Focal Plane Array) detector are calculated and assessed by the spaceborne blackbody. It will be a thorny problem to assess the performance index of the infrared FPA detector, if the performance of the blackbody and calibration mechanism is degenerated. The detectors Performance changes have a direct impact on the optical remote sensor due to that the detectors are the key components of the optical remote sensor. Based on a project, the paper introduced an in-orbit evaluation method of infrared FPA detector using blackbody and typical features on the earth as radiation sources. It provided an effective evaluation method for other remote sensors with FPA detectors.

8533-59, Session PS

Research on breadboard spectrometer for measuring 1.61um CO2 band

Wei Peng, Shanghai Institute of Technical Physics (China); Shixiang Wu, Vision Engineering Ltd (China); Yuxuan Liu, Lei Ding, Xianghua Wang, Shanghai Institute of Technical Physics (China)

This paper introduces the design of a short-wave infrared breadboard spectrometer which is built to prove the scheme that would be implemented into an atmospheric CO2 measuring instrument. The instrument which embraces three spectrometers is designed to get spectral information on atmospheric CO2 from space. These three spectrometers take spectral band of 0.76μm, 1.61μm and 2.06μm, respectively. Two different techniques have been taken to acquire information on CO2 sources and sinks in the atmosphere. Both techniques are able to get high spectra resolution and high signal-to-noise ratio (SNR). The basic method for the breadboad spectrometer is in principal identical with the approach used for NASA's OCO. The short-wave infrared breadboard spectrometer is built to detect 1.61μm CO2 absorption band. Taking a 640?512 pixel Indium Gallium Arsenide (InGaAs), the spectrometer might cover spectra from 1.591μm to 1.621μm with spectra resolution of 0.1nm. Continuum spectra are covered as well as the CO2 absorption spectra, because these spectra can provide important information about factors which interfere with the 1.61μm absorption band. The breadboard spectrometer is a fast grating system with F/1.8 and a planar reflective grating. In order to achieve the requirement for high SNR, the optics and electronics have been designed very carefully. Recently, the design of optics has been finished and components have been procured or customized. The 640x512 pixel InGaAs system is able to take snapshots, but is still need to reduce its noise and correct its non-uniformity and non-linearity. After finishing the breadboard spectrometer, a series of tests will be conducted to gain significant data, such as SNR, the polarization sensitivity, Instantaneous Field Of View (IFOV), spectral response and so on. These data will reflect performance of the spectrometer and provide a significant reference for further works.

8533-60, Session PS

A method of FPGA implementation FTS phase correction based on CORDIC algorithm

Jiaqing Liu, Laboratory of Infrared Detection and Imaging,,CAS (China) and Shanghai Institute of Technical Physics (China); Lei Ding, Laboratory of Infrared Detection and Imaging,CAS (China) and Shanghai Institute of Technical Physics (China)

Ultra-spectral atmospheric remote sounding has been under development since the late 1970's.With many advantges,Michelson interferometer is a good candidate sounder.The operational polar orbiting satellite implementation has already been initiated with IASI(2006) on European MetOp-A satellite and this is to be followed by the CrIS(2011) on US NPOESS NPP. The evolution towards the ultimate goal of a global system of geostationary ultra-spectral sounders has progressed through the successful ground demonstration of GIFTS.Because of budget problem , the GIFTS for a space demonstration has been canceled.Europe is proceeding with the development of an operational GIFTS-like instrument IRS(2017) to fly aboard the MTG satellites.China also planned to fly Michelson interferometer aboard FY-3D (2015) and FY-4A(2014).

In some case, the interferograms are processed by an on-board digital processing subsystem which performs the inverse Fourier transform and the radiometric calibration (mainly phase correction) in order to decrease the transmission rate.

FPGA such as Xilinx Virtex-4 and Virtex-5 series that providing a flexible hardware and software co-design architecture to meet the on-board data-processing challenges of such missions while reducing the essential resources of mass and volume of earlier computing platforms such as the BAE Rad750 SBC.

Phase correction is one of the basic processing steps required by almost any Fourier transform spectrometer(FTS). There are many causes for phase error, like e.g. electronic delays in the acquisition chains or chromatism of the optics, but the main reason is that the interferogram sample used as the centre point for performing the inverse FFT does not necessary correspond to the position of Zero Path Difference (ZPD). So after inverse Fourier transform of the interferograms, the recovery spectrum in the complex plane, we have the computed spectrum given by:

(1)

Where , , are respectively the computed spectrum, the actual spectrum, the phase error, and is the wavenumber.

If we separate the computed inverse Fourier transform in Eq.(1) into its real and imaginary parts and, respectively, and take the square root of the product of with its complex conjugate, we have

(2)

So, any linear phase error in wave number can be exactly eliminated by computing the square root of the computed spectrum. The most obvious disadvantage is that double-sided interferograms are required and the process of obatining the absolute value by the square root of the sum of two squares is nonlinear,and the noise in the final spectrum is no longer constant but increasures as the signal decreases and is always positive.

This promble can be improved by data acquision and radiometric / spectrum calibration.

This metod is simple and suited for implemention with FPGA.But there have some problem to computing the square root, so we introucted CORDIC (Cordinate Rotation Digital Computer) algorithm to do this.

The CORDIC algorithm is an iterative convergence algorithm that performs a rotation iteratively using a series of specific incremental rotation angles selected so that each iteration is performed by shift and add operation.The CORDIC equations (Vectoring mode) used for computing the square root can be written as:

(3)

If with initialization : x[0]= Br(v),y[0]= Bi(v),z[0]=0, after a series of iteratives, we have

Where k is the scale facor.

So with CORDIC algorithm, we can have a metod of FPGA implementation phase correction. which with high speed and little FPGA using ratio, and can be parallel in a chip.

8533-61, Session PS

Preliminary study of the stereo geolocation accuracy of ZY-3 satellite

Li-ping Zhao, Satellite Surveying and Mapping Application Ctr. (China) and School of Resource and Environmental Science, Wuhan University (China); Xin-ming Tang, Xing-ke Fu, Yu-xing Li, Xian-hui Dou, Satellite Surveying and Mapping Application Ctr. (China)

ZY-3 satellite is the first high resolution civilian stereo mapping satellite of China, which is mainly used in vertical system diagram, resources investigation, disaster prevention and reduction. In the satellite it carries forward (F) and backward (B) stereo cameras, one nadir (N) camera and one multispectral (M) camera, with resolution up to 3.6 m, 2.1 m and 5.8 m respectively, and the width is 52 km.In this paper, ZY-3 stereo positioning method is discussed based on rational function model, and the positioning accuracy of stereo pair composed by B-F-N and B-F has been researched as well, furthermore, related experiments are carried out using imaging data in Harbin and Yan-An of China respectively. In the result, it shows that the accuracy of three-line array (B-F-N) stereo pair could be within 50 m in plane, and 50 m in altitude without any ground control point; While with the support of a few ground control points, accuracy turns to be better than 3 m in both plane and altitude, which is sub-pixel accuracy, and the accuracy of stereo pair composed by back and forward cameras (B-F) is quite close to that of three-line array.

8533-62, Session PS

Stray light analysis of nearby slot source using integrated ray tracing technique

Eunsong Oh, Korea Ocean Research & Development Institute (Korea, Republic of) and Yonsei Univ. (Korea, Republic of); Jinsuk Hong, Samsung Thales Co., Ltd. (Korea, Republic of); Sug-Whan Kim, Yonsei Univ. (Korea, Republic of); Seongick Cho, Korea Ocean Research & Development Institute (Korea, Republic of) and Yonsei Univ. (Korea, Republic of); Joo-Hyung Ryu, Korea Ocean Research & Development Institute (Korea, Republic of)

Step and stare method is one of the frequently used observation techniques in the remote sensing. This method makes no stripe pattern from a scanning technique and monitors a large field of view with mosaic several snap shots using 2-D detector. With those merits, the Geostationary Ocean Color Imager (GOCI) takes 16 step-by-step slots (4/EW * 4/NS) to cover the target area of 2500 km * 2500 km centered at 130°E * 36°N with the pointing mirror with 2 axes circular mechanism. When acquiring the imagery data in the low Sun elevation angle, the radiance level discrepancy was noticed in the cloudy circumstance next to each other slot. In order to find out those phenomena, firstly, we suggested that unwanted radiations from the Earth bright target or the atmosphere such as cloud are major candidates of stray light in the problematic images. Secondly, the internal opto-mechanical system design and its material can be affected to the image performance. In the in-depth study, we performed the realistic simulation for the stray light analysis. For embodying GOCI operational concept, we constructed the Integrated Ray Tracing model consisting of the Sun model as a light source, a target Earth model, and the GOCI optical system model. We then combined them in Monte Carlo based ray tracing computation. Light travels from the Sun and it is then reflected from the Earth section of roughly 2500km * 2500km in size around the Korea peninsula with 16 slots. It is then fed into the instrument before reaching to the detector plane. Trial simulations consisted with three case studies mainly. Firstly, we estimated how much the stray light according to the targets suggested clouds affects near-by slot image. Two ways including East-West and North-South effect were progressed at each slot. Secondly, the spectral results for 8 bands were compared with varying filter wheel mechanical structure and glass material characteristic. Lastly, we check the influence on the Sun elevation angle to the GOCI instrument at the observational time. This study results prove that the changeable bright source is candidate of stray light source and disturb to close slot image from the next slot target, and that the IRT end-to-end simulation technique introduced here can be applicable for high accuracy simulation of stray light analysis of GOCI and of other earth observing satellite instruments.

8533-63, Session PS

COMS normal operation for Earth observation mission

Young-Min Cho, Korea Aerospace Research Institute (Korea, Republic of)

Communication Ocean Meteorological Satellite (COMS) for the hybrid mission of meteorological observation, ocean monitoring, and telecommunication service was launched onto Geostationary Earth Orbit on June 27, 2010 and it is currently under normal operation service since April 2011. The COMS is located on 128.2° East of the geostationary orbit. In order to perform the three missions, the COMS has 3 separate payloads, the meteorological imager (MI), the Geostationary Ocean Color Imager (GOCI), and the Ka-band antenna. Each payload is dedicated to one of the three missions, respectively. The MI and GOCI perform the Earth observation mission of meteorological observation and ocean monitoring, respectively. For this Earth observation mission the COMS requires daily mission commands from the satellite control ground station and daily mission is affected by the satellite control activities. For this reason daily mission planning is required. The Earth observation mission operation of COMS is described in aspects of mission operation characteristics and mission planning for the normal operation services of meteorological observation and ocean monitoring. And the first year

normal operation results after the In-Orbit-Test (IOT) are investigated through statistical approach to provide the achieved COMS normal operation status for the Earth observation mission.

The mission operation characteristics of meteorological observation and ocean monitoring for the normal operation services are discussed in the point of overview. The discussions deal with the operational imaging areas, daily mission schedule characteristics, and special observations for calibration and instrument performance monitoring. The COMS Mission Planning Subsystem (MPS) is a part of the satellite operation system of COMS ground station. The MPS synthesizes the user mission requests for 'meteorological observation and ocean monitoring' and the satellite orbit and attitude control mission, resolves conflicts between missions, and establish daily mission plan of the Earth observation and the satellite control. The first year normal operation results are analyzed through statistical approach for the study of the mission operation status of COMS and the satellite image reception status which are achieved during the first year normal operation. The meteorological observation mission is operated continuously for 24 hours a day and 365 days a year. The meteorological mission schedules have been investigated to obtain the average values of daily satellite operation rate for the meteorological mission operation modes of Earth Imaging, Non-Earth Imaging, Mission Standby, and Satellite Maneuver. The satellite image reception status is summarized for each MI image type. The ocean monitoring mission is fulfilled by the daytime ocean imaging and the GOCI calibration. The ocean monitoring mission schedules have been investigated to obtain the average values of daily satellite operation rate for the ocean mission operation modes of Earth Imaging, Calibration, Mission Standby, and Satellite Maneuver. The satellite image reception status is summarized for GOCI image and calibration. The COMS mission operation results show that the COMS Earth observation mission have been operated successfully during the first year normal operation after IOT with respect to the requirement that the meteorological mission is to be continued 24 hours a day and 365 days a year and the ocean mission is to be operated 8 times a day and 365 days a year.

8533-64, Session PS

Novel high sensitivity sensor design based on cascaded long-period fiber gratings

Zhengtian Gu, Univ. of Shanghai for Science and Technology (China)

Long-period fiber gratings (LPFGs) have been intensively investigated for the chemical sensing applications due to their high sensitivity to the surrounding refractive index (RI) change. The methods of enhancing the sensitivity of LPFG-based RI sensors have being drawn people's attention, such as cladding etching, overcladding deposition, or photonic crystal fiber. All these improvement methods aim at an increase in the interaction between cladding modes and the surrounding material to be measured.

In this paper, a cascaded LPFG sensor with film coating is presented. Two LPFGs are cascaded to form Mach-Zehnder interferometer(LPFG-MZI). The cladding mode coupled by a grating can be recoupled by another grating, which gives a sinusoidal channelled spectrum within the attenuation bands. Further, the cascade chirped LPFG is also presented to study its sensing performance. Due to the introduction of the chirp distribution, there is a series of sharp interference fringe patterns in a periodic transmission spectrum. The interaction between the cladding modes and the surrounding will results in obvious shifts of the interference fringes.

The optical transmission spectrum and the sensing characteristics for ambient refractive index measurement of the cascaded LPFG sensor are analyzed in a form of transfer matrix based on rigorous coupled mode theory. The results indicate that it is highly sensitive to the film refractive index and surrounding refractive index, so it can be used as gas sensor or solution sensor. For gas or solution sensor, the sensitivity is defined as the ratio between the relative change of interference peak wavelength of the cascade LPFG and relative change of the film or the surrounding refractive index. In addition, the influence of the film optical parameters on the sensitivity are analyzed. By using optimization method, the optimal film optical parameters and the grating structure parameters are obtained. Data simulation shows that the resolution of the refractive index of the films is predicted to be more than 10^-7. In practical application, the width and amplitude of interference peak will influence the measurement precision of the resonant wavelength. Among the mode reorganization region, the interference peak will decrease and disappear, which must be avoided for selecting the film parameters. The theoretic analysis provides straightforward foundation for the actual highly sensitive film sensors.

Further, the influence of the chirp coefficient and structural parameters on the transmission spectrum of cascade chirped LPFG is analyzed with the transfer matrix method based on the coupling theory. For this LPFG film gas sensor, the sensitivity is defined as relative gradients of transmissivity to the refractive index of the films. By analyzing the relationship between the sensitivity and the thin film optical parameters, the optimal design parameters can be obtained. Data simulation shows that the resolution of the refractive index of the films is predicted to be more than 10^-9. In contrast to conventional measurement method based on interrogating the wavelength change, the intensity interrogation of this LPFG sensor means that no optical spectrum analyser is required in the measuring system, which is favourable for practical applications, especially for in situ environmental motoring.

8533-65, Session PS

The Radiance Standard RASTA of DLR's calibration facility for airborne imaging spectrometers

Thomas Schwarzmaier, Peter Gege, Deutsches Zentrum für Luft- und Raumfahrt e.V. (Germany)

The German Aerospace Center (DLR) operates the Calibation Home Base (CHB) as a facility for the calibration of airborne imaging spectrometers and for field spectrometers. Until recently, absolute radiometric calibration was based on an integrating sphere that is traceable to SI units through calibration at the German Metrology Institute PTB. However, the stability of the radiance output was not monitored regularily and reliably. This was the motivation to develop a new radiance standard (RASTA) which allows monitoring of small changes in the wavelength range from 380 to 2500 nm. Radiance source is a diffuse reflector illuminated by a tungsten halogen lamp. Five radiometers mounted in a special geometry are used for monitoring. This setup improves twofold the uncertainty assessment compared to the previously used integrating sphere. Firstly, lamp irradiance and panel reflectance have been calibrated at PTB additionally to the radiance of the complete system. This calibration redundancy allows to detect systematic errors and to reduce calibration uncertainty. Secondly, the five radiometers form a redundant control system to measure changes of the spectral radiance. This enables long-time monitoring of the radiance source including assessment of the uncertainty caused by aging processes. Further advantages concern maintenance, applicability and flexibility. Since RASTA uses a single lamp while the integrating sphere uses four, the probability of lamp failure is reduced and hence the interval of lamp exchange. Because a calibrated lamp is available as backup, it can be installed any time, eliminating periods of non-availability. Since the spectral radiance can be calculated using the irradiance of the lamp and the reflectance of the panel, only new components need to be calibrated, but not the entire system. The area of the used reflectance panel is much bigger than the exit port of the integrating sphere, which makes the new source applicable to sensors with larger field of view. Radiance sources of different intensity and spectral shape can be realised easily by exchanging the diffuse reflector. RASTA has been calibrated at PTB in November 2011 in the wavelength range from 350 to 2500 nm. The expanded uncertainty (k=2) is below 1.7 % in the range 525 to 1700 nm and increases steadily towards shorter and longer wavelengths (3.4 % at 350 nm, 15 % at 2500 nm).

8533-66, Session PS

Rigorous geometrical modeling of ALSAT-2A Algerian satellite

Issam Boukerch, Mohammed Hadeid, Redouane Mahmoudi, Bachir Takarli, Kamel Hasni, Ctr. National des Techniques Spatiales (Algeria)

The use of imagery data produced by the Algerian national very high resolution satellite Alsat-2A have a significant technological and economical impact by assuring a strength autonomy in terms of availability and covered area, allowing to Algeria the improvement and the update the basic and thematic mapping throughout the national territory which is the base of the Algerian sustainable development program.

This work starts by an overview of ALSAT-2A characteristics, namely the images and the imaging system with a brief history of ALSAT program.

Knowing the internal and external parameters is essentials for the modelling of the geometry of imaging satellite. From metadata given by the images distributor and the collected ground control points a rigorous geometrical model can be developed, a description of the most important elements provided in the metadata and their characteristics are then presented.

The mathematical model is then explained; after the analysis of the metadata provided with ALSAT-2A images, the rigorous pushbroom camera model can be developed. This model has been successfully applied to many very high resolution imagery systems based on the well known colinearity equation. The internal parameters are presented in a polynomial form of the line of sight vector, and the external parameters are derived from the attitude quaternions and the keplerian parameters calculated from the position / velocity vector, these external parameters were considered as an initial solution and refined by least square using the known coordinates of the ground control points.

Several tests are described and the results are then presented and discussed. The test images are supplied by ASAL (Algerian Space Agency), the first dataset comprise a panchromatic image over the region of El Bayadh in the North West of Algeria equipped with nine GPS surveyed points. The second dataset is an along track stereoscopic panchromatic 1A level images over the town of sevilla in the south of Spain with 24 GCPs.

The first test is about the absolute accuracy, the level 2A of the images provide 33.42m RMSE with a bias of 351.32m an affine transformation using 4 GCPs can improve this RMSE to 19.6m. The 1A level is a product intended for photogrammetric use, the analysis of the metadata provided with this level of image product permit to achieve a better accuracy.

The developed model is based on 26 parameters that can be grouped in three groups which are orbital, Translation and attitudes parameters. In the second test different sets of parameters are used to identify the minimum number of adjustable parameters to achieve a higher accuracy. This test indicate that the use of a second order polynomials correction of attitudes provide an 1.69m in vertical and 2.89m in horizontal accuracy.

The last test is about the influence of GCP number on the achieved accuracy; here we conclude that an accuracy of 3.39m in horizontal and 3.03m can be obtained using only four GCP with a first order polynomials correction of attitudes

8533-67, Session PS

One-year operation of in-orbit radiometric calibration for geostationary ocean color imager

Seongick Cho, Eunsong Oh, Sun-Ju Lee, Yu-Hwan Ahn, Joo-Hyung Ryu, Youngje Park, Korea Ocean Research & Development Institute (Korea, Republic of)

After the successful launch and in-orbit test of GOCI(Geostationary Ocean Color Imager), one of main payloads of COMS(Communication, Ocean and Meteorological Satellite), the new era of ocean color remote sensing has begun with the world's first ocean color observation sensor in geostationary orbit, GOCI.

In order to retrieve the quality controlled radiance from the RAW data in DN(Digital Number), in-orbit radiometric calibration with reference light source is required. In case of GOCI, Sun is the reference light source for the in-orbit radiometric calibration. Solar Diffuser(SD) and Diffuser Aging Monitoring Device(DAMD) as a second solar diffuser are implemented on GOCI for in-orbit solar calibration. SD and DAMD of GOCI are QVD(Quasi-Volumic Diffuser) type solar diffusers made of fused silica which are very well-known for the low solar UV sensitivity. Two Diffusers of GOCI are made of same material in the same fabrication conditions. The only difference between SD and DAMD is the size. Diameter of SD and DAMD is 14cm and 7cm, respectively.

GOCI radiometric model defined in 3rd order polynomial after the correction of dark current to retrieve radiance from DN in GOCI RAW data was characterized in on-ground test campaign, and verified in in-orbit test campaign. GOCI linear gain(G) and 3rd order non-linear gain(b), coefficients of GOCI radiometric model can be acquired from the solar calibration images observed with two diffusers at local night time. The GOCI linear gain value is about 0.49 for Band 1(412nm) and non-linear gain value is about -1.38E-9 for Band 1(412nm) from the pre-launch GOCI on-ground test results with Sun-simulated integrating sphere. After the 6-month in-orbit test campaign, it was found that the gain difference between on-ground tests and in-orbit tests is about 3.3% in linear gain(G).

In this paper, we report one-year operation results of GOCI in-orbit radiometric calibration with two solar diffusers. GOCI radiometric gain variation during the year of 2011 is about 1.8% for linear gain(G). One technical issue to be resolved is that radiometric gain derived from calibration image acquisition with solar diffuser has a seasonal variation. We found that these seasonal variation is highly correlated with the transmittance variation of solar diffusers with respect to azimuth angle. After the brief correction of azimuth angle variation of solar diffuser which was characterized during on-ground test campaign, the azimuth angle corrected radiometric gain variation for linear gain(G) is about 0.3%.

The characterization model of two solar diffusers is planned to be improved with implementation of enhanced azimuth angle correction algorithm.

8533-68, Session PS

Pre-launch spatial response calibration of the Landsat Data Continuity Mission thermal infrared sensor

Brian Wenny, Sigma Space Corp. (United States); Kurt Thome, Dennis Reuter, NASA Goddard Space Flight Ctr. (United States); Taeyoung Choi, Matthew Montanaro, Sigma Space Corp. (United States); Zelalem Tesfaye, Johns Hopkins Bayview Medical Ctr. (United States)

The Thermal Infrared Sensor (TIRS) for the Landsat Data Continuity Mission (LDCM) platform was designed and built at NASA Goddard Space Flight Center (GSFC). TIRS data will extend the data record for thermal observations from the heritage Landsat sensors, dating back to the launch of Landsat 4 in 1982. The two-band (10.8 and 12.0 micrometer) pushbroom sensor with a 185 km wide swath uses a staggered arrangement of quantum well infrared photodetector (QWIPs) arrays. The required spatial resolution is 100 m for TIRS, with the assessment of crop moisture and water resources being science drivers for that resolution. Evaluation of spatial resolution typically relies on a straight knife-edge technique to determine the spatial edge response of a detector system and such an approach was implemented for TIRS. Flexibility in the ground calibration equipment used for TIRS thermal-vacuum chamber testing also made possible an alternate strategy that implemented a circular target moved in precise sub-pixel increments across the detectors to derive the edge response. Results for both in-track and across-track edge response analysis are presented in terms of edge slope and extent, Line Spread Function (LSF) and Modulation Transfer Function (MTF). A comparison with the modeled spatial response shows good agreement.

8533-69, Session PS

Study on modeling and simulation techniques based on the whole imaging chain of optical remote sensing

Ningjuan Ruan, Haibo Zhao, Xuxia Zhuang, Chunxiao Xu, Beijing Institute of Space Mechanics and Electricity (China)

The reality of modeling is the precondition of space optical remote sensing image modeling and simulation, which plays a great importance on simulation accuracy. So the modeling of space optical remote sensing image should cover integrated composition and effect. The imaging chains include scenario, atmosphere, illumination, platform, sensor, compression/ transmission/ decompression/, ground image restoration and so on. The influences of signal, noise and MTF should also be considered in the modeling.

The models based on the composing and effects of the whole imaging chain were established and simulations were completed on the paper. The simulation images were presented on the paper, involving scenario of 0.3m to 10m resolution, images after the influence of atmosphere and illumination of different season and imaging time, visible and infrared remote sensor, platform of different satellite imaging angle and stability, compress ratio from 1:4 to 1:16, different ground image restoration method. Based on the models and simulation results, the keys of space optical remote sensor modeling and simulation were

sum up and presented on the paper, which will be reference for the simulation of the whole imaging chain of remote sensing in space.

8533-70, Session PS

Test results of adaptive optics system with deformable mirror for remote sensing telescope

Norihide Miyamura, The Univ. of Tokyo (Japan)

In small satellites remote sensing, high spatial resolution has to be achieved by a lightweight sensor. To realize these contrary requirements, adaptive optics system (AOS) is used. In remote sensing, it is difficult to use a reference point source unless the satellite controls its attitude toward a star, so image-based wavefront estimation method without reference source, phase diversity, is used. We propose to estimate wavefront aberration and calibration parameters of deformable mirror (DM) simultaneously. We describe the laboratory test results of the adaptive optics system using deformable mirror to validate the estimation and control algorithm.

8533-71, Session PS

Development of a large-size gold coated integrating sphere

Masatomo Harada, Fumihiro Sakuma, Yasuji Yamamoto, Yasuhiro Nakajima, Haruyoshi Katayama, Japan Aerospace Exploration Agency (Japan)

Remote sensing optical sensors are usually radiance calibrated against an integrating sphere with an internal halogen light source.

Barium sulfate is generally used as the inner wall of an integrating sphere. Barium sulfate is an ideal material in the VNIR range due to its high reflectance (98%) and Lambertian behavior, which produces a uniform light source at the aperture of the integrating sphere. However, in the SWIR range, a barium sulfate integrating sphere is unsuitable for the working standard, i.e., the calibration light source, because of the hydrophilic nature of barium sulfate. The uniformity degrades. The spectral radiance spectrum of the barium sulfate integrating sphere is not smooth and has many bumps caused by water absorption in the SWIR range though the spectrum is smooth with no bumps in the VNIR range. These bumps degrade the calibration accuracy of the spectral radiance and it is difficult to evaluate the uncertainty. Furthermore, the radiance stability near water absorption bands greatly depends on the temperature and moisture in the room, which also degrades the calibration accuracy.

To accomplish the high calibration accuracy in the SWIR range, we've been studying integrating spheres which is made from materials that are not hydrophilic such as gold instead of barium sulfate. Gold has a flat reflectance spectrum of 95% between 1 and 20 um and is not hydrophilic. Therefore, gold is an ideal material for the sphere's inner wall in the SWIR range.

We've developed a gold coated integrating sphere with an inner diameter of 1 m and an aperture diameter of 40 cm. This integrating sphere is expected to be used for the radiometric calibration of sensors such as SGLI (Second generation Global Imager) and HISUI (Hyperspectal Imager Suite).

In this presentation we show the initial results of the gold coated integrating sphere system.

8533-72, Session PS

ALSAT-2A power subsystem behavior during launch, early operation and in-orbit test

Nacera Larbi, Mehdi Attaba, Centre des Techniques Spatiales (Algeria); Eric Beaufume, EADS Astrium (France)

In 2006, Algerian Space Agency (ASAL) decided to design and built two optical Earth observation satellites. The first one, ALSAT-2A, was integrated and tested as a training and cooperation program with EADS Astrium Toulouse. The second satellite ALSAT-2B will be integrated by ASAL engineers in the Satellite Development Center (CDS) at Oran in Algeria. On 12th July 2010, Algeria has launched ALSAT-2A onboard an Indian rocket PSLV-C15 from the Sriharikota launch base, Chennaï. ALSAT-2A is the first Earth observation satellite of the AstroSat-100 family; the design is based on the Myriade platform and comprising the first flight model of the New Astrosat Observation Modular Instrument (NAOMI). This Instrument offers a 2.5m ground resolution for the PAN channel and a 10m ground resolution for four multi-spectral channels which provides high imaging quality. The operations are performed from ALSAT-2 ground segment located in Ouargla (Algeria) and after the test phase ALSAT-2A provides successful images. ALSAT-2A electrical power system (EPS) is composed of a GaAs solar array generator (SAG with 180 W end of life), a Li-ion battery (15 Ah) dedicated to power storage and energy source during eclipse or high consumption phases and a Power Conditioning and Distribution Unit (PCDU), it uses an unregulated power bus. This paper focuses primarily on ALSAT-2A electrical power system behavior during Launch and Early OPeration (LEOP) as well as In Orbit Test (IOT). The telemetry data related to the solar arrays voltage, current and temperature will be analyzed in addition to battery temperature, voltage, charge and discharge current. These parameters will be carefully studied in function of satellite power consumption.

8533-73, Session PS

A 1550-nm time-of-flight laser ranging system based on 1.5-GHz sine-wave gated InGaAs/InP APD

Min Ren, Guang Wu, Yan Liang, Weibin Kong, Heping Zeng, East China Normal Univ. (China)

Laser ranging systems at 1550 nm have attracted lots of attention in long distance remote sensing applications because of their ease for compactness with fiber devices, low atmospheric loss and particularly, working in the eye-safe wavelength region. On the other hand, single-photon detectors are going to be used for ultra long-distance laser ranging, such as the satellite laser ranging. InGaAs Geiger-mode avalanche photodiodes (InGaAs GAPDs) have been mostly used to realize single-photon detection at 1550nm. However, InGaAs/InP GAPDs are usually operated in gated Geiger mode to suppress dark noise and afterpulses, where the gate width is only several nanoseconds at multi-megahertz repetition rate. It will take a very long time to scan the delay of the gate to catch the reflecting photons, due to the low duty cycle ratio of the detecting gate. Recently, self-cancellation and sine-wave techniques have been proposed to increase the gating repetition rate to multi-gigahertz [1]. In this case, the InGaAs GAPD is operated in quasi-continuous mode, and useful for applications without synchronized trigger.

We demonstrated an eye-safe laser ranging system based on InGaAs/InP GAPD single-photon detector at 1550 nm [2], which was operated in 1.5-GHz sine-wave gated mode. A DFB laser was used with the pulse width of ~50 ps and the energy of 0.5 nJ per pulse. A 140-mm diameter Newtonian telescope was used to receive the reflecting photons. The daylight background and other stray noise were blocked by an optical band pass filter (FWHM ~ 6 nm). The reflecting photons were collected to the single-photon detector through a 62.5/125 micro-meter multi-mode fiber. The total timing jitter of the single-photon detector was about 350 ps. The time data recorded by a Time-Correlation-Single-Photon-Counter system (TCSPC) was the round-way flight time of the photons from the laser source to the targets. The depth resolution of this ranging system was better than 6 cm corresponding to 400 ps time-of-flight of the photons. Thanks to the single-photon-level sensitivity, the laser ranging system can measure the non-cooperation reflective objects 1000 m away. Moreover, it is able to realize 400-km laser ranging with the laser energy of only 81 micro-joules per pulse.

References

[1] R. E. Warburton, A. McCarthy, A. M. Wallace, S. Hernandez-Marin, R. H. Hadfield, S. W. Nam, and G. S. Buller, "Subcentimeter depth resolution using a single-photon counting time-of-flight laser ranging system at 1550 nm wavelength," Opt. Lett. 32, 2266-2268 (2007).

[2] Z. L. Yuan, A. W. Sharpe, J. F. Dynes, A. R. Dixon, and A. J. Shields, "Multi-gigahertz operation of photon counting InGaAs avalanche photodiodes," Appl. Phys. Lett. 96, 071102 (2010).

[3] M. Ren, X. Gu, Y. Liang, W. Kong, E. Wu, G. Wu, and H. Zeng, "Laser ranging at 1550 nm with 1-GHz sine-wave gated InGaAs/InP APD single-photon detector,"Opt. Express 19, 14, 13497-13502 (2011).

8533-74, Session PS

A Laser Ranging System Operating at 1036 nm with Geiger-mode Silicon Avalanche Photodiode

Guang Wu, Min Ren, Yan Liang, Zhiyuan Wang, Haifeng Pan, Heping Zeng, East China Normal Univ. (China)

In recent years, improvements in Geiger-mode avalanche photondiode (GAPD) based single-photon detection technology have brought many advantages to remote sensing applications. The single-photon detector based on silicon GAPD has many inherent advantages, such as less dark noise, operation at room temperature, small overall size. All these advantages make it a good sensor for space based remote sensing system. However, the detection efficiency goes down very fast when the wavelength of the source light exceeds 1000 nm. Meanwhile, near-infrared lasers have many superiors in space remote sensing applications, due to the low background radiation and low atmospheric loss [1]. One of the most wildly used near-infrared lasers work at 1064 nm, because it is very convenient to get high output in Yb-doped laser system at this wavelength. But the detection efficiency of the Si-GAPD based single-photon detector is only about 2% at this wavelength. 1036 nm is another high gain output wavelength of Yb-doped laser system, and the detection efficiency is about 6%. Thus, the 1036-nm laser source is a better choice for near-infrared laser remote sensing systems. Furthermore, Yb-doped fiber laser systems perform well on shock resistance testing and thermal independence testing.

We demonstrated a laser ranging system working at 1036 nm with a Si-GAPD based single-photon detector. The laser source employed here is an Yb-doped fiber laser actively mode-locked by an acoustic optical modulator. The max output energy per pulse is 100 micro-Joules, and the line width is 25 nm. With a 400-mm diameter telescope to collect the return photons, the longest working distance would achieve 730 km theoretically. By using the time-of-flight time correlation single photon counting approach, we obtained 15-cm minimal surface-to-surface resolution, corresponding to 400-ps timing jitter of the detector, under daylight background. It provides a simple way to build a high sensitive 1036 nm laser ranging system, suitable for space based applications. As the single photon detector is designed to detect light with extremely weak energy up to the lowest energy level of optical information carrier, the ranging systems with single photon detectors are able to reach the highest sensitivity. Benefit from low power consumption of the devices used in this system, it provides a reasonable chance for developing this system into hundreds kilometer working distance.

References

[1] M. Ren, X. Gu, Y. Liang, W. Kong, E. Wu, G. Wu, and H. Zeng, Opt. Express 19, 14, 13497-13502 (2011).

8533-45, Session 10

The impact of time scales to calibration and validation for the CERES Earth radiation budget decadal record

Kory J. Priestley, NASA Langley Research Ctr. (United States); G. Lou Smith, National Institute of Aerospace (United States); Audra Bullock, NASA Langley Research Ctr. (United States); Susan Thomas, Science Systems and Applications, Inc. (United States)

The Clouds and the Earth's Radiant Energy System (CERES) Flight Model-6 (FM-6) instrument will fly on the Joint Polar Satellite System (JPSS) -1 spacecraft, which has a launch-readiness date of December, 2016. This mission will continue the critical Earth Radiation Budget Climate Data Record (CDR) begun by the Earth Radiation Budget Experiment (ERBE) instruments in the mid 1980's and continued by the CERES instruments currently flying or scheduled to fly on the EOS Terra, EOS Aqua, and NNPP spacecraft.

The largest source of uncertainty in the interpretation of decadal Climate Records is due to latent artifacts which reduce the ability to maintain radiometric precision/traceability over the lifetime of the record. If radiometric precision is not maintained with sufficient knowledge, it increases the chance that the community will interpret uncorrected instrument drifts as a climate signal. In contrast to this, withholding the data from the scientific community until the traceability is perfectly understood, precludes both valuable independent review of the dataset, as well as the conclusion of scientific results which do not require the same level of accuracy as a decadal record.

Rigorous pre-launch ground calibration is performed on each CERES flight unit to achieve a 1-sigma absolute accuracy goal of 1% for reflected solar, and 0.5% for emitted thermal radiance observations. Any ground to flight or in-flight changes in radiometer response are monitored using a protocol employing both onboard and vicarious calibration sources and experiments. Each of these experiments has unique sampling constraints (i.e. spatial, spectral, and temporal).

Balancing the production of an accurate record against the need of the community to have access to the data in a timely fashion involves sound scientific and engineering judgment. The CERES Edition_2 product release schedule has provided the community calibrated radiances on ~ 6 month centers over the lifetime of the mission. This periodicity however is on the same time scale as many phenomena which can influence an instruments response: Beta angle, Earth sun distance, Orbital shifts/drifts, Instrument operational mode. This greatly increases the possibility that latent artifacts reside within the data as the separation of climate signal from instrument artifact as determined using the cal/val procedure is very difficult.

The current effort describes the process and protocols used by the CERES Science Team to prevent the introduction of latent instrument artifacts into the record and attempts to quantify the magnitude of artifacts which could reside in the released products in the hope that the frequency of inaccurate scientific being drawn is reduced.

8533-46, Session 10

Comparing radiances from ScaRaB-3 and CERES scanning radiometers

George L. Smith, Z. Peter Szewczyk, Science Systems and Applications, Inc. (United States); Kory J. Priestley, NASA Langley Research Ctr. (United States)

Clouds and Earth Radiant Energy System (CERES) scanning radiometers Flight Models 1 and 2 have flown on the Terra spacecraft since December 1999 and Flight Models 3 and 4 have operated on the Aqua spacecraft since May 2002. The calibrations of these instruments have been maintained by use of an Internal Calibration Module in each instrument and the validation protocol has relied on comparisons of measurements from each instrument, in addition to Earth scenes such as deep convective clouds. Flight Model 5 was placed into orbit in October 2011 aboard the NPP spacecraft, now named the Suomi spacecraft (NPP). Comparisons of the FM-5 measurements with those from the other four CERES instruments are needed to provide information about the current calibrations of FM-1 through -4.

The ScaRaB-3 scanning radiometer was placed in an orbit with 20o inclination in September 2011 aboard the Megha-Tropique satellite. ScaRaB gives a unique opportunity to increase our ability to compare the CERES instruments by acting as a transfer radiometer among the CERES instruments. Also, these measurements will give researchers the relations between ScaRaB-3 measurements and thoe from CERES instruments.

The Suomi orbit has the same Equator crossing time and nearly the same inclination as the Aqua orbit, but with a greater altitude. Consequently Aqua periodically underpasses Suomi. At these times the measurements of FM-3, -4 and -5 can be compared. During northern Summer Solstice the FM-2 and FM-3 are operated so as to scan in the east-west plane as the orbits cross at local noon at 70o North, thereby providing data for tying the calibrations of FM-2 and -3 together. There are many times when the Terra and Aqua spacecraft underpass Megha-Tropique at any time of the year, so that CERES instruments can be operated to measure radiances which are also measured by ScaRaB and thus related to each other. This paper presents the conditions for which the CERES instruments must be operated to obtain data with which to compare calibrations.

For both instruments to be measuring the same radiance, they must observe the same scene from the same direction at the same time. Practically, the footprints for the observations must overlap or cover the same region. The direction of observation must coincide within 5 degrees in view zenith angle, solar zenith angle and relative azimuth angle. The passes must be within 7.5 minutes of each other. Finally, the CERES instruments may not operate to scan in the direction of spacecraft motion, to avoid degrading the optics with atomic oxygen or other contaminants.

Before the CERES crosses the orbit of ScaRaB, it will be rotated in azimuth such that its scan plane coincides with that of ScaRaB. As CERES moves along its orbit, it will view scenes which are viewed by ScaRaB at angles within the constraints. The geometry for this matching of observations is described in the scan plane and in terms of the orbit crossing.

8533-47, Session 10

Development of dedicated target tracking capability for the CERES instruments through flight software: enhancing radiometric validation and on-orbit calibration

Kelly K. Teague, Science Systems and Applications, Inc. (United States)

Five CERES scanning radiometers have been flown to date. The Proto-Flight Model flew aboard the Tropical Rainfall Measurement Mission spacecraft in November 1997. Two CERES instruments, Flight Models (FM) 1 and 2, are aboard the Terra spacecraft, which was launched in December 1999. Two more CERES instruments, FM-3 and FM-4, are on the Aqua spacecraft, which was placed in orbit in May 2002. These instruments continue to operate after providing over a decade of Earth Radiation Budget data. The CERES FM-5 instrument on the Suomi-NPP spacecraft, launched in October 2011. The CERES FM-6 instrument is manifested on the JPPS-1 spacecraft to be launched in December, 2016. A successor to these instruments is presently in the definition stage. This paper describes the evolving role of flight software in the operation of these instruments to meet the Science objectives of the mission and also the ability to execute supplemental tasks as they evolve.

In order to obtain and maintain high accuracy in the data products from these instruments, a number of operational activities have been developed and implemented since the instruments were originally designed and placed in orbit. These new activities are possible because of the ability to exploit and modify the flight software which operates the instruments. The CERES Flight Software interface was designed to allow for on-orbit modification, and as such, constantly evolves to meet changing needs.

The purpose of this paper is to provide a brief overview of modifications which have been developed to allow dedicated targeting of discrete geo-location's as the CERES sensor flies overhead on its host spacecraft. This new observing strategy greatly increases the temporal and angular sampling for specific targets of high scientific interest. In particular, these modifications enable the following

- More efficient field campaign and intercomparison coverage: taking into account increased sampling, and ability to look at certain stable sites (e.g. Dome C, Sonora desert, etc.).

- Targeting high-probability locations of Deep Convective Clouds which may serve a stable target for the emitted thermal bands, as well as enabling increased three channel intercomparison opportunities.

- Lunar calibration may be completed with large statistics.

- With CERES pointing ability proven, one can then consider future operational instrument designs which expand upon this capability

8533-48, Session 11

In-orbit calibration strategy for Sentinel-1

Paul Snoeij, Ignacio Navas-Traver, Dirk Geudtner, Allan Østergaard, Bjorn Rommen, Michael Brown, Ramon Torres, European Space Research and Technology Ctr. (Netherlands); Marco Schwerdt, Björn Döring, Manfred Zink, Deutsches Zentrum für Luft- und Raumfahrt e.V. (Germany)

The ESA Sentinels constitute the first series of operational satellites responding to the Earth Observation needs of the EU-ESA Global Monitoring for Environment and Security (GMES) programme. The GMES space component relies on existing and planned space assets as well as on new complementary developments by ESA. ESA is developing the Sentinel-1 European Radar Observatory, a constellation of two polar orbiting satellites for operational SAR applications. The two C-band radar satellites will provide continuous all-weather day/night imagery for user services, especially those identified in ESA's GMES service elements programme and on projects funded by the European Union (EU) Framework Programmes.

Radiometric calibration must be performed as part of the normal operation of the SAR. The calibration process is divided into two components: internal and external calibration. Internal calibration provides an assessment of radar performance using internally generated calibrated signals, especially in the context of pre-flight testing and in-orbit verification and during the nominal operational phase.

The Sentinel-1 SAR instrument has demanding requirements for measurement stability (0.5dB, 3σ). Considering in orbit conditions and ageing effects, the hardware alone cannot provide sufficient stability to fulfill these requirements. Therefore an internal calibration system is implemented to measure the actual instrument gain and phase changes in order to apply them later, in the ground processing, for correction of the image data. The parameter to be derived by internal calibration is the so-called PG product, a quantity proportional to the product of transmit power of a polarization channel and gain of both the co- and cross-polarization receiver. It is to be noted that the PG product is complex and allows correcting both amplitudes and phases of the image data.

External calibration makes use of ground targets of known RCS to render an end-to-end calibration of the SAR system, thereby assessing the impact of those elements that are difficult, if not impossible, to assess using internal methods. External calibration methods can involve the use of: passive and precisely constructed targets, such as corner reflectors and spheres; natural terrain with known backscattering properties, such as the Amazon rainforest; or active transponders. The most important point with respect to the in-orbit calibration and performance verification of this flexible SAR system is the tight performance with an absolute radiometric accuracy of only 1 dB (3 σ) for all operational modes. Never before such a strong requirement (a few tenths of dB) has been defined for a satellite SAR system.

For interferometric application of the Sentinel-1 SAR the accuracy of InSAR measurements is controlled by the orbit accuracy (ground track repeatability) and the phase stability over a data take. The phase stability over a data take is monitored by internal calibration. Ground targets with stable phase of the reflected signal can be used as references to determine the repeatability of phase measurements.

Following the experience gained with ERS and ENVISAT it is necessary to have a set of precision radar transponders to act as point targets which can be automatically programmed and accessed during the Sentinel-1 commissioning phase and the remainder of the mission lifetime in order to achieve the absolute radiometric and polarimetric accuracy requirement.

This paper will describe aspects of the in-orbit calibration and performance verification of the Sentinel-1 constellation.

8533-49, Session 11

Robust in-flight multi-angular calibration for the PROBA-V mission

Stefan Livens, Sindy Sterckx, Stefan Adriaensen, VITO NV (Belgium)

To ensure the data quality of the PROBA-V global vegetation monitoring satellite, a comprehensive system for vicarious radiometric calibration has been developed. Multiangular calibration covers one aspect of this: the estimation and compensation of sensitivity variations of individual detectors. High frequency pixel to pixel variations are typical for line sensors which can result in unwanted striping effects. If the sensitivity variations profiles are accurately known, correction is straightforward. To achieve this throughout the duration of the mission, it is very desirable to perform in-flight assessment of the variations in addition to preflight calibration.

We propose a method which relies on large, bright and uniform areas, such as those found in the Dome C area on Antarctica. A set of images will be used together to cover the wide field of view of the PROBA-V satellite (three cameras, covering 875km or 500km each).

The method first estimates sensitivity profiles for every image separately. For this, a high frequency relative response (HFRR) image is computed as the ratio between an original and a low pass filtered image. The HFRR image represents the local high frequency variations. Per HFRR column, a trimmed mean value (mean of the 50% central values in the distribution) is computed. This results in a multiangular profile for the image. The robust mean computation ensures that the result is not influenced by small nonuniformities. As long as less than half of the image is non-uniform, the influence remains minimal.

A large enough set of single-image profiles covers the whole field of view and offers values from multiple profiles for every sensor pixel. The overall profile is obtained by computing per pixel a trimmed mean of the single-image profile values.

The method is validated on a test set of 100 images of Dome C Antarctica, captured with the SPOT-VGT 2 instrument. Validation was performed in different ways. First, the image set was split in two equal subsets and sensitivity profiles calculated separately for both.

Comparison showed that both results are very strongly correlated which indicates that they represent sensor characteristics and not target nonuniformities. The profiles were also used to correct the images of the other subset:

frequency analysis shows that the strong peak in high frequency (corresponding to variations at 1 pixel distance) is almost completely removed. Visual inspection of corrected images confirms that the striping is removed almost completely. Finally, the profiles were compared to original multiangular calibration results of the SPOT-VGT 2 mission. Again, a high degree of correlation was observed.

The validation tests show that the proposed method works well and allows accurate multiangular calibration, even from images which are not completely uniform and much smaller than the instruments field of view.

8533-50, Session 11

Characterisation methods for the hyperspectral sensor HySpex at DLR's calibration home base

Andreas Baumgartner, Peter Gege, Claas Köhler, Karim Lenhard, Thomas Schwarzmaier, Deutsches Zentrum für Luft- und Raumfahrt e.V. (Germany) and Remote Sensing Technology Institute (IMF) (Germany)

The German Aerospace Center's (DLR) Remote Sensing Technology Institute (IMF) operates a laboratory for the characterisation of imaging spectrometers. Originally designed as Calibration Home Base (CHB) for the imaging spectrometer APEX, the laboratory can be used to characterise nearly every airborne hyperspectral system. Characterisation methods will be demonstrated exemplarily with HySpex, an airborne imaging spectrometer system from Norsk Elektro Optikks A/S (NEO). Consisting of two separate devices (VNIR-1600 and SWIR-320m-e) the setup covers the spectral range from 400 nm to 2500 nm. Both airborne sensors have been characterised at NEO. This includes measurement of spectral and spatial resolution and misregistration, polarisation sensitivity, signal to noise ratios and the radiometric response. The same parameters have been examined at the CHB and were used to validate the NEO measurements. Additionally, the line spread functions (LSF) in across and along track direction, the spectral response functions (SRF) for certain detector pixels, the radiometric response, spectral straylight and nonlinearity were measured. The LSFs were measured by imaging a scanning slit on the detector. The SRFs were gained by illuminating sensor channels with scanned monochromatic light. A tuneable laser was used to extract spectral straylight. The radiometric response was measured with an integrating sphere, which was also used to obtain information about the linearity of the detector by changing neutral filters or integration times. The high degree of lab automation allows the determination of the SRFs and LSFs for a large amount of sampling points. Despite this, the measurement of these functions for every detector element would be too time-consuming as typical detectors have ~10^5 elements. But with enough sampling points it is possible to interpolate the attributes of the remaining pixels. The knowledge of these properties for every detector element allows the quantification of spectral and spatial misregistration (smile and keystone) and a better calibration of airborne data. Further laboratory measurements are used to validate the models for the spectral and spatial properties of the imaging spectrometers. Compared to the future German spaceborne hyperspectral Imager EnMAP, the HySpex sensors have the same or higher spectral and spatial resolution and also two detector arrays. This makes it possible to use the system as an EnMAP simulator. The acquired airborne data will be used to prepare for and validate the spaceborne system's data.

8533-51, Session 11

Laboratory test simulation for non-flat response calibration of global Earth albedo monitor

Sehyun Seong, Sug-Whan Kim, Dongok Ryu, Yonsei Univ. (Korea, Republic of); Jinsuk Hong, Samsung Thales Co., Ltd. (Korea, Republic of); Mike Lockwood, The Univ. of Reading (United Kingdom)

In this report, we present laboratory test simulation for directional responsivity of a global Earth albedo monitoring instrument. The sensor is to observe the Sun and the Earth, alternately, and measure their shortwave (< 4?m) radiations around the L1 halo orbit to obtain global Earth albedo. The instrument consists of two channels (a broadband scanning radiometer, an imager with ±2° field-of-view). In the case of the energy channel instrument, radiations arriving at the viewing ports from the Sun and the Earth are directed toward the pyroelectric detector via two spherical folding mirrors and a 3D compound parabolic concentrator (CPC). They have different ray paths along the radiometer optical train and the directions of the incident lights are fed with scanned images obtained from the F/4 Cassegrain telescope with linear CCDs of the visible channel instrument. The instrument responsivity is defined by the ratio of the incident radiation input to the instrument output. The radiometer's directional responsivity needs to be characterized across the field-of-view to calibrate output signal. The spatial responsivity is to measure before and after the flight. In both cases, a distant small source (DSS) configuration is needed. For the laboratory test, the DSS configuration consists of an off-axis Newtonian collimator and the energy channel instrument with directional adjustable mounts. The collimating beam is produced by the Lambertian point source and the F/3.8 Newtonian telescope. Light source from a tungsten halogen lamp with controlled color temperatures from 2,700K to 3,000K illuminates an integrating sphere, internally. The diffused lights from the integrating sphere exit port are passed through a pinhole having several hundred micron aperture. The beam is transmitted via band pass filter, reflected by a flat folding mirror, and directed to an off-axis parabolic (OAP)

mirror. After reflecting by the OAP mirror, the lights are collimated with an order of arc minute beam divergence angle. The energy channel instrument can be rotated on x- and y-field axes and this makes the incident lights have field angles for directional responsivity measurement. The incident lights are focused in front of the 3D CPC entrance aperture by two spherical folding mirrors, and chopped at the focused position by shutter. The modulated lights are concentrated on the pyroelectric detector surface by the 3D CPC. The laboratory test simulation for predicting the instrument directional responsivity was conducted by a radiative transfer computation with Monte Carlo ray tracing techniques and an analytic signal computation with flux-to-signal conversion algorithms while considering pyroelectric detector properties. In the radiometric simulation, especially, measured BRDF of the 3D CPC was used for scattering effects on radiometry. With diamond turned 3D CPC inner surface, the anisotropic surface scattering model from the measured data was applied to ray tracing computation. The technical details of the laboratory test simulation are presented together with future plan.

Conference 8534A: Remote Sensing of Clouds and the Atmosphere

Monday - Tuesday 24–25 September 2012 • Part of Proceedings of SPIE Vol. 8534 Remote Sensing of Clouds and the Atmosphere XVII; and Lidar Technologies, Techniques, and Measurements for Atmospheric Remote Sensing VIII

8534-1, Session 1

Preliminary results of a Lidar-Dial integrated system for the automatic detection of atmospheric pollutants

Pasquale Gaudio, Michela Gelfusa, Maria Richetta, Univ. degli Studi di Roma Tor Vergata (Italy)

In the last decades, atmospheric pollution in urban and industrial areas has become a major concern of developed countries. In this context, surveying relative large area in an automatic way is an increasing common objective of public health organisations. The Lidar-Dial technology is widely recognised as a cost-effective approach to monitor the atmospheric and for example, has been successful applied to the early detection of forest fire.

The investigation described in this paper are concerned with the development of a Lidar-Dial integrated system to detect suddenly release in air of harmful and polluting substances.

The approach consists of continuous monitoring of the surveillance area with a Lidar type measurement. Once a significantly increase in density is revealed, the Dial technique is used to identify the released chemicals.

In the paper, the specifications and the requirements of the measurements are discussed. The most stringent specification is the need for a very compact system with a range of at least 600-700 m. Of course, the optical wavelengths must be in an absolute eye-safe range for humans. A conceptual design of the entire system is described and the most important characteristic of the main elements are provided. In particular as sources it is planned to use either a solid state a CO2 lasers after a carefully assets of their competitive performance. Since the detection of dangerous substances must be performed in an automatic way, the monitoring station will be equipped with an adequate set of control and communication devices for independent autonomous operation.

The results of the first preliminary tests illustrate the potential of the chosen approach.

8534-2, Session 1

Ozone vertical profile measurements with the Ozone Mapper Profiler Suite (OMPS) Limb Profiler

Didier F. Rault, NASA Langley Research Ctr. (United States)

The Ozone Mapper Profiler Suite (OMPS) was launched in October 2011 on board of the Suomi NPP sun-synchronous space platform. The aim of the OMPS mission is to continue monitoring the global distribution of the Earth's middle atmosphere ozone and aerosol. OMPS is composed of three instruments, namely the Total Column Mapper (heritage: TOMS, OMI), the Nadir Profiler (heritage: SBUV) and the Limb Profiler (heritage: SOLSE/LORE, SAGE III, OSIRIS, SCIAMACHY).The focus of the paper will be on the Limb Profiler (LP) instrument. The LP instrument measures the Earth's limb radiance, from which ozone vertical profiles are retrieved from the upper tropopause up to 60 km. Pre-launch end-to-end studies of the sensor and retrieval algorithm have predicted ozone accuracy of 5% or better (from the tropopause up to 50 km), precision of about 3-5% from 18 to 50 km, vertical resolution of 1.5-2 km, with vertical sampling of 1 km and along-track horizontal sampling of 1 deg latitude. The paper will describe the on-orbit performance of the sensor and the retrieval algorithm. Early validation of the retrieved ozone and aerosol products will be discussed with comparison of OMPS/LP products with correlated measurements from space-borne and Earth-based sensors.

8534-3, Session 1

Preliminary validation of CERES instruments aboard the NPP and TERRA/AQUA satellites

Zbigniew P. Szewczyk, Science Systems and Applications, Inc. (United States)

The main focus of this paper is a comparison of unfiltered radiances measured by CERES instruments operating on three different platforms, namely the NPP, Terra and Aqua satellites. Data for the comparison have been continuously collected since the launch of the NPP satellite in the fall of 2011, and several strategies can be employed for this purpose. Using a special scanning mode, viewing geometries of instruments (FM5 and FM3, and also FM5 and FM2) can be matched to enable comparison at the unfiltered radiance level, and to provide a large data set for comparing all three channels. In addition, using a special elevation scan profile on FM5 and FM3, an unprecedented high precision dataset can be collected for a more stringent test of the consistency between the two instruments.

In order to compare CERES instruments on the NPP and Terra/Aqua satellites, several data collecting strategies have been designed. They are based on orbit characteristics and scanner capabilities. They are referred to as (i) simultaneous Earth observations, (ii) matched sites targeting, and (iii) a minor plane radiation measurements; they are briefly described in the next section. Calculations are based on a satellite ground track prediction file available for 14 days in advance. Satellite locations are given in one-minute intervals, and then are interpolated to the duration of a single scan or 6.6 sec.

Simultaneous Earth observations. This is a strategy that is readily available for the instruments on board the NPP and Aqua satellites. The NPP and Aqua satellites are in 98.6o and 98.2o sun-synchronous, ascending orbits, respectively, and their altitudes are 825km and 705km. Their equatorial crossing time is 1:30PM, therefore, every 64 hours they fly "in tandem" only separated by a few degrees in the geolocation of their ground-tracks. Specifically, for about 1 minute, or 10 full scans, the groundtracks of both satellites are within 0.25o latitude and 2o longitude. Data collected within this strategy are processed on a 1o ? 1o grid for an average difference.

Matched sites targeting. A unique comparison opportunity is available when groundtracks of the NPP and Aqua satellites are within a 0.25o, and less than 5 minutes apart. These opportunities present themselves less than 10 times per months; however, they offer a comparison of very high precision data. Each opportunity lasts up to 5 minutes, and the comparison is at a footprint level. Scanners on both satellites are operating in a nadir dwell scan profile that produces 330 footprints along their respective groundtracks.

Minor plane radiation measurements. This strategy is devised for comparing measurements taken by FM5 and FM1 or FM2. Since there is common projection point on the groundtracks of both satellites about 68oS and 68oN within 5 minutes, this configuration offers another comparison opportunity. The best comparison viewing direction is in the plane normal to the principal plane, which is designated as the minor plane. The instrument head is kept at the same relative azimuth during the comparison data collection period of about two minutes using a normal scan profile.

A paper will further elaborate on comparison data collection as details become available when FM5 is in a full operational mode. Further details will be also provided regarding data processing, results and statistics for the first six months of data collection.

8534-4, Session 1

Construction of NOAA/NESDIS/STAR AMSU-A-only atmospheric temperature thematic climate data records

Wenhui Wang, Cheng-Zhi Zou, National Oceanic and Atmospheric Administration (United States)

The Advanced Microwave Sounding Unit A (AMSU-A) onboard the National Oceanic and Atmospheric Administration (NOAA), the

European Meteorological Operational satellite programme (MetOp), and the National Aeronautics and Space Administration (NASA) polar orbiting satellites observes layers of atmospheric temperatures from the surface up to the top of the stratosphere since 1998. AMSU-A observations are essential to construct consistent long-term satellite-based temperature climate data records. It is a direct successor of the Microwave Sounding Unit (MSU, 1978-2006) and a predecessor of the Advanced Technology Microwave Sounder onboard the current NPP and the future JPSS satellites. AMSU-A data are also important for extending the historical Stratospheric Sounding Unit (1978-2006) observations to present time and the future.

We have previously inter-calibrated AMSU-A atmospheric temperature channels using the simultaneous nadir overpass and global ocean mean temperatures time series. AMSU-A channel 5, 7, and 9 has been merged to the MSU to generate 30+ years of atmospheric temperature datasets (Zou and Wang, 2011). In this study, we focus on methodologies to construct consistent, AMSU-A-only upper atmospheric temperature thematic climate data records (TCDRs). Most high quality AMSU-A channel observations were not used in our previous study and the methods employed then were inadequate to address problems encountered in all AMSU-A upper air channels. In this study, we developed a new general frame work that is based on extensive radiative transfer simulation and NASA MERRA reanalysis to address a variety of pre-merging issues. These issues include corrections of limb effect, sensor zenith angle drift, diurnal drift, and adjustments of frequency drift in NOAA-15 channel 6 and between MSU and AMSU-A channels. After the pre-merging corrections and adjustments, grid-based (Zou and Wang, 2011) and zonal mean (Mears and Wentz, 2009) methods for merging AMSU-A data from different satellites will be evaluated. The well performed merging method will be used to generate the NOAA/NESDIS/STAR AMSU-A atmospheric temperature TCDRs.

Totally 14 channels of 13-year (1998-2011) global gridded AMSU-A atmospheric temperature TCDRs will be constructed in this study: (1) AMSU-A channels 5-14 atmospheric temperatures (from mid-troposphere to top-stratosphere); (2) MSU equivalent measurements from AMSU-A at mid-troposphere, upper-stratosphere, and lower-stratosphere; (3) MSU equivalent lower tropospheric temperatures (Christy et al., 2003; Mears and Wentz, 2009) from AMSU-A channel 5. AMSU-A observations from 6 satellites, including NOAA-15 through 18, NASA Aqua, and MetOp-A will be merged. Figure 1 shows global mean temperatures time series and trends generated using our preliminary AMSU-A channels 5-14 atmospheric temperatures TCDRs and grid-based merging method. Figure 2 shows AMSU-A channels 5 and 7-13 averaged temperature trends around latitude circles for 1998-2011.

References

Christy et al. (2003) Error estimates of version 5.0 of MSU-AMSU bulk atmospheric temperatures, J. Atmos. Oceanic Technol., 20(5), 613-629.

Mears and Wentz (2009) Construction of the Remote Sensing Systems V3.2 atmospheric temperature records from the MSU and AMSU microwave sounders, J. Atmos. Oceanic Technol., 26(6), 1040-1056.

Zou and Wang (2011). Intersatellite calibration of AMSU-A observations for weather and climate applications. J. Geophys. Res., 116(D23), D23113

8534-5, Session 1

Snowfall retrieval by the combination of CloudSat-CPR and AQUA/AMSR-E data: a preliminary study

Nari Kim, YangWon Lee, YoungSeup Kim, Pukyong National Univ. (Korea, Republic of)

Snowfall retrieval algorithm was developed by combining two data source; reflectivity of CloudSat-CPR as an active microwave sensor and brightness temperature of AMSR-E as a passive microwave sensor, and investigated an application possibility. The vertical reflectivity values of 20 from surface observed by Cloudsat and brightness temperature for 9 channels (10.75GHz, 18.7GHz, 23.8GHz, 36.5GHz, 89.0 GHz) of AMSR-E. Study area is located from 30°N to 45°N in latitude and from 120°E to 135°E in longitude. The orbit of CloudSat is corresponded with AQUA and they observed Korea region by a margin of about 90 seconds. Thus, data when satellites passed through Korea region composed the dataset. Reflectivity from Cloudsat was averaged because CloudSat has higher horizontal resolution than AMSR-E, the resolution of two data was matched.

First, AMSR-E data was classified into clear sky and snowfall. The brightness temperature observed by 9 channels of AMSR-E is influenced by surface and atmosphere. In order to remove such effect, we performed the Principle Components Analysis (PCA) about clear sky data. Of mode values of 9 calculated by PCA we used the rest mode values after removing mode 1 and 2 that represented effect on surface. Using the calculated mode values, weighted brightness temperature (wtT) was computed.

Second, we performed the PCA for 20 vertical reflectivity values to extract the components that strongly affects snowfall effect. Using mode 1 values, weighted reflectivity (Z') was computed.

Through the regression analysis for wtT and Z' values, we set up the linear regression equation, and performed the snowfall retrieval using only brightness temperature of AMSR-E finally. The case study carried out by snowfall retrieval algorithm. Images for each of AMSR-E channels, snowfall was not able to identify. On the other hand, images using snowfall retrieval algorithm was able to detect for snowfall on the sea but unidentifiable on the land.

In this study, snowfall retrieval algorithm was highly applicable to the ocean regions, but it needed additional researches for the land region.

8534-6, Session 1

Preliminary results of the PreViBOSS project: description of the fog life cycle by ground-based and satellite observation

Thierry G. Elias, Dominique Jolivet, Hygeos (France); Jean-Charles Dupont, Martial Haeffelin, Ecole Polytechnique (France); Frédéric Burnet, Meteo-France CNRM (France)

The PreViBOSS project consists in using observation to improve visibility forecast in the fog life cycle (on a time scale of few hours). Ground-based instrumentation is set up at the SIRTA Observatory (http://sirta.ipsl.fr/) to sound microphysical and optical properties of the boundary layer aerosols and droplets during three seasons of the ParisFog field campaign (2010-2013), and satellite observation provides documentation of the cloud field above and around the SIRTA. The EUMETSAT NWC/SAF (Nowcasting / Satellite Application Facilities) cloud type product will be exploited to provide an indicator of the cloud field impact on the fog life cycle.

The PreViBOSS project will be presented as well as preliminary results. First, the fog life cycle is described with in situ data from a meteorological mast, a visibilimeter, a ceilometer as well as aerosol and droplet counters. The fog life cycle is defined as the chronological sequence 'clear sky - mist - n(fog - mist) - clear sky', where the 'fog-mist' sub-sequence may be observed several times (n can be included between 1 and 3). During both 2010-2011 and 2011-2012 seasons, around 400 hours of fog are observed (visibility smaller than 1000 m) as well as around 1700 hours of mist (visibility included between 1000 and 5000 m). Around 50% of fogs form after stratus lowering while other 50% of fogs form exclusively after radiative cooling. In November 2011, averaged visibility in the fog is 350±250 m.

Second, NWC/SAF cloud type is compared to ground-based observation of the cloud cover with radiometers, lidars and radars set up at the SIRTA. A focus is thrown on 1) the ground-based observation of the cloud cover when 'Very Low Cloud' type is identified by the satellite instrument; 2) the cloud typology defined by the satellite instrument during the fog life cycle identified by ground-based observation.

8534-7, Session 1

Multi-year satellite and surface observations of AOD in support of Two-Column Aerosol Project (TCAP) field campaign

Evgueni I. Kassianov, Duli Chand, Larry K. Berg, Jerome Fast, Jason Tomlinson, Pacific Northwest National Lab. (United States); Richard Ferrare, Chris Hostetler , John Hair , NASA Langley Research Center (United States)

Satellite and ground-based observations of atmospheric aerosols have been available for several decades and have provided many opportunities to analyze the temporal and spatial variability of the properties of atmospheric aerosols that are relevant to understanding

climate. In this presentation, we will present an analysis of satellite-derived aerosol optical depth (AOD) and discuss its variability as a function of: i) proximity to a large urban area, ii) season and iii) time of day; these results will be compared to observations from a nearby AERONET station. Our analysis is based primarily on observations from the MODIS Terra satellite and the MODIS Aqua satellite. Use is also made of the CALIPSO system to identify elevated aerosol layers which contribute to changes in the AOD. The motivation for this study is two-fold. First, observations such as these are of intrinsic interest to understanding the energy budget within a column of air, and hence are directly related to many climate issues. Second, these observations are now playing a key role in defining flight plans and sampling strategies for the 2012-2013 Two Column Aerosol Program (TCAP), during which a combined set of in situ air aircraft measurements supplemented by a High Spectral Resolution Lidar (HSRL) will be made. These measurements will provide detailed information with which to evaluate the ability of climate models to simulate AOD.

8534-8, Session 2

Results from long-term detection of mixing layer height: different ceilometer sites and comparison with Radio-Acoustic Sounding System

Klaus Schäfer, Stefan Emeis, Carsten Jahn, Karlsruher Institut für Technologie (Germany); Christoph Münkel, Vaisala GmbH (Germany)

The mixing layer height (MLH) is an important factor which influences exchange processes of ground level emissions. The continuous knowledge of MLH is supporting the understanding of processes directing air quality. If the MLH is located near to the ground, which occurs mainly during winter and night-time, air pollution can be high due to a strongly limited air mass dilution.

Since 2006 different methods for long-term continuous remote sensing of mixing layer height (MLH) are operated in Augsburg. The Vaisala ceilometers LD40 and CL31 are used which are eye-safe commercial mini-lidar systems. The ceilometer measurements provide information about the range-dependent aerosol concentration; gradient minima within this profile mark the borders of mixed layers. Special software for these ceilometers provides routine retrievals of lower atmosphere layering from vertical profiles of laser backscatter data. The radiosonde data from the station Oberschleissheim near Munich (about 50 km away from Augsburg city) are also used for MLH determination. The profile behaviour of relative humidity (strong decrease) and virtual potential temperature (inversion) of the radiosonde agree mostly well with the MLH indication from ceilometer laser backscatter density gradients.

A RASS (Radio-Acoustic Sounding System) from Metek is applied which detects the height of a turbulent layer characterized by high acoustic backscatter intensities due to thermal fluctuations and a high variance of the vertical velocity component as well as the vertical temperature profile from the detection of acoustic signal propagation and thus temperature inversions which mark atmospheric layers. These data of RASS measurements are the input for a software-based determination of MLH. A comparison of the results of the remote sensing methods during simultaneous measurements was performed. The information content of the different remote sensing instruments for MLH in dependence from different weather classes was analysed further. A special focus is the continuous determination of MLH.

Since 2010 a LD40 is installed to determine MLH at the site Höglwald (about 15 km away from Augsburg city). The performance of the ceilometers is sufficient to detect convective layer depths exceeding 2000 m and nocturnal stable layers down to 50 m. The remote sensing of the MLH in Augsburg and at the site Höglwald are compared to find an enhancement of MLH above the urban area.

8534-9, Session 2

Detection of mixing layer height by ceilometer and air pollution in urban area

Klaus Schäfer, Stefan Emeis, Carsten Jahn, Karlsruher Institut für Technologie (Germany); Patrick Wagner, Univ. Duisburg-Essen (Germany); Christoph Muenkel, Vaisala GmbH (Germany)

Ceilometers are applied by KIT/IMK-IFU to detect layering of the lower atmosphere continuously. This is necessary because not only wind speeds and directions but also atmospheric layering and especially the mixing layer height (MLH) influence exchange processes of ground level emissions. It will be discussed how the ceilometer monitoring information is used to interpret the air pollution near the ground.

The information about atmospheric layering is continuously monitored by uninterrupted remote sensing measurements with the Vaisala ceilometer CL51 which is an eye-safe commercial mini-lidar system. Special software for this ceilometer provides routine retrievals of lower atmosphere layering from vertical profiles of laser backscatter data. The air pollution is detected by the University of Duisburg-Essen (UED) for some volatile organic compounds (VOC) with a gas chromatograph. The meteorological data are collected by the UDE and the monitoring station Essen of the German National Meteorological Service (DWD).

An intensive measurement period during the winter 2011/2012 is studied. The weather situations are characterized, the meteorological influences upon air pollutant concentrations like wind speed and wind direction are studied and the correlations of ceilometer MLH with VOC concentrations are determined.

8534-10, Session 2

Assessing the relations between spectral sensitivity and integrated water vapor for NDSA processing applied to a radio link between two LEO satellites

Luca Facheris, Fabrizio Cuccoli, Univ. degli Studi di Firenze (Italy); Susanne Schweitzer, Karl-Franzens-Univ. Graz (Austria)

The concept of Normalized Differential Spectral Attenuation (NDSA) was introduced years ago by the first two authors, and related studies for tropospheric water vapor sounding utilizing a couple of LEO satellites (one carrying a transmitter, the other a receiver and operating in the Ku/K bands) in a limb geometry were supported by ESA. A basic reason was that NDSA proved to be a valid candidate to reduce tropospheric scintillation effects. NDSA is based on the conversion of a spectral parameter (the spectral sensitivity S), into the total content of water vapor (hereafter IWV, Integrated Water Vapor) along the propagation path between the two LEO satellites. To measure S, it is required that the total attenuations at two relatively close frequencies, symmetrically placed around a reference frequency fo , are simultaneously estimated.

In particular, the potential of S to provide direct estimates of IWV along LEO-LEO tropospheric propagation paths in the 15 to 25 GHz interval was shown, accounting for the natural variations of the atmospheric conditions in ideal measurement conditions (no disturbance at the receiver nor propagation impairments). Such variations were obtained based on real radiosonde data, on the Liebe atmospheric propagation model and on a spherically symmetric atmosphere: IWV was computed along the radio path, S simulated separately and finally the IWV-S relationships at various altitudes obtained. These could then be used as empirical relationships to directly convert S measurements into IWV estimates.

During further studies it was envisaged that frequencies from 179 to 182 GHz (M band) have a great potential for estimating IWV at the highest tropospheric altitudes (from 10 km upwards). Also, the 30 GHz channel was identified as the optimal one to detect the presence of liquid water in the LEO-LEO link.

However, two basic problems affect the reliability of the empirical IWV-S relations found so far: the first is the fact that the accuracy of the radiosonde data used to derive them were not uniformly distributed in the northern and southern hemisphere; the second is the limited amount of radiosonde data available at the highest altitudes (above 10 km), and its scarce reliability. The second problem evidently affects the reliability analysis of the IWV-S relations in the M band.

In this paper we present the results of a global scale analysis of the IWV-S relations made utilizing the ECMWF global atmospheric model. We prepared a global database including three-dimensional fields (5° latitude x 5° longitude, vertical sampling about 1 km, up to 20 km altitude, step 0.5 km) of pressure, temperature, humidity, liquid water, ice water and wind components. Eight global datasets in the four seasons and at dedicated time layers (12:00 UTC and 24:00 UTC) were compiled on the basis of ECMWF T511L91 analyses. S and IWV were simulated and computed at all altitudes from 0 to 20 km as described above, obtaining IWV-S relations for 17, 19, 21, 179 and 182 GHz.

Also the relations between Integrated Liquid Water (ILW) and S at 30 GHz have been considered, confirming the potential of this frequency to detect and possibly correct for errors on IWV estimates due to liquid water along the LEO-LEO propagation path.

8534-11, Session 2

The development of air quality indices through image-retrieved AOT and PM10 measurements in Limassol Cyprus

Kyriacos Themistocleous, Diofantos G. Hadjimitsis, Cyprus Univ. of Technology (Cyprus); Adrianos Retalis, National Observatory of Athens (Greece); Nektarios Chrysoulakis, Foundation for Research and Technology (Greece)

Research indicates that aerosol optical thickness (AOT) values and particulate matter (PM10) measurements can be used as indicators of atmospheric pollution. The problem of relating AOT with suspended particulate matter near the ground is still an open question. While satellite images can provide reliable and synoptic measurements from space, comparisons with monitoring surface level air pollution continues to be a challenge since satellite measurements are column-integrated quantities. In this study, in-situ spectroradiometric measurements were taken during satellite overpass using field spectrometers to obtain the reflectance values of the calibration targets used. Sun photometer measurements were taken with the Microtops hand-held sun photometer to measure AOT. Meteorological data was collected from nearby meteorological stations and PM10 measurements were collected from local mobile air pollution stations. Following, the darkest pixel method of atmospheric correction was applied to a series of Landsat satellite images. The reflectance values of the atmospherically-corrected image were used in the radiative transfer equation to solve for AOT. Thematic maps were generated in order to develop air quality indices. The image-derived AOT values were examined for a positive correlation with PM10 measurements. It appears there exists a significant correlation between AOT and PM10 measurements. This study was conducted as part of the LIFE09 ENV/CY/000252-PM3 study and is supported by the European Commission under the LIFE+ Environment and Governance Programme.

8534-12, Session 2

Local distribution of PM2.5 concentration over Osaka based on space and ground measurements

Itaru Sano, Sonoyo Mukai, Makiko Nakata, Kinki Univ. (Japan); Nobuo Sugimoto, National Institute for Environmental Studies (Japan); Brent N. Holben, NASA Goddard Space Flight Ctr. (United States)

This work intends to estimate PM2.5 concentration over mega city Osaka in Japan based on both satellite and ground measurements. Our work is composed of the following steps. At first the relationship between PM2.5 and aerosol optical thickness (AOT) is derived by using the measurements with ground sun photometer and PM-sampler. In addition vertical concentration of aerosol particles are also investigated by LIDAR measurements. The second step is to retrieve columnar AOT distribution from the space-based reflectance information with CAI (cloud aerosol imager) on GOSAT (greenhouse gases observing satellite). Note that, the PM2.5 measurements indicate the surface level concentration of the atmospheric particles, and hence the columnar AOT distribution should be converted to the surface level aerosol optical depth (AOD) based on the aerosol extinction profile with LIDAR. Finally, PM2.5 distribution is obtained from the relationship derived at the first step. The estimated PM2.5 distribution is partially validated with the sampling of PM2.5 at the surface.

8534-13, Session 2

Remote sensing of BVOC isoprene retrieval based on ambient concentrations and ecosystem type

Man Sing C. Wong, Janet E. Nichol, The Hong Kong Polytechnic Univ. (Hong Kong, China); Latifur Sarker, Univ. of Teknologi Malaysia (Malaysia)

This paper presents an interactive model to relate Biogenic Volatile Organic Compounds (BVOC) isoprene emissions to ecosystem type, as well as environmental drivers such as light intensity, temperature, landscape factor and foliar density. Data and techniques have recently become available which can permit new improved estimates of isoprene emissions over Hong Kong. The techniques are based on Guenther et al.'s (1993, 1999) model. The spatially detailed mapping of isoprene emissions over Hong Kong at a resolution of 100m and an interactive database are constructed for retrieval of the map for any day of the year upon input of the prevailing climatic parameters. This approach assigns emission rates directly to ecosystem types not to individual species, since unlike in temperate regions where one or two single species may dominate over large regions, Hong Kong's vegetation is extremely diverse with up to 300 different species in one hectare. Field measurements of emissions by canister sampling obtained a range of ambient emissions according to different climatic conditions for Hong Kong's main ecosystem types in both urban and rural areas, and these were used for model validation. Results show the model-derived isoprene flux to have moderate to high correlations with field observations (i.e. r2=0.45, r2=0.64, r2=0.50 for all 53 field measurements, subset for summer, and winter data respectively) which indicate the robustness of the approach when applied to tropical forests at detailed level, as well as the promising role of remote sensing in isoprene mapping. The interactive raster database provides a simple and low cost estimation of the BVOC isoprene in Hong Kong at detailed level. City planners and environmental authorities may use the derived models for estimating isoprene transportation, and its interaction with anthropogenic pollutants in urban areas.

8534-14, Session 3

Cloud detection and characterization using topological data analysis

Chona S. Guiang, Robert Y. Levine, Spectral Sciences, Inc. (United States)

The presence of cirrus clouds introduces a net heating effect on the atmosphere and can also interfere with high altitude or satellite remote sensing. Previous work on detection and characterization of cirrus clouds have been based on observing spectral signatures across spectral channels with significant water absorption [Gao 1995], or calculation of radiant intensity ratios over a water band to a reference spectral channel [Adler-Golden 1999].

Our proposed approach is based on applying computational homology to characterize the topological properties of cloud reflectance. We utilize an application called JPLEX [JPLEX] to study the persistent homology of multi-dimensional simplicial complexes built from available hyperspectral or multispectral data. The technique has been successfully applied to discriminate subtle features in high dimensional noisy data. Previous examples include pixel classification and anomaly detection in hyperspectral images. JPLEX analysis makes use of the entire multidimensional data set (not just one or a combination of spectral bands) which may offer advantages in discriminating among various cloud types in a scene, as well as determining other characteristics of cirrus clouds such as altitude and thickness. The JPLEX input consisted of the LandSat six spectral bands in an unprocessed data cube of 8261 x 7261 pixels. Simplicial complexes are built as a function of scale s, in the abstract 7-dimensional radiance-spectral band space. Each complex is then characterized by a set of topologically invariant parameters called Betti numbers. The appearance and disappearance of simplicial k-complexes over the length scale s are catalogued by a set of k Betti numbers defined over intervals, which produce characteristic patterns of "bar codes." The resulting bar codes capture discriminating shape features in the high dimensional data cube. For example voids in the cube space, which may be due to unobserved physical constraints, alter the bar codes. Our initial computational experiment with a LandSat ocean scene has demonstrated that JPLEX can discriminate between cumulus and cirrus clouds, and that similar bar code patterns are observed for the same cloud type.

Next, we will perform the same topological analysis for cirrus clouds at different altitudes, using JPLEX to generate sets of bar codes, interpret the results in terms of higher-dimensional structures in the data (e.g., formation of voids), and then associate the calculated bar codes with observables that correlate with cloud altitude (e.g., water column amount above the cloud.) For a more compact and revealing representation of the "birth and death" of topological structures, as

well as a mathematical framework in which to evaluate the similarities and differences among bar codes, we will consider Harer's formal definition of the space of persistence diagrams [Mileyko 2011]. Validation of retrieved altitudes and cloud thickness will be made against established cirrus detection and characterization algorithms. Finally, we will assess the robustness of this topological approach against noise and background clutter.

References:

B. C. Gao and Y. J. Kaufman, "Correction of Thin Cirrus Effects in AVIRIS Images Using the Sensitive 1.375 m Cirrus Detecting Channel," Summaries of the Fifth Annual JPL Earth Science Workshop, JPL Publication 95-4, 1, 1995, pp. 59-62

S. M. Adler-Golden, R. Y. Levine, A. Berk, L. S. Bernstein, G. P. Anderson and B. Pukall, "Detection of Cirrus Clouds at 1.13 m in AVIRIS Scenes Over Land," SPIE 3756, 1999, 368-373.

JPLEX: http://comptop.stanford.edu/u/programs/jplex/ Y. Mileyko, S. Mukherjee and J. Harer, "Probability Measures on the Space of Persistence Diagrams," Inverse Problems, 27, 2011, 124007.

8534-15, Session 3

Fast Monte Carlo-assisted simulation of cloudy Earth backgrounds

Steven Adler-Golden, Steven Richtsmeier, Alexander Berk, James W. Duff, Spectral Sciences, Inc. (United States)

The design of optical remote sensing systems and projection of their performance require good estimates of the expected radiance levels and their spectral and spatial distributions. In particular, there is a need for software that can rapidly generate a wide, representative variety of radiometrically accurate images of the earth's atmosphere and surface at arbitrary optical wavelengths in views from aircraft and spacecraft.

The biggest challenge is the quantitative modeling of cloud fields and their effects, which require calculations with a 3-D radiation transport (RT) code. Such calculations are typically very time-consuming, making them prohibitive for on-the-fly use and limiting the ability to assemble a comprehensive pre-calculated database. The input variables that specify a scene are numerous, and include surface properties, which are geographically and seasonally dependent, observer line-of-sight variables, solar illumination angles, wavelength, atmosphere model and cloud type and coverage. An image library that fully covers the scenarios of interest might require around 104 monochromatic images, each of which might take an hour or more to compute on a PC processor with a 3-D Monte Carlo RT code such as MCScene [1].

Here we describe a practical solution in which the image radiance is decomposed into components that each depends on only a small number of input variables, thereby reducing the required calculations by orders of magnitude. A first-principles RT model is used to combine pre-calculated cloud field databases with separate surface and upper atmospheric descriptions to build the desired scene. The model is a generalization to 3-D atmospheres of an equation used for atmospheric compensation in clear sky conditions [2]. The cloud fields are described by direct and diffuse transmittance and path radiance images, which are calculated by MCScene using a voxelized cloud model. A local correlation-based data fusion method is used to suppress Monte Carlo "photon" noise, dramatically speeding the convergence of the MCScene calculations and enabling assembly of an extensive cloud image database in reasonable time. In addition, the observed low spectral dimensionality of the cloud field database allows the use of sparse pixel sampling to extend the simulations from the multispectral domain (several to tens of bands) to the hyperspectral domain (hundreds of bands) with little or no additional computational effort.

In this paper we will present a discussion on the radiation transport model for above-cloud viewing and outline the MCScene cloud field calculations that provide the model inputs. We also describe the noise reduction and sparse sampling methods used to reduce computation time. Finally, the new technique and "exact" direct Monte Carlo simulation are compared for several scenes.

References:

[1] Sundberg, R., S. Richtsmeier, and R. Haren, "Monte Carlo-Based Hyperspectral Scene Simulation," Second Annual WHISPERS Conference, Reykjavik, Iceland, 14-16 June (2010).

[2]

[3] Matthew, M. W., S. M. Adler-Golden, A. Berk, G. Felde, G. P. Anderson, D. Gorodetzky, S. Paswaters and M. Shippert, "Atmospheric Correction of Spectral Imagery: Evaluation of the FLAASH Algorithm with AVIRIS Data," SPIE Proceeding, Algorithms and Technologies for Multispectral, Hyperspectral, and Ultraspectral Imagery IX (2003).

8534-16, Session 3

Numeric modeling in non-stationary problems of laser sensing of scattering media: new effective Monte Carlo code

Boris A. Kargin, Yevgeniya Kablukova, Institute of Computational Mathematics and Mathematical Geophysics (Russian Federation)

Non-stationary problems of laser sensing are of great interest in connection with the wide practice of using laser sensors (LIDARs) placed on the ground, on aircraft and in space to quickly diagnose aerosol contaminants in the atmosphere, the space-time transformation of aerosols' microphysical properties and various types of cloud particles, to determine remotely the hydrophysical properties of the ocean, to discover the upper and lower boundaries of cloudiness and to solve a variety of other problems of optical remote sensing of the natural medium. It's possible to get acquainted in more detail with a list of certain modern physical problems' statements for problems of laser sensing of the atmosphere and ocean and corresponding methods of statistical modeling in the quite recent review [1]. The justification of using the Monte-Carlo methods as well as elaboration of corresponding algorithms for solving non-stationary problems of transfer theory of optical radiation in scattering and absorbing media have been performed quite a long time ago in a series of early works, which were summarized in [2]. The laser sensing problems under consideration are different from many other problems of atmosphere optics because of the complex boundary conditions related to the finite size of the source radiation beam and small phase volume of the detector as well as the principally non-stationary character of the transfer process being modeled. This condition is responsible for typical requirements to the technique of statistical modeling and determines the necessity of using local estimates which, though labor-intensive, are the only possible method of calculating sought for radiation properties registered by a detector with a small phase volume. Such problems belong to the class of so-called "big" problems of mathematical physics and for their solution serious computing resources, including multiprocessor computer systems, are required. That's why one topical issue in solving practical problems of remote laser sensing of natural media by the Monte-Carlo method is the problem of reducing an algorithm's "the cost of computation". For this issue a new optimization of local estimates by means of integrating based upon a discrete-stochastic version of "importance sampling" and using a variation of the "splitting" method is presented in the paper. The computation formulae are presented in detail, including those used to estimate optimal splitting parameters and the node grid for discrete-stochastic integrating of local estimates. The results of a great series of numerical calculation of a laser signal reflected off a cloud layer in dependence on algorithm optimization parameters as well as on optical-geometrical properties of the problem in the scheme of bistatical laser sensing of lowest-layer clouds are presented.

1. Krekov G.M. Monte Carlo method in problems of atmospheric optics / Atmospheric and Oceanic Optics. 2007.Vol. 20, No. 09, pp. 757-766.

2. Marchuk G.I., Mikhailov G.A., Nazaraliev M.A., Darbinian R.A., Kargin B.A., Elepov B.S. Monte Carlo Methods in Atmospheric Optics / SpringerVerlag. 1980. - 208p.

8534-18, Session 3

Infrared measurements throughout polar night using two AERIs in the Arctic

Zen H. Mariani, Kim Strong, Mareile A. Wolff, Univ. of Toronto (Canada); Penny Rowe, Von P. Walden, Univ. of Idaho (United States); Pierre F. Fogal, Univ. of Toronto (Canada); Thomas J. Duck, Glen Lesins, Dalhousie Univ. (Canada); David S. Turner, Environment Canada (Canada); Christopher J. Cox, Univ. of Idaho (United States); Edwin W. Eloranta, Univ. of Wisconsin-Madison (United States); Jim R. Drummond, Dalhousie Univ. (Canada); Claude B. Roy, Richard L. Lachance, ABB Analytical Measurement (Canada); David D. Turner, National Oceanic and

Atmospheric Administration (United States); David R. Hudak, Environment Canada (Canada); Iosif A. Lindenmaier, Univ. of Toronto (Canada)

The Atmospheric Emitted Radiance Interferometer (AERI) is a moderate resolution (1 cm–1) Fourier transform infrared spectrometer used worldwide to characterize the properties of the atmospheric column at the planetary boundary layer and lower tropospheric levels. This remote sensing tool measures absolutely calibrated atmospheric radiance using NIST traceable components, allowing traceability and uncertainty quantification. The Extended-range AERI (E-AERI) version of the instrument can measure the downwelling infrared spectral radiance from the atmosphere between 400 and 3000 cm-1. The extended spectral range of the instrument is particularly useful for monitoring the 400-550 cm-1 (20-25 μm) region, where most of the infrared surface cooling currently occurs in the dry air of the Arctic. Spectra from the E-AERI provide information about radiative balance, trace gases, and cloud properties in the Canadian high Arctic. The instrument was installed at the Polar Environment Atmospheric Research Laboratory (PEARL) Ridge Lab at Eureka, Nunavut, in October 2008. Measurements are taken every seven minutes year-round (precipitation permitting), including polar night when the solar-viewing spectrometers at PEARL are not operated. A similar instrument, the University of Idaho's Polar AERI (P-AERI), was installed at the Zero-altitude PEARL Auxiliary Laboratory (0PAL), 15 km away from the PEARL Ridge Lab, from March 2006 to June 2009. During the period of overlap, these two instruments provided calibrated radiance measurements from two altitudes. A fast line-by-line radiative transfer model is used to simulate the downwelling radiance at both altitudes; the largest differences (simulation - measurement) occur in spectral regions strongly influenced by atmospheric temperature and/or water vapour. The two AERI instruments at close proximity but located at two different altitudes are well-suited for investigating cloud forcing. As an example, it is shown that a thin, low ice cloud resulted in a 6% increase in irradiance. The presence of clouds creates a large surface radiative forcing in the Arctic, particularly in the 750-1200 cm-1 region where the downwelling radiance is several times greater than clear-sky radiances, which is significantly larger than in other more humid regions.

Retrievals of total columns of various trace gases are currently being evaluated using a prototype version of the retrieval algorithm SFIT2 [Pougatchev et al., 1995, Rinsland et al., 1998] modified to analyze emission features. Total columns of O3, CO, CO2, CH4, N2O, HCN, and C2H4 using SFIT2 can be retrieved from E-AERI spectra during clear-sky conditions. Recently, retrievals of CO with high sensitivity to the lower troposphere have been demonstrated for the AERI systems [Yurganov et al., 2010]. In contrast to solar absorption measurements of atmospheric trace gases, which depend on sunlit clear-sky conditions, the use of emission spectra allows measurements year-round (except during precipitation events or when clouds are present). This capability allows the E-AERI to provide temporal coverage throughout the four months of polar night, when the PEARL Bruker 125HR solar absorption FTIR spectrometer is not operated [Batchelor et al., 2009]. This presentation will describe the E-AERI instrument, its measurement site, and the new prototype SFIT2 retrieval code adapted for emission spectra.

8534-19, Session 3

Estimation of aerosol properties from airborne hyperspectral data: a new technique designed for industrial plume characterization

Adrien Deschamps, Rodolphe Marion, Commissariat à l'Énergie Atomique (France); Pierre-Yves Foucher, Xavier Briottet, ONERA (France)

During the last decades, tropospheric aerosols have been widely studied using remote sensing instruments. The growing recognition of the importance of aerosols for climate and global change studies has enabled the development of a number of very significant techniques to estimate their properties from satellite data such as AVHRR, MODIS, MISR, POLDER [1]. However, all these satellites acquire data at relatively low spatial resolution (from 250m for MODIS to several kilometers for POLDER). The characterization of aerosols emission sources at this scale is a challenge, especially for industrial sources.

Therefore, we propose in this study to use airborne hyperspectral imagers to estimate aerosols properties inside an industrial plume. These instruments (e.g. CASI, HyMap, AHS) acquire data in several dozens of spectral bands in the Visible Near Infrared (VNIR) domain with a spatial resolution from one to several meters. Some techniques have been already developed to retrieve information about composition, size and concentration of particles into a thick plume from hyperspectral data [2-3]. However, from now, they can not be applied to industrial plumes, and particularly to thin plumes containing metallic particles.

Indeed, the approach used in these estimation methods is based on Look-Up Tables and requires a physical description of the aerosols mixture (number of components in the mixture, complex refractive index of the components, number of modes in the size distribution). But anthropogenic metallic aerosols - major constituents of industrial emissions - have rarely been studied. The lack of knowledge concerning the properties of this kind of particles did not enable the development of an aerosols model, suitable for particles emitted by a metallurgical plant for instance. Moreover, the developed aerosols retrieval algorithm has been validated for vegetation plumes mostly, which are bright and thick plumes for which the AOT can reach 5. The application of this inversion method to darker and thinner plumes requires modifications in the retrieval procedure.

To bridge this gap, we have conducted a two-step study. Firstly, we have used information provided by recent studies [4-6] to propose a model of physical and optical properties in the VNIR of industrial aerosols mixture containing metallic components, not available from now in the literature. From this model, the radiative properties of an industrial plume and its impact on hyperspectral data have been investigated. Examples of extinction coefficient and single scattering albedo simulated from our aerosols model are given in Fig. 1.

Secondly, the performances of the current aerosols estimation methods have been assessed for industrial plume characterization using synthetic hyperspectral data. From these simulations, a new estimation technique, specially designed for optically thin plumes, has been developed. Also based on Look-Up Tables, this technique separately treats the bright and dark surfaces, to estimate aerosols absorption on one hand and aerosols scattering on another. Moreover, the transitions between different kinds of grounds are used to separate the contribution of ground and aerosol in the radiance signal. After validating the method on data simulated with MODTRAN, we applied it to a real hyperspectral dataset, acquired over the heavy industrialized area of Fos-sur-Mer, France, by the CASI sensor in 2010 through the EUFAR program. Preliminary results are shown in Fig.2

8534-20, Session 3

Aerosol properties from multi-spectral and multi-angular aircraft 4STAR observations: Expected advantages and challenges

Evgueni I Kassianov, Connor Flynn, Pacific Northwest National Lab. (United States); Jens Redemann, Bay Area Environmental Research Institute (United States); Beat Schmid, Pacific Northwest National Lab. (United States); Philip B. Russell, NASA Ames Research Ctr. (United States); Alexander Sinyuk, NASA Goddard Space Flight Ctr. (United States)

Multi-spectral remote sensing applications of the airborne 14-Channel NASA Ames Airborne Tracking Sunphotometer (AATS-14) have mostly focused on extracting important information about atmospheric aerosol and gas constituents from direct solar beam transmission at 14 wavelengths. Recently, the NASA Ames Research Center in collaboration with the Pacific Northwest National Laboratory have made impressive technical improvements and developed the next airborne generation of AATS-14, named the Spectrometer for Sky-Scanning, Sun-Tracking Atmospheric Research (4STAR) with continuous spectral coverage spanning ultraviolet, visible and near-infrared wavelengths with an increased number of channels (more than 1500 pixels) and the sky-scanning ability similar to the ground-based AERONET sun/sky photometers. The upcoming Two-Column Aerosol Project will start in summer 2012 and involve for the first time airborne 4STAR observations in two regions off the coast of North America. We apply a sensitivity study for illustrating both advantages and challenges associated with the airborne multi-spectral and multi-angular observations. One of these challenges is that the 4STAR entrance optics are considerably shorter than those of the ground-based AERONET instruments. As a result, an apparent enhancement of sky radiance can occur at small scattering angles (closer than 6 degrees from the sun). For the sensitivity study, we select cases with a wide range of observational conditions, including different aerosol loadings and types, obtained from multi-year AERONET climatology at a number of sites around the world.

8534-21, Session 4

The comparison of the darkest pixel and empirical line atmospheric correction methods to retrieve aerosol optical thickness using the radiative transfer equations

Kyriacos Themistocleous, Diofantos G. Hadjimitsis, Cyprus Univ. of Technology (Cyprus); Adrianos Retalis, National Observatory of Athens (Greece); Nektarios Chrysoulakis, Foundation for Research and Technology-Hellas (Greece)

This paper presents a comparison of the darkest pixel (DP) and empirical line (EL) atmospheric correction methods in order to examine their effectiveness to retrieve aerosol optical thickness (AOT) using the radiative transfer (RT) equations. Research has found that the DP and the EL methods are the two simplest and most effective methods of atmospheric correction; however, which of the two atmospheric correction methods is more effective in deriving accurate AOT values remains an open question. The accuracy of the DP and EL atmospheric correction methods were examined using pseudo-invariant targets in the urban area of Limassol in Cyprus, by using reflectance values before and after atmospheric correction. Eleven Landsat 5 and Landsat 7 satellite images were atmospherically corrected using both the DP and EL methods. The reflectance values following the DP and EL method of atmospheric correction were used in the radiative transfer equation to derive the AOT values. Following, an accuracy assessment was conducted comparing the in-situ AOT values as measured from sun photometers with the AOT values derived from the RT equations in order to determine the effectiveness of the DP and EL methods for retrieving AOT. The study found that the EL atmospheric correction method provided more accurate AOT values than the DP method.

8534-22, Session 4

The use of volcanic beach sand as a pseudo-invariant target for atmospheric correction using Landsat images

Kyriacos Themistocleous, Diofantos G. Hadjimitsis, Cyprus Univ. of Technology (Cyprus); Adrianos Retalis, National Observatory of Athens (Cyprus); Nektarios Chrysoulakis, Foundation for Research and Technology-Hellas (Greece)

Pseudo-invariant targets are often used for atmospheric correction, as their reflectance values are stable across time. Sand is often used as a pseudo-invariant target, although there is conflicting research about its effectiveness as a pseudo invariant target. This study will examine the effectiveness of volcanic sand as a pseudo-invariant target. The study area is a 250x250 meter area of volcanic beach sand near Limassol, Cyprus. In-situ spectroradiometric measurements were taken using field spectrometers to obtain the reflectance values of volcanic sand over wet and dry conditions. The varying saturation levels of the sand due to rainfall, humidity and high temperatures was considered. A series of Landsat-5 TM and Landsat-7 ETM+ satellite imagery were atmospherically corrected using the darkest pixel method in order to assess the effectiveness of the volcanic sand as a pseudo-invariant target. The mean in-situ in-band reflectance values as found from the ground measurements were compared with the at-satellite reflectance values following atmospheric correction. It was found that precipitation conditions such as rainfall affected the reflectance values of sand. The study found that wet sand had a significantly lower reflectance value compared to dry sand. Further, salinization also affected the reflectance value of volcanic sand. Therefore, precipitation conditions need to be considered when using sand as a non-variant target for atmospheric correction.

8534-23, Session 4

Remote sensing of chemical gas cloud emission by passive infrared scanning imaging system

Liang Xu, Minguang Gao, Jianguo Liu, Yang Jiao, Mingchun Feng, JingJing Tong, Sheng Li, Anhui Institute of Optics and Fine Mechanics (China)

Passive Fourier-transform infrared (Passive-FTIR) spectroscopy allows rapidly identification of the air pollution. However, for the localization of a leak and a complete assessment of the situation in the case of the release of a hazardous chemical gas or biological cloud, information about the position and the spatial distribution of a cloud is very important. In this work, a scanning imaging passive FTIR system, which composed of an interferometer, a data acquisition and processing software, a scanning system, a video system, and a laptop has been developed. The concentration retrieval algorithm for the passive FTIR remote measurement of gas cloud is presented, which involves the infrared radiative transfer model, radiometric calibration and absorption coefficient calculation. The concentration of the object gas is retrieved by using the nonlinear least squares method. And no background spectra are required. The remote sensing experiment of SF6 was carried out. The measuring result shows that, the column densities of all directions in which a target compound has been identified may be retrieved by a nonlinear least squares fitting algorithm and algorithm of radiation transfer, a false color image is displayed. The results are visualized by a video image, overlaid by false color concentration distribution image. The system has a high selectivity, and it allows visualization and quantification of pollutant clouds. The system allows mobile, real-time and fast measurements of chemical gas and biological clouds.

8534-24, Session 4

Mapping of Methane from Scanning Imaging Absorption Spectrometer for Atmospheric Cartography (SCIAMACHY)

Mohd Zubir M Jafri, Hwee San Lim, Kok Chooi Tan, Univ. Sains Malaysia (Malaysia)

Among all the greenhouse gases, methane is the most dynamic and abundant greenhouse gas in the atmosphere. The global concentrations of atmospheric methane has increased more than doubled since pre-industrial times, with a current globally-averaged mixing ratio of ~ 1750 ppbv. Due to its high growth rate, methane brings significant effects on climate and atmospheric chemistry. There has a significant gap for variables between anthropogenic and natural sources and sinks of methane. Satellite observation of methane has been identified that it can provide the precise and accurate data globally, which sensitive to the small regional biases. We present measurements from Scanning Imaging Absorption Spectrometer for Atmospheric Cartography (SCIAMACHY) included on the European environmental satellite ENVISAT, launched on 1st of March 2002. Main objective of this study is to examine the methane distribution over Peninsular Malaysia using SCIAMACHY level-3 data. They are derived from the near-infrared nadir observations of the SCIAMACHY at the University of Bremen through scientific WFM-DOAS retrieval algorithm version 2.0.2.Maps of time averaged (yearly, tri-monthly) methane was generated and analyzed over Peninsular Malaysia for the year 2003 using PCI Geomatica 10.3 image processing software. The maps show dry-air column averaged mixing ratios of methane (denoted XCH4). It was retrieved using the interpolation technique. The concentration changes within boundary layer at all altitude levels are equally sensitive through the SCIAMACHY near-infrared nadir observations.Hence, we can make observation of methane at surface source region. The results successfully identify the area with highest and lowest concentration of methane at Peninsular Malaysia using SCIAMACHY data. Therefore, the study is suitable to examine the distribution of methane at tropical region.

8534-17, Session PS

Atmospheric correction models for high resolution WorldView-2 multispectral imagery: A case study in Canary Islands, Spain.

Javier Martín Abasolo, Anabella Medina, Francisco Eugenio González, Javier Marcello Ruiz, Univ. de Las Palmas de Gran Canaria (Spain); Juan Antonio Bermejo, Fundación Observatorio Ambiental de Granadilla (Spain); Manuel Arbelo, Univ. de la Laguna (Spain)

The atmospheric correction has proven to be a crucial aspect in the pre-processing of remote sensing images applications. There are various simple algorithms, but it has been shown that the use of more

elaborated atmospheric models have significantly improved the results of the corrections. The launch of high-resolution WorldView-2 satellite, with new spectral channels and the ability to change its viewing angle, has highlighted the importance of properly modeling the surface characteristics and the directional reflectance phenomenon due to different surface textures depending of the viewing angle (Bidirectional reflectance Distribution Function, BRDF).

The 6S atmospheric correction model, based on radiative transfer theory, provides patterns which describe atmospheric conditions in a specific study area. The selection of parameters directly affects the result of the atmospheric correction, being the most significant parameter the optical thickness. 6S allows calculating the reflectivity depending on the type of surface to be studied enabling, as well, modeling the directional effect depending on the viewing angle of the satellite. In this study we have proceeded to make the correction of the eight multispectral and panchromatic bands of WorldView-2 by the 6S model, defining the geometry of the satellite observation and viewing angle. The spectral response of the nine bands has been defined and the weather conditions more suited to the study area (Canary Islands) were properly included. We have set the correct model for the directional effects of different areas like sand and sea coast. Figure 1 shows the 6s input parameters configuration file for WorldView-2 Coastal channel, which defines the correction for sea surface directional effects (wind, salinity and pigments).

The true reflectance value arc is obtained from the model output by using the following formula,

arc= y/(1+x_c*y) with y= x_a*R - x_b

where R is the observed radiance (w/m2*sr*μm), x_a, x_b, and x_c are the coefficients obtained from the model. x_a is the inverse of the transmittance, and x_b is the scattering term of the atmosphere and x_c is the reflectance of the atmosphere for isotropic light.

To check the proper functioning of the atmospheric correction in situ measurements were performed in different parts of the study area, with similar weather and lighting conditions. Figure 2 shows the WorldView-2 image of area under study, showing the locations where samples were obtained.

The results show a great similarity between the values of reflectivity obtained by the in situ radiometer and the values obtained by the eight multispectral satellite channels after the 6S atmospheric correction. Figure 3 shows the comparison between the reflectivity obtained by the radiometer (values with 1 nm steps) and the reflectivity obtained for eight channels of the WorldView-2 with bandwidths close to 50 nanometers.

In summary, the atmospheric correction methodology implemented, using the 6s model, has demonstrated an excellent performance and accuracy for WorldView-2 data of coastal areas.

8534-26, Session PS

Study of the topside electron density profiles obtained by COSMIC satellites and ionosondes over Europe during a four-year period

Haris Haralambous, George Dekoulis, Frederick Univ. (Cyprus)

The determination of the ionospheric electron density profile below the electron density peak (termed as bottomside electron density profile) has been traditionally conducted on a relatively local basis by ground-based ionosondes which are special types of radar used for monitoring the electron density at various altitudes in the ionosphere. Since ionosondes can only probe the ionosphere up to the maximum electron density the determination of the profile above the peak (termed as topside electron density profile) is represented by models which extend the profile above the peak. An alternative modern technique for measuring electron density profiles is the GPS Radio Occultation conducted by means of signals transmitted by GPS satellites (orbiting the Earth at ~ 20200 km) and received by LEO satellites. The profiles based on this technique are inferred indirectly exploiting radio signals crossing the Earth's ionosphere and undergoing refraction. The FORMOSAT-3/COSMIC (Constellation Observing System for Meteorology, Ionosphere, and Climate) satellite constellation is such a system based on 6 satellites (at an orbit of ~ 800 km) and has been in operation since 2006 providing excellent spatial coverage with more than 2000 occultations per day. In this paper a comparison of the topside electron density profiles over the European area is investigated in terms of these two different measurement techniques, within a period of four years. A subsequent comparison is therefore presented based on the values retrieved by radio occultation measurements and ionosondes systematically monitoring the ionosphere over Europe exploiting the inherently excellent spatial coverage provided by the COSMIC satellite constellation and the relatively uniform distribution of ionosonde stations in operation over European latitudes. In an effort to ensure that the comparison between COSMIC and ionosonde measurements is as accurate as possible, the distance between the ionosonde and GPS occultation at the peak of the F layer is limited to 1o within a time interval of 15 min. Furthermore only electron density profiles values during geomagnetically quiet conditions are taken into account, as ionopsheric electron density irregularities give rise to erroneous determination of profiles from GPS occultations due to significant fluctuations of the electron density profile.

8534-27, Session PS

Magnetospheric substorm measurements using PRIAMOS and NASA's THEMIS cluster satellites

George Dekoulis, Haris Haralambous, Frederick Univ. (Cyprus)

This paper describes the recent results obtained from the new PRIAMOS interferometer system designed for Space Weather studies. The results are being compared to data from NASA's THEMIS mission to study the variability and motion of the geomagnetic plasma that occur during strong activity. PRIAMOS remotely senses the interaction of the solar wind and the precipitation of highly energetic particles through the inner magnetosphere to the ionosphere. The vast three dimensional area of the planetary plasma environment, up to date, has been partially sampled despite the various in-situ and ground-based measurements. The generated signatures on the different data fusion products, before and after post-processing, indicate that the precipitation of the electrons produces distinct waveforms that are directly proportional to the measured azimuthal gradient displacement of the magnetic field dipolarization region. These results are seriatim paired to correlate the dipolarization region with the induced dipolarization effects recorded during strong geomagnetic plasma disturbances.

8534-28, Session PS

A feasibility study of cloud screening with neural networks with Aura/OMI data

Giulia Saponaro, Pekka Kolmonen, Gerrit de Leeuw, Johanna Tamminen, Finnish Meteorological Institute (Finland)

Over the last centuries, industrial activities, that our modern civilization relies on (burning fossil fuels, occupying lands for agriculture and industry), have greatly been affecting the composition of the atmosphere. The emission of anthropogenic nature contributes to altering concentrations of trace gases and particulate matter determining, for example, the well-known greenhouse effect. Nowadays, human's impact on climate change and air quality is considered a hot topic, since governments aim to regulate it with consecutive effects on global economy.

Earth orbiting satellites have enabled scientists to collect global atmospheric composition data. The TROPOspheric Monitoring Instrument (TROPOMI) is expected to provide high-quality information of daily-global observations of atmospheric parameters for climate and air quality applications. TROPOMI is the payload of the ESA/GMES Sentinel 5 Precursor to be launched in 2014, extending the data records from Aura/OMI and ENVISAT/SCIAMACHY. Retrievals of trace gas concentrations and aerosol properties require precise cloud screening which represents a challenge at TROPOMI's spatial resolution and without thermal infrared measurements. The cloud imagery will be obtained from the VIIRS instrument onboard the NPP-mission, flying in constellation with S5P/TROPOMI. Most of the cloud detection methods are based on thresholding radiances by suitable values that are empirically estimated based on training sets or physically defined, e.g. through radiative transfer models.

In this study cloud screening is analyzed with a neural networks algorithm (Extreme Learning Machine) to develop an automated cloud clearing method for the upcoming TROPOMI instrument. Owing to the fact that cloud properties are difficult to detect, neural networks, with their adaptive learning nature, offer an alternative to operator-dependent solutions. The developed algorithm employs Aura/OMI data for preliminary studies. EOS/Aura is the last satellite in the "A-train" satellite constellation. Fifteen minutes ahead of Aura, EOS/

Aqua has onboard MODIS instrument. Since both follow the same ground track, MODIS data are useful to validate OMI cloud products. Training the neural network requires a training dataset. The input data is the reflectance computed from OMI L1 radiance in the visible band, while the co-located MODIS cloud fraction represents the target-reference data. In order to extract salient spectral information from 751 channels, a singular values decomposition (SDV) is applied to the input data. OMI offers the so called small-pixel-data-read-out with five time higher spatial sampling than the standard which provides information on spatial inhomogeneity of the scene. The variance of the small pixel reflectance has been added to the input dataset, with the solar zenith angle. Several orbits in different season have been processed. Results are encouraging: the performances are good on ocean surfaces while still fails when reflectance measurements detect other target like desert's sand or ice covers. The next step to proceed is to add to the input dataset the Aura/OMI surface reflectance climatology data product (OMLER).

In this paper an automated cloud-detection method is proposed. The algorithm based on "ELM neural network" is characterized by low computation requirements and good screening performances. These combined features make the ELM NN a favorable solution for processing large amount of satellite scientific data.

8534-29, Session PS

Individual particle analysis in suburban Osaka

Makiko Nakata, Itaru Sano, Sonoyo Mukai, Kinki Univ. (Japan)

Anthropogenic small particles dominate the air over urban areas because of local emissions. The distribution of atmospheric particles is complicated due to the increasing emissions of sulfuric, nitric, carbonaceous and other aerosols in association with economic growth in East Asia. Also dust events cause increase on particulate matter and serious atmospheric turbidity. In this work, we intend to demonstrate variation of atmospheric particles around Higashi-Osaka in Japan. Higashi-Osaka is suburban area located on the east of Osaka city. We equip various ground measurement devices in Higashi-Osaka campus of Kinki University. The data supplied by the Cimel instrument are analyzed with a standard AERONET (Aerosol Robotics Network) processing system. It provides us with Aerosol optical thickness and the Ångström exponent. We set up an SPM sampler and a standard instrument of NIES/LIDAR network attached to our AERONET site. The SPM sampler provides particle information about the concentrations of PM2.5, PM10 and OBC separately. It is found from the simultaneous measurements and analyses that clear atmosphere with few small particles is not too often, usually polluted particles from diesel vehicles and industries are suspended at Higashi-Osaka. Aerosol properties at Higashi-Osaka site are roughly into two classes by applying a clustering method to the AERONET data. The first shows small aerosols are dominant attributed to the background aerosols at Higashi-Osaka. The second shows large aerosol optical thickness and small Ångström exponent values, and can be attributed to the dust event. The result indicates the characterization of atmospheric particles varies especially in dust phenomenon. Then we performed detailed analysis of atmospheric particles in dust days. We analyzed aerosols with scanning electron microscope (SEM) coupled with energy dispersive X-ray analyzer (EDX). This instrument can detect contain elements of sample by X-ray emanated from the surface of the sample. In order to investigate change of particle properties before and after dust event, we select three cases as before dust reaches to Higashi-Osaka, peak of dust event and after dust event and after dust passes. For comparison to dust days, we also analyzed particles on normal day. The results of analyses for each case indicate that nonspherical particles with large particle size are dominant and the main component becomes silicon derived from soil particles at the peak of dust event and soil particles remain after dust event. It is found that sometimes anthropogenic pollutant is transported to Higashi-Osaka before dust comes and components from anthropogenic source increase before dust event.

8534-30, Session PS

Algorithms for radiative transfer simulations of aerosol retrieval

Sonoyo Mukai, Itaru Sano, Makiko Nakata, Kinki Univ. (Japan)

Aerosol retrieval work from satellite data, i.e. aerosol remote sensing, is divided into three parts as: satellite data analysis, aerosol modeling and multiple light scattering calculation in the atmosphere model which is called radiative transfer simulation. The aerosol model is compiled from the accumulated measurements during more than ten years provided with the world wide aerosol monitoring network (AERONET). The model of the Earth's atmosphere is based on the AFGL code, which provides the aerosol and molecule distributions with height. The radiative transfer simulations take Rayleigh scattering by molecules and Mie scattering by aerosols in the atmosphere, and reflection by the Earth surface into account. Thus the aerosol properties are estimated by comparing satellite measurements with the numerical values of radiation simulations in the Earth-atmosphere-surface model. It is reasonable to consider that the precise simulation of multiple light-scattering processes is necessary, and needs a long computational time especially in an optically thick atmosphere model. Therefore efficient algorithms for radiative transfer problems are indispensable to retrieve aerosols from space.

This work is aimed at developing the practical and efficient algorithms for retrieving aerosol characteristics. The standard radiative transfer problem in a case of finite optical thickness is treated first, and then the problem in aerosol events such as dust storms or biomass burning plumes that are associated with excessive loading of aerosols in the atmosphere is considered. Finally our algorithms are practically applied for various type of space-based measurements by MODIS (The Moderate Resolution Imaging Spectroradiometer), GLI(Cloud and Aerosol Imager), CAI(Cloud and Aerosol Imager), and so on.

Conference 8534B: Lidar Technologies, Techniques, and Measurements for Atmospheric Remote Sensing

Thursday 27–27 September 2012 • Part of Proceedings of SPIE Vol. 8534 Remote Sensing of Clouds and the Atmosphere XVII; and Lidar Technologies, Techniques, and Measurements for Atmospheric Remote Sensing VIII

8534-47, Session PS

Studies on the crystallisation behaviour of erbium doped phosphate glasses

Nupur Prasad, Billy D. Richards, Univ. of Leeds (United Kingdom); Malcolm Glendenning, Martyn Marshall, Paul Sharp, Glass Technology Services (United Kingdom); Animesh Jha, Univ. of Leeds (United Kingdom)

Phosphate glasses can dissolve high concentrations of rare earth ions and have excellent spectroscopic properties making them useful solid-state laser materials. Solid-state lasers doped with different rare-earth ions find applications in a wide range of LIDAR (Light Detection and Ranging) and sensing applications; phosphate glasses are useful host materials for many applications in the visible and near-infrared spectral regions. For example, trivalent erbium (Er3+) doped phosphate glasses operate at the eye-safe wavelength of 1.54 μm and are used for range finding and sensing applications. Tm3+ doped solid-state lasers operating at ~2 μm can be used for wind-shear and turbulence monitoring. Similarly, Nd-doped metaphosphate glasses are the preferred gain medium for high-peak-power lasers used for fusion energy research because they can store optical energy at greater densities than other glass-types and can be fabricated in large sizes with high rare-earth ion concentration. The University of Leeds in partnership with Glass Technology Services is developing new phosphate laser glass compositions for advanced glass processing techniques. As part of this work, issues affecting the glass quality have been evaluated, with particular focus on defect formation, especially crystallisation. Avoiding crystallisation during processing is essential to form high quality laser gain materials. The work presented explores some of the factors controlling these defects including contamination during melting. The crystallisation behaviour of the glass was investigated for several different phosphate glass compositions and different melting conditions, including melting duration, temperature and crucible material.

8534-53, Session PS

High-power infrared fiber frequency comb

Wenxue Li, Ming Yan, Kangwen Yang, Xuling Shen, Heping Zeng, Jian Zhao, East China Normal Univ. (China)

High-repetition-rate high-power carrier envelope phase stabilized ultrashort pulse is urgently desired for many applications such as precision spectroscope, laser material processing, accurate laser synchronization and low phase noise RF generation; it will also be of great benefit for improvement of precision remote laser ranging in which the phase shift between laser pulses after passing a certain medium could reveal the information of accurate distance. The precision and ambiguity range for absolute distance measurement have been greatly improved using fiber-laser frequency comb source by Professor N. R. Newbury's group. In this paper, we demonstrated the generation of high-power infrared fiber frequency comb with millihertz-level phase noise and timing jitter less than one rad. The infrared spectrum centre around 1030 nm from a broadband Ti:sapphire femtosecond laser was power scaled up to 100 W by a cascade four-stage ytterbium-doped large-mode-area photonic crystal fiber amplifier. The repetition rate and carrier envelope phase offset frequency were stabilized by compensating the variation during fiber amplification process via electronic feedback loops. The repetition rate could be changed by modulating the length of piezoelectric ceramics mounted in one of the output mirror of the Ti:sapphire cavity while the carrier envelope phase offset frequency were changed by controlling the output power from acoustic optical modulator of Ti:sapphire oscillator. There was no obvious power decay and spectral distortion of amplified laser pulses were observed, indicating the amplified spontaneous radiation noise was sufficiently suppressed during power scaling processes. The standard deviation of the locked offset frequency at an output power of 100 W was estimated to be 4.71 mHz, which already included both system and detection noise within a recording time of 30 minutes. The standard deviation of the counts for beat frequency increased from 1.86 mHz at 10 W to 3.88 mHz at 30 W and maintained around 4.30 mHz when the output power rising from 40 W to 100 W. The linewidth of locked offset frequency was maintained at 2.62 mHz and had a variation of less than 0.2 mHz when the output power rising from 10 W to 100 W. Comparing with the carrier envelope stabilization, the noise of the locked repetition rate for high-power ultrashort pulse was relatively minor. The standard deviation of the locked repetition rate was less than 1 mHz and maintained unchanged with its linewidth kept at 2.52 mHz when the output power increased. The high-power fiber comb could maintain more than half an hour without significant variation, indicating effective compensation of phase noise for fiber amplifier by the electronic feedback loops. This high-power infrared fiber comb will become a powerful tool for remote laser ranging with accurate resolution and longer distance.

8534-54, Session PS

Generation of phase-stabilized high-power fiber comb for long distance ranging

Wenxue Li, Ming Yan, Kangwen Yang, Xuling Shen, Heping Zeng, East China Normal Univ. (China)

Fiber-based optical frequency comb has become an attractive near-infrared light source for precise and rapid distance measurements due to its compactness, high precision in time and frequency domains and long-term stability. Furthermore, the ultra-short pulses with stabilized carrier-envelope (CE) phase make the comb compatible for both the time-of-flight measure and the high-precision interferometric distance measurement. On the other hand, the rapid development in large-mode-area ytterbium-doped double-clad photonic crystal fibers (LMA-YDCF) greatly promotes amplification power up to hundreds of watts, which provides high average power as well as high pulse peak intensity required in long distance ranging. Note that the LMA-YDCF amplifier also shows high threshold of nonlinear effects including stimulated Raman and Brillouin scattering and therefore is particularly useful for low-noise amplification. Usually, in order to stabilize the CE phase of the high-power lasers, either a phase servo loop or a difference-frequency-generation scheme has been employed. However, the limited feedback bandwidth and the inevitable 1/f noise seriously limit the frequency and phase accuracy offered by the two approaches. Recently, a self-referenced feed-forward scheme based on an acousto-optic frequency shifter (AOFS) has been reported to reduce phase noise of a Ti:Sapphire laser to shot-noise-limited level with arbitrary offset frequency. And a similar scheme was employed for successfully stabilizing CE phase of a ytterbium-doped fiber laser.

In this paper, we demonstrate a high-power ytterbium-doped fiber frequency comb centered at 1030 nm for precise long-distance ranging. Its repetition rate was locked at 65.3 MHz with sub-mHz line-width. By using a large-mode-area (LMA) ytterbium-doped double-clad photonic-crystal fiber amplifier, the seed laser pulses were amplified to 20 W with recompressed pulse width of ~140 fs. For cancelling phase noise caused by the laser oscillator and amplifier, a AOFS was used to instantly stabilize the CE phase of the high-power laser pulses. Consequently, the CE phase frequency was locked on the laser repetition rate with a relative linewidth of ~1.4 mHz. The integrated phase noise (from 4 mHz to 100 kHz) was measured to be ~370 mrad, corresponding to a timing jitter of ~120 as.

8534-55, Session PS

Air quality monitoring in Cyprus using Lidar, sun-photometer, PM10 and MODIS data

Paraskevi Perdikou, Frederick Institute of Technology (Cyprus); Argyrw Nisatzi, Diofantos G. Hadjimitsis, Cyprus Univ. of Technology (Cyprus)

Particulate matter (PM) concentration has become an important index of air pollution. In-situ PM measurements are local measurements and not numerous enough to provide information on large spatial scales, since aerosol concentrations are highly variable in space. Benefiting from the large spatial and temporal coverage, satellite remote sensing

has been used to observe the characteristics of aerosols, such as AOD (aerosol optical depth), over the years. This study is part of the research project 'AIRSPACE' aiming at extracting an algorithm for relating satellite MODIS AOD retrievals and ground-based PM10. To achieve this, ground measurements from Lidar, CIMEL sun photometer (NASA/AERONET network) and DustTrack (PM10) on a site in the city of Limassol were used and compared with MODIS AOD retrievals. A site in the city of Nicosia was also used for validation purposes where hand-held sun-photometer and DustTrack (PM10) ground data were also collected. Since AOD reflects the aerosol loading of the atmosphere and PM concentration is usually measured at surface level, the correlation between them is severely influenced by the vertical distribution of aerosols and the Relative Humidity (RH) that impacts aerosol extinction coefficient. To reduce uncertainties, meteorological data such as the height of Planetary Boundary Layer (HPBL) retrieved from the second derivative of the Range Corrected Signal (RCS) of Lidar, RH at the ground at 08.00 LST, hourly wind direction and hourly wind speed, were also considered.

8534-56, Session PS

An unsupervised classification for full-waveform LiDAR point data using IHSL transform and the FCM algorithm

Jinhu Wang, Chuanrong Li, The Academy of Opto-Electronics (China)

Airborne laser scanning (ALS), is an active remote sensing technique where a laser emits short infrared pulses towards the Earth's and Object's surface and a photodiode records the backscattered echo. A timer measures the round-trip time of the laser pulse that allows calculating the range (distance) between the laser scanner and the object that generated the backscattered echo. Thereby, information about the geometric structure of the Earth's surface is obtained[1]. Since 2004, new ALS commercial systems called full-waveform LiDAR have appeared with the ability to record the complete waveform of the backscattered signal echo. Thus, in addition to range measurements, further physical properties of objects included in the diffraction cone1 may be derived with an analysis of the backscattered waveforms[2]. This paper first present a waveform decomposition method based on B-spline initiated EM algorithm, taking Gaussian function as kernel function. Then the accuracy of waveform decomposition is presented. Based on the full-waveform LiDAR data, we decomposed the backscattered pulse waveform and abstracted each component in the waveform after the preprocessing of noise detection and waveform smoothing. And by the time flag of each component acquired in the decomposition procedure we calculated the three dimension coordination of the component. Then the components' waveform properties, including amplitude, width and cross-section, were uniformed respectively and formed the Amplitude/Width/Section space. We apply the IHSL colour transform to the above space to find a new space, RGB colour space, which has a uniform distinguishability among the parameters and contains the whole information of each component in Amplitude/Width/Section space. After the process mentioned above, the Fuzzy C-means algorithm is used to complete ground feature classification. The advantage of this approach is that the correlation between components can be removed and the interclass distinguish ability is maintained as well. So it could achieve a high performance in the point segmentation algorithm, and since we could treat the parameters in the same way, the classification procedure can be simplified. A general classification accuracy is given. The experiments show that this method could provide an improved classification result compared with the method which uses the Amplitude/Width/Section space directly during the segmentation procedure. The experiments show that a high accuracy classification result is efficiently achieved using this method. The classification result could probably be better applied in later target detection and identification.

[1] Wolfgang Wagner, Andreas Ullrich,Vesna Ducic, Thomas Melzer, Nick Studnicka. Gaussian decomposition and calibration of a novel small-footprint full-waveform digitizing airborne laser scanner, ISPRS Journal of Photogrammetry & Remote Sensing. 60 (2006) 100-112

[2] C. Mallet and F. Bretar, "Full-waveform topographic lidar: State-of-the-art," ISPRS Journal of photogrammetry & Remote Sensing, vol. 64, no. 1, pp. 1-16, 2009.

[3] H. Gross, B. Jutzi, and U. Thoennessen, "Segmentation of tree regions using data of a full-waveform laser," in Symposium of ISPRS Photogrammetric Image Analysis (PIA), Munchen, Germany, sep 2007, ISPRS, vol. XXXVI Part(3/W49A).

[13]Li Guo, Nesrine Chehata, Clement Mallet, Samia Boukir. Relevance of airborne lidar and multi-spectral image data for urban scene classification using Random forest. ISPRS Journal of Photogrammetry and Remote Sensing. 66 (2011) 56-66

8534-40, Session 5

Pulsed 2-micron direct detection Integrated Path Differential Absorption (IPDA) Lidar for CO2 column measurement *(Invited Paper)*

Upendra N. Singh, Jirong Yu, Mulugeta Petros, NASA Langley Research Ctr. (United States)

The mid-IR wavelength regions at 1.57μm and 2.05μm are considered suitable for CO2 IPDA measurements. Two instruments operating at 1.57μm have been developed and deployed as airborne systems for atmospheric CO2 column measurements. One instrument is based on an intensity modulated CW approach, the other one a high PRF, pulsed approach. Although both the wavelengths at 1.57μm or 2.05 μm are suitable for the CO2 concentration measurement, current modeling efforts show that the weighting function at 2.05 μm is more favorable for measurements in the lower troposphere, including the boundary layer. With support from NASA Earth Science Technology Office, under NASA Laser Risk Reduction Program, NASA Langley Research Center has developed a high energy double-pulsed 2-micron CO2 lidar system and has recently performed a ground test demonstration of coherent detection of CO2. NASA LaRC seeks to advance that heritage to a 2-micron pulsed direct detection IPDA lidar system to meet the requirements for CO2 column measurement from space-based platform using direct detection, an alternate approach to measure CO2 concentrations with significant advantages.

8534-41, Session 5

High energy optical parametric sources for multi-wavelength DIAL: a generic approach

Jessica Barrientos Barria, Jean-Baptiste Dherbecourt, Myriam Raybaut, Antoine Godard, Jean-Michel Melkonian, Michel Lefebvre, ONERA (France)

Spectroscopic applications, such as remote detection of greenhouse gases by differential absorption LIDAR (DIAL), require the use of narrow linewidth (single longitudinal mode), high-peak-power, pulsed sources, with high beam quality and wide and fast tuning procedures. Indeed, the accuracy of the measurements is strongly impacted by the transmitter performances.

In such context, we have been involved, for several years, in the development of parametric sources for DIAL, i.e. optical parametric oscillators (OPO) and amplifiers (OPA). Indeed, parametric converters are very advantageous as laser transmitters, since they allow high peak power generation in the nanosecond regime; given their wide tuning range, they allow to design transmitters for the detection of various gas species (CO2, CH4, N2O, H2O, SO2).

The main issue with conventional basic OPO schemes is the emitted linewidth, which stands around several nanometers under pulsed operation, which is too broad for remote sensing applications. To be able to fully control the spectral content of pulsed OPOs, we have developed a doubly resonant OPO architecture, in which signal and idler cavities can be separately adjusted in a nested-cavity configuration (NesCOPO). The main interests of this resonator are i) its frequency versatility, ii) its low oscillation threshold, iii) the specific tuning properties of the dual cavity approach.

Indeed, the tuning range of the NesCOPO is not limited by the availability of seeding sources and can thus be designed to address any specie having absorption lines within the transparency range of available non linear materials. Here we will present micro-laser pumped devices covering the 3.2-3.8 and 3.7-4.3μm range.

Also, owing to its low oscillation threshold, micro-laser pumped laser transmitters can be build-up using this device, for short range, portable LIDAR instruments, as well as high power architectures (OPO-OPA), pumped by high energy pump lasers for long range applications. Performances of a specific 2.05 μm transmitter for CO2 will be presented, emitting more than 15 mJ of single frequency radiation, based on a NesCOPO, followed by OPA stages.

Finally, making use of the specific dual cavity arrangement, specific tuning procedures can be implemented, allowing to generate

sequences of wavelengths with narrow linewidth (Fourier transform limited) and adjustable frequency spacing (down to a few tens of MHz) and span (up to several hundreds of GHz - without temperature tuning of the device). Demonstration experiments on CO2 remote sensing using a portable - microlaser pumped - integrated path DIAL bench will be presented, with either dual wavelength operation or multi-line sampling for a complete coverage of several CO2 absorption lines with sequences of tens of emitted wavelengths. Generation of recurrent sequences of two (λon and λoff) or three reproducible wavelengths by a high-energy 2.05 µm DIAL emitter will also be presented.

8534-42, Session 5

A flexible eye-safe lidar instrument for elastic-backscatter and DIAL

Iain Robinson, James W. Jack, Cameron F. Rae, John Moncrieff, The Univ. of Edinburgh (United Kingdom)

Developments in lidar have been driven largely by improvements in two key technologies: lasers and detectors. We describe here a lidar instrument for atmospheric remote sensing using the elastic-backscatter and differential-absorption lidar (DIAL) techniques. The instrument features an all-solid-state laser source combined with photon-counting detection providing portability, eye-safe operation and high sensitivity.

The system is built around a custom-designed Newtonian telescope with a 0.38 m diameter primary mirror. Laser sources and detectors attach directly to the side of the telescope allowing for flexible customization with a range of equipment.

We report the operation of the system with a laser source based on an optical parametric oscillator. The OPO is pumped by an Nd:YLF laser at a wavelength of 1.057 µm. It is angle-tuned by rotating the crystal providing output wavelengths tunable to a maximum extent of 1.6 µm for the signal wave and 3.1 µm for the idler. This provides a wide range of available wavelengths suitable for lidar, all within a spectral region with a relatively high exposure limit for eye safety. The OPO delivers 1 mJ output pulse energy which is expanded and then transmitted coaxially from the telescope.

The use of the 1.6 µm wavelength region provided by the signal wave allows for several direct detection schemes. Tests of the instrument were made with indium gallium arsenide (InGaAs) photodiode detectors and a custom-built multi-stage transimpedance amplifier. These tests demonstrated that the system achieves a ranging precision better than 0.3 m. Whilst photodiode detectors are a very low-cost solution their limited sensitivity restricts the maximum range over which a signal can be detected. We therefore outline the adaptation of the instrument to support photon-counting detectors such as avalanche photodiodes (APDs) and single-photon avalanche diodes (SPADs).

Our goal is to make vertically-resolved measurements of greenhouse gas concentrations using DIAL. A gas cell within the laser source allows the wavelength to be tuned to match a specific absorption feature of CO2 near 1.6 µm. The source can rapidly be tuned between the on-line and off-line wavelengths to make a DIAL measurement.

There is significant interest in the application of lidar to the study of greenhouse gas concentrations. Whilst satellite-borne instruments provide global coverage they generally make column-integrated measurements and therefore provide little information on greenhouse gas concentrations in the boundary layer where sources and sinks reside. Aircraft sampling provides direct measurements of vertical concentration profiles, but is too costly for routine deployment. Ground-based lidar provides the capability to measure vertical profiles of CO2 and other greenhouse gases through the boundary layer. By maintaining the instrument as both low-cost and portable we envisage the possibility of continuous lidar monitoring and the deployment of a network of instruments. Applying the data collected to our atmospheric models would allow for the determination of the locations sources and sinks of greenhouse gases, contributing to our understanding of fluxes.

8534-43, Session 6

Diode-pumped Alexandrite laser: a bright prospect for future space Lidar missions *(Invited Paper)*

Michael J. Damzen, Imperial College London (United Kingdom) and Midaz Lasers Ltd. (United Kingdom); Ara Minassian, Midaz Lasers Ltd. (United Kingdom)

Diode-pumped Alexandrite laser technology has the potential to be a laser source with superior electrical-to-optical efficiency and broad wavelength tuning capabilities compared to current Nd:YAG based laser systems. These capabilities can provide significant benefits for future Earth Observation Lidar missions as well as more general spectroscopic sensing applications. However, until now all commercial Alexandrite is flashlamp pumped with resulting low efficiency. Recent advent of high power, reliable red diode lasers has enabled the prospect of high efficiency diode-pumped Alexandrite laser technology. We present breakthrough results of the world's first multi-Watt (6.4 W cw operation) diode-pumped Alexandrite laser and QCW mode high energy (23.4mJ) with high slope efficiency ~42%, showing that this technology could have wide applicability as a compact high efficiency, high energy and tunable laser source.

The experimental diode-pumped Alexandrite laser incorporated a 0.21 at. % Cr doped Alexandrite slab amplifier crystal with dimensions 2 x 2 x 30 mm. The two 2 x 2 mm lasing faces were AR coated for 760nm, near the peak lasing wavelength of Alexandrite. The Alexandrite slab was dual side pumped by a pair of red diode stacks at 635nm through the side faces (2 x 30 mm) and with polarisation parallel to the b-axis of the crystal. The laser cavity was formed by a plane output coupler with reflectivity 99% and a high reflectivity rear mirror with radius of curvature 100 mm. The diode pumping was performed in both quasi-CW mode and CW mode.

In QCW mode with pump pulse duration of 1ms, output pulse energy of ~ 23.4 mJ (at ~ 760nm) was achieved at 94 mJ incident pump energy. The slope efficiency was s~ 31.2% with respect to incident pump energy or ~ 42% with respect to absorbed pump. When pump repetition rate was varied from 25 Hz - 100 Hz no change in pulse energy was observed showing no effects of thermal roll-over and indicating that output is scalable and only limited currently by available pump power. At 100 Hz repetition rate average output power was 2.34 W. With diode pumping in CW mode, a CW output power of 6.4 W was produced at an incident pump power of 58 W.

In conclusion, we have designed, constructed and demonstrated the World's first multi-Watt (6.4 W), multi-milli-Joule (23.4 mJ) diode-pumped Alexandrite laser. By diode side pumping an Alexandrite slab architecture, we have demonstrated high efficiency and in a system that is not optimised, with the possibility of further efficiency improvement to ~ 60% optical-to-optical. This demonstrates the exciting prospect for a high efficiency, high energy Alexandrite laser source to supersede Nd:YAG in future Earth Observation satellite missions, with the added benefit of wavelength tunability for superior scientific flexibility and data acquisition in the near-IR, or UV (by harmonic generation).

8534-44, Session 6

The Titan laser family: high pulse energy, high repetition rate and excellent beam quality for Lidar applications

Martin D. Ostermeyer, Artur Napiwotzki, Karsten Schmidt, Frank Massmann, IBL Innovative Berlin Laser GmbH (Germany)

The Titan Series of IB-Laser is designed for applications like e.g. Lidar or particle imaging velocimetry (PIV) that need simultaneously higher pulse energies in the sub-Joule range, high repetition rates up to 1kHz combined with an excellent beam quality. The series has an air cooled branch with pulse energies up to 50mJ at repetition rates of 100Hz and a water cooled branch with pulse energies of up to 400mJ in a transverse fundamental or multimode mode. The Titan series consists of diode pumped Nd:YAG master oscillator power amplifier systems (MOPA). They are built in a hybrid fashion of end and side pumped laser heads. Next to the fundamental wavelength at 1064nm higher harmonics at 532nm, 355nm or 266nm are available. Injection seeding with pulse build up time method is optionally available for these laser systems. The pulses have durations between 8 - 20ns.

Examples of the Titan series will be introduced: The Titan 50FM SHG produces 50mJ at 1064nm and 25mJ at 532nm with an M2 < 1.4 at repetition rates of 1kHz. The Titan 250FM emits 250mJ pulses at 1064nm with 500Hz repetition rate and an M2 < 1.5 whereas the Titan 400FM generates 400mJ pulses at 1064nm with an M2 < 1.7 at 300Hz repetition rate. The transverse multimode systems are designed for top hat like beam profiles with M2-numbers ranging around 7 - 15.

An example of the air cooled branch of the series is the Titan AC 30

4WL. This model can emit up to 30mJ 1064nm, 15mJ 532nm, 6mJ 355nm and 2.5mJ 266nm at 100Hz repetition rate. It is a multimode system with an M2-number ranging around 5.

8534-45, Session 6

Broadband spectroscopic lidar for SWIR/MWIR detection of gaseous pollutants in air

Simon Lambert-Girard, Nicolas Hô, Bruno Bourliaguet, INO (Canada); Michel Piché, Univ. Laval (Canada); François Babin, INO (Canada)

A broadband SWIR/MWIR spectroscopic lidar for detection of gaseous pollutants in air is presented for doing differential optical absorption spectroscopy (DOAS). One of the distinctive parts of the lidar is the use of a picosecond or sub-nanosecond OPG (optical parametric generator) capable of generating broadband and tunable SWIR/MWIR light. The tunability comes from the fact that high intensity light from a 1064-nm pump laser is passed through a spatially variable period and temperature tunable PPMgO:LN OPG. The generated broadband light has a full width at half maximum (FWHM) that goes from 10 to >100 nm and is tunable between 1.5 and 3.9 µm. The resulting pulse energies, conversion efficiencies, beam quality and spectra of the output light (both the idler and the signal) will be presented for an 8 ps input pulsewidth along with results from 700 to 1300 ps pulsewidths at both low and high pulse repetition frequencies (400 Hz to >10 KHz). The optical source layout is presented, along with a description of the lidar breadboard. Results from indoor simulated typical operation of the lidar will be discussed, the operation consisting in emitting the broadband coherent light along a line of sight (LOS) and measuring the returns from back-scattering by aerosols or from back-scattering by a topographic feature. The results presented will be for methane. A second distinctive feature is the detector used in the output plane of the grating spectrograph of the lidar system. It is a gated MCT-APD (HgCdTe - Avalanche Photo-Diode) focal plane array detector with in-house electronics. The whole of the returned spectra is measured, within a very short time gate, at every pulse and at a resolution of a few tenths of a nm. Light inputted to the spectrograph is collected by a variable focus telescope for maximum coupling. A programmable volume of space along the laser beam path is imaged at the entrance of the spectrograph and 320 spectral channels can be measured simultaneously, attenuating the effects of atmospheric instabilities on measurements. Since all wavelengths are emitted and received simultaneously, the atmosphere is “frozen” during a path integrated measurement and this ultimately reduces the baseline drift, a problem inherent in low concentration measurements of pollutants using DOAS methods. The resulting path integrated absorption spectra and gas concentrations are retrieved by fitting the molecular absorption features present in the measured spectra. The use of broadband pulses of light and of DOAS fitting procedures make it possible to measure more than one molecule at a time, including interferents and complex molecules. The OPG approach enables the generation of moderate FWHM continua with high spectral energy density which can be tailored by choosing the pulsewidth, the pulse energy, the PPMgO:LN period and temperature. Moreover, the source tunability allows selection of different appropriate rovibrational absorption features of a great number of molecules. Proposed follow-on work and applications will also be presented.

8534-46, Session 6

Mid-infrared emission from Dy3+ doped tellurite bulk glass and waveguides

Billy D. Richards, Toney Teddy-Fernandez, Animesh Jha, Univ. of Leeds (United Kingdom); David J. Binks, The Univ. of Manchester (United Kingdom)

We present the fabrication and characterisation of Dy3+-doped tellurite glasses and waveguides for applications in the mid-IR. The low phonon energy and large rare-earth ion solubility of tellurite glasses, as well as having infrared transmission ranges up to >5 µm, make them promising candidates for new mid-IR solid-state laser host materials. This paper presents recent achievements in the fabrication of tellurite glasses, glass characterisation and rare-earth ion spectroscopy which is compared to other glass hosts relevant to the mid-IR such as fluoride and germanate glasses. When excited with an 808 nm laser diode source, Dy3+ doped tellurite bulk glasses exhibited very broad fluorescence from the 6H13/2 - 6H15/2 transition which extends from 3 µm to 3.6 µm FWHM compared to 2.9 µm to 3.1 µm in Dy3+ doped ZBLAN glass. This broad and red-shifted fluorescence band in tellurite glass may find use in LIDAR and sensing applications as it coincides with an atmospheric transmission band, compared to the ~3 µm emission of Dy3+ doped ZBLAN lasers which is absorbed by atmospheric water. Channel waveguides were inscribed by a femtosecond laser operating at 800 nm, 1 kHz repetition rate and 100 fs pulse width. Laser inscription was carried out with a 0.65 NA aspheric lens objective with various powers ranging from 300 nJ to 5 µJ and speeds from 0.01 to 6 mm/s and the waveguide was buried at a depth of 140 µm. A 1600 nm laser mode was propagated through the channels. Figure 2-A and 2-B show waveguides written using a single scan technique, while waveguides shown in 2-C and 2-D were written by the stress induced method, (two waveguides were written close enough to produce a positive index change due to the densification via high stresses). In all cases confined guiding behaviour was observed. When pumped using an 808 nm laser diode source, the Dy3+ doped tellurite waveguide exhibited amplified spontaneous emission (ASE) in the 3-3.6 µm range which matched the fluorescence from the bulk glass samples.

8534-57, Session 6

First attempt to monitor atmospheric glyoxal using differential absorption lidar

Liang Mei, Lund Univ. (Sweden); Alexandros D. Papayannis, National Technical Univ. of Athens (Greece)

Volatile organic compounds (VOCs) are key species present in the Earth’s atmosphere and contribute significantly to atmospheric chemistry, although most of these compounds have extremely low mixing ratios. Once emitted to the atmosphere, VOC species are removed via gas-phase reactions with radicals like hydroxyl (OH), nitrate (NO3), halogen and halogen oxides and compounds like ozone. The end-products of VOCs oxidation are formaldehyde (HCHO) and glyoxal (CHO.CHO) and ultimately carbon monoxide (CO) [1]. CHO.CHO is one of the most prevalent carbonyl compounds in the atmosphere. It is the smallest alphadicarbonyl formed by chemical reactions following the initial elementary oxidation of VOC. CHO. CHO is also a short lived trace gas. As the overwhelming majority of the VOC sources are close to the surface, the glyoxal in the boundary layer will dominate the column amount of CHO.CHO. Therefore glyoxal columns are a surrogate for the rate of VOC oxidation and large CHO.CHO columns can be used as a marker of air masses, which are photochemical “hot spots” [2]. The main objective of the present work is to measure for the first time the profiles of glyoxal using differential absorption lidar (DIAL) technique [3], in order to provide a comprehensive assessment of its temporal and spatial variation.

The strongest absorption line of CHO.CHO in the blue wavelength region is at 455.1 nm. However, nitrogen dioxide (NO2) also absorbs the broadband blue light. In order to compensate the effect of absorption cross-section variations of the NO2 around 455.1 nm, three-wavelength DIAL measurements were performed, i.e., CHO.CHO and NO2 were measured simultaneously. The absorption peaks for NO2 and CHO.CHO are at 457.9 nm and 455.1 nm, respectively, while both two gases share the same off-line wavelength, i.e., 456.9 nm. The laser source is a Nd:YAG (355 nm, 20 Hz) pumped optical parametric amplifier (OPA). The linewidth of the signal beam is typically around 0.2 nm, which is narrower than the full width at half maximum (FWHM) of the absorption cross section of both CHO.CHO and NO2. The three wavelengths were tuned shot-by-shot, performed by quickly tuning the angle of the BBO crystal using a piezoelectronic transducer (PZT). The laser beam was first expanded to around 7-cm diameter and then transmitted into the atmosphere. The backscattered light was collected by a Newtonian telescope, detected by a photomultiplier tube (PMT), and finally recorded by a transient digitizer.

The measurements were performed in Lund, Sweden, during July, 2012. The obtained DIAL curves indicate that the background concentration of CHO.CHO was very low, actually below the current detection limit of the system, which is around 6 ppb. The local concentration of NO2 was at the time of measurement also very low, as confirmed by parallel DOAS measurements. In spite of the extremely low CHO.CHO concentrations in Scandinavia determined by satellite measurements [1], we note that significantly higher concentrations are expected in warm climate regions as Guangdong, China. Therefore, we plan for further measurements at this location, using a newly developed and advanced DIAL system.

REFERENCES

[1] M. Vrekoussis, F. Wittrock, A. Richter, and J. P. Burrows, Atmospheric Chemistry and Physics 10 (2010).

[2] S. Myriokefalitakis, M. Vrekoussis, K. Tsigaridis, F. Wittrock, A. Richter, C. Bruhl, R. Volkamer, J. P. Burrows, and M. Kanakidou, Atmospheric Chemistry and Physics 8 (2008).

[3] Z. G. Guan, P. Lundin, L. Mei, G. Somesfalean, and S. Svanberg, Appl Phys B 101, 465 (2010).

8534-48, Session 7

Measurement of tropospheric aerosol in São Paulo area using a new upgraded Raman LIDAR system *(Invited Paper)*

Fabio J. da Silva Lopes, Eduardo Landulfo, Walter M. Nakaema, Instituto de Pesquisas Energéticas e Nucleares (Brazil)

Elastic backscatter lidar systems have been use to determine aerosol profile concentration in several areas such as weather, pollution and air quality monitoring. In order to determine the aerosol extinction profiles from those is applied the Klett inversion method, however, this procedure suffers from the lack of information since there are two unknowns, the aerosol backscatter and extinction coefficients, to be determined using only one measured lidar signal. It is only possible using a priori assumptions of the relations between the two coefficients. When a Raman lidar system is used the inelastic backscatter signal is affected by aerosol extinction but not by aerosol backscatter. The Raman lidar technique allows the determination of the extinction and backscatter coefficients without any priori assumptions or any other collocated instruments.

The MSP-Lidar system, set-up in a highly dense suburban area in the city of São Paulo, are been upgrading to a Raman Lidar, and in its present 6-channel configuration it allows to monitor elastic backscatter at 355 and 532 nm together with nitrogen and water vapor Raman backscatters at 387 and 608 nm and 408 and 660 nm correspondingly. Thus, the measurements of aerosol backscattering, extinction coefficients and water vapor mixing ratio in the Planetary Boundary Layer will become available. The system will provide the important meteorological parameters such as Aerosol Optical Depth (AOD) and will be used for the study of aerosol variations in lower troposphere over the city of São Paulo, air quality monitoring and for estimation of humidity impact on the aerosol optical properties, without any priori assumptions. This study will present the first results obtained with this upgraded lidar system, demonstrating the high quality of obtained aerosol data.

8534-49, Session 7

The effective use of Doppler LiDAR in wind power applications

Peter J. M. Clive, SgurrEnergy Ltd. (United Kingdom)

Doppler LiDAR is finding an increasingly central role in wind assessments for wind power projects as a result of the availability of units suitable for wind power applications. The requirements of these projects influence the development of new techniques because they place quite different demands on LiDARs compared to other meteorological applications, in terms of the parameters being obtained, the degrees of precision and accuracy required, and the instrument configurations necessary to achieve this. Conversely, the acquisition of datasets which were not available to wind analysts and applied eolicists prior to the advent of LiDAR are influencing the methods with which wind project sites are assessed both during the resource assessment and operational phases. High financial stakes, narrow margins and technical risks associated with wind projects are driving a need for accuracy in LiDAR data and leading to assumptions, approximations and received wisdom regarding wind flow features such as turbulence and shear to be challenged as a result of the datasets becoming available. This presentation reviews the interface between LiDAR techniques and wind power studies and the interactions that have led to on-going significant developments in both fields.

8534-50, Session 7

Roadside remote sensing of vehicle exhaust

John S. Hager, HEAT, LLC (United States)

LIght Detection And Ranging (LIDAR) systems have been used extensively to remotely measure pollutants and chemical constituents from a remote platform. We have developed a LIDAR system to measure quantities of vehicle exhaust.

Unfortunately, the tendency of a gaseous plume to change shape and size as it expands makes it difficult to quantify a plume's constituent amounts using traditional infrared and ultra-violet absorption techniques. We have developed an innovative new system, which can remotely measure quantities and relative amounts of target molecules in an exhaust plume (Patent No.: 8,134,711).

We have developed a system that measures different gases simultaneously. This allows us to measure relative amounts and quantities of different gases concurrently. The EDAR (Emission Detection And Reporting) system is simple and inexpensive.

The measurement of absolute quantities in vehicle emissions is desirable in many applications. Quantities measured from real-world driving conditions would greatly improve vehicle emissions statistics. Our device will hopefully be economical enough for multi-point setups in order to measure the same vehicle multiple times along the same stretch of roadway. Measuring quantities under real-world loading conditions, along with cumulative emissions at different sites, would help scientists, pollution modelers, and urban planners alike. Our EDAR system remotely measures the optical masses of vehicle exhaust constituents such as CO2, CO, HC, NOX, and NH3. As a result, we can report the desirable unit of mass-per-distance of exhaust left behind by a vehicle on the open road.

Relative amounts are calculated using the measurements of the exhaust plume taken at different wavelengths simultaneously. By scanning the laser over the plume one can choose the location with the most of the target gas in its' path. In this way we can maximize the signal to noise ratios of our measurements. Also, one can use the CO2 image, which will have the largest percent of the exhaust and also the largest absorption, to infer the concentrations of the lesser percentage gases, even though their concentrations have dropped below the noise.

Data has been collected using certified gas mixtures. Also, data has been collected on vehicles equipped with an Emission Systems Inc. (EMS) exhaust analyzer and flow meters. Also real-world testing has been done on random vehicles at the time of submission of this abstract. Results from this data will be presented.

8534-51, Session 7

Numerical simulation of the Doppler measurements for the scheme with two lidars

Evgeniya A. Shelekhova, Alexander P. Shelekhov, Institute for Monitoring of Climatic and Ecological Systems (Russian Federation)

In this paper the numerical simulation results of the Doppler measurements for high horizontal spatial resolution using the scheme with two lidars are presented. It is assumed that the Doppler lidars have different location, and they are located in diametrically opposite corners of selected area. The Doppler lidars measure the components of mean wind velocity in the points corresponding grid cells and the horizontal spatial resolution of the Doppler measurements is defined the grid sizes. We simulate the variances, which characterize the measurement uncertainty of components of mean wind velocity for two lidars. It is shown that the variances are different for oppositely located lidars and depend strongly on state of the atmospheric turbulence and the number and sizes of grid cell. Also the variances are the complex functions of the signal-to-noise ratio, VAD sector scan angle, elevation angle, and direction sensing. For the first lidar the measurement uncertainty of component of mean wind velocity U decreases with increasing cell number for in the direction sensing of East and horizontal spatial resolution of 1x1 km. The measurement uncertainty increases with increasing cell number for resolution equal to 1x1 km. The variance for the component U is a maximum and the component V has a minimum uncertainty of measurement in the directions of North and South. The variance for the component U is a minimum and the component V has a maximum measurement uncertainty in the directions of East and West. The variance for the components U and V have the same values in the directions of North-East, North-West, South-East, and South-West. For the second lidar the measurement uncertainty of component of mean wind velocity has the opposite behavior. For example, the variance for the component U is a minimum and the component V has a maximum uncertainty of measurement in the directions of North and South. Thus the

measurement precision of component of mean wind velocity can be significantly increased if we use the scheme with two Doppler lidar at one and the same time.

8534-52, Session 7

Flare monitoring for refining process efficiency assessment using the Lidar technique

Renata F. Da Costa, Eduardo Landulfo, Instituto de Pesquisas Energéticas e Nucleares (Brazil); Roberto Guardani, Escola Politecnica da Univ. de São Paulo (Brazil); Riad Bourayou, Instituto de Pesquisas Energéticas e Nucleares (Brazil); Paulo F. Moreira Jr., Escola Politecnica da Univ. de São Paulo (Brazil); Juliana Steffens, URI (Brazil)

Real-time measurement of atmospheric emissions from industrial stacks is a very difficult task due to stack height, sensor calibration difficulties, and the dynamics of oscillations in the emission patterns. Optical remote sensing techniques have obvious advantages for gas pollutant detection, e.g., they enable fast operation over large distances, and in hostile environments with large fluctuations of temperature and pressure.

Lidar techique has special capabilities for remote sensing of different components of the atmosphere. Besides being a valuable tool for process monitoring and control, a Lidar-based monitoring system provides an innovative means to validate dispersion models used in most cases of environmental impact studies. In this sense, a Lidar-like system was applied to the monitoring of particle emissions by an industrial flare stack. Backscattered light intensity measurements were carried out at three wavelengths with a Nd:YAG laser (355, 532 and 1064 nm) by scanning the Lidar over a delimited area around the stack tip. The recorded data were correlated with vertical profiles of the wind field measured by Sodar.

The remote sensing system will be further implemented with the addition to the existing Lidar of a combination of laser-induced incandescence (LII) and fluorescence (LIF) and Fourier transform infrared spectroscopy (FTIR) in order to enable quantitative estimations of characteristic properties of soot aggregates and combustion gases.

The experiment has been carried out at CEPEMA, an Environmental Research Center of the University of São Paulo, in Cubatão. The area is surrounded by a large industrial complex responsible for a large inventory of particle and gas emissions into the city area whose climate and topography are unsuitable to pollution dispersion. Thus, all efforts in improving the efficiency of industrial processes by minimizing pollutant emissions can indirectly mitigate the environmental and health problems caused by the intense industrial activity in the area.

Conference 8535: Optics in Atmospheric Propagation and Adaptive Systems

Tuesday 25–25 September 2012 • Part of Proceedings of SPIE Vol. 8535 Optics in Atmospheric Propagation and Adaptive Systems XV

8535-1, Session 1

Characteristics of long-range scintillation data over maritime coastal areas

Arie N de Jong, TNO Defence, Security and Safety (Netherlands)

The knowledge on scintillation, caused by atmospheric turbulence, is of vital importance for the performance prediction of threat detection systems and for the development of associated detection algorithms. During the FATMOSE trial, held over the False Bay (South Africa) from November 2009 until October 2010, day and night (24/7) scintillation data were collected for point sources at a range of 15.7 km. For this kind of ranges, being of great operational interest, the theory of weak turbulence is generally no longer valid, so short range scintillometer data cannot be used for the prediction of long-range scintillation. Therefore we used simultaneously our MSRT transmissometer (in scintillation mode) and a high resolution imager for the scintillation measurement. Because of the large source and receiver aperture, corrections were made for the effect of pupil averaging, determined by the transverse coherence length. In the paper examples are shown of scintillation spectra in comparison with Kolmogorov's -5/3 power law and of the log-intensity character of the scintillation. Attention is spent on the saturation effect, occurring in cases of small apertures. By using the multiband scintillation data, we were able to investigate the color dependence of scintillation, of which examples are shown. Measured scintillation data are also compared with predictions from our marine boundary layer based TARMOS model. It appears that the performance of these predictions is hampered by the inhomogeneity of the weather parameters along the path. In the paper several data series out of the large amount of available data are presented, covering a few consecutive days of data with examples of extremely low scintillation levels, probably occurring in cases of near-zero Air-Sea Temperature Difference along the total pathlength.

8535-2, Session 1

Joint French-German radar measurements for the determination of the refractive index in the maritime boundary layer

Helmut W. Essen, Andreas J. Danklmayer, Fraunhofer FHR (Germany); Mario Behn, Joerg Förster, WTD 71 (Germany); Yvonick Hurtaud, Ctr. d'Expertise Parisien (France); Vincent Fabbro, Laurent Castanet, ONERA (France); Stefan Sieger, Fraunhofer FHR (Germany)

To predict the performance of maritime radars, it is essential to assess the propagation characteristics of electromagnetic waves in the maritime boundary layer. Usually parabolic equation models are employed to simulate the propagation factor. Besides the geometry between radar sensor and target and the RMS sea height the refractive index of the maritime boundary layer within the transmission path is of essential importance. In this environment, the spatial and temporal variations in air-sea temperature difference lead to refractive index gradients and gives reason for atmospheric ducts. These events modify the radar coverage in low troposphere.

The test program has the aim to deliver knowledge to improve radar performance in maritime environment, namely improve the detection of stealthy targets and of asymmetric threats, like small boats. The latter has also applications for blue border protection, which is a most recent topic. For a scientific analysis of radar performance it is necessary to gain a better knowledge of the environmental influences, like atmospheric stratification in the maritime boundary layer, the sea clutter dependence according to sea waves characteristics, wind, frequency and grazing angle.

The result of the study should provide new techniques to give radar operators a realtime knowledge of the presence of atmospheric structures, which have an impact detection of targets at low altitude and thereby improve the power of future tactical decisions.

A method to retrieve the refractive index gradients in the low troposphere is Refractivity from Clutter (RFC) algorithm. The propagation factor is computed from the received clutter power, then it is iteratively processed in order to retrieve the refractive index profiles.

Under a respective French-German technical agreement a measurement program has been initiated, with contributions from ONERA-CERT, DGA MI / TN and Fraunhofer-FHR, WTD 71. Experimental and operational Radars are involved using a wide frequency range, namely L-, C-, X- to Ku, Ka and W-band and different radar heights above sea level. Experiments are conducted at the German North Sea coast (Island of Sylt) to cover atlantic sea conditions and at SESDA (Saint Mandrier sur Mer) at the Mediterranean coast for a different maritime environment.

The evaluation is done in the following way: From the clutter measurement for different sea states, grazing angles and radar frequencies the spatiotemporal fluctuations of clutter at high resolution are derived as well as amplitude distributions, sea Doppler spectra and occurrence of spikes. To validate the indirect method it is essential to have full knowledge over environmental conditions given by the sea wave and direction spectrum, wind speed and direction, M-Profile in the boundary layer. For the organisation of the trials, information of meteorological and sea wave forecast is necessary. A detailed meteorological and environmental characterization is performed using a wide range of instrumentation on board a vessel and on the shore. The paper gives an overview on the RFC method with examples from the previous campaigns. It describes the experimental set-up and its methodology and shows first experimental results from the Sylt campaign.

8535-3, Session 1

Measurements of IR propagation in the marine boundary layer in cool atmospheric conditions

Eirik Glimsdal, Arthur D. van Rheenen, Lars T. Heen, Norwegian Defence Research Establishment (Norway)

A multinational field trial (SQUIRREL) was held at Eckenförde / Surendorf, Germany, during September 2011 to study both infrared ship signature and atmospheric propagation effects close to the sea surface. In this paper, infrared camera recordings of ship mounted sources are analyzed. The cameras were positioned about 4 m above mean sea level. Several meteorology stations - mounted on land, on a pier and on a buoy - were used to characterize the propagation environment, while sensor heights were logged continuously. Both sub- and super-refractive conditions were studied. Measurements are compared to results from an earlier field trial performed in USA under warm and humid conditions, and differences between medium wave and long wave infrared are emphasized. The ship mounted sources - two calibrated blackbody sources operating at 100 oC and 200 oC - were used to study contrast intensity and intensity fluctuations as a function of distance. The distance to the apparent horizon is also determined. Measurement results are compared to results from the IR Boundary Layer Effects Model (IRBLEM).

8535-4, Session 1

Field deployable TDLAS for long path atmospheric transmission

Christopher A. Rice, Glen P. Perram, Air Force Institute of Technology (United States)

A tunable diode laser absorption spectroscopy (TDLAS) device with narrow band (~300 kHz) diode laser fiber coupled to a pair of 12.5" Ritchey-Chrétien telescopes was used to study atmospheric propagation. The ruggedized system has been field deployed and tested for propagation distances of greater than 1 km. By scanning the diode laser across many free spectral ranges, many rotational absorption features are observed. Absolute laser frequency is monitored with a High Fineese wavemeter to an accuracy of 2 MHz. Phase sensitive detection is employed with absorbance of < 1%

observable under field conditions. More than 50 rotational lines in the molecular oxygen A-band X-b (0,0) transition near 760 nm were observed. Temperatures were determined from the Boltzmann rotational distribution to within 1.3% (less than ±2 K). Oxygen concentration was obtained from the integrated spectral area of the absorption features to within 1.6% (less than ± 0.04 x 1018 molecules / cm3). Pressure was determined independently from the pressure-broadened Voigt lineshapes to within 10%. A Fourier Transform Interferometer (FTIR) was also used to observe the absorption spectra at 1 cm-1 resolution. The TDLAS approach achieves a minimum observable absorbance of 0.2%, whereas the FTIR instrument is almost 20 times less sensitive. Applications include atmospheric characterization for high energy laser propagation and validation of monocular passive raging. The Cesium Diode Pumped Alkali Laser (DPAL) operates near 894 nm, in the vicinity of atmospheric water vapor absorption lines. Water vapor concentrations are accurately retrieved from the observed spectra using the HITRAN database.

8535-5, Session 1

Retrieving atmospheric turbulence features from differential laser tracking motion data

Dario G. Perez, Pontificia Univ. Católica de Valparaíso (Chile); Luciano Zunino, Ctr. de Investigaciones Opticas (Argentina) and Univ. Nacional de La Plata (Argentina); Gustavo Funes, Damian Gulich, Ctr. de Investigaciones Opticas (Argentina); Angel Fernandez, Pontificia Univ. Católica de Valparaíso (Chile)

We have previously introduced the Differential Laser Tracking Motion Meter (DLTMM) [Proc. SPIE textbf{7476}, 74760D (2009)] as a robust device to determine many optical parameters related to atmospheric turbulence. It consists of two thin laser beams---whose separations can be modified---that propagate through convective air, then each random wandering is registered with position detectors, sampling at $800~$Hz. The hypothesis that analyses of differential coordinates is less affected by noise induced by mechanical vibration was tested. Although we detected a trend to the Kolmogorov's power exponent with the turbulence increasing strength, we were unable to relate it to the Rytov variance. Also, analyzing the behavior of the multi-fractal degree estimator (calculated by means of multi-fractal detrended fluctuation analysis, MFDFA) at different laser-beam separations for these differential series resulted in the appreciation of characteristic spatial scales; nevertheless, errors induced by the technique forbid an accurate comparison with scales estimated under more standard methods. In the present work we introduce both an improved experimental setup and refined information theory quantifiers that eliminate many of the uncertainties found in our previous study. A new version of the DLTMM employs cross-polarized laser beams that allows us to inspect more carefully distances in the range of the inner-scale, thus even superimposed beams can be discriminated. Moreover, in this experimental setup the convective turbulence produced by electrical heaters previously used was superseded by a chamber that replicates isotropic atmospheric turbulence---anisotropic turbulence is also reproducible. Therefore, we are able to replicate the same state of the turbulent flow, specified by Rytov variance, for every separation between beams through the course of the experience. In this way, we are able to study the change in our MFDFA quantifiers with different strengths of the turbulence, and their relation with better known optical quantities. The movements of the two laser beams are recorded at $6~$kHz; this apparent oversampling is crucial for detecting the turbulence's characteristics scales under newly developed quantifiers form the information theory: permutation complexity and entropy. The estimated characteristic scales and multi-fractal nature detected by this experiment provides insight into the non-gaussian nature of propagated light.

8535-6, Session 1

Long-term measurements of refractive index structure constant in atmospheric boundary layer

Otakar Jicha, Pavel Pechac, Stanislav Zvanovec, Czech Technical Univ. in Prague (Czech Republic); Martin Grabner, Vaclav Kvicera, Czech Metrology Institute (Czech Republic)

With increasing interest in atmospheric sensing of the Earth, and newly proposed wireless links, either from the ground to remote sensing satellites, or between deep space and earth, it is necessary to measure aerosols, water vapour, clouds, winds, trace constituents, and temperature to understand the complex mechanisms governing the atmosphere. Scintillation and wandering of transmitted optical beams, together with distortions of their phase fronts, are mainly caused by thermal turbulence within the transmission medium and non-homogeneities of the refractive index. With respect to LIDAR sensing, turbulence consequently produces spatial and temporal irradiance scintillation in the target plane and results in an average target-plane beam size that is larger than the diffraction-limited beam size. To predict scintillations due to propagation in a turbulent atmosphere, a refractive index structure constant of air has been introduced. In the optical region the parameter is primarily related to fluctuations of the temperature of air in the atmosphere.

Although several height dependent models have been derived from measurements over the last few decades, more often by using classical measurements by radiosondes, it is still difficult to obtain structure constant characteristics with sufficient spatial and temporal resolution in the lowest troposphere below 100 m. Results from analyses of a long-term measurement campaign are introduced in the paper with vertical profiles of air temperature and relative humidity being measured on the 150-m-high Podebrady mast located near the city of Prague at an altitude of 188m above sea level. Combined Vaisala HMP45D sensors located at 19 heights between 0 and 150 m above the ground level with average spacing of about 7.5 m are utilized. Atmospheric pressure is also recorded by a Vaisala PTB100A sensor. The vertical profiles have been recording every minute since 2008.

Long-term statistics using cumulative distribution functions (CDFs) of the structure constant were generated under the assumptions of the Kolmogorov model of turbulence. First, the vertical profiles of the structure constant were studied and the empirical results were compared to the existing models. Annual statistics of the structure constant were generated separately at each height forming height profiles given for the selected quantiles of 0.1%, 50%, 90%, and 99% of time. It was observed that the structure constant is decreasing with height on average. It is shown that in the boundary layer the logarithm of the constant as a function of frequency can be approximated by a simple linear function with two empirical parameters which were derived and tabled for each selected quantile. Secondly, seasonal variations of the structure constant were analysed at two selected heights, 39.7 and 79.8 metres above the ground, respectively and the CDFs were processed separately for each calendar month with the changes plotted for the selected quantiles with generally higher values being reported during the summer season and slight differences between the two heights observed and analysed. The results of this study can be utilized for any remote sensing application in a moderate climate where the optical turbulence in the atmospheric boundary layer needs to be addressed.

8535-7, Session 1

Remote sensing of atmospheric turbulence profiles by laser guide stars

Xiwen Qiang, Northwest Institute of Nuclear Technology (China) and Xi'an Jiaotong Univ. (China); Junwei Zhao, Shuanglian Feng, Min Wu, Jinyong Chang, Fei Zong, Jing-ru Liu, Northwest Institute of Nuclear Technology (China); Jianping Song, Xi'an Jiaotong Univ. (China)

Characteristics of atmospheric turbulence varies temporally and spatially, so remote sensing of atmospheric turbulence profiles in real time is important and necessary for applications such as performance analysis of astronomical adaptive optics systems, astronomical site surveys and selection, validation of atmospheric turbulence prediction models, free space laser communication, and laser beam propagation in the atmosphere.

The astronomical and adaptive optics communities have established several optical techniques for remote sensing Fried parameters, a value of path-integrated structure constant of refractive index of atmospheric, but it is necessary to remote sensing ranged-resolved information of atmospheric turbulence. Laser guide star technique is used commonly in adaptive optics community, and differential image motion method is a matured technique in astronomical community. So, a new technique is put forward for remote sensing atmospheric turbulence profiles.

Combined with laser guide stars and differential image motion method, remote sensing of atmospheric turbulence profiles in real time is realized in experiments effectively. The configure of experiment

consists of a powerful pulsed lasers, a beam-expanding lens and a negative lens for beam-focusing, a reflective mirror for beam-projecting, a optical device for receiving and imaging of returned signals, a ICCD camera for recording images of laser guide stars, and a computer for controlling and data processing.

By expanding and focusing laser beams projected from a powerful pulsed lasers, laser guide stars are formed at several successive altitudes. A optical system with two receiving telescopes is developed based on differential image motion method. The laser guide stars are observed with the optical system developed, and images of laser guide stars with two spots at a receiving ICCD camera.

The images with two spots at the same altitude are processed and centroids of two spots at every images are given. Differential image motion variance of distance of centroids could be derived from the images at the same altitude. So, the motion of the images of the laser guide stars from each altitude is characterized as the differential image motion variance. Based on a inversion algorithm, atmospheric turbulence profiles could be retrieve from differential image motion variance of distance of centroids at various altitudes.

Experiments of remote sensing have been performed, and the profiles of atmospheric turbulence are obtained. The structure constants of refractive index of the atmosphere range from 10-14m-2/3 at lower altitudes to 10-16m-2/3 at higher altitude. The results show it is a effective method that combined laser guide stars with differential image motion and could sense atmospheric turbulence profiles remotely in real time.

8535-8, Session 1

GPS derived spatial ionospheric total electron content variation over South-Indian latitudes during intense geomagnetic storms

Sampad K. Panda, Shirishkumar S. Gedam, Indian Institute of Technology Bombay (India)

Geomagnetic storms are turbulence in geomagnetic field when interplanetary magnetic field driven by solar wind move southward and continue for extended period of time. Although these occur less frequently, but may energize ionospheric electrons and particles to result ionospheric abnormality, consequently causing damage to satellites, power grids and radio communications. Ionosphere at higher latitude is more prone to geomagnetic storms, but in low latitude regions i.e., India-subcontinent even if less effect is expected, but exhibit many distinctive characteristics, such as scintillations, equatorial ionization anomaly (EIA), fountain effect and equatorial electrojets (EEJ). Free electrons in ionosphere introduce delay global positioning system (GPS) satellite signals resulting mismeasurement of exact locations during GPS positioning. With the opportunity of full constellation GPS satellites wrapping around the globe, now it has become possible to inspect regional even global ionosphere from signature stamps on its signals. From the simultaneous observations of carrier phase and pseudorange measurements in a dual frequency GPS receiver, the line integral of free electron density along the pathway of signal through ionosphere (i.e., Total Electron Content, TEC) can be estimated. The TEC is measured in terms of TECU where, 1 TECU = 1 x10^16 electrons/m^2. In the present paper, dual frequency GPS data are taken from three low latitude GPS stations in India located at Bangalore (near the geomagnetic equatorial region), Hyderabad (subtropical region), and Mumbai (near crest of anomaly) to study the TEC responses during intense geomagnetic storms. The epoch-wise vertical TEC in terms of TECU is derived from signals of all visible satellites and 2-sigma iterated mean vertical TEC is calculated at every 0.1 hr interval at each station during the storm days. From the event occurred during 29th October 2003 (Disturbance Storm index in nanotesla, Dst = 353 nT), it is observed that TEC limit reaches a maximum value of ~104.9 over Bangalore, where as the values over Hyderabad and Mumbai are ~133.2 and ~132.4 respectively. In the same year, another severe storm occurred on 20th November (Dst = -383 nT) increasing the TEC value to ~68.4, ~84.5, and ~92.9 over Bangalore, Hyderabad, and Mumbai respectively. Similarly, due to storm on 7th November 2004 (Dst = -374 nT) the estimated TEC rises to ~80.8, ~78.6, and ~83.3 and subsequently after two days another intense storm (Dst = -263 nT) increased the TEC to maximum of ~63.7, ~74.2, and ~84.1 from Bangalore to Mumbai through Hyderabad. One more intense storm occurred during 15th May 2005 (Dst = -247nT) resulting increased TEC value of ~54.5 at Bangalore, ~74.9 at Hyderabad, and ~81.6 units at Mumbai. The consequences of TEC variation from equator towards anomaly region is analyzed and correlated with 4-minute averages of Z-component of interplanetary magnetic field (IMF-Bz) recorded by Advanced Composition Explorer (ACE) spacecraft and 3-hourly geomagnetic K-indices (Kp-index) to investigate intense storm effect and its abnormal variation due to interaction of IMF with earth's magnetometer. The behavior of TEC during the occurrence is compared to previous and successive quiet days to estimate its influence during positioning measurements.

8535-9, Session 1

Application of independent component analysis method in real-time spectral analysis of gaseous mixtures for acousto-optical spectrometers based on differential optical absorption spectroscopy

Alexander V. Fadeyev, Vitold E. Pozhar, Scientific and Technological Ctr. for Unique Instrumentation (Russian Federation)

The paper presents a new approach based on statistical independent component analysis (ICA) method to improve the efficiency of methods for chemical analysis of multicomponent gaseous mixtures by means of spectrometers based on acousto-optical tunable filters (AOTFs).

The unique feature of AOTF-based spectrometers is random spectral access (RSA). This property provides the possibility of rapid selective spectral analysis that is effective for such applications as the control of technological processes, monitoring of object evolution, in particular variations of individual components of objects, and other procedures, in which important information is correlated with a few characteristic spectral lines. Differential spectroscopy, in particular the method of differential optical absorption spectroscopy (DOAS), is suited to such kind of spectra. The essence of DOAS method is the decomposition of measured absorption spectra into a linear combination of absorption spectra of its components. The spectral pattern of each component is restricted to only a few spectral lines.

The more the sparsity of spectra, the more efficient the use of RSA-based methods. But from the other hand the reliability of analysis becomes lower because of possible loss of important information during the spectral lines selection. The error may be caused by the presence of unexpected substances in the mixture, as well as the presence of noise. To solve this problem an algorithm based on ICA is proposed. By using the proposed algorithm in conjunction with an existing algorithm for quantitative analysis it is possible to create real-time gas-analytical systems based on acousto-optical spectrometers with adaptive features.

It is proposed an algorithm for qualitative analysis based on statistical ICA method. By using ICA the spectral data of mixture can be decomposed into independent components (spectral sources), whose spectra could be used as the reference spectra for regression analysis. Unlike most of conventional qualitative methods, for example methods based on Bayesian approach, the proposed ICA-based algorithm does not require any a priori information about the object. The only requirement is the assumption of statistical independence of reference spectra. The algorithm can be used as a preprocessing step aimed at detection of some extra components in the mixture and the post-processing operation for estimation of measurement accuracy and uncertainty by means of residuals analysis.

It is feasible to apply ICA to spectra consisting of a limited set of characteristic lines (e.g. DOAS spectra), because ICA is known to be the most effective in application to sparse spectra. Implementations of the algorithm are proposed for RSA-spectrometers. It is reported the comparison of the proposed ICA analytical procedure to conventional Bayesian algorithms. The simulation was accomplished using spectra measured by gas-analyzer GAOS [1]. GAOS has been developed as an absorption spectrometer for real-time ambient trace-gas monitoring by DOAS technique. This movable instrument is based on double-stage collinear AOTF made of SiO2, demonstrating following characteristics: spectral range 0.25-0.45 mcm, spectral resolution 9 cm-1. It is targeted at simultaneous detection of such pollutants as some simple oxides (NO2, SO2, HCHO) and aromatic hydrocarbons (C6H6, C6H5CH3, C6H5OH, etc.).

Proposed approaches will be applied in the construction of adaptive systems based on acousto-optical tunable filters.

[1] Pustovoit, V. I., Pozhar, V. E., "Long-path optical spectral AOTF-based gas analyzer," Proc. SPIE 4574, 174-178 (2001).

8535-10, Session 2

GPU-based simulations of optical propagation through turbulence for passive and active imaging applications *(Invited Paper)*

Goulven Monnier, François-Régis Duval, Solène Amram, ALYOTECH France (France)

The usual numerical approach for accurate, spatially resolved simulation of optical propagation through atmospheric turbulence involves Fresnel diffraction through a series of phase screens. When used to reproduce instantaneous laser beam intensity distribution on a target, this numerical scheme may get quite expensive in terms of oth CPU and memory resources, due to the many constraints to be fulfilled to ensure the validity of the resulting quantities. In particular, computational requirements grow rapidly with higher-divergence beam, longer propagation distance, stronger turbulence and larger turbulence outer scale. Our team recently developed IMOTEP, a software which demonstrates the benefits of using the computational power of the Graphics Processing Units (GPU) for both accelerating such simulations and increasing the range of accessible simulated conditions. By comparison with a CPU implementation, speedup factors ranging from 40 to 60 are demonstrated for the execution of the basic propagation phase-screen algorihm.

Simulating explicitly the instantaneous effects of turbulence on the backscattered optical wave is even more challenging when the isoplanatic or totally anisoplanatic approximations are not applicable. Two methods accounting for anisoplanatic effects have been implemented in IMOTEP. The first one, dedicated to narrow beams and non-imaging applications, involves exact propagation of spherical waves for an array of isoplanatic sources in the laser spot. The second one, designed for active or passive imaging applications, involves pre-computation of the DSP of parameters describing the instantaneous PSF. PSF anisoplanatic statistics are “numerically measured” from numerous simulated realisations. Once the DSP are computed and stored for given conditions (with no intrinsic limitation on turbulence strength), which typically takes 5 to 30 minutes on a recent GPU, output blurred and distorted images are easily and quickly generated. Comparison with real images of distant targets show an overhall agreement, but also some discrepancies whose origins are discussed. It appears that more realistic models of the parametric PSF should be evaluated, in order to account for the transcient high-frequency information present in speckled images. Here again, the use of GPU could help maintain acceptable computing time.

The paper gives an overview of the software with its physical and numerical backgrounds. The approach developed for generating anisoplanatic instantaneous images is emphasized.

8535-11, Session 2

Transmitter and receiver modules for free-space optical transmission links in the mid-infrared

Myriam Raybaut, Sophie Derelle, ONERA (France); Johan Rothman, CEA-LETI (France); Antoine Godard, Joël Deschamps, Aurélie Bonnefois, Nicolas Védrenne, Anne Durécu, ONERA (France)

So far, most free-space optics (FSO) links have been performed in the telecom wavelength bands; however, it may be convenient to use other atmospheric transmission windows, especially in the mid-infrared range (3-5 µm).

In this context, we have thus investigated the feasibility of a long range FSO link in the mid-infrared. It appeared that an emission wavelength around 4 µm presents several advantages compared to the usual wavelength, i.e. 1.55 µm. We have thus specifically developed source and detector modules, offering performances compatible with FSO transmission links at 3.6 µm.

The transmitter source is based on the frequency conversion of a telecom 1.5 µm diode laser into the 3.6 µm range by parametric mixing. Indeed, we perform difference frequency generation (DFG) between the radiation emitted by a commercial continuous wave 1.08 µm fiber laser and the 1.5µm telecom radiation in periodically poled lithium niobate. Providing that the DFG stage is properly designed, i.e. as long as the DFG phase-matching bandwidth is larger than the signal bandwidth, the modulation properties of the 1.5 µm radiation are directly transposed to the emitted 3.6 µm DFG radiation. Several DFG stages have been designed and tested, based on either bulk or waveguide non linear crystals solutions, and we managed to generate several mW at 3.6 µm.

The receiver is based on a cooled HgCdTe avalanche photodiode manufactured by the CEA LETI and a commercial amplifier at ambient temperature. The cut-off wavelength of the detector is equal to 4.2µm at 80K and 3.9µm at 200K. We measured a multiplication gain equal to 185 at 80K and 9V and to 20 at 200K and 6V. The excess noise factor is very weak ~1.25 and independent of the multiplication gain. The response time of the detector has been measured using a mid-infrared picosecond parametric source and varies from a few nanoseconds to 1ns depending on the detector size and for temperatures between 80K and 160K. The fall time is strongly limited by diffusion of the carriers generated quite far from the junction. It is important to note that, up to now, no particular technological development has been performed to improve the bandwidth of the detector itself.

We performed a free-space optical transmission link in laboratory conditions (5 m). The source was modulated at 0.12 Gb/s, the signal was successfully received by the receiver. The details of the experiments will be presented, along with the improvement potentialities of the set-up.

This is nevertheless to our knowledge the first demonstration of a mid-infrared optical link based on direct detection in the mid-infrared.

8535-12, Session 2

The nonlinear OPC technique for laser beam control in turbulent atmosphere

Vladimir B. Markov, Advanced Systems & Technologies, Inc. (United States); Anatoliy Khizhnyak, Advnaced Systems & Technologies, Inc. (United States)

Optimal laser energy delivery on a remote image-resolved target trough turbulent medium is a task that is difficult to achieve. For example, propagation of the laser beam through turbulent atmosphere results in increased spot size, beam jitter and substantial degradation of its power density at the target plane. Mitigation of these effects can be achieved by pre-distorting the wavefront of the output beam. To be effective, this technique requires information on the inhomogeneity of the atmospheric layer along the propagation path between the laser system and the target. These data can be collected, for instance, by using a localized beacon on the target. In order to incur an adequate phase disturbance the laser beacon beam should propagate through the same turbulent atmosphere as the laser beam to corrected. Thus, formation of the diffraction limited beacon on the target is an important goal.

Early we discussed the approach for compensating phase disturbance due to atmospheric turbulence based on the target-in-the-loop (TIL) scheme. In this presentation we report the results of the laboratory realization of the proposed approach of beacon formation through turbulent medium in TIL-scheme with optical phase conjugation. The laboratory realization of the TIL-scheme includes the diffuse target, turbulent atmosphere simulator, laser amplifier and a non-linear optical phase conjugate mirror. In the current experimental setup, the turbulence simulator is made off a group of random phase screens with Kolmogorov spectrum and it enables to imitate a controlled-level strength of turbulence (scintillation index).

This presentation provides formation on experimental results of the lab-tests and operational performance of the TIL-system and comparison of these data with the results of the computer simulation.

8535-13, Session 2

Laser beam propagation through an ensemble of vortex rings in air

Fedor V Shugaev, Ludmila S Shtemenko, Oksana A Nikolaeva, Oksana A Solenaya, Lomonosov Moscow State Univ. (Russian Federation); Evgenii N Terentiev, Lomonosov Moscow state university (Russian Federation)

The problem of the evolution of an ensemble of vortex rings (5-10 in number) in air has been solved. The full system of the Navier -Stokes equations was used. The parametrix method was applied (the 2nd and 3rd iterations, the linear solution being considered as the first

iteration). The calculations were performed for a wide range of the ring parameters (circular and elliptic cross-sections, various diameters of the rings, their different orientation in the space etc.). The initial value problem is as follows. The vorticity has non-zero value only inside the rings at initial instant, the density and the temperature being constant everywhere at t=0. We considered two cases of the initial distribution of the vorticity in the core of a ring: (i) the vorticity is constant; (ii) its variation is proportional to the distance from the axis of the ring. First of all we calculate the vorticity at t>0, and then the velocity and the dissipation function. After that we determine the density. If this quantity is known, then it is possible to find the refractive index. The solution to the Navier-Stokes equations is an oscillating one. Thus the refractive index is an oscillating function with respect to time. These results enable to model turbulence in an adequate way without using the Taylor frozen turbulence hypothesis. The evolution of the frequency spectrum of the density fluctuations was obtained. These results were compared with Tatarskii's data. Solutions to the Navier-Stokes equations in an isolated system decay as time increases. But they may be useful in order to model the atmospheric turbulence, if one considers a short period of time.

The intensity of a laser beam propagating through the ensemble of vortex rings in air was found with the aid of the parabolic equation method. The corresponding value of the refractive index was determined from the Navier-Stokes equations.

A numerical procedure is set forth which allows to solve the problems of superresolution without using regularization methods. The task is as follows. There is a set of experimental data (with some errors) and an instrument function (with some error). It is possible to find the corresponding modulation transfer function (MTF). The problem is solved within a bounded domain. We change the domain in such a manner that the MTF has nowhere zero values. Besides, we reduce the noise. The procedure enables to solve problems of focusing in the turbulent atmosphere and those of target indications.

8535-14, Session 2

Scintillation of pseudo-partially coherent Gaussian beam in atmospheric turbulence: application for free-space optical communications

Xianmei Qian, Wenyue Zhu, Ruizhong Rao, Anhui Institute of Optics and Fine Mechanics (China)

By using wave optics numerical simulation, the scintillation of pseudo-partially coherent Gaussian beam propagating in atmospheric turbulence is investigated. The effects of partial coherence on scintillation index are analyzed as a function of the correlation length of beam source. The reduction of the aperture averaging scintillation index, on-axis and off-axis scintillation are shown for a horizontal propagation path. The aperture averaging factor of pseudo-partially coherent beam is compared with that of fully-coherent beam. And how the pseudo-partially coherent Gaussian beam behaves like partially coherent Gaussian Schell-model beam is also discussed. It was found that the on-axis scintillation index and off-axis scintillation index of pseudo-partially coherent beam can be reduced greatly by decreasing the coherence degree of beam source. The results of aperture averaging scintillation index also revealed the advantage of using pseudo-partially coherent beam compared to fully coherent beam. However, the aperture averaging factor of a pseudo-partially coherent beam is smaller than that of the fully coherent beam at the same receiving aperture diameter. This implies that the aperture averaging effect of scintillation index may be weakened by reducing the coherence degree of beam source. This work may provide a basis for the utilization of pseudo-partially coherent beam in free-space optical communications.

8535-15, Session 3

Holographic wavefront sensing with spatial light modulator in context of horizontal light propagation

Andreas Zepp, Fraunhofer-Institut für Optronik, Systemtechnik und Bildauswertung (Germany)

For correction of atmospheric effects on the propagation of (laser) light by adaptive optics, the wavefront deformations can be detected with adequate sensors. Established wavefront sensors (WFS), like Shack-Hartmann sensor, provide indeed good results, but for some applications insufficient measurement speed. Often time-consuming detector readouts as well as extensive signal post-processing are necessary, so that the detection rate is limited to well below 10kHz. For scenarios with challenging conditions like laser communication through strong turbulence these sensors are not reasonably usable.

A promising alternative is the Holographic Wavefront Sensor (HWFS). Core of the sensor is a holographic created grating as diffractive optical element. By illuminating this element with the wavefront of interest it generates two light spots for each present Zernike mode at defined locations. The amplitude of the respective mode can be determined from the intensity difference of both foci. Hence the decomposition of the wavefront in its Zernike components is realized in hardware and is in principle carried out in speed of light. There is no need of time-consuming software-based calculations. The detection of the modes can be made with fast photodiodes at the focus positions.

For the sensor fabrication a multiplex-hologram is recorded. Herein exactly two interference pattern are stored for every wavefront aberration, which is to be analyzed. Therefor a convergent wave is taken as object beam, focused in a specific object point. As reference beam once a wave with the positive amplitude of the interesting wavefront aberration is used and once with the negative. These recordings are made for any relevant Zernike mode each with differing object point locations.

The use of an analog hologram plate to record the interference pattern has the advantage of a high resolution (more than 3000 lines/mm). Drawbacks are the sources of error during the hologram recording, since the quality of the hologram is significant dependent on its exposure and the chemical processing.

A very flexible alternative to the hologram plate is the use of a Spatial Light Modulator (SLM) as sensor. The hologram recording is replaced by calculation of the interference pattern. Such a computer-generated hologram (CGH) can afterwards be displayed with the SLM and functions by illuminating as phase grating. With CGHs the symmetric alignment of the object foci can be realized error-free und the results are independent of the analog exposure parameters. Furthermore according to the application a fast switch between different CGHs is possible, to detect just one selected Zernike mode with increased sensitivity temporary for instance.

For this reason we realized the HWFS with the SLM Holoeye Pluto-NIR-2 (1920x1080 pixels of 8µm size) and studied a further important property: The theoretic independence from scintillation. Any region of the (computer-generated) hologram contains a part of the interference pattern as diffraction grating. Consequently fractional shadowing of the sensor should reduce the absolute intensity of the reconstructed foci but have no influence on the intensity difference of the two foci of one Zernike mode. Our corresponding experiments show promising results. Parallel the behavior of the Sensor with scintillation was simulated in open loop.

8535-16, Session 3

New wavefront sensing concepts for adaptive optics instrumentation

Kacem El-Hadi, Lab. d'Astrophysique de Marseille (France); Thierry Fusco, ONERA (France); Brice Le Roux, Lab. d'Astrophysique de Marseille (France)

Key words: adaptive optics, wavefront sensing, MEMS deformable mirror, liquid crystal corrector, Spatial Light Modulator.

The developement of new instrumentations for the future European Extremely Large Telescope (E-ELT) will require new developments in adaptive optics in terms of simulation (end-to-end simulator for an ELT), optimisation of control laws (traditional Kalman filter methods will show limitations because of the power of necessary computation, multi-stages correction) and experimental validation of new wavefront concepts.

In order to address these key aspects, a new multi-purpose experimental Adaptive Optics (AO) bench is developed at Laboratory of Astrophysics of Marseille. It is based on two stages of wavefront control and correction using a Shack-Hartmann wavefront sensor in front of a MEMS deformable mirror (140 actuators from Boston Micromachines) for "low orders" modes correction, while a Pyramid wavefront sensor (PWFS) will be combined to a Liquid Crystal Spatial Light Modulator to correct the "high orders" frequencies. Both systems could be merged in a two stages AO concept allowing us to study the coupling of a telescope pre-correction with a dedicated large M4 deformable mirror and a post focal high order AO system. Analysis and optimisation of the spatial and temporal split of the AO correction

between the two systems is therefore essential.

Finally, we will use the world's fastest and most sensitive camera system OCAM2 (developed at LAM) with the pyramid concept (proposed by R. Ragazzoni), to demonstrate a homemade fast and hyper-sensitive PWFS (up to 100x100 sub-apertures) dedicated to the first generation instruments for ELTs.

All these studies are led in collaboration with ONERA and L2TI.

8535-17, Session 4

Remote sensing on a stellar surface *(Invited Paper)*

Oskar von der Lühe, Kiepenheuer-Institut für Sonnenphysik (Germany)

The Sun is the only star where physical processes can be observed directly at their intrinsic scales. Solar surface structure appears with scales ranging from several 105 km to a few dozen km, taxing the resolution limit of today's largest - i. e., meter-class - solar telescopes. Many processes which can be observed at the solar surface are connected with the solar magnetic field, which also causes the solar magnetic cycle and which produces violent eruptions and mass ejections that affect the space near the earth. Understanding solar magnetism is therefore vital for human activity in space, and requires observations of the Sun which are highly resolved in space and time.

Solar astronomers now operate telescopes with apertures exceeding one meter, with a spatial resolution approaching 50 km on the solar surface. Telescopes with 4m apertures which resolve some 20 km are under construction in the US and in the planning stage in Europe. These facilities are equipped with high resolution spectrographs and sensitive polarimeters to extract the maximum of information from the Sun's radiation. They also require high order adaptive optics and multi-conjugate adaptive optics systems in order to overcome the influence of turbulence in the Earth's atmosphere. The combination of active control and image processing has proved a viable path towards remote sensing of the solar surface with diffraction limited resolution in recent years.

This talk provides an overview of current goals and recent results of high resolution solar observations and illustrates the techniques which are used by solar astronomers.

8535-18, Session 4

Simulation of atmospheric turbulence for a qualitative evaluation of image restoration algorithms

Claudia S. Huebner, Fraunhofer-Institut für Optronik, Systemtechnik und Bildauswertung (Germany)

Many remote sensing applications are concerned with observing objects over long horizontal paths and often the atmosphere between observer and object is quite turbulent, especially in arid or semi-arid regions. Depending on the degree of turbulence, atmospheric turbulence can cause quite severe image degradation, the foremost effects being temporal and spatial blurring.

The software-based mitigation of degradation effects caused by atmospheric as well as artificial turbulence in various spectral bands and the consequent image restoration by means of iterative blind deconvolution has been subject of our study in the past. However, an unbiased qualitative evaluation of the respective restoration results proves difficult if little or no additional information on the "true image" is available.

Therefore, in this paper a turbulence simulation method is proposed and used to produce image data on which restoration algorithms can be tested. In addition, a qualitative evaluation of our image restoration algorithms is given.

8535-19, Session 4

Image reconstruction of extended objects: demonstration with the Starfire Optical Range 3.5m telescope

Szymon Gladysz, Fraunhofer-Institut für Optronik, Systemtechnik und Bildauswertung (Germany); Roberto Baena Galle, Royal Academy of Sciences and Arts of Barcelona (Spain) and Univ. de Barcelona (Spain); Robert L. Johnson, Lee Kann, Air Force Research Lab. (United States)

Using data from the 3.5m SOR telescope we have benchmarked a number of image restoration techniques: multi-frame blind deconvolution, Richardson-Lucy restoration, bispectrum-based speckle imaging, deconvolution with regularization, and maximum-likelihood, wavelet-based deconvolution. The input data consists of short exposures, typically less than 10ms, either uncompensated, or after adaptive-optics correction with the new 24by24-subaperture system. The data was recorded simultaneously in two channels: I-band (650-1000 nm) and J-band (1100-1350 nm) and typically consists of one thousand images per object. The imaged objects were planetary-type bodies, e.g. moons of Jupiter.

We discuss the possibility of extracting the PSF of the observations directly from the uncompensated speckle images and using it for deconvolution. For AO-compensated images a reference PSF from a stellar point-source was employed for image restoration.

We describe some of the encountered shortcomings of the methods: incapability of the most widely-used optimization criterion to capture perceptual image quality, limited capability of the myopic/blind codes to perform PSF update, and effect of the adaptive-optics image stabilization on the performance of multi-frame blind codes which rely, to some extent, on PSF diversity.

We have also tested the algorithms on simulated AO data. In these controlled tests, with known "ground truth", we have presented the algorithms with simulated AO images of Saturn and also with a first-guess PSF characterized by a varying level of mismatch relative to the target observations. We have also investigated the effect of varying the level of noise in the observations. The maximum-likelihood, wavelet-based algorithm with a static PSF produces results which are generally better than the results obtained with the myopic/blind approaches (for the images we tested and up to the ~20% level of mismatch in the Strehl ratio) thus showing that the ability of a method to suppress the noise and to track the underlying iterative process is just as critical as the capability of the myopic/blind approaches to update the PSF.

We discuss future directions like maximum-a-posteriori deconvolution with statistical PSF prior: in the pupil-, image-, or Fourier domain. We aim to produce a deconvolution algorithm which automatically extracts PSF from the observations and updates it while conforming to the known statistical properties of the turbulence or AO-corrected residuals.

8535-20, Session 4

Multi-frame restoration of turbulence degraded underwater images *(Invited Paper)*

Andrey V Kanaev, U.S. Naval Research Lab. (United States)

The ability to image underwater is highly desired for scientific and military applications, including optical communications, situational awareness, diver visibility, and mine detection. However, underwater imaging is severely impaired by scattering and optical turbulence associated with refraction index fluctuations. Naturally, the approaches taken to solve the underwater image restoration problem have their origin in atmospheric turbulence compensation algorithms.

There is certain similarity between the atmospheric and underwater image degradations but the difference in the scales of refraction index fluctuations in two media brings out the need for significant modifications of atmospheric techniques to be applicable to underwater imagery. Significantly stronger underwater image distortions resulting in large local shifts and warping of the image features require robust tracking using, for example optical flow estimation, even under relatively benign underwater conditions.

Comparative performance of multi-frame nonlinear gain “lucky patch” algorithms with variable degree of optical flow technique sophistication is presented for underwater imagery collected in a laboratory tank and in a field exercise. Reliance of image restoration on accuracy of the optical flow algorithm is revealed and one approach to enhance restored image quality using confidence measures of optical flow estimation is proposed.

8535-21,

Laser illuminated image estimation in the presence of atmospheric scintillation

David C. Dayton, Applied Technology Associates (United States); John-Paul Sena, Jeremy S. Oliver, Gregory Fertig, Air Force Research Lab. (United States); Rudolph Nolasco, Applied Technology Associates (United States)

No Abstract Available

8535-22,

Modified Cessna T206H with retractable MX15HDI turret for airborne ISR applications

Rudolph Nolasco, Applied Technology Associates (United States); Gregory Fertig, John-Paul Sena, Jeremy S. Oliver, Air Force Research Lab. (United States); David C. Dayton, Applied Technology Associates (United States)

No Abstract Available

Conference 8536: SAR Image Analysis, Modeling, and Techniques

Wednesday - Thursday 26–27 September 2012 • Part of Proceedings of SPIE Vol. 8536 SAR Image Analysis, Modeling, and Techniques XII

8536-2, Session JS2

An experimental setup for multiresolution despeckling of COSMO-SkyMed image products

Bruno Aiazzi, Istituto di Fisica Applicata Nello Carrara (Italy); Luciano Alparone, Fabrizio Argenti, Univ. degli Studi di Firenze (Italy); Stefano Baronti, Istituto di Fisica Applicata Nello Carrara (Italy); Tiziano Bianchi, Alessandro Lapini, Univ. degli Studi di Firenze (Italy)

8536-3, Session JS2

Multi-chromatic analysis of a single SAR image for absolute ranging

Fabio Bovenga, Consiglio Nazionale delle Ricerche (Italy); Leonardo Gallitelli, Davide O. Nitti, Politecnico di Bari (Italy)

The Multi-Chromatic Analysis (MCA) uses interferometric pairs of SAR images processed at range sub-bands located at different spectrum positions, and explores the phase trend of each pixel in the frequency domain. The phase of stable scatterers evolves linearly with the sub-band central wavelength, the slope being proportional to the absolute optical path difference. Consequently, both phase uwrapping as well as height computation can be performed on a pixel by pixel basis without spatial integration.

Results obtained through theoretical modeling as well as by processing airborne wideband SAR data indicate that at least 300 MHz seems to be required to provide reliable results. Thus, the technique appears optimally suited for the new generation of satellite sensors as TerraSAR-X (TSX) or COSMO-SkyMed (CSK), which operate with larger bandwidths than previously available instruments, generally limited to few tens of MHz. Recently the technique has been used to derive ground elevation by processing interferometric pairs acquired in Spotlight mode by both TSX and CSK satellite missions. However, further potential applications are possible. In particular, this work is aimed at experimenting the use of MCA for measuring the optical path between the SAR sensor and the imaged scene by processing a single SAR acquisition.

The optical path depends on the Euclidean distance between the sensor and a target on the ground as well as on the delay induced by the interaction between the microwave SAR signal and atmosphere. The first contribution amounts to hundreds of kilometers, while the second one is in the order of few meters depending mainly on the dry component of the troposphere. In this configuration, the slope of the phase trend along frequencies depends on the full optical path, and therefore, to avoid aliasing, it would be required to split the full band into an unfeasible number of sub-bands. Thus, in order to reduce the range of measuring distance, we adopted a processing scheme which consists in subtracting from the SAR image phase a term proportional to the Euclidean distance computed through inverse geocoding. The residual term is proportional to the sum of the atmospheric delay and of a term which accounts for errors in Euclidean computation due to inaccurate knowledge of both satellite and target positions. This residual term can be measured through MCA by using a limited and feasible number of sub-bands. Assuming negligible the positioning errors, the validation of this approach can be performed by comparing the distance measured by MCA with the atmospheric delay computed through analytical models and in situ records. First, we carried out a feasibility study aimed at evaluating the maximum value for the errors in satellite and target positions, allowed to perform the reliable validation. Then, in order to reduce the error in the target positions and to guarantee good phase stability, we selected SAR acquisitions which include artificial corner reflectors to be used for MCA processing and the following validation procedure.

8536-4, Session JS2

Ultra-wide band ISAR imaging by Laguerre Gauss tomographic reconstruction

Elio D. Di Claudio, Giovanni Jacovitti, Univ. degli Studi di Roma La Sapienza (Italy); Alberto Laurenti, GIAL S.r.l. (Italy)

Ultra Wide Band (UWB) Inverse Synthetic Aperture Radar (ISAR) imaging techniques are today interesting not only for classical long-range target recognition purposes , but also for short range applications, such as ground penetrating radar, vehicle tracking and classification, non-invasive sub-surface sensing, etc...

ISAR image techniques are based on the collection of several radar echoes from the target, taken at different angles and providing different range profiles (RPs). Whenever the angle under which the target is observed is sufficiently narrow, the plane wave assumption can be accepted, corresponding to line integration along the cross range direction. This amounts to say that the ISAR imaging problem can be formulated as a tomographic reconstruction process, where RPs are regarded as tomographic projections of a synthetic target backscattering map (STBM). By fact, classical Fourier transformation methods for ISAR inversion are based on the well known Fourier slice theorem, even though techniques become more and more sophisticated as long as complex and unknown target motion takes place during the signal acquisition process.

The ISAR imaging approach presented here is inherently UWB oriented, and provides tomographic reconstruction of the STBM as a linear combination of RPs samples taken at different angles. These appealing features essentially depend on the peculiar mathematical properties of the representations adopted for the RP and the STBM, consisting of the two-dimensional (2-D) Hermite Gauss (HG) and Laguerre Gauss (LG) polynomial expansions. In fact, the 2-D HG functions are Cartesian separable and the LG functions are polar separable, but they span exactly the same 2-D signal space and are block-wise linearly related.

The idea leading to the present method stems from the theory developed in [1], where the cross sections of linear patterns were optimally estimated by the LG expansion of the observed image. Such a process is based on the fact that the coefficients of a one-dimensional Hermite expansion of the line integral (tomographic sections) along a given direction of the image plane are linear combinations of the coefficients of the 2-D HG expansion, and by consequence of the LG expansion coefficients. Owing to the angular harmonic modulation of the LG functions, this linear relationship depends in a very simple way on the given view angle.

Inverting this process leads to calculate the STBM image through a linear estimation of its LG expansion coefficients from any set of RP signals. The resulting resolution of the STBM image is determined by the maximum LG expansion order allowed by the numerical rank of the linear system matrix itself, which in turn depends on the number of available ISAR views and their angles.

The method is candidate for developing both high quality ISAR imaging and automatic target classification techniques, using appropriate LG expansion orders.

In the paper, the STBM image obtained from a simple set of static omni-directional scatterers, using UWB pulses and a 32th order LG expansion, will be shown to give a first idea of the results achieved by such a method.

[1] E. D. Di Claudio, G.Jacovitti, and A. Laurenti, “Maximum Likelihood Orientation Estimation of 1-D Patterns in Laguerre-Gauss Subspaces,” IEEE Trans. on Image Processing, vol. 19, No. 5, May 2010, pp. 1113-1125.

8536-5, Session 1

Compact polarimetry for C-band land-use classification: a pre-study for the Canadian Radar Constellation Mission (RCM)

Shane R. Cloude, AEL Consultants (United Kingdom); David G. Goodenough, Hao Chen, Natural Resources Canada (Canada)

RCM, the proposed Canadian follow up to the successful Radarsat-2 satellite imaging radar, proposes a new wide-swath polarimetric mode, compact [1], which comprises a hybrid mode, single transmit polarization (circular) and simultaneous coherent orthogonal linear receive. On a single pixel SLC level, the system will then measure only a projection of the complex scattering matrix [S]. The main advantages of such a system are the simpler transmitter architecture requirements, the wider swath capability and lower data rate compared to quadpol. However, it remains to be seen how the loss of information through projection affects the quality of classification products. Here we investigate this for land-use forestry applications.

In this talk we first highlight a new approach to the analysis of compact polarimetric data [2]. In most analyses of compact polarimetry, interest is centered on the multi-looked 4-element real Stokes vector (SV) of the scattered wave [1]. This is then the basis for one of the most popular compact techniques, the m-δ classification [3]. All these are well known features of compact polarimetry, but here we extend the analysis to consider a wider brief, namely how to relate the basic SV observables obtained from compact to classical decomposition methods, as used in full quadpol systems [4]. We outline a new approach to compact analysis based on decomposition theory [2]. We treat both the entropy/alpha and model based decomposition methods before summarizing our proposed new approach to decomposition parameter estimation from compact data.

We then use a time series of Radarsat-2 quadpol data acquisitions collected over the autumn and winter of 2011/12 for a well-calibrated test site near Hinton in Alberta, Canada, which contains a mixed forest, semi-natural vegetation and mountainous terrain environment. This data is collected in the new wide swath quadpol mode FQW of Radarsat-2, which matches the wider range swath capability of any future compact mode. This data is first used to simulate compact mode data using circular polarization transmit and dual linear receive and the co-registered multi-temporal stack then employed for a rule based classifier to determine land use types compared against a reference land-use map. We then compare the information obtained against a standard dualpol linear transmit and dual linear receive, as proposed in the ESA Sentinel missions, to confirm the utility of using circular polarization for enhanced land-use products.

[1] R. K. Raney “Dual Polarized SAR and Stokes Parameters”, IEEE Geoscience and Remote Sensing Letters, Vol. 3, No. 3, pp 317-319, July 2006

[2] S. R. Cloude, D. Goodenough, H. Chen, “Compact Decomposition Theory”, IEEE Geoscience and Remote Sensing Letters, Vol. 9 (1), pp 28-32, Jan 2012

[3] F. J. Charbonneau, B. Brisco, R. K. Raney, H. McNairn, C. Liu, P. Vachon, J. Shang, R. DeAbreu, C. Champagne, A. Merzouki, T. Geldsetzer, “Compact Polarimetry Overview and Applications Assessment”, Can. J. Remote Sensing, Vol. 36, Suppl. 2, 2010

[4] S.R. Cloude, E. Pottier, “A Review of Target Decomposition Theorems in Radar Polarimetry”, IEEE Transactions on Geoscience and Remote Sensing, Vol. 34 No. 2, pp 498-518, March 1996

8536-6, Session 1

Comparison of alternative parameters to dual polarimetric SAR data

Mitsunobu Sugimoto, Kazuo Ouchi, National Defense Academy (Japan)

In this study, we investigated possible alternative parameters for dual polarization data. Synthetic aperture radar (SAR) has been proven to be one of the most useful sensors in remote sensing because of its high resolution and all-weather day-and-night observation capabilities. In early days, most SAR systems operated on single polarization. However, recent technological advancements allowed us to develop and operate SAR systems with multi-polarization observation capability. Multi-polarization data have shown the potential to increase further the ability of extracting physical quantities of observation targets. Quad-polarization data have more information than the others, but they are relatively few in number compared with single or dual polarization data. Although there are many SAR systems capable of quad-pol observation, most of them are operated mainly on single or dual polarization mode because of the operational cost and system restriction. Thus, there is a certain trade-off between data availability and multi-polarization. Therefore, we focused on dual-polarization data as a good compromise between single and quad polarization data. Coherence analysis and modified entropy/alpha decomposition are used in this study and they are one of the methods that can effectively utilize dual polarization data. The goal of this study is to examine the possibility of deriving information comparable to quad-polarization data from dual-polarization data.

We tested possible candidates that can be derived from HH-VV dual polarization data and can serve as substitutes for cross-polarization component in quad-pol data. Experiments are performed using the Advanced Land Observation Satellite-Phased Array L-band SAR (ALOS-PALSAR) quad-polarization data. The cross-polarization component is used as a benchmark for the alternative parameters. In Pauli decomposition, which is used for quad-polarization data, the data are decomposed into three components: odd-bounce scattering, even- bounce scattering, and volume scattering. Among them, the odd-bounce and even-bounce components can be obtained from HH-VV dual polarization data. The remaining component, the cross-polarization (closely related to volume scattering) component, cannot be directly obtained from HH-VV dual polarization data. In place of the cross-polarization component, we compare several parameters derived from the coherence analysis and modified entropy/alpha decomposition.

The backscattering of cross-polarization component is relatively large in urban or forested areas and small on the sea. Entropy has a similar trend to cross-polarized scattering. On the other hand, HH-VV coherence is expected to be high on ocean surface or bare soil where surface scattering is dominant and volume scattering is little, and it is low in the areas such as forests where volume scattering is dominant. Thus, HH-VV coherence shows an opposite tendency to the cross-polarization component. In this case, we modified coherency so that it shows similar trend to the cross-polarized scattering. We compared entropy, alpha, modified coherence, and HH-VV phase difference to the cross-polarization component in quad-pol data. The correlation coefficients between the cross-polarization component and them were higher than the correlation coefficient between the components of Pauli decomposition and the corresponding components of the four-component scattering power decomposition. Although dual polarization data are often considered to be inadequate compared with quad polarization data, our study showed the possibility that dual polarization data can be as capable as quad polarization data.

8536-7, Session 1

Synergy of Cassini SAR and altimeter acquisitions for retrieval of dunes height on Titan

Marco Mastrogiuseppe, Univ. degli Studi di Roma La Sapienza (Italy) and Consiglio Nazionale delle Ricerche (Italy) and EURAC research (Italy); Valerio Poggiali, Univ. degli Studi di Roma La Sapienza (Italy)

Since 2004, Cassini RADAR provides a vast amount of data, suggesting new scenarios for Titan’s morphology and evolution. Cassini RADAR operates at 13.8 GHz as a radiometer, scatterometer, altimeter and synthetic aperture radar (SAR). Several features, reflecting a complex morphology typical of an active land-atmosphere interaction, have been detected in these flybys: impact craters, fluvial channels, “sand dunes” and lakes.

This work focuses on the retrieval of dune field shape characteristics using different sensors. During the last six years (January 2005 to September 2011) Cassini has performed 77 Titan’s flybys and several observations of dunes fields have been collected in altimetry mode. Assuming general shape of a dunes field similar to that of a surface with a Gaussian heights distribution, we estimate the dunes heights from altimetry data via Maximum Likelihood Estimation (MLE) procedure applied along with a non-coherent Cassini EM signal model. Application of this method over Fensal dune field where the altimetry path went across during the T30 flyby (May 2007), led to a dunes peak - trough heights estimation in order of 80 - 120 meters, these values match with previously estimations given by radarclinometry and SAR - stereo. Titan dunes were simulated taking into account the morphology shown by SAR images, the estimations over this synthetic surface allow to evaluate the method accuracy in determining dunes heights.

For the analysis of dune fields also images from SAR acquisitions can be exploited. There are several cases in which SAR and altimeter modes have been acquired over same areas covered by dune fields such as during T28 and T30 flybys.

SAR backscattering coefficients in synergy with electromagnetic models (such as Integral Equation model, IEM) can provide hints on the dielectric and morphological properties of dune fields. A preliminary analysis has been carried out over dune fields observed during T7 flyby. Backscattering coefficients and incidence angle records have been extracted for some profiles of the dunes, maximum and minimum values identified and plotted vs the incidence angle. The difference between minimum and maximum, due to the variation of the local incidence angle, determined by the tilt angle of the dune, is compared to the trend observed as a function of the incidence angle, giving an estimate of 6°-7° for the tilt angle of the dune. Average periodicity and height are estimated in, respectively, 3 km and 140 m. The main purpose of the proposed work is to provide estimates of dune field characteristics by exploiting synergy between SAR and altimeter acquisitions modes. The steps of the processing include:

- Collocation of the altimeter tracks over the SAR images for the areas covered by dune fields;
- Estimation of dune parameters by using altimeter mode
- Estimation of dune parameters by using SAR mode
- Comparison of results and accuracy assessment of the estimates

8536-9, Session 1

Georeferencing and geological structures analysis approach in radarSat2 images

Hafifa Fatima Zohra Haddoud, Mostafa Belhadj-Aissa, Univ. des Sciences et de la Technologie (Algeria)

Abstract---Target geolocation in radar images is becoming more crucial with the advent of high-resolution sensors and the variety of acquisition modes. Each image acquisition system produces specific geometric distortions in its raw images and consequently the geometry of these images does not correspond to the terrain or to a specific map projection of end-users. The geometric distortions vary according to different factors such as the acquisition system (the platform, the sensor and other measuring instruments), as well as the observed surface (problem of earth model, effects of its rotation and the problems inherent to the relief [8]). Nevertheless, it is possible to make general categorizations of these distortions. For RADARSAT 2, image acquisition can be achieved in a wide range of viewing directions [6], and at different resolutions, which implies different geometric distortions, specific to each type of acquisition mode. We also have to take into account the range nonlinearities caused by both the height of target regions and the side-looking acquisition mode of SAR images. We propose a georeferencing process for RADARSAT 2 images, using image metadata. Three levels of treatment were achieved: extracting and restructuring the orbital data from the header file; global modelling of the random distortions to achieve georeferencing, and finally rectifying the range position error caused by elevation in the slant range plane. The process was tested on a set of image data acquired by the RADARSAT2 satellite in both quadri and bipolarisation, covering an area of the capital “Algiers” (Algeria).

8536-10, Session 2

Environmental parameters retrieval through SAR tomography: an airborne application

Erwan Renaudin, Bryan Mercer, Univ. of Calgary (Canada)

A major goal of nowadays research is to focus on understanding temporal climatic variations that are related to the carbon cycle. According to United Nations development Group (UNDG) estimates, the destruction of forest on a global basis is responsible for 20% of annual CO2 uptake into the atmosphere. Forests are directly involved in the regulation of the rate of carbon into the atmosphere. All the world forest covers 30% of the continental surface and assimilates carbon dioxide from the air. Continental Biomass, which represents the quantity of carbon contained in vegetation, is mainly contained in the forests. In turn, knowing the forest’s biomass and its evolution are key elements for determining the capacity of a particular area to act as a carbon sink, soaking up carbon-based gases and cleaning the atmosphere of major types of pollution blamed for the greenhouse effect and global warming.

Remote sensing systems are ideal tools for studying the Earth’s surface because they provide a worldwide coverage and continuous monitoring in time. However, monitoring biomass from space is still driving much of the efforts of the research community with moderate success. If we consider the global deforestation and agricultural impact against biomass, one has to consider the problem around a half hectare, close to the size of a local human interaction, or “farmer impact”. The need for an airborne remote sensing system monitoring at this resolution without saturation is indeed a strong requirement to meet the UN expectations within this “resolution”.

The SAR (Synthetic Aperture Radar) imaging radar is mapping through clouds, thus its performance is essentially independent of the weather conditions. This approach is based on the estimation of forest height by means of complementary polarimetric and interferometric SAR (POLInSAR) to ensure the retrieval of the biomass on a wider range of values (above the saturation) using SAR Tomography. However, the principal limitation of any Tomographic reconstruction techniques from radar is to synthesize the vertical dimension with large numbers of repeat flight tracks, making the technique highly operationally expensive. The objective of this research is to determine forest biomass volume through the measurement of the 3D vegetated structure of forests, namely the Tomograms, without requiring multiple flight tracks over the same area. In our approach, vertical biomass profiles were calculated using the particular methodology of Polarisation Coherence Tomography (PCT) with a single pass dual baseline airborne system. The scattering function over the vertical was assessed by decomposing the biomass profiles by means of Legendre polynomials. Relating biomass through direct in situ measurements showed the quintessence of forest monitoring, since a particular highlight is placed on sensitivity of vertical structure to biomass.

The expected derivation of environmental parameters such as biomass is demonstrated in this research. There are indeed strong relationship between the generated tomograms and the vertical distribution of biomass. Forest monitoring will certainly gain at getting another dimension. The future challenge will dwell on the application of the techniques over different range of species and forest habitat.

8536-12, Session 2

Rating curve from SAR imagery

Giovanni Corato, Consiglio Nazionale delle Ricerche (Italy); Renaud Hostache, Patrick Matgen, Ctr. de Recherche Public - Gabriel Lippmann (Luxembourg); Tommaso Moramarco, Consiglio Nazionale delle Ricerche (Italy); Tullio Tucciarelli, Univ. degli Studi di Palermo (Italy)

Reliable discharge estimates at a river site depend on local hydraulic conditions, which are usually defined by recording water level. In fact, stage monitoring is relatively inexpensive, especially when compared to the cost necessary to carry out flow velocity measurements. However, there is a need for converting stage records into discharge values. This task is generally addressed through a reliable rating curve, which can be unknown, in the case of gauged sites wherein velocity measurements cannot be carried out, or limited to low flows. In addition, a rating curve differs from the one-to-one stage-discharge relationship when unsteady flows occur. In order to relate stage and discharge hydrographs at a selected river section also during unsteady flow conditions, 1D hydraulic modelling can be adopted. Nevertheless, a reliable use of hydraulic modelling is strictly related to the availability of riverbed geometry data along with an accurate Manning’s roughness coefficient calibration. For the latter, many studies show that it is possible to use remote sensing derived (RSD) information to calibrate a hydraulic model. The most frequently used sensors are the Synthetic Aperture Radars (SAR), due to their high spatial resolution and the all weather and day-and-night capability. Therefore, a reliable continuous discharge monitoring system can be obtained using a hydraulic model and combining the in situ information provided by a stream gauge with RSD information, stemming from SAR sensors.

In this work, a new procedure for continuous discharge estimation is proposed. The procedure is based on the use of the DORA hydraulic model to convert recorded stages into discharges by exploiting RSD information in terms of water levels for Manning’s roughness calibration. This last issue is addressed on the basis of the ensemble of water levels estimated from the SAR image. The main advantage of this procedure consists in the fact that the RSD information coming from SAR sensors is globally available, without any limitation related to site accessibility or weather conditions. These features makes the procedure suitable for gauged sites not equipped for velocity measurements or located in areas not easily accessible by the operators.

The flood event of January 2003, on the Alzette River in Luxembourg, is investigated by using two available SAR images. The results show that RSD information is suitable for an efficient hydraulic model calibration, oriented to discharge estimation at a river site where only stages are recorded. A good match between observed and computed discharge hydrographs has been obtained using both images. Future missions, like SWOT, promise to provide more accurate and frequent water stage information that might be used also for bathymetry modelling, thereby reducing the need of topographic cross-section surveys.

8536-13, Session 2

Analysis of ground deformation using SBAS-DInSAR technique applied to COSMO-SkyMed images, the test case of Rome urban area

Francesca Ardizzone, Consiglio Nazionale delle Ricerche (Italy); Manuela Bonano, Istituto per il Rilevamento Elettromagnetico dell'Ambiente (Italy); Alessandro Giocoli, Istituto di Metodologie per l'Analisi Ambientale (Italy); Riccardo Lanari, Istituto per il Rilevamento Elettromagnetico dell'Ambiente (Italy); Maria Marsella, Univ. degli Studi di Roma La Sapienza (Italy); Antonio Pepe, Istituto per il Rilevamento Elettromagnetico dell'Ambiente (Italy); Angela Perrone, Sabatino Piscitelli, Istituto di Metodologie per l'Analisi Ambientale (Italy); Silvia Scifoni, Marianna Scutti, Univ. degli Studi di Roma La Sapienza (Italy); Giuseppe Solaro, Istituto per il Rilevamento Elettromagnetico dell'Ambiente (Italy)

Remote sensing is a key tool for environmental monitoring due to its outstanding capabilities to provide unique and timely information about Earth surface. In particular, differential SAR interferometry (DInSAR) represents nowadays a well-established remote sensing technique for the investigation of surface deformation phenomena. Among the variety of DInSAR techniques that have been developed over the years, a very popular approach is represented by the Small BAseline Subset (SBAS) algorithm, which exploits a two-scale strategy, as detailed in and allows the detection and monitoring of very localized deformation signals that may affect, for instance, single buildings or man-made structures in urban areas.

This work is aimed at investigating the capability improvement of SBAS-DInSAR technique to map deformation phenomena affecting urban areas by exploiting SAR data acquired by the X-band sensors of the Cosmo-Skymed (CSM) constellation with respect to those of the ERS/ENVISAT radar systems, operating at the C-band. To this aim, we have applied the SBAS-DInSAR approach to three different archives of SAR images gathered by the CSM, the ERS and the ENVISAT platforms over the area of Roma (Italy) from 1992 to 2010. From the available SAR data-sets, we have accordingly obtained three mean deformation velocity maps of the area, as seen by the three different radar systems in the relevant observation time intervals; furthermore, for each coherent pixel, we have retrieved the corresponding displacement time series. The achieved DInSAR products have then used to perform the proposed comparative analysis, which has also benefited from the availability of external information, such as electrical resistivity tomography data, geological maps, leveling time series and building structural data.

We focused on the Torrino area, in the south-eastern sector of Roma, where independent studies had already revealed that significant deformation signals were present, testified by the serious damages which have affected many buildings in the area. However, this signal was not detectable into the ERS deformation time series being such buildings of recent construction. On the contrary, the analysis of the ENVISAT DInSAR products, spanning the time interval between 2002 to 2008, has clearly evidenced the presence in the investigated areas of such a deformation signal in correspondence to one of the new buildings. Finally, the CSM deformation time series have definitely evidenced that buildings in this area are clearly affected by significant displacement signals with a rate reaching up to 5 cm per year. Two geoelectrical surveys have been executed to reconstruct the geological setting of the subsoil in order to investigate the causes of the observed ground settlements and to attempt a more detailed reconstruction of each single buildings behavior.

Additional investigations were also done on the urban area of Rome characterized by the presence of recent alluvial deposits (bed of the Tiber River and its tributaries), representing a critical element for the buildings stability; we remark that all the area located in alluvial deposits is affected by a major trend with significant velocity of subsidence that have in the past irreversibly damaged many buildings. The retrieved DInSAR products have revealed particularly helpful to perform simplified damage assessment analyses on each building, allowing us to study their stability conditions and to make some hypotheses on their possible critical evolutions in time.

8536-14, Session 2

Study of movement and seepage along levees using DInSAR and the airborne UAVSAR instrument

Cathleen E. Jones, Jet Propulsion Lab. (United States); Gerald Bawden, U.S. Geological Survey (United States); Steven Deverel, HydroFocus, Inc. (United States); Joel Dudas, California Dept. of Water Resources (United States); Scott Hensley, Sang-Ho Yun, Jet Propulsion Lab. (United States)

We have studied the utility of high resolution SAR for levee safety and health monitoring using UAVSAR data collected along the levees in California's Sacramento-San Joaquin Delta and along the lower Mississippi River during the floods of Spring 2010. Our study has focused on detecting and tracking changes that are indicative of potential problem spots, namely deformation of either the levee crown or toe and seepage through or beneath the levees. Here we present the results of that study.

Since July 2009 we have collected UAVSAR data over California's Sacramento Delta near monthly to evaluate the utility of high resolution airborne L-band SAR remote sensing for consistent monitoring of the region with wide scale spatial and temporal coverage. The Sacramento-San Joaquin Delta, located immediately east of San Francisco Bay, is the primary water source for the state of California and contains the 2nd largest levee system in the United States, surpassed only by the levee system along the Mississippi River. The area is comprised of tidal marshland and levee-rimmed islands used primarily for agriculture, with scattered urban communities built on the flood plain. Since the islands' formation in the 1800s, subsidence has steadily decreased the land elevations to between 3 and more than 7 meters below mean sea level. The current average subsidence rates for each island varies, with 1.23 cm/yr in the western Delta and 2.2 cm/yr in the central Delta, as determined by ground-based instruments at isolated points.

We use differential interferometry (DInSAR) for measuring surface deformation on and near earthen levees and to measure yearly subsidence rates throughout the area. Because land in the delta is primarily used for agriculture, temporal decorrelation is potentially a major problem for DInSAR studies of the area depending upon the frequency of the imaging SAR. With L-band data, we find that the levees and much of the land within the islands do not usually decorrelate over the 1-month repeat interval and that we can successfully measure consistent deformation along the levee toe in areas of recent repair. Our studies of the California and Mississippi levees show promising results for detecting seepage using both DInSAR and multi-polarization, single pass SAR. We will discuss the results and the methods we have developed to detect seeps and movement. We have found in this study that the signals indicating movement or seeps can easily be mistaken for false positive signals arising from different sources, so we will also discuss the procedures used to identify false positive signals that otherwise masquerade as change in the levee condition.

This research was conducted in part at the Jet Propulsion Laboratory, California Institute of Technology, under contract with the National Aeronautics and Space Administration.

8536-32, Session PS

Lessons learned using COSMO-SkyMed imagery for flood mapping: case studies

Nazzareno Pierdicca, Luca Pulvirenti, Univ. degli Studi di Roma La Sapienza (Italy); Marco Chini, Istituto Nazionale di Geofisica e Vulcanologia (Italy); Frank S. Marzano, Saverio Mori, Univ. degli Studi di Roma La Sapienza (Italy)

Floods are the most frequent weather disasters in the world and the most costly in terms of economic losses. Mapping flood extension is

fundamental to ascertain the damages and for relief efforts. Satellite synthetic aperture radar (SAR) systems are particularly suitable for flood mapping, thanks to the capability to operate in cloudy conditions and during both day and night time and the sensitivity of the microwave radiation to water.

Although the temporal repetitiveness of SAR imagery was a critical issue for their operational use for flood monitoring, so far, the COSMO-SkyMed constellation of four satellites is presently fully deployed, giving the opportunity to obtain a large amount of daily radar images that can be used to produce frequent inundation maps (revisit time in the order of some hours) characterized by high spatial resolution, thus representing a fundamental source of data for operational flood management systems.

COSMO SkyMed has been activated in the last few years several times during the occurrence of flood events all over the world. The task of generating flood maps in a pre-operational framework foreseen in the OPERA Pilot Project funded by Italian Space Agency has offered the opportunity to gain a significant experience in this field. A review of the mechanisms which determine the imprints of the inundation on the radar images and of the fundamental simulation tools able to predict these imprints and help image interpretation is provided. The approach developed to process the data and to generate the flood maps is also summarized. Then, the paper illustrates the experience gained with COSMO-SkyMed by describing and discussing a number of significant examples.

Among others, the COSMO-SkyMed SAR observations of the area hit by the 2011 Japan tsunami are discussed. The interpretation of the available data has allowed us to detect the flooded areas, as well as the receding of the floodwater from March 12 to March 13, 2011 and the presence of the debris floating above the water surface. Moreover, thanks to the high spatial resolution of the COSMO-SkyMed images, the presence of floodwater in some urban areas in the Sendai harbor has been revealed by exploiting the information on the coherence.

Another interesting case study regarding a recent severe weather event that occurred in Northwestern Italy is discussed. Heavy rainfall occurred in some areas of the Liguria and Piedmont regions from November 3, 2011 till November 8, 2011 and numerous flash floods were reported. The event was monitored by using a number of CSK images provided by the Italian Space Agency (ASI) and some observations were performed when heavy rainfall, causing an attenuation of the X-band radar signal, occurred. The analysis of this case study aims at highlighting the difficulties that have to be tackled to discriminate among permanent water bodies, flooded areas and areas affected by significant rainfall and that increase if the area of interest is characterized by a complex large scale topography because of the shadowing effects and the possible presence of wet snow (in winter) that absorbs X-band radiation.

8536-34, Session PS

On the Appropriate Feature for General SAR Image Registration

Dong Li, Graduate Univ. of the Chinese Academy of Sciences (China) and Ctr. for Space Science and Applied Research (China); Yunhua Zhang, Ctr. for Space Science and Applied Research (China)

Profited from a number of SAR missions, the available SAR imagery of one region increases dramatically, which makes the joint processing of multiple images to accurately sense and understand the scene possible, and this may become a potential direction for SAR image processing. Since SAR images may be acquired from different imaging geometries and/or by different sensors, there is always a geometrical warp between the images and this should be aligned first to enable further application. The task of image registration is to estimate the warp function between images so that the same pixel position in each image can be mapped to the same target position in the global coordinate system. Lots of registration algorithms for SAR images have been hitherto proposed. In this paper, we concentrate on the registration algorithms based on image feature. It seems that many existing feature-based algorithms are introduced from the optical image registration area in a sense. This poses some open problems which have not been perfectly solved. This paper is dedicated to investigate the appropriate feature for SAR image registration. We give a comprehensive evaluation to the commonly-used features such as tie points, Harris corner, the scale invariant feature transform (SIFT), and the speeded up robust feature (SURF) in terms of several criteria such as the geometrical invariance of feature, the extraction speed, the localization accuracy, the geometrical invariance of descriptor, the matching speed, the robustness to decorrelation, and the flexibility to image speckling. It is shown that SURF outperforms others. Among these criteria, we particularly address the feature's flexibility to the unavoidable SAR speckle which degrades the image information and should be suppressed. Since the speckle filtering may change the feature position and impact the subpixel feature localization in turn, thus a good feature detector should be robust to speckle. We find that the Fast-Hessian detector of SURF has a potential relation with the refined Lee speckle filter, which indicates that SURF can extract image feature at different scales even under the influence of image speckling. This observation is validated when we oversample the image with increasing sampling rate, i.e. refine the image pixel, it means much more severe speckle would be suffered, unlike SIFT, the numbers of extractable correct correspondences by SURF and the matching false alarm rate, however, are still improved accordingly. In consideration of some applications with strict requirement for registration accuracy, we suggest using the original Fast-Hessian detector on the oversampled image with unaltered sampling step to extract the feature. The registration experiments on some SAR image pairs demonstrate that the suggested SURF can significantly improve the subpixel registration accuracy and speckle immunity. Therefore, we think SURF is more appropriate and competent for general SAR image registration.

8536-35, Session PS

The Appropriate Parameter Retrieval Algorithm for Feature-Based SAR Image Registration

Dong Li, Graduate Univ. of the Chinese Academy of Sciences (China) and Ctr. for Space Science and Applied Research (China); Yunhua Zhang, Ctr. for Space Science and Applied Research (China)

Image registration is to estimate the geometrical warp between images. Many registration algorithms which conduct warp estimation by fitting the geometrical feature correspondences have been recently proposed for SAR. This paper is dedicated to investigate the appropriate parameter retrieval algorithm for feature-based SAR image registration. Since the SAR images are acquired spatial or temporal separately, together with the influences from the non-robustness of feature descriptor and matching algorithm, there are always unavoidable mismatches in the constructed correspondences. Besides this, since SAR acquires the target scattering with a slant range geometry which can not be transformed to a central projection model, the SAR geometrical warp can not be modeled as the global epipolar geometry as optical images. However, we can conventionally approximate the warp function as a low-order polynomial when the images are acquired from gently topographic area with relatively short baseline. This indicates that we focus on the global registration but neglecting the local discontentment. Therefore, in order to achieve an accurate estimation, the retrieval algorithm should be robust to outliers and local image distortion. The robust random sample consensus (RANSAC) is the widely-used retrieval algorithm in the existing literatures for SAR image registration. It performs the estimation by randomly sampling a minimal sampling set (MSS) to achieve an estimation of the warp, and the entire dataset are then checked for finding those correspondences which are consistent with the estimation to construct a consensus set (CS). These two steps are repeated in an iterative fashion until the probability of finding a larger CS drops below a certain threshold. However, this estimation strategy may magnify the local distortion which may result in estimation uncertainty and damnify the global registration accuracy although the largest CS is achieved. This uncertainty is validated when we execute the algorithm on a RadarSat interferometric SAR (IFSAR) image pair 100 times but slightly different estimations are obtained with each execution. Besides this, an interest phenomenon is observed that even for the executions with the same cardinality of CS, the obtained parameters are also different. This indicates that the extracted correct matches which compose the CS are actually still varied otherwise the parameters would be stable because they are retrieved by just LS fitting the inliers. All of these demonstrate that RANSAC is instable for SAR image registration for its inappropriate estimation mechanism and loss function. Thus in order to enable stable and robust registration for SAR images, an extended fast least trimmed squares is proposed, which conducts the registration by fitting at least half of the correspondences to minimize the squared polynomial residuals instead of fitting the MSS to maximize the cardinality of CS. Experiment on IFSAR image pair demonstrates that the proposed

algorithm works very stably and the obtained registration is averagely better than that by RANSAC in terms of cross-correlation and spectral SNR. By this algorithm, a stable estimation for any kind of 2D polynomial warp model with high robustness and accuracy can be efficiently achieved, thus it is more appropriate for SAR image registration.

8536-36, Session PS

Oil rigs in full polarization SAR imges

Chen Peng, Jingsong Yang, The Second Institute of Oceanography, SOA (China)

Oil rig in Off-shore area is an important oil production facility. It is a fixed structure in ocean. In this paper, we want to study the relationship between the oil rig shapes and full polarization SAR image. We had got the full polarization SAR images in Bohai Sea, in China. At the same time, we also get double of pictures about the oil rigs. The polarimetric signature and feature of rigs will be compared. Then pauli-decomposition will be done to get different components of backscatters. Then, the polarimetric entropy alpha anisotropy decomposition and classification will be done. So we try to find some relationship between features of rigs in SAR images and real rigs shapes.

8536-37, Session PS

Movement velocity and snow line estimation in glacier area from interferometric and polarimetric SAR

Zhen Li, Jianmin Zhou, Bangsen Tian, Lei Huang, Ding Shen, Ctr. for Earth Observation and Digital Earth (China)

Glacier is sensitive indicators of climate fluctuations. More observations of glacier mass balance, surface melt patterns and snowline position are needed for climate change monitoring, natural hazard assessment and water supply purposes. In the paper, methods of moving velocity and snow line identification for glacier are presented using interferometric and polarimetric SAR from ALOS/PALSAR and RadarSat/SAR data in the Qinhai-Tibetan Plateau.

Utilizing repeat two-pass D-InSAR approach, with an external DEM, we extracted the motion of the glacier surface. The amount of “glacier surface” decorrelation is increased by the longer spatial baseline of the interferometric pair, the longer time separation of the SAR images acquisition, more complex terrain, and more noise sources. The longer wavelength SAR data (ALOS L-band) are better to avoid decorrelation phenomenon. The movement parameter of the Dongkemadi glacier is resolved using a 46 day-separation ALOS InSAR pair acquired from ascending orbit at Dec. 10, 2007 and Jan. 25, 2008 in the Dongkemadi Glacier (33.08N, 92.09E) in Qinghai-Tibet Plateau. The five corner reflectors were fixed in the glacier surface in October 2007, and are continually measured by GPS-RTK (Real Time Kinematic) technology each year. The velocities of the CR derived from the GPS-surveyed are compared with from InSAR measure, the estimation differences (between GPS and ALOS) are all <8 cm year–1.

The snow line identification is carried out from full polarization RADARSAT-2 SAR imagery at same area in Aug.30, 2009. Before classification, the correction of the topographical distortions inherent, which induced by the slant projection of SAR systems and the highly variable terrain, is performed for polarimetric image of rugged terrain. Methods for terrain correction of PolSAR developed using polarimetric signature to refine the location accuracy and perform the pixel size normalization on each element of the coherency matrix by the backward integration. Also, azimuth-slope correction is immediately following after radiometric correction. A supervised classification is performed on the orthorectified image, and the snow line is delineated on the orthorectified image too. With polarimetric characteristics from SAR targets decomposition, several classification methods were compared, which are the decision tree method, SVM (Support Vector Machine) classifier, maximum likelihood classifier, minimum distance classifier and Wishart classifier. From the classification map at the end of melt season, the snow line at glacier area can be identification. These results show that it’s an effective way to identify the snow line on glaciers in mountainous environment at later summer using PolSAR data.

8536-38, Session PS

Monitoring of mining-induced land subsidence by PALSAR and TerraSAR-X

Tomonori Deguchi, Nittetsu Mining Consultants Co., Ltd. (Japan)

In this study, we applied InSAR time series analysis to Zonguldak Hardcoal Basin in Republic of Turkey using PALSAR and TerraSAR-X data in order to monitor mining induced surface displacement. Zonguldak coal area is located along the Black Sea 240 km away from Istanbul to the east. Recently, ground deformation caused by underground exploration has come to the surface, and it has been destroying roads and buildings. In the past research using JERS-1/SAR data observed on May and September 1995 and RADARSAT-1 between September 2005 and October 2006, small phase anomalies with several hundred-meter of spatial scale were clearly detected over the mining tunnels of coalfields. It was determined that these deformations were caused by the activity of coal mining.

We utilized PALSAR and TerraSAR-X data for the detail analysis on the recent mining induced land subsidence. Because the backscatter of X-band microwave adopted for TerraSAR-X sensor is disturbed by plants, urban areas near Kozlu coalfield are focused. PALSAR data in fine beam mode were obtained from an ascending orbit, TerraSAR-X data in the StripMap mode were from a descending orbit. The vertical and east-west displacement were calculated by the composition of the deformation vectors of PALSAR and TerraSAR-X. Additionally, the source depth of the main anomaly detected near the campus of Zonguldak Karaelmas University was estimated by vector analysis using the vertical and east-west displacement vectors. As a result, it was approximately 80 to 100 meters under sea level. On the other hand, the depth of coal production zones is recorded 300 to 560 meters under sea level. Thus, it was supposed that the anomaly near the university had been caused by not only mining activities but also the other factor in the shallower geological formation.

8536-40, Session PS

Analysis of terrain influences in Pol-InSAR forest height estimation and attempts to the correction

Chuanrong Li, Academy of Opto-Electronics, Chinese Academy of Sciences (China); Yonghe Zhang, Information Institute, the Equipment Academy of the Air Force (China) and Institute of Tracking and Telecommunication Technology (China); Yongsheng Zhou, Academy of Opto-Electronics, Chinese Academy of Sciences (China); Wen Hong, Institute of Electronics, Chinese Academy of Sciences (China)

Polarimetric Interferometric Synthetic Aperture Radar (Pol-InSAR) technique is a combination of Polarimetric SAR (PolSAR) and Interferometric SAR (InSAR) and has been demonstrated its success in the estimation of forest height [1-4]. Terrain slope is a factor that always prevents the wide application of SAR technique, especially the forestry application, because great majority of forest locates on mountainous region.

Firstly, the terrain influences on Pol-InSAR forest height estimation are analyzed. Terrain slope affects the estimation accuracy in several ways, e.g., 1) Variation in terrain slope could induce the change of polarization orientation angle, which would distort the Pol-InSAR complex coherence, and thus affect the accuracy of forest height estimation; 2) When the terrain slope exists, the local incidence angle is no longer equal to the radar look angle, which yields misestimating of forest height if using radar look angle as the local incidence angle.

In practical, all these factors influence the final estimated forest height all together. In order to facilitate studying, we present the analysis of terrain influences in view of polarimetric orientation shift and local incidence angle, respectively. For the former, the relation of forest height estimation error with polarimetric orientation shift is derived by a simulation approach. The results show that when polarimetric orientation shift is within +/-18 degree, estimation error is smaller than 10%. For the latter, an equation is derived to describe the relation between true and estimated forest height. When the range slope is positive (i.e., slope surface faces toward radar), forest height is underestimated; when negative, overestimated. Larger radar look angles yield to larger estimation errors.

Furthermore, methods for correcting terrain influences are presented,

which including: 1) Design airborne experiment flight track along mountain ridge, since the polarimetric orientation angle shift is mainly induced by the azimuth slope and less affected by the range slope. 2) Utilize Pol-InSAR optimal coherences for forest height inversion if the computational efficiency is not an issue, because the optimal coherences are not affected by the polarimetric orientation angle shift. 3) Revise the estimated forest height from RVoG model inversion, where the range slope can be calculated by InSAR dataset or a priori DEM.

REFERENCES:

[1] S. R. Cloude and K. P. Papathanassiou, "Three-stage inversion process for polarimetric SAR interferometry," IEE Proc.-Radar Sonar Navig., vol. 150, no. 3, pp. 125-134, June 2003.

[2] F. Kugler and I. Hajnsek, "Forest characterisation by means of TerraSAR-X and TanDEM-X (polarimetric and) interferometric data," in Proc. IGARSS 2011, Vancouver, Canada, July 24-29, 2011, pp. 2578-2581.

[3] Y. S. Zhou, W. Hong and F. Cao, "Investigation on the applications of decorrelation analysis in polarimetric SAR interferometry," in Proc. IGARSS 2009, Capetown, South Africa, July 12-17, 2009, pp. 254-257.

[4] M. Neumann, "Remote sensing of vegetation using multi-baseline polarimetric SAR interferometry: theoretical modeling and physical parameter retrieval," Ph.D. dissertation, University of Rennes 1, France, 2009.

8536-41, Session PS

Exact RCS reconstruction of interested targets from SAR images

Dandan Gu, Xiaojian Xu, BeiHang Univ. (China)

Radar cross section (RCS) measurement and prediction are of great importance for studying radar target signature and automatic target recognition (ATR). Point scatterer model based schemes were proposed to reconstruct and predict RCS by extracting scattering centers from synthetic aperture radar (SAR) and inverse SAR (ISAR) images. However, it became difficult to extract scattering centers when the images were blurred, such as a resolution cell containing multiple scattering centers. Another way to predict far-field RCS is based on the mathematical transform relationship between RCS and ISAR image. The resulting RCS of simple targets from ISAR images show the validation of the technique, although several factors affecting RCS calculation, such as window function, zero-padding, etc., were not considered strictly.

Large scene SAR images often contain various manmade or natural targets of interest, background clutter, speckle noises, etc. Moving targets appear defocused or at wrong positions depending on the direction of the target motion. Moreover, other factors in data processing, including system over-sampling, window function, zero-padding and image calibration, have influence on the resulting images as well. Therefore, a procedure is proposed to reconstruct RCS of interested targets exactly via considering all these aspects.

The overall process for exact target RCS reconstruction from large scene SAR images is as follows: the region of interest (ROI) is first selected to obtain an image chip containing the target image. For moving targets, refined SAR image processing is then performed on the image chip for further motion compensation and image refocusing. Target segmentation algorithm is performed on the refined SAR image chip to find the exact region of the interested target and suppress any background clutter. The resulting target image chip is finally utilized for exact RCS reconstruction using the procedure proposed in the current paper.

The paper is organized as follows. A detailed mathematical analysis for RCS conversion from SAR and ISAR images are presented in Section 2. In Section 3, the procedure and implementation are discussed. Examples with satisfactory RCS reconstruction are illustrated in Section 4. Both numerically calculated ISAR image and practical spaceborne SAR image are used to demonstrate the effectiveness and applicability of the procedure. It is shown that exact RCS reconstruction over a wide range of frequencies and azimuth angles can be made, even for target containing multiple interactions.

8536-42, Session PS

Imaging and target-location algorithms for airborne bistatic SAR system

Yong Li, Ya Li, Nanjing Univ. of Aeronautics and Astronautics (China)

Bistatic synthetic aperture radar (BiSAR) systems have been attracting considerably increasing interests in these decades. The real-time location of stationary ground targets in BiSAR images from a general bistatic configuration, when the transmitter and receiver move along nonparallel trajectories with different velocities, is more complicated than a monostatic case, because the range-Doppler history of the bistatic SAR used to determine the coordinates of the targets of interests are double hyperbolic which involving the solution of nonlinear equations.

In this paper, we present a modified imaging algorithm and the target-location methods for airborne BiSAR under a general geometric configuration. As a step to a numerically efficient processor, a computational efficient image formation method, namely linear range-Doppler (LRD) algorithm is firstly generalized from the monostatic SAR to BiSAR imaging, which also enable the ground-target location processing to be feasible.

The LRD algorithm, originated from the basic theory of rotating-object imaging, has been tested to be robust for mid-resolution monostatic SAR imaging, because the overall processing is achieved by fast Fourier transform and vector-multiplication operations. However, the original LRD algorithm needs to be modified before being used in processing bistatic SAR data, because there are distinct differences in the phase history of the received signal and the sample location of spatial frequency.

With a detailed analysis of the double hyperbolic range-Doppler equations in the signal processing flowchart of the proposed BiSAR LRD algorithm, we adopt two methods in linearizing the nonlinear equation and tailor them to our problem. Specifically, we select the Newton iteration and the dichotomy methods to solve the nonlinear equations and compare the performances of them in locating the ground-targets for the general case of BiSAR system.

As shown in this paper, the Newton iteration method that approximates the root of a nonlinear equation in one variable using the value of the function and its derivative, because of its robustness and higher rate of convergence, becomes an attractive solution. The dichotomy method just requires that the function values of the two terminals in the finite interval are contrary, hence, leading to a larger region of convergence.

We evaluate the proposed methodologies by a set of point-target simulations using the parameters in regard to a classical mid-resolution airborne BiSAR system. The simulation results are given and analyzed to demonstrate their validity in providing accurate positions of any stationary ground-target in the BiSAR image.

8536-43, Session PS

An expermient of one-stationary bistatic SAR

Xiong Songya, Institute of Electronics (China)

In the recent years, bistatic SAR has been the spotlight since its flexible configurations and its great potential value in military compared with mono-SAR. A lot of bistatic SAR experiments have been performed, including various bistatic configurations.

On August 1st of 2011, IECAS has performed an X-band one stationary bistatic SAR experiment. The experiment was designed to do further research on the bistatic SAR. The bandwidth of the transmitter is 100MHz. We use strip mode SAR with the resolution is <1m in theory.

In this paper, the X-band bistatic experiment is described. First the bistatic configuration and the synchronization is considered. After, the back projection algorithm is presented and the simulated results prove its correctness. Finally, the experiment result processing with back projection proves the algorithm.

8536-44, Session PS

Unsupervised change detection in very high spatial resolution Cosmo-Skymed SAR images

Nicola Acito, Salvatore Resta, Giovanni Corsini, Marco Diani, Alessandro Rossi, Univ. di Pisa (Italy)

Change Detection (CD) in Very High Spatial Resolution (VHSR) SAR images is a challenging task aimed at detecting a set of pixels that have undergone a relevant change with respect to a previous acquisition. In surveillance applications, the goal is the detection of changes understood as insertion, deletion or movement of man-made objects between the two acquisitions. In a typical wide area surveillance system CD process has to be considered as the first task to be accomplished. Given the image pairs collected over the monitored scene, the CD process allows the regions of the scene corresponding to anomalous changes to be enhanced and highlighted. Such regions may contain changes concerning the targets of interest and typically guide the user in a more detailed exploration accomplished by using the VHSR SAR image pairs or, if available, VHSR optical images of the same scene acquired at the same time.

In this work we propose a novel pixel-wise CD technique inspired by the RX Anomaly Detection (AD) algorithm, proposed to deal with AD in optical images. Denoting with x[i,j] and y[i,j] the pixels of two amplitude images X and Y occupying the same spatial position, the proposed algorithm (called RX-CD) measures the degrees of anomalousness (T[i,j]) of each pixel x[i,j] with respect to the local background. Particularly, local estimates of the first and the second order statistics of the background are adopted in computing T[i,j]. These estimates are obtained from a given neighbourhood of the pixel y[i,j] in the second image (Y). In this way, the image Y is assumed as background and T[i,j] measures the anomalousness of x[i,j] with respect to Y. In applying the RX-CD algorithm false changes could be detected when the amplitude levels of the same pixel in the two images sensibly differ due to dissimilar acquisition conditions. To mitigate the false detection problem, instead of using Y, we use a suitable pre-processing algorithm aimed at deriving the best (in the minimum mean squared error sense) linear prediction of X from the observation Y. The coefficient of the linear predictor are estimated from all the pixels of the two images.

In order to test and validate the proposed method we analyse a spot light (VHSR) amplitude Cosmo-Skymed image pair at one-meter spatial resolution acquired on a very complex urban scenario. The analysis is focused on two regions of the scene where a ground truth (GT) concerning the changes occurred between the two acquisitions is available. The GT on the two regions is used to quantitatively evaluate the performance provided by the RX-CD algorithms. Particularly, the experimental Receiver Operating Characteristics (ex-ROC) are derived by computing the fraction of detected changes (FoDT) and the false alarms rate (FAR) over the considered operating scenario.

8536-45, Session PS

A four component decomposition based on the compact polarimetry mode using RADARSAT2 data

Boularbah Souissi, Mounira Ouarzeddine, Aichouche belhadj-aissa, Univ. des Sciences et de la Technologie (Algeria)

Recently, dual-mode partially polarimetric SAR systems (DP) have been proposed such us ENVISAT ASAR , Japanese L-band PALSAR, the European X-band TERRASAR-X, and the Canadian C-band RadarSAT 2, where one polarization (H or V) is transmitted, whereas two are received. These dual-pol modes collect only half of the full scattering matrix, either (HH, VH) or (VV, HV). This reduces both the data processing requirements and the information content of the polarimetric imagery. The acquired data set has the same coverage as for the single transmit polarization, but provides added information due to the two independent channels on-receive. From a mission standpoint, the dual-pol imaging modes collect a wider swath width, and hence greater area coverage, as compared to quad-pol imagery. However, the per-pixel information content is less for dual-pol imagery than for quad-pol imagery, which tends to favor quad-pol data collection.

Other system configurations have been also proposed and called compact polarimetry. In these polarimetric configurations, only one transmit/receive cycle is required instead of two in a full quad-pol system, reducing the pulse repetition frequency and data rates by a factor of two for a given swath width. Souyris et al. introduced the π/4 compact polarimetric mode, in which the transmitted polarization is the superposition of linear horizontal and vertical polarizations H + V, resulting in a linear polarization oriented at 45◦ with respect to the horizontal. The radar receives returns in horizontal and vertical polarizations. Another hybrid dual-pol mode is the circular transmit, linear receive (CTLR) mode. As the name suggests either a left or right circularly-polarized signal is transmitted and both H and V polarizations are coherently received. The polarimetric models employed assume both reflection symmetric scattering, and a relationship between the linear coherence and the cross-polarization ratio to construct a full reflection symmetric polarization matrix from the 2?2 mode covariance data. An equivalent covariance or coherency matrix may be reconstructed to produce the so-called pseudo quad-pol data that accurately reproduces the full quad-pol data.

The compact polarimetry was proposed to assess various architecture designs that could be implemented on low-cost/low-mass. In that context, the comparison between full polarimetry (fp) versus dual polarimetry (dp) is a subject of most importance.

This paper provides a comparison of the information content of full quad-pol data and the pseudo quad-pol data derived from compact polarimetric SAR modes. A pseudo-covariance matrix can be reconstructed following Souyris's approach and si shown to be similar to the full polarimetric (FP) covariance matrix. Both the polarimetric signatures based on the kennaugh matrix and the Freeman and Durden decomposition in the context of this compact polarimetry mode are explored. The Four component decomposition is used in our study because of the use of the most known scattering mechanisms which are the surface, double, volume and helix targets.

We illustrate our results by using the polarimetric SAR images of Algiers city in Algeria acquired by the RadarSAT2 in C-band.

8536-47, Session PS

Automatic and semi-automatic extraction of curvilinear features from SAR images

Emre Akyilmaz, Osman Erman Okman, Fatih Nar, SDT A.S. (Turkey); Müjdat Çetin, Sabanci Univ. (Turkey)

Extraction of curvilinear features, including fences surrounding various buildings, from synthetic aperture radar (SAR) images is important for various automatic target recognition (ATR) tasks. Unfortunately, the sequence of bright pixels which ideally constitutes the curvilinear feature is usually disrupted, causing significant amount of discontinuities in the feature of interest observed in the image. In addition to the curvilinear feature being disrupted, SAR images also contain high amount of speckle noise which makes accurate extraction of such curvilinear features very difficult. Despeckling mostly causes formation of new discontinuities in curvilinear features since some parts of the curvilinear features are very thin or not bright enough so they may be treated as noise and therefore suppressed through the despeckling operation.

In this study, extraction of curvilinear features from SAR images is developed as a post-processing approach which follows despeckling. Image despeckling is realized using feature preserving despeckling (FPD) which preserves edges of regions and bright point scatterers while smoothing homogenous regions, but at the same time it could over-smooth thin structures especially having low intensity values. Curvilinear features may enlarge at the locations of bright point scatterers. Such bright point scatterers also cause sudden intensity changes over the curvilinear feature which complicates the problem further. Conventional edge and line detection methods mostly fail to capture such curvilinear features.

After despeckling, our approach starts by finding the regional maxima in the image and expanding these points to apply region based constant false alarm rate (RB-CFAR) thresholding. This produces regions that potentially contain targets and features of interest. The number of regions is reduced by applying predefined rules based on size and eccentricities of the regions. This process produces a "reduced regional maxima image" that usually contains less than 1% of the pixels in the original SAR image. Dijkstra's graph search algorithm is used to find the optimum path crossing over all the determined points. Edge paths are defined dynamically during search between each pair of pixels in the reduced regional maxima image if the length of the edge path is within a predefined range. Edge paths with average intensity values greater than a threshold are used within search. The threshold is selected loosely in order not to miss any real edges. The cost of travelling over an edge is defined in terms of

pixel intensities, neighbors' intensities, curve smoothness, and the length of the edge. If only a single point is used then a curvilinear feature starting from that point and ending at that point is extracted. Points on the curvilinear feature can be selected by the user in the semi-automatic mode of our approach or points can be determined by finding strong line components in the automatic mode. Dijkstra's optimum path is declared as a curvilinear feature using a ratio of average (ROA) operator over the whole path. The proposed method has moderate computational complexity and provides near real-time solutions in the semi-automatic mode. Our experimental results demonstrate the effectiveness of the proposed algorithm in extracting curvilinear features.

8536-15, Session 3

New land masking methods in SAR images for ship detection

Ezz E Ali, Tarek Ahmed Mahmoud, Ahmed Saleh Mashaly, Military Technical College (Egypt)

Following are the steps for the two proposed methods:

Morphological method:

1)SAR image of the littoral regions is processed by morphological Tophat filter to enable detection of land area and to reduce speckle noise.

2)The resultant image then convertered to a binary image according to certain threshold that can be computed from its histogram.

3)The binary image then processed to remove small isolated particles. This is done by using a sequence of morphological erosion for binary images. This sequence of morphological erosion operation is performed with structuring element size that is greater than the size of biggest isolated particle. As a result of this erosion operation all of the isolated particles will be successfully removed.

4)Finally, the output image produced from the last step will be processed to fill holes that appear in the detected land regions. Filling holes process will be performed by a sequence of morphological dilation for binary images with structuring element size that is greater than the smallest hole size. As a result of this dilation operation all of the holes will be filled to get the final form of the land masking map for littoral regions.

Proposed mean estimator method:

1) First, the input SAR image is pre-processed twice by Sigma filter with window size (5*5). Each filtered pixel value is represented by the average of those pixels within the range of two standard deviations (2σ) of the centeral pixel.

2) The speckle has been reduced considerably as the result of the previous step, while coastline edges remain unaffected. Sobel operator for edge detection is then applied to the output image of Sigma filter to generate preliminary edge map.

3)A simple procedure is implemented which generates an approximation to the land boundary. To fill the gaps between neighboring pixels the edge map is processed by applying a (5*5) mean filter that is a linear filter where the centered pixel value in its window depends on the average value of the grey levels neighborhood defined by the filter window.

4) A threshold is then set and applied to the output of the previous step to get a binary image of coastlines. Enhancement step will be added to this method using a sequence of morphological erosion for binary images to remove isolated particles as explained before.

The main advantage of this proposed method is to produce the final land masking map by using only one step (mean estimator test) as compared to large number of steps introduced in other land masking methods.

8536-16, Session 3

A new automatic technique for coastline extraction from SAR images

Daniele Latini, Fabio Del Frate, Univ. degli Studi di Roma Tor Vergata (Italy); Francesco Palazzo, SERCO S.P.A. (Italy); Andrea Minchella, RSAC Ltd (United Kingdom)

To date different papers can be found describing techniques for supervised or unsupervised SAR segmentation or single object extraction. However, so far, rather weak responses have been given to the challenge represented by the new VHR X-band SAR sensors. Indeed the extremely high spatial resolution and the scattering characteristics of the X-band introduce new issues in the analysis of the data. While in remotely sensed imagery including visible bands the specific coastline extraction task may be recognized as not particularly complex, this does not hold for SAR images. Besides the speckle problem, the difficulties in SAR images stem from the fact that the backscattering from the water can be influenced by different effects due to wind and wave modulation. This can determine a not easy discrimination between sea and land. While coastline extraction from SAR data can be attempted by means of photo-interpretation, the use of more automatic techniques may play a crucial role especially in real-time or near-real time operational scenarios, or when a huge amount of data is available, as it is the case with the COSMO-SkyMed constellation. In automatic coastline detection specific knowledge concerning the boundary is used to form rules that guide the grouping of pixels. Moreover, the local edge tracing in coastline detection must be guided by the global information about the coastline; that is, information extending over the whole image. In this paper the results obtained considering PCNN, Pulse Coupled Neural Networks, will be presented and discussed. PCNN is a relatively new and unsupervised NN, based on the implementation of the mechanisms underlying the visual cortex of small mammals

8536-17, Session 3

First demonstration of GMTI for maritime application with TerraSAR-X Dual Receive Antenna mode

Matteo M. Soccorsi, Deutsches Zentrum für Luft- und Raumfahrt e.V. (Germany)

The campaign conducted by the German Aerospace Center in April and May 2010 with the TerraSAR-X satellite made available for the first time dual channel data. The Dual Receive Antenna (DRA) mode is an experimental acquisition mode which exploits the hardware redundancy. The antenna is split into two halves which receive at the same time, but independently, the transmitted signal. The configuration allows to generate two images acquired at the same time where the phase difference carries information about the projected across track velocity component of the illuminated targets.

In this work a processor for processing the data is presented in order to detect the target and to retrieve the line of sight velocity component. A hybrid technique (CFAR and GMTI) is adopted for detection of moving and non-moving targets. A scene over the Strait of Gibraltar is processed and the results are compared to the AIS information.

The data are affected by strong ambiguity due to the PRF, thus a technique which maximize the signal to clutter ratio is presented and applied for ambiguity suppression. The false alarms due to the ambiguities are extremely reduced. Subsequently, the interferogram is generated and the phase is used in order to detect moving targets (GMTI). The intensity information is also used to detected moving and non-moving target exploiting a classical CFAR technique. The results derived by the two techniques are combined to provide the output quicklook and detected vessel record.

8536-18, Session 3

Sea clutter contamination test with log-cumulants

Ding Tao, Anthony P. Doulgeris, Camilla Brekke, Univ. of Tromsø (Norway)

Polarimetric synthetic aperture radar (SAR) imagery is useful for oceanographic applications, such as ship detection, because of the complementary information contained in different channels. This work investigates the contamination of ocean clutter statistics due to potential targets within the clutter estimation region (secondary data). The aim of this study is to detect the contaminated ocean clutter using log- cumulant tests and eliminate its effect on the clutter estimate. Experiments are performed on several Radarsat-2 quadrature polarimetric (quad-pol) SAR datasets.

The ocean clutter contamination issue has been observed during our study of the polarimetric whitening filter (PWF). The PWF [1,2] is known as an effective speckle reduction method for ship detection, which usually is implemented using the sliding window technique.

An inherent problem in ocean clutter estimation is the reduction in sensitivity due to contamination. It appears as darker values in the PWF output, and increases the risk of missing any real targets in the dark regions.

Log-moments and log-cumulants were introduced by Nicolas along with the second kind statistics (or Mellin kind statistics) [3], as an effective way to measure and visualize non-Gaussian statistics. In preliminary investigations, the second and third order log-cumulants were measured for each polarimetric channel in several ocean clutter regions. For uncontaminated ocean clutter, the cross-polarization and co-polarization channel log-cumulants are statistically similar. Contaminated ocean clutter shows both an absolute deviation and a significant difference between the cross-polarization and co-polarization channel log-cumulants. Our statistical test is designed to exploit the observed effects. The ocean clutter estimation region is first divided into sub-blocks. For each sub-block, log-cumulants for each polarimetric channel are measured. The distance between the average cross-polarization and average co-polarization log-cumulants are compared for statistical significance [4]. Then the contaminated sub-blocks are eliminated from the ocean clutter estimation region, which improves the ship detection performance.

References:

[1] L. Novak and M. Burl, “Optimal speckle reduction in polarimetric SAR imagery,” Aerospace and Electronic Systems, IEEE Transactions on, vol. 26, no. 2, pp. 293-305, Mar 1990.

[2] L. Novak, M. Burl, and W. Irving, “Optimal polarimetric processing for enhanced target detection,” Aerospace and Electronic Systems, IEEE Transactions on, vol. 29, no. 1, pp. 234-244, Jan 1993.

[3] J.-M. Nicolas, “Introduction aux statistiques de deuxie`me espe`ce: applications des logs-moments et des logs-cumulants a` l’analyse des lois d’images radar,” Traitement du Signal, vol. 19, no. 3, pp. 139-167, 2002.

[4] S. Anfinsen, A. Doulgeris, and T. Eltoft, “Goodness-of-fit tests for multilook polarimetric radar data based on the Mellin transform,” Geoscience and Remote Sensing, IEEE Transactions on, vol. 49, no. 7, pp. 2764-2781, July 2011.

8536-19, Session 4

Soil moisture retrieval from ASAR Wide Swath mode observations as demonstrator for the future GMES Sentinel-1 capabilities

Simonetta Paloscia, Istituto di Fisica Applicata Nello Carrara (Italy); Rogier van der Velde, Bob Su, Univ. Twente (Netherlands); Jun Wen, Cold and Arid Regions Environmental and Engineering Research Institute (China); Yaoming Ma, Institute of Tibetan Plateau Research (China)

The amount of water stored in the soil is a key state variable controlling many biophysical processes that impact water, energy and carbon exchanges at the land-atmosphere interface. In-situ soil moisture measurements are labour intensive and site-specific. Yet, frequent spatial soil moisture distributions are desired because of its variability in nature. The possibility of observing soil moisture from space is, therefore, regarded as being extremely attractive.

In this context, microwave remote sensing have received most attention because microwaves have the unique ability to return information on media (atmosphere, vegetation, soil) that are opaque to the much shorter visible/near-infrared and thermal wavelength. As a part of the European Global Monitoring for Environment and Security (GMES) programme, the Sentinel-1 will provide high resolution microwave observations acquired via the Synthetic Aperture Radar (SAR) technique on an operational basis at a global scale. As such, the development of the Sentinel-1 space infrastructure paves the way for operational soil moisture monitoring at high spatial resolutions. However, among the challenges of retrieving soil moisture from SAR are correcting for effects of vegetation, surface roughness and incidence angle when using the ScanSAR products. In recent years, several algorithms have been developed to cope with these challenges. Various assumptions are adopted posing different inherent uncertainties on the retrieved soil moisture.

In this study, we evaluate two recently developed soil moisture retrieval algorithms using a long-term Advanced SAR (ASAR) Wide Swath mode data sets collected over the Central Part of the Tibetan Plateau. One algorithm is based on the Integral Equation Method (IEM) surface scattering model that explicitly simulates the backscatter as a function of the incidence angle and surface roughness. With the surface roughness as input, the soil moisture is retrieved by matching the IEM simulated and ASAR observed backscatter. The other algorithm adopts an Artificial Neural Network (ANN) for describing the backscatter as a function of land surface variables and retrieve soil moisture at low computational costs. The ANN was trained by using several electromagnetic models able to simulate the backscattering on bare and vegetated soils (i.e. AIEM, Oh and RTT models). The retrievals obtained with both algorithms are validated against several years of soil moisture measurements collected at different sites across the Tibetan Plateau.

8536-20, Session 4

Future use of the data from the ESA Sentinel-1 mission for operational soil moisture mapping: a multitemporal algorithm

Nazzareno Pierdicca, Luca Pulvirenti, Univ. degli Studi di Roma La Sapienza (Italy)

Soil moisture content (mv) is a key parameter that influences both global water and energy budgets because it controls the redistribution of rainfall among infiltration, runoff, percolation in soil, and evapotranspiration. Its knowledge is therefore essential for hydrological applications.

Synthetic Aperture Radar (SAR) measurements are sensitive not only to soil moisture, but also to surface roughness and, in the presence of vegetation, to biomass and canopy structure. This implies that mv retrieval is generally an ill-posed problem, especially if the observations from a single configuration (i.e. single frequency, polarization and incidence angle) system are used. Recent works have proved that such an ill-posedness can be tackled if a time-series of SAR observations is available. In these works both change detection techniques as well as Bayesian approaches [1] have been used.

The future European Space Agency (ESA) Sentinel-1 mission, foreseen in the framework of the European GMES program, will provide C-band radar data characterized by short revisit time (the two-satellite constellation will offer six days exact repeat), thus permitting the application of multitemporal inversion algorithms, that are expected to strongly increase the quality and the reliability of the mv retrievals, and to develop an operational mv product.

In this paper, a multitemporal algorithm conceived to be operationally used to map mv from Sentinel-1 data is presented. It has been designed in the framework of the “GMES Sentinel-1 Soil Moisture Algorithm De-velopment” project funded by ESA [2]. The algorithm is based on the hypothesis that a statistical relation exists among the soil conditions at the different times of the series (i.e., among some of the geophysical parameters involved in the problem). In particular, it is assumed that, considering a specific temporal interval in which a number of images is available, the average characteristics of surface roughness do not substantially change, as opposed to soil moisture, whose temporal scale of variation is shorter than that of roughness.

As for the effects of vegetation canopy on the radar signal, they are taken into account by applying the well-established “Cloud Model”. The temporal series of radar data, possibly corrected for the vegetation effects, is integrated within the retrieval algorithm that is based on the Bayesian maximum posterior probability (MAP) statistical criterion.

In this paper some new comparisons of the algorithm estimates with ground truth are presented thanks to the availability of multitemporal SAR sequences during some international campaigns organized by ESA.

Preliminary results show that the performances of the multitemporal algorithm are better than those provided by a standard monotemporal one.

[1] Pierdicca, N.; Pulvirenti, L.; Bignami, C.: Soil moisture estimation over vegetated terrains u-sing multitemporal remote sensing data. Remo-te Sensing of Environment. Vol. 114, pp. 440-448, 2010

[2] S. Paloscia, S. Pettinato, E. Santi, N. Pierdicca, L. Pulvirenti, C. Notarnicola, G. Pace, A. Reppucci, “Soil moisture mapping using Sentinel 1 images: the proposed approach and its preliminary validation carried out in view of an operational product”, Proc. SPIE 8179, 817904 (2011);

8536-21, Session 4

COSMO SkyMed X-band SAR imagery for snowpack characterization in mountain areas

Emanuele Santi, Simonetta Paloscia, Simone Pettinato, Istituto di Fisica Applicata Nello Carrara (Italy); Claudia Notarnicola, Luca Pasolli, Mattia Callegari, EURAC research (Italy)

In the last few years the remote sensing community has shown a growing interest in the new generation X-band Synthetic Aperture Radar (SAR) satellites, such as COSMO-Skymed (CSK) and Terra-SARX (TSX). Thanks to the higher operational frequency with respect to the sensors available in the past (mainly working at L and C-bands), X-band SAR systems acquire signals that have a higher interaction with water and ice particles within the snowpack. CSK, due to the 4-satellite constellation, makes it also possible to have a low revisit time over the same area, which is a crucial feature for monitoring applications.

The characterization of snowpack parameters is a challenging task. First, the backscattering coefficient is sensitive to various snow parameters (e.g. grain radius, snow density, liquid water content) in different way depending on frequency, incidence angle and polarization. Secondly, the capability of the signal to penetrate the snow layer depends on the status of the snowpack itself (e.g. on the amount of free liquid water content). The combination of X-band with higher frequencies, as Ku-Band, would be a significant improvement for operative snow investigations, as suggested by the ESA Cold Regions Hydrology High-resolution Observatory (CoReH2O) mission proposal. However, such systems are not available from satellite SAR systems yet. Further research is required for a better understanding and exploitation of currently available X-band satellite SAR systems.

In this work, the characterization and extraction of snowpack parameters from X-band SAR imagery has been addressed by comparing two methods. Both are based on a preliminary sensitivity analysis, based on datasets of snowpack parameters (depth, density, snow grain radius, temperature and wetness) collected from the available meteorological stations on two test sites in the Italian Alps. This is a crucial step, since it provides indications on the sensitivity of the input features (i.e., remote sensing signals and ancillary data) to variations in the target snow parameters. After this phase, the retrieval process is addressed. The first method is based on a Neural Network retrieval algorithm, trained by using a DRTM electromagnetic model in order to estimate the snow depth. The second one, which combines SAR and optical thermal satellite data, retrieves some of most important parameters of the snow cover (i.e. density, wetness and grain radius) with an algorithm based on the Support Vector Machine technique and trained with the use of the IEM electromagnetic model. Both methods make use of the threshold criterion for detecting the snow cover extent on which the two algorithms are applied.

The comparison of the two methods was carried out on the Cordevole test site located in the Dolomites, Eastern Italian Alps, by using ground data collected by the Avalanche Center in Arabba and meteorological data collected by a network of automatic stations.

Both methods were developed and implemented in the framework of two projects funded by the Italian Space Agency (HYDROCOSMO and SNOX) for the exploitation of X-band satellite SAR data for the analysis and characterization of snow in mountain areas.

8536-22, Session 4

Mapping spatial and temporal patterns of soil moisture with ASAR imagery in the Alps

Luca Pasolli, Claudia Notarnicola, EURAC research (Italy); Lorenzo Bruzzone, Univ. degli Studi di Trento (Italy); Giacomo Bertoldi, Marc Zebisch, EURAC research (Italy)

The Alpine environment is suffering the effects of climate changes and in particular of the global warming. For the future much drier and warmer conditions together with higher inter-annual variability can be expected. This means increasing drought periods in summer, while higher probability of heavy rain in winter [1]. These variations may have a strong impact on the water availability for agricultural and human purposes and may be strongly related to natural hazards such as floods and landslides [2]. Soil moisture content is fundamental for studying and monitoring such phenomena, provided that accurate, spatially and temporally distributed information on this variable are available [3].

An efficient and effective solution is the mapping of this variable from satellite remote sensing data. In particular the use of microwave Synthetic Aperture Radar (SAR) signals has been widely investigated and exploited since many years with promising results. Most of the currently operational satellite SAR sensors (Radarsat2, Envisat ASAR, ERS-2) operate at C-band, which is not the optimal one for the retrieval of soil moisture. Indeed, at this frequency surface roughness and vegetation coverage strongly affects the backscattering coefficient. Advanced retrieval algorithms together with data processing and fusion techniques have been proposed to deal with the complexity and non-linearity of the retrieval problem [4], [5]. The retrieval process becomes even more challenging moving in mountain areas, such as the Alps, were the topography and the heterogeneity of the landscape introduce further ambiguity in the SAR backscattering [6].

The possibility to retrieve soil moisture content from satellite SAR imagery in alpine areas has been deeply investigated in a previous contribution [7]. The analysis pointed out the strong influence of topography and vegetation coverage on the SAR backscattering signal. To deal with the retrieval process in this challenging scenario, an advanced algorithm based on the Support Vector Regression (SVR) technique and the integration of ancillary data was successfully proposed. The achieved results pointed out the possibility to effectively estimate soil moisture in mountain areas in terms of both quantitative accuracy and capability to reproduce local spatial patterns.

On the basis of the promising results already achieved, in this study the analysis is extended to temporal series of SAR data. The interest in this kind of analysis is motivated by the fact that temporal patterns of soil moisture content can provide useful indications for the application domains cited above. Moreover, upcoming satellite missions (e.g., the Sentinel family) will provide the scientific community with continuous and frequent acquisitions of the Earth surface. It is thus important to investigate and develop algorithm able to effectively handle these data. Up to now, however, such an analysis has not been carried out in the specific case of mountainous landscapes. More in detail, this work aims at: i) assessing the effectiveness of the proposed retrieval algorithm to effectively reproduce temporal (seasonal and inter-annual) patterns of the target variable in mountain areas; and ii) investigating the evolution of the estimated spatial and temporal patterns of soil moisture together with meteorological and ancillary distributed data, to derive useful indication about the inter-correlation among these environmental variables and eventually improve the retrieval of soil moisture in this operational scenario.

The experimental analysis will be carried out with the use of a two years long Envisat ASAR Wide Swath (WS) C-band satellite imagery time series. Despite the reduced spatial resolution with respect to the data used in the previous analysis, WS imagery can be acquired with reduced temporal delay with respect to high resolution data. Moreover, the swath width easy allows covering large portions of the earth surface. These two features are important for monitoring purposes and for properly capturing temporal trends of the target variable. Moreover, the use of this data allows investigating the effect of the reduced spatial scale on soil moisture retrieval with the proposed algorithm. The test site is a small Alpine catchment located in the Mazia valley, Alto Adige, Italy. This area is mainly covered by grassland and has also some forest stands. It is particularly suitable for the analysis thanks to the well representative topographic, climatic and soil conditions. In addition to this, numerous and reliable field reference data (including temporal series of meteorological variables and soil characteristics) are available. In the final paper, a thorough description of the experiments and results achieved will be provided.

References

[1] Brunetti, M., Maugeri, M., and Nanni. T. (2001). Changes in total precipitation, rainy days and extreme events in northeastern Italy. Int. J. of Climatology, vol. 21, pp. 861-871.

[2] Horton, P. et al. (2006). Assessment of climate-change impacts on alpine discharge regimes with climate model uncertainty. Hydrological Processes, vol. 20, pp. 2091-2109.

[3] Rodriguez-Iturbe, I., D'Odorico, P., Porporato, A., et al. (1999). On the spatial and temporal links between vegetation, climate, and soil moisture. Water Resources Research, vol. 35-12, pp. 3709-3722.

[4] Notarnicola, C., and Posa, F., 2006. "Combination of X, C and L band for retrieval of surface parameters," in Proc. SPIE vol. 6746.

[5] Paloscia, S., Pampaloni, P., Pettinato, S., and Santi, E., 2008. "A comparison of algorithms for retrieving soil moisture from ENVISAT/ASAR images," IEEE Transaction on Geoscience and Remote Sensing, vol. 46, no. 10, pp. 3274-3284.

[6] Luckman, A.J., (1998). The effect of topography on mechanisms of radar backscatter from coniferous forest and upland pasture. IEEE

Transaction on Geoscience and Remote Sensing, vol. 36, no. 5.

[7] Pasolli, L., Notarnicola, C., Bruzzone, L., Bertoldi, G., Della Chiesa, S., Hell, W., Niedrist, G., Tappeiner, U., Zebisch, M., Del Frate, F., and Vaglio Laurin, G. (2011). Estimation of soil moisture in an alpine catchment with RADARSAT2 images. Applied and Environmental Soil Science, vol. 2011, Article ID 175473, 12 pages.

8536-23, Session 4

A Bayesian approach to retrieve soil parameters from SAR data: Effect of prior information

Matias Barber, Martin Maas, Pablo Perna, Francisco M. Grings, Haydee Karszenbaum, Instituto de Astronomía y Física del Espacio (Argentina)

Orbiting microwave synthetic aperture radar (SAR) systems offer the opportunity of monitoring soil moisture content at different scales and under any kind of weather conditions, through the known sensitivity that backscattered signal exhibits to soil parameters, including soil moisture. In this framework, soil parameter retrieval can be considered an inference problem, where one essentially wants to infer soil condition given a set of measured backscatter coefficients and ancillary information.

A wide range of forward models, ranging from experimental fittings to physically-based models have been developed in order to assess the dependency of soil parameters to backscattered signal. These models are important to understand the soil backscattering physics, but they can also be a key tool to the retrieval of soil condition from measurements. This is particularly important since one of the main problems of SAR-based soil moisture retrieval is the limited performance of inverse models. This poor performance is mostly related to measurement errors, the heterogeneity of the target's surface, the difficulty to parameterize the models in terms of the soil parameters and the difficulty to measure them on the field [1, 2, 3]. Furthermore, another phenomenon degrades SAR-based soil moisture retrieval: speckle noise [4]. It is characteristic of SAR images, and it is usually reduced in a post-processing stage by averaging neighboring pixels (multi-looking process) at the expense of spatial resolution. Nevertheless, averaging implicitly assumes that soil properties inside the average window are constant, which is usually not the case. Therefore, a tradeoff between averaging and soil heterogeneity is usually accepted.

In general, the retrieval model and the speckle noise are considered as independent problems, whereas they are indeed a part of the same inference problem. In a recent paper [5], this issue was addressed by a Bayesian retrieval methodology, which incorporates the speckle and the terrain heterogeneity as sources of uncertainty that degrade the soil moisture estimate. That study focused mainly on the effect that multi-looking and prior information have on the accuracy of soil moisture retrieval.

In this paper, a further numerical investigation is carried out to assess the specific effect of the prior information about soil condition on the accuracy of the retrieved parameters. In particular, the question to be answered here is which are the necessary requirements of the prior information to ensure an acceptable estimate of soil moisture. This is particularly important for soil moisture retrieval from SAR measurements, where soil roughness depends on the tillage system applied, but from which it is feasible to obtain useful a priori information to improve the retrieval.

REFERENCES

[1] N. E. C Verhoest, H. Lievens, W. Wagner, J. Álvarez-Mozos, M. S. Moran, and F. Mattia, "On the Soil Roughness Parameterization Problem in Soil Moisture Retrieval of Bare Surfaces From Synthetic Aperture Radar", Sensors, pp. 4213-4248, July 2008.

[2] M. Callens, N. E. C Verhoest, and M. W. J. Davidson, "Parameterization of tillage-induced single-scale soil roughness from 4-m profiles", IEEE Transactions on Geoscience and Remote Sensing, pp. 878-888, April 2006.

[3] Z.S. Haddad, P.D. Dubois, and J.J. van Zyl, "Bayesian Estimation of Soil Parameters from Radar Backscatter Data", IEEE Transactions on Geoscience and Remote Sensing, pp. 76-82, January 1996.

[4] J.S. Lee, K. W. Hoppel, S. A. Mango, and A. R. Miller, "Intensity and Phase Statistics of Multilook Polarimetric and Interferometric SAR Imagery", IEEE Transactions on Geoscience and Remote Sensing, pp. 1017-1028, September 1994.

[5] M. Barber, F. Grings, P. Perna, M. Piscitelli, M. Maas, C. Bruscantini, J. Jacobo Berlles, H. Karszenbaum, "Speckle noise and soil heterogeneities as error sources in a Bayesian soil moisture retrieval scheme for SAR data", IEEE Journal of Selected Topics in Applied Earth Observations and Remote Sensing, 2012. (In press).

8536-24, Session 5

Sea state measurements using TerraSAR-X data

Miguel Bruck, Susanne Lehner, Deutsches Zentrum für Luft- und Raumfahrt e.V. (Germany)

Synthetic Aperture Radar (SAR) provides information on the two dimensional ocean surface. Due to its high resolution, daylight, weather independency and global coverage, SAR is suitable for ocean observation. TerraSAR-X (TS-X) and his twin brother satellite Tandem-X acquire data of the sea surface with resolution up to 1 m. Individual ocean waves with wavelengths under 30 m are detected. For c-band SAR data, algorithms to derive sea state information were developed. To use TS-X SAR data for ocean applications, algorithms have been developed to extract meteo-marine information from the x-band SAR data: the XWAVE algorithm for estimation of integrated wave parameters. The XMOD algorithm was developed for the estimation of fine wind speed fields, with a resolution of a few meters. It provides an accurate estimate on wind speed information between 3 and 17 m/s with standard deviation of 1.5 m/s.

The XWAVE algorithm for X-band SAR uses an empirical approach. It is based on Fourier analyses of TS-X data and uses a geophysical model function with coefficients that are fitted with collocated hindcast wave height wave model results provided by the German Weather Center (DWD) and in-situ buoy measurements.Significant wave height is derived by the XWAVE combining wind information estimated by the XMOD algorithm. The ocean wave information derived from SAR data on sea state obtained by Fourier analyses and the wind information are combined, taking into account wind sea waves and wind influence on ocean waves imaged by the SAR. The XWAVE depends also in incidence angle and wave peak direction.

TS-X data were acquired over wave measuring buoy devices and integral wave parameters were estimated from TS-X and TD-X data by integration of two-dimensional image spectra using the algorithm proposed. Significant wave height derived from TS-X data using the XWAVE algorithm was verified with a 120 TS-X Stripmap collocated in-situ deep water buoy measurement data-set with an Si of 0.20. Wave in-situ measurements are provided by NOAA, for many different locations providing this way diversity in ocean wave conditions necessary for the tuning and testing of the algorithm. The tuning/validation data-set were analyzed for homogeneous areas, which are areas free of artifacts not related to ocean wind generated waves, e.g. oil, ice, atmospherics effects, and internal waves. Similar results were obtained with different collocated data-sets with different in-situ buoy data and wave model results. The SAR integrated one dimensional spectra is also analyzed and compared to the wave spectra provided by the buoy. The wave direction derived from the TS-X data is also compared to the one given by directional buoys. Comparison of sea state parameters derived from TS-X data acquired overall the ocean is made to wave model results in regions were in-situ data is unavailable.

TS-X SAR due to higher resolution to conventional c-band SAR is particularly useful to characterize sea state in the spatial domain, especially where sea state variability is high, as is the case of coastal areas with complex bathymetry. The changes of sea state properties are investigated. Results are compared to a wave spectral model designed for coastal applications and buoy measurements where available.

8536-25, Session 5

Deepwater Horizon oil slick characterization with UAVSAR

Cathleen E. Jones, Benjamin M. Holt, Jet Propulsion Lab. (United States); Brent Minchew, California Institute of Technology (United States)

In June 2010, the UAVSAR platform was deployed to the Gulf of Mexico in response to the Deepwater Horizon (DWH) oil spill. We have analyzed the quad-polarized L-band SAR data collected over the main oil slick to develop and validate algorithms for improved discrimination of oil slicks on water and identification of oil properties. Our results

show that radar backscatter from both clean water and oil in the slick is predominantly from a single surface scatterer, consistent with the tilted Bragg scattering mechanism across the incidence angle range of 26-60°. We find that the change of backscatter over the main slick is due to both a damping of the ocean wave spectral components by the oil and an effective reduction of the dielectric constant resulting from a mixture of 65-90% oil with water in the surface layer. These results support the use of synthetic aperture radar in quantifying oil volumetric concentration in a thick slick of emulsified oil.

We performed a Cloude-Pottier polarimetric decomposition to determine whether this formulation of the results enhanced oil detection/characterization. Using the H/A/α parameters, we show that surface scattering is dominant for oil and water whenever the data are above the noise floor and that the entropy (H) and α parameters for the DWH slick are comparable to those from the clean water. The anisotropy, A, parameter shows substantial variation across the oil slick whenever the backscatter in all channels is above the instrument noise floor. We find the most reliable indicator for slick detection to be the major eigenvalue of the coherency matrix, which is equivalent to the total backscattered power for both oil in the slick and clean seawater.

Our results are unique in that they quantify specific properties of thicker emulsified oil rather than simple slick extent, so are potentially useful for guiding spill clean-up. The improved sensitivity of UAVSAR compared to other aircraft and satellite SAR is due primarily to the low noise floor of ~-50 dB, which is at least 20 dB below that of most radars in use over the DWH spill. With UAVSAR we can discriminate small variations in the radar signature within the oil slick, from which we have extracted bulk estimates of the volumetric concentration of the surface oil. Our results conflict with several previous polarimetric SAR studies of marine oil slicks. While it is possible that the conflicts are attributable to different characteristics of the studied oil slicks, such as thickness, weathering, degree of emulsification, and use of dispersants, we found through a thorough analysis of the UAVSAR instrument noise floor that our results are in agreement with those previous studies only in areas where the data had low signal-to-noise ratio.

This research was conducted in part at the Jet Propulsion Laboratory, California Institute of Technology, under contract with the National Aeronautics and Space Administration.

8536-26, Session 5

Ocean surface slick characterization by multi-polarization Radarsat-2 data

Stine Skrunes, Camilla Brekke, Torbjørn Eltoft, Univ. of Tromsø (Norway)

Marine oil spills are an important environmental problem, and satellite SAR remote sensing have become a valuable tool for the detection and monitoring of these spills. An oil spill can be detected by SAR due to the reduced backscatter from the oil-covered sea surface, as the oil will dampen the surface waves. However, a number of natural phenomena, called look-alike phenomena, will produce similar dark features in the SAR images, in some cases leading to false detections. One example of a look-alike phenomena is biogenic surface films produced by marine organisms. Recent developments in the satellite SAR sensors allow for multi-polarization image acquisitions, and the added information in dual- or quad-polarization measurements could provide more information about the possible oil spill and improve the discrimination between oil spills and their look- alikes.

Since the early 1980s, the Norwegian Clean Seas Association for Operating Companies (NOFO) has conducted oil-on-water (OPV) exercises, where oil is released onto the sea surface in order to test procedures and equipment for oil spill cleaning up operations. A large-scale oil-on-water exercise, OPV-2011, was carried out in June 2011 at the Frigg field in the North Sea. Three different types of oil (crude oil, oil emulsion and plant oil) were released, and the resulting surface slicks were imaged within the same scenes by both Radarsat-2 and TerraSAR-X, separated in time by only 16 minutes. The data set from OPV-2011 has been analysed by studying multi-polarization features, e.g. anisotropy, entropy, mean scattering angle [1] [2], standard deviation of co-polarized phase difference [3] [7] and the correlation between HH and VV [4]. Interesting variations between the different oil types and within the individual slicks are seen. Classifications based on a feature sub set show potential for discrimination between mineral oils and the biogenic film produced by the plant oil. A zoning in the classified mineral slicks are revealed, possibly related to zones of different thicknesses [5] [6].

This years exercise, OPV-2012, will be conducted 11-15 June in the North Sea. Crude oil and/or oil emulsion will be released. In addition, a release of plant oil and/or oleyl alcohol (OLA) for simulation of natural biogenic slicks are planned. SAR data from several sensors, i.e. Radarsat-2, TerraSAR-X and Cosmo-SkyMed, matching the time and place of the exercise, have been ordered. In addition, multi-spectral data will be obtained. If everything goes according to plan, both mineral oils and biogenic slicks will also this year be imaged within the same SAR scenes, and with several sensors close in time. Hence, both a multi-polarization and a quasi-multi-frequency analysis of oil spills and biogenic look-alikes can be done.

An analysis similar to that performed on the OPV-2011 data set, will also be done on the new data acquisitions. Hence, more certain conclusions can be drawn on the ability of multi-polarization SAR imagery for oil spill characterization and oil vs look-alike discrimination. Results from the two oil-on-water exercises will be presented and compared in the final paper.

Acknowledgement:

Thanks to Total E&P Norge AS for funding this study, thanks to NOFO for letting us participate in the exercise, and thanks to KSAT, InfoTerra and The Norwegian Meteorological Institute for providing the Radarsat-2, TerraSAR-X and weather data respectively.

References:

[1] Cloude, S.R. and Pottier, E.: An Entropy Based Classification Scheme for Land Applications of Polarimetric SAR, IEEE Trans. on Geosci. and Rem. Sensing, Vol. 35, No. 1, 1997.

[2] Migliaccio, M., Gambardella, A. and Tranfaglia, M.: SAR Polarimetry to Observe Oil Spills, IEEE Trans. on Geosci. and Rem. Sensing, Vol. 45, No. 2, 2007.

[3] Migliaccio, M, Nunziata, F. and Gambardella, A., On the co-polarized phase difference for oil spill observation, Int. J. of Rem. Sens., Vol. 30, No. 6, p. 1587-1602, 2009.

[4] Nunziata, F., Gambardella, A. and Migliaccio, M., On the Mueller Scattering Matrix for SAR Sea Oil Slick Observation, IEEE Geosc. and Rem. Sens. Letters., Vol. 5, No. 4, p. 691-695, 2008.

[5] Skrunes, S., Brekke, C., and Eltoft, T., An Experimental Study on Oil Spill Characterization by Multi-Polarization SAR, To be presented at EUSAR 2012, Germany (accepted based on draft paper).

[6] Skrunes, S., Brekke, C., and Eltoft, T., Oil Spill Characterization with Multi-Polarization C- and X-band SAR, To be presented at IGARSS 2012, Germany (accepted based on full paper).

[7] Velotto, D., Migliaccio, M., Nunziata, F. and Lehner, S., Dual-Polarized TerraSAR-X Data for Oil-Spill Observation, IEEE Trans. on Geosc. and Rem. Sens., Vol. 49, No. 12, p. 4751-4762, 2011

8536-27, Session 5

Confidence levels in the detection of oil spills from satellite imagery: from research to the operational use

Guido Ferraro, European Commission Joint Research Ctr. (Italy); Olaf Trieschmann, European Maritime Safety Agency (Portugal); Marko Perkovic, Univ. of Ljubljana (Slovenia); Dario Tarchi, European Commission Joint Research Ctr. (Italy)

Detected oil spills are usually classified according to confidence levels. Such levels are supposed to describe the probability that an observed dark feature in the satellite image is related to the actual presence of an oil spill. The Synthetic Aperture Radar (SAR) derived oil spill detection probability estimation has been explored as an intrinsic aspect of oil spill classification, which fundamentally computes the likelihood that the detected dark area and its extracted features are related to oil spill. However, the SAR based probability estimation should be integrated with additional criteria in order to become a more effective tool for the End User. As example, the key information for the final users is not the confidence level of the detection “per se” but the alert (i.e. the impact) that such a detection could generate.

This topic was deeply discussed in the framework of the R&D European Group of Experts on remote sensing Monitoring of marine Pollution (EGEMP) and a paper was published in 2010. Following this paper, the newly established EMSA CleanSeaNet service (2nd generation) provides the alert level connected to the detection of an potential oil spill in a satellite image in a different way.

8536-28, Session 5

Slicks in SAR imagery of the sea surface

Stanislav A Ermakov, Institute of Applied Physics (Russian Federation)

An overview of studies on the problem of marine slicks and their SAR signatures carried out at the Institute of Applied Physics RAS is given. SAR signatures of slicks related to different oceanic/atmospheric processes are considered, including slicks due to oceanic internal waves, non uniform currents, wind fronts, algae bloom, oil spills.

SAR signatures of oceanic internal waves occur typically as groups of periodic bands characterized by different types of SAR image intensity variations: double sign signatures (amplifications and depressions of the radar backscatter) and single sign signatures - negative (depression) or positive (amplification) sign bands. The double sign signatures are surface manifestations of internal waves in the absence of surfactant films, while the negative sign signatures are formed when the sea surface is covered with films, the positive sign bands correspond to the case of very low, near threshold wind velocities. Results of field studies of the surface manifestations of internal waves are discussed, including investigations of film characteristics in slick bands simultaneous with measurements of characteristics of internal waves and short wind waves. Variations of the spectrum of short wind waves are analyzed theoretically and theory is shown to explain at least qualitatively SAR signatures of internal waves.

Another typical feature in SAR imagery is “filamentary” slicks which can be related to marine currents. Field measurements of film characteristics and current velocities inside/outside the “filaments” have shown that these slicks are characterized by the accumulation of surfactants, and that the filaments are located in the zones of convergency of weak transverse current components thus marking the zones of non uniformity of surface currents. Surfactant redistribution and slick formation due to non uniform surface currents are analyzed theoretically to explain the physical mechanism of filamentary slicks formation.

Slick structures associated with atmospheric processes, wind fronts, due to surfactant compression by inhomogeneous wind drift currents are also discussed and are illustrated by observations of periodic and solitary slick bands in the field of oscillating and step-like wind fronts.

Examples of algae bloom manifestations in SAR images are discussed. The influence of algae bloom on radar backscattering has been studied in field experiments and in laboratory. It is shown that the intensity of X-band radar backscattering decreases with phytoplankton concentration in the upper water layer. The effective water viscosity and film elasticity values have been measured and their increase in the presence of algae is considered as the main physical reason of enhanced wind wave damping and radar backscatter depression.

To investigate quantitatively possibilities of slick detection with SAR numerous field studies of wind wave damping and radar backscatter depression by films have been carried out at IAP RAS, including simultaneous SAR observations and platform and boat measurements of wind waves with scatterometers and optical spectrum analyzers. Physical characteristics of films have been studied in detail for artificial films (including oil films) used in the experiments. Dependencies of the damping degree (spectrum contrast) on radar wavelength are obtained at different wind conditions and for films with different elasticity values. A model of wave damping is developed and is shown to describe satisfactory experiment. Recommendations on using radar (SAR) of different bands are given.

This work has been supported by RFBR (projects 11-05-00295, 11-05-97027, 10-05-00101, 11-05-97029) and by the RF Ministry of Education and Science (Contracts №11.G34.31.0048, №11.G34.31.0078).

8536-29, Session 6

Fully automatic oil spill detection from COSMO-SkyMed imagery using a neural network approach

Ruggero G. Avezzano, Fabio Del Frate, Daniele Latini, Univ. degli Studi di Roma Tor Vergata (Italy)

The increased amount of available Synthetic Aperture Radar (SAR) images acquired over the ocean represents an extraordinary potential for improving oil spill detection activities. On the other side this involves a growing workload on the operators at analysis centers. In addition, even if the operators go through extensive training to learn manual oil spill detection, they can provide different and subjective responses. Hence, the upgrade and improvements of algorithms for automatic detection that can help in screening the images and prioritizing the alarms are of great benefit. In the framework of an ASI Announcement of Opportunity for the exploitation of COSMO-SkyMed data, a research activity aiming at studying the possibility to use neural networks architectures to set up fully automatic processing chains using COSMO-SkyMed imagery has been carried out and results are presented in the paper. The automatic identification of an oil spill is seen as a three step process based on segmentation, feature extraction and classification. We observed that a PCNN (Pulse Coupled Neural Network) was capable of providing a satisfactory performance in the different dark spots extraction, close to what it would be produced by manual editing. For the classification, a Multi-Layer Perceptron (MLP) Neural Network was employed.

8536-30, Session 6

Targets observation at sea exploiting reflection symmetry extracted from X-band dual-polarimetric SAR data

Domenico Velotto, Deutsches Zentrum für Luft- und Raumfahrt e.V. (Germany); Ferdinando Nunziata, Maurizio Migliaccio, Univ. degli Studi di Napoli Parthenope (Italy); Susanne Lehner, Deutsches Zentrum für Luft- und Raumfahrt e.V. (Germany)

Targets over the ocean surface (i.e. ships or man-made objects like oil rigs) being complex metallic structures call for all the three scattering processes: single-bounce returns due to direct backscattering from surfaces perpendicular to the radar beam; double-bounce scattering due to the dihedral formed by the vertical ship’s conducting plates and the sea surface; multiple-bounce caused by the ship’s structure (e.g. deck and cables). Synthetic Aperture Radar (SAR) observation of such targets relies on the fact that the measured Normalized Radar Cross Section (NRCS) is higher than the one from the surrounding sea surface and therefore they are imaged as bright spots over SAR images.

The information content provided by the NRCS collected by a single-polarization SAR (the horizontal polarization is assessed to perform better respect to the vertical one) is in general quite poor to efficiently observe metallic targets at the sea. The increased interest towards polarimetric SAR data along with a recent development of SAR missions equipped with high resolution X-band sensors (e.g. TerraSAR-X, Tandem-X and COSMO-SkyMed) have driven the scientific community to conceive more effective observation techniques.

In order to reduce false alarms, physically based approaches based on the Cloude-Pottier decomposition parameters or on the Cameron’s coherent target decomposition (CTD), have been developed for ship detection purposes. However, these algorithms are quite complex to be implemented operationally and they require a high computational load.

In this study, a physically-based approach that exploits the intrinsic symmetry properties that characterize the sea surface with and without metallic targets is proposed. Sea surface target-free, being a distributed natural target, is expected to satisfy the reflection symmetry while sea surface target-covered, being a complex structures, is expected to break the reflection symmetry. An effective measure of the departure from the reflection symmetry is given by the cross-correlation (i.e. the correlation between like- and cross-polarized channels). A sensitivity study of the cross-correlation is performed and a simple but very effective filter is developed to observe metallic targets at sea in dual-polarimetric SAR data

Experiments undertaken over X-band Single look Slant range Complex (SSC) TerraSAR-X SAR data confirm the soundness of the approach. The filter is tested on both HH/HV and VV/VH dual-polarimetric combinations and the outputs are verified through available Automatic Identification System (AIS) data.

8536-31, Session 6

Three-dimensional monopulse radar imaging simulation of ships on sea surfaces

Diao Guijie, Xiaojian Xu, BeiHang Univ. (China)

Synthetic aperture radar and inverse synthetic aperture radar (SAR/ISAR) images are two-dimensional (2-D) projections of three-

dimensional (3-D) targets scattering on the radar imaging plane. For ships on sea surfaces in complex motion, SAR/ISAR images can not always reveal the true aspects of the targets. This makes it difficult to realize the automatic target recognition (ATR). To overcome the drawback of the 2-D radar images, the three-dimensional (3-D) monopulse radar imaging model and algorithm are studied in this paper.

A raw signal model for wideband monopulse radar is developed according to spotlight synthetic aperture radar (SAR) geometry, and applied to the three-dimensional (3-D) imaging for ships on sea surfaces. For the electromagnetic (EM) signals received by the monopulse radar, multi-path EM scattering model is adopted to simulate the EM interactions between the ship and the sea surface. Both the reflection coefficient of the time-evolving sea surface and the ship motion dynamics derived by sea waves are introduced into the multi-path EM scattering calculation to simulate the time-variant scattering characteristics of a ship.

One-dimensional (1-D) high resolution range profiles (HRRPs) and 2-D radar images can be obtained from the calculated raw signals. And then, the 3-D images of a target can be reconstructed with the 1-D HRRPs or the 2-D radar images. Comparing the two traditional methods, the one based on 1-D HRRPs is more efficient and more convenient for real-time realization. The later one based on 2-D radar images can provide more scattering information for 3-D contour reconstruction of the target and the angle glint will be weakened, since the scatters are discriminated in Doppler domain. However, for a ship in motion of six degrees of freedom (6-DOF), i.e., surge, sway, heave, roll, pitch and yaw, complex calculations are needed to get a focused 2-D radar image, which is difficult for real-time realization. For these reasons, an optimized 3-D monopulse imaging algorithm based on multi-frame 1-D HRRPs is proposed. Several frames of 3-D image are reconstructed from several single-frame 1-D HRRPs at different intervals, and assembled to a final 3-D image via coordinate translating and position shifting. Due to the relative motion between the radar and the target within the synthetic aperture time, the 3-D images from different 1-D HRRPs reflect the time-variant scattering characteristics of the target. So the assembled final 3-D image will present more details of the target 3-D contour than the images based on single-frame 1-D HRRPs. This algorithm does not need complex phase compensation, so it is more efficient compared to the method based on 2-D radar images.

Simulation results validate the algorithm and show that the 3-D monopulse image is less affected by target motion. This demonstrates promising features for target classification and recognition.

Conference 8537: Image and Signal Processing for Remote Sensing

Monday - Wednesday 24–26 September 2012 • Part of Proceedings of SPIE Vol. 8537
Image and Signal Processing for Remote Sensing XVIII

8537-1, Session 1

Image sharpening: solutions and implementation issues *(Invited Paper)*

Andrea Garzelli, Univ. degli Studi di Siena (Italy)

No Abstract Available

8537-2, Session 1

Color and spatial distortions of pan-sharpening methods in real and synthetic images

Anabella Medina Machín, Javier Marcello Ruiz, Francisco Eugenio González, Dionisio Rodríguez Esparragón, Javier Martín Abasolo, Univ. de Las Palmas de Gran Canaria (Spain)

The purpose of pixel level fusion (pan-sharpening) is to improve the spatial resolution of the original multispectral image, by enhancing structural and textural details, and simultaneously retaining the spectral fidelity. Various pan-sharpening methods have been proposed in the literature, mainly based on high-pass filtering, algebraic operations, component substitution or multi-resolution analysis.

A set of indicators have been proposed to quantitatively assess the images quality. To measure the spectral distortion, each fused image is compared to the multispectral one using different indices, usually the correlation coefficient, the root mean square error, the relative dimensionless global error, the universal image quality index, the structure similarity index or the spectral angle mapper. Unfortunately, some disagreement has been demonstrated in quantitative measurements using the mentioned quality indicators. To assess the spatial quality, the detail of the fused image must be compared to that present in the panchromatic image. Very few quantitative measures are available to evaluate the spatial quality and usually the spatial correlation coefficient (Zhou) is considered.

This work addresses the challenging topic of the quality evaluation of pan-sharpened multispectral images. A database of GeoEye satellite images having different spectral and spatial characteristics was created and several pan-sharpening methods were implemented and tested. In particular, the fusion techniques analyzed were the Brovey transform, Intensity-Hue-Saturation (IHS), extended IHS (e-IHS), principal component analysis (PCA), Mallat discrete wavelet transform (TWD), à trous additive wavelet algorithm (atrousaw) and combination of à trous with IHS (atrousawi) and PCA (atrousawpc) were also analyzed.

After the evaluation of these fusion algorithms we can conclude that, in general, the à trous wavelet methods achieve the best spectral performance while those attaining the best spatial accuracy are e-IHS and PCA, with the Mallat wavelet transform being the worst. We also found some interesting results about the color and the spatial distortions of each method. It was demonstrated that some colors bands are more affected than others depending on the fusion techniques considered.

In order to analyze in more detail such distortions, a multispectral synthetic image was created, including the primary colors and different spatial structures with diverse shapes and sizes. The complete quantitative assessment was again conducted and complemented by a detailed visual analysis plus the generation of error images to provide local information on areas with more and less distortion for each individual multispectral channel. In general, wavelet methods are highly satisfactory in spectral terms. PCA causes the worst distortions, mainly in the green, red and white colors; while Brovey severely affects the blue band; and IHS the blue and black colors. On the other hand, wavelet-based algorithms significantly alter edges, specially the TWD on curved shapes.

In summary, a new C++ tool has been implemented to assess the quality of 8 pan-sharpening methods using qualitative and quantitative indices. After a thorough analysis, employing real and synthetic data, spectral and spatial conclusions have been extracted. Finally, we can state that the à trous additive wavelet and the extended IHS provide the best compromise between spectral and spatial distortion.

8537-3, Session 1

Advantages of Laplacian pyramids over ‘’à trous” wavelet transforms for pansharpening of multispectral images

Bruno Aiazzi, Istituto di Fisica Applicata Nello Carrara (Italy); Luciano Alparone, Univ. degli Studi di Firenze (Italy); Stefano Baronti, Istituto di Fisica Applicata Nello Carrara (Italy); Andrea Garzelli, Univ. degli Studi di Siena (Italy); Massimo Selva, Istituto di Fisica Applicata Nello Carrara (Italy)

Pansharpening techniques based on multiresolution analysis (MRA) substantially split the spatial information of the MS bands and of the Pan image into a series of bandpass spatial frequency channels. The high frequency channels of Pan are inserted into the corresponding channels of the interpolated MS bands. The ‘’à trous” wavelet (ATW) transform and the generalized Laplacian pyramid (GLP) are most widely used to perform MRA. In both cases, if the reduction lowpass filter is designed in such a way that its frequency response matches the modulation transfer function (MTF) of the spectral channel into which details will be injected, the spatial enhancement provided by MRA techniques becomes comparable to that of component-substitution (CS) techniques.

In this paper, we investigate on the advantages provided by adopting GLP in MRA-based pansharpening. Apart from computational issues (GLP is slightly slower than ATW because of extra steps of decimation and interpolation), the most notable difference in performances depends on the way GLP and ATW deal with aliasing possibly occurring in the MS data. Aliasing of MS, which is originated by insufficient sampling step size, or equivalently by a too high amplitude value of MTF at Nyquist frequency, may lead to annoying jagged edges in the sharpened image. In this paper we prove that GLP is capable of compensating the aliasing of MS, unlike ATW and analogously to CS methods, thanks to the decimation and interpolation steps present in its flowchart.

Experimental results will be presented in terms of quality/distortion global score indexes for increasing amounts of aliasing, measured by the amplitude at Nyquist frequency of the Gaussian-like lowpass filter simulating the average MTF of the individual spectral channels of the instrument. GLP and ATW-based methods, both using the same MTF filters and the same global injection gain, will be compared to show the advantages of GLP over ATW in the presence of aliasing of the MS bands. The above two MRA-based methods will be compared also with a CS-based method, the enhanced Gram-Schmidt spectral sharpening (GS+) that is a modified version of ENVI’s GS with improved spectral quality, thanks to a least squares (LS) calculation of the spectral weights defining the generalized intensity.

We will present experimental results on SAM, ERGAS and Q4 indexes between fusion products at 4 m, achieved from MS and Pan data spatially degraded by four along rows and columns, and original 4 m MS. Progressively increasing amounts of aliasing are generated by applying Gaussian-shaped lowpass filters with moduli of frequency responses at cutoff Nyquist frequency increasing from 0.1 to 0.6. All fusion methods benefit from aliasing up to a simulated MTF approximately equal to 0.3. After that value GS+ steadily follows the same trend leading to better and better fusion performances. Conversely the two MRA-based methods, ATW and GLP, follow opposite trends leading to poorer and poorer performances of ATW and better and better performances of GLP, as the amount of aliasing increases.

8537-4, Session 1

Multiresolution image fusion using compressive sensing and graph cuts

V. Harikumar, Manjunath Joshi, Mehul Raval, Prakash P Gajjar, Dhirubhai Ambani Institute of Information and Communication Technology (India)

Multiresolution fusion refers to the enhancement of low spatial

resolution (LR) of multispectral (MS) images to that of Panchromatic (Pan) image without compromising on the spectral details. In this paper we propose a new approach for multiresolution fusion which is based on the theory of compressive sensing and graph cuts. We first estimate a close approximation to the fused image by using the sparseness in the given Pan and MS images. Assuming that the Pan and LR MS image have the same sparseness, the Initial estimate of the fused image is obtained as the linear combination of the Pan blocks. The low resolution MS image is modeled as the degraded and noisy version of the fused image in which the degradation matrix entries are estimated by using the initial estimate and the MS image. A regularization based approach is used to obtain the final solution. We use the truncated quadratic prior for the preservation of the discontinuities and graph cuts for optimization. The advantage of the proposed method is that it does not require the registration of Pan and MS data. Also the spectral characteristics are well preserved in the fused image since we are not directly operating on the Pan digital numbers. Effectiveness of the proposed method is illustrated by conducting experiments on synthetic as well as on real satellite images. Quantitative comparison of the proposed method in terms of ERGAS, Correlation Coefficient, RASE and SAM with the state of the art approaches indicates superiority of our approach.

8537-5, Session 2

Multitemporal evaluation of topographic correction algorithms using synthetic images

Ion Sola, María González-Audícana, Jesús Álvarez-Mozos, Jose Luís Torres, Univ. Pública de Navarra (Spain)

Land cover classification and quantitative analysis of multispectral data in mountainous regions is considerably hampered by topographic effects on the spectral response pattern. In the last years different topographic correction (TOC) algorithms have been proposed to correct the illumination differences between sunny and shaded areas observed by optical remote sensors.

Although the available number of TOC methods is high, the evaluation of their performance usually relies on the existence of precise land cover information, and a standardised and objective evaluation procedure has not been proposed yet. Besides, previous TOC assessment studies only considered a limited set of illumination conditions, commonly images taken under favourable illumination conditions.

This paper presents a rigorous, objective and accurate procedure to assess the accuracy of these TOC methods based on a variety of synthetically generated images. These images represent the radiance an optical sensor would receive under specific geometric and temporal acquisition conditions and assuming a certain land-cover type, and they are generated considering different periods of the year, which entails a variety of solar angles, in order to assess the performance of TOC methods under different scenarios considering topographic, geometrical and temporal acquisition conditions.

A method for creating synthetic images using state-of-the-art irradiance models has been proposed, considering the real topography of a specific area (Synthetic Real image, SR) or considering the relief of this area as being completely flat (Synthetic Horizontal image, SH). The comparison between the corrected image obtained applying a TOC method to a SR image and the SH image of the same area, considered the ideal correction, allows assessing the performance of each TOC algorithm. This performance of TOC is quantitatively measured through the widely accepted Structural Similarity Index (SSIM) proposed by Wang et al.

This approach has been applied to a set of six synthetic scenes generated over a mountainous area (Pyrenees) of the North-Eastern side of Navarre, Spain, for different dates between February and December 2009.

The most frequently used topographic normalization methods have been tested in this work. Among them, Statistic-Empirical correction, proposed by Teillet et al., has ranked first, giving satisfying results in the majority of the cases, while other algorithms show a good performance in summer but give worse results in winter, when images are taken under poor illumination conditions. On the contrary, it can be observed that the simplest method tested, the Cosine correction, gives clearly poorer results than some of the other methods, especially in winter images. In the future this approach could be used to analyse the influence of land-cover spatial variability on the performance of TOC algorithms and also the influence of sensor configuration.

8537-6, Session 2

An automated method for relative radiometric correction performed through spectral library based classification and comparison

Ciro D'Elia, Simona Ruscino, Univ. degli Studi di Cassino e del Lazio Meridionale (Italy)

In this paper we propose a method to perform automated radiometric correction of remotely sensed multispectralhyperspectral images. Indeed, as noticed, when the earth's surface backscatters the incident solar radiation, not the whole reflected energy reaches the satellite's sensors, but part of it is absorbed by the atmosphere, which in effect behaves as a selective filter at different wavelengths. The effects of atmosphere, as well as the calibration errors which the satellite sensors may present, may be compensated by performing the radiometric correction operation in order to achieve good performances in different applications, such as classification and change detection. As far as the change detection is concerned, relative radiometric correction is particularly interesting since it deals with images which have to be compared and since in this context an absolute correction may be characterized by a high complexity. In previous works [1],[2] we have proposed a change detection algorithm which can be implemented in both pixel-based and data mining object-based contexts. In this case, we performed radiometric correction of multispectral images by using a least-square approach: considering one image as the reference one and the other as a linearly scaled version of the reference one, the linear coefficients can be calculated by using a set of control points conveniently chosen. Unfortunately, the choice of control points is a tricky operation, strictly connected to the specific application. In [1] and [2] these points were chosen depending on their level of change, i.e. pixels or objects belonging to the unchanged areas were good candidates for the control subset of points. However different methods can be used: for instance, in [3] control points are chosen by using a correlation procedure performed on sliding windows of 21x21 pixels. In this paper we propose an automated method for performing relative radiometric correction of multispectral remotely sensed images, in which the choice of the control points is based on a comparison of the spectral content of those images to the spectral response of known materials. In order to do this we used the spectral library kindly offered by USGS Spectroscopy Lab [4]. Specifically, we perform a vector quantization of the images separately, considering N quantization levels represented by N known materials' signatures properly selected. Then the quantized images are compared in order to identify the areas classified as belonging to the same class, so identified by the same quantization index which will make the subset of control points that should be used for performing relative radiometric correction. Experimental results showed that choosing points characterized by an homogeneous spectral content for radiometric correction improves the performances of specific image processing algorithms, such as change detection and classification algorithms.

8537-7, Session 2

A linear approach for radiometric calibration of full-waveform Lidar data

Andreas Roncat, Norbert Pfeifer, Technische Univ. Wien (Austria); Christian Briese, Technische Univ. Wien (Austria) and Ludwig Boltzmann Institute for Archaeological Prospection and Virtual Archaeology (Austria)

During the past decade, small-footprint airborne full-waveform lidar systems have become increasingly available. The primary output of these systems is high-resolution topographic information in the form of three-dimensional point clouds over large areas. However, recording the temporal profile of the transmitted laser pulse and of its echoes enables to detect more echoes per emitted pulse than in the case of discrete-return lidar systems, resulting in a higher point density over complex terrain. Furthermore, full-waveform instruments also allow for retrieving radiometric information of the scanned surfaces, commonly as an amplitude value and an echo width stored together with the 3D coordinates of the single points. However, the radiometric information needs to be calibrated in order to combine datasets acquired at different altitudes and/or with different instruments, so that the radiometric information becomes an object property independent of the flight mission and instrument properties.

State-of-the-art radiometric calibration techniques for full-waveform lidar data are based on Gaussian Decomposition to overcome the ill-posedness of the inherent inversion problem, i.e. deconvolution. However, these approaches make strong assumptions on the temporal profile of the transmitted laser pulse and the physical properties of the scanned surfaces, represented by the differential backscatter cross-section. In this paper, we present a novel approach for radiometric calibration using uniform B-splines. This kind of functions is of widespread use in industrial geometry and computer-aided design. Uniform B-splines can be constructed by recursive convolution which allows for linear inversion without constraining the temporal shape of the modeled signals. The theoretical derivation and error analysis are illustrated by examples recorded with a Riegl LMS-Q560 and an Optech ALTM 3100 system, respectively.

8537-8, Session 2

Spectral discrimination based on the optimal informative parts of the spectrum

Seyed Enayat Hosseini Aria, Massimo Menenti, Ben Gorte, Technische Univ. Delft (Netherlands)

Developments in sensors technology boost information content of imagery collected by space- and airborne hyperspectral sensors. Unfortunately, the increasing number of bands causes data dimensionality to raise the processing issues. On the other hand, narrow bands next to each other may be highly correlated, which leads to data redundancy. Moreover, the correlated bands may change from one scene to another. This paper shows a newly developed method to identify the most informative spectral regions of the spectrum with the minimum correlation with each other, and evaluates the land cover classes separability on the given scenes using the constructed spectral bands.

This method, applied to hyperspectral datasets, identifies the most informative parts of the spectrum between 400 and 2500 nm based on Shannon's information theory. This theory expresses implicitly that by having more independent data, information content is increasing. So, in the splitting method we have tried to find the spectral regions which have less dependency. Hence, based on the information theory, the method finds the regions of the spectrum which have the minimum relation with other regions to maximize the information content with the minimum number of bands.

In this method, named Spectral Region Splitting (SRS), one starts with a single very wide spectral band covering the complete measured spectral range. Then this wide band is split in two parts. The optimum location of the split is determined by measuring the correlation of the new bands, and by selecting that location where this is minimum. The splitting continues recursively until reconstruction of the full reflectance spectrum using the selected bands is possible with 99% accuracy. In this process, contiguous and correlated narrow bands may be selected at different stages of the procedure, which does not give much additional information. Therefore, the correlation between them was also re-evaluated at the end of the first selection and highly correlated bands were eliminated.

This SRS method was applied to hyperspectral scenes with different land cover, acquired by AVIRIS with 220 bands. These scenes include vegetation, bare soil, and different types of water; and each area led to a specific set of bands with different widths showing the most informative parts of the spectrum with the required accuracy. For example in a vegetated scene, SRS selected just one narrow band at the red edge (694-704 nm), which is most sensitive to pigment concentration in most leaves and canopies. In addition, the near infrared plateau, where the reflectance is higher than in the other regions of the spectral range in the vegetated area, is also selected as a very wide band by the SRS method. It seems these regions are very significant to increase the potential for correct classification of vegetation types (Fig.1).

After the selection of most informative bands by SRS in different scenes, the separability distance in spectral space of different classes was investigated, using Transfer Divergence (TD) and Jeffries-Matusita (JM) distance measures. The potential of accurate classification of land cover types using hyperspectral remote sensing is predicted by these distance measures.

8537-9, Session 2

A stripe noise removal method of interference hyperspectral imagery based on interferogram correction

Chuanrong Li, Chuncheng Zhou, Lingling Ma, Lingli Tang, Xinhong Wang, The Academy of Opto-Electronics (China)

An Spatially Modulated Fourier Transform Hyperspectral Imager (named HSI) aboard on the Chinese Huan Jing-1A (HJ-1A) satellite has a spectral coverage of 0.459-0.956?m with 115 spectral bands. In practical, periodical and directional stripe noise was found distributing in the HSI imagery, especially at the first twenty shortwave bands. To fully utilize all information contained in hyperspectral images, it is demanded to eliminate the stripe noise. This paper presents a new method to deal with this problem.

Firstly, possible sources of HSI stripe noise are analyzed based on interference imaging mechanism. Traditional noises, e.g. device position changes due to launch, non-uniformity in the instrument itself and aging degradations, are directly recorded at the focal plane array and thereafter in the interferogram. After inverse Fourier transform exerted on the interferogram, the spatial dimension of the interference hyperspectral image is restored with complicated and untraceable stripe noises. Therefore traditional image processing methods based on spectral image will not be effective for removing the HSI stripe noise. In order to eliminate this effect, a stripe noise removal method based on interferogram correction is necessary.

Then, the implementation process of the interferogram correction method is presented, which mainly contains three steps: 1) Establish relative radiometric correction model of the interferogram based on relatively homogeneous ground scenes as much as possible; 2) Correct the response inconsistency of CCD array by carrying out relative radiometric correction on the interferogram; 3) Convert the corrected interferogram to obtain the revised hyperspectral images. An experiment is conducted and the new method is compared with several traditional methods. The results show that the stripe noise of HSI image can be more effectively removed by the proposed method, and meanwhile the texture detail of original image and the correlation among different bands are finely reserved.

Reference:

[1] Bin Xiangli, Zhonghou Wang, Xuebin Liu, Yan Yuan, Zhongying Ji, and Qunbo Lv. "Spatially Modulated Fourier Transform Hyperspectral imager for HJ-1A Satellite". Spacecraft Engineering, 2009. vol. 18(6), pp. 43-49.

[2] Juanjuan Jing, Bin Xaingli, Qunbo Lv, Min Huang, and Jinsong Zhou. "Advance in Interferogram Data Processing Technique". Spectroscopy and Spectral Analysis, 2011. vol. 31(4), pp. 865-870.

[3] Lele Yao, Wei Zhao, and Shiming Fan. "Study on On-orbit Data Relative Radiometric Calibration of Hyper-spectral Imager on HJ-1A Satellite". Spacecraft Engineering, 2009. vol. 18(2), pp. 42-47.

[4] M. P. Dierking, and M. A. Karim. "Solid-block stationary Fourier-transform spectormeter". Applied Optics. 1996, vol. 35 (1): 84-89.

[5] L. Mertz. "Auxiliary computation for Fourier spectrometry". Infrared Physics. 1967, vol. 7 (1): 17-23.

[6] M. L. Forman. "Correction of Asymmetric Interferograms Obtained in Fourier Spectroscopy". Journal of The Optical Society America. 1966, vol. 56 (1): 59-63.

[7] G. Corsini, M. Diani, and T. Walzel. "Striping Removal in MOS-B Data". IEEE Transactions on Geoscience and Remote Sensing. 2000, vol. 38 (3): 1439-1446.

[8] Jinsong Chen, Yun Shao, and Boqin Zhu. "Destriping in CMODIS Data by A Improved Moment Matching". Remote Sensing Technology and Application. 2003, vol. 18 (5): 313-316.

8537-10, Session 3

Active contours with edges: combining hyperspectral and grayscale segmentation

Alex Chen, University of North Carolina, Chapel Hill (United States)

The problem of classification in hyperspectral imagery has an extensive background. Much of this literature focuses on the large amount of spectral information available in each pixel. One drawback of hyperspectral data, however, is that the spatial resolution of the data is often lower than the spatial resolution typically used with

grayscale or color imagery. Thus, many approaches to classification make little use of spatial information.

In this work, we treat the image segmentation problem by using a high spatial resolution grayscale image and a high spectral, but low spatial resolution hyperspectral image. This result can then further be used to register the two data sets.

First, we use a modified Chan-Vese segmentation algorithm (Chen 2012). A multiple level set approach is used to segment the image into N classes, each with a representative spectral signature.

This segmentation uses a normalized L^2 distance, which more accurately characterizes hyperspectral data. Furthermore, spatial information is utilized by balancing the length of the total boundary. For the second step, we introduce a novel segmentation algorithm on the two images, adjusting the segmentation result from the first part. The addition of an edge detector on the grayscale image drives the segmentation result toward high gradients in the grayscale image, which has more finely resolved edges and is more accurate in space.

While the original Chan-Vese segmentation algorithm did not make use of a edge detector, other works have incorporated the edge detector for faster convergence. In this case, an edge detector is not used for the hyperspectral data due to the imperfect knowledge of edge locations and inaccuracy with the georegistration process. In other words, the segmentation algorithm trusts the spectral information from the hyperspectral image and trusts the spatial/edge information from the grayscale image.

This second segmentation result differs from the first only slightly. By placing a small weight on the edge detector term, the second segmentation is kept close to the first. The slight differences, however, are significant in that the segmentation is much more accurate than can be obtained with either data set alone.

The set of algorithms is also efficient since the first algorithm is run on low spatial resolution data, while the second algorithm does not need to be run for many iterations.

Since dual segmentation results are obtained, they can be compared to register interesting features. The registration of these two data sets is of particular relevance for the image fusion problem, in which a high resolution grayscale image and a low resolution hyperspectral image are fused to create a high spatial resolution hyperspectral image.

Image fusion requires that the hyperspectral image and panchromatic image are co-registered to lie in the same spatial domain. However, the registration process is often imperfect, resulting in slight differences between the locations of objects. In fact, many image fusion results show significant blurring of spectral signatures near edges. Thus, the segmentation algorithm not only gives a more accurate segmentation result, but also has interesting applications to registration and image fusion.

8537-11, Session 3

A modular image processing chain for feature extraction from multispectral satellite images

Marc Wieland, Massimiliano Pittore, Helmholtz-Zentrum Potsdam Deutsches GeoForschungsZentrum GFZ (Germany)

Following an object-based approach to image analysis we propose an automated image processing chain to extract objects of interest from high resolution multi-spectral satellite images. The processing chain is based on open-source solutions and consists of several modules including image segmentation, segmentation optimization and evaluation, feature selection and machine learning based classification. An automated extraction of detailed built-up masks from Quickbird and WorldView-2 images is presented to illustrate the approach.

In an initial processing stage an efficient graph-based image segmentation algorithm is deployed and combined with a specifically developed multi-scale optimization and evaluation procedure. The optimization procedure iteratively merges a hierarchical set of segmentations into a single multi-scale segmentation based on the mean percentage difference of the weighted brightness values between sub-segments and super-segments. A supervised evaluation of segmentation qualities is used to quantitatively select segmentation parameters and optimization thresholds. The multi-scale segmentation procedure is able to reduce over- and under-segmentation as well as the number of segments needed to describe the desired objects of interest appearing at different scales within the same image. It can therefore provide with an improved input for further object-based image analysis steps. In the proposed work the segmentation is trimmed to optimize the delineation of building footprints.

A Support Vector Machines (SVM) statistical learning algorithm is deployed to label the delineated segments according to their landuse/landcover. The input feature vector used to describe the segments is composed of spectral, textural and geometrical features. To reduce the dimensionality of the feature space a systematic and quantitative feature selection is carried out using a ReliefF algorithm. The SVM model is trained on a pan-sharpened Quickbird image with an extensive set of training samples for five urban landuse/landcover classes (building, other sealed surface, bare soil, vegetation, shadow). SVM parameters are selected during the training phase using a k-fold cross-validation, where training samples are randomly split into ten-fold subsets and one subset is used to train the model while the others form the test samples. An optimal SVM parameter selection is reached when the cross-validation estimate of the test samples error is minimal. The trained SVM model is applied to each segment of the full Quickbird image to automatically derive a landuse/landcover classification. In a post-classification stage segments labelled as building are extracted from the five class output and are subjected to a connected components analysis to derive a detailed binary built-up mask.

The proposed processing chain has been applied to a Quickbird image of Bishkek, Kyrgyzstan resulting in a built-up mask that proves to be highly accurate with an overall accuracy of 90.24% and a kappa value of 0.65. Due to its flexible modular structure and the use of statistical learning the developed procedure can be easily applied to different objects of interest and image types. Besides the Bishkek test case an application of the procedure to a WorldView-2 image scene will be presented. All modules are developed on an open-source basis and are currently being implemented into a plugin to the open-source software QGIS to allow for a high degree of transparency and usability.

8537-12, Session 3

Automatic segmentation of textures on a database of remote-sensing images and classification by neural network

Philippe Durand, Conservatoire National des Arts Métiers (France); Dariush Ghorbanzdeh, Conservatoire National des Arts et Métiers (France); Luan Jaupi, Conservatoire National des Arts et Metiers (France)

Analysis and automatic segmentation of texture is always a delicate problem. Objectively, one can opt, quite naturally, for a statistical approach.

These techniques very reliable mathematically based study of higher order moment is very accurate but very expensive experimentally.

We propose in this paper, a well-proven approach for texture analysis in remote sensing, based on morphological and geostatistics. The labeling of different textures like ice, clouds, water, forest on a sample test image is then learned by a neural network. The texture parameters are extracted from the shape of the autocorrelation function, calculated on the appropriate window sizes for the optimal characterization of textures. a mathematical model from fractal geometry is particularly well suited to the characterization of the cloud texture. It provides a very fine segmentation between the texture and the cloud from the ice. The geostatistical parameters are entered as a vector of size ten entries individualized by characterizing the textures. A neural network and robust multilayer is then asked to rank all the images in the database from a training set correctly selected. In the design phase, several alternatives were considered and it turns out that a network has three layers is very suitable for the proposed classification. It therefore contains a layer of input neurons, an intermediate layer and a layer of output. With the coming of the learning phase the results of the classifications are very good. This approach can within a geographic information system, bringing precious information. such as the exploitation of the cloud texture (or disposal) if we want to focus on other thematic deforestation, changes in the ice...

The best results were obtained for a network with $10-10-10$ a success rate of 75 %. This gives good results after a relatively short computation time when the hidden layer has between 5 and 20 neurons.

The results on test images are exactly those desired. The success rate limited to 75 % is explained by the fact that the corrected was very rough and it was set to a window $32 times 32$. Had we obtained a success rate of 100%, It would meant that our system was not working. The interest of the backpropagation algorithm, it is also

possible to reject a high error rate in the fixed. The system reacts properly on unlearned. He sometimes combine multiple textures to a particular window where the texture does AVAT not been defined. His answer is always relevant to their learning.

Classification can be considered correct. We obtain a very thin separation between different textures. many images has not been learned. The boundaries between textures are observed and two textures are labeled correctly: The ice and rocks. On the board 4 we see that the noisy ice by cloud cover is well separated from the ice first, water second. The tools developed should permit the expert to properly assess the rate of cloud cover in SPOT images

8537-13, Session 3

Improved boundary tracking by off-boundary detection

Alex Chen, University of North Carolina, Chapel Hill (United States)

Chen et al. 2011 introduced a boundary tracking method that was particularly useful for the analysis of hyperspectral data. Due to its large size, the processing of hyperspectral data can be very computationally expensive. With new sensors that are able to capture both high spatial and high spectral resolution data, efficient methods for boundary and edge detection become even more important.

By only sampling points near the boundary of an object, the boundary tracking algorithm is able to detect object boundaries with a high degree of precision. For the fractal-like coastlines especially prevalent in hyperspectral data, high precision tracking allows the detection of coastal features in great detail.

A significant drawback to boundary tracking in comparison with more traditional image segmentation algorithms, however, is its relatively weak performance in the presence of noise or textures. As a local algorithm, it is particularly sensitive to patches of noise, which can lead the tracker astray. Once off of the boundary, only a chance movement back toward the boundary allows the boundary to be tracked again.

One improvement is the use of a change-point detection algorithm such as Page's CUSUM algorithm to ``average'' noise. Weighted intensities along the path of the tracker are summed, and a boundary detection is assigned only when a certain threshold of this statistic is reached. This adaptation significantly improves tracking in noisy and textured data. However, the problem of off-boundary movement still remains.

In this work, we introduce a second CUSUM statistic to track the characteristic behavior of off-boundary movement. Qualitatively, movement along a boundary should consist of alternating values characteristic of both sides of the boundary. On the other hand, movement away from the boundary consists of values primarily from only one region.

To this end, we employ a two-sided CUSUM test of the likelihood ratio of the density functions between the two regions. If estimates for the density functions are unknown, they can be estimated from samples. The null hypothesis corresponds to a mean value of 0, indicating movement along the boundary. The alternative hypothesis is that either an increase or decrease in the mean occurs.

Once off-boundary movement is detected via the CUSUM test, a backtracking procedure is used to move to the last detected boundary point. Fortunately, the CUSUM test also provides a good estimate for the detection delay in off-boundary movement. Experimentally, it was found that slight perturbations in the position and trajectory vectors result in new paths that may ultimately track the boundary through the problem areas.

One of the most significant applications for boundary tracking is high dimensional or high resolution data such as hyperspectral images. By sampling only along a path, boundary tracking gives a fast method to detect the boundaries of an object. Numerical experiments show that the use of the two-sided CUSUM test for off-boundary movement and backtracking results in fewer tracking failures. This mitigates the most significant weakness in boundary tracking.

8537-14, Session 3

Extending the fractional order Darwinian particle swarm optimization to segmentation of hyperspectral images

Pedram Ghamisi, University of Iceland (Iceland); Micael S. Couceiro, Univ. de Coimbra (Portugal); Jon Atli Benediktsson, The Univ. of Iceland (Iceland)

Hyperspectral remote sensing allows capturing images using a wide range of spectra from ultraviolet to visible to infrared. These hyperspectral images can be used, for instance, to detect and identify objects such as surface minerals or buildings employing image segmentation techniques. However, due to the high dimensional complexity of hyperspectral data, it is difficult to create accurate image segmentation algorithms for hyperspectral imagery. Image segmentation is defined as the process of dividing an image into disjoint homogenous regions and it could be regarded as the fundamental step in various image processing applications. There are a few methods for image segmentation such as texture analysis based, histogram thresholding based, clustering based and region based split and merging methods. One of the most famous methods for image segmentation is thresholding method, which is commonly used for segmentation of an image into two or more clusters. One way for finding the optimal set of thresholds is the exhaustive search method. The exhaustive search method based on the Otsu criterion is simple, but it has a disadvantage that it is computationally expensive. Exhaustive search for n - 1 optimal thresholds involves fitness evaluation of n(L-n+1)n-1 combinations of thresholds, so this method is not suitable from the computational cost's point of view. The task of determining n - 1 optimal thresholds for n-level image thresholding could be formulated as a multidimensional optimization problem. For this purpose, each solution is formed as Population(i) = {t1, t2 ,... , tn} where t is the threshold value. PSO-based method can be considered as one of the most significant methods in the field of image thresholding based segmentation. However, a general problem with the PSO and other optimization algorithms is that of becoming trapped in a local optimum such that it may work well on one problem but may fail on another problem.

In this paper, a novel multilevel thresholding segmentation method is proposed for grouping the pixels of hyperspectral images into different homogenous regions. The new method is based on Fractional-Order Darwinian Particle Swarm Optimization (FODPSO) which is used for finding the optimal set of threshold values and uses many swarms of test solutions which may exist at any time. In the FODPSO, each swarm individually performs just like an ordinary PSO algorithm with rules governing the collection of swarms that are designed to simulate natural selection. Moreover, the concept of fractional derivative is used to control the convergence rate of particles. In a previous work, the FODPSO was successfully compared to other PSO variants using benchmark optimization functions, thus presenting a superior performance in both speed and solution. As a result, using many swarms at the same time and fractional calculus to control the convergence rate of swarms suggest the successful use of the FODPSO algorithm in image segmentation problems.

Experimental results compare the FODPSO with the classical PSO within multi-level segmentation problems in hyperspectral images from different points of view such as CPU time, optimal threshold value and corresponding fitness value. Results indicate that FODPSO is more robust than PSO and has a higher potential for finding the optimal set of thresholds with more between-class variance in less computational time, especially for higher segmentation levels and for images with a wide variety of intensities. Results indicate that the FODPSO based method improves the PSO based segmentation method in fitness value and CPU process time points of view by 11.63 percent and 84.40 percent respectively.

8537-15, Session 4

Target attribute-based false alarm rejection in small infrared target detection

Sungho Kim, Yeungnam Univ. (Korea, Republic of)

The main objective of infrared search and track (IRST) system is to detect distant infrared targets as quickly as possible for ship defense. Previous spatial filters can detect small infrared targets very well. However, they also produces a lot of false alarms around cloud and ground clutter. In this paper, we present a novel method of false alarm rejection method based on target attribute and machine

learning approach. First, a set of target attribute features is extracted from intensity distribution and segmented region. According to the database inspection, small infrared targets has Gaussian intensity distributions and circularly symmetric region. From these findings, we can extract eight kinds of target attribute features. Then an optimal classifier is learned using machine learning by adaboost. Target chips and false alarm chips are automatically generated from a real infrared dataset using well-designed spatial detector. Adaboost learns weak classifiers by maximizing classification rate for a training set. Experimental results on a set of test set and test sequences validate the robustness and usefulness of the proposed false alarm rejection method.

8537-17, Session 4

Computationally efficient strategies to perform anomaly detection in hyperspectral images

Alessandro Rossi, Univ. di Pisa (Italy); Nicola Acito, Accademia Navale di Livorno (Italy); Marco Diani, Giovanni Corsini, Univ. di Pisa (Italy)

In the field of remote sensing, hyperspectral imagers are employed in both civilian and military applications to accomplish target detection and recognition on the basis of their capability to determine the spectral signature of the materials observed within a scene. Spectral signatures characterize materials in a unique manner thus allowing the discrimination and leading to two major applications: target classification and target detection. When no a priori information about the spectrum of the targets of interest is provided, the task of target detection turns into anomaly detection (AD). The goal of AD is to find objects in the image that are anomalous with respect to the background, i.e., observations that deviate from the background clutter spectral distribution.

In an operational scenario, potential anomalies are first detected by means of moderate resolution hyperspectral imaging sensors that examine wide areas and search for anomalies that are subsequently classified and identified employing an additional higher resolution imager. In many applications, the task of AD has to be performed in real-time to quickly furnish information to the operator responsible of the decision process. In this context, an emerging field of research in the design of anomaly detection algorithms for hyperspectral images consists of finding out strategies to reduce the computational load in order to assure real-time, or nearly real-time, in-flight processing.

In this work, a sub-class of AD algorithms is considered, i.e. those algorithms aimed at detecting small rare objects that are anomalous with respect to their local background. This local approach allows the design of real-time strategies that at the same time acquire data and process them for anomaly detection. Among such techniques, one of the most-established AD techniques is the RX algorithm which is based on a local Gaussian model for background and computes local estimates of its parameters from the pixels within a window around the pixel under test.

In the previous literature, the RX decision rule has been employed to develop computationally efficient algorithms tested in real-time operating systems. Initially, a recursive block-based parameter estimation procedure was adopted that makes the RX processing and the detection performances differ from those of original RX. More recently, an update strategy has been proposed which relies on a line-by-line processing without altering the RX performance.

In this work, a survey of computationally efficient methods to implement the RX detector is presented focusing on the line-by-line and the recursive block-based approaches, both improved with algebraic strategies to speed up the estimation of the covariance matrix for the computation of the RX statistic. The analysis has been carried out showing the advantages and the limitations of each examined configuration. A real hyperspectral image of a scene with deployed targets has been employed to perform a comparison in terms of both computational load and anomaly detection performances related to the different analyzed strategies to perform the RX algorithm.

8537-18, Session 4

Concentration measurements of complex mixtures of broadband absorbers by widely tunable optical parametric oscillator laser spectroscopy

Keith Ruxton, M Sqaured Lasers Ltd. (United Kingdom); Neil Macleod, Damien Weidmann, Rutherford Appleton Lab. (United Kingdom); Graeme P. A. Malcolm, Gareth T. Maker, M Squared Lasers Ltd. (United Kingdom)

The ability to obtain accurate vapour parameter information from a compound's absorption spectrum is an essential data processing application in order to quantify the presence of an absorber. Concentration measurements can be required for a variety of applications including environmental monitoring, pipeline leak detection, surface contamination and breath analysis. These applications target the strong fundamental absorption bands in the mid-infrared (MIR) region present in the majority of volatile organic compounds (VOCs). Absorption features are present in this region due to stretching vibrations of oxygen-hydrogen (O-H), carbon-hydrogen (C-H), nitrogen-hydrogen (N-H) and carbon-nitrogen (C-N) bonds. The vapour-phase absorption spectrum may be a combination of different vibrations depending on what organic functional groups are present.

This work demonstrates sensitive concentration measurements of complex mixtures of VOCs using broadly tunable MIR laser spectroscopy. Due to the high absorption cross-sections, the MIR spectral region is ideal to carry out sensitive concentration measurements of VOCs by tunable laser absorption spectroscopy (TLAS) methods. However, when a complex mixture of VOCs with additional interfering species (e.g. water) is probed by TLAS, spectral band overlap can result in a complicated spectrum, from which retrieval of accurate, unambiguous, individual concentration information becomes challenging.

Absorption spectra of mixtures of VOCs were recorded using a MIR optical parametric oscillator (OPO), with a tuning range covering 2.5 µm to 3.7 µm. The output of the MIR OPO was coupled to a multi-pass astigmatic Herriott gas cell that can provide up to 200 m of absorption pathlength, with the cell laser transmission output being monitored by a detector. The resulting spectra were processed by a concentration retrieval algorithm derived from the optimum estimation method, taking into account both multiple broadband absorbers and interfering molecules that exhibit narrow multi-line absorption features.

In order to assess the quality of the concentration measurements and assess the capability of the spectral processor, experiments were conducted on calibrated VOCs vapour mixtures flowing through the spectroscopic cell. Custom-built permeation sources were characterised through gravimetric calibration, and installed in a gas generator to produce concentrations of VOCs ranging from parts per billion (ppb) to parts per million (ppm) within a nitrogen carrier gas.

Validation of the spectral processor offers interesting prospects for the detection of complex broadband absorbers mixtures, either by in-situ or remote-sensing methods. The authors consider this work as a first step in an effort to develop and apply a similar concentration fitting algorithm to hyperspectral images in order to provide concentration maps of the spatial distribution of multi-species vapours. Adapting the algorithm for the analysis of hyperspectral images requires additional optimisation and performance tests. Since the algorithm is applied to each individual pixel, the hyperspectral cube size dictates the level of computation required. The reported functionality of the novel fitting algorithm makes it a valuable addition to the existing data processing tools for parameter information recovery from recorded absorption data.

8537-19, Session 4

A regularization based method for spectral unmixing of imaging spectrometer data

Jignesh Bhatt, Manjunath Joshi, Mehul Raval, Dhirubhai Ambani Institute of Information and Communication Technology (India)

In spectral unmixing, the imaging spectrometer data is unmixed to yield underlying abundance maps of the constituent materials after extracting (estimating) their spectral signatures (endmembers). Under linear mixing model, we consider a supervised spectral unmixing wherein given the extracted endmembers, the task is to

estimate the abundances. This is a severe ill-posed problem, as the hyperspectral signatures are strongly correlated resulting in the ill-conditioned signature matrix which makes the constrained least squares estimation highly sensitive to the noise. Further, the acquired data often do not fully satisfy the simplex requirement imposed by the linearity, resulting in inaccurate extraction of endmembers. This in turn may lead to unstable solution in the subsequent estimation of abundances. In this paper, we adopt the regularization alternative to achieve stable solution by improving the conditioning of the problem. For this purpose, we propose to use Tikhonov regularization within the total least squares (TLS) estimation framework. The functional is formulated as a sum of the TLS as its data-term which takes care of the possible modeling errors and the Tikhonov prior which imposes the smoothness requirements. The resultant energy function being convex is minimized by gradient based optimization technique. The solution space is restricted to yield nonnegative abundances. The experiments are conducted for different levels of noise on the simulated data, and the results are compared with the state-of-art approaches; quantitatively using the different measures as well as perceptually. Finally the proposed approach is applied on the real AVIRIS data to obtain abundance maps of the constituent materials.

8537-20, Session 5

Application of MODIS NDVI time series data for land cover classification at European scale

Francesco Vuolo, Florian Gabas, Clement Atzberger, Univ. für Bodenkultur Wien (Austria)

This study investigates the potential of MODIS 250-m NDVI (16-day composites) time series and gridded (bio)climatic indicators to derive land cover (LC) maps at European scale. The approach involves the use of support vector machines (SVM) trained on reference samples obtained through visual interpretation of Google Earth (GE) high resolution imagery. Within the available training samples, a small set of suitable support vectors is identified using a random selection approach to optimize class separability. Based on this approach, a previous study indicated an overall accuracy of 73% (95% C.I.: 68%, 77%). with a large number of independent validation samples spread over three contrasting regions in Europe (Eastern Austria, Macedonia and Southern France).

This paper aims at confirming preliminary findings with a focus on seven additional test sites located in Portugal, Spain, Italy, France, Germany, Scotland and Norway. Classification accuracies are presented for the resulting SVM maps and three (globally available) reference land cover products: GLC2000 (1 km), MODIS LC (500 m) and GlobCover 2009 (300 m). Results confirm that the accuracy of areas where the three reference maps disagree can be notably improved. Results are discussed, in view of an operative LC mapping application with a focus on vegetation monitoring at Europe scale.

8537-21, Session 5

A novel active learning method for support vector regression to estimate biophysical parameters from remotely sensed images

Begüm Demir, Lorenzo Bruzzone, Univ. degli Studi di Trento (Italy)

This abstract presents a novel active learning (AL) technique for the estimation of biophysical parameters, i.e., tree stem diameter and volume, from remotely sensed images. The biophysical parameters can be obtained by supervised regression methods [1]. Such approaches require the availability of ground truth information in order to train the algorithm. However, the collection of labeled samples is time consuming and costly, and therefore to acquire a adequate number of labeled training samples is a difficult task in real applications. To deal with this problem, AL approaches have gained a significant interest in the RS literature particularly in the context of classification of RS images [2]. AL methods automatically select the most informative unlabeled samples to be manually labeled by a human expert in order to obtain a non-redundant and effective training set. However it is marginally considered in the RS community in the context of RS regression problems.

Here, we focus our attention on AL extending its use to the framework of RS regression problems. In greater detail, we propose a novel AL technique based on Support Vector Machine (SVM) for regression problems to estimate tree stem diameters and volume from multireturn light detection and ranging (LIDAR) data. The proposed AL method aims to select the most informative unlabeled samples by i) firstly eliminating the most certain samples (whose parameters have the highest probability to be correctly estimated by the considered regression model, and thus non-informative) from a pool of unlabeled samples, and ii) then choosing the most diverse unlabeled samples among the uncertain ones that present in the high density regions. The most certain unlabeled samples, which are most likely to be inside the tube of the SVM regression model, are found based on a clustering method. The basic assumption in the proposed method is that since the training samples that are not support vectors (i.e., non SVs) are inside the tube, the unlabeled samples that fall in the same clusters with non SVs are most probably lie in the tube as well. Accordingly, the kernel k-means clustering [2] is applied to both all unlabeled samples and the training samples that are non SVs, and thereafter clusters with non SVs are eliminated. Then, the density of the retained clusters is assessed in order to select the samples from high density regions to avoid choosing outliers. Density of each cluster is measured according to the ratio between the number of samples and the distance of the furthest two samples present in the cluster. To reduce the redundancy between the selected samples, only the medoid samples of the highest density clusters are chosen as the most informative ones to be added to the training set. Experimental results show the effectiveness of the proposed technique for the estimation of forest parameters from multireturn LIDAR data. These results will be presented in the full paper.

REFERENCES

[1]M. Dalponte, L. Bruzzone, and D. Gianelle, “A system for the estimation of single tree stem diameters and volume using multireturn LIDAR data,” IEEE Transactions on Geoscience and Remote Sensing, vol. 49, no. 7, pp. 2479-2490, 2011.

[2]B. Demir, C. Persello, and L. Bruzzone, “Batch mode active learning methods for the interactive classification of remote sensing images,” IEEE Transactions on Geoscience and Remote Sensing, vol. 49, no.3, pp. 1014-1031, 2011.

8537-22, Session 5

Reduction of training costs using active classification in fused hyperspectral and LiDAR data

Sebastian Wuttke, Hendrik Schilling, Wolfgang Middelmann, Fraunhofer-Institut für Optronik, Systemtechnik und Bildauswertung (Germany)

This paper presents a novel approach for reducing the training costs in classification with co-registered hyperspectral (HS) and Light Detection and Ranging (LiDAR) data using an Active Classification framework.

Fully automatic classification can be achieved by unsupervised learning, which is not suited for adjustment to specific classes. On the other hand, supervised classification with predefined classes needs a lot of training examples which need to be labeled with the ground truth, usually at a significant cost.

The concept of Active Classification alleviates these problems by reducing the number of examples needed for the training of the classification algorithm. Since no predefined classes are required, great flexibility is retained. The main difference to classical supervised machine learning approaches is the use of a selection strategy: only selected samples are ground truth labeled and used as training data. One common selection strategy is to incorporate the current state of the classification algorithm and choose the examples for which the expected information gain is maximized. In this paper the user is strongly involved in the active selection strategy. He is shown a visual representation of the remotely sensed area with additional aid in form of suggestions from the classification algorithm according to its current training state. Then he can define training samples to introduce new classes or further improve the accuracy of existing ones.

In the second step a conventional classification algorithm, in this case the k-NN algorithm, is trained using this data.

By alternating between these two steps the algorithm reaches high classification accuracy results with less training samples and therefore lower training costs. This principle is not constrained to one specific classification algorithm and there are multiple choices for the selection strategy. The proposed framework allows a simple change of these core elements.

The results further benefit from fusing the heterogeneous information of HS and LiDAR data within the classification algorithm. For this purpose, several HS features, such as Vegetation Indices, and LiDAR features, such as relative height and roughness, are extracted. This increases the separability between different classes and reduces the dimensionality of the HS data. Those features can be easily integrated in the Active Classification framework.

The practicability and performance of this framework is shown for the detection and separation of different kinds of vegetation, e.g. trees and grass in an urban area of Berlin. This area was chosen due to the strong mixture of trees, buildings and flat areas. The HS data was obtained in May 2011 by the SPECIM Aisa Eagle 2 sensor. The used binning provides 127 spectral channels with a resolution of 4.5 nm and 512 pixels across track with a ground resolution of approximately 1 m. LiDAR data was recorded in August 2011 with the Riegl LMS Q560. This sensor provides measurement rates of 240 kHz and a range accuracy of 20 mm.

8537-23, Session 5

Detection of built-up areas in ASTER and SAR images using conditional random fields

Benson K. Kenduiywo, Jomo Kenyatta Univ. of Agriculture and Technology (Kenya); Valentyn A. Tolpekin, Alfred Stein, International Institute for Geo-Information Science and Earth Observation (Netherlands)

The current increase in population has resulted in widespread spatial changes, particularly rapid development of built-up areas, in cities and its environs. Up-to-date spatial information is requisite for the effective management and mitigation of the effects of built-up area dynamics. Spectral heterogeneity in built-up areas, however, remains a challenge to existing classification methods. This study developed a method for detecting built-up areas from SAR and ASTER images using conditional random field (CRF) framework. CRF modelled context in form of spatial dependencies of both class labels and data in a statistical manner using class quantitative measures (features). A feature selection approach and a novel data dependent term of CRF was designed and used to classify blocks of merged pixels in a defined window size. Mean, standard deviation and variogram slope features were used to characterize training areas with slope describing spatial dependencies within blocks of a given class. CRF association potential was designed using support vector machines (SVM) Gaussian Radial Basis Function (RBF) kernel, which can handle redundant data with any form of distribution while inverse of transformed euclidean distance was used as a data dependent term of CRF interaction potential. The latter maintained stable accuracy when subjected to a range of small to large smoothness parameters using different image block sizes, while preserving class boundaries and aggregating similar labels during classification. This enforced a discontinuity data adaptive model that moderated smoothing given data evidence unlike MRF, which penalizes every dissimilar label indiscriminately. After several experiments 8?8 image blocks were used to detect built-up areas in Nairobi. The accuracy of detecting built-up areas using CRF exceeded that of markov random field (MRF), SVM and maximum likelihood classification (MLC) by 1.13%, 2.22% and 8.23% respectively. It also had the lowest false positives. The method illustrated that built-up areas increased by 98.9 hectares while 26.7 hectares were converted to non-built-up areas. Thus, it can be used to detect and monitor built-up area expansion; hence provide timely spatial information to urban planners and other relevant professionals.

8537-24, Session 5

A new approach to automatic road extraction from satellite images using boosted classifiers

Umut Cinar, Ersin Karaman, Ekin Gedik, Ugur Halici, Yasemin Yardimci, Middle East Technical Univ. (Turkey)

Automatic road extraction from electro-optic satellite images is studied in the remote sensing literature since road networks have great importance on effective decision making for navigation support, urban planning, map updating, emergency and military applications. In this study, a supervised method for automatic road detection based on spectral indices and structural properties is proposed. Adaboost learning algorithm is utilized for extracting road structures in the satellite image.

The current literature on automatic road extraction includes different approaches which benefit from basic image processing methods, frequency based methods, knowledge bases and segmentation. Most of the works present in the literature are also supervised methods which utilize the common spectral characteristics of roads as features. These approaches generally fail on different satellite images since spectral characteristics of roads tend to vary between satellites. EVI and NDVI are used for detecting vegetation in the satellite image and consistent among different type of satellite images. For roads, those indices are not discriminating as they are for vegetation extraction, but they guarantee similar valuation among different satellites. Therefore, instead of directly using spectral band reflection of roads, spectral indices are taken as features of the roads. However, those indices do not guarantee correct classification of road regions alone since different type of roads such as soil, concrete and asphalt also show different spectral characteristics which result in different index values. We also use discriminating structural properties of roads as features in this study. For this purpose, input images are segmented using Mean-Shift Algorithm. Each one of the resulting segments is scored according to their elongatedness properties. Each segment is also classified into eight classes regarding their orientation values and neighboring segments which belong to same class are favored in the scoring process. By this approach, similar oriented segments are evaluated together, ensuring the continuity of road network. The proposed method uses these spectral indices and structural features to train a strong classifier using the Adaboost (Adaptive Boosting) algorithm. Adaboost algorithm has good generalization properties which makes it an excellent candidate for extracting roads with varying spectral characteristics.

To demonstrate the performance of the proposed method, a total of 30 IKONOS and GEOEYE satellite images are used. Both satellites provide panchromatic and multispectral (Blue, Green, Red, Near Infrared) bands with different resolutions. For training of the classifier and tests, Ground Truth (GT) data are prepared manually for all images. It should be noted that the classifier is trained with GEOEYE and IKONOS images, to show the classifiers independency from the satellite type. The preliminary results are promising and final quantitative and visual results will be given in the final version of the paper.

8537-25, Session 6

Automatic registration of multimodal views on large aerial images

Anna Pelagotti, Istituto Nazionale di Ottica (Italy); Francesca Uccheddu, Univ. degli Studi di Firenze (Italy); Pasquale Ferrara, Istituto Nazionale di Ottica (Italy)

Remote sensing data are inherently multispectral. Views acquired in different bands need to be registered among each other in order to provide a meaningful data set to be further exploited.

In order to reliably relate remotely sensed images to terrain views, a further step is required. A depth image of the terrain surface may be used as reference image to combine all data coherently, like in Geographic Information System (GIS) programs.

This last phase deals with images with very different content, and possible geometrical relative deformations.

When “a priori data” are available, this procedure is easly performed. When instead this information is missing, an a posteriori registration is needed, capable of coping with such different data.

Automatic techniques are to be preferred since they are not subjective and can be applied to big image data sets.

Cross Correlation (CC) methods are widely used to register remotely sensed multispectral images, however they are known to be content-dependent and are not readly appliable to multimodal image sets.

Scale-invariant feature (SIFT) transform algorithms can help to find similar features between two images, but if such images come from different sensors or are synthetically generated this approach does not always work.

Maximization of Mutual Information (MMI) methods proved to be highly reliable even when the shared content is low, like in case of terrain maps and Lidar images, or multispectral image sets acquired at different times or with different devices. However MMI methods are computationally expensive. When a complex model, like an affine model is cosidered for the relative deformation, and an exhaustive search is performed over large ranges for each parameter of the set,

the number of required operations grows rapidly.

In this paper a new automatic method capable of registering multimodal images like terrain maps and multispectral data is presented. The method exploits a multiresolution approach with adaptive strategy to select the similarity measure to be applied.

In order to fully exploit the possibilies offered by the various similarity measures, a thorogh study of their performance on images of different resolution and size has been evaluated and is described.

The adaptive strategy is designed to make use of the strenghts and overcome the limitations of the criterions considered.

At low resolution and with small image size, MMI proved to be underperforming, while CC is giving reliable results; on the other hand, at higher resolution and with large data set, CC is prone to fail, while MMI is accurate.

This information lead us to design the algorithm so that at the lowest resolution step CC is applied to downsampled images. Its relatively low computational cost makes it possibile to explore large ranges for the affine parameter search. At higher resolution the MMI criterion is avandageously used over a limited range search, thus reducing the overall algorithm complexity.

8537-26, Session 6

Unsupervised mis-registration noise estimation in multi-temporal hyperspectral images

Salvatore Resta, Univ. di Pisa (Italy); Nicola Acito, Accademia Navale di Livorno (Italy); Marco Diani, Giovanni Corsini, Univ. di Pisa (Italy)

Hyperspectral remote sensing is a promising approach to detect changes occurred in multitemporal images collected from airborne platforms. In this work, we focus on the Anomalous Change Detection (ACD) problem, whose goal is the detection of small changes occurred between two images of the same scene. When data are collected by airborne platforms, perfect registration between images is very difficult to achieve, and therefore a residual mis-registration (RMR) error should be taken into account in developing ACD techniques. The RMR can be viewed as a per pixel shift in both the directions of the image coordinate system, whose magnitude is typically in the order of few pixels. Recently, the Local Co-Registration Adjustment (LCRA) approach has been proposed to deal with the performance reduction due to the RMR, providing excellent performance in ACD tasks. The LCRA approach employs a spatial “uncertainty window” (UW) whose size in both the spatial directions has to be chosen in accordance with the magnitude of the RMR. Unfortunately, the estimation of the RMR magnitude is actually an open issue, and therefore the ACD task has to be accomplished for different size of the UW. As a consequence, the computational load strongly increases and the detection output is not unique.

In this paper we propose a novel method that allows the characterization of the first and second order statistics of the RMR, permitting to precisely define the UW size in the LCRA approach. Moreover, depending on the specific distribution of the RMR, the estimates provided by the proposed method allow directional UWs with different size to be designed. The technique is based on a sequential strategy that exploits the well known Scale Invariant Feature Transform (SIFT) algorithm cascaded with the Minimum Covariance Determinant (MCD) algorithm. The SIFT procedure was originally developed to work on gray level images. The proposed method adapts the SIFT procedure to hyperspectral images so as to exploit the complementary information content of the numerous spectral channels, further improving the robustness of the outliers filtering by means of a highly robust estimator of multivariate location. The RMR is modelled as a unimodal bivariate random variable whose mean value and covariance matrix have to be estimated from the data. Such estimates are obtained from the coordinates of the key-points extracted by the SIFT algorithm, after properly filtering the false matches between couples of descriptors which do not belong to the same spatial feature. In order to assess the performance of the proposed method, an experimental analysis has been carried out on different real hyperspectral datasets with very high spatial resolution. We assumed as a benchmark the RMR statistics obtained by means of a supervised technique aimed at selecting couples of corresponding pixels in the image pair. The comparison between the benchmark and the estimated RMR highlighted the effectiveness of the proposed approach, providing reliable and very accurate estimation of the RMR statistics, indeed resulting in a consistent improvement of the ACD algorithms performance.

8537-27, Session 6

Short-term change detection for UAV video

Günter Saur, Wolfgang Krüger, Fraunhofer-Institut für Optronik, Systemtechnik und Bildauswertung (Germany)

The change detection of e.g. parking cars is a task of short time scale, i. e. the observations are taken in time distances from several minutes up to few hours. Each observation is a short video sequence corresponding to the near-nadir overflight of the UAV over the interesting area. We distinguish this task from video motion detection (shorter time scale) and from long term change detection, e.g. based on time series of still images for several days up to years.

As a prerequisite, a precise image-to-image registration is needed. According to the interesting scenes, the images are selected on the basis of the geo-coordinates of the sensor’s footprint and with respect to a certain minimal overlap. The automatic image-based fine-registration adjusts the image pair to a common geometry by using a robust matching approach to cope with outliers caused by e.g. 3D objects, changed objects, changed shadows, moving objects, compression and transmission artefacts.

The change detection algorithm, too, has to be robust against image differences caused by such influences, i.e. to distinguish between relevant and not relevant changes (3D structure, changed length of shadows).

For the core task of change detection based on image pairs we implemented several algorithms: (1) an iconic correlation based approach, (2) a feature based approach, and (3) an approach based on multivariate analysis of texture or color channels. The change detection algorithms are evaluated with several examples covering both semi-urban scenes and open landscape.

The algorithms are implemented in the ABUL video exploitation system and are adapted for a semi-automatic workflow, see [1], [2]. In a further step we plan to incorporate more information from the video sequences to the change detection input images, e.g. by image enhancement, by along track stereo, or by other capabilities which are available in the ABUL system.

[1] Image exploitation algorithms for reconnaissance and surveillance with UAV, N. Heinze; M. Esswein; W. Krüger; G. Saur, SPIE Airborne Intelligence, Surveillance, Reconnaissance (ISR) Systems and Applications VII, 26 April 2010

[2] Detection and classification of moving objects from UAVs with optical sensors, Michael Teutsch; Wolfgang Krüger; Norbert Heinze, SPIE Signal Processing, Sensor Fusion, and Target Recognition XX, 5 May 2011

8537-28, Session 6

Integrating multi-interferometry and change detection techniques: a SAR-based method for improving landslide detection

Christian Iasio, EURAC research (Italy); Gabriele Moser, Univ. degli Studi di Genova (Italy); Claudia Notarnicola, EURAC research (Italy); Sebastiano B. Serpico, Univ. degli Studi di Genova (Italy)

The development of methods for fast detection of features related to or generated by natural hazards, such as co-seismic deformation maps made by SAR interferometry, became usual early assessment tools in the last years. At the same time, with the higher and more disparate availability of SAR data sources, also the processing techniques based on this type of images are evolving very fast. In the context defined by both these circumstances, we are investigating and proposing a methodology for assisting early landslide detection, taking advantage from different approaches to SAR data analysis: change detection and multi-interferometry.

The difficulties in the interpretation of SAR derived products for this purpose, mainly represented by velocity field maps obtained by means of Persistent Scatterer Interferometry (PSI), are related to the relationship among the different point measures composing the dataset and to the extent and distribution of the velocities indicated by each PS. The aim of the proposed methodology is to provide an improved kind of output, where the solutions to these issues are partially supplied, or at least suggested, in order to make the SAR-based outputs for landslide detection more easily interpretable and immediately usable.

The opportunity to investigate this methodology is provided by

projects funded by the Italian Space Agency (ASI) for the feasibility study of COSMO-SkyMed (CSK) data for civil usage. The improvement of slope deformation dynamics by X-band CSK data was already analyzed on a slow earth-flow occurring near Corvara in Badia, in the Dolomites (Alps), Northern Italy. Here a large stack of CSK images was acquired in the last year and PSI analysis was already carried out by the solid, industry standard, methodology provided by T.R.E.. The original improvement to this work already done, consists in coupling these data with maps of change detection obtained by processing part of the same data stack through algorithms able to delineate deformations occurred during the monitored period. The change-detection task is addressed by recent techniques, specifically developed to deal with very high-resolution SAR data, such as those acquired by the CSK mission. Given a multitemporal pair of CSK images acquired over the same area at different times, such methods combine Bayesian unsupervised image analysis, non-Gaussian parametric density function estimation, and Markov random field models in order to discriminate changed and unchanged areas, while favoring, at the same time, robustness to speckle.

This experiment remarked the capability to detect a number of changed areas in the considered image. Further results about the possibility to get new information by coupling this new output with PSI products and a thorough discussion of their relevance with respect to the monitored landslide will be detailed in the full paper.

The envisaged refinement of this methodology consists in the iterative process of defining time frames which have to be considered for the change detection analysis, on the basis of anomalies detected by the time series recorded in the PS dataset, in order to optimize the integrated output of homogenous velocity field maps.

8537-30, Session 7

A rooftop extraction method using color feature, height map information and road information

Yongzhou Xiang, Ying Sun, Chao Li, National Univ. of Singapore (Singapore)

Rooftop extraction from satellite images is a key element in various applications such as urban planning. However, due to the presence of occlusion and shadows, lack of contrast, and uncertainty in building structures, it still remains a difficult task to automatically extract the outline of rooftops with good accuracy. This paper presents a new method for rooftop extraction that integrates color features, height map, and road information in a level set based segmentation framework. By incorporating the height map and road information, it can not only reduce the false detection rate, but also improve the segmentation accuracy significantly.

The proposed method consists of two steps: rooftop detection and rooftop segmentation. In the first step, rooftops are detected according to not only the color features but also the height map derived from a stereo pair of satellite images. In the second step, a level set based segmentation approach is used to achieve more accurate rooftop extraction results.

The first step requires the user to provide a few example rooftops from which the color distribution of rooftop pixels is estimated. For better robustness, we obtain superpixels by applying the quick shift algorithm to the input satellite image, and then classify each superpixel as rooftop or non-rooftop based on its color features. Since a real rooftop has a relatively large height value, those detected rooftop candidates with small height values are likely to be falsely detected and therefore should be removed. Hence, we calculate the average height value of each rooftop candidate based on the height map, and remove those candidates with a below-threshold height value.

Level set based segmentation is then performed in the neighborhood of each detected rooftop. The level set energy function consists of four terms: region-based, shape prior, length, and penalizing term. For better discriminability between rooftop and non-rooftop pixels, we use the CIE Lab space instead of RGB space to model color distribution. Besides color features, height is also used as an independent feature. The shape prior term allows the evolving level set contour to take on a desired shape. In our application, rectangle rooftops are of greater interest compared to other shapes. Thus, the calculation of the shape-prior term requires performing rectangle fitting to the evolving contour. In urban areas, the orientation of most rooftops is either aligned with or perpendicular to the orientation of the closest road. Therefore, road information can be used to guide rectangle fitting and improve the fitting accuracy.

The performance of the proposed rooftop extraction method has been evaluated on a satellite image of 1 km?1 km in area, with a resolution of one meter per pixel. The method achieves detection rate of 88.0% and false detection rate of 9.5%. The average Dice's coefficient over 433 detected rooftops is 73.4%. These results demonstrate that by integrating the height map in rooftop detection and by incorporating road information and rectangle fitting in a level set based segmentation framework, the proposed method provides an effective and useful tool for rooftop extraction.

8537-31, Session 7

Integration of photogrammetric DSM and advanced image analysis for the classification of urban areas

Mauro Dalla Mura, Francesco Nex, Fabio Remondino, Michele Zanin, Fondazione Bruno Kessler (Italy)

The classification of urban areas from aerial images or DSM (Digital Surface Model) is one of the main topics in the Remote Sensing and Photogrammetric research community, as this process is the main step for several tasks such as feature extraction, change detection, etc. Several authors have already proposed a huge variety of supervised and unsupervised image-based classification algorithms. On the one hand, most of these approaches exploit multispectral images as input in order to improve their performances (only few approaches use RGB images) but the final accuracy of the classification results depends on the image resolution, illumination conditions, presence of shadows, etc.. On the other hand, several range-based segmentation and classification algorithms have been developed: most of these approaches consider LiDAR point clouds as input data exploiting multi-echo, full-waveform and signal intensity information as features considered to classify the data. However, very few approaches consider DSM generated by image matching techniques as an input because this kind of data does not give any additional information (such as multi-echo and intensity) and it can be affected by noise especially in shadowed and occluded areas. The integration of both image and range data has already shown to improve the results in terms of classification accuracy in several applications, exploiting the complementary nature of the provided information. Anyway, a classification considering a joint integration of range and image information has not been fully exploited yet.

In this paper, a new approach of integration between image and point cloud for urban areas classification is presented. A set of aerial RGB overlapping images are used as input. A photogrammetric DSM is firstly generated by using multi-image matching techniques and the classification of points according to their geometrical properties is initially performed: each point of the DSM is classified into ground and off-ground classes and an evaluation of its position reliability is given considering the variation of the normal vector to the DSM surface in its neighbourhood.

Subsequently, we propose to perform a thematic classification of the surveyed areas by considering the surface's reflectance in the visible spectrum (provided by all the optical overlapping), altitude information, and the directions of the vectors orthogonal to the 3D surfaces as features. The geometrical constraints given by the photogrammetry allows to define a direct correlation between pixels of each image and their position (and classification too) in the space. In this way, the thematic classification of the land cover can be improved by considering simultaneously the height information of the DSM and the values of reflectance sensed by the multiple images available.

In order to associate each pixel to the most suitable class, we define a cost function according to the quality of the generated DSM and the ambiguities between the classification results and the topological characteristics of the DSM.

In this work, the proposed classification algorithm is detailed and the achieved results with a set of aerial images over a dense urban area are shown. Finally, the conclusion and the future development will be analysed and discussed.

8537-32, Session 7

Tracking image features using three-dimensional edge detection

David A. Schug, Alec E. Forsman, Naval Air Warfare Ctr. Aircraft Div. (United States); Glenn R. Easley, System Planning Corp. (United States)

The availability of volumetric data has increased the need to develop better analysis tools for three-dimensional data sets. These volumetric data sets provide information beyond that contained in standard two-dimensional images. Previous work with such data sets has been based on sequential use of two-dimensional analysis tools. In this work, we use an extension of the wavelet transform known as the shearlet transform for the purpose of edge analysis and detection in three-dimensions. This method takes advantage of the shearlet transform's improved capability to identify edges compared to wavelet-based approaches. Furthermore we apply three dimensional edge detection in the context of two dimensional tracking of image features. We show that three dimensional edge detection provides better tracking capability in noise and lighting variations even for objects with complicated structure.

We begin by describing the background necessary to integrate 3D edge detection methods into a two dimensional tracking algorithm. Complications with the general 2D tracking problem will be presented. Common approaches to solve the 2D tracking problem using both time domain and frequency domain methods are contrasted. We review previous work demonstrating the improved performance of both 3D wavelet and 3D shearlet edge analysis techniques to extract image features. The positive results achieved from 3D edge detectors provide solid justification for our proposed tracking solution using 3D edge analysis.

The implementation section defines the integration of 3D edge detection into three dierent 2D tracking algorithms. The tracking algorithms will use the 3D Canny, 3D wavelet, and 3D shearlet edge analysis methods respectively. The 2D Canny algorithm will be used as a standard to compare the other methods against.

The experiment section will set up different image sequence scenarios necessary to generate test data. We begin with synthetic data to serve as absolute truth data to compare the results from each dierent 2D tracking algorithm. The structure and center point location of the track object is known as it follows a set trajectory from frame to frame. Each tracking method will process the test image sequence independently to generate its own computed trajectory of the track object. The tracking methods will be subject to increasing levels of identically distributed noise and lighting variations. Also variations in track object trajectory dynamics and different track object shapes will be considered. Error analysis with synthetic truth data will grade each algorithm and help to characterize their true performance. Also each algorithm will then be evaluated using real-world image sequences.

8537-33, Session 7

Performance evaluation of DTM area-based matching reconstruction of Moon and Mars

Cristina Re, Centro Interdipartimentale Studi e Attività Spaziali (CISAS)–G. Colombo, University of Padova (Italy); Riccardo Roncella, Gianfranco Forlani, Dept. of Civil Engineering, University of Parma (Italy); Gabriele Cremonese, INAF - Astronomical Observatory Padova (Italy); Giampiero Naletto, Department of Information Engineering, University of Padova (Italy) and 2CNR-Institute for Photonics and Nanotechnologies UOS Padova LUXOR (Italy) and INAF - Astronomical Observatory Padova (Italy)

The importance of high resolution DTMs in the geomorphological studies of planets and asteroids has established stereo coverage and photogrammetric reconstruction of the body surface as a standard among the scientific goals of space missions. For example, HiRISE, the pushbroom image sensor onboard the Mars Reconnaissance Orbiter, provides images with ground resolution of 0.3 m. These data represent an enormous potential for the automatic generation of Digital Terrain Models (DTMs) thanks to the high level of details and its stereo capability. Another example are the instruments on board the Lunar Reconnaisance Orbiter (LRO) that, together, enable the extraction of DTMs: LROC (Lunar Reconnaissance Orbiter Camera) consists of a Wide Angle Camera (WAC) for synoptic multispectral imaging, and two Narrow Angle Cameras (NAC) to provide high-resolution images (0.5 to 1.5 m pixel scale) of key targets. Presently, existing stereo processing techniques still require an extensive human intervention and it is clear that a lot of efforts have to be dedicated to reach a high level of automation. Our research group is currently concentrating its efforts in improving our proprietary developed matching software comparing it with the capabilities of Ames Stereo Pipeline (ASP) (Broxton et al, 2008). In our tests NASA's Planetary Data System (PDS) images (pre-elaborated with the Integrated Software for Imagers and Spectrometers, ISIS) and orientation parameters (recorded in the cube files also with ISIS) were given as input to two DTM generation programs: either Dense Matcher (DM) developed at the University of Parma, and the ASP tools. The goal of this paper is to highlight where improvements are necessary in matching strategies: for example the use of different matching algorithms as well as different transformation models between the stereo images can lead to very different results both in terms of accuracy and computational efforts; also the influence of bundle adjustment procedures to eliminate the geometric inconsistencies among the images and to produce an easier object reconstruction is investigated.The comparison of just the image matching procedure being the main objective of this work, all other steps of the DTM generation procedure (pre-processing, orientation by bundle adjustment or navigation, data and computation of object coordinates by triangulation) have been made independent of the matching software by using the ASP framework. Two types of tests have been performed. In the first, applied to real Hirise and NAC images, the matching accuracy of DM has been checked against that of ASP both with respect to reference DTMs of Mars produced by the USGS with Socet Set and of the Moon by DLR of Berlin with their proprietary software. In a second series of tests, synthetic images were generated with a 3D modelling software, matched with DM and triangulated to measure the effect on accuracy of the texture of the real images. Simulating the acquisition environment inside a 3D modelling software allows the isolation of the different error sources as well as provide an error-free comparison DTM, that is considered essential to interpret the results obtained with real image data.

8537-34, Session 7

Automatic generation of digital terrain models from LiDAR and hyperspectral data using Bayesian networks

Dominik Perpeet, Wolfgang Gross, Wolfgang Middelmann, Fraunhofer Institute of Optronics, System Technologies and Image Exploitation IOSB (Germany)

Various tasks such as urban development, terrain mapping or waterway and drainage modeling depend on digital terrain models (DTM) from large scale remote sensing data. Common DTM generation methods require extensive manual input and corrections. Previous attempts at automation are mostly based on determining the non-ground regions via fixed thresholds followed by smoothing operations. We propose a novel approach to automatically deduce a DTM from a digital surface model (DSM) with the aid of hyperspectral data. For this, advantages of a scanning LiDAR system and a pushbroom hyperspectral sensor are combined.

Starting point for the presented method is a DSM, generated from an airborne LiDAR system, onto which the hyperspectral data has already been mapped. While a DSM directly depicts the measured data and is readily acquired using airborne remote sensing, a DTM requires further processing. As a preprocessing step, hyperspectral information is used to determine and adjust regions where reverberations of the LiDAR data occur, such as contours of bodies of water. This is achieved via comparison of the underlying spectral signatures with information on elevation and elevation gradients. In the next step, obstructions have to be detected and replaced with estimated terrain elevation. These obstructions can be artificial, e.g. buildings and vehicles, or natural, e.g. forests. True terrain elevation is estimated using local measurements as well as contextual information. For this, a set of features is extracted from the merged LiDAR and hyperspectral data. These include vegetation indices to separate soil and manmade structures from vegetation. Additionally, elevation gradients of the DSM can be combined with material classification results as supporting information. More complex terrain such as slopes, embankments, and extended forests would still require manual corrections using only these features. Since geometric as well as semantic information has to be taken into account simultaneously, Bayesian networks lend themselves to aid DTM generation. We construct a hybrid Bayesian network (HBN), where modeled nodes can be discrete or continuous, and incorporate our already determined features. Using this network, original measurements from the DSM are processed together with the selected features, providing an estimated elevation value for each original LiDAR point. Additionally, we calculate the local reliability depending on the estimated robustness of the features used and the distance to unchanged measurement points.

An urban scenario with noticeable terrain variations, including a general slope and a river, is used to demonstrate the method. Local accuracy of the generated DTM is estimated for each measurement point based on used features, sensor specifications and neighboring measurements.

The presented automatic DTM generation successfully combines advantages of the LiDAR single point measurements with hyperspectral image data. At the same time, Bayesian networks provide flexibility, since they can readily be adapted to specific scenarios such as mountainous or urban regions.

8537-35, Session JS1

Classification of polarimetric SAR data using dictionary learning

Jacob S. Vestergaard, Anders L. Dahl, Rasmus Larsen, Allan A. Nielsen, Technical Univ. of Denmark (Denmark)

This contribution deals with classification of multilook fully polarimetric synthetic aperture radar (SAR) data by learning a dictionary of crop types present in the Foulum test site. The Foulum test site contains a large number of agricultural fields, as well as lakes, forests, natural vegetation, grasslands and urban areas, which make it ideally suited for evaluation of classification algorithms.

Dictionary learning centers around building a collection of image patches typical for the classification problem at hand. This requires initial manual labeling of the classes present in the data and is thus a method for supervised classification. Sparse coding of these image patches aims to maintain a proficient number of typical patches and associated labels. Data is consecutively classified by a nearest neighbor search of the dictionary elements and labeled with probabilities of each class.

Each dictionary element consists of one or more features, such as spectral measurements, in a neighborhood around each pixel. For polarimetric SAR data these features are the elements of the complex covariance matrix for each pixel. We quantitatively compare the effect of using different representations of the covariance matrix as the dictionary element features. Furthermore, we compare the method of dictionary learning, in the context of classifying polarimetric SAR data, with standard classification methods based on single-pixel measurements.

8537-36, Session JS1

A novel approach to building change detection in very high resolution SAR images

Francesca Bovolo, Univ. degli Studi di Trento (Italy); Carlo Marin, Lorenzo Bruzzone, Univ degli Studi di Trento (Italy)

No abstract available.

8537-37, Session JS1

Blind whitening of correlated speckle to enforce despeckling of single-look high-resolution SAR images

Alessandro Lapini, Tiziano Bianchi, Fabrizio Argenti, Luciano Alparone, Univ. degli Studi di Firenze (Italy)

No abstract available.

8537-38, Session JS2

Maritime surveillance with synthetic aperture radar (SAR) and automatic identification system (AIS) onboard a microsatellite constellation

Erica H. Peterson, Robert E. Zee, Univ. of Toronto (Canada); Georgia Fotopoulos, The Univ. of Texas at Dallas (United States)

New developments in small spacecraft capabilities will soon enable formation-flying constellations of small satellites, capable of performing cooperative distributed remote sensing operations at a fraction of the cost of traditional large spacecraft missions. As part of ongoing research into applications of formation-flight technology, recent work has explored the benefits of a mission based on combining SAR with AIS (automatic identification system) data. In this mission concept, two or more microsatellites would trail a large SAR transmitter in orbit, each carrying a SAR receiver antenna and one carrying an AIS antenna. Spaceborne AIS can receive and decode AIS data from a large area, but accurate decoding is limited in high traffic areas, and the technology itself relies on voluntary vessel compliance. SAR images, as opposed to optical imagery, can be acquired independently of weather conditions and solar illumination. However, vessel detection amidst speckle, a noise-like characteristic of SAR imagery, can be challenging. In this constellation, voluntary broadcasts of vessel position and velocity via AIS are received and decoded, and used in combination with SAR observations to form a more complete picture of maritime traffic and identify potentially non-cooperative vessels. Due to the limited transmit power of the microsatellite platform as well as limited ground station downlink time, data will be processed onboard the spacecraft. Herein we present the onboard data processing portion of the mission concept, including methods for automated SAR image registration, vessel detection, and fusion with AIS data. Georeferencing in combination with a spatial frequency domain correlation method is used to register the processed SAR imagery. Wavelet-based speckle reduction facilitates vessel detection via a standard CFAR (Constant False Alarm Rate) algorithm, while still leaving sufficient detail for registration of the filtered and compressed imagery. Moving targets appear offset from their actual position in SAR imagery, depending on their velocity and the image acquisition geometry; multiple SAR images acquired from different locations are used to determine the actual positions and velocities of these targets. Finally, a probabilistic inference model is then used to combine the SAR target data with transmitted AIS data, taking into account nearest-neighbor position matches and uncertainty models of each observation.

8537-39, Session JS2

GLRT-entropy joint location of low-RCS target in heavy sea clutter

Jianing Wang, Xiaojian Xu, BeiHang Univ. (China)

Detection and location of low radar cross section (RCS) targets in heavy sea clutter are of great significance in military and civilian applications. Most of the existing work used a generalized likelihood ratio test (GLRT) detector whose performance heavily depends on the estimated probability. However, when target location is considered, techniques based on estimated probability cannot work well since more accurate estimates of sea clutter are required. Range images vary a lot before and after clutter suppression when a target is present, meaning that entropy can also be used in the detection and location of target. A GLRT-entropy joint target location approach for heavy sea clutter is proposed in this paper, which takes the advantage of using both estimated probability and localized entropy of the range image.

The radar scene considered in the current work is a sea surface having at most one point target. Complex Gaussian (CG) model is used to statistically describe the sea clutter. All the statistical parameters are estimated using the expectation-maximization (EM) method. After obtaining the covariance matrix of the clutter, subspace based method is employed for mitigation of sea clutter. The received signal after a matched filter is projected onto the subspace that is orthogonal to clutter's dominant eigenvetors. Signals after clutter suppression are then used in the target location.

For simplified calculation, a slightly modified GLRT is adopted for target detection. Instead of calculating the log-likelihood ratio between the hypotheses that target is present or not in the whole area directly, the proposed approach detects target bin by bin.

As long as a target is detected, the range bin for that target is identified. With a probability based approach, the target is considered to locate in the range bin whose probability of containing a target is the maximum. Unfortunately, sea clutter in the target range bin is overestimated. This makes the estimated probability of each bin departures from the real value and further leads to a bad location performance. For accurate location, the proposed approach takes localized entropies of range images into consideration. Range images before and after clutter suppression noticeably vary when a target exists in a specified bin, and localized entropies of the two range images also differ greatly, especially in the target range bin. Target location is then performed by comparison of localized entropies before and after clutter suppression respectively.

Monte Carlo simulation is conducted for performance evaluation. Simulation results demonstrate performance advantages of the

proposed approach over those where only information of estimated probability or entropy is used.

8537-40, Session PS

Detection of hedges based on attribute filters

Gabrielle Cavallaro, Univ. of Iceland and Univ. degli Studi di Trento (Italy); Benoit Arbelot, Gipsa-lab (France); Mathieu Fauvel, DYNAFOR Lab., INRA, and Univ. of Toulouse (France); Mauro Dalla Mura, Fondazione Bruno Kessler (Italy); Jon Atli Benediktsson, The Univ. of Iceland (Iceland); Lorenzo Bruzzone, Univ. degli Studi di Trento (Italy); Jocelyn Chanussot, Lab. des Images et des Signaux (France); David Sheeren, DYNAFOR Lab., INRA, and Univ. of Toulouse (France)

Hedges are narrow vegetated areas composed of shrubs and/or trees that are usually present at the boundaries of adjacent agricultural fields. The detection of hedges is a very important task for the monitoring of a rural environment and aiding the management of their related natural resources.

In this paper, a technique for detecting hedges is presented. It exploits their spectral and spatial characteristics. In details, spatial features are extracted with attribute filters, which are connected operators defined in the mathematical morphology framework. Attribute filters are flexible operators that can perform a simplification of a grayscale image driven by an arbitrary measure. Such measure can be related to the scale, shape, contrast etc. characteristics of regions in the scene. It is proposed to compute attribute filters on the inclusion tree which is a hierarchical dual representation of an image. Since the filtering exploits the inclusion tree structure, it is possible to process simultaneously both bright and dark regions (with respect to their surroundings graylevels). Hence, a better spatial characterization of the hedges can be obtained since their local relative contrast is not accounted. Detection of the hedges is then performed by classifying simultaneously spectral and spatial features in a stack vector architecture.

8537-42, Session PS

A FPGA-based automatic bridge over water recognition in high-resolution satellite images

Sebastian Beulig, Maria von Schönermark, Felix Huber, Deutsches Zentrum für Luft- und Raumfahrt e.V. (Germany)

In the following a new algorithm for recognizing bridges over water in high-resolution satellite images is presented. The main advantage of this algorithm is, that it is implemented in reconfigurable hardware, so called Field Programmable Gate Arrays (FPGA). Due to the very limited resources of the FPGA, the algorithm is computationally easy. And because of their ability to execute program parts in parallel, a very high processing speed can be reached.

In addition, no a-priory knowledge about the bridge is needed. Even bridges with an irregular shape, e. g. with balconies, can be detected.

These characteristics make this method suitable for an image evaluation on board of satellites. The extracted image information is submitted to the on board data handling unit (OBDH). The OBDH can influence the image processing chain, e. g. initiate a direct downlink, and/ or arrange the camera for a second shot of the scene. This is a useful scenario in case of natural hazards.

For the development and analysis of the algorithm two kinds of satellite data are used. At first panchromatic images from the ESA Satellite Proba-1. And secondly near-infrared images from the satellite system RapidEye. Both data sources have a spatial resolution of 5m. So the majority of common bridges should be detectable.

The algorithm consists of two parts. In the first part a water mask is derived from the satellite image. This is based on the known characteristics of water. Low thresholds for the roughness and the gray level values can separate water from background (land or clouds). A binary map is generated. Due to the appearance of small falsely classified water segments an additional post processing is realized. That means the water segments are eroded and dilated for several times.

Because of that, thin rivers and small river segments are also removed. Therefore only bridges with a minimum length of ~65m can be detected.

The second part of the algorithm recognizes bridges in the binary map. Possible bridge regions, where two water segments are at close quarters, are selected. Distinctive points at the water rim are labeled and connected. A search for straight lines is not applicable. Then their arrangement is analyzed. If it fits a certain pattern, then as a result the center of the bridge will be marked.

By now, 20 images from each satellite are analyzed. In these 40 images a total number of 155 bridges of all different sizes are visible. Thereof 99 are fully or partly recognized. 56 bridges could not be detected. And in 34 cases the labeling was wrong. The two main error reasons are thin rivers and the partially poor water classification. With the used FPGA configuration (Spartan 3E with a clock frequency of 12.5 MHz) a 900x900 pixel image is processed in 8-10 seconds, depending on the number of water segments.

Hence, this is a promising first step towards an automatic bridge recognition realized on a small microchip.

8537-43, Session PS

Web-based data acquisition and management system for GOSAT validation Lidar data analysis

Hiroshi Okumura, Shoichiro Takubo, Takeru Kawasaki, Indra N. Abdullah, Saga Univ. (Japan); Osamu Uchino, National Institute for Environmental Studies (Jordan); Isamu Morino, Tatsuya Yokota, National Institute for Environmental Studies (Japan); Tomohiro Nagai, Tetsu Sakai, Takashi Maki, Meteorological Research Institute (Japan); Kohei Arai, Saga Univ. (Japan)

Global warming has become a very serious issue for human beings.

Scientists have suggested that, at the rate the Earth's temperature is rising, an extreme form of global climate change could occur in a few centuries.

In 1997, the Kyoto Protocol was adopted at the Third Session of the Conference of the Parties to the United Nations Framework Convention on Climate Change (COP3), making it mandatory for developed nations to reduce carbon dioxide emissions by six to eight per cent of their total emissions in 1990, and to meet this goal sometime between 2008 and 2012.

Furthermore, the Global Climate Observation System (GCOS) has been proposed by the World Meteorological Organization (WMO) and the United Nations Environment Program (UNEP) in order to strengthen observations of land, ocean, and space conducted by each country.

So far, the number of ground-based carbon dioxide observation points has been limited, and they have been distributed unequally throughout the world.

Greenhouse gas Observation SATellite (GOSAT) enables the precise monitoring of the density of carbon dioxide by combining global observation data sent from space with data obtained on land, and with simulation models. In addition, observation of methane, another Greenhouse gas, has been considered.

For validation of GOSAT data products, we have continued ground-base observation with Fourier Transform Spectrometer (FTS), aerosol Mie lidar and ozone-DIAL lidar at Saga University, JAPAN since March, 2011.

For lidar data analysis, not only acquired lidar data but also meteorological data are required.

We develop an web-base data acquisition and management system for effective acquisition of meteorological data and management of acquired lidar data.

The system consists of data acquisition part and data management part.

Data acquisition part written in Perl language acquires AMeDAS ground-level meteorological data, RawinSonde high altitude meteorological data, ground-level oxidant data, skyradiometer data, skyview camera images, meteorological satellite IR image data and GOSAT validation lidar data.

AMeDAS (Automated Meteorological Data Acquisition System) is a high-resolution surface observation network developed by Japan Meteorological Agency (JMA) used for gathering regional weather data and verifying forecast performance. Begun operation on November 1, 1974, the system consists of about 1,300 stations with automatic

observation equipment. These stations, of which more than 1,100 are unmanned, are located at an average interval of 17 km throughout Japan.

These AMeDAS meteorological data are acquired from Saga city station every hour.

RawinSonde are essential to obtain high altitude temperature and air pressure data.

These RawinSonde meteorological data are acquired from Fukuoka city station twice (00Z and 12Z) a day.

Ground-level oxidant data are required for analysis of ozone-DIAL lidar data.

These ground-level oxidant data are acquired from Saga city station every hour.

Skyradiometer is required to observe optical thickness.

Skyradiometer data are acquired every hour.

Skyview camera images and meteorological satellite IR image data are required to confirm clouds above lidar.

Skyview camera images are acquired every 5 minutes in daytime and meteorological satellite IR image data are acquired every hour.

GOSAT validation lidar data are manually uploaded via secure FTP.

Data management part written in PHP language demonstrates satellite-pass date and all acquired data and provides interactive graphical user interface.

8537-44, Session PS

Recognition and quantification of temporal profiles of land cover changes in south-western Colombia by image analysis of Landsat-7 ETM+ samples

Tatiana Solano-Correa, Apolinar Figueroa-Casas, Leonairo Pencue-Fierro, Univ. del Cauca (Colombia)

The study of land cover that form a region and evaluation of its dynamics, is an important issue to be prerequisite for the sustainable management of natural resources, environmental protection, and basic data monitoring and modeling, specifically in the case of southwestern Colombia have prominence because it is a high mountain area with a large variability of vegetation cover and land use. Knowing the amount and distribution in spatial and temporal control is important for agriculture, deforestation, environmental degradation and climate change.

Today it is possible to access to all kinds of information from remote sensing satellites providing access to almost anywhere and any data. In this case we have used multispectral satellite images Landsat7 ETM+ from NASA that primarily allow coverage for a considerable spectral range, an appropriate spatial resolution.The images are obtained for the same study area every 16 days, but due to the specific characteristics of the studied system, much time is covered with clouds, causing difficulties when sorting by ignorance or by identifying areas of coverage erroneous due to cloud shadows.

This study presents the implementation of image processing techniques in satellite bands of the visible and infrared spectrum for the differentiation of land cover in the Colombian Andes, which is dominated by high mountain systems, using methods of texture analysis, principal component analysis, discrete cosine transform, combination of color spaces and vegetation indices.

An analysis of the characteristics to differentiate viable coverage was done, obtaining a separability visible for about eleven classes. The characteristics obtained are combined so as to allow to obtain separate zones in the feature space that would ensure a correct discrimination in the classification stage. In the classification module were used different approaches: neural networks by using the feature space allowed us to determine whether or not a pixel belongs to a type of coverage and an expert system based on a binary tree that took the decision to classify each pixel within a coverage rate based on previously entered conditions.

These results were aligned time profiles for the evolution quantification of the different coverages, obtaining conclusions about local and regional dynamics in order to project future scenarios and establish corrective measures where necessary.

Finally, validation was performed with data obtained in-situ in a cross-correlation approach and allowed to establish an accuracy of 95% correct results. This methodology can be applied to larger extensions and to obtain reliable trends measures in the coverage of interest in different areas, specifically in regard to the Andean countries ecosystems (Colombia, Ecuador, Peru, Chile, Bolivia).

8537-45, Session PS

Segmentation of remote sensing images for building detection

Hamid Moayeri, Islamic Azad Univ. (Iran, Islamic Republic of)

Image segmentation can be used as an important basic operation for meaningful analysis and interpretation of High resolution images of remote sensing. This process is regarded as a mandatory preprocessing step in many computer vision based applications and it's useful in extracting interested object from acquired images from different sources, by separating them from different other objects in each image. Proposed algorithm in this research is used on the urban remote sensing images for segmenting them to detect buildings area, with consider images histogram as input parameter. The main objective in the threshold based segmentation process is determining an efficient threshold's value for bi-level segmentation that is simplest case for this operation or several threshold's values for multi- level segmentation. However the problem gets more and more complex when we try to do segmentation with greater details by employing multilevel thresholding. In such cases, image segmentation technique changes to multiscale classification problem, where depend on determined threshold's values, image's pixels that had gray-level values within a specified range of thresholds are grouped into one class. Usually, this is not simple to determine exact locations of distinct valleys (threshold's points) in a multimodal image's histogram, to segment them for extracting interested objects or regions effectively. Several algorithms have so for been proposed that have addressed the issue of histogram thresholding. While many of them address the issue of bi-level thresholding, either has considered the multilevel problem. This paper proposes a new optimal multilevel thresholding algorithm, which is especially suitable for applying to multimodal image's histogram. To do optimization process in this algorithm, we used special kind of particle swarm optimization algorithm which is called hybrid PSO algorithm. The performance of proposed algorithm is evaluated and then compares with improved variant of Genetic Algorithm, which is another popular stochastic global optimization technique.

8537-46, Session PS

Learnable hyperspectral measures

Abdulrahman Galal, Arab Administrative Development Organization (Egypt); Hesham Hassan, Cairo Univ. (Egypt); Ibrahim Imam, Virginia Polytechnic Institute and State Univ. (United States)

Hyperspectral similarity measures are static threshold based measures. Such measures require extensive expert intervention. The proposed approach developed learnable hyperspectral measures to relax expert engagement. This is done through using hyperspectral measures values as similarity patterns and employing a classifier. The classifier acts as an adaptive similarity threshold. Two similarity patterns are proposed. The first pattern is the cosine similarity vector for the second spectral derivative pair. The second pattern is a composite vector of different similarity measures values. The resulting patterns are classified by SVM. The proposed approach is applied on full hyperspectral space and subspaces. The experimental evaluation showed that the proposed approach outperformed PCA and NCA approaches. The results of version 2.2 of the proposed approach are statistically significant compared to NCA approach - the best competitive approach.

PCA performance was poor. This is because PCA kept high variance bands and ignored low order bands containing discriminatory information. In addition, PCA failed to classify small size classes of the test dataset. Unlike PCA which is not directly related with the final classification performance, NCA was designed to directly optimize the expected leave-one-out (LOO) classification error on the training data. Therefore, NCA performance was far better than PCA. NCA developed a learnable distance metric by finding a linear transformation of input data to enable KNN to perform well in this transformed space. Although NCA achieved good results, it is computationally expensive.

The proposed approach versions were capable of capturing the specific notion of similarity that is appropriate for each spectral region. The different similarity measures values vector versions performed

better than cosine similarity vector versions as they were able to combine different discriminatory characteristics powered by different similarity measures. The proposed versions applied on hyperspectral subspace performed better than their counterparts applied on the full hyperspectral space. This is because decomposing the hyperspectral into subspaces maximized the information discrimination within each subspace, and minimized the statistical dependence between subspaces. In doing so, potentially useful spectral response information was not discarded. In addition, it overcame the small-sample size problem, since the number of training signatures required per subspace was substantially low. Utilizing One-against-One SVM and RBF Kernel boosted the classification accuracies of the proposed approach versions.

The results imply that using simple learnable hyperspectral measures overcome complex or manually tuned techniques used in classification tasks.

8537-47, Session PS

A new coastline extraction in remote sensing images

Kun Xing, Beijing Institute of Space Mechanics and Electricity (China); Yili Fu, Harbin Institute of Technology (China); Feng Zhou, Beijing Institute of Space Mechanics and Electricity (China)

Extraction of coastline from remote sensing image is of great significance for automatic navigation, marine rescue, ocean pollution monitoring, shoreline mapping, ship positioning, spacecraft position and attitude control, remote sensing image registration and cruise missile guidance. With the advent of ocean observing satellites, coastline detection technology from SAR image is rapidly becoming a hot field in remote sensing image processing, but research works about optics image are few. There are two ways for SAR images to detect coastlines: one is low level image processing technique that smoothing, segmentation and tracking are applied, the other is high level image processing technique such as multi-resolution and wavelet transform. Unlike SAR images, visible images are formed with higher resolution, no speckle noises, large amounts of data and the gray level of water are closer to the gray level of land. So the above-mentioned methods are not strong reliability and accuracy for visible images. This paper presents a solution to the problem of extracting coastlines accurately and rapidly in high-resolution panchromatic remote sensing images. Active contour models, also called snakes, were proposed by Kass et al., and since then have been successfully applied in a variety of problems in computer vision and image analysis, such as edge and subjective contours detection, motion tracking and segmentation. There are several key difficulties with original snakes. Many works has been proposed to improve snake models: Balloon model, GVF Snake, greedy algorithm for snake, ACO Snake, Loop Snake and R-Snake. However, most of the methods proposed to address problems solve only one problem while creating new difficulties. The basic goal of this paper is to present the snake model as an effective coastline extraction technique. In order to improve motion performance, we develop better energy functions. Firstly, coastlines are detected by water segmentation and boundary tracking, which are considered initial contours to be optimized through active contour model. As better energy functions are developed, the power assist of snakes becomes effective. New internal energy has been done to reduce problems caused by convergence to local minima, and new external energy can greatly enlarge the capture region around features of interest. After normalization processing, energies are iterated using greedy algorithm to accelerate convergence rate. The experimental results encompassed examples in images and demonstrated the capabilities and efficiencies of the improvement.

8537-48, Session PS

De-striping algorithm in ALOS satellite imagery based on adaptive frequency filter

Yutian Cao, Dongmei Yan, Gang Wang, Ctr. for Earth Observation and Digital Earth (China); Shucheng You, China Land Surveying and Planning Institute (China); An Li, Ctr. for Earth Observation and Digital Earth (China)

ALOS satellite carries a panchromatic remote-sensing instrument for stereo mapping (PRISM), an advanced visible and near infrared radiometer type 2 (AVNIR-2), and a phased array type L-band synthetic aperture radar (PALSAR). Among these three kinds of remote sensing sensors, PRISM can acquire image products level 1 with obvious image scanning trace, which results in the periodic stripe noises.

Stripe noises in ALOS PRISM imagery can be seen as symmetrical directional peaks in image frequency domain. Accordingly, the de-striping algorithm in ALOS satellite imagery based on adaptive frequency filter firstly calculates the column accumulative distribution curve, which is formed along the horizontal axis of the image energy spectrum. Then this algorithm looks for the critical points between the high and low frequency components of the curve to construct an adaptive filter and applies the filter to remove vertical stripe noises in ALOS satellite imagery data. This algorithm is proved to effectively detect and remove vertical stripes in ALOS satellite imagery to make images not only more interpretable but also more suitable for post-processing.

Moreover, in view of existence of oblique stripes in ALOS imaging products level 2, which have been geometry corrected, the above de-striping algorithm is improved to increase the universality. Based on the theory that image inclination angle is the angle contained by the axis with strongest intensity in Fourier spectrum and vertical axis, the algorithm is improved by taking inclination angle computation as the first step. Experimental image is processed by a 2D Fourier transform at first. Then the obtained spectrum amplitude is transformed into Log-Polar space. The next step is calculation on inclination angle of oblique stripes making use of peaks statistics of projection in angular axis and image content. Whereafter, the improved algorithm just takes advantage of the calculated angle to rotate the experimental image for ensuring stripe noises vertical and proceeds automatic image clipping in the rotated image for an effective area. With this, the vertical de-striping algorithm mentioned above can be implemented in the effective image area to remove stripe noises.

The results show that the improved algorithm of oblique stripes removal is able to figure out stripes' inclination angle and realize automated image processing. Meanwhile, this algorithm is proved to have the remarkable robustness. In order to verify the result of the algorithm, this paper compares the algorithm results with the official processing results. Comparison is carried out by quantitatively evaluations of both these two kinds of processing results, indicated by mean value, standard deviation and inverse coefficient of variation. The results of evaluation demonstrate that the image quality has been improved after de-striping, adopting the algorithm based on adaptive frequency filtering in this paper, without losing important information.

8537-49, Session PS

Segmentation of vegetation scenes: the SIEMS method

Alexandre Alakian, ONERA (France)

This paper presents an unsupervised segmentation method dedicated to vegetation scenes with decametric or metric spatial resolutions. The proposed algorithm, named SIEMS, is based on the iterative use of the Expectation–Maximization algorithm and o?ers a good trade-o? between oversegmentation and undersegmentation. Moreover, the choice of its input parameters is not image–dependent on the contrary to existing technics and its performances are not crucially determined by these input parameters. SIEMS consists in creating a coarse segmentation of the image by applying an edge detection method (typically the Canny–Deriche algorithm) and splitting iteratively the undersegmented areas with the Expectation–Maximization algorithm. The method has been applied on two images and shows satisfactory results. It notably allows to distinguish segments with slight radiometric variations without leading to oversegmentation.

8537-50, Session PS

Selection of interpolation methods used to smile correction of SWIR hyperspectral images

Lin Li, Shanghai Institute of Technical Physics (China) and Graduate University of the Chinese Academy of Sciences (China); Yong Hu, Cailan T. Gong, Shanghai Institute of Technical Physics (China); Mingsheng Peng, Shanghai Univ. (China)

Spectral smile is widely referred as an optical distortion in the cross-track direction that affects hyperspectral images. Limited by the dispersive optical systems, smile effect usually presented in pushbroom sensors, such as hyperspectral imagers. Smile effect destroys the alignment between slit light and the across-track pixels and makes both central wavelength and spectral resolution non-homogenous along the across-track position, as a result, spectrum is mixed in the images. The smile effect alters the pixel spectral that affects quantitative remote sensing applications, for example, it reduces the accuracies of recognition of the red-edge position and leads to misclassification. Smile effect becomes observable when the image is transformed into Minimum Noise Fraction (MNF), for images with significant smile, a brightness gradient appears in the first eigenvalue image of MNF space. Apart from MNF transformation, another way to inspect for the smile effect is to look at the band difference images around atmospheric absorption feature such as Oxygen feature near 760nm.Traditional correction methods of smile effect include adapt the MNF component that embodies the cross-track effects before rotating the MNF data set back to the radiance space, make the mean DN of each band as all column DN value etc. Among all techniques, only the resampling method gives a satisfactory result. In this paper, we focus on the SWIR hyperspectral images, illustrate the smile effect as well as the consequence in the images, analyze the smile effect on the application of remote sensing and propose several interpolations to resample the spectrum so as to correct the smile effect. The paper is organized in four steps: first of all, give an analysis of the wavelength shifts between onboard and in the laboratory spectral calibration results, conduct the wavelength correction according to the offset results and retrieve the central wavelength of each detector element in the detector array from the corrected calibration data records. Second, a series of pre-processing are carried out, such as removing the black level and abnormal pixels in the images, non-uniformity correction etc. Then, according to the onboard spectral calibration data records, six different types of interpolation are tested to the SWIR hyperspectral images, they are linear interpolation, three points quadratic polynomial interpolation, four points three-order Lagrange interpolation, five points four-order Lagrange interpolation, piecewise cubic Hermite interpolation and cubic spline interpolation. Finally the performance of those interpolation methods to resample the spectrum was assessed in three ways: a qualitative comparison is obtained from images of MNF fraction before and after smile correction; an accurate analysis of terrain classification is proposed and the surface reflectance curves of images before and after smile correction are compared. The results indicate that four-point cubic Lagrange interpolation and cubic spline interpolation are better than other four interpolation methods, the smile effect is overcome and the noise increase is minimized. However some strong absorption bands are likely to be so corrected that introduce new errors by applying to the linear and three points quadratic polynomial interpolation.

8537-51, Session PS

Junction extraction on road masks by pruned skeletons

Umut Cinar, Ersin Karaman, Ekin Gedik, Ugur Halici, Yasemin Yardimci, Middle East Technical Univ. (Turkey)

Road junction extraction from remotely sensed images is not a widely studied topic, yet there are some attempts to detect/classify road junctions. One study [1] mainly tries to extract road arms before constructing the resultant intersection polygon between the road arms. In a recent work[2], the road network is found by simply thresholding the grayscale image, and then inspecting the orientation features of road skeleton which leads to the final result. However, non-enhanced skeleton causes many false alarms. Similarly, the study[3] uses road skeleton to detect intersection points after applying an improved ridge detector to extract road mask. Their study tries to decrease false alarm rate by pruning road mask before morphological thinning operation. Another study [4] employs a road junction extraction operator using a feed-forward neural network for classification. In their study, road edges from grayscale images are used as feature vectors for corresponding search windows. In[5], an unsupervised learning algorithm is employed with pre-defined rules to deal with junction extraction problem.

In this study, the skeleton of the given road mask is used to detect junctions. There are two main challenges for distinguishing road junctions from skeleton imperfections of a road network. First challenge is the presence of spurious branches due to thinning operation. These branches are falsely identified as road junctions by standard junction extraction algorithms. The second is the spurious loops on the skeleton caused by the misalignment of road arms. Especially, these two problems degrade the performance of junction extraction dramatically when automatic road extraction algorithms are used as they are more vulnerable to environmental effects such as vegetation and shadow resulting in corrupted road masks. Therefore, special purpose pre- or post- processing methods are needed to overcome these problems. There are three major steps of the proposed method:

i. Preprocessing:

At this stage, the road mask is skeletonized by the help of morphological thinning operation. After that false branches of skeleton are removed by using recursively following endpoints until the junction points are reached. Moreover, small loops of skeleton are eliminated by firstly filling them before further skeletonization operations are applied. By this way, a pruned version of initial skeleton can be acquired, which will be used as input for latter stages.

ii. Vectorization, junction detection and junction type classification:

Firstly, vectorization of the preprocessed skeleton is achieved by the method proposed by P.Kovesi. After this operation, a piecewise linear representation of the road network is obtained. By using this representation, the points where more than two vectors intersect are gathered as potential junction points. For each potential junction, a vector set is formed by using intersecting vectors of the point. Afterwards, the junctions are classified as T-type, Y-type and X-type according to their vector sets' geometric features.

iii. Postprocessing:

At the last step, morphological dilation followed by shrink operation is applied to merge junctions close to each other. A minimum distance threshold value is used to merge close junctions.

8537-52, Session PS

Integrating region similarity to MRF Model for image segmentation

Tiancan Mei, Xuebing Guo, Sidong Zhong, Wuhan Univ. (China)

Image segmentation aims to divides an image into disjoint parts that are homogeneous with respect to a chosen property such as reflectivity, texture etc. The performance of image segmentation is of paramount importance for many subsequent image based applications, such as information extraction based on remote sensing image. Once the segmentation result is obtained, relevant properties of the segmented region, such as shape, brightness, texture, etc can be used for further image understanding and interpretation.

Due to ambiguity of image data that contain complex scenes, the segmented region rarely corresponds directly with objects in the input image. In order to get meaningful segmentation results, it is necessary to take into account the contextual information about the image under analysis. Bayesian approach is a simple, yet effective tool to integrate both the contextual information and image data statistical property in the segmentation process. Under the framework of Bayesian approach, the Markov random field(MRF) is used to model the contextual knowledge about the image. MRF is a probabilistic graphical model, which provides a statistical way to model the spatial contextual constraints of an image, and obtains the segmentation results by maximizing a posterior probability of the label random variables given the image observations.

The MRF model was initially used to segment the image at the pixel level. Because the neighboring relationship among pixels is regular on the 2D lattice, the pixel-based MRF methods could conveniently model the spatial contextual information. However, the calculation of the pixel-based MRF is time-consuming. Hence, many researchers have extended the MRF model based on initial segmentation results. Generally speaking, the region-based MRF methods usually divide an image into several segmented regions first. Then, the region-based MRF model is defined on these initial regions to obtain the finally segmentation results by integrating prior information. Most of the region based MRF model used POTTS model to describe the contextual information by considering whether the class label of neighboring site is identical with each other. Thus it gives preference to the segmentation results that have large uniform regions. The POTTS model describes the interaction between the neighboring sites without taking observed image data into account, which leads to poor segmentation results.

In this paper, we propose a segmentation method based on region based MRF model. Complex contextual behavior can be captured through this method. By taking into account statistical interaction

between neighboring regions, this method enhance the power of modeling class label interaction. Differentiating from the traditionally POTTS model which processes the class label interaction independent of the image data, we estimate the class label interaction by taking into account the contribution of image data. Specifically, we calculate the statistically similarity between neighboring regions. Then it is used to modify the class label interaction based on POTTS model. The method of how to incorporate statistical similarity of neighboring region into MRF model is detailed in this paper.

The proposed image segmentation method consists of two main components. The first component is to perform initial image segmentation. Then the region feature is calculated. Also at this stage, the region adjacency graph(RAG)is built to represent the spatial topological relationship between neighboring regions. The initial segmentation is carried out by using mean-shift algorithm. The second component is refine the initial segmentation by using MRF model to describe the contextual information. The statistical property of segmented region is represented by Gaussian model. Under the Bayesian framework, the posterior probability is the product of the likelihood of observed field and prior probability of label field. In this paper, the contribution of observed field is modeled by Gaussian distribution. The contribution of label field is represented by modified POTTS model. By introducing statistical similarity of neighboring region into POTTS model, the contribution of label field is associated to observed image data. The more similar neighboring regions, the more probable they will share the same class label. The final segmentation is obtained by maximizing posterior probability by using ICM algorithm.

Region based MRF model is a powerful image segmentation tool. By introducing the statistical similarity into the POTTS model, the performance of segmentation is improved. The proposed scheme was tested on remote sensing images, and the results show that the segment results are quite promising.

8537-53, Session PS

Imaging and target-location algorithms for airborne bistatic SAR system

Yong Li, Ya Li, Nanjing Univ. of Aeronautics and Astronautics (China)

Bistatic synthetic aperture radar (BiSAR) systems have been attracting considerably increasing interests in these decades. The real-time location of stationary ground targets in BiSAR images from a general bistatic configuration, when the transmitter and receiver move along nonparallel trajectories with different velocities, is more complicated than a monostatic case, because the range-Doppler history of the bistatic SAR used to determine the coordinates of the targets of interests are double hyperbolic which involving the solution of non-linear equations.

In this paper, we present a modified imaging algorithm and the target-location method for airborne BiSAR under a general geometric configuration. As a step to a numerically efficient processor, a computational efficient image formation method, namely linear range-Doppler (LRD) algorithm is firstly generalized from the monostatic SAR to BiSAR imaging, which also enable the ground-target location processing to be feasible.

The LRD algorithm, originated from the basic theory of rotating-object imaging, has been tested to be robust for mid-resolution monostatic SAR imaging, because the overall processing is achieved by fast Fourier transform and vector-multiplication operations. However, the original LRD algorithm needs to be modified before being used in processing bistatic SAR data, because there are distinct differences in the phase history of the received signal and the sample location of spatial frequency.

With a detailed analysis of the double hyperbolic range-Doppler equations in the signal processing flowchart of the proposed BiSAR LRD algorithm, we adopt two methods in linearizing the nonlinear equation and tailor them to our problem. Specifically, we select the Newton iteration and the dichotomy methods to solve the nonlinear equations and compare the performances of them in locating the ground-targets for the general case of BiSAR system.

As shown in this paper, the Newton iteration method that approximates the root of a nonlinear equation in one variable using the value of the function and its derivative, because of robustness and higher rate of convergence, becomes an attractive method. The dichotomy method just requires that the function values of the two terminals in the finite interval are contrary, hence, leading to a larger region of convergence.

We evaluate the proposed methodologies by a set of point-target simulations using the parameters in regard to a classical mid-resolution airborne BiSAR system. The simulation results are given and analyzed to demonstrate their validity in providing accurate positions of any stationary ground-target in the BiSAR image.

8537-54, Session PS

The study of optical fiber communication technology for space optical remote sensing

Jun Zheng, Sheng-quan Yu, Xiao-hong Zhang, Rong-hui Zhang, Jian-hua Ma, Beijing Institute of Space Mechanics and Electricity (China)

The latest trends of Space Optical Remote Sensing are high-resolution, multispectral, and wide-swath detecting. High-speed digital image data transmission will be more important for remote sensing.

At present, the data output interface of Space Optical Remote Sensing, after performing the image data compression and formatting, transfers the image data to Data Storage Unit of the Spacecraft through LVDS circuit cables, which consist of some low voltage differential signal output ports. One port is dedicated to one data valid signal; one port is dedicated to one transmit clock signal using to synchronize image data transmission on the interface; and some ports are dedicated to image data signal.

But this method is not recommended for high-speed digital image data transmission. This type of image data transmission, called source synchronization, has the low performance for high-speed digital signal, because it will introduce too much jitter for clock and data during operation at high rates. There will be arbitrary phase differences and skew between the clock and data or among the data ports. Besides, it is difficult for cable installing and system testing in limited space of vehicle, because of mass volume, mass weight of many LVDS circuit cables.

To resolve these issues as above, this paper describes a high-speed interconnection device for Space Optical Remote Sensing with Spacecraft through optical fiber. To meet its objectives, this device is comprised of Virtex-5 FPGA with embedded high-speed series and power-efficient transceiver, called Rocket-IO GTX transceiver, fiber-optic transceiver module, the unit of fiber-optic connection and single mode optical fiber, which are adapt to harsh space environments. For proper high-speed operation, the GTX transceiver requires a high-quality, low-jitter, reference clock.

First, Parallel image data with synchronizing clock and data valid signal flows into the FPGA TX interface, through the PCS which has built-in PCS features, such as 8B/10B encoding, through the PMA, and then out the TX driver as high-speed serial data. High-speed serial data flows from traces on the board into the PMA of the RX, whose Clock Data Recovery (CDR) circuit in GTX transceiver extracts a recovered clock from incoming data. Then flows into the PCS, and finally into the FPGA logic.

Second, the special communication protocol is performed for image data transmission system, according to the characteristics of unilateral communication for Space Optical Remote Sensing with Data Storage Unit of the Spacecraft.

Third, the unit of fiber-optic connection with high reliability and flexibility is provided for transferring high-speed serial data through optical fiber between Space Optical Remote Sensing and Spacecraft.

It is evident that this method provides many advantages for Space Optical Remote Sensing in the aspect of image data high-speed transmission:

1. Improving the speed of image data transmission of Space Optical Remote Sensing;

2. Enhancing the reliability and safety of image data transmission, such as the elimination of cable-to-cable and box-to-box electromagnetic-interference (EMI) effects;

3. Space Optical Remote Sensing will be reduced significantly in size and in weight;

4. System installing and system testing for Space Optical Remote Sensing will become easier.

8537-55, Session PS

Elastic band-to-band registration for airborne multispectral scanners with large field of view

Feng Li, ChuanRong Li, LingLi Tang, The Academy of Opto-Electronics (China); Yi Guo, Commonwealth Scientific and Industrial Research Organization (CSIRO) (Australia)

Multispectral scanners (MSS) with large field of view improve efficiency in Earth observation. It, however, may bring a problem: different none-linear warping and inconsistent local transformation exist between bands. This is caused by air turbulence; self-propelled vibration of airborne platforms; as well as the systematic design of MSS. Variation of the intensity of spectral bands makes the problem even more challenging.

In this paper, an elastic image registration is proposed for solving the registration problem brought by airborne multispectral line scanners with large field of view. Rather than carrying out registration between bands straightforwardly, corresponding featured images of each band are created. The idea of the inverse compositional algorithm is borrowed and expended in dealing with local warping of the featured images. Rather than warping the source image towards the reference image step by step with a first order Taylor Series expansion, warping the reference image towards the source image, a Hessian matrix can be calculated outside of the iterations. The Hessian matrix is calculated once only for each scale image. A 7-dimensional vector is used to describe the warp and the brightness variation between the source and reference images. After resolving the global affine transform, two images can be coarsely aligned. Then, dealing with local warping between local regions needs to be considered. As many other methods, for each location within the two images, boxes or blocks are used to deal with the local warping individually. The smaller the box size, the better the approximation with translation for the complex none rigid warping. Therefore, a 3-dimensional vector is adopted to describe the translation and brightness variation between the source image box and the reference image box. This improved elastic image registration method can deal with a global affine warping and local shift translations based on from coarse to fine pyramid levels. A pyramid scaling model is built into this image registration method to deal with possible large spatial variations within images.

Experimental data was captured by flying a big Unmanned Aerial Vehicle (UAV) with a new type of multispectral line scanner (red, green, blue and near inferred) and a visible light CCD array camera on board. The new MSS is composed of four off axle sphere reflectors with FOV of 61.93° and IFOV of 0.18mrad. Common rigid or global registration methods fail to solve the registration problem, because each band suffers different nonlinear warping, though the flight was carried out under good weather condition. Results show that our new elastic registration method can well solve the problem with less time and high accuracy. Both numerical and visual results will also be included in the paper.

8537-56, Session PS

Remote sensing image classification by mean shift and color quantization

Hind Taud, Instituto Politécnico Nacional (Mexico); Stéphane Couturier, José Joel Carrillo-Rivera, Univ. Nacional Autónoma de México (Mexico)

Remote sensing imagery involves large amounts of data acquired by several kinds of airborne, sensors, wavelengths spatial resolutions, and temporal frequencies. To extract the thematic information from these data, many algorithms and techniques for segmentation and classification have been proposed. In fact, various algorithms has been used for both image segmentation and classification. The representation of the different multispectral bands as true or false colour imaging has been widely employed for visual interpretation and classification. On the other hand, the colour quantization, which is a well-known method for data compression, has been utilized for colour image segmentation and classification in computer vision application. The number of colours in the original image is reduced by minimizing the distortion between the quantified and the original image with the aim of conserving the representation of pattern. Considering the density estimation in the colour or feature space, similar samples are grouped together to identify patterns by any clustering techniques. Mean shift algorithm has been successfully applied to different applications as the basis for nonparametric unsupervised clustering techniques. Based on an iterative way, mean shift detects modes in a probability density function. In this article, the contribution consists in providing an unsupervised colour quantization method for image classification based on mean shift. To avoid the high computational cost of mean shift, the integral image is used. The method is evaluated on Landsat satellite imagery as a case study to underline forest mapping. A comparison between the proposed method and the simple mean shift is carried out. The result proves that the proposed method is useful in multispectral remote sensing image classification study.

8537-57, Session PS

Object-based image analysis and data mining for building an ontology of informal urban settlements

Dejrriri Khelifa, Ctr. National des Techniques Spatiales (Algeria) and EEDIS Laboratory, University of Sidi Bel Abbes (Algeria); Malki Mimoun, Univ. of Sidi Bel Abbes (Algeria)

During recent decades, unplanned settlements have been appeared around the big cities in most developing countries and as consequence, numerous problems have emerged. Thus the identification of different kinds of settlements is a major concern and challenge for authorities of many countries. Very High Resolution (VHR) Remotely Sensed imagery has proved to be a very promising way to detect different kinds of settlements, especially through the using of new object-based image analysis (OBIA). The most important key is in understanding what characteristics make unplanned settlements differ from planned ones, where most experts characterize unplanned urban areas by small building sizes at high densities, no orderly road arrangement and Lack of green spaces. Knowledge about different kinds of settlements can be captured as a domain ontology that has the potential to organize knowledge in a formal, understandable and sharable way. In this work we focus on extracting knowledge from VHR images and expert's knowledge. We used an object based strategy by segmenting a VHR image into regions of homogenous pixels at adequate scale level and then computing spectral and spatial attributes for each region to create objects. A genetic based data mining was used to generate high predictive and comprehensible classification rules based on selected samples from the OBIA result. Optimized intervals of relevant attributes are found, linked with land use types for forming classification rules. The unplanned areas were separated from the planned ones, through analyzing of the line segments detected from the input image. Finally a simple ontology was built based on the previous processing steps. The approach has been tested to VHR images of one of the biggest Algerian cities, that has grown considerably in recent decades.

8537-58, Session PS

A parametric statistical model over spectral space for the unmixing of imaging spectrometer data

Jignesh Bhatt, Manjunath Joshi, Mehul Raval, Dhirubhai Ambani Institute of Information and Communication Technology (India)

Under linear mixing model, imaging spectrometer data are considered to be linear combinations of constituent endmembers signatures. Spectral unmixing techniques attempt to estimate underlying abundance maps of the endmembers from the data with a set of endmember signatures. However, it should be noted that the abundance are not uniformly distributed over the entire scene and their proportions are varied based on the scene contents. Due to the noise in the remotely sensed satellite data, the estimated abundance values are inaccurate with the use of conventional maximum-likelihood based estimation techniques. In this paper, we propose a maximum a posteriori - Huber-Markov random field (MAP-HMRF) method in order to achieve better estimation of the abundance. A MAP estimation is obtained by incorporating the HMRF as the prior along with the data-term. A Huber function is defined based on the first order difference among abundance at each location, across the contiguous spectral space. The Huber function is quadratic for homogeneous regions and it becomes linear for the regions having significant variations in the mixture. This way of modeling the abundance as HMRF over the measured spectral space preserves the sudden variations in the

abundance as well as the homogeneity in the abundance values. The final MAP energy function to be minimized is (attached in. pdf file) formulated as the sum of the data-term and the HMRF prior term. This function is convex but non-quadratic and hence can be easily minimized by using a simple gradient based optimization method. While optimizing, the solution space of the estimated abundance is restricted to lie between 0 and 1.

The proposed method is tested by conducting experiments on simulated as well as on real data (AVIRIS). A 224-band data is generated by using linear combinations of three endmember spectra. These are Ammonioalunite NMNH145596, Brucite HS247.3B and Andradite WS487 available from the USGS spectral library. The simulated data (scene) is constructed to yield nine different regions having different proportions of the mixture of the three spectral signatures. While experimenting, we add additive white Gaussian noise in the data. At each location, the estimated abundance maps using the proposed method are compared with the ground truth as well as with the results obtained using the state-of-the art approach. The experimental results demonstrate that the proposed method outperforms the fully constraint least squares (FCLS) approach and show better matches with the ground truth values. The results with the real data (AVIRIS) demonstrate the potential of the proposed method to preserve the spectral variations among the abundance.

8537-59, Session PS

The inpainting of hyperspectral images: a survey and adaptation to hyperspectral data

Alex Chen, University of North Carolina, Chapel Hill (United States)

Image inpainting has become one of the most important problems in image processing. It deals with the restoration of missing or damaged data over an image domain. In this work, we will survey some of the most common grayscale and color inpainting algorithms and study their suitability for adaptation to hyperspectral inpainting. One of the principal applications is the recovery of missing regions due to gaps in hyperspectral data obtained from airborne sensors.

The most common inpainting methods involve the propagation of information from nearby regions into the unknown region through some diffusion process. Other effective methods use the comparison of similar neighborhoods to partially known regions. Many of these methods are readily generalizable to vector-valued data, mainly RGB color data.

Many inpainting algorithms introduce an energy functional that penalizes undesirable characteristics such as excessive variation away from edges. Variational inpainting methods evolve a PDE to minimize this functional.

One of the earliest effective variational inpainting algorithms is the total variation (TV) algorithm, which preserves edge sharpness in contrast to isotropic diffusion, which tends to produce too much blurring.

Nonlocal algorithms that compare similar neighborhoods are particularly effective on images with repeated structure. Such methods often search in a nearby window for similar-looking patches.

Then unknown pixels can be filled using the corresponding known pixels in the similar patch. For a more robust algorithm, several similar patches can be averaged.

Inpainting in hyperspectral imagery, however, remain relatively less explored. There are clear differences between hyperspectral data and color images that make a direct conversion from color inpainting to hyperspectral inpainting not always advisable. While total intensity remains a dominant factor in classifying objects in color images--as in grayscale images--spectral content becomes much more important for hyperspectral data.

It is well-known that spectral shape is significant in hyperspectral data; the intensity of each spectral band should not be considered separately. One simple method to deal with this observation is to decouple illumination and spectral shape. More generally, inpainting on a transformed coordinate space, such as from Principal Components Analysis (PCA), can give more accurate results.

Tschumperle and Deriche consider inpainting on vector-valued images, obtaining impressive results on color images, but their method is not as effective for hyperspectral data. Rial et al. treats the problem of inpainting hyperspectral data, pointing out that spectral information is relatively more important than spatial information due to the wealth of spectral information in hyperspectral data.

Finally, hyperspectral data with high spatial resolution has become increasingly available. We thus explore the possibilities on such data. Fourth-order inpainting methods evolve a fourth-order PDE to propagate information. While more computationally expensive, these methods have been shown to reduce staircasing of diagonal edges and connect edges that have been broken by the unknown region.

For hyperspectral data with high spatial resolution, spatial information such as edge quality becomes more significant. Thus, fourth-order inpainting methods that preserve edges often outperform their second-order counterparts.

8537-61, Session PS

Unsupervised classification of hyperspectral images using an Adaptive Vector Tunnel classifier

Suleyman Demirci, Turkish Air Force Academy (Turkey); Isin Erer, Istanbul Technical University (Turkey)

Hyperspectral image classification is one of the most popular information extraction methods in remote sensing applications [1]- [7]. These methods use multiple regions of electromagnetic spectrum, and consist of a variety of algorithms involving supervised, unsupervised or fuzzy classification, etc. In supervised classification, reference data with known a priori class information is used. Various supervised classification algorithms may be used to assign unknown pixels to their classes. Parametric classification algorithms assume that the observed data have predefined statistical nature. Although nonparametric classification algorithms do not make this assumption, their calculation costs remain high [8]. In unsupervised classification, computer based clustering algorithms are used to group pixels which have similar spectral characteristics according to some statistical criteria. Among the most powerful techniques for understanding hyperspectral image clustering, K-means is one of the most used iterative approaches [9], [10]. It is a simple though computationally expensive algorithm, particularly for clustering large hyperspectral images into many categories.

In this study, a new adaptive unsupervised classification technique is presented. It is a kind of vector tunnel around the training pixel spectra that changes according to spectral variation with respect to hyperspectral bands. This adaptive vector tunnel classifier does not need a priori class information or heavy mathematical calculation just like in standard software implementation of K-means which uses floating-point arithmetic, Euclidean distances or vector angel [9], [10]. It also does not need any other parameters such as covariance matrix which has computationally expensive calculation. Comparing to Euclidean distance algorithm, proposed method uses multiple distance and can follow instantaneous changes in the spectra. But Euclidean Distance algorithm can not detect the location of changes in spectra. Unnecessity of dimension reduction except omitting poor bands preserves additional information in multidimensional spectral signature. Contrary to spectral angle method, it is possible to take into account the materials that have different reflectance level but similar spectral shape.

The proposed method may be summarized as in the following:

Step1: A random pixel is selected in the hyperspectral image.

Step 2: According to this pixel spectra, n-dimensional vector tunnel is formed by using predefined tunnel parameters.

Step 3: Whole pixels in the image are tested if they lie in the tunnel or not. According to test result, the pixels in first tunnel are assigned as the members of the first class.

Step 4: The parameters of the vector tunnel are adapted with respect to mean and standard deviation of the first class.

Step 5: A second random pixel is selected and Steps 2-4 are repeated to assign the members of the second class.

Step 6: Steps 1-5 are repeated for all the remaining pixels to assign the members of the following classes. The class number is equal to the tunnel number. Amount of tunnel is roughly defined by adjusting tunnel threshold parameter.

The proposed method is tested on AVIRIS Indiana's Pine and HYDICE Urban data. Although vector tunnel classifier does not need intensive mathematical calculation, classification results are comparable to K-Means Classification Algorithm. Because of lack of HYDISE ground truth data, Quantitative test results will be given for only AVIRIS data in full paper.

8537-63, Session PS

Range-azimuth decoupling framework for CS-ISAR imaging

Xiaochun Xie, Gannan Normal Univ. (China); Ling-Juan Yu, Jiangxi Univ. of Science and Technology (China)

By using compressive sensing technique, the data rate needed in radar imaging can be remarkably reduced. But in most of CS-ISAR imaging methods, target is reconstructed in 2D directly, which need huge storage space and computation time. In traditional ISAR imaging, the processing on range and azimuth are decoupled. This method increases the imaging speed and reduces the storage space. So we want to find a CS-ISAR imaging method with decoupled range and azimuth processing step. To achieve this goal, phase reservation in range compression is the key issue.

In this paper, we propose a phase-reservation CS based pulse compression algorithm by analyzing the sparse characteristics of complex base-band echo signal from a target using chirp signal as transmitted signal. After CS range compression, the recovered scatters can keep their phase information. The phase information is a function of distance between radar and scatter, and can be used in 2D/3D radar imaging. Based on the traditional methods, we can get 2D and 3D ISAR imaging framework, as shown in Figure 1.

To verify the proposed framework, we carry out two experiments. One experiment is designed to valid 2D ISAR imaging with real data. The echo data of a moving train is acquired by a ground stationary Ka-band radar system and CS based range compression is carried on the acquired data with a down-sampling rate of 50. The imaging results in Figure 2 shows that 2D CS-ISAR imaging method can represent the same detail information of the train as traditional method. Another experiment is designed to valid 3D InISAR imaging with simulation data. The reconstruction result confirmed that the 2D ISAR images gotten from CS method can be used for 3D InISAR imaging and the framework we proposed in Figure 1 is feasible, and the phase information reserved by the proposed algorithm can guarantee the quality of 3D radar imaging. The experiment results also showed that the proposed framework can increase the imaging speed and reduce the storage space of CS-ISAR imaginf system remarkably.

8537-64, Session PS

A comparison study of object-based and pixel-based classification techniques for high resolution urban land-cover mapping

Mohammad Rezaei, Univ. of Tehran (Iran, Islamic Republic of)

The launch of new high-resolution earth observation satellites (e.g. WorldView-2 and GeoEye-1) provides potential resources for Land Cover classification. The remotely sensed images acquired by these sensors benefit of higher spectral and spatial resolution characteristics which lead to more effectively detect, classify and quantify the earth surface features.

In this paper, we evaluated four different classification methods in two main categories: Rule-based which performed in object-based paradigm (Bouziani & Goita, 2010), Support Vector Machines (SVM) as a pixel-based method that we run in both pixel-based and object-based paradigm [2][3], Classification And Regression Tree (CART) which we use as an object-based techniques and Maximum Likelihood Classification (MLC) as a common pixel-based one. Object-based methods were implemented using commercial software, eCognition (Baatz & Schäpe, 2000). These techniques have been applied to a very high-resolution image dataset acquired by WorldView-2 from an urban area in Rio de Janeiro, this imagery was provided by DigitalGlobe for the IEEE-IGRARSS 2011's Data Fusion Contest. The spatial resolutions of panchromatic and multispectral image bands are 0.46-0.52 and 1.8-2.4 meter respectively. The multispectral sensor is a unique system able to collect images in 8 bands ("The Benefits of the 8 Spectral Bands of WorldView-2," 2009).

For a better discrimination, some new features have been extracted from new bands of WorldView-2. The normalize differences of non-homogenous feature introduced using Coastal and Red edge bands, which can discriminate buildings and road more precisely (Wolf, 2010). Extraction of vegetation has been done using NDVI, but instead of using NIR-1, we use NIR-2 to increase the differences of vegetation and other land covers (Chávez & Clevers, 2010). Also, for determining the shadow, Principal Component Analysis (PCA) of whole image has been done and differences of blue band and PC-1 imported as a new feature (Nobrega & Quintanilha, 2006).

Figure 2 shows the overall accuracy of methods. Results show that the rule-based classifications achieved a high overall accuracy, 96.62%, whereas the CART and SVM reached a lower accuracy, 92.63% and 90.81 respectively. SVM and MLC as most common methods in pixel-based paradigm produced lower accuracy in comparison to object-based, 87.31% and 72.37% respectively.

8537-65, Session PS

A quaternion-based method for satellite images pan-sharpening

Chahira Serief, Habib Mahi, Moussa Sofiane Karoui, Ctr. National des Techniques Spatiales (Algeria)

To date, several pan-sharpening methods have been proposed in the literature. However, conventional Pan-sharpening processes are based on color separation (RGB decomposition for example) of color (spectral) images resulting in significant loss of color information. The aim of this work is to investigate the potential of hypercomplex numbers representation of color images, in particular Quaternion model, for satellite images pan-sharpening. Quaternion model allows color images to be handled as a whole, rather than as color-separated components. That is, the values of the color components (R, G and B for example) of each pixel of a color image are represented as a single pure quaternion valued pixel. The proposed fusion method is based on Quaternion intensity-hue-saturation (QIHS) transform and consists of three steps. First, the color (spectral) image is represented as a pure quaternion image to take into account its particular nature. Then, the IHS transform is applied to the pure quaternion image resampled at the scale of panchromatic (Pan) image. Finally, the image fusion process is done by IHS-based component substitution. The efficiency of the proposed method is tested on Quickbird dataset. A comparative evaluation among the proposed technique and the standard IHS-based method is then conducted.

8537-66, Session PS

Hierarchical watershed segmentation based on gradient image simplification

Mauro Dalla Mura, Fondazione Bruno Kessler (Italy); Francois Cokelaer, Jocelyn Chanussot, Gipsa-lab (France)

Watershed is one of the most widely used algorithms for segmenting remote sensing images. This segmentation technique can be thought as a flooding performed on a topographic relief in which the water catchment basins, separated by watershed lines, are the regions in the resulting segmentation. A popular technique for performing a watershed relies on the flooding of the gradient image in which high level values correspond to watershed lines and regional minima to the bottom of the catchment basins.

In general, the intrinsic variability of the spectral dynamics in real images leads to a fine partition of the scenes (i.e., over-segmentation) with this segmentation approach. A possible way to contrast this well known effect relies on a filtering phase applied to the original image for defining regions (i.e., markers) that will not be split in the segmentation phase. The simplification of the input image leads to a more coarser partition of the scene.

In this paper, we propose to perform a simplification on the gradient image by removing high contrast edges. In this way, regions in the subsequent watershed segmentation get to be merged. The filtering of the gradient image is performed applying length filtering (using morphological path-based operators) and attribute filters. In this way, it is possible to drive the simplification (and thus, the resulting way to merge regions) according to some characteristics of the high contrast regions in the image that are accounted by the filters.

By applying a sequence of progressively more aggressive filters (leading to greater simplifications of the image) it is possible to generate a hierarchy of segmentations.

Conference 8538A: Earth Resources and Environmental Remote Sensing/GIS Applications

Tuesday - Thursday 25–27 September 2012 • Part of Proceedings of SPIE Vol. 8538
Earth Resources and Environmental Remote Sensing/GIS Applications III

8538-1, Session 1

Monitoring of changes in areas of conflicts: the example of Darfur

Holger Thunig, Ulrich Michel, Pädagogische Hochschule Heidelberg (Germany)

Rapid change detection is used in cases of natural hazards and disasters. This analysis leads to rapid information on areas of damage. In certain cases the lack of information after catastrophe events is obstructing supporting measures within disaster management. Earthquakes, tsunamis, civil war, volcanic eruption, droughts and floods have much in common: people are directly affected, landscapes and buildings are destroyed. In every case geospatial data is necessary to gain knowledge as basement for decision support. Where to go first? Which infrastructure is usable? How much area is affected? These are essential question which need to be answered before appropriate, eligible help can be established.

This paper focuses on change detection applications in areas where catastrophic events took place which resulted in rapid destruction especially of manmade objects. Standard methods for automated change detection prove not to be sufficient; therefore a new method was developed and tested. The presented method allows a fast detection and visualization of change in areas of crisis or catastrophes. While often new methods of remote sensing are developed without user oriented aspects, organizations and authorities are not able to use these methods because of lack of remote sensing knowledge. Therefore a semi-automated procedure was developed. Within a transferable framework, the developed algorithm can be implemented for a set of remote sensing data among different investigation areas. Several case studies are the base for the retrieved results. Within a coarse dividing into statistical parts and the segmentation in meaningful objects, the framework is able to deal with different types of change. By means of an elaborated Temporal Change Index (TCI) only panchromatic datasets are used to extract areas which are destroyed, areas which were not affected and in addition areas where rebuilding has already started.

8538-2, Session 1

Detection and assessment of land use dynamics on Tenerife (Canary Islands): the agricultural development between 1986 and 2010

Sebastian Günthert, Pädagogische Hochschule Heidelberg (Germany) and Ruprecht-Karls-Univ. Heidelberg (Germany); Simone Naumann, Pädagogische Hochschule Heidelberg (Germany); Alexander Siegmund, Pädagogische Hochschule Heidelberg (Germany) and Ruprecht-Karls-Univ. Heidelberg (Germany)

Since Spanish colonial times, the Canary Islands and especially Tenerife have always been used for intensive agriculture. Today almost 1/4 of the total area of Tenerife are agriculturally affected, whereas especially mountainous areas with suitable climate conditions are drastically transformed for agricultural use by building of large terraces. In recent years, political and economical developments lead to a further transformation process, especially inducted by an expansive tourism, which caused concentration- and intensification-tendencies of agricultural land use in lower altitudes as well as agricultural set-aside and rural exodus in the hinterland. The main aim of the research is to address the agricultural land use dynamics of the past decades and to statistically assess the causal reasons for those changes.

Therefore an object-based classification procedure for recent RapidEye data (2010), Spot 4 (1998) as well as SPOT 1 (1986-88) imagery was developed, followed by a post classification comparison (PCC). A key benefit of this classification technique is the possibility to deal with image objects or segments and not pixel. The object based approach thereby offers high potential for the identification of agricultural land use in medium resolution satellite imagery, as agricultural parcels are besides its spectral characteristics also detectable on the basis of geometrical attributes (e.g. rectangular fit, size etc.) of the segments. However, the information obtained from the medium resolution data has its limits. Older agricultural fallow land or agricultural set-aside with a higher level of natural succession can hardly be acquired in the used satellite imagery. For this reason, a second detection technique was generated, which allows an exact identification of the total agriculturally affected area on Tenerife, also containing older agricultural fallow land or agricultural set-aside. The method consists of an automatic texture-oriented detection and area-wide extraction of linear agricultural structures (plough furrows and field boundaries of arable land, utilised and non-utilised agricultural terraces) in current orthophotos of Tenerife. Once the change detection analysis is realised, it is necessary to identify the different causal factors, which are responsible for the agricultural land use dynamics. In general, these so called driving forces can be subdivided into (1) socioeconomic drivers, for example population growth, the increase of the tourist sector, rural migration, settlement expansion; (2) proximate drivers, which can be seen as land management variables, for example regional planning or the establishing of nature protection areas and (3) location-specific drivers which do not ‘drive’ land use changes directly, but can influence land use abandonment decisions, for example misconnexion of agricultural areas to infrastructure units like streets etc. The statistical connections between agricultural land use changes and these driving forces are identified by the use of correlation and regression analyses, followed by a causal proof to avoid statistical but not causal interactions of the correlations.

8538-3, Session 1

Assessing the spatial fidelity of resolution-enhanced imagery using Fourier analysis: a proof-of-concept study

Daniel L Civco, Chandi Witharana, Univ. of Connecticut (United States)

Pan-sharpening of moderate resolution multispectral remote sensing data with those of a higher spatial resolution is a standard practice in remote sensing image processing. This paper suggests a method by which the spatial properties of resolution merge products can be assessed. Whereas there are several accepted metrics, such as correlation and root mean square error, for quantifying the spectral integrity of fused images, relative to the original multispectral data, there is less agreement on a means by which to assess the spatial properties, relative to the original higher-resolution, pan-sharpening data. In addition to qualitative, visual, and somewhat subjective evaluation, quantitative measures used have included correlations between high-pass filtered panchromatic and fused images, gradient analysis, wavelet analysis, among others. None of these methods, however, fully exploits the spatial and structural information contained in the original high resolution and fused images. This paper proposes the use of the Fourier transform as a means to quantify the degree to which a fused image preserves the spatial properties of the pan-sharpening high resolution data. A high-resolution 8-bit panchromatic image was altered to produce a set of nine different test images, as well as a random image. The Fourier Magnitude (FM) image was calculated for each of the datasets and compared ? via FM to FM image correlation. Furthermore, the following edge detection algorithms were applied to the original and altered images: (a) Canny; (b) Sobel; and (c) Laplacian. These edge-filtered images were compared, again by way of correlation, with the original edge-filtered panchromatic image. Results indicate that the proposed method of using FTMI as a means of assessing the spatial fidelity of high-resolution imagery used in the data fusion process outperforms the correlations produced by way of comparing edge-enhanced images.

8538-4, Session 2

Change detection in time series of high resolution SAR satellite images

Markus Boldt, Karsten Schulz, Fraunhofer-Institut für Optronik, Systemtechnik und Bildauswertung (Germany)

In the last few years, change detection based on remote sensing data has become a high frequented field of research with multiple applications for practical use. To detect changes between temporarily different satellite image data is of interest for example in terms of urban monitoring and disaster management. In the latter case, accurate information about the dimension and the category of the change has to be available as fast as possible. Change detection in general is not only the detection of changes between two temporarily different images. Furthermore, categorization of the detected changes into classes representing the kind of change is an important step of change detection (e.g. post-processing classification).

The change detection method described in this paper aims at the fully automatic detection of small scaled, abrupt changes in time series of SAR amplitude image data which are caused for example by different kinds of vehicles or building sites. To create a robust method which is simple to generalize, only a single parameter has to be set by the operator. This parameter is used in a sequential morphological filter approach encoding the size of the detected changes.

Changes between interferometric TerraSAR-X image pairs (original image data: courtesy of Astrium Services / Infoterra GmbH) of Greding, Germany (11 day repeat pass cycle) are investigated over a time period of almost half a year (August to December of 2008), both in ascending and descending orbit image data. By this, temporarily stable (> 11 days) and unstable changes (11 days) are classified resulting in a visualization named ActivityMap.

For evaluation purposes, this method is compared to the CoVAmCoh analysis which represents another change detection method considering phase information visualized as coherence image. In general, both methods are able to detect changes, but they partially provide complementary information. Therefore, the CoVAmCoh method is sensitive to even very small areas of changes.

In a final evaluation step, the ActivityMaps of both orbit directions and one exemplary CoVAmCoh image of the same area are integrated in the software tool Google™ earth.

8538-5, Session 2

Evaluating remote sensing image fusion algorithms for use in humanitarian crisis management

Chandi Witharana, Civco L. Daniel, Univ. of Connecticut (United States)

Image fusion is inextricably linked to satellite-based rapid mapping workflows. Fused images form the basis for manual, semi-, and fully-automated classification steps in the crisis information retrieval chain. This study investigated how different fusion algorithms perform when applied to very high spatial resolution (VHSR) satellite images that encompass ongoing- and post-crises scenes. The evaluation entailed twelve fusion algorithms: Brovey transform, color normalization (CN) spectral sharpening, Ehlers fusion, Gram-Schmidt fusion, high-pass filter (HPF) fusion, local mean matching, local mean variance matching, modified intensity-hue-saturation (IHS) fusion, principal component analysis (PCA) fusion, subtractive resolution merge (SRM) fusion, the University of New Brunswick (UNB) fusion, and wavelet-PCA (WV-PCA) fusion. These fusion methods are commonly encountered in literature and most are built into commercial software packages. The selected algorithms were applied to GeoEye-1 satellite images taken over three different geographical settings representing natural and anthropogenic crises that had occurred in the recent past: earthquake-damaged sites in Haiti, flood-impacted sites in Pakistan, and armed-conflicted areas and internally-displaced persons (IDP) camps in Sri Lanka. Fused images were assessed using an array of quantitative quality indicators and visual inspection methods. Spectral quality metrics included: correlation coefficient, root-mean-square-error (RMSE), relative difference to mean, relative difference to standard deviation, spectral discrepancy, deviation index, peak signal-to-noise ratio index, entropy, mean structural similarity index, spectral angle mapper, and relative dimensionless global error in synthesis. The spatial integrity of fused images was assessed using Canny edge correspondence, high-pass correlation coefficient, and RMSE of Sobel-filtered edge images. Under each metric, fusion methods were ranked and best competitors were identified. Ehlers, WV-PCA, and HPF reported the best values for the majority of spectral quality indices. Under spatial metrics, UNB and Gram-Schmidt algorithms reported the optimum values. The CN sharpening and SRM algorithms exhibited the highest spectral distortions where as the WV-PCA algorithm showed the weakest spatial improvement. With respect to subjective and objective assessments there is no single fusion method which exhibited superior performances simultaneously for color preservation and spatial improvement. In conclusion, we recommend the University of New Brunswick algorithm if visual image interpretation is involved, whereas the high-pass filter fusion is recommended if semi- or fully-automated feature extraction is involved, for pansharpening VHSR satellite images of on-going and post crisis sites.

8538-6, Session 2

Comparison of 3D representations depicting micro folds: Overlapping Imagery vs. Time of Flight Laser Scanner

Aristidis D. Vaiopoulos, University of Athens (Greece); Andreas Georgopoulos, National Technical University of Athens (Greece); Stylianos G. Lozios, University of Athens (Greece) and University of Athens (Greece)

A relatively new field of interest, which continuously gains grounds nowadays, is digital 3D modeling and environments. However, the methodologies, the accuracy and the time and effort required to produce a high quality 3D model have been changing drastically the last few years. Whereas in the early days of digital 3D modeling, 3D models were only accessible to computer experts in animation, working many hours in expensive sophisticated software, today 3D modeling has become reasonably fast and convenient.

On top of that, with online 3D modeling software, such as 123D Catch, nearly everyone can produce 3D models with minimum effort and at no cost. The only requirement is panoramic overlapping images, of the (still) objects the user wishes to model. This approach however, has limitations in the accuracy of the model. An objective of the study is to examine these limitations by assessing the accuracy of this 3D modeling methodology, with a Terrestrial Laser Scanner (TLS).

Therefore, the scope of this study is to present and compare 3D photorealistic models, produced with two different methods: 1) Traditional TLS method with the instrument ScanStation 2 by Leica and 2) Panoramic overlapping images obtained with DSLR camera and processed with 123D Catch free software. The main objective of the study is to evaluate advantages and disadvantages of the two 3D model producing methodologies.

The area represented with the 3D models, features multi-scale folding in a cipollino marble formation. The most interesting part and most challenging to capture accurately, is an outcrop which includes vertically orientated micro folds. These micro folds have dimensions of a few centimeters while a relatively strong relief is evident between them (perhaps due to different material composition and/or tectonic stress). The area of interest is located in Mt. Imittos, Greece.

Technically, the two utilized methodologies have important differences:

1a) In TLS, the distance of a certain point from the sensor is calculated by measuring the time required by the laser beam to meet the surface of the object and travel back to the sensor, divided by 2 (time of flight).

1b) When processing overlapping images (stereopairs) to obtain 3D model, parallax is used. Parallax is the displacement in the apparent position of an object viewed along two different lines of sight (provided by stereopairs). Parallax can be used to measure distances, since nearby objects have larger parallax than distant objects, when viewed from different angles.

2a) With TLS, the instrument was mounted in five places perimetrically of the area of interest, acquiring respectively five point clouds. The point clouds were later processed in the software for the instrument, Cyclone, in order to be tied precisely (best fit method). Draping of the imagery onto the point cloud was carried out with different software.

2b) With stereopair imagery, overlapping images were acquired with DSLR camera and the extraction of the point cloud and textured 3D model was carried out by 123D Catch software automatically.

3) TLS has superior accuracy (~8 mm), but requires more time and effort. The opposite happens with the stereopair method.

Since TLS has greater accuracy, we can assess the accuracy of the stereopair method and discuss its suitability for certain applications.

8538-7, Session 2

Analysis of time series geospatial data for seismic precursors detection in Vrancea zone

Maria A Zoran, Roxana S Savastru, Dan M Savastru, National Institute of Research and Development for Optoelectronics (Romania)

According to classical earthquake theory, small earthquakes should continue to grow into large earthquakes until they spread all along the fault line. The mechanical processes of earthquake preparation are always accompanied by deformations, afterwards complex short- or long term precursory phenomena can appear. Earthquake prediction has two potentially compatible but distinctly different objectives: (a) phenomena that provide information about the future earthquake hazard useful to those who live in earthquake-prone regions and (b) phenomena causally related to the physical processes governing failure on a fault that will improve our understanding of those processes.

Rock microfracturing in the Earth's crust preceding a seismic rupture may cause local surface deformation fields, rock dislocations, charged particle generation and motion, electrical conductivity changes, gas emission, fluid diffusion, electrokinetic, piezomagnetic and piezoelectric effects. Space-time anomalies of Earth's emitted radiation (radon in underground water and soil , thermal infrared in spectral range measured from satellite months to weeks before the occurrence of earthquakes etc.), ionospheric and electromagnetic anomalies are considered as pre-seismic signals. Satellite remote sensing data provides a systematic, synoptic framework for advancing scientific knowledge of the Earth complex system of geophysical phenomena which often lead to seismic hazards. The GPS data provides exciting prospects in seismology including detecting, imaging and analyzing signals in regions of seismo-active areas. Most earthquakes have precursors (defined as changes in the Earth physical-chemical properties that take place prior to an earthquake). Earthquake precursors emerging as a strong earthquake approaches are fuzzily differentiated by the characteristic lead-time between precursor and the strong earthquake: long-term (LT), tens of years; intermediate-term (IT), years, short-term (ST), months; and immediate (Im), days and less. This gradation reflects a more general phenomenon: unfolding of seismicity in a cascade of earthquakes' clusters, culminated by a strong earthquake. Most of the precursory phenomena also exhibit patterns in which systematic growth takes place during the pre-seismic period, corresponding to the local stress build-up. This is followed by a relatively rapid return to near equilibrium conditions following the earthquake event. This paper aims at investigating thermal seismic precursors for some major earthquakes in Romania in Vrancea area, occurred in 1977, 1986, 1990 and 2004, based on time series satellite data provided by NOAA and MODIS. Quantitative analysis of air (T) and land surface temperature (LST) and sensible surface latent heat net flux (SLHF) data extracted from satellite and in-situ monitoring available data recorded before and during the occurrence of earthquake events shows the consistent increasing in the air and land surface in the epicentral locations several days before earthquake, and at different distances of hypocenters function of registered earthquake moment magnitude. The purpose of this paper is to show complementary nature of the changes observed in land surface temperature, surface latent heat net flux, atmospheric and meteorological parameters associated with the investigated earthquake events in Vrancea zone. The present results show existence of coupling between lithosphere-atmosphere associated with preparation and seismic event occurring. Such results of pre-earthquake signals are promising and can contribute significantly in future towards forecasting the impending earthquakes in tectonically active regions.

8538-8, Session 3

Assessment of Rapid Eye's Red-Edge capabilities to characterize vegetation types and status

Pablo H. Rosso, RapidEye AG (Germany)

RapidEye's constellation of five identical satellites are multispectral sensors with five bands (blue, green, red, red-edge and near infra-red) able to produce images at 5-m spatial resolution. One of the distinctive features of RapidEye's satellites is the presence of a Red_Edge band, which has been included in the design of the satellites to enhance their capabilities of detecting and analyzing vegetation characteristics. Despite this, a deep understanding of the Red-Edge potential and its capability as a tool to monitor vegetation is still incomplete. Most of the previous research on the red-edge spectral response in vegetation has been done with hyperspectral sensors and the translation of this knowledge into multispectral systems has not been yet effectively done. For example, an important amount of research has been based on changes in slope between the red absorption and the near-infrared peak reflection in relationship to changes in both, chlorophyll content and leaf structure in plants. This however, has a limited application to multispectral systems that can capture the entire spectral area with only one (or two) broad band(s).

A complete series of spectral indices, mostly utilizing the Red, Red-Edge and Near Infrared (NIR) bands, derived from RapidEye images were tested to assess their capabilities to characterize different vegetation cover types (mainly forest and crops) at different levels of health status and percent plant cover. The aim was to determine the potential of bands and band combinations to characterize and discriminate between different vegetation types and status from the point of view of the user of satellite images as a monitoring tool. Despite this apparent variability of plant systems and disturbance agents, the expectation was to find a common thread around the fact that in all cases there would be detectable differences in chlorophyll content and plant leaf structure. Ancillary data, such as ground surveys and high spatial resolution imagery, were used as base information to choose areas of interest in different environments, and statistical analyses were used to compare the performance of several indices, which were chosen based on available literature and previous knowledge.

Preliminary results indicate that band and index performance varies with the plant system considered and with the type of feature to be discriminated. For example, in trees, indices that include the Red band seem to be more efficient to separate health or vitality status. Combinations of Red and NIR seem more effective to separate crop types, whereas Red and Red-Edge can mostly contribute to separate crop status. Indices that include NIR are the most effective for discriminating plant from non-plant features. Interestingly, it was observed that bands that separately have good discrimination ability can cancel each other when combined into indices.

Results are expected to assist multispectral imagery analysts to devise more suitable tools for vegetation monitoring based on the already available base research.

8538-9, Session 3

Data service platform for MODIS Vegetation Indices time series processing at BOKU Vienna: current status and future perspectives

Francesco Vuolo, Anja Klisch, Clement Atzberger, Univ. für Bodenkultur Wien (Austria)

Continuous observations of the land surface from medium to coarse spatial resolution satellite sensors provide input to a variety of ecosystem models and environmental applications. They also provide an opportunity to investigate the potential of existing and new methodologies for land surface characterization.

Most of the analysis and interpretations at global and regional scale have been based on time series of the Normalised Difference Vegetation Index (NDVI) initially derived from the NOAA Advanced Very High Resolution Radiometer sensor and successively from SPOT VEGETATION, MODIS and MERIS.

The integration of NDVI time series in various modelling frameworks is nowadays facilitated by readily available and standardized (in time and space) products. Such global composites have a high potential for continuous and real time updating. Despite the continuous effort for making these products globally available in near real time (for example from the MODIS team), various processing steps are still required before complete and efficient integration in any modelling framework is possible. For instance, temporal and spatial sub-setting, mosaicking, reprojection and data smoothing are routine operations that are not yet completely automatized. This holds even more for derived products such as phenological indicators and vegetation anomalies.

The aim of this paper is to present a freely available data service platform for managing and executing pre-processing operations of archived MODIS NDVI time series on request. The system is based on the integration of various software and hardware components: a

web-user interface and a MySQL database are used to collect and store requests from users. A server side application schedules the user's requests and checks out the results. The core of the processing system is based on the "MODIS" package developed in R, which provides data acquisition, mosaicking and reprojection. Smoothed and gap-filled data sets are derived using the state-of-the-art Whittaker filter implemented in Matlab. After the processing, data are stored locally and can be downloaded directly via ftp.

An analysis of the performance of the system, along with processing and storing capacity is presented. Results are discussed, in particular in view of an operative platform for real time filtering, phenology and land cover mapping applications with a focus on Europe.

8538-10, Session 3

Development of a low altitude airborne remote sensing system for supporting the processing of satellite remotely sensed data intended for archaeological investigations

Athos Agapiou, Diofantos G. Hadjimitsis, Cyprus Univ. of Technology (Cyprus); Andreas Georgopoulos, National Technical Univ. of Athens (Greece); Kyriacos Themistocleous, Dimitris D. Alexakis, Cyprus Univ. of Technology (Cyprus); Giorgos C. Papadavid, Agricultural Research Institute (Cyprus)

Remote sensing has been successfully used in the last years, for the detection of shallow buried relics such as archaeological remains. The detection is based mainly in photointerpretation of crop marks from high resolution satellite or aerial data. It has been shown by several researchers that remote sensing data may have a significant potential for archaeological investigations. Indeed, many studies have used different multispectral and hyperspectral satellite sensors. However, in most of these studies there is lack of ground verification for all these satellite investigations. Satellite images need to be atmospherically and geometrically corrected, before being subjected to any post-processing techniques, while some other corrections taken into account are sun elevation, elevation of the area of interest e.t.c. Therefore, in situ spectroradiometric measurements can provide more accurate results (ground "truth"data) regarding the reflectance of each target.

Furthermore the use of low altitude airborne system for archaeological research is very limited. "ICAROS" project funded by the Cyprus Research Promotion Foundation aims to develop an airborne system for archaeological investigations. The system will incorporate both a field spectroradiometer such as the GER1500 and NIR camera, in a balloon. The GER 1500 spectroradiometer has the capability to record the reflectance from 400 nm up to 1050 nm (blue/green/red and NIR band). The Field of View (FOV) of the instrument is 4o while a calibrated spectralon panel will be used in order to minimize illumination errors during the data collection. During the experimental works existing atmospheric conditions will be monitored using sun-photometer and meteorological station.

The overall methodology of the project, the calibration procedure of the system and preliminary results from different cases studies in Cyprus, are also presented and discussed in this paper. Calibration includes both geometric and radiometric calibration. Some practical problems are also discussed and the overall results are compared either with satellite or ground measurements.

Spectroradiometric measurements and NIR images will be taken from different heights from the balloon system. The results will be compared with different satellite images acquired from Landsat, ASTER, Chris-Proba etc.

8538-11, Session 3

Using remote sensing imagery to display geographical places automatically coming from a geoparsing web service

Erick López-Ornelas, Rocio Abascal-Mena, Sergio Zepeda-Hernández, Univ. Autónoma Metropolitana (Mexico)

This paper explores new ways to analyze and visualize geographical information from the web in a remote sensing image. In web pages, we usually find many geographic locations associated to regular information on the site. This geographic information is very valuable and is rarely used and exploited on the website. An interesting example is the cover of the newspapers online, where there is always an interesting relationship between the news and its location. Thus, we propose an approach to extract geographic locations from web pages and then visualize this information in a remote sensing image automatically.

Geographic Information Retrieval (GIR) typically has focused on extracting geospatial information from documents and utilizing such information to filter documents or to provide a geographic focus of a document [1]. In this way, the motivation of our work is the fact that all information on the web, like the newspaper covers, typically happen at some location.

Our approach is based on the use of a Geoparsing Web Service (GWS), it enriches content with geographic metadata by extracting places from unstructured text from any online web page [2], [3]. Geoparsing offers the ability to turn text documents into geospatial databases. This process is done in two steps: 1) entity extraction and 2) disambiguation, which is also known as grounding or geotagging. Geospatial entity extraction uses natural language processing to identify place names in text, while disambiguation associates a name with its correct location. To access the GWS we have used the Yahoo Query Language (YQL) which is a query influenced by the Structured Query Language (SQL) but diverges from it as it provides specialized methods to query, filter, and join data across web services. Once geographic coordinates are extracted by using eXtensible Markup Language (XML) [4], [5], we draw the geo-positions and link the documents into a remote sensing image in order to visualize the extracted information.

Our approach, not only extracts the places with their latitude and longitude, but also it is capable to show them in a map, in our case we use a Landsat 7 image. This satellite image can easily be added as a layer into a GIS.

The contribution of this work includes (1) the use of a Geoparsing Web Service for analyzing a global collection of web pages, (2) the use of XML tags to visualize the information extracted in a remote sensing image and (3) the integration of this remote sensing image into a Geographical information System.

REFERENCES

[1] Martins, B., Manguinhas, H. And Borbinhna, J. "Extracting and Exploring the Geo-Temporal Semantics of Textual Resources." IEEE ICSC, pp. 1-9, 2010.

[2] Strötgen, J. "Extraction and Exploration of Spatio-temporal Information in Documents." Proceedings of the 6th Workshop on Geographic Information Retrieval 2010.

[3] Yamamoto, M. "Extraction and Geographical Navigation of Important Historical Events in the Web." Web and Wireless Geographical Information Systems - 10th International Symposium, W2GIS 2011, Kyoto, Japan, March 3-4, 2011.

[4] Gohr, A., Spiliopoulou, M., and Hinneburg, A. "Visually Summarizing the Evolution of Documents Under a Social Tag." Proceedings of the KDIR 2010- International Conference on Knowledge Discovery and Information Retrieval, 2010.

[5] Anastacio, I., Martins, B., and Calado, P. "Classifying Documents According to Location Relevance." Proceedings of the 14th Portuguese Conference on Artificial intelligence: Progress in Artificial intelligence. Lecture Notes in Computer Science. pp. 598-609, 2009.

8538-12, Session 3

A new time-to-digital converter for the 3D imaging lidar

Chunsheng Hu, Zongsheng Huang, Shiqiao Qin, Xingshu Wang, National Univ. of Defense Technology (China)

The research of the 3D imaging lidar (light detection and ranging) is a key area in the 3D information acquisition research. It has so many successful applications at present. For the civil uses, it has been applied to terrain mapping, disaster monitoring, environmental monitoring, resources survey, forest survey, and etc. For the military uses, it has been applied to battlefield reconnaissance, obstacle avoidance of helicopters, active laser guidance, and etc.

The time-to-digital converter is a key part in the 3D imaging lidar, which determines the precision of measurement and ranging of the 3D imaging lidar. The previous 3D imaging lidar usually adopts ASIC (Application Specific Integrated Circuit) chip as the time-to-digital converter. Recently, the recent 3D imaging lidar begins to use the interpolating converter based on FPGA (field programmable gate array), which has some advantages: high measurement frequency,

adequate measurement precision, easy realization, low cost, and etc. In the interpolating converter, FPGA logical cells are used as time delayers. The delay time of the logical cell changes with FPGA temperature and voltage, which decreases the measuring precision of time interval.

In order to reduce the negative influence caused by the temperature and voltage variations of the FPGA (Field Programmable Gate Array), we propose a new FPGA-based time-to-digital converter. The proposed converter adopts a high-stability TCXO (Temperature Compensated Crystal Oscillator), a FPGA and a new algorithm, which can significantly decrease the negative influence due to the FPGA temperature and voltage variations. This paper introduces the principle of measurement, main framework, delayer chain structure and delay variation compensation method of the proposed converter, and analyzes its measurement precision and the maximum measurement frequency. The proposed converter is successfully implemented with a Cyclone I FPGA chip and a TCXO. And the implementation method is discussed in detail. The measurement precision of the converter is also validated by experiments. The results show that the mean measurement error is less than 260 ps, the standard deviation is less than 300 ps, and the maximum measurement frequency is above 10 million times per second. The precision and frequency of measurement for the proposed converter are adequate for the 3D imaging lidar.

If Cyclone IV FPGA is adopted, the precision and frequency of measurement for the proposed converter can be enhanced more than 2 times. For the 3D imaging lidar, the proposed converter has some advantages: easy application, adequate measurement frequency and precision. The proposed converter is used and tested in a high-speed 3D imaging lidar. As well as the 3D imaging lidar, the proposed converter can be applied to the pulsed laser range finder and other time interval measuring areas.

8538-13, Session 4

Object-based urban change detection analyzing high resolution optical satellite images

Markus Boldt, Fraunhofer-Institut für Optronik, Systemtechnik und Bildauswertung (Germany); Antje Thiele, Karlsruher Institut für Technologie (Germany) and Fraunhofer-Institut für Optronik, Systemtechnik und Bildauswertung (Germany); Karsten Schulz, Fraunhofer-Institut für Optronik, Systemtechnik und Bildauswertung (Germany)

Nowadays, change detection in urban areas by investigating image data of high-resolution remote sensing satellites has become an extreme important topic. To detect changes is of interest, for example, in terms of monitoring and disaster management, where accurate information about dimension and category of changes are frequently high requested.

This paper treats the development of rule sets for object-oriented multispectral classification to differentiate between traffic infrastructure, water areas, vegetation and non-vegetation area. Additionally, changes are detected by analyzing multi-temporal classification results, where the identification of areas of high construction activity is focused. Hence, changes due to different viewing geometry, especially observable at elevated objects (e.g. trees and buildings), have to be classified and eliminated.

The processing workflow is realized by use of the software tools Definiens Developer and ERDAS Imagine for multiresolution segmentation and fuzzy-based classification. The rule sets are set up on a training area, and later evaluated on additionally areas. Furthermore, the setting of processing parameters such as segmentation level is varied to evaluate the robustness of the developed rule set.

For this study, high-resolution multi-temporal satellite images of QuickBird covering the city Karlsruhe (10th June of 2005 and 15th April of 2007) as well as LiDAR Digital Surface Model (DSM) data of the same area are used to detect areas of high construction activity. Moreover, the detection results are evaluated by several Ground Truth data. For this, one on-site inspection was performed in the July of 2007.

8538-14, Session 4

Integrated data processing of remotely sensed and vector data for building change detection

Natalia Sofina, Manfred Ehlers, Univ. Osnabrück (Germany); Ulrich Michel, University of Education Heidelberg, Germany (Germany)

In the last years natural disasters have had an increasing impact involving immense economical and human losses. Remote sensing technologies are being used more often for rapid registration and visualization of changes in the affected areas providing essential information for damage elimination, planning and coordination of recovery activities. A number of image processing methods have been proposed to automate a detection of changes on the Earth's surface. Most of the methods focus on the comparison of remotely sensed images of the same area acquired at different dates. However, atmospheric influences (e.g., clouds covering the objects of interest) make the observations often ineffective in the optical domain. In addition, the accuracy of the change detection analysis decreases if the images are acquired with different acquisition angles. These situations can be frequent in the case of sudden catastrophes (e.g., earthquakes, landslides or military actions), when there is no time to wait for the perfect conditions to acquire the data. This study presents a GIS-based approach for detection of destroyed buildings. The methodology is based on the integrated analysis of vector data containing information about the original urban layout and remotely sensed image obtained after a catastrophic event.

For identification of a building condition a new feature 'Detected Part of Contour' (DPC) was developed. The basic idea behind the proposed feature is the assessment of building contour integrity. The feature defines a part of the building contour that can be detected in the remotely sensed image. It reaches maximum value (100%) if the investigated building is intact. Furthermore, several features based on the analysis of textural information are analyzed. Finally, a binary classification of building state concludes the change detection analysis.

The integrated data processing enables, on the one hand, the minimization of the influence of the atmosphere and illumination effects and, consequently, the improvement of the damage detection. On the other hand, the object oriented GIS technology makes it possible to concentrate on the investigation of the specified objects, thereby reducing false alarms due to natural changes that occur around the investigated objects (e.g., seasonal changes of vegetation). Additionally, GIS based change detection analysis produces a tangible end product - a damage maps.

The proposed method for damage mapping was applied to the 2010 earthquake in Qinghai (China). GIS information was obtained by digitizing from pre-earthquake images. The performed experiments indicate that employing a GIS-based analysis for change detection can essentially improve the potential for remotely sensed data interpretation and can be considered a powerful tool for the detection of destroyed building.

The proposed methodology has been developed solely within the Open Source software environment (GRASS GIS, Python, Orange). The use of Open Source software implies an innovative, flexible and cost-effective solution for change detection analyses.

8538-15, Session 4

Ad-hoc model acquisition for combat simulation in urban terrain

Dimitri Bulatov, Peter Solbrig, Peter Wernerus, Fraunhofer-Institut für Optronik, Systemtechnik und Bildauswertung (Germany)

Because of the geo-politic developments of the last two decades, the strategic tasks and areas of applications for the members of the North Atlantic Alliance have been dramatically changed. From the originally assigned task of acting as national and allied defense forces within the partners' own borders, their range of action has been extended by out-of-area missions under conditions of an asymmetric conflict. Ambushes, urban operations, snipers hiding behind obstacles and necessity to be considerate with civilian population and infrastructure are those complicated challenges that military forces, particularly in urban environment, are exposed to during their deployment on peace-keeping and peace-enforcing missions. For a soldier participating in

a patrol or involved in urban warfare, it is very difficult to take right decisions within a short time and under enormous pressure. However, there is a justified hope that these decisions can be taken more easily if they are extensively trained in an environment that is tailored to the concrete situation. The task of simulation of military missions for soldiers in different levels of command motivated us to fill the gap between the authentic 3D models, obtainable by the state-of-the-art methods of sensor-data evaluation and the computer games for combat simulation, such as Virtual Battle Space 2 (VBS2) that is already being employed, however, mostly in invented environments. Beside authenticity (and, as a consequence, an up-to-date character) of the obtained model, we strive for a highest possible level of automation, that is, a simulated mission should be ideally possible to create with several mouse-clicks a short-time after sensor data acquisition has been carried out.

Due to their low cost and easy, riskless use, small unmanned aerial vehicles (UAVs), or micro UAVs (MUAVs) in particular, with passive sensors onboard have become an increasingly attractive tool for ad-hoc data acquisition. However, the two steps of image orientations and generation of dense 3D point cloud can be omitted if a laser point cloud is given. The building detection procedure from dense point clouds includes modeling DTM and DSM, separation of buildings and vegetation and filtering the elevated regions of the difference between DTM and DSM by height, area and elongation. The building reconstruction procedure, applied on each of the remaining regions, performs boundary extraction, roof detail analysis and texturing building roofs. Afterwards, polygonal models of buildings and trees, whose appearance can be adjusted according to seasonal changes, are exported into an FBX-format. This data can be automatically converted into the VBS2-proper format. p3d. In the thus instantiated model of 3D-urban terrain, we will present a typical scenario, realized in VBS2, of a military mission in a non-cooperative 3D environment.

8538-16, Session 4

Integrating machine learning techniques and high-resolution imagery to generate GIS-ready information for urban water consumption studies

Nils Wolf, Angela Hof, Ruhr-Univ. Bochum (Germany)

A recent study by the European Environment Agency has pointed to Southern Europe's leading role in urban sprawl. On Mediterranean coasts, suburban natures have evolved around and in between established tourist zones. This urban sprawl is driven by shifts in tourism development. Residential tourism, second homes and a proliferation of water-intensive leisure infrastructure, including golf courses, are the most striking artefacts of this urban landscape transformation. This process of urbanization has produced new landscapes of water consumption, threatening the local water supply systems and exacerbating water scarcity. Ornamental, 'Atlantic' gardens and swimming pools are the main water-demanding outdoor uses driving the recent increase in urban water consumption levels. In the face of climate change, urban landscape irrigation is becoming increasingly important from a resource management point of view. Integrated water management demands information on the relevance of urban structure types for water demand and consumption, yet this type of data often eludes statistical observation or is masked in consumption data on coarse spatial levels.

This paper adopts urban remote sensing towards a targeted mapping approach using machine learning techniques and high-resolution imagery (WorldView-2) to generate GIS-ready information for urban water consumption studies. By combining image analysis with research questions from urban studies, the paper moves beyond measuring and monitoring of physical properties of urban areas and looks into the extraction of swimming pools, vegetation and - as a subgroup of vegetation - turf grass. These surface features are important determinants of water consumption and urban environmental studies related to water demand, irrigation and the role of green spaces in urban landscapes can take advantage of new remote sensing imagery and analysis techniques. For image analysis, the complex nature of urban environments suggests spatio-spectral classification, i.e. the complementary use of the spectral signature and spatial descriptors. Multiscale image segmentation provides means to extract the spatial descriptors - namely object features - which can be concatenated at pixel level to the spectral signature. In this study, we assess the predictive power of object features and investigate the interplay of different machine learning techniques (kernel methods and tree-based ensembles), data dimensionality and the distribution and size of training and test data. The results from the image analysis are combined with calculations of evaporative water loss from pools and a method based on reference evapotranspiration to estimate net landscape irrigation requirements. Visualized in maps, the results are support for powerful communication means in water conservation campaigns that already address gardens and swimming pools tentatively and encourage the use of more Mediterranean species in gardening, adequate irrigation technology, and pool covers. Another application of the information is in urban microclimate studies looking into the spatial patterns of urban vegetated cooling as ecosystem service, the potential water requirements to supply these services, and differential access to these services between residential neighbourhoods.

8538-17, Session 4

3D campus modeling using LiDAR point cloud data

Yoshiyuki Kawata, Satoshi Yoshii, Yukihiro Funatsu, Kazuya Takemata, Kanazawa Institute of Technology (Japan)

The needs of having a 3D model of urban city are increasing in a wide range of practical applications, such as risk and disaster managements, various city mapping and planning and others. The main objective of this study is to find appropriate and effective procedures which can make a 3D modeling of urban area efficiently, using the airborne LiDAR point cloud data. In this study we selected our KIT campus as such a target, consisting of many complicated buildings like the urban city in the residential environment. The 3D modeling of the campus was made, using the point cloud data as basic information on the shape and height of the buildings. Since the point cloud data provides little information on the side of the buildings, we had to use many building pictures from different directions, in the practical realization of the 3D campus. Nevertheless, the use of point cloud data was very attractive to make an accurate modeling of 3D campus, because of many advantages of the point cloud data, such as a wide coverage of the area and high accuracy of target registration. In the completion of the 3D model campus we had to manipulate several software applications, including GRASS GIS, FUSION, and AutoCAD Civil 3D. We found a few capabilities of AutoCAD Civil 3D 2011 were particularly useful in dealing with the point cloud data. Making the use of importing and exporting capabilities from and into Google Earth, we successfully exported a 3D KIT campus into Google Earth and a walkthrough simulation of 3D campus was demonstrated. Finally, we clarified many merits and faults of these applications in the procedures of 3D modeling. The discussion on the point clouds from MVS(Multi-View Stereo Software) using a set of target pictures was also given in comparison of LiDAR point clouds.

8538-18, Session 5

Multitemporal satellite data in mine waste monitoring of Medet copper deposit

Denitsa Borisova, Hristo Nikolov, Doyno Petkov, Space Research and Technology Institute (Bulgaria); Banush Banushev, Univ. of Mining and Geology (Bulgaria)

The anthropogenic impact of the mining industry on the environment is seen all over the world. Two types of pollution from tailing dumps are observed - airborne pollution through dusting, and waterborne due to direct dumping and accidental releases. In the last decades several mining areas and corresponding waste disposal sites in Bulgaria are being monitored for ongoing reclamation processes. In this research we were focused on one environmental status of one of the most important copper producing fields for our country - Medet deposit. This mining complex consists of an open cast mine, the overburden dumps and a processing plant.

The objectives of the study were: (1) to analyze multispectral satellite images for 1980 - 2000 in order to assess the environmental pollution from the mining activity in the Medet open pit mine in temporal perspective; (2) to prove that by means of remote sensing an integrated environmental impact assessment can be made.

After ceasing its exploitation in 1994 a rehabilitation program for soil cover and hydrographic network was established and launched. A continuous task is the monitoring of these activities from the beginning for at least 15 years period. We consider that revealing the potential of satellite multispectral and multitemporal imagery will provide valuable information on the impact of this long-term mining activity on the

environment. One of the first tasks was to prepare thematic maps for several, non-successive years of the affected areas at regional scale. On the next step change detection methods were used to assess the short-term reclamation activities by examination of vegetation cover status in the areas surrounding the mine. To complete this tasks data from Landsat TM/ETM+ instruments combined with in-situ measured data was used. For data processing several techniques, both standard, such as basic and advanced statistics, image enhancement and data fusion, and novel methods for supervised classification were used. The results obtained show that used data and the implemented approach are useful in environmental monitoring and economically attractive for the company responsible for the ecological state of the region. The polluted water surface amounted to at least 150 km2 through dumping in 1978 and to 106 km2 in 1986 due to dusting. Thus, the impact from the mining and concentrate production activities should be recognized as more significant than it was officially reported. In the past the main mechanism of pollution was the direct dump of the waste water into closest river. Today and in the near future, airborne pollution caused by dust storms will dominate and for this reason field work for the level of heavy metals concentration into the soil must be foreseen. The effective rehabilitation of the tailing dumps will be a long-term process during which monitoring of the close areas on regular basis are intended by the team. In this long term activities an we plan to increase effectiveness of the assessment of the impact caused by the mining and concentration production industry by complementing the remote sensing methods by in-situ measurements and laboratory tests.

8538-19, Session 5

Statistical frameworking of deforestation models based on human population density and relief energy

Ryuei Nishii, Daiki Miyata, Kyushu Univ. (Japan); Shojiro Tanaka, Shimane Univ. (Japan)

Worldwide decrease of forest area is chiefly due to negative impact of human activities, but that is restricted to topographical circumstances. In this research, we consider statistical modeling of forest area ratio F observed on a grid-cell system, taking values from zero to one. The F will be predicted by covariates: population density (N) and relief energy (R), where R is the difference between the maximum and minimum altitudes in each site.

Tanaka and Nishii (2009, IEEE Transaction on Geoscience and Remote Sensing) explored a regression model of logit-transformed forest area ratios, where the mean function is given by the sum of two non-linear parametric functions of the covariates. We will consider the following problems:

1) Classification: Observed sites are classified into three types: completely-deforested (F =0), fully-forest-covered (F =1), or remaining (0< F<1) sites. Our problem is to derive a classification method using the population density and the relief energy at the current site and its neighbors.

2) Regression: For the forest ratios with 0< F<1, the problem is to find the best regression model for predicting the ratio using the covariates. For this modeling, we must take spatial dependency of the ratio into account. Also, flexible mean functions of the regressions are required.

For the classification problem 1), we proposed the followings.

(a) Modeling categorical responses with the covariates N and R at the current site as well as its neighborhood is considered.

(b) Box-Cox power transforms of the covariates are used.

For the regression problem 2), we proposed the followings.

(a) An extended transform of F including logit-transform is proposed. The transform is applied to the forest ratio: target variable in regression.

(b) The mean functions are given by piece-wise cubic polynomials of the logarithmic-transformed covariates. The number of nodes is determined by minimizing Akaike Information Criterion (AIC).

(c) The model specifies the effect from completely-deforested or fully forest-covered neighbors.

(d) The error terms of the regression models have spatial dependency from the first- and second-order neighborhoods.

The joint distribution is derivable in a closed form, and the procedure for deriving the maximum likelihood estimates is given.

The proposed models were applied to Japanese test field with grid-cell sites each measuring about 1 square km. The field has 159 sites with F =0 and 1713 sites with F =1. The remaining 6825 sites have the ratios 0< F<1.

Concerning to 1), it was seen that the classification using the neighbors' covariates shows high performance. Also, the power transforms to the covariates are effective. Concerning to 2), the spline-based functions were much superior in detecting the small changes of regression functions to the former parametric model. Also, spatially dependent models improve the regression significantly by the evaluation of AIC.

8538-20, Session 5

Object-oriented industrial solid waste identification using HJ satellite imagery: a case study of phosphogypsum

Zhuo Fu, Wenming Shen, Rulin Xiao, Wencheng Xiong, Yuanli Shi, Ministry of Environmental Protection (China); Baisong Chen, Chinese Academy of Fishery Sciences (China)

The increasing volume of industrial solid wastes presents a critical problem for the global environment. In the detection and monitoring of these industrial solid wastes, the traditional field methods are generally expensive and time consuming. It is thus difficult for the corresponding administrative departments to understand the overall spatial distribution of the industrial solid wastes in time. With the advantages of quick observations taken at a large area, remote sensing provides an effective means for detecting and monitoring the industrial solid wastes in a large scale.

In this paper, we employ an object-oriented method for detecting the industrial solid waste from Advanced Spaceborne Thermal Emission and Reflection Radiometer (ASTER) images. We select phosphogypsum which is a typical industrial solid waste as our target. Our study area is located in Fuquan in Guizhou province of China, which is a typical clustering area of different industrial solid wastes mainly including phosphogypsum. The ASTER data we used consists of 14 bands: 3 bands in the visible and near infrared (VNIR) with 15m resolution, 6 bands in the short wave infrared (SWIR) with 30m resolution and 5 bands in thermal bands (TIR) with 90m resolution. The object-oriented method we adopted consists of the following steps.

1) Transform the pixel-based images into the object-based ones. Initially, the optimal segmentation parameters are determined through many segmentation experiments. Based on these segmentation parameters, multi-scale segmentation method is adopted to segment the remote sensing images. The object-based images are thus obtained.

2) Build the feature knowledge set of the object types. From the object-based ASTER images, we explore the features of industrial solid waste and other typical objects based on sample training. The features we used include spectral features as well as shape features, texture features, spatial features, etc. The spectrums of the samples of typical objects are extracted from ASTER object-based images in all the 14 bands. And spectral features of different types of objects are analyzed using statistical indicators. Due to the resolutions of VNIR bands are higher than those of other bands. We choose VNIR bands of ASTER object-based images to extract other features of the typical objects. Based on these features of objects and additional priori knowledge from ground surveys, we build a feature knowledge set which is important in building the decision tree rule set.

3) Detect the industrial solid wastes based on object-oriented decision tree rule set. We analyze the heterogeneity in features of different objects. According to the feature heterogeneity, an object-oriented decision tree rule set is then built for aiding the identification of industrial solid waste. Then, based on this decision tree rule set, the industrial solid waste can be identified automatically from remote sensing images.

Finally, the identification results are validated using ground survey data. Experiments and results indicate that the object-oriented method provides an effective method for detecting industrial solid wastes.

8538-21, Session 6

Land cover classification using remote sensing imagery and random forests with anisotropic diffusion

Xuan Zhu, Monash Univ. (Australia)

Various image classification methods have been developed for land cover mapping. Among them classification and regression trees (CART) and their new modifications such as random forests (RF) have proven effective. However, these CART-based methods perform per-pixel classification, which often produces suboptimal results with scattered misclassifications. This paper introduces an anisotropic diffusion technique to address the problem and combines this technique with RF for land cover classification using remote sensing imagery and ancillary data. RF is used to produce probability maps for each type of land cover, the anisotropic diffusion technique is employed to smooth the probability maps and then independent maximum probability rules are applied on the smoothed probability maps to generate a land cover map. This method was applied to land cover classification for the Jiuzhaigou Nature Reserve in China using Landsat TM Images and topographic data and its classification accuracy was assessed. The results demonstrated that the combined use of RF and anisotropic diffusion improved the overall accuracy by 6% over the land cover classification without a smoothing process.

8538-22, Session 6

Assessing regrowth and deforestation processes in western Amazonia (Rondônia, Brazil) using high frequency time series of high spatial resolution remote sensing data

Joao M. Carreiras, Joana B. Melo, Instituto de Investigação Científica Tropical (Portugal); Richard M. Lucas, Aberystwyth Univ. (United Kingdom); Yosio E. Shimabukuro, Instituto Nacional de Pesquisas Espaciais (Brazil)

The Brazilian Legal Amazon (BLA), covering an area of ~5,000,000 km2, consists primarily of primary tropical forest (rainforest and seasonal forest). Currently, most of the deforested area is under agricultural use, but over 35% has been abandoned and often supports regenerating forest. However, up-to-date and timely spatial maps of regrowth and the growth stage are required to better understand the past, present and future role of these forests in regional carbon budgets and in the recovery of biodiversity.

The objective of this research was to test a combination of high frequency time series of Landsat 5 Thematic Mapper (TM) data to assess regrowth and deforestation processes in a settlement located in the Western BLA (Machadinho d'Oeste, Rondônia). In total, 21 Landsat 5 TM scenes covering a 27-year period (1984-2011) were acquired, pre-processed and classified into three classes: mature forest (MF), secondary succession forest (SSF), non-forest (NF). Using 10-fold cross-validation, the overall accuracy in the classification ranged from 96.6-99.7%; the omission and commission errors of the class with higher misclassification errors (SSF) ranged from 0.69-7.58% and 1.72-7.11%, respectively. A number of metrics associated with the areas undergoing regrowth in the last date (2011) were calculated including the period of active land use (PALU) prior to abandonment to regenerating forests, age of regenerating forest (ARF) and frequency of clearance (FC). Also, deforestation and regrowth rates were calculated between consecutive dates.

The analysis of the time series of classified images showed that, in 1984 (the first date), 99% of the study area was occupied by MF, with the remainder occupied by NF. No SSF was present. In 2011, 38% (66,813 ha) of the area was occupied by NF, followed by MF (35%, 60,634 ha) and SSF (27%, 47,887 ha). This dramatic change was a consequence of high deforestation and regrowth rates in the period since 1984. Deforestation rates in areas previously occupied by MF ranged from 1.21 %yr-1 to 9.95 %yr-1, while deforestation rates in areas previously occupied by SSF were even higher, from 2.48 %yr-1 to 88.05 %yr-1, indicating reclearance. Regrowth rates ranged from 3.68 %yr-1 to 84.18 %yr-1. Approximately 50% of the area with SSF in 2011 had a PALU of one year whilst around 90 % had a PALU not exceeding four years. Around 45 % of the area with SSF in 2011 was less or equal than 5 years of age and 40 % between 6 and 15 years. About 55 % of the area with SSF in 2011 had been cleared once and around 95% was cleared a maximum of three times. In Machadinho d'Oeste, SSF in 2011 have established on land with a short PALU and have been cleared several times prior to abandonment. Based on previous studies, these observations suggest that the regenerating forests are likely to support a reasonably high level of tree species but if future reclearance operations and extended periods in active use prevail, the capacity of the forests to recover tree species diversity may be reduced.

8538-23, Session 6

Impacts of land use land cover (LULC) changes on land surface temperature (LST) in Addis Ababa city in Ethiopia using satellite images of December 1986 and 2010 respectively

Daniel M. Mbithi, Kenya Meteorological Services (Kenya)

Urbanization has been a major force of Land Use Land Cover (LULC) throughout human history that has had a great impact on climate change.

To evaluate the effects of atmospheric correction, NDVI was calculated from both the original image and atmospherically corrected image by using the following formula:

To derive emissivity image the equation below was written in the spatial modeler of ERDAS as can be seen below:

This study has examined LULC changes in the capital of Ethiopia, Addis Ababa from 1986 to 2010. Urban/built-up areas expanded dramatically, while agricultural land and forest declined.

Barren land increased, mainly in the boundary areas between forest and dry agricultural fields, especially in steeply sloping areas. The observed changes in LULC were largely attributed to population pressure on the land, a rapidly growing infrastructure and poor land use planning. Changes in LULC were accompanied by changes in Land Surface temperature (LST). This could lead to an intensified urban heat island (UHI) effect in the urban areas. The abundance of forest was an important factor influencing LST.

Moreover, temperature differences between the urban/built-up and the surrounding rural areas significantly widened.

The study assessed the UHI spatial patterns and temporal variations in the Addis Ababa city.

The urban-rural temperature differences between the urban core and its surrounding areas show a maximum difference of >20 degrees centigrade.

Greening of the urban set up is highly recommended in this study.

8538-24, Session 6

A comparison of selected machine learning classifiers in mapping a South African heterogeneous coastal zone: Testing the utility of an object-based classification with WorldVeiw-2 Imagery

Elhadi E. Adam, Riyad Ismail, Onisimo Mutanga, Univ. of KwaZulu-Natal (South Africa)

Land -cover mapping has increasingly been identified as one of the vital data components for many aspects of local and global changes and environmental applications. Remote sensing has been the most commonly data source used for determining land cover thematic mapping and providing valuable information about the extension, changes, and risk analysis of land- cover at various spatial, spectral and temporal resolutions. The classification of land cover /use from remotely sensed imagery can be divided into two general image analysis methods; pixel-based classification and object-based classification. Multispectral remotely sensed data and traditional pixel-based classification has long been the mainstay for classifying land- cover/use. However, it was recognized that traditional pixel-based image analysis is limited due to many problems such as; image pixels are not true geographical objects and pixel topology is limited, pixel-based image analysis overlooks the spatial photo-interpretive elements such as texture, context and shape. Moreover, in the high spatial resolution imagery, the variability implicit within the class sometime confuses the pixel-based classifiers and results in lower accuracy. Therefore, the land cover maps are often judged to be of insufficient quality for operational applications due to the disagreements between the reference data set and predicted classes derived from the remotely sensed data.

The advent of new generation satellites with moderate resolution is seen as a trade-off between the advantages of multispectral resolution satellite data and hyperspectral data. WorldView-2 is one such sensor which contains a reasonable number of spectral bands that are configured in unique portions of the electromagnetic

spectrum, including the red edge. This study explored the possibility of object-based image analysis approach for mapping land- cover/ use in a heterogeneous coastal zone using WorldView-2 imagery. WorldView-2 image comprised eight multispectral bands with spatial resolution of 2 m. The spectral ranges of the eight bands are 400-450 nm (B1-coastal), 450-510 nm (B2-blue), 510-581 nm (B3-green), 585-625 nm (B4-yellow), 630-690 nm (B5-red), 705-745 nm (B6-red edge), 770-895 nm (B7-near infrared-1), and 860-1040 nm (B8-near infrared-2) (Fig 1). Two relatively modern and robust supervised machine learning algorithms (random forest (RF) and support vector machines (SVM)) were also compared. Image segmentation was performed (Fig 1A), and eleven broad land cover classes were identified in a heterogeneous coastal area in KwaZulu-Natal-South Africa. Subsequently, we assessed the performance of object-based image analysis method and each of the selected machine learning algorithms in mapping these land cover classes. The validation of the developed land-cover/use maps form RF and SVM were performed through error matrix statistics using independent test dataset generated from a field work data and an aerial photography. Results showed that both the machine learning classifiers in combination with object-based approach are useful in mapping land-cover/use in heterogeneous coastal areas. However, SVM achieved the best overall accuracy (86%) and kappa statistic (0.84) than RF which produced an overall accuracy of 80% and kappa value of 0.77 (Fig 1). Overall, the study underline the utility of WorldView-2 imagery and the combination of object-based image analysis and machine learning classifiers in mapping land-cover/use in high heterogeneous coastal areas - a previously challenging task with broad band satellite sensors and traditional pixel-based image classification.

8538-25, Session 6

Sustainable management of coastal resources in Nigeria

Henry O Odunsi, Earth Info Services (Nigeria)

Sustainable management of the coastal zone is crucial because of its productive level in total global primary production. The coastal area is a very important part of a nation's territorial boundary. Globally, many coastal systems are being impacted at present by anthropogenic driving forces of global change. About 50% of world's coastal ecosystems are at risk of degradation from threat of sea level rise, flooding, erosion and ecological destruction. Nigerian coastline extends for about 853km and lies within the Atlantic Ocean. It is a promising environment for rapid socio-economic development due to the abundance of food, energy, mineral resources and economic activities. Coastal states of Nigeria accounts for 25% of the country's population which is about 150 million. The basic ecological zones in Nigerian coastal environment include mangrove swamps, forests, estuaries and beaches. Coastal resources in Nigeria constitute the aquatic flora and fauna, mangroves, forests and fisheries resources which are mainly found along the coastal states of the country. The non-renewable resources in Nigerian coastal zone include oil and gas, solid minerals, gravel, sand and clay. Airborne LIDAR bathymetry is a survey technique that is faster and cheaper for mapping the coastal zone. It is a remote sensing method of surveying that is ideal for coastal waters and usually displays improved resolution and accuracy when it comes to coastal aerial mapping. However, the need for sustainable management is to ensure conservation of natural resources that abound in this environment. Remote sensing mapping of Nigerian coastal ecosystem will facilitate the acquisition of data within a fraction of a second accurately and is essential for sustainable management of biodervisity in the region. Furthermore, due to the dynamic nature of the coastal areas, airborne LIDAR bathymetry and remote sensing technique will be useful in identification of critical areas along the Nigerian coastal boundary that require urgent attention and solution. Because of the increase in coastal populations and the degrading nature of anthropogenic activities, there is the urgent need for sustainable management of Nigeria's coastal resources which is presently threatened and endangered.

8538-26, Session 7

Per-field crop classification in irrigated agricultural regions in middle Asia using random forest and support vector machine ensemble

Fabian Löw, Julius-Maximilians-Univ. Würzburg (Germany); Gunther Schorcht, Julius-Maximilians-University (Germany); Ulrich Michel, Pädagogische Hochschule Heidelberg (Germany); Stefan W. Dech, Deutsches Zentrum für Luft- und Raumfahrt e.V. (Germany); Christopher Conrad, Julius-Maximilians-Univ. Würzburg (United States)

Irrigated agricultural regions in Middle Asia are characterized by different environmental and crop management settings. Crop yield and irrigation water demand modeling is a critical task and requires that both, the total surface that is cultivated and the distribution of crops is known. This in turn requires accurate crop identification at the field-scale.

This study presents an improved mapping procedure for crops of irrigated areas in Middle Asia. A hybrid classifier approach using Random Forest (RF) and Support Vector Machine (SVM) is tested with RapidEye time series to classifying crops in the four study sites. The time series consist of eight RapidEye images and were acquired over the growing period in 2011. Depending on the diversity of different crops in the test sites five up to eight classes were distinguished. A comprehensive set of spectral, textural features from the grey-level co-occurrence matrix, and semivariogram derived features were calculated for each field and time step as classification input.

A set of rules was developed to combine the results of the individual RF and SVM classifications and assign final class labels based on maximum classification probability and other rules. Classification confidence estimates at the field level for the discrete crop maps coincides with the combined membership of the assigned classes by the RF and the classification confidence of the SVM.

The potential synergistic use of the two classifiers is explored and compared with the results from the single classifiers. Three major outcomes were derived among each study site: a hybrid classification map, classification confidence maps, and assessment of the feature usefulness in the classification. The latter was derived by the RF internal computation of the variable importance for each candidate predictor based on the out-of-bag (OOB) observations as mean decrease of accuracy. In this context the 50 top-ranked features (most important candidate predictor variable) were used as input for the SVM to reduce possible negative effects of the feature space size on classification accuracy (Hughes effect), and speed up classification process.

Experimental results indicate an improved overall accuracy of the hybrid classifier, expect for one site where a slightly reduced overall accuracy was observed. Overall accuracies of RF and SVM in the study sites range between 84%-87% and 85%-94%, respectively, indicating a better performance of the SVM. The ensemble classifier results in increased overall accuracies over the test sites (89%-94%). Predictive errors of the two single classifiers tend to be different among the classes and the study sites: agreement of the two single classifiers in classifying crops ranges between 72% and 85%.

The hybrid approach seems suitable to improve classification accuracy in most of the study sites and provides field based information on classification confidence which might aid stakeholders in the region in making more informed decisions and incorporate uncertainty information in decision support systems.

8538-27, Session 7

Spatio-temporal robustness of fractional cover upscaling: a case study in semi arid savannah's of Namibia and Western Zambia

Julian Zeidler, Martin Wegmann, Julius-Maximilians-Univ. Würzburg (Germany); Stefan W Dech, Deutsches Zentrum für Luft- und Raumfahrt e.V. (Germany)

Vegetation cover is a key parameter in analysing the state and dynamics of ecosystems. Savannah ecosystems are defined by their small scale patches of woody and herbaceous vegetation inter-spaced with bare soil, resulting in a spatially highly heterogeneous landscape. Africa's semi-arid savannah's are particularly prone to degradation, due to increasing population pressure as well as ongoing climatic changes.

However in most large scale land cover classifications inhomogeneous areas are aggregated into few discrete classes and therefore often deliver unsatisfying results in highly variable biomes, like savannahs. The benefits for monitoring and decision making can be vastly increased if the inherent information on the underlying land covers are retained. This can be archived by a fractional cover classification, which provides an estimate of sub-pixel continuous cover percentages

of underlying land cover classes, and are therefore often a better thematic representation compared to discrete classes. Prior research utilised a multi-scale Fractional Cover (FC) approach, starting with a simple classification (tree/shrubs, herbaceous vegetation, bare soil, water) of very high resolution optical data (Worldview, IKONOS, Quickbird) for a very small subset of the study area, which was then aggregated to the cover fractions at an intermediate (e.g. Landsat) resolution grid and used as input for a random forest regression tree ensemble to extrapolate the fractions to the whole scene. This can in turn used as input for a second up-scaling to 250m MODIS resolution.

In this case study the robustness of the up scaling approach and the limits of the spatial and temporal transferability at the very high and intermediate resolution were analysed for a study area situated in the Caprivi Strip in Namibia and the adjacent Western Province of Zambia. The key research questions were to quantify i) the robustness of the upscaling, ii) the loss of accuracy depending on the lag in image acquisitions, iii) the loss of accuracy dependent on the time of image acquisition in the phenological cycle. To this end 18 Worldview (WV) images, covering all phases of the vegetation cycle,as well as all usable Landsat TM (4) and ETM+ (7) images were obtained. All combinations of WV and LS images were used as input for the FC regression-tree. Furthermore a choice subset of WV and LS were taken to regress against multi-temporal LS data.

The analysis showed that continuous fractional cover mapping is a highly suitable concept for semi-arid ecosystems with their gradual transitions. The optimal time for WV acquisition was at the beginning of the dry season , when overall class separability was best. While the RMSE proved unusable for images recorded in the rainy season between November and March, it was otherwise usable, even for larger lags of up to a month, with deviations below 15%, which is comparable to similar studies.

The spatial subset(s) used as training data have to cover the whole range of occuring vegetation densities to receive reliable up-scaling results for the whole image, as the resulting range is limited to that observable in the training areas. If this demand can be met, comparably small (and therefore readily available) very high resolution data is sufficient to reliably scale to regional results.

8538-29, Session 7

Remote sensing of the hydrology of the Tibetan Plateau

Volker Hochschild, Eberhard Karls Univ. Tübingen (Germany); Jan Kropacek, Technical Univ. Dresden (Germany); Niklas Neckel, Sebastian Hoerz, Eberhard Karls Univ. Tübingen (Germany)

Climate change and its potential effects are of global interest. Lake ice and snow coverage act as effective indicators of climate change due to their sensitivity to climate elements (like air temperature in the case of the lake ice), and can be observed on a large-scale with the help of remote sensing. The lakes on the Tibetan Plateau are important indicators for the development of the high mountain ecosystems facing the impacts of future climatic warming on runoff from snow and ice. Many of these Tibetan lakes are remote and hard to access, so multisensoral remote sensing is a valuable tool to generate hydrological relevant information as modeling input (land cover, soil moisture, trends in mountain lake ice cover, etc.) or validation base (lake level changes).

For the monitoring of the lake ice, the first and the last day of the partial ice cover and the period of total ice cover are defined on the basis of temporal high resolution MODIS data. The larger lakes were compared and put into regional groups in order to delineate and define different local trends.

For obtaining a better spatial resolution for the calculation of the ice covered area, additional medium and high resolution optical and microwave data (ERS-1, ERS-2, ENVISAT A-SAR, LANDSAT, Kompsat-2, RapidEye) are being considered, which at the same time, have a smaller temporal resolution. By means of correlating the different data, the respective advantages of each data type are merged and then used for the exact iced surface area calculation.

The study is enhanced by the use of passive microwave data (SSM/I, AMSR-E) which provides very high temporal resolution information as validation input. Simultaneously TerraSAR-X ScanSAR data is analysed currently for the whole winter period 2011 (December until April) in order to derive the spatial distribution of different ice types.

The snow cover is an important intermediate storage of water and plays a crucial role in the water budget of the Tibetan endorheic lakes since their contribution to runoff is mostly unknown as well as the loss through sublimation. It is observed by multitemporal MODIS 8-day snow cover composites, which were split into three different seasons and displayed as RGB synthesis of snow distribution (RSD, Kropacek et al. 2010). The different colors indicate the spatial distribution of the dominant precipitation mechanism within the large Tibetan Plateau. Further multisensoral remote sensing analysis include the observation of lake level alterations by satellite altimetry as well as the investigation of the ice thickness or the glaciated area inside the basins with time series of IceSat data.

The study is financed by the German Research Association (DFG) within the priority program 1372 (TiP) “Tibetan Plateau: Formation - Climate - Ecosystems” as well as from the German Ministry of Research (BMBF) within the WET (Variability and Trends of water balance components in benchmark-catchments of the Tibetan Plateau) scientific cooperation.

8538-30, Session 7

Modeling the distribution of aboveground biomass in Miombo ecosystems (Mozambique, Southeast Africa) using L-band Synthetic Aperture Radar data

Joao M. Carreiras, Joana B. Melo, Instituto de Investigação Científica Tropical (Portugal)

The importance of accurately reporting the carbon content of forested lands has been acknowledged and stressed by several studies and international conventions, e.g., the United Nations Framework Convention on Climate Change (UNFCCC). The quantification of forest aboveground biomass is important for forest management, carbon sequestration credits and scientific applications such as carbon cycle modeling. However, there is a great uncertainty related to the estimation of forest aboveground biomass, especially in the tropics. Miombo woodlands are the largest savanna in the world and dominate southern Africa. They are strongly influenced by anthropogenic fires and support the livelihoods of over 100 million people. However, it is threatened by desertification processes, deforestation, degradation of land and water resources, and loss of biodiversity.

The main goal of this study was to test a combination of field data and Japan’s Advanced Land Observing Satellite (ALOS) Phased Array L-band Synthetic Aperture Radar (PALSAR) backscatter intensity data to reduce the uncertainty in the estimation of forest aboveground biomass in the Miombo woodlands of Mozambique (East Africa). The penetrative capability of L-band synthetic aperture radar (SAR) data and the resulting interaction with vegetation structure is the main motivation for using these data for modeling forest aboveground biomass with a view to reduce the uncertainty in their estimation.

A detailed field campaign took place in July 2011 in a Miombo woodland region of the Zambézia province, Mozambique (East Africa). A set of 51 plots were selected based on a stratified sampling approach on the basis of three tree crown cover classes: 10-30%, 30-40%, 40-50%. A 20 meter radius plot was used, structural attributes collected (e.g., diameter at breast height, species identification), and used in combination with species-specific and generalized allometric equations to estimate the forest aboveground biomass of all sampled plots. ALOS PALSAR fine beam dual (FBD; HH and HV polarizations) data were acquired in 21 June 2010 to cover the study area. The data were acquired with an off-nadir angle of 34.3o (ascending orbit) and were provided by the European Space Agency in level 1.1 (single look complex, SLC).

A machine learning algorithm, based on bagging stochastic gradient boosting (BagSGB), was used to model forest aboveground biomass as a function of ALOS PALSAR FBD backscatter intensity metrics. The application of this method resulted in a coefficient of correlation (R) between observed and cross-validation predicted forest aboveground biomass values of 0.95 and in a root mean square error (RMSE) of 5.03 Mg ha-1. Furthermore, the BagSGB model produced also a measure of forest aboveground biomass prediction variability (coefficient of variation) on a pixel-by-pixel basis, with values ranging from 7 to 148 % (mean = 25 %) across the study area. Some issues were identified as potential source of uncertainty that must be tackled in future studies, namely the heterogeneity of forest structural types and the dimension of field plots.

8538-31, Session 7

SPOT 5 imagery for soil salinity assessment in Iraq

Sergio Teggi, Sofia Costanzini, Francesca Despini, Univ. degli Studi di Modena e Reggio Emilia (Italy); Francesco Immordino, ENEA (Italy); Paolo Chiodi, Univ. degli Studi di Modena e Reggio Emilia (Italy)

Soil salinization is a form of topsoil degradation due to the formation of soluble salts at deleterious levels. This phenomenon can seriously compromise vegetation health and agricultural productivity, and represents a worldwide environmental problem. Remote sensing is a very useful tool for soil salinization monitoring and assessment. In this work we show some results of a study aimed to define a methodology for soil salinity assessment in Iraq based on SPOT 5 imagery.

This methodology allows the identification of salinized soils primarily on bare soils. Subsequently some soil salinity assessment can be done on vegetated soils.

On bare soil the identification of salt is based on spectral analysis, using the Minimum Noise Fraction transformation and several indexes found in literature.

In case of densely vegetated soils the methodology for the discrimination of salinized soils has been integrated with the results obtained from the classification of vegetation coverage.

8538-32, Session 8

Object-based identification of cropland degradation: a case study in Uzbekistan

Olena Dubovyk, Gunter Menz, Rheinische Friedrich-Wilhelms-Univ. Bonn (Germany); Christopher Conrad, University of Wuerzburg (Germany); Asia Khamzina, Rheinische Friedrich-Wilhelms-Univ. Bonn (Germany)

Sustainability of irrigated agriculture is threatened by cropland degradation, particularly in irrigated agriculture-based economies, such as in Central Asia. The field-based identification of the degraded agricultural areas is important for developing land rehabilitation and monitoring programs. In heterogeneous irrigated agro-ecosystems, traditional pixel-based analysis of satellite data could lead to inaccurate mapping of degraded cropland due to mixed pixels and pixel heterogeneity. In contrast, object-based image analysis can handle these issues, at the same time providing parcel-specific information on the land's state. Assessment of vegetation cover decline, as a main indicator of the land degradation for sparsely vegetated areas, could be challenging with conventionally-applied vegetation indices, due to, for example, their sensitivity to soil background. Spectral mixture analysis (SMA), which provides an accurate quantitative estimation of proportional vegetation cover at a subpixel level, is, therefore, suitable for monitoring vegetation changes in irrigated agricultural areas.

We combined the object-based image analysis and SMA to develop an approach for identifying parcels of irrigated degraded cropland in Northern Uzbekistan, Central Asia, where ongoing land degradation is acute due to soil salinization. For the years 1987 and 2010, the multiple Landsat TM images were acquired to capture the crop growing season. The datasets were geometrically and radiometrically preprocessed. This was followed by a linear spectral unmixing approach and the object-based image classification. The derived maps were spatially compared to quantify the observed changes. A spatial pattern of degraded cropland was further interpreted in regard to specific agricultural land use and using supplementary datasets. A field campaign was conducted for validation of the results. Considering the spectral dimensionality of Landsat TM, a multiple 4-endmember (green vegetation, water, dark soil, and bright soil) model was set up for the analysis. The spectral unmixing results were valid, as indicated by the overall root mean square errors of <2.5% reflectance for all images. The results of classification revealed an increase in area of degraded croplands by 2% during last 14 years, while 5821 fields (241 km2) were affected by degradation processes, to varying degrees. During the observation period, spatial distribution of degraded fields was mainly associated with the abandoned croplands (R2=0.82) and lands with low inherent fertility (R2=0.98). This indicates that the lands, poorly suitable for cropping, tended to be abandoned from agricultural practices and experienced vegetation degradation. The proposed approach was successful in object-based identification of degraded and abandoned fields, yielding overall accuracies of the maps exceeding 78%. It could be further elaborated for a field-based monitoring of cropland degradation, thus revealing areas, which should be primarily targeted by rehabilitation measures in similar landscapes of Central Asia and elsewhere.

8538-33, Session 8

Spatiotemporal object-based image analyses in the Blue Nile area using optical multispectral imagery

Mustafa M. El-Abbas, Elmar Csaplovics, Technische Univ. Dresden (Germany)

Considering the dramatic change occurred in the Blue Nile region of Sudan, this study is of great value of developing a method for identification of forestland cover extents, integrating rate of changes and causes. The study utilized three consecutive optical multispectral images, two Landsat TM images of 1990 and 1999 as well as Aster image of 2009 to evaluate forest-cover dynamics during the period 1990 to 2009. The method adopted in this research consists in cross operation of classified images from different points in time, which utilizes the overlaying images to be compared for change detection. The post-classification change detection technique was performed here for the following reasons: Firstly, to eliminate the atmospheric effects and spectral variation in vegetation classes due to the different phenological properties since each image classified separately. Secondly, it can not only locate whether there is a change or not, but also provides detailed change (from-to) information classes. And thirdly, to reduce the effect due to the variation between images acquired from different sensors. For the purpose of post-classification change detection technique, classified maps for corresponding dates were required. The two well known image classification approaches (object-based and pixel-based) were performed to address the ability of each to generate accurate results. Due to the dramatically changes observed in the region, the topographic maps are not suitable for result validation. Instead, the accuracy of Landsat TM 1990 and 1999 images were assessed by visual selection of random points from the raw images data. Following the much precise result obtained from the classification approaches, in addition to unavailability of neither aerial photograph nor field survey data to be used as training areas for the Landsat images 1990 and 1999, the rule-based method in object-based approach was found to be the much fitted method to classify the images required for the post-classification change detection, which they were achieved with overall accuracy of 91 %, 93 % and 95 % for the years 1990, 1999 and 2009 respectively. Nine Land Use Land Cover (LULC) classes were generated from each, i.e. agriculture (rain-fed), bare-land, crop-land, dense-forest, grassland, orchard, scattered-forest, settlements and water body. Therefore, and considering the dramatic change observed in the area, the fusion operation of multi-temporal data results initially in quite numerous change "from-to" information classes, which allows for aggregation of these classes at any hierarchical level of details. New layers of segments were created representing the change areas as well as the overlapped areas of each pair of classified images. Subsequently, a series of optimized algorithms have been developed to estimate the change in LULC. Thus, the developed approach allows the operator to effectively know the spatial pattern of changes, trend and magnitude of the dynamics occurred in each of the classified LULC classes. While many change-detection techniques have been developed, a little has been done to assess the quality of these techniques. However, in order to quantitatively evaluate the accuracies of the change maps, the accuracy assessment based on best classification results were performed in eCognition software, which reveals that, the accuracies of the change maps for the two time intervals were consistently high.

8538-35, Session 8

Total ozone column distribution over peninsular Malaysia from Scanning Imaging Absorption Spectrometer for Atmospheric Cartography (SCIAMACHY)

Mohd Zubir M. Jafri, Hwee-San Lim, Kok Chooi Tan, Univ. Sains Malaysia (Malaysia)

Increasing of atmospheric ozone concentrations have received great attention around the whole because of its characteristic, in order to degrade air quality and brings hazard to human health

and ecosystems. Ozone, one of the most pollutants source and brings a variety of adverse effects on plant life and human being. Continuous monitoring on ozone concentrations at atmosphere provide information and precautions for the high ozone level, which we need to be established. Satellite observation of ozone has been identified that it can provide the precise and accurate data globally, which sensitive to the small regional biases. We present measurements from Scanning Imaging Absorption Spectrometer for Atmospheric Cartography (SCIAMACHY) included on the European environmental satellite ENVISAT, launched on 1st of March 2002. Main objective of this study is to examine the ozone distribution over Peninsular Malaysia using SCIAMACHY level-2 of total ozone column WFMD version 1.0 with spatial resolution 1° x 1.25°. Maps of time averaged (yearly, tri-monthly) ozone was generated and analyzed over Peninsular Malaysia for the year 2003 using PCI Geomatica 10.3 image processing software. It was retrieved using the interpolation technique. The concentration changes within boundary layer at all altitude levels are equally sensitive through the SCIAMACHY near-infrared nadir observations. Hence, we can make observation of ozone at surface source region. The results successfully identify the area with highest and lowest concentration of ozone at Peninsular Malaysia using SCIAMACHY data. Therefore, the study is suitable to examine the distribution of ozone at tropical region.

8538-36, Session 8

Combine MODIS and HJ-1 CCD NDVI with logistic model to generate high spatial and temporal resolution NDVI data

Jingyi Jiang, Jinling Song, Jingdi Wang, Zhiqiang Xiao, Beijing Normal Univ. (China)

High spatial and temporal resolution Normalized Difference Vegetation Index (NDVI) data can be used to describe vegetation dynamics and provide the variation of surface for monitoring phenology and land cover change quantitatively. However, the NDVI products provided by the satellite-based sensors like AVHRR, SPOT/VEGETATION, MODIS have the low spatial resolution and contain erratic fluctuations especially in cloudy and snowy areas. These fluctuations are inconsistent with vegetation growth process which is known to be gradually and continuously. This paper presents a method using MODIS NBAR NDVI to simulate vegetation dynamics and combining curves with few HJ-1 CCD NDVI data to get the High spatial and temporal resolution data. The data we used include the 8-day MODIS NBAR product (MOD43B4, 1 km) from 2004 to 2010, the MODIS Land Cover data (MOD12Q1, 1 km), the high spatial land use and land cover(LULC) map(30m) and the HJ-1 CCD NDVI (30m). First, using MODIS Land Cover data with 30m LULC map to calculate the percentage of every classes in the MODIS pixel. And the mean MODIS NDVI can be got through the average value of pure pixels using MODIS NBAR product from 2004 to 2010. Then the logistic model which is usually used to describe the phenology of ecosystems is fitted to the average MODIS NDVI to simulate the variation in NDVI time series and the intra-annual vegetation dynamics for every types are achieved. Specifically, temporal variation in NDVI data for a multiple growth or senescence cycle can be modeled using multi-logistic functions. This seasonal cycle is consistent with the known processes of vegetation and is continuous in time series. So the simulated NDVI time series of all vegetation types are extracted as background values and the HJ-1 CCD NDVI is used to adjust the curve of time-series NDVI to estimate the NDVI at high spatial and temporal resolution. The method is applied to the Heihe River basin. And the results are compared with some filed measured data, which shows the high feasibility of the method to generate accurate and reliable data. The method is also used in other typical area to estimate its practical applicability. It is proved that the method can be used in small scales to lager regions. The high spatial and temporal resolution NDVI time series data is significative for climate, hydrology and biogeochemical models and can be used to analysis the characteristics of NDVI spatial and temporal changes in large scales or compare the differences of NDVI time series in various regions.

8538-37, Session 8

Remote sensing indices for monitoring land degradation in a semiarid to arid basin in Jordan

Jawad T. Al-Bakri, Hani Saoub, The Univ. of Jordan (Jordan); William Nickling, Univ. of Guelph (Canada); Ayman Suleiman, The Univ. of Jordan (Jordan); Mohammad Salahat, The Hashemite Univ. (Jordan); Saeb Khresat, Jordan Univ. of Science & Technology (Jordan); Tareq Kandakji, The Univ. of Jordan (Jordan)

The use of remote sensing data to map the biophysical indicators of land degradation and desertification has become increasing as improvements in spatial, spectral and temporal resolutions are advancing with time. For research communities, tradeoffs between spatial and spectral resolution are often arising when satellite remote sensing data is used to map land degradation. In this study, spectral reflectance measurements for more than one hundred locations were recorded using a 16-bands multispectral radiometer that includes both narrow and wide spectral bands in the visible, near infrared (NIR) and shortwave infrared (SWIR) wavelengths.

Measurements, with an instantaneous field of view (IFOV) of 3-4 m, were focused on degraded soils and vegetation of the semiarid basin of Yarmouk river in Jordan. Spectral reflectance measurements were arranged in spreadsheets and spectral profiles were plotted for the different types of soils and vegetation. Linear regression analysis was made between soil spectral reflectance and soil surficial properties of salinity, sand, silt and clay. A linear spectral unmixing was applied to mixed pixels to eliminate the effects of vegetation and rocks on soil spectral reflectance. For vegetation, spectral measurements for rainfed wheat and barley were correlated with biomass and cover for both crops to identify the suitable remote sensing indicators for monitoring vegetation, as a biophysical indicator of land degradation in the study area. The same procedures were followed to correlate spectral reflectance extracted from ASTER image with soil salinity, vegetation biomass and cover. This was carried out to investigate the use of medium resolution (15-m) images to map those biophysical indicators.

Results showed that vegetation types were differentiated in the near infrared parts of electromagnetic spectrum and were well separated from the degraded soils in the shortwave infrared wavelength at 1480 nm. For most sites, the differences in the bandwidths (in the range of 8.5 nm to 90 nm) did not improve the differentiation of vegetation types. For all wavelengths, stronger correlations (maximum R2 = 0.85) values were obtained for vegetation cover when compared with biomass (maximum R2 = 0.54). For soil, significant correlations were observed between salinity and spectral reflectance. In all visible to NIR bands, soil spectral reflectance tended to increase with salinity. The maximum correlations were obtained in the blue wavelengths (470±10 nm, 485±90 nm), followed by green and the NIR bands, where R2 values were around 0.60. All SWIR bands, except the 1480±14.5 nm, were significantly correlated with soil salinity, with slightly higher correlation in the narrow wavelength than the broad wavelength of the SWIR.

The relationship between soil salinity and ASTER bands was significant but with relatively low correlation (maximum R2 = 0.31) when compared with the results obtained for the radiometer at the same wavelengths. The correlations between ASTER bands and vegetation cover were slightly lower (maximum R2 = 0.62) when compared with results of radiometer. Results of the study showed that the use of remote sensing indicators related to vegetation and soil salinity would be recommended to map the extent of land degradation in the study area and similar environments.

8538-38, Session PS

The application of remote sensing in the environmental risk monitoring of tailings pond: a case study in Zhangjiakou area of China

Rulin Xiao, Wenming Shen, Wencheng Xiong, Zhuo Fu, Yuanli Shi, Fei Cao, Ministry of Environmental Protection (China)

As a kind of huge environmental risk source, tailings pond could cause a huge environmental disaster to the downstream area once an accident happened on it. Therefore it has become one focus of the environmental regulation in china. Especially, recently, environmental emergencies caused by tailings pond are growing rapidly in China, the environmental emergency management of the tailings pond has been confronting with a severe situation. However, the regulatory agency is badly weak in the environmental regulation of tailings pond, due to the using of ground surveys and statistics which is costly, laborious and time consuming, and the lacking of strong technical and information support.

Therefore, in this paper, according to the actual needs of the environmental emergency management of tailings pond, we firstly make a comprehensive analysis of the characteristics of the tailings pond and the advantages and capability of remote sensing technology, and then proposed a comprehensive and systematic indexes system and the method of environmental risk monitoring of tailings pond based on remote sensing and GIS. The indexes system not only considers factors from the upstream area, the pond area and the downstream area in a perspective of the risk space theory, but also considers factors from risk source, risk receptor and risk control mechanism in a perspective of risk systems theory. Given that Zhangjiakou city has up to 580 tailings pond and is nearly located upstream of the water source of Beijing, so finally we apply the proposed indexes system and method in Zhangjiakou area in China to help collect environmental risk data of tailings pond in that area and find out it works well. Through the use case in Zhajiakou, the technique of using remote sensing to monitor environmental risk of tailings pond is feasible and effective, and would contribute to the establishment of 'Space-Ground' monitoring network of tailings pond in future.

8538-39, Session PS

Identification of physical geographical borders of Khorezm oasis and its ecosystems through Landsat images

Muzaffar J. Matchanov, Urgench State Univ. (Uzbekistan) and Univ. do Porto (Portugal); Ana C. Teodoro, Neftalí P. Sillero, Univ. do Porto (Portugal)

Khorezm oasis is one of the ancient agricultural and cultural centers in Asia. It is served as a study area of various scientific directions (1), especially ecological and geographical investigations (2,3). Therefore, they have been conducting in administrative area or in phenomenon sphere without considering ecosystem complexity/unique in geographical sciences, difficulties indicating its clear physical geographical borders among scientists.

The main objective of this study is determining physical geographical borders of the Khorezm oasis and classifying its ecosystems. Terms in relation to "oasis" were reviewed and summarized (4,5). Landsat 4-5 TM (level 1) images covering the period of 1987-2010 were used to classify ecosystems and the oasis borders were indicated by analyzing agricultural lands, vegetation index, and administrative borders. The Landsat images are all geometrically corrected and orthorectified. Shuttle Radar Topography Mission (SRTM) data were used to analyze and review other offered borders of the oasis. Six ecosystem classes based on three different supervised classification algorithms (Minimum-Distance, Parallelepiped, and Maximum Likelihood): Irrigated, Desert, Inner desert, Lakes, River (and river bank), Urban were classified. The selection of ecosystem was based on reference data (topographic maps, Google Earth data, field observations and field data). The pixel-based classification algorithm presented a very good performance, demonstrated by the results of overall accuracy (>90%) and Kappa statistics (>0.90). Geographical Information Systems (GIS) techniques were used to compute the oasis area. The use of Landsat images to determining ecosystem borders and their dynamics is an appropriate approach in physical geographical sciences.

References:

1. Vlek P.L.G., Martius C., Wehrheim P., Schoeller-Schletter A., and John Lamers (2001): Economic Restructuring of Land and Water Use in the Region Khorezm (Uzbekistan) (Project Proposal for Phase I). ZEF Work Papers for Sustainable Development in Central Asia. No. 1, pp.75.

2. Khamroev,M.O.2009. Social Ecology of Khorezm region and geographical features of population health. PhD Thesis, SRHYI of Uzhydromet. Tashkent, pp.-166.

3. Matchanov, M.J.2009. Ecological safety and its physico-geographical aspects (in case of Kharezm region). PhD Thesis, SRHYI of Uzhydromet. Tashkent, pp.-129.

4. Gvozdetskiy, N.A., Mixaylov, N.I.1987.Physical Geography of SSSR. М.

5. Uzbek-Soviet Encyclopedia.1972.Edited by Muminov,I.M. Volume 3, Tashkent.-215 p.

8538-40, Session PS

Interannual variability of surface albedo over east Asia according to land cover

Chang-Suk Lee, Kyung-Soo Han, Kyoung-Jin Pi, In-Hwan Kim, Min-Ji Lee, Pukyong National Univ. (Korea, Republic of)

Land surface albedo is key parameter for anticipating climate. Especially, now a day land surface albedo that show flux of radiation between the land surface and the atmosphere is became more important due to climate change by global warming. Therefor a lot of studies about land surface albedo have been performed and are underway using various remotely sensed data. In this study, we analysis variation of land surface albedo over East Asia (20° ~ 50° N, 100° ~ 145° E) during 10 years (2001 ~ 2010) using Moderate Resolution Imaging Spectroradiometer (MODIS) albedo product. MODIS has provided surface albedo 1 km spatial resolution product in the form of 16 day composite and global land cover. Among the albedo data set, three broadband data (visible, near infrared, short wave) was used for analysis which was conducted according to land cover. There are not only various land cover (crop, forest, shrub, grass, barren etc.) but also dessert (Gobi), and ongoing desertification areas are included in study area.

8538-41, Session PS

Satellite remote sensing data for urban heat waves assessment and human health impacts

Maria A. Zoran, National Institute of Research and Development for Optoelectronics (Romania); Mariana R. Dida M.D., Univ. of Medicine and Pharmacy of Craiova (Romania)

Remote sensing is a key application in global-change science and urban climatology. Urbanization, the conversion of other types of land to uses associated with growth of populations and economy has a great impact on both micro-climate as well as macro-climate. By integrating high-resolution and medium-resolution satellite imagery with other geospatial information, have been investigated several land surface parameters including impervious surfaces and land surface temperatures for Bucharest metropolitan area in Romania. The aim of this study is to examine the changes in land use/cover pattern in a rapidly changing area of Bucharest metropolitan area in relation to urbanization since the 1990s till 2011 and then to investigate the impact of such changes on the intensity and spatial pattern of the UHI (Urban Heat Island) effect in the region in relation with heat waves assessment. Investigation of radiative properties, energy balance, heat fluxes and NDVI, EVI is based on satellite data provided by various sensors Landsat TM, ETM+, MODIS and IKONOS.

The aim of this study is to examine the changes in land use/cover pattern in a rapidly changing area of Bucharest metropolitan area in relation to urbanization since the 1990s till 2011 and then to investigate the impact of such changes on the intensity and spatial pattern of the UHI effect in the region with heat waves conditions. Our analysis showed that higher temperature in the UHI was located with a scattered pattern, which was related to certain land-cover types. In order to analyze the relationship between heat waves, UHI and land-cover changes, this study attempted to employ a quantitative approach in exploring the relationship between temperature and several vegetation indices, including the Vegetation Index NDVI and EVI extracted from time-series satellite data. Such analysis is very helpful in urban mesoscale models and urban climate studies. An interesting correlation analysis was done regarding human health effects of summer 2003, 2007 and 2010 years heat wave events in Bucharest and periurban areas.

In Bucharest urban and periurban areas, the range of average net radiation extracted from MODIS data during summer was in the order of 690- 810 Wm-2, function of the subregion tested areas as the net radiation is partitioned to sensible heat and storage heat. During summer heat wave events of 2003, 2007 and 2010 years, the average extracted net radiation was in the range of 800- 950 Wm-2. This paper demonstrates the potential of moderate-and high resolution, multispectral imagery to map and monitor the evolution of the physical urban environment in relation with micro and macroclimate conditions. So called effect of "urban heat island" must be considered mostly for summer periods conditions and large European scale heat waves. The rates of urbanization are characterized by creating a typology of urbanization trends based on quantities that are indicative to the

potential environmental impacts. As future climate trends have been predicted to increase the magnitude and negative human health impacts of urban heat waves in metropolitan areas, there is an urgent need to be developed adequate strategies for societal vulnerability reducing.

8538-42, Session PS

Visualization and GIS Analyse of Marine Disasters based on Globe Model

Linchong Kang, Suixiang Shi, Haiyan Huang, Feng Zhang, National Marine Data and Information Service (China)

Skyline is one of the popular sphere model software platforms, which is an interactive environment established by aero image, satellite data, digital elevation model and other 2D or 3D information sources. It can integrate data rapidly and support large database and real-time information flow communications technique effectively. In this paper,firstly, based on globe model of Skyline software, remote sensing imagery and terrain elevation of islands and Coastal Zones in china are implemented using multi- resolution level of details(MLOD). The imagery includes Spot 5 imagery which spatial resolution is 2.5m and Aerial Images which spatial resolution is 0.5m. Secondly, integrates flood forecasting models based on data flow in disaster process analysis, uses the GIS technology in flood disaster impact analysis, and adopts the globe model as a platform for results show of sea level rise modeling and impact analysis. Thirdly, the predicton flow and data structure of storm surge was analyzed,then virtualization and analysis based on series presentation technology as field data.

8538-43, Session PS

A new time discrimination circuit for the 3D imaging lidar

Chunsheng Hu, Zongsheng Huang, Xingshu Wang, Dejun Zhan, National Univ. of Defense Technology (China)

The research of the 3D imaging lidar is a key area in the 3D information acquisition research. The time discrimination circuit is a key part in the 3D imaging lidar, which determines the precision of the measurement and imaging in the 3D imaging lidar. At present, the CFD (constant fraction discriminator) is the main time discrimination method used in the 3D imaging lidar. The CFD circuit is usually composed of a time delayer, an attenuator and a comparator. The time delayer in the previous CFD circuit is generally implemented with a delay line. The signal distortion of the delay line is very small. However, the delay line has some shortcomings: big volume, difficult adjustment, and etc. Recently, the delay line is replaced by a low-pass or high-pass filter which is usually implemented with resistors and capacitors. This method reduces the volume and adjustment difficulties of the delay line, but increases the signal distortion, resulting in the time discrimination precision reduction.

In order to reduce the signal distortion and enhance the time discrimination precision, we propose a new time discrimination circuit, which improves both the time delayer and the attenuator in the previous CFD circuit. The proposed circuit mainly includes a time delayer, a low-pass filter, a comparator and a pre-discriminator. The time delayer is implemented with a series of inductors and capacitors, replacing the delay line in the previous CFD circuit. The time delayer has some advantages: low signal distortion, small volume, easy adjustment, and etc. The low-pass filter replaces the attenuator in the previous CFD circuit, which attenuates the signal amplitude and broadens the signal width. The low-pass filter reduces the noise by decreasing the equivalent noise bandwidth, and increases the signal slope at the discrimination time. Therefore, the time discrimination error is decreased significantly.

This paper carried out a theoretical analysis for the noise and time discrimination error in the proposed circuit and compares them to the previous CFD circuit. The comparison shows that the proposed circuit reduces the time discrimination error about 50 percent under the same noise level. The proposed circuit is discussed in detail, which adopts the MAX9601 comparator, a RC (resistor and capacitor) low-pass filter and a time delayer implemented with a LC (inductor and capacitor) network.

To test the time discrimination precision and time delay of the proposed circuit, some experiments have been carried out. The experiments show that the time delay of the circuit is about 14ns, and the time discrimination error due to signal amplitude variation is less than 112 ps when the signal amplitude ranges from 0.2 V to 1.86 V. The tested time discrimination error complies well with the theoretical calculation. The time discrimination error is less than 250 ps when the SNR (signal-to-noise ratio) is above 18.5, less than 112 ps when the SNR above 54.5. The time discrimination circuit is used and tested in a high-speed 3D imaging lidar. Besides the 3D imaging lidar, the circuit can be applied to the pulsed laser range finder and other time discrimination system.

8538-44, Session PS

Long term seismic noise acquisition and analysis with tunable monolithic horizontal sensors at the INFN Gran Sasso National Laboratory

Fausto Acernese, Univ. degli Studi di Salerno (Italy); Rosangela Canonico, Uni. degli Studi di Salerno (Italy); Rosario De Rosa, Univ. degli Studi di Napoli Federico II (Italy); Gerardo Giordano, Rocco Romano, Fabrizio Barone, Univ. degli Studi di Salerno (Italy)

In this paper we present the scientific data recorded by tunable mechanical monolithic horizontal seismometerslocated in the Gran Sasso National Laboratory of the INFN, within thermally insulating enclosures onto concrete slabs connected to the bedrock. The main goals of this long term test are a preliminary seismic characterization of the site in the frequency band 10–7 Hz ÷ 1 Hz and the acquisition of all the relevant information for the optimization of the sensors.

8538-45, Session PS

Low frequency/high sensitivity horizontal monolithic sensor

Fausto Acernese, Rosangela Canonico, Univ. degli Studi di Salerno (Italy); Rosario De Rosa, Univ. degli Studi di Napoli Federico II (Italy); Gerardo Giordano, Rocco Romano, Fabrizio Barone, Univ. degli Studi di Salerno (Italy)

This paper describes a new mechanical implementation of a folded pendulum based inertial sensor, configurable as seismometer and as accelerometer.1 The sensor is compact, light, scalable, tunable (< 100mHz), with large band (10–6 Hz ÷ 10 Hz), high quality factor (Q > 1500 in air) instrument and good immunity to environmental noises, guaranteed by an integrated laser optical readout. The measured sensitivity curve is in very good agreement with the theoretical one (10–12 m/√Hz in the band (0.1 ÷ 10 Hz). Typical applications are in the field of earthquake engineering, geophysics, and in all applications requiring large band-low frequency performances coupled with high sensitivities.

8538-46, Session PS

Performance of commercial and open source remote sensing/image processing software for land cover/use purposes

Ana C. Teodoro, Dário Ferreira, Neftali P. Sillero, Univ. do Porto (Portugal)

The developments in computer science applied to remote sensing allows monitoring and mapping the land cover/use, health farming crops status, forestry-areas burned, floods surfacing, coastal areas, etc. The firsts remote sensing/image processing software were created by commercial companies, the GTE corporation and ESL Inc.. Nowadays, there is a new philosophy of remote sensing/image processing software: the philosophy of open source software. The main objective of this work was to compare the potentialities and list the available tools of four remote sensing/image processing softwares. For this study, we assessed the performance of several algorithms available in: PCI Geomatic V8.2, Envi 4.7, Spring 5.1.8, and Orfeo toolbox integrated in Monteverdi 1.10.0. The PCI Geomatic and Envi are commercial softwares and Spring and Orfeo are open source softwares.

In this work, two images were used: one image Landsat 5 Thematic

Mapper from October 2011 (path 204; row 32) and one IKONOS image from September 2005. Both images cover the same area. The images were already geometrically corrected (UTM projection zone 29N and WGS89 datum).

A list with all the classification algorithms available in PCI Geomatic, Envi, Orfeo and Spring software were listed, and divided into the different approaches of classification (pixel-based, object-oriented, learning algorithms, and principal components analysis). The two images were classified with each algorithm in the four softwares. Then, the time of performance and classification results were assessed and compared between the four softwares. The classes of image classification were based in CORINE Land Cover, and were the same for the Landsat 5 TM and IKONOS image.

The PCI Geomatic was the software that presented a higher number of classification algorithms, followed by Envi, Spring, and Orfeo, respectively. The PCI and Envi contained more algorithms that Spring, however did not present object-based classification algorithms (for the versions analyzed). The Spring was the only software that contains both pixel-based and object-oriented classification algorithms. The higher number of segmentation algorithms were available in Orfeo. The accuracy of the classification algorithms in the different software's were evaluated trough the confusion matrix (overall accuracy) and Kappa statistics. The performance of classification algorithms are identically in all softwares.

This work could be very important for the researchers because it provides a qualitative and quantitative analysis of different image processing algorithms available in different software (commercial and open source).

8538-47, Session PS

Mechanical monolithic tiltmeter for low frequency measurements

Fausto Acernese, Rosangela Canonico, Univ. degli Studi di Salerno (Italy); Rosario De Rosa, Univ. degli Studi di Napoli Federico II (Italy); Gerardo Giordano, Rocco Romano, Fabrizio Barone, Univ. degli Studi di Salerno (Italy)

The paper describes a tilt meter sensor for geophysical applications, based on Folded Pendulum (FP) mechanical sensor. Both the theoretical model and the experimental results of a tunable mechanical monolithic FP tilt meter prototype are presented and discussed. Some of the most important characteristics, like the measured resolution of $\approx$ 0.1 nrad at 100mHz, are detailed. Among the scientific results, earth tilt tides have been already observed with this monolithic FP tilt meter prototype.

8538-48, Session PS

Monitoring the burst-out of Enteromorpha prolifera in the Yellow Sea of China

Haiying Li, Hongchun Peng, Hui Zhang, Huaihai Institute of Technology (China); Chunling Huang, Cold and Arid Regions Environmental and Engineering Research Institute, Chinese Academy of Sciences (China)

In the eve of the Beijing Olympics Games, Qingdao in China, as the host city of OSC of Beijing 2008 Olympic Games, was surrounded by Enteromorpha prolifera, which was followed with interest by whole China and the world. In 2009, Enteromorpha disaster struck the north-central of Yellow Sea once again, resulting in extremely negative impact to the ocean activities. It became an important issue to monitor and prevent the burst-out of Enteromorpha prolifera for the inshore Provinces of the Yellow Sea. The focuses were where the source of Enteromorpha prolifera was, what the drift course was , when the time of burst-out was, and where it bursted out. The Enteromorpha often comes from other ocean, monitoring the drifting path of the Enteromorpha will become very important.

The Study area is located at 31-41°N, 117-127°, mainly the Yellow Sea. And the data sources are Terra MODIS 1B images from 2000-2010 years, because it has high temporal absolution of 0.5 day, and spatial absolution of 250m in band 1 and 2. We used NDVI as an indicator of Enteromorpha prolifera.

The MOIDS data must be preprocessed before used to derive information of Enteromorpha prolifera, which include BOW-TIE processing, image registration, clip, merge, and masking. The images preprocessed were used to calculate the index of NDVI and get the range of Enteromorpha prolifera, and get that of dynamic change with time. And the results show that:

1) Appear year of Enteromorpha prolifera: they were founded firstly in 2001, and there are little appearance in the following years of 2003 and 2005. However, we did not find any Enteromorpha prolifera in study area in the subsequent three years of 2002,2004 and 2006. The first outbreak is in 2007 and subsequent four years remained the tread of outbreak.

2) Place and time: The sea area of Yancheng is usually the first place that we find Enteromorpha prolifera, and sometimes in esat of Yangtze estuary.

3) Drift path: Generally, they appeared in south area of Yellow sea, and moved northward in the process of gradually breeding. The area covered by Enteromorpha prolifera increased year by year, and Shandong is the mainly affected waters.

4) Growth cycle: From the data analysis, the distribution of Enteromorpha prolifera not only has changed, its density also has the change; the smaller density is in front of the range in drift process. And its life cycle is about 15 days, but which still need further work to validate.

8538-49, Session PS

The feasibility of landscape pattern analysis within the alpine steppe of the Yellow River source based on historical CORONA panchromatic imagery

Quanjun Jiao, Bing Zhang, Liangyun Liu, Ctr. for Earth Observation and Digital Earth (China)

Multi-scale analysis of landscape statistics is very important to research ecological processes. However, it was lack of high-resolution data to extract the landscape pattern features of suspected ecological degradation region a few decades ago. CORONA panchromatic film photos acquired between 1960 and 1972 provide the historical high-resolution image resource in small-scale ecological pattern research. The purpose of this research was to assess the feasibility of landscape pattern analysis within the alpine steppe area of the Yellow River source through historical CORONA panchromatic imagery. Histogram analysis result shows that the swamp meadow is difficult to be distinguished from water, but there is a potential of mapping four patch types in alpine steppe in gray imagery. Through segmentation image of alpine steppe area, different landscape pattern metrics were calculated in several selected areas. The result also shows that landscape pattern metrics are closely related to NDVI level of alpine grassland. It can be concluded that historical CORONA panchromatic imagery is a potentially valuable high-resolution remote sensing source for long-time ecological monitoring.

8538-50, Session PS

Spatio-temporal analysis for the correlations between meteo-hydrological factors and malaria infection in South Korea

DonJeong Choi, Young Cheol Suh, Pukyong National Univ. (Korea, Republic of)

Malaria is globally increasing due to the neglect of management system, increasing resistance of mosquitoes to insecticides, population growth and migration, land use change, global warming, El Niño, logging, construction of the dam and various factors. Malaria is the most important vector-borne disease and the most sensitive disease in long-term climate change. In South Korea, all the malaria infection cases cause by P. vivax that had vanished 1970s and rediscovered after 1993. Especially, a steady increase since 2000 and the spatial distribution of infection have spreading to cities range after 2005. Accordingly, in Korea, the necessity of research is increasing for the relationship between meteorological factors and malaria infection. However, meteorological studies are relatively few because most studies have been conducted in the field of medicine or public health. In addition, few studies have been conducted even reveals the limitations levels in application of meteorological factors and expertise of spatial analysis. Therefore, we performed spatio-temporal analysis for the correlation between 2001 and 2011 monthly meteorological data and malaria infection. The malaria data came from

2001~2011 claim data from the Centers for Korean Disease Control and Prevention. NDVI (Normalized Difference Vegetation Index) index using SPOT5 satellite sensors, USGS 30M * 30M DEM was carried out the hydrological environmental factor which represent habitat of malaria infection and mosquito breeding site.

Climate factors replaced the activity of malaria-carrying mosquito; monthly rainfall products from TRMM satellite data, monthly surface temperature using MODIS and monthly maximum, minimum and average value of absolute humidity was calculated using kriging the station data, were calculated and used in this study. GEE (Generalized Estimating Equation) model of Poisson distribution is applied to reflect the outbreak of malaria and seasonality of meteo-hydrological factors, and the cluster analysis was performed to detect the spatio-temporal Hotspot of calculated regression coefficients.

The results of this study showed that the statistically reasonable correlation was found. However, it needed additional researches for the exposure of source of infection on North Korea using satellite images, considering the spread of the disease and distribution of local meteo-hydrological factors are continuous and most of areas affected by malaria are adjacent to the Demilitarized Zone (DMZ).

8538-51, Session PS

Evaluation of wind flow computational models using multi-resolution remote sensing datasets in a high complexity terrain domain

John Koutroumpas, Konstantinos Koutroumpas, Infometrics Ltd. (Greece)

Wind flow estimation over complex terrain is a crucial procedure for several applications such as prediction of wind energy resources, pollution dispersal estimation and bridge design. Numerous flow models of different type and complexity have been developed in order to reconstruct a steady-state wind field based on initial experimental data. These computational models are divided into two main categories: a. linearized models and b. mass-consistent models. Linearized models are based on simplified steady-state solutions of the Navier-Stokes equations for boundary layer wind profile. On the other hand, mass-consistent models are based on adjustment of interpolated field of wind flows to satisfy mass conservation equations. In both cases the accuracy of wind flow estimation strongly depends on the complexity of terrain domain and consequently on resolution and accuracy of topographical input data, that describe terrain characteristics. In this work we evaluate three wind flow computational models (MS-3DJH/3R, WaSP and 3D-RANS) in a complex terrain domain in Southern Greece using three remote sensing datasets of different spatial resolution. The study area is a mountainous region with frequent changes of terrain slope and land cover. The evaluation is based on a pair-wise intercomparison of results derived from two meteorological stations. The first anemometer mast is used as a predictor and the second is used for evaluation of wind speed predictions. For the simulation of the wind field, terrain characteristics are described by a terrain roughness map and by a digital elevation model. Object-oriented segmentation techniques have been applied to Landsat, ASTER and IKONOS images in order to derive terrain roughness maps with spatial resolution of 30 meter, 15 meter and 1 meter respectively. Furthermore, two DEMs with global coverage (SRTM and ASTER GDEM) and a high-resolution DEM, derived from digital photogrammetric techniques, paired with corresponding terrain roughness maps produce three different resolution input data to wind flow computational model. The influence of the topographical input data on the accuracy of wind flow estimation over complex terrain has been tested with three computational models: MS-3DJH/3R, WaSP and 3D-RANS. From the results, it has been found that the spatial resolution of topographic input data is a crucial factor in achieving accurate wind flow estimation over complex terrain. Moreover non-linear 3D-RANS computational model with topographical input data derived from high resolution remote sensing images results to higher accuracies in wind flow estimation. It is remarkable that wind speed predictions from the simplest linear model MS-3DJH/3R with high resolution input data are more accurate than results from the sophisticated 3D-RANS solver with low resolution input data.

8538-52, Session PS

Coastal morphodynamic features/patterns analysis through a video based system and image processing

Fábio Santos, Joaquim Pais-Barbosa, Ana C. M. Teodoro, Hernâni Gonçalves, Paolo Baptista, António Moreira, Fernando Veloso-Gomes, Francisco Taveira-Pinto, Paulo Gomes-Costa, Vítor Lopes, Filipe Neves-Santos, Univ. do Porto (Portugal)

The Portuguese coastline, like many other worldwide coastlines, is often submitted to several types of extreme events resulting in flooding, infrastructure, habitats and coastal defenses destruction, dunes breaching and erosion. Thus, acquisition of high quality field measurements has become a common concern for scientists and coastal managers, and coastal monitoring is a key issue to follow, observe, understand and forecast the phenomena/processes that may occur both in the present and in the future.

The nearshore survey systems have been traditionally based on in situ measurements or in the use of satellite and aircraft mounted remote sensing systems. Other technique, that is gathering importance since their first implementations in the early 1990s, is the video-monitoring systems, which proved to be an economic, efficient and successful way to collect useful and continuous data and also to document extreme events such as storms.

In this context, Portugal is a country with a significant coastline and with a huge lack of coastal monitoring programs. Therefore, one way to overcome this problem is to develop a low cost video monitoring system.

This idea led to the development of the project MoZCo (Advanced Methodologies and Techniques Development for Coastal Zone Monitoring), which intends to implement and develop monitoring techniques for the coastal zone, collecting continuous data and increasing the current knowledge on Portugal coastal morphodynamics, hydrodynamics and hydromorphology behavior.

The pilot study area is Ofir beach (north of Portugal), a critical coastal area. In the beginning of this project, in 2010, a monitoring video station was developed, with low-cost cameras, and installed on the top of a building with about 40 meters height, collecting snapshots and 10 minutes videos every hour.

In order to process the data, several video image processing algorithms were implemented and a Graphical User Interface (GUI) was developed in Matlab®, allowing the achievement of the main products of a video-monitoring system, such as image rectification, time exposure (timex), variance images, time series of pixel intensities (timestack images) and shoreline detection.

The extraction and analysis of shoreline variability and its evolution is fundamental to a broad range of investigations. In this work, an algorithm for the shoreline detection was developed based on image processing techniques using both snapshots and timex images. The HSV color space was used, since better results were achieved than with the RGB color space. The idea is to select a study and a sample area, containing pixels associated with dry (dry sand) and wet (wet sand and water) regions, over which a thresholding and some morphological operators are applied. A manual digitalization of the shoreline for some images was used for checking purposes.

After comparing the results obtained from the automatic procedure with the manual digitalization, promising results were achieved despite the simplicity of the method, which is still in continuous development in order to optimize the results. Furthermore, new techniques for shoreline detection are being tested and new applications are being developed in order to provide a wide range of features necessary for coastal zone monitoring.

8538-53, Session PS

Land cover data from Landsat single-date archive imagery: an integrated classification approach

Sofia Bajocco, Tomaso Ceccarelli, Simone Rinaldo, Antonella De Angelis, Luca Salvati, Luigi Perini, Agricultural Research Council (Italy)

The analysis of land cover dynamics and of the underlying patterns of socio-environmental interactions, provides insight into many environmental problems. However, there are few data sources which

can be used to derive consistent time series, remote sensing being one of the most valuable ones. Due to their multi-temporal and spatial coverage needs, such analysis is usually based on large land cover datasets, which requires automated, objective and repeatable procedures. The USGS Landsat archives provide free access to multi-spectral, high-resolution remotely sensed data starting from the mid-eighties; in many cases, however, only single date images are available. This paper suggests an objective approach for generating land cover information from 30m resolution and single date Landsat archive satellite imagery. A procedure was developed integrating pixel-based and object-oriented classifiers, which consists of the following basic steps: i) pre-processing of the satellite image, including radiance and reflectance calibration, texture analysis and derivation of vegetation indices, ii) segmentation of the pre-processed image, iii) its classification integrating both radiometric and textural properties. The integrated procedure was tested for an area in Sardinia Region, Italy, and compared with a purely pixel-based one. Results demonstrated that a better overall accuracy, evaluated against the available land cover cartography, was obtained with the integrated (86%) compared to the pixel-based classification (68%) at the first CORINE Land Cover level. Furthermore the integrated approach showed its potentiality in identifying a number of classes also at the second CORINE Land Cover level. The proposed methodology needs to be further tested for evaluating its trasferability in time (constructing comparable land cover time series) and space (for covering larger areas).

8538-54, Session PS

Landslide detection using ALOS optical data: the case of Sykies Village in Andritsena, Greece

Konstantinos G Nikolakopoulos, University of Patras / Department of Geology (Greece)

One of the newest satellite sensors with stereo collection capability is ALOS. ALOS has a panchromatic radiometer with 2.5m spatial resolution at nadir and a multispectal radiometer with 10m spatial resolution. Two ALOS Prism data sets and two ALOS AVNIR collected over the same area within a year were used. The same ground control points were used for the creation of two DSMs and the orthorectification of the multispectral data. The elevation difference between the DSMs and the difference of the NDVI images created from the multispectral data were used in order to detect landslides.

8538-55, Session PS

GIS4schools: A new approach in GIS education

Timo Demharter, Ulrich Michel, Pädagogische Hochschule Heidelberg (Germany)

From a didactic point of view the procurement and the application of modern geographical methods and functions become more and more important. Although the integration of GIS in the classroom is repeatedly demanded, inter alia in Baden-Württemberg, Germany, the number of GIS users is small in comparison to other European countries or the USA. Possible reasons for this could, for instance, lie in the lack of GIS and computer knowledge of the teachers themselves and the subsequent extensive training effort in Desktop-GIS.

Today you have the technological possibilities to provide the broad public with geoinformation and geotechnology: Web technologies offer access to web-based, mobile and local applications through simple gateways.

The objective of this project is to generate a service-based infrastructure, which can be operated via mobile clients as well as via Desktop-GIS or a Browser. Due to the easy availability of the services the focus is in particular on students. This circumstance is a novelty through which a differentiated approach to the implementation of GIS in schools is established. Accordingly, the pilot nature of this project becomes apparent as well as its greater importance beyond its actual content especially for the sector of media development at colleges of education.

The continuity from Web-GIS to Desktop-GIS is innovative: The goal is to create an adapted multi-level solution which allows both, an easy introduction if desired or a detailed analysis - either to be achieved with a focus especially on students and their cooperation among one another.

8538-56, Session PS

Discomfort level and at-satellite land surface temperature: case study of Klang Valley

Illyani Ibrahim, Azizan Abu Samah, Univ. of Malaya (Malaysia)

The rapid urbanization increases impervious surfaces has altered the energy balance of the environment. This research attempts to study on the relationship between the discomfort level and temperature in order to mitigate the heat effect to the environment. The satellite imagery of Landsat was retrieved on 2nd February 2006 and according to its date and time, five variables were retrieved from air quality and weather stations for identification of discomfort level. Atmospheric and geometric corrections are applied to the image to remove the effects of the atmosphere on the reflectance values of image and to avoid geometric distortion of the image used. Land surface temperature was extracted by using mono window algorithm which was developed by Qin et al. (2001). The discomfort index was measured the whole year of 2006. The calculated discomfort level was evaluated by using Thom's index based on the ground station and compared to the retrieved land surface temperature.

8538-58, Session PS

Monitoring land cover dynamics in the Aral Sea region by remote sensing

Giorgi Kozhoridze, Leah Orlovsky, Nikolai Orlovsky, Ben-Gurion Univ. of the Negev (Israel)

The Aral Sea ecological crisis resulted from the USSR government decision in 1960s to deploy agricultural project for cotton production in Central Asia. Consequently water flow in the Aral Sea decreased drastically due to the regulation of Amydarya and Syrdarya Rivers for irrigation purposes from 55-60 km3 in 1950s to 43 km3 in 1970s, 4 km3 in 1980s and 9-10 km3 in 2000s. In 1987 the fourth biggest inland water body in the world was divided into two parts: northern - Small Aral and southern - Big Aral (the latter in 2009 had separated into deep Western and shallow Eastern parts). Its level decreased from 53.4 MSL in 1960 to 29 MSL (Big Aral) and 41 MSL (Small Aral Sea) in 2006. The analysis of the recent satellite images evidences that in August 2011 the area of the dried bottom of the Aral Sea was 57,529 km2. The water bodies' area was 2,317 km2, 4,411 km2 and 3,243 km2 for Eastern, Western and Small Arals respectively. Vulnerability of the region and the local inhabitants increased to the crucial level. The dried bottom of the Aral Sea and adjacent deltaic areas are characterized by the high changeability. Timely reliable information on Land Cover and Land Use (LC/LU) in different formats and scales is significant assistance for the solution of wide range of ecological problems and implementing contingency planning. Remote sensing is essential instrument performing land classification and monitoring for large, distant and difficult of access areas. The main goal of the study was implementation of various research approaches (decision tree, statistical analyses, fuzzy classifiers, and image algebra) for monitoring and classification land cover changes in the Aral Sea region in the last two decades.

Expert land cover classification approach gives the opportunity to use the unlimited variable for classification purposes. Thus the band algebra (band5/band4 and Band4/Band3) and remote sensing indices (Normalized differential Salinity Index (NDSI), Salt Pan Index (SPI), Salt Index (SI), Normalized difference Vegetation Index (NDVI), Albedo, Crust Index were utilized) utilized for the land cover classification has shown satisfactory result with classification overall accuracy 86.9 % and kappa coefficient 0.85.

After the sea desiccation, the exposed bottom turned mostly to the solonchaks (salty pans). On the other hand areas of former deltaic rivers' branches are covered by sands with sparse vegetative cover, which are transported/spread by wind from eastern part of the former Aral Sea contour to the south-western and western directions. The area of agricultural fields in the deltaic regions decreases permanently. Abandoned fields are transforming into solonchaks in Amudarya delta (56%) and sandy massifs in Syrdarya delta (8%).

Desiccation of the Aral Sea results mainly in formation of solonchaks of different types and constant accumulation of salts in the upper soil horizons. Thus, the Aral Sea turned from accumulator of salts in the region to its distributor to the atmosphere and adjacent areas. The further pathway of exposed bottom transformation is: marsh solonchaks, coastal solonchaks, dry solonchaks (puffy, crusty, white salt on top surface) with relatively low ground water table sparsely

overgrown with halophytic vegetation. The other prevailing process is expanding of “new” (young) sands prone to wind erosion and their mixing with solonchak soils. Consequently, vast bared areas prone to the wind erosion processes turn to the powerful emission sites of salty dust storms.

8538-61, Session PS

A research framework of payments for environmental services of island based on remote sensing

Li-an Wang, The Second Institute of Oceanography, SOA (China) and Guangdong Ocean Univ. (China); Jianyu Cheng, Qiong Liu, Dongyang Fu, The Second Institute of Oceanography, SOA (China)

From 1960 to 2000, the Millennium Ecosystem Assessment (MEA) revealed that nearly two-thirds of global ecosystem services are on the decline. Island is the most vulnerable element in the marine ecological environment. With the rapid development of economy and the continual growth of population, some problems, which threaten the ecosystem of island, has drawn a world-wide attention in the 21st century, including reclamation of the coastal area, coastal marine pollution, rising sea levels, sea water encroachment, diseases and red tide. China,with varied islands covering an area of three million square kilometers, takes the ninth place in the world. Remote sensing technology as a means to observe the earth for large area, is particularly suitable for island ecological environment monitoring and evaluation. The issue of measuring the evolution of space and time in ecosystem services of island from multi-sensor,multi-channel, multi-temporal remote sensing data available to the protection of island ecological health, is considered one of the critical problems crying out for solutions in the ocean ecosystem research. Based on principle of social equity, Payments for Environmental Services(PES) has, by far, become an effective means of internalization to settle the external problems of public goods in recent years.The current application of PES cases has been globally widespread throughout America, the Caribbean, Europe, Africa, Asia and Oceania. The ecological compensation of the land resource has been put into effect at certain extent, but not much has been done for the marine. Taking islands as the object, this paper is to expound the cocept of island PES , and to reveal the mechanism of island PES with the purpose of constructing the PES mechanism of island with multidisciplinary methods, such as the marine ecology, ecological economics combined with remote-sensing data. This study will lay the theoretical foundation for ameliorating island environmental protection policy, and provide guidance to the government in making island development strategy and PES programs.

Conference 8538B: Special Joint Session on Remote Sensing and Natural Disasters: Remote Sensing 2012

Monday 24–24 September 2012 • Part of Proceedings of SPIE Vol. 8538 Earth Resources and Environmental Remote Sensing/GIS Applications III

8538-70, Session 10

An automated approach to flood mapping

Weihua Sun, Donald Mckeown, David W. Messinger, Rochester Institute of Technology (United States)

Heavy rain from Tropical Storm Lee resulted in a major flood event for the southern tier of New York State in early September 2011 causing evacuation of approximately 20,000 people in and around the city of Binghamton. In support of the New York State Office of Emergency Management, a high resolution multispectral airborne sensor (WASP) developed by RIT was deployed over the flooded area to collect aerial images. One of the key benefits of these images is their provision for flood inundation area mapping. However, these images require a significant amount of storage space and the inundation mapping process is conventionally carried out using manual labor. In this paper, we design an automated approach for flood inundation mapping from the WASP airborne images. This method employs Spectral Angle Mapper (SAM) for color RGB or multispectral aerial images to extract the flood binary map; then it uses a set of morphological processing and a boundary vectorization technique to convert the binary map into a shapefile. This technique is relatively fast and only requires the operator to select one pixel on the image. The generated shapefile is much smaller than the original image and can be imported to most GIS software packages. This enables critical flood information to be shared with and by disaster response managers very rapidly, even over cellular phone networks.

8538-72, Session 10

Remote Sensing and GIS for the management of interactions between natural risks and major hazard industrial activities

Alessandra Marino, Mariano Ciucci D.V.M., Istituto Superiore per la Prevenzione e la Sicurezza del Lavoro (Italy)

In the Italian territory about 1/3 of municipalities are located in areas exposed to seismic hazard. At the same time most of the Italian territory is subject to hydrogeologic events (i.e. landslides and floods). The area object of this study, Sulmona Basin and upper Pescara Valley, is characterized by potential exposition to these hazards, with a particular attention to seismic hazard and landslide hazard. Furthermore the area is characterized by the presence of major hazard industrial plants.

For this paper a dedicated GIS database has been built in order to evaluate the interactions between specific natural hazards and industrial hazard and the related vulnerability of territory and population. For this research MIVIS hyperspectral (at a 1500 and 3000 m elevation) images have been used. The obtained images have been georeferenced. From the processing and classification of these images some information layer have been obtained: thematic maps of land-use (industrial areas identification), vegetation conditions, thermal pollution, quality parameters (temperature, organic matter, chlorophyll, sediments) for river waters. Thematic maps obtained from remote sensing have been inserted in a GIS, that means a system to insert, store, integrate, extract, retrieve, manipulate and analyze georeferenced data layers in order to produce interpretable information. Then the data base has been integrated with further information inserted as continuous layers; thematic layers; vector layers; punctual data; attributes. Among inserted layers: location and information regarding industrial plants, seismic classification, landslides and landsliding hazard maps. Some specific operators (overlaying, proximity analysis, recoding, matrix analysis) have been applied that allowed to integrate the information contents and therefore to obtain final thematic maps (hazard maps, vulnerability maps, events scenarios). The innovative technologies proposed facilitate and optimize the management of data and information obtained from different methodologies. The possible interactions between industrial facilities, urban areas and other environment components have been studied. This allowed to obtain different thematic layers showing environment quality, hazard, impact. The vulnerability of the possible sensitive targets located in the areas surrounding the major hazard plants has been analyzed. Furthermore the visualization of damage models (provided according to regulation by plant operator) related to accidents has been obtained, constituting a valid support for land-use planning and natural and industrial hazard management. In complex and vulnerable environments it is basic to find ways to convert data into information. Remote sensing and GIS represent useful methodology aimed to that, and at the same time can play an important function in monitoring and management. These methodologies facilitate ad optimize the performance of tasks required by current regulations. Then it is useful to develop methodologies to support all parties involved, in particular industry and Competent Authorities.

8538-73, Session 10

Flood delineation from synthetic aperture radar data with the help of a priori knowledge from historical acquisitions and digital elevation models in support of near-real-time flood mapping

Stefan Schlaffer, Markus Hollaus, Wolfgang Wagner, Technische Univ. Wien (Austria); Patrick Matgen, Ctr. de Recherche Public - Gabriel Lippmann (Luxembourg)

Mapping flood events with satellite data has attracted a considerable amount of attention during the last decade, owing to the growing interest in using space- and airborne spatial data in near-real time flood management. Active microwave sensors play an essential role because of their night-and-day operability and their capability to penetrate clouds, which is critical under the extreme weather conditions during which flood events mostly occur. The utility of synthetic aperture radars (SAR) - albeit their relatively high spatial resolution in comparison to scatterometers - is limited by their low revisit times of 5-30 days. This is expected to change with the forthcoming two-satellite Sentinel-1 constellation which is foreseen to feature an almost daily revisit time over Europe and Canada and a spatial resolution of 22 m.

Another issue concerns the variety of factors influencing flood extent delineation from radar backscatter measurements. Most existing algorithms exploit the fact that calm water surfaces represent specular reflectors from which only a low amount of energy is returned to the sensor. Thresholding is one of the most commonly used methods due to its simplicity and low computational cost and has yielded good results under calm wind conditions. Wind-induced waves, however, often increase the roughness of water surfaces. Flooding occurring under dense vegetation or between buildings also leads to higher backscatter due to so-called double-bounce effects. Another problem often encountered with thresholding is overestimation of the flooded area due to low backscatter from either melting snow or dry, flat areas.

Another commonly used method is region growing, which can help to overcome the overestimation problem by only adding pixels to the flooded extent which are connected to a seed region. Defining suitable seed regions is critical for this operation but can be problematic as it again involves thresholding or another means of classification from which to derive the centres of water bodies.

In this paper, we propose a method which combines these two approaches and additionally takes into account a freely available digital elevation model (DEM) and historical SAR data. As a first step, an ENVISAT ASAR scene with a spatial resolution of 150 m acquired during a flood event is classified using the threshold approach. Then the seed for the subsequent region growing is defined by overlaying this pre-classified map with a permanent water body (PWB) mask and a river network derived from a modified version of the DEM from the Shuttle Radar Topography Mission (SRTM). The PWB mask is extracted from a multi-temporal ASAR image stack, which in this case contains pre- and post-flood observations.

As result, a map of the flooded extent and a mask showing areas where no retrieval is possible due to, e.g., vegetation cover or dense buildings is obtained. The proposed approach is applied to the November 2007 flood in Tabasco, Mexico. The derived results are

validated with high-resolution flood maps derived from TerraSAR-X. The data used by the proposed algorithm is available for a large portion of the world, which makes the approach suitable for automated near-real time flood mapping.

8538-74, Session 10

Anomalously strong bora events in the NE part of the Black Sea imaged and studied with SAR and optical imagery

Anna Yu. Antonyuk, SCANEX Research and Development Ctr. (Russian Federation) and Lomonosov Moscow State Univ. (Russian Federation); Andrey Yu Ivanov, P.P. Shirshov Institute of Oceanology (Russian Federation)

The Northeast part of the Black Sea regularly runs the danger of strong winds from the northeast during winter and summer periods. In particular, near the Russian town of Novorossiysk the winds can be quite strong (above 20-30 m/s). They are called bora winds. Bora is one of the famous local winds, which blow in Europe from coasts onto the Adriatic Sea and the Black Sea. These events have a strong effect on the coastal and marine environment of the Black Sea and even on infrastructure and social-economic life along the region coast. In the coastal zone the bora is also known to have multiple surface wind jets related to the surrounding mountain relief and strong gustiness that had been focused on in many meteorological studies. But it is not possible to describe these features using in situ observations.

Two very strong bora events (wind up to 40-45 m/s) occurred in the end of January and in the beginning of February 2012 have been imaged and studied using synthetic aperture radar (SAR) images acquired by the Envisat, Radarsat-1 and Radarsat-2 satellites as well as the optical images of MERIS (Envisat) and MODIS (Aqua &Terra) sensors. In addition, meteorological data also have been used from the weather stations at the Black Sea coast. The SAR images reveal the spatial structure of the bora winds in unprecedented details, showing several different features as footprints on the sea surface. Optical images revealed patterns associated with bora. Whereas combined use of SAR and optical images showed that the sea surface roughness and cloud patterns associated with these bora events yields information on the spatial extent and the structure of the bora winds, which cannot be obtained by other in situ observations. Moreover using the manifestations of atmospheric gravity waves (AGW) or cross-wind linear features, the bora pulsation period can be extracted.

Quantitative information on the near-surface wind field can be derived from the SAR images by using the CMOD-type wind scatterometer model for converting radar backscatter values into wind speeds. These fine-resolution wind fields extracted from SAR images can be used to validate and improve mesoscale and local atmospheric models.

Finally it is concluded that the multisensor and multiband satellite imagery together with contact measurements and CMOD modelling yield complete information on the bora winds, especially during anomalously strong events, which cannot be obtained by other instruments.

8538-75, Session 11

Contribution of ocean radar for tsunami warning

Thomas Helzel, HELZEL Messtechnik GmbH (Germany)

A review of the potential and a summary of required next steps to integrate this technique into existing Tsunami Early Warning Systems

The high frequency (HF) surface wave radar is a well established remote sensing technique to monitor ocean currents and waves of the coastal environment far beyond the horizon. It is used for more than 20 years from the scientific community for various applications. The first paper about the potential of this technique for Tsunami warning was published in 1972 [1]. The ocean radar should be able to detect the surface current signature induced by an approaching Tsunami at the continental shelf.

Even if this was common knowledge on December 26th 2004 when the Aceh Tsunami shocked the world, none of the ocean radar systems installed in this region measured a Tsunami induced ocean current signature. This initiated a research project to simulate the back-scattered radar signal in case of a typical Tsunami induced current at the continental shelf edge. This international study used the oceanographic model (HAMSOM) to simulate the surface current signature, converted this current signature into modulated radar signals, and superposed this onto real ocean radar signals. This results in a realistic signal to noise characteristic of the simulated results showing clearly the sensitivity of the radar observation to the specific operational radar parameter as resolution in range, azimuth and time [2].

With this know-how the ocean radar community was able to extract the Tsunami induced current signatures of the Honshu Tsunami in 2011. Various stations from three different manufacturers using slightly different techniques were able to measure the Tsunami signals. The most impressive result was that on the other side of the Pacific the first little wave of just 0.6 m height was detected 8 minutes before it reached the coast of Chile [3]. This indicates that ocean radar would be useful for Tsunami warning for all coastlines where the distance to the continental shelf edge would allow to issue an Tsunami alert several minutes before the waves reaches the coast.

Now the scientific challenge is to use the data that an ocean radar can deliver to provide a reliable wave height forecast for specific regions. This requires an intensive co-operation between oceanographers working with numerical models, seismic experts, radar engineers and the operators of national Tsunami warning networks.

References

[1] D. Barrick, “First-order theory and analysis of MF/HF/VHF scatter from the sea”, IEEE Trans. Ant. and Prop., vol. AP-20, pp. 2-10, January 1972

[2] A. Dzvonkovskaya, et al, “ Simulation of Tsunami Signatures in Ocean Surface Current Maps Measured by HF Radar”, Proceeding of IEEE Oceans Conference, Bremen 2009

[3] K.-W. Gurgel, et al, “Observing the 2011 Honshu Tsunami at the Coast of Chile by HF radar”, Geophysical Research Abstracts Vol. 14, No. 7584, EGU General Assembly 2012

8538-76, Session 11

A new automatic synthetic aperture radar-based flood mapping application hosted on the European Space Agency’s Grid Processing of Demand Fast Access to Imagery environment

Patrick Matgen, Laura Giustarini, Renaud Hostache, Ctr. de Recherche Public - Gabriel Lippmann (Luxembourg)

There is a clear need for developing innovative processing chains for generating remote sensing-based products supporting near real-time flood management. A collaborative research and development effort between remote sensing scientists and hydrologists is necessary for extracting flooding-related information from remote sensing data streams. This paper introduces an automatic flood mapping application that is hosted on the Grid Processing on Demand (G-POD) Fast Access to Imagery (Faire) environment of the European Space Agency. The main objective of the online application is to deliver operationally flooded areas using both recent and historical acquisitions of SAR data. Having as a short-term target the flooding-related exploitation of data generated by the upcoming ESA SENTINEL-1 SAR mission, the flood mapping application consists of two building blocks:

1) A set of query tools for selecting the “crisis image” and the optimal corresponding pre-flood reference image from the G-POD archive

2) An algorithm for extracting flooded areas via change detection using the previously selected “crisis image” and “reference image”.

Stakeholders in flood management and service providers are able to log onto the flood mapping application to get support for the retrieval, from the rolling archive, of the most appropriate pre-flood reference image. Potential users will also be able to apply the implemented flood delineation algorithm. We propose a simple but effective flood detection algorithm based on image differencing. This hybrid methodology combines histogram thresholding, region growing and change detection as an approach enabling the automatic, objective and reliable flood extent extraction from SAR images. The method is based on the calibration of a statistical distribution of “open water” backscatter values inferred from SAR images of floods. SAR images acquired during dry conditions enable the identification of areas that are not “visible” to the sensor (i.e. regions affected by ‘layover’ and

'shadow') and that behave as specular reflectors (e.g. smooth tarmac, permanent water bodies). Change detection with respect to a pre-flood reference image thereby reduces over-detection of inundated areas. The algorithms are computationally efficient and operate with minimum data requirements, considering as input data a flood image and a reference image.

Case studies of several high magnitude flooding events (e.g. July 2007 Severn River flood, UK and March 2010 Red River flood, US) observed by high-resolution SAR sensors as well as airborne photography highlight advantages and limitations of the proposed online application. We show that the fully automated SAR-based flood mapping technique overcomes some limitations of manual approaches.

The online flood mapping application on G-POD can be used sporadically, i.e. whenever a major flood event occurs and there is a demand for SAR-based flood extent maps. In the long term, a potential extension of the application could consist in systematically extracting flooded areas from all SAR images acquired on a daily, weekly or monthly basis.

8538-79, Session 11

Monitoring El Hierro submarine volcano with low and high resolution satellite images

Francisco Eugenio, Francisco Javier Marcello Ruiz, Javier Martin, Univ. de Las Palmas de Gran Canaria (Spain)

Satellite remote sensing technologies provide large amounts of data about the state and evolution of terrestrial environments. The usefulness of these data, collected to address particular problems at the Earth's surface, depends on the capability to extract useful information on the processes of interest and to interpret them. Multitemporal and multi-satellite studies or comparisons between satellite data and local ground measurements require nowadays the establishment of a hierarchy of processes that allow the generation of operational products and the development of processing algorithms characterised by its precision, autonomy and efficiency.

The recent eruption of a submarine volcano at the El Hierro Island (27.78N, -18.04W) has provided a unique and outstanding source of tracer that may allow us to study a variety of structures. The island off the Atlantic coast of North Africa-built mostly from a shield volcano-has been rocked by thousands of tremors and earthquakes since July 2011, and an underwater volcanic eruption 300 meters below sea level started on October 10, 2011. The eruption is the first in the island chain in nearly 40 years. A milky green plume in the water stretches 25-30 kilometers at its widest and, approximately, 100 kilometers long, from a large mass near the coast to thin tendrils as it spreads to the southwest. The plume is likely a mix of volcanic gases and a blend of crushed pumice and seafloor rock.

Monitoring submarine volcano is not an easy task compared with land volcano because it is covered by seawater and located in remote area. Satellite remote sensing is a powerful tool for monitoring submarine volcanic activities such as discolored seawater, floating material and volcanic plume. This paper illustrates the capabilities of satellite remote sensing systems to improve understanding of volcanic processes and volcanic hazards by providing more frequents observations and scientific information at a wide variety of wavelengths.

Thanks to this natural tracer release, medium and high-resolution satellite images obtained from MODIS, MERIS, Aster or WorldView sensors have been processed to provide information on the concentration of a number of marine parameters: chlorophyll, phytoplankton, suspended matter, yellow substance, CDOM, particulate organic and inorganic, etc. So, this oceanographic remote sensing data has played, as well, a fundamental role during field campaigns guiding the Spanish government oceanographic vessel to the appropriate sampling areas.

The favorable results from this study have spawned a follow-up project that consists on the upgrade of the developed oceanographic techniques to study these submesoscale structures and their possible relationship with lateral mixing and biological effects, combining medium and high-resolution multisensor satellite images of El Hierro tracer with in situ observations, and implementing a surface motion model using optical flow algorithms applied in satellite image sequences.

8538-80, Session 12

Research study on appropriate interpretation techniques of satellite images for natural disaster management

Mohammadreza Poursaber, Yasuo Ariki, Kobe Univ. (Japan); Mohammad Safi, Abbaspour Univ. (Iran, Islamic Republic of)

This study addressed the problem of change detection for the purpose of natural hazard mitigation in general and demonstrated the feasibility of employing remotely sensed images for this purpose. Due to the limited access to actual registered imagery data, scaled structural models are constructed and their images are used for experiments. Some of the major technical challenges involved in the problem of structural change/damage were also identified and successfully dealt with.

In this paper, the assumption of employing registered images is made which in practice might be difficult to achieve. Employing ground control points (GCP) and an imaging pro¬cessing software like ENVI with GIS technique should be helpful for improving registration accuracy.

The authors believe that processing time has a lower priority compared to the precision of the results as long as the near real-time nature of the algorithm is maintained. Algorithms developed for pipelines have been modified and validated to choose optimal GIS mesh dimen¬sions and contour intervals for vi¬sualizing post-disaster damage patterns. Statistically significant regressions have been developed at any dam¬age state. Such work improves loss estimation sig¬nificantly and also creates advanced technology to visualize post-disaster damage patterns for rapid decision support and de¬ployment of emergency services.

8538-81, Session 12

Detecting spatio-temporal changes in the extent of seasonal and annual flooding in South Asia using multi-resolution satellite data

Giriraj Amarnath, Mohamed Ameer, Vladimir Smakhtin, International Water Management Institute (Sri Lanka); Pramod Kumar Aggarwal, International Water Management Institute (India)

This paper presents two algorithms for flood inundation mapping to understand seasonal and annual changes in the flood extent and in the context of emergency response. Time-series profiles of Land Surface Water Index (LSWI), Enhanced Vegetation Index (EVI), Normalized Difference Vegetation Index (NDVI) and Normalized Difference Snow Index (NDSI) are obtained from MOD09 8-day composite time-series data (resolution 500m; time period: 2000-2011). The proposed algorithm was applied for MODIS data to produce time-series inundation maps for the ten annual flood season over the period from 2000 to 2011. The flood product has three classes as flood, mixed and long-term water bodies. The MODIS flood products were validated via comparison with ALOS AVINIR / PALSAR and Landsat TM using the flood fraction comparison method. Compared with the ALOS satellite data sets at a grid size of 10km the obtained RMSE range from 5.5 to 15 km2 and the determination coefficients range from 0.72 to 0.97. The spatial characteristics of the estimated early, peak and late and duration of inundation cycle were also determined for the period from 2000 to 2011. There are clear contracts in the distribution of the estimated flood duration of inundation cycles between large-scale floods (2008-2010) and medium and small-scale floods (2002 and 2004).

In another algorithm that specifically uses medium resolution satellite datasets (e.g. EO-1 ALI, Landsat) with the spectral properties having bands of shortwave infrared (SWIR), near-infrared (NIR) and green spectral bands to develop a suitable band rationing technique for detecting surface water changes. This technique is referred to as Normalized Difference Surface Water Index (NDSWI). The NDSWI-based approach produces the best results for mapping of flood inundated areas when verified with original satellite data. Analysis of results reveals that NDSWI has the potential to detect floodwater turbidity, which was verified using principal component analysis. The application of the technique is informative about flood damages, which are illustrated using the floods in Pakistan in 2010 as an example.

Examples on the analysis of spatial extent and temporal pattern of flood-inundated areas are of prime importance for the mitigation of floods. The generic approach can be used to quantify the damage caused by floods, since floods have been increasing each year resulting in the loss of lives, property and agricultural production.

8538-82, Session 12

The effects of orography on win, cloud and Rainfall patterns during typhoon Ketsana (2009)

Mohd Zubir MatJafri, Hwee-San Lim, Tan Fuyi, Khiruddin Bin Abdullah, Univ. Sains Malaysia (Malaysia)

The objective of this study is to investigate the effects of orography on the rainfall, wind, and cloud systems of the TCs in Malaysia and Indochina. Remote sensing techniques have been used to study the impacts of TCs. Using data from the Fengyun 2D (FY-2D) satellite, we observed the development and structure of Typhoon Ketsana, which occurred from September 21 to October 4, 2009. To determine the relationship of the typhoon with the orographic effect, remote sensing techniques such as the Global Digital Elevation Model (GDEM) from the Advanced Spaceborne Thermal Emission and Reflection Radiometer (ASTER) satellite, wind information from the Navy Operational Global Atmospheric Prediction System (NOGAPS), and radiosonde data were applied in this study. This study provides an example of how the orographic effect is important to weather forecasters, as high mountain ranges were able to influence the distribution of the cloud, rainfall and even wind flow patterns during the typhoon season; but how significant or obvious the relationship between the orography and the typhoon's impacts were depended on the intensity of the typhoon system and its movement. From this study, the following conclusions can be drawn: 1) rainfall tends to be distributed over high mountain regions; 2) wind flow will change its direction upon encountering any restrictions, especially those of high terrain regions; and 3) cloud patterns are deformed by high mountains and tend to flow with the mountains' structure because of the orographic effects. The regions most affected by Typhoon Ketsana in the study area were Vietnam in Indochina, Sabah in East Malaysia (EM), Kelantan and Terengganu in Peninsular Malaysia (PM). From the comparison among the study areas, it was found that Indochina had the most significant results for the orographic effects on typhoon activity, followed by the tail effects in EM. This phenomenon was found in PM, although it was not as significant as the other study areas. This remote sensing technique allows tropical cyclones to be forecasted and their impacts to be defined, and it allows disaster zones to be determined.

8538-83, Session 12

Volcanic precursors retrieval by the synergy of spaceborne sensors and ground instrumentations

Mohd Nadzri Md Reba, Nor Khairunnisa Abd Latip, Mazlan Hashim, Univ. Teknologi Malaysia (Malaysia)

The 400-year long dormant Mount Sinabong, Sumatra, Indonesia finally exhibited massive eruption after several days of rumbling and ejected powerful bursts of ash on 29 August, 30 August, 3 September and 7 September 2010. It was reported that the eruption has affected a total economic loss of about USD 4 millions and interrupted few air traffics and airport operations for several days. It is therefore critical to monitor evolution of the eruption and by determining precursory parameters would help one to predict the distribution of volcanic clouds and thus to minimize the total hazardous impact. Basically, volcano shows some pre-eruptive indications prior to the summit in which continuous emission of ash and small plumes is evident. Remote sensing demonstrates great advantages to synoptically measure the volcanic ash and small plumes in term of their optical, chemical and physical properties. Ground instrumentation as the remote sensing counterpart provides continuous and actual measurement of all properties on ground at local scale. Space-based sensors onboard the A-train satellites; Ozone Monitoring Instrument (OMI), Moderate Resolution Imaging Spectroradiometer (MODIS) and Cloud-Aerosol Lidar and Infrared Pathfinder Satellite Observations (CALIPSO), spaced at few minutes apart are used to collect high-resolution three-dimensional images of volcanic tracers.

This paper highlights advantages of the synergy between space-based sensors and ground instrumentations to determine the optical, chemical and physical properties of Mount Sinabung precursory evident based on measurements taken in Peninsular Malaysia. Aerosol optical thickness (AOD), attenuated backscatter and extinction are the optical properties while the physical properties are particulate matter of 10 and 20 micron (i.e. hereafter PM10 and PM20 respectively). Chemical properties to be measured are sulphur dioxide (SO2) and nitrogen dioxide (NO2). Ground measurement retrieves most of the variants from 50 distributed meteorological stations in respect to the time of A-train satellites overpass. MODIS and CALIPSO measure the optical and physical properties while OMI observes the chemical one. Linear optimization is applied by defining the mean square error between ground and remote sensing measurements at certain statistical error thresholds (e.g., 1-sigma, 2-sigma and 3-sigma of Gaussian distribution). This paper aims to estimate optical, physical and chemical properties as the volcanic precursors from the synergy of both instruments by using the linear approximation error. This paper also highlights the major challenge which is to correlate the satellite-footprint measurement (MODIS and OMI) with the point-based ground measurement and addresses the point-spread function (PSF) approximation as a solution. There is a good agreement between satellite and in-situ measurements particularly for satellite data with less cloud cover, low anthropogenic effects and high data availability. This study found that series of provisional ash trajectories and plume movements towards the western Peninsular Malaysia are present. All in all, this paper demonstrates the significance of collaboration between ground- and space-based measurements to map volcanic precursory parameters which would improve early warning system practicalibility.

8538-84, Session 12

Estimation of Mount Sinabong SO2 emission using Kalman filter

Mohd Nadzri Md Reba, Nor Khairunnisa Abd Latip, Univ. Teknologi Malaysia (Malaysia)

Mount Sinabong in Sumatera, Indonesia is a volcanic mountain that was inactive and dormant for more than 400 years. In August 2010 this long-dormant volcano finally had shown signs of eruption and ejected a powerful burst of volcanic ash into the sky. Sulphur dioxide (SO2) is significantly evident particularly in the presence of volcanic clouds that can be easily transported and distributed to other places. Meteorological stations in the Peninsular Malaysia have recorded an increasing amount of SO2 which has been assumed to be originated from Mount Sinabong by long-range transportation of volcanic clouds. Satellite-based sensor offers great means to monitor SO2 at the ultraviolet (UV) band by exploiting the uniqueness of SO2 properties as an obvious target that can be distinguished between other gases during the eruption. Ozone Monitoring Instrument (OMI) is a remote sensing sensor onboard the EOS AURA platform designed to quantify SO2 emission by unprecedented spatial resolution of 13 x 24 km at nadir and in daily observation to map contiguous emission of volcanic SO2.

This paper focuses on mapping column SO2 emission using OMI to spatially study the distribution and amount of SO2 over Peninsular Malaysia during the Mount Sinabong eruption. Four types of OMI SO2 data product (OMISO2) are used; Planetary Boundary Layer (PBL), Lower tropospheric (TRL), Middle tropospheric (TRM) and Upper tropospheric and stratospheric (STL), to measure column SO2 emission at different layer of altitudes. However, mapping of column SO2 emission from each OMISO2 is limited to void pixels due to processing flags; flag of effective cloud fraction and off nadir measurement and data quality flag. PBL pixels with less than 20% of cloud fraction represent high accuracy of column SO2 emission retrieval of which less contribution by cloud induce error in the retrieval algorithm. Yet, this is a challenge as Peninsular Malaysia experiences cloud cover throughout the year. Besides, the PBL product requires near-nadir viewing angles of 20 to 40 at each pixel to obtain high sensitivity of column SO2 emission. For all data products, good quality column SO2 emission is denoted by quality flag with bit equals to 0.

This paper aims to estimate the void pixels of OMISO2 by applying the Kalman filter and thus to map column SO2 emission distribution in Peninsular Malaysia. Different filtering kernel sizes are designed and applied on single snapshot to determine parameters for prediction state and measurement state. In the a-priori state, state vector estimates and state variance are defined based on low pass filter and high pass filter respectively while measurement variable is computed in the a-posteriori one. Estimation determines Kalman gain in several iterations and finally finds the estimated SO2 when the estimated variance converged with the expected error. This paper highlights good agreement between the estimated SO2 pixels and in-situ measurement for PBL data product. However, this result shows impact of anthropogenic SO2 is more evident than the volcanic SO2. Nevertheless TRL, TRM and STL products give some indicators of the presence of volcanic clouds in the Peninsular Malaysia. OMI data is proved to be the most sensitive towards column SO2 emission and thus, it is convenient for early warning and mitigation of Mount Sinabung hazards.

Conference 8539: High-Performance Computing in Remote Sensing

Wednesday - Thursday 26–27 September 2012 • Part of Proceedings of SPIE Vol. 8539 High-Performance Computing in Remote Sensing II

8539-1, Session 1

High-performance computing in image registration

Mauro Dalla Mura, Claudio Andreatta, Tobia Francesco, Michele Zanin, Fabio Remondino, Fondazione Bruno Kessler (Italy)

Thanks to the recent technological advances, a large variety of image data is at our disposal with variable geometric, radiometric and temporal resolution. In many applications the processing of such images needs high performance computing techniques in order to deliver timely responses e.g. for swift decisions or real-time actions. Thus, parallel or distributed computing methods, DSP microprocessors, GPU/CUDA programming and FPGA devices have become essential tools for the challenging issue of processing large amount of geo-data.

The article focus on the processing and registration of large datasets of terrestrial and aerial images for 3D reconstruction and diagnostic purposes. Terrestrial images are acquired with Single-Lens Reflex (SLR) digital cameras, aerial images are acquired from airborne or UAV platforms.

For the image alignment procedure, sets of corresponding feature points need to be automatically extracted in order to successively compute the geometric transformation which aligns the data. The feature extraction and matching are ones of the most computationally demanding operations in the processing chain thus, a great degree of automation and speed is mandatory. In this paper, the details of the implemented operations exploiting parallel architectures and GPU are presented. The innovative aspects of the implementation are (i) the effectiveness on a large variety of unorganized and large datasets, (ii) capability to work with high-resolution images and (iii) the speed of the computations.

8539-2, Session 1

GPU-parallel performance of the community radiative transfer model (CRTM) with the optical depth in absorber space (ODAS)-based transmittance algorithm

Jarno Mielikainen, Bormin Huang, Allen H. L. Huang, Univ. of Wisconsin-Madison (United States); Tsengdar J. Lee, NASA Headquarters (United States)

The Community Radiative Transfer Model (CRTM) is a fast model for simulating the infrared (IR) and microwave (MW) radiances of a given state of the Earth's atmosphere and its surface. The CRTM radiances has been used for satellite data assimilation in numerical weather prediction. Many IR and MW sensors are supported within the CRTM. The CRTM takes into account the radiance emission and absorption of various atmospheric gaseous as well as the emission and the reflection of various surface types. Two different transmittance algorithms are currently available in the CRTM OPTRAN: Optical Depth in Absorber Space (ODAS) and Optical Depth in Pressure Space (ODPS). ODAS in the current CRTM allows two variable absorbers (water vapor and ozone). The current paradigm shift toward many-core architectures highlights the need to parallelize scientific codes. In the future, even CPUs will gain additional computational power through increase in the number of cores rather than higher clock frequencies. Thus, parallel approach to CRTM, as exemplified by the research presented in this paper, will be necessary even on future CPUs to fully utilize them. Using commodity graphics processing units (GPUs) for accelerating CRTM means that the hardware cost of adding high performance accelerators to computation hardware configuration are significantly reduced. In this paper, we examine the feasibility of using GPUs to accelerate the CRTM with the ODAS transmittance model. Our results show that GPUs can provide significant speedup over conventional processors for the 8461-channel IASI sounder. In particular, a GPU on the dual-GPU NVIDIA GTX 590 card can provide a speedup 339x for the single-precision version of the CRTM ODAS compared to its single-threaded Fortran counterpart running on Intel i7 920 CPU.

8539-3, Session 1

Real-time progressive band processing of linear spectral unmixing

Chein-I Chang, Kenhao Liu, Univ. of Maryland, Baltimore County (United States); Chao-Cheng Wu, National Taipei Univ. of Technology (Taiwan)

Band selection (BS) has advantages over data dimensionality in satellite communication and data transmission in the sense that the spectral bands can be tuned by users at their discretion for data analysis while keeping data integrity. However, to materialize BS in such practical applications several issues need to be addressed. One is how many bands required for BS. Another is how to select appropriate bands. A third one is how to take advantage of previously selected bands without re-implementing BS. Finally and most important one is how to tune bands to be selected in real time as number of bands varies. This paper presents an application in spectral unmixing, progressive band selection in linear spectral unmixing by resolving all the above-mentioned issues where data unmixing can be carried out in a real time and progressive fashion with data updated recursively band by band in the same way that data is processed by a Kalman filter.

8539-4, Session 1

Fast Fourier Transform Co-processor (FFTC): towards embedded GFLOPs

Christopher T. F. Kuehl, Uwe Liebstueckel, Felix Witte, EADS Astrium GmbH (Germany); Martin Suess, European Space Research and Technology Ctr. (Netherlands); Nicholas Kopp, Hybrid DSP Systems (Netherlands); Isaac Tejerina, Michael Uemminghaus, EADS Astrium GmbH (Germany); Michael Kolb, University of Applied Sciences (Germany); Roland Weigand, European Space Research and Technology Ctr. (Netherlands)

2.1 Applications

The intended applications for the FFTC are Interferometry, Radar, Synthetic Aperture Radar (SAR) imaging, Sonar, Pulse Compression, Doppler Processing, Medical Imaging, Communications, Spectrum Analysis, Image Recognition, Geophysical Imaging, Acoustics, Ultrasound, and much more.

2.2 General description

The standalone FFT chip is capable of executing sustained FFT processing, vector multiplication convolutions and correlations on 1D complex data sets of up to 1K samples. The FFT chip has additional data ports for 4 SDRAM banks for long FFT processing or multidimensional FFT-based processing. Port 0 is the 64 bit primary input port, Port 5 is the 64 bit primary output port, and Port 1...4 can be connected to SDRAM banks to handle corner turning operations or act as double buffers.

An addressing FPGA takes care of the SDRAM addressing (including refresh if necessary), such that the FFT processor is independent of external memory type. The choice of the external memory can be a trade-off of performance, price and availability. FFT processor programming is performed through instruction sets. The instructions determine the data flow and the memory addresses to be generated by the addressing FPGA.

Depending on the user calls (one call can be, for example, the convolution of a 256 X 256 kernel with a 512 x 512 data set), a proper instruction set is selected for the FFT chip. Basically, one instruction contains the following information:

- mode of the FFT core / vector multiplier;
- length of the data vectors;

• data transfer settings:

• target port of the input Port 0 data vector;

• source port of the output Port 5 data vector;

• source and target port of the vector to be processed.

In this way many FFT operations can be mapped on the FFTC processor by sequencing FFTC instructions. Basic instruction sets for representative operations, such as listed in the table, are preprogrammed. User-/application-specific multidimensional FFT-based operations are implemented through downloading specific instruction sets.

2.3 General operation

The execution of FFT-based algorithms is based on multi-dimensional FFT processing of large data sets. The multidimensional nature of these algorithms requires large memory for so-called “corner turning” operations (transposition of data sets). To keep the continuous throughput of the FFTC for the multidimensional processing, the FFTC has 4 SDRAM banks. This allows double buffering and corner turning operations through proper addressing of the SDRAM banks.

The input and output data rate of the FFTC are independent of the processing clock. In fact, to eliminate the need of external input and output FIFOs, it is often more convenient to match the I/O data rate to the effective processing data rate. For example, a 1K complex FFT has an effective 100 MSPS data rate and matches with 100 MHz I/O data rate, whereas a 1K X 1K complex 2D FFT has an effective 50 MSPS data.

The FFTC has 4 basic instruction sets. Instruction 0 is a single-phase instruction, instruction 1, 2, and 3 are two-phase (two sequences of the same length are entered into the chip) instructions:

1. single FFT / IFFT

2. FFT seq1 / FFT seq2 / multiply / IFFT

3. FFT / multiply / IFFT

4. multiply / FFT

Each instruction can be preceded or followed by a complex multiplication. All multiplications can be normal or conjugated. A batch mode for FFTs below 512 points avoids wait states between subsequent FFTs and prevents degradation of performance. In practice, this allows to feed the processing core with the next sequence, whereas the previous sequence is still in the pipeline registers.

8539-5, Session 1

GPU implementation of a neural network-based classifier for hyperspectral data

Jose J. Gomez Franco, Javier Plaza, Antonio J. Plaza, Univ. de Extremadura (Spain)

In this paper we analyze the performance of a GPU-based parallel implementation of a feedforward neural network classifier in the context of hyperspectral data classification. Specifically, we focus on the training phase of the backpropagation algorithm, which is the most expensive step in computational terms. Our proposed strategy on commodity graphics processing units (GPUs) reduces the computational cost over previous implementations of the same classifier. Experimental validation is based on the analysis of hyperspectral data collected by the NASAs Airborne Visible InfraRed Imaging Spectrometer (AVIRIS) over the Indiana Pines region in the Northwestern Indiana, United States. The proposed approach is implemented using CUDA (compute device unified architecture), and tested on a GPU architecture by NVidia: Tesla C1060. Results reveal considerable speedup factors while retaining the same classification accuracy for the neural classifier.

8539-6, Session 2

Progressive hyperspectral imaging

Chein-I Chang, Univ. of Maryland, Baltimore County (United States)

Progressive hyperspectral imaging (PHSI) is a new concept that has never been explored in the past. It decomposes data processing into a number of stages and processes data stage-by-stage progressively in the sense that the results obtained by previous stages are updated and improved by subsequent stages only using new innovations information that is not available in previous stages. This is quite different from a sequential processing which processes data samples in a sequential manner where each data sample is fully processed. Specially, the idea of PHSI is believed to be the first ever materialized to utilize available information in a best possible means to process massive data by updating data processing via using the new innovations information provided by each spectral band. As a result, the PHSI can significantly reduce computing time and in the mean time can be also realized in real-time in many application areas such as hyerspectral data communications and transmission where data can be communicated and transmitted progressively. Most importantly, the PHSI allows users to screen preliminary results before deciding to continuously complete the data processing.

8539-7, Session 2

Accelerating WRF 5-layer thermal diffusion model on a NVidia Fermi GPU

Melin Huang, Univ. of Wisconsin-Madison (United States); Jarno Mielikainen, Univ. of Eastern Finland (Finland); Allen H. L. Huang, Univ. of Wisconsin-Madison (United States); Mitchell D. Goldberg, National Oceanic and Atmospheric Administration (United States)

The Weather Research and Forecasting (WRF) is a numerical weather prediction and atmospheric simulation system with dual purposes for forecasting and research. The WRF software infrastructure consists of several components such as dynamic solvers and physical simulation modules. WRF includes several Land-Surface Modes (LSMs). The LSMs uses atmospheric information, radiative forcing and precipitation forcing from the surface layer scheme, the radiation scheme and the microphysics/convective schemes, respectively, together with the land’s state variables and land-surface properties, to provide heat and moisture fluxes over land points and sea-ice points [W. C. Skamarock et al., 2008]. The WRF 5-layer thermal diffusion simulation is a LSM based on the MM5 5-layer soil temperature model [J. Dudhia, 1996] with the energy budget including radiation, sensible, and latent heat flux. The WRF LSM model is very suitable for massively parallel computation as there are no interaction among horizontal grid points. More and more scientific applications have adopted graphics processing units (GPUs) to accelerate the computing performance. In this study, we will demonstrate our GPU massively parallel computation efforts on the WRF 5-layer thermal diffusion model.

8539-8, Session 2

GPU implementation of attribute profiles for remote sensing image classification

Sergio Bernabe, Univ. de Extremadura (Spain); Prashanth R. Marpu, Masdar Institute of Science and Technology (United Arab Emirates); Mauro Dalla Mura, Fondazione Bruno Kessler (Italy); Antonio J. Plaza, Univ. de Extremadura (Spain); Jon A. Benediktsson, The Univ. of Iceland (Iceland)

Attribute Profiles (APs), which are built using the versatile morphological attribute filters based on the max-tree (and min-tree) representation of an image have shown to be promising tools for spectral-spatial classification of remote sensing data. However, the application of APs is restricted by the computational load while generating the max-tree representation. There were earlier efforts to generate the max-tree by using high performance computing environments based on distributed computing over several nodes in a parallel architecture. In this work, we investigate the feasibility of an implementation of the max-tree data structure using GPUs by means of tiling. In this way, the overheads due to sharing memory resources in a distributed computing architecture are overcome. Moreover, the proposed architecture would make feasible to compute the max-tree with a reasonable computational load on a single node.

8539-9, Session 2

An efficient watermarking technique for satellite images using discrete cosine transform

Saeed H AL-Mansoori, Emirates Institution for Advanced

Science and Technology (United Arab Emirates)

Nowadays, with the rapid growth of technologies and the prevalence of network communication, new challenges raises to protect the multimedia data transmission on the World Wide Web (internet). Data security is one of the main important needs these days, especially in the field of remote sensing. Emirates Institutions for Advanced Science and Technology (EIAST) as an example, provides a satellite images captured by DubaiSat-1 satellite to customers inside the UAE including government agencies, universities, research centers, and distributed also outside the region. To deal with the issue of data security, the concept of watermarking has been introduced. The idea of watermarking is to embed a secret message, watermark inside an image and to increase the digital data security. The aim of this study is to hide an entire pattern as a watermark such as an organization's logo (or trademark) directly into the original DubaiSat-1 satellite image. This will prevent any unauthorized manipulation to the image data. This secret watermark is used for copyright protection and ownership authentication for (EIAST). This study will based on Discrete Cosine Transform (DCT) to provide an excellent protection and highly robust under flipping, noise, resize and rotation attacks. Watermarking is a combination of electrical (image and signal processing) and computer science fields which is the process of hiding information (i.e data) which can be a signature, logo, image, label, text into a multimedia object such as text or image or audio or video in such away it can be extracted later to show the ownership and authentication of an object. Generally, there are three main parts for watermarking scheme; the watermark, encoder, and decoder. Figure 1 below shows a basic block diagram of watermarking process.A block diagram (figure1) shows the basic principles stages in digital image watermarking process; starting from generating and embedding the watermarked logo and information into the original image to produce a watermarked signal and this process called "encoding", then the watermarked signal transmitted to somebody. If any modification done on that transmitted signal, this process is called "attack". There are many types of attack such as flipping, rotation, cropping, JPEG compression, and scaling. This stage will examine the robustness of the algorithm implemented. Finally, detection process is applied to watermarked signal to extract the information embedded into the original image.

8539-10, Session 2

GPU acceleration of simplex volume algorithm for hyperspectral endmember extraction

Haicheng Qu, Junping Zhang, Zhouhan Lin, Hao Chen, Harbin Institute of Technology (China)

Simplex volume method is an algorithm based on a special geometrical structure called convex simplex polytope in the feature space of hyperspectral image. By utilizing a specific formula for simplex volume in high dimensional space, the algorithm extracts endmembers from initial hyperspectral image directly. Due to the fact that it has no relation to the dimensions of dataset, this method overcomes an inherent flaw of dimension constraint in N-FINDER. And it can also ward off loss of the small targets information possessed by rare vectors effectively. However, a large amount of calculation for simplex volume is invoked in the algorithm such as finding the value of a determinant constructed by two spectral vectors in the feature space of a hyperspectral image. Fortunately the computational complexity is dependent on the number of endmembers and there exists no dependency between pixels, so this algorithm is suitable for parallel implementation. The high-performance computation based on GPU techniques have brought a novel access to acceleration for hyperspectral image processing with its enhanced computing capabilities, higher cost-performance and lower energy consumption, as compared to its CPU counterpart. By fully utilizing the SIMD architecture of GPU, we assign the complicated simplex volume calculation task to GPU, through which method the total speedup of the whole algorithm is accessed. What's more, a concept called the endmember structure influence function is given in the implementation of the algorithm, by which we can estimate the importance of each endmember. As the extracted endmembers increase, new endmember impairs less to the structure of the hyperspectral image in the spectral dimension, which suggests that the former few endmembers can prop up a general simplex volume structure in that spectral dimension.

8539-11, Session 2

Real-time causal processing of anomaly detection

Yulei Wang, Harbin Engineering Univ. (China); Shih-Yu Chen, Univ. of Maryland, Baltimore County (United States); Chunhong Liu, China Agriculture Univ. (China); Chein-I Chang, Univ. of Maryland, Baltimore County (United States)

Anomaly detection generally requires real time processing to find targets on a timely basis. This paper develops a real time causal processing to perform anomaly detection. It is an innovational processing which makes use of Woodbury's identity to update information only provided by the pixel currently being processed without re-processing previous pixels. Experimental results demonstrate these two versions significantly improve processing time compared to conventional anomaly detection without real time causal processing.

8539-12, Session 2

Further optimizations of the GPU-based pixel purity index algorithm for hyperspectral unmixing

Xin Wu, Xiaopeng Shao, Xidian Univ. (China); Antonio J. Plaza, Univ. de Extremadura (Spain); Bormin Huang, Univ. of Wisconsin-Madison (United States)

Spectral unmixing is a very important analysis tool for remotely sensed hyperspectral data exploitation. It amounts at automatically finding the signatures of pure spectral components (called endmembers in the hyperspectral imaging literature) and their associated abundance fractions in each pixel of the hyperspectral image. Over the last few years, many algorithms have been proposed to automatically find spectral endmembers in hyperspectral data sets. One of the first and most successful approaches has been the pixel purity index (PPI), which finds endmembers after performing iteratively projections of the pixels in the data onto a set of ramdomly generated unit vectos (called skewers) which partition the high-dimensional space given by the hyperspectral image pixels, thus allowing to identify the endmembers as the pixels with maxima projection values after projections onto a large skewer set. Although this algorithm has been widely used in the hyperspectral unmixing community, it is highly time consuming as its precision increases asymptotically (i.e., the more skewers used in the process, the better the obtained results). Due to its high computational performance, the PPI algorithm has been implemented in several high performance computing architectures including commodity clusters, heterogeneous and distributed systems, field programmable gate arrays (FPGAs) and graphics processing units (GPUs). However, the algorithm has been never reported to perform in real-time for hyperspectral image data, which is an important exploitation goal. In this paper, we develop an optimized version of the PPI algorithm which has been specifically tuned for GPU architectures resulting in real-time analysis results. Our experimental results, conduced using both simulated and real hyperspectral data sets and using NVidia GPU platforms, indicate both the endmember extraction accuracy and the improved computational performance of the proposed implementation.

8539-13, Session 3

Visualization tools for extremely high resolution DEM models from the LRO and other orbiter satellites

J. Montgomery, Georgetown Univ. (United States); John McDonald, DePaul Univ. (United States)

Advances in NASA's satellite instrumentation have provided a dramatic increase in the size and resolution of remotely sensed data. Each of NASA's recent missions, from the Mars Global Surveyor (MGS) to the Lunar Reconnaissance Orbiter (LRO) to the Mercury Messenger Orbiter, have provided increasingly higher resolution imagery. Satellite sensors collect visual, altimeter, spectrographic and other data.

Data from these orbiters have been used by researchers in fields such as astronomy and geophysics, providing a wealth of information

on the formation and evolution of these bodies. For example, geophysicists have used data from the MGS laser altimeter to study surface features for sites that were likely formed by fluid flow. The lunar altimeter dataset shows great promise for aiding the identification, classification and cataloging of craters and ridges. Such studies could benefit greatly from the increased resolutions of recent data.

Unfortunately this dramatic increase in resolution has caused increasing difficulty for data processing and visualization. The Lunar Orbiter's Laser Altimeter (LOLA) digital elevation model (DEM) is a prime example of this. It is currently available in resolutions up to 1024 pixels/degree, yielding approximately 68 billion data points, and with individual file segments generally around 2GB in size. Such files will not fit into the onboard memory of most graphics cards for display and may not even fit into a single process' main memory on many small computers. As instrumentation improves, this problem will only be exacerbated.

Several software tools are publicly available to assist users with these large data sets, however the current suite of software tools are either geared toward off-line processing, provide low fidelity visualization or require substantial delay between rendering and user interactions. To mitigate these shortcomings we introduce mVTK, a novel software tool that is capable of dynamically creating equidistant cylindrical map projections from altimetry data publicly available through NASA PDS nodes. mVTK can process low-resolution DEM files (4 - 64 pixels/degree) to high-resolution DEM files (128 - 1024 pixels/degree) in real-time.

The cartographic projections dynamically created by mVTK provide 2D shade-relief renderings with false coloring and are an accurate rendering using unmodified NASA DEM data. mVTK has a simple graphical user interface that provides a user with a whole planet projection, where they can interactively and selectively zoom in/out to the minimum/maximum resolution supported by the underlying DEM files. Additionally, mVTK supports a collection of simple tools for measuring distance, height and slope on the dynamically rendered map projections.

We discuss rendering, visualization and data management techniques that allow mVTK to render gigabyte size DEM files in real-time. In addition, we compare the load times, rendering times and visual fidelity of mVTK to previous visualization packages and discuss some of the challenges encountered in rendering such large data sets. mVTK runs on commodity hardware and GPU's that support OpenGL v2.1 or later running Windows 7 or Apple's Mac OSX 10.6.6 operating systems.

8539-14, Session 3

Modified full abundance-constrained spectral unmixing

Shih-Yu Chen, Englin Wong, Chein-I Chang, Univ. of Maryland, Baltimore County (United States)

Fully constrained least squares (FLCS) has been widely used for spectral unmixing. A modified FCLS (MFCLS) was also proposed for the same purpose to derive two iterative equations for solving fully abundance-constrained spectral unmixing problems. Unfortunately its advantages have not been recognized. This paper conducts a comparative study and analysis between FCLS and MFCLS via custom-designed synthetic images and real images to demonstrate that while both methods perform comparably in unmixing data, MFCLS edges out FCLS in less computing time.

8539-15, Session 3

Implementation of prediction-based lower triangular transform on the graphics processing unit

Shih-Chieh Wei, Tamkang Univ. (Taiwan); Bormin Huang, Univ. of Wisconsin-Madison (United States)

The prediction-based lower triangular transform (PLT) is a special case of generalized triangular decomposition. PLT features the same coding gain as the Karhunen-Loeve transform but with a lower design and implementational cost. With its good decorrelation and perfect reconstruction properties, PLT has been applied to lossless compression of sounder data with high compression ratio. As PLT involves many matrix computations which are good candidates for parallel processing, this work will use the graphics processing unit which has hundreds of cores for speedup of the PLT compression time.

8539-16, Session 3

Evolutionary techniques for sensor networks energy optimization in marine environmental monitoring

Francesco Grimaccia, Politecnico di Milano (Italy); Ron Johnstone, University of Queensland (Australia); Marco Mussetta, Politecnico di Milano (Italy); Andrea Pirisi, UP – Underground Power (Italy); Riccardo E. Zich, Politecnico di Milano (Italy)

The sustainable management of coastal and offshore ecosystems, such as for example coral reef environments, requires the collection of accurate data across various temporal and spatial scales. Accordingly, monitoring systems are seen as central tools for ecosystem-based environmental management, helping on one hand to accurately describe the water column and substrate biophysical properties, and on the other hand to correctly steer sustainability policies by providing timely and useful information to decision-makers.

Notably, however, remote sensing is an indirect monitoring technique and it is currently limited to just a few characteristics of aquatic environments based on the measurement of ocean color (different constituents of water column absorb specific wavelengths of light). By contrast, field surveys provide far more accurate measurements than image data and the number of parameters that can be measured in situ is much larger.

A robust and intelligent sensor network that can adjust and be adapted to different and changing environmental or management demands would revolutionize our capacity to wove accurately model, predict, and manage human impacts on our coastal, marine, and other environments.

Even in this field, in the last few years advances in sensor technology, wireless communications and digital electronics have made realistic to produce on a large scale miniaturized low-cost sensors which integrate sensing, processing, and communication capabilities. The advantages comprise not only the size reduction, but also the increasing in functionality and system reliability.

In this paper advanced evolutionary techniques are applied to optimize the design of routing architecture for wireless sensor networks, guaranteeing at the same time a full network connectivity and a minimum energy consumption. The proposed techniques have been tested in respect of the most known test functions with good results obtained in all the considered cases, especially for optimization of large domain objective functions.

In order to maximize the network lifespan, the authors implement an enhanced hybrid technique developed in order to exploit in the most effective way the uniqueness and peculiarities of two classical optimization approaches, Particle Swarm Optimization (PSO) and Genetic Algorithms (GA).

Here, this procedure is applied to energy harvesting buoys for marine environmental monitoring in order to optimize the recovered energy from sea-wave, by selecting the optimal device configuration.

8539-17, Session 3

Acceleration the electromagnetic composite scattering based on GPU

Zhen-sen Wu, Xiang Su, Xidian Univ. (China)

The electromagnetic composite scattering of target and environment, such as sea or ground, is meaningful and challenges. However in practical problems when the frequency of incident wave is high, the number of unknowns in the traditional numerical methods, such as method of moments (MoM) and finite difference time domain (FDTD), increase dramatically even beyond the computing capacity of existing computer. Therefore the reasonable approximation of high frequency method, physical optics (PO), is used to solve this problem in this paper. Although by introducing shaded and lighting areas the number of unknowns is effectively reduced. But when the problem is complex, distinguish every patch belongs to lighting or shaded area is also need to cost a lot of time. This paper first introduces the Z-Buffer method from computer graphics to reduce the time of distinguishing all the

patches. The Z-Buffer method is that store the patches to buffer by any order, if the point correspond to patch is closer than that in buffer, use the value of the color and depth of the new point to replace the old value. The number of patches is huge and the order is not limited, that is, the patch can be seen as independent of each other, therefore this method is especially suitable for massively parallel processing. The graphic process unit (GPU) with computing unified device architecture (CUDA) is advantage of a large number of data parallel computing. This paper we use GTX590 with Fermi architecture to solve the problem and effectively reduce the time.

8539-18, Session 4

A unified theory for virtual dimensionality of hyperspectral imagery

Chein-I Chang, Univ. of Maryland, Baltimore County (United States)

Virtual dimensionality (VD) is defined to specify the number of spectrally distinct signatures in hyperspectral data. Unfortunately, there is no provided specific definition of what “spectrally distinct signatures” are. As a result, many techniques developed to estimate VD have produced various values for VD. This paper develops a unified theory for VD of hyperspectral imagery where the value of VD is completely determined by the spectral statistics of targets of interest. Using this new developed theory the VD techniques can be categorized according to targets characterized by various orders of statistics into 1st order statistics, 2nd order of statistics and high order statistics (HOS) where a binary composite hypothesis testing problem is formulated with a target of interest considered as a desired signal under the alternative hypothesis while the null hypothesis represents absence of the target. With this interpretation many VD estimation techniques can be unified under the same framework, for example, Harsanyi-Farrand-Chang (HFC) method, maximum orthogonal complement algorithm (MOCA).

8539-19, Session 4

On the acceleration of Eta Ferrier Cloud Microphysics Scheme in the Weather Research and Forecasting (WRF) Model using a GPU

Jun Wang, Bormin Huang, Allen H. L. Huang, Univ. of Wisconsin-Madison (United States); Mitchell D. Goldberg, National Oceanic and Atmospheric Administration (United States)

More and more scientists and engineers are using Graphics Processing Units (GPUs) instead of CPUs for scientific computing. On the other hand, the Weather Research and Forecasting (WRF) model which is a numerical weather prediction and atmospheric simulation system, has been designed for both research and operational applications. WRF code can be run in different computing environments ranging from laptops to massively-parallel supercomputers. The Eta Ferrier microphysics scheme is a sophisticated cloud microphysics module in the Weather Research and Forecasting (WRF) model. In this paper, we present the approach and the results of accelerating the Eta Ferrier microphysics scheme on many-core NVIDIA Graphics Processing Units (GPUs). We discuss how our GPU implementation takes advantage of the parallelism in Eta Ferrier scheme, leading to a highly efficient GPU acceleration. We implement the Eta Ferrier microphysics scheme on a low-cost personal supercomputer with 512 cores on a GPU. Our GPU implementation achieves an overall speedup of 37x compared to a single thread CPU. Since Eta Ferrier microphysics scheme is only an intermediate module of the entire WRF model, the GPU I/O should not occur, i.e. its input data should be already available in the GPU global memory from previous modules and its output data should reside at the GPU global memory for later usage by other modules. The speedup without host-device data transfer time is 272x.

8539-20, Session 4

Review of high performance computing requirements in hyperspectral image processing

Prashanth R. Marpu, Masdar Institute of Science and Technology (United Arab Emirates); Antonio J. Plaza, Univ. de Extremadura (Spain)

Hyperspectral images are characterized by hundreds of spectral bands and hence leading to large data size. Processing hyperspectral images is a computationally intensive task and high performance computing (HPC) environments are increasingly being employed to process the data. In this study, we review three processing tasks which are commonly associated with hyperspectral data, namely classification, spectral unmixing and change detection, and further describe the parallel processing techniques generally adopted in each case giving examples. By analyzing the commonly used methods, we investigate the suitability of different methods in different HPC environments such as clusters, multi-core systems or specialized hardware devices such as field programmable gate arrays (FPGAs) and graphics processing units (GPUs). To this effect guidelines are provided for transition to HPC for processing large volumes of data in different application contexts.

8539-21, Session 4

Hyperspectral image feature extraction accelerated by GPU

HaiCheng Qu, Harbin Institute of Technology (China) and Liaoning Technical Univ. (China); Ye Zhang, Zhouhan Lin, Hao Chen, Harbin Institute of Technology (China)

PCA (principal components analysis) algorithm is the most basic method of dimension reduction for high-dimensional data, which plays a significant role in hyperspectral data compression, decorrelation, denoising and feature extraction. With the development of imaging technology, the number of spectral bands in a hyperspectral image is getting larger and larger, and the data cube becomes bigger through these years. As a consequence, operation of dimension reduction is more and more time-consuming nowadays. Fortunately, GPU-based high-performance computing has opened up a novel approach for hyperspectral data processing. This article is concerning on the two main processes in hyperspectral image feature extraction: (1) calculation of transformation matrix; (2) transformation in spectrum dimension. These two processes belong to computationally intensive and data-intensive data processing respectively.

On the basis of previous GPU-accelerated generic PCA algorithm, we use GPU to accelerate SPCA and KPCA, further on which we optimize the acceleration strategies. That is, comparing with previous acceleration strategies based on Cublas Library, a numerical algorithm of eigenvalue computing are rewritten to improve the efficiency.

In the second process, transformation in spectrum dimension, the first step is to divide the image into slices on spectral dimension. A strategy of loading the massive hyperspectral image asynchronously is taken to implement co-processing of GPU and CPU, by which processing efficiency is improved. Originated from two aspects of speedup and calculation accuracy, a set of experimental parameters are designed to get insight into performance improvement of GPU implementation on SPCA and KPCA. All the codes are written under the framework of CUDA, in both Windows and Linux platforms. What’s more, a Matlab edition is implemented for compare.

From the aspect of feature extraction, we analyze the suitability of linear and non-linear methods. Moreover, we verify the robustness of this algorithm by adding noises.

The results of the experiment shows that the asynchronous co-processing of CPU and GPU can hide the latency of data transmission effectively. For the more computationally intensive KPCA algorithm, the total acceleration of GPU implementation is more than 10 times(The C implementation is using GSL library, without which the acceleration ratio will be higher.). This result is better than SPCA. As for platform factor, the execution time of the same code shows that Linux seems to be faster than Windows.

8539-22, Session 4

High performance cluster system design for remote sensing data processing

Yuanli Shi, Wenming Shen, Wencheng Xiong, Zhuo Fu, Rulin Xiao, Ministry of Environmental Protection (China)

The development of computationally efficient techniques for transforming the massive amount of remote sensing data into scientific understanding is critical for space-based earth science and planetary exploration. Operating on large remote sensing data sets with a single computer system sometimes means simplifying approximations used to limiting the efficiency of data processing and the precision of the final results. The application of High Performance Computing (HPC) technology to remote sensing data processing is one solution to meet the requirements of remote sensing real- or near-real-time processing capabilities. Compared to the other HPC technology, cluster systems have played a more important role in the architecture design of high-performance computing area during recent years which is cost-effective and efficient parallel computing system able to satisfy specific computational requirements in the earth and space sciences communities. In this paper, we present a powerful cluster system built by Satellite Environment Center, Ministry of Environment Protection of China (SEC, MEP) that is designed to process massive remote sensing data of HJ-1 satellites automatically everyday.

Like the typical cluster system, there is five-layer architecture of our designed cluster system of remote sensing data processing, including hardware device layer, network layer, OS/FS layer, middleware layer and application layer. We build the cluster system with eight computing, one login/management and two I/O nodes, which are mainly delivered by IBM Microsystems, H3C and EMC companies, and they are installed in the cabinets respectively. Two different kinds of networks: Local Area Network (LAN) with Gigabit Ethernet and Storage Area Network (SAN) with FC network are built together to play their different advantages. SUSE Linux Enterprise Server 10 SP2 as the operating system and StorNext File System as the parallel file system are installed to ensure the best support for all hardware components. LAM/MPI as the MPI implementation and open source batch system OpenPBS as Task scheduler are adopted to perform parallel computing applications that are suitable for remote sensing data processing.

To verify the performance of our cluster system, image registration has been chose to experiment with one scene of HJ-1 CCD sensor. The HJ-1 CCD data is consists of four spectral bands, with a space resolution of 30 meters and a band swath of 360 kilometers. One scene is nearly 900 MB. The data is corrected systemically in both geometry and radiation prior to our imagery registration processing. The method of polynomial algorithm and linear interpolation are applied in our experiments. From the results of the imagery registration with different number of processor range from 1 to 16, we can see that the processing time decreases rapidly with the increasing of number of processors in the front fifth, changes slowly in the middle and almost has no change in the latter among 10 to 15. Based on the figure and analysis, the power function of monotone decreasing would be used to describe the relationship between the processor number and processing time. The consuming time is opposite proportion to the processor number. That's to say the scalability is almost well. And also there is an approximate minimum value with the processor increasing. We can regard the seventh as a high cost performance in this experiment which is significant for resource arrangement. The test results show that the speedup varies with the number of processor in power function of monotone increasing. First, the slope of the trend line decrease slightly. Due to the characteristic of imagery registration, there are some fixed serial procedures increasing the overhead. Second, the speedup is not ascended unlimitedly and the slope tends to approximate one. Once the task reaches its max parallel speed, the time will not reduce. This trend of speedup is a well pattern of all parallel computing.

The experiments of imagery registration shows that it is an effective system to improve the efficiency of data processing, which could provide a response rapidly in applications that certainly demand, such as wild land fire monitoring and tracking, oil spill monitoring, military target detection, etc. Further work would focus on the comprehensive parallel design and implementations of remote sensing data processing.

Conference 8540: Unmanned/Unattended Sensors and Sensor Networks

Wednesday - Thursday 26–27 September 2012 • Part of Proceedings of SPIE Vol. 8540
Unmanned/Unattended Sensors and Sensor Networks IX

8540-1, Session 1

Fusion, planning and humans in sensor networks *(Keynote Presentation)*

Mark E. Campbell, Cornell Univ. (United States)

No Abstract Available

8540-2, Session 2

Modelling systems of weakly characterised sensors

Christopher J Willis, BAE Systems (United Kingdom)

Systems designed for surveillance and reconnaissance applications are frequently comprised of multiple sensors, and often multiple platforms. However, the effects of individual sensor performance, operational approaches and sensor interaction can mean some surprising results are observed for the system as a whole. Therefore, the modelling of multiple sensor systems is important, but can also be challenging. It is possible that the sensing system may be comprised of sensors of several different types, including active and passive approaches in, for example, the radio frequency or optical portions of the spectrum. Some may have well-understood performance, whereas others may be only poorly characterised. Applications of a modelling approach can be useful in the selection of sensors or sensor combinations of sufficient performance to achieve operational requirements or; for understanding how the system might be best exploited in the fulfillment of mission requirements.

A simulation framework has been developed for examining sensor options across different sensor types, parameterisations, search strategies, and applications. The framework is based around a scheme outlined in the literature. This utilises Bayesian Decision Theoretic principles, along with simple sensor models and Monte-Carlo simulation to derive the expected performance of single deployed sensors and of sensor combinations. The basic framework has been significantly extended to include recognition and identification problems along with the detection problem for which it was originally designed. The performance of each sensor is represented by simple performance statistics. For a detection sensor these statistics may be the probabilities of correct detection and of false alarm, or; for a recognition sensor, they may be related to the expected confusion matrix. The framework has also been expanded to treat cases in which the sensors are poorly characterised, and recommendations for parameterisation in this mode are made.

The sensor system modelling framework has been applied to a number of illustrative problems. These range from simple target detection problems using sensors of differing performance, or of different regional search schemes, through to examinations of: the number of measurements required to reach threshold performance; the effects of sensor measurement cost; issues relating to the poor characterisation of sensors within the system, and; the performance of a more elaborate combined detection and recognition sensor system. Generally, these results tend to show that the method is able to quantify qualitative expectations of performance, and is sufficiently powerful to highlight some unexpected aspects of operation.

Experiments are presented which consider the number of samples used to assess sensor performance. These reveal the limitations in having only small sets of data with which to characterise sensor performance. The simulations demonstrate that, where only small samples are available to assess the sensor, strong sensor performance might be expected, but only mediocre levels achieved. Further results consider systems comprised of both detection and recognition sensors. These again treat cases in which the sensors are well understood, and when only poorly understood. It is noted that, in some situations, a pair of weak sensors can work together to correct each other's limitations and ultimately achieve a good system performance.

8540-3, Session 2

Design of re-locking algorithm using target modeling of histogram ratio during coast tracking mode in infrared image

Sohyun Kim, Agency for Defense Development (Korea, Republic of); Junmo Kim, KAIST (Korea, Republic of)

Coast mode is one of tracking modes that deals with the target occlusion, where tracking is halted for a while and the servo slew rate is maintained according to the target movement just before the occlusion. As the last step of the coast mode tracking, this paper presents a target re-locking algorithm to resume the target tracking after the blind time. First, during the normal image tracking stage, as a target model, a gray-level histogram ratio of the target and background is computed for each frame of the normal stage images thereby updating the target model at each time step. When entering the coast mode due to occlusion, we run the re-locking algorithm for each frame of the coast mode images so that it can immediately resume the tracking right after the end of the blind time. The re-locking algorithm divides the input image into blocks and for each block of the image, it takes an average of histogram ratios over the block and selects candidate target blocks of large histogram ratios, where the histogram ratio is evaluated at the gray-level of each pixel in the block and those histogram ratios are averaged over the pixels in the block. Due to the block-based averaging, the overall decision is robust to noise in the IR image, and the re-locking process afterward is of reduced computational complexity. With the target candidate blocks, a clustering is performed to make target candidate clusters, where each cluster is a set of connected blocks of large histogram ratios. As a final step, the first-ranked target candidate cluster is selected by computing an overall score that combineds the histogram ratios and the prior knowledge of the target sieze, location, and variation of the intensity obtained during the normal tracking stage. We present experimental results based on both computer simulation and test under real environment with EOTS demonstrating the effectiveness of the proposed algorithm.

8540-4, Session 2

Global electronic dominance

Peter S. Sapaty, National Academy of Sciences of Ukraine (Ukraine)

A high-level control technology will be revealed that can dynamically establish overwhelming dominance over any distributed networked systems with electronic devices and any communications between them. It is based on implanting of universal control modules (which may be concealed) into key system points which, communicating, collectively interpret mission scenarios in a special high-level Distributed Scenario language (DSL). Self-evolving and self-spreading in networks, covering them in a super-virus mode, DSL scenarios can analyze their structures and states and set up any needed behavior, including creation, jamming or elimination of unwanted infrastructures. Details of the technology implementation and numerous system scenarios related to electronic warfare, cyber warfare and counterterrorism will be revealed in the presentation. This Spatial Grasp Technology (SGT), known as WAVE in the past, has a long history. Being much older than Java (born behind the "iron curtain") it has been used in different countries for intelligent network management, simulation of distributed battlefields, distributed virtual reality, distributed knowledge bases, and cooperative robotics. Along with useful applications in various areas, some of its uncontrolled and simplified & degenerated implementations could have supposedly been used as computer viruses (like Distributed Denial of Service attacks) or for illegal hacking in public networks.

8540-5, Session 3

Evaluation of range parameters of the cameras for security system protecting the selected critical infrastructure of seaport

Mariusz Kastek, Jaroslaw Barela, Marek Zyczkowski, Rafal Dulski, Piotr Trzaskawka, Krzysztof Firmanty, Juliusz Kucharz, Military University of Technology (Poland)

There are many separated infrastructural objects within a harbor area that may be considered „critical", such as gas and oil terminals or anchored naval vessels. Those objects require special protection, including security systems capable of monitoring both surface and underwater areas, because an intrusion into the protected area may be attempted using small surface vehicles (boats, kayaks, rafts, floating devices with weapons and explosives) as well as underwater ones (manned or unmanned submarines, scuba divers). The cameras used in security systems operate in several different spectral ranges in order to improve the probability of detection of incoming objects (potential threats). The cameras should then have adequate range parameters for detection, recognition and identification and those parameters, both measured and obtained through numerical simulations, will be presented in the paper.

The range parameters of thermal cameras were calculated using NVTherm software package. Parameters of four observation thermal cameras were also measured on a specialized test stand at Institute of Optoelectronics, MUT. This test stand makes it also possible to test visual cameras. The parameters of five observation cameras working in the visual range were measured and on the basis of those data the detection, recognition and identification ranges were determined. The measurement results and simulation data will be compared. The evaluation of range parameters obtained for the tested camera types will define their usability in the real security system for the protection of selected critical infrastructure of a seaport.

8540-7, Session 3

MOCVD growth and characterization of ZnO nanowire arrays for advanced ultraviolet detectors

Abdiel Rivera, Univ. of Connecticut (United States); John Zeller, Naval Undersea Warfare Ctr. (United States) and Magnolia Optical Technologies, Inc. (United States); Tariq Manzur, Naval Undersea Warfare Ctr. (United States); Ashok Sood, Magnolia Optical Technologies, Inc. (United States); A.F.M. Anwar, Univ. of Connecticut (United States)

Zinc oxide (ZnO) provides a unique wide bandgap biocompatible material system exhibiting both semiconducting and piezoelectric properties, and is a versatile functional material that has a diverse group of growth morphologies. Bulk ZnO has a bandgap of 3.37 eV that corresponds to emissions in the solar blind ultraviolet (UV) spectral band (240-280 nm). We have grown highly ordered vertical arrays of ZnO nanowires using a metal organic chemical vapor deposition (MOCVD) growth process. This growth process has distinct advantages over other methods that require incorporation of metal catalysts as seed layers, which can introduce undesired defects to the structure that decrease crystal quality. For the MOCVD nanowire growth, diethylzinc (DEZn) is used as zinc precursor and nitrous oxide (N2O) as the oxygen precursor, with nitrogen (N2) as the carrier gas. The nanowires were grown on Si(111), SiO2, and m-plane sapphire substrates. The structural and optical properties of the grown vertically aligned ZnO nanowire arrays were characterized by scanning electron microscopy (SEM), X-ray diffraction (XRD), and photoluminescence (PL) measurements. The diameters of the grown nanowires were estimated from SEM based measurements to be in the range of 20-30 nm for sapphire, 90-150 nm for Si (111), and 70-90 nm for SiO2. The unique diffraction pattern for ZnO (002) concurred with the SEM inspection indicating vertical orientation of the nanowires. ZnO nanowires show predominant peaks commonly observed at 379 nm and 385 nm, attributed to the recombination of excitons through an exciton to exciton collision process, and band to band acceptor transition, respectively. Additional shallows peaks are also exhibited in the blue light spectrum region ascribed to 2LO phonon interaction and oxygen interstitial vacancies. In the case of the ZnO nanowires grown on Si (111), and SiO2, only exciton to exciton recombination was observed. UV detectors based on ZnO nanowires offer high UV sensitivity and low visible sensitivity for applications such as missile plume detection and threat warning. An analytical model that can predict sensor performance in the UV band using p-i-n, p-n, and Schottky detector configurations with and without gain for a desired UV band of interest has also been developed that has the potential for substantial improvements in sensor performance and reduction in size for a variety of threat warning applications. Using this model, signal-to-noise ratios can be modeled from illuminated targets at various distances with high resolution under standard MODTRAN atmospheres in the UV band and the solar blind region using detector arrays with and without high gain. In addition, testing and characterization of photomultiplier tubes (PMTs) exposed to eight individual UV LEDs having peak wavelengths ranging from 248 nm to 370 nm has been performed to provide a relative UV detection performance benchmark. Compared to PMTs, the nanowires arrays are expected to exhibit low noise, extended lifetimes, low power requirements, and can be coupled with microlens arrays to further improve their sensitivity for UV detector applications.

8540-8, Session 3

Development of a variable climate controlled portable storage facility

Mitchel Timmins, Kamal Yadav, Kennedy Iroanusi, Andrew J. Tickle, Coventry Univ. (United Kingdom)

This paper focuses on the development of a portable variable climate controlled system that can be tailored to the requirements of the item to be stored by manipulating the temperature, humidity and light levels within the controlled area. This could be used to store anything from bio-chemical samples (to preserve them from field work) to cooled electronics (prior to deployment in a given situation) to foodstuffs (such as wine and other alcohols). In this situation however, to provide a relatively simplistic example, the environment will be used to store wine. The system is adaptive in that anything can be stored within it, assuming the storage parameters are known in order to correctly configure the environment. In this paper a microcontroller (PICF4520) is connected to a fridge with various sensors attached to monitor and manipulate the environment and adjust it accordingly. For the chosen item to be stored, a temperature of 13oC is required, a high humidity level and a non-Ultraviolent (UV) light source. This work thus allows for a small handheld unit that could be used to control the climate within without the need for the traditional 12 - 16 foot size portable units traditionally used. Additional features to be considered are connecting a mobile phone to the system in order to provide the ability to alter the system parameters and receive updates by the use of SMS text messages. The latter means that a unit could be left in the field and run off a solar cell to assist in longer term studies. This paper presents how the microcontroller is connected to the fridge and its sensors, how it manipulates the environment and the process by which the temperature and other factors can be changed without having to edit and re-compile the C code, this allows for a much more friendly device interface.

8540-9, Session 3

Monitoring/sensing applications on AirPON

Ilja Kopacek, SQS Vláknová optika a.s. (Czech Republic); Michael Pisarik, Czech Technical University in Prague, Dept. of Electromagnetic Field (Czech Republic) and SQS Vláknová optika a.s. (Czech Republic)

Main characteristics of our MLS (monitoring line system):

- Monitoring of physical layer (optical fiber).
- Modular design enables customization for wide spectrum of applications.
- Local or remote control of the equipment via Ethernet - TCP/IP protocol.
- Monitoring of dark as well as lit fibers.
- Management of the system via web interface.
- Event setting and data logging as well as customized management and reporting.
- Event notification via variety of media channels such as e-mail and SMS.
- Failure prediction - monitoring on longer, more sensitive wavelength.

Different types of MLS

1. Transmissive monitoring (TM) - this is a direct method of measurement (optical source and optical receiver)

Advantages:

• Continuous measurement of predetermined level of attenuation and its changes.

• Exact time-wise power level measurement of very short lasting interruptions.

• Large dynamic range of the system = 60dB (transmitter Tx=0dBm, receiver Rx from -60 up to 0dBm).

Disadvantages:

• Impossible to identify the location of disruption.

2. RFTS (Remote Fiber Test System) monitoring - reflectometric measurement (OTDR)

Advantages:

• Identification of the location and degree of disturbance (of measured quantity IL, IL/km and length)

• Graphical relation plotting between IL level and the distance.

Disadvantages:

• Switched, interrupted method of measurement.

• Impossible to detect short interruptions.

3. ARFTS (Advanced Remote Fiber Test System) monitoring - combination of TM and RFTS

Advantages:

• TM monitoring with automatic switchover to RFTS monitoring if change in IL level it detected.

• Periodic reflectometric measurements of optical fibers.

• Mapping of long term IL trends of certain elements in optical fiber (splices, connectors...).

Disadvantages:

• Switched, interrupted method of measurement.

8540-34, Session 3

Uncooled silicon carbide sensor producing optical signal *(Invited Paper)*

John W. Zeller, Tariq Manzur, Naval Undersea Warfare Ctr. (United States); Aravinda Kar, CREOL, The College of Optics and Photonics, Univ. of Central Florida (United States)

Crystalline silicon carbide (SiC) is a wide bandgap covalent semiconductor material with excellent thermo-mechanical and optical properties. While the covalent bonding between the Si and C atoms allows n-type or p-type doping by incorporating dopant atoms into both the Si and C sites, the wide bandgap enables fabrication of optical detectors over a wide range of wavelengths. To fabricate a Mid-Wave Infrared (MWIR) detector, an n-type 4H-SiC substrate is doped with Ga using a laser doping technique. The Ga atoms produce an acceptor level of 0.30 eV which corresponds to the MWIR wavelength of 4.21 ?m. Photons of this wavelength excite electrons from the valence band to the acceptor level, thereby modifying the electron density, refractive index, and reflectance of the substrate. This change in reflectance constitutes the detector response. The dynamics of the detector response are studied by placing a chopper at a constant angular velocity between the MWIR radiation source and the detector. The imaging capability of the detector is established by reflecting incoherent light at a wavelength of 633 nm, which is produced by projecting illumination from a light-emitting diode (LED) off the detector towards a CMOS camera and examining the digital output of the camera to determine the relative intensity of the incident radiation. In addition, a mathematical model is presented to analyze the dynamic response and determine the electron density and lifetime in the acceptor level.

8540-10, Session 4

Advances in free-space laser communications at the Naval Research Laboratory *(Invited Paper)*

Rita Mahon, William S. Rabinovich, Mike S. Ferraro, Peter G. Goetz, James L. Murphy, Harris R. Burris Jr., Christopher I. Moore, U.S. Naval Research Lab. (United States); L.M. Thomas, Fibertek, Inc. (United States); Michael J. Vilcheck, U.S. Naval Research Lab. (United States)

No Abstract Available

8540-11, Session 4

Free-space optical communication at 1.55 μm and 4.85 μm and turbulence measurements in the evaporation layer

John W. Zeller, Naval Undersea Warfare Ctr. (United States) and Magnolia Optical Technologies, Inc. (United States); Tariq Manzur, Naval Undersea Warfare Ctr. (United States)

Free-space optics (FSO) holds the potential for high bandwidth communication in situations where landline communication is not practical, with relatively low cost and maintenance. For FSO communication in maritime environments, laser beams propagating through the evaporation layer near the sea surface are affected by turbulence, the scattering coefficients of the water particles, and the salt water itself. The short-wave infrared (SWIR) and mid-wave infrared (MWIR) bands contain atmospheric transmission windows spanning approximately 1.50-1.75 μm and 4.6-4.9 μm, respectively, making lasers emitting in these ranges suited for high bandwidth covert FSO communication. An InP based quantum cascade laser with a ring-shaped cavity exhibiting 0.51 W room temperature emission at ~4.85 μm has been developed for FSO applications. This surface emitting laser is an ideal choice for FSO due to its small footprint, symmetrical high beam quality, near diffraction limited performance, and the relatively low atmospheric attenuation. Transmission coefficients and losses were modeled using MODTRAN for optical path lengths of up to 2 km for various atmospheric conditions. The determination of the refractive index structure parameter Cn2 is useful in calculating the time-dependent Fried parameter, r0, which provides an indication of the magnitude of the phase distortion of an optical wavefront by scintillation in accordance with the Kalomogorov model. To better gauge and understand the effects of turbulence on FSO communication, Cn2, which relates to scintillation strength, may be estimated from a database of environmental parameters experimentally measured near the sea surface. By determining how Cn2 and r0 data relate to FSO transmission under the same environment, measures can be implemented to reduce the bit error rate and increase data throughput, enabling more efficient and accurate communication links. Commercial 1.55 μm FSO transceivers at have been acquired that provide up to 155 Mbps digital data transmission at a range of up to 3 km in typical operating conditions. Likewise, FSO transmitter and receiver circuits for relaying analog video and audio signals were developed in-house using low-cost COTS components and determined capable of providing communication over path lengths of up to ~5 km. FSO beam optimization is achievable through adaptive optics using a deformable mirror and Shack-Hartmann wavefront sensor, whereby wavefront distortion of a transmitted beam is measured and the wavefront is modulated in real time to compensate for the effects of turbulence to provide optimized FSO reception through the evaporation layer. The Kalman filter method may also be employed to reconstruct an original undistorted image from a series of sequential transmitted images altered by turbulence. Additionally, a dedicated automatic target recognition and tracking optical correlator system using advanced processing technology has been developed. Rapidly cycling data-cubes with size, shape, and orientation are employed with software algorithms for this system to isolate correlation peaks and enable tracking of targets in maritime environments with future track prediction. Using advanced techniques and compensation methods, limitations associated with infrared FSO transmission and reception in the evaporation layer may be overcome or circumvented to provide high bandwidth communication through turbulence or adverse weather conditions.

8540-12, Session 4

Probability of fade and BER performance of FSO links over the exponentiated Weibull fading channel under aperture averaging

Ricardo A. Barrios, Federico Dios, Univ. Politècnica de

Catalunya (Spain)

Recently a new proposal to model the fading channel in free-space optics (FSO) links, following the statistics of the exponentiated Weibull (EW) distribution, was made [1]. It has been suggested that the EW distribution can model the probability density function (PDF) of the irradiance under weak-to-strong turbulence conditions in the presence of aperture averaging. Here, we carry out an analysis of probability of fade and bit error-rate (BER) from numerical simulation results and experimental data. The bit error-rate analysis is made considering intensity modulation/direct detection with on-off keying. Data is assumed to follow the statistics of the EW distribution, and compared with the Gamma-Gamma (GG) and Log-normal (LN) distributions, as they are the most widely accepted models in FSO nowadays. It is shown how the proposed EW model is valid in all the tested conditions, and outperforms the GG and LN distributions, which are only valid under certain scenarios.

[1] Barrios, R. and Dios, F., "Exponentiated Weibull distribution family under aperture averaging for Gaussian beam waves," Opt Express (to be published).

8540-13, Session 4

Adaptive inverse control for gyro-stabilized platform of electro-optical tracking system

Yun-Xia Xia, Qiliang Bao, Zhijun Li, Institute of Optics and Electronics (China); Qiongyan Wu, Institute of Optics and Electronic, Chinese Academy of Sciences (China)

Electro-optical acquisition, tracking and pointing system (ATP) is widely used in high-energy lasers weapons, laser communications and so on. Line-of-sight stabilized system, which can be used to isolate the vibration of the moving bed and the disturbance of atmosphere, is the most important part of ATP system. The capability of tracking input signal and disturbance rejecting are the key issues. In this paper, a novel control approach so called Adaptive Inverse Control (AIC) is proposed for line-of-sight stabilized system. There are three adaptive elements, including plant model, tracking controller and disturbance cancel controller. All the adaptive control loop is based on recursive least squares lattice filter. An inverse model of the plant is used as the open-loop tracking controller. The control signal drives both the plant and plant model to estimate disturbance and another inverse model of plant is used to cancel disturbance. So it processes the input signal tracking and disturbance rejecting separately. In addition, because the plant model is identified on-line, the control system has strong robustness. Based on this novel method, simulation and experiment are both carried out for a gyro stabilized platform of electro-optical tracking system. The experiment includes a shaking platform which can generate vibration as the moving bed and a gyro stabilized platform which is mounted on the shaking platform. Both the simulated and experimental results indicate that the gyro stabilized platform using AIC method is accurate and effective. Comparing with PID control method, the tracking precision and disturbance cancel error are both greatly improved at low-frequency and mid-frequency by adopting AIC method. It can be concluded that the AIC method is a new approach for the high-performance gyro stabilized platform system and might have broad application prospect.

8540-14, Session 4

The impact of sunlight on the performance of visible light communication systems over the year

Mahmoud H. Beshr, Ivan Andonovic, Univ. of Strathclyde (United Kingdom); Moustafa H. Aly, Arab Academy for Science, Technology & Maritime Transport (Egypt)

Visible light communications (VLC) is a valuable addition to future generations of networks, utilizing light for illumination for the purposes of advanced service provisioning at high speed. Low energy consumption, license free and RF interference free operation are compelling advantages. VLC systems are affected by sunlight limiting connection availability and reliability. The paper presents an analysis of the performance of VLC systems at different locations around the world over the cycle of a year; the evaluation considers the impact of sunlight as a function of location, time and for different surfaces over the four seasons of the year. 47% of the sunlight spectrum lies within the visible light frequency band, the band of network operation. To date the evaluation of the performance of VLC systems has not rigorously considered the impact of sunlight. In previous research, sunlight has been treated as Gaussian noise; this research takes into consideration the variation of sunlight intensity over the year of 2011. Hourly sunlight irradiance for two representative hospital environments, Cairo, Egypt and Glasgow, Scotland are considered and the calculation of solar irradiance, considers the longitude and latitude of locations, day of year and time of day. VLC impulse response has to date been determined solely for single reflection for standard room sizes. Here an evaluation of the impulse response for relatively large room sizes for both line-of-sight (LOS) and non-line-of-sight (NLOS) components up to the fifth reflection will be presented. Signal to Noise Ratio (SNR) and bit error rate (BER) will be evaluated for each season over the year. Monte Carlo simulations together with a Matlab routine is used to model the system simulate and evaluate the system performance.

The results of the impact of sunlight irradiance on VLC system performance for 2011 are presented in Table I. The evaluation presented the achievable BER for the four seasons of year for a range of surfaces; plaster walls, floors, plastic walls and ceilings; the attainable BER ranges from 10-9 to 10 -12. All simulations were conducted using hourly calculations (8760 hours) of sunlight irradiance and it is found that the lowest SNR (and BER) occurred for summer days in Cairo where sunlight intensity reaches its maximum.

In summary, the availability of VLC systems is a strong function of the level of natural sunlight and indeed the performance may be compromised under high intensity scenarios such as encountered during summer periods.

8540-15, Session 4

High speed GaN micro-light-emitting diode arrays for data communications

Scott Watson, Univ. of Glasgow (United Kingdom); Jonathan J. D. McKendry, Shuailong Zhang, David Massoubre, Univ. of Strathclyde (United Kingdom); Bruce R. Rae, The Univ. of Edinburgh (United Kingdom); Richard P. Green, Univ. College Cork (Ireland); Erdan Gu, Univ. of Strathclyde (United Kingdom); Robert K. Henderson, The Univ. of Edinburgh (United Kingdom); Anthony E. Kelly, Univ. of Glasgow (United Kingdom); Martin D. Dawson, Univ. of Strathclyde (United Kingdom)

Micro light-emitting diode (micro-LED) arrays based on an AlInGaN structure have attracted much interest recently as light sources for data communications. Both visible light communication (VLC) and plastic optical fibre (POF) communication have become very important techniques in the role of data transmission. The micro-LEDs which have been used contain pixels ranging in diameter from 14 to 84μm (in increments of 10 μm) and can be driven directly using a high speed probe or via complementary metal-oxide semiconductor (CMOS) technology. The CMOS arrays allow for easy, computer control of individual pixels within arrays containing up to 16 x 16 elements. The micro-LEDs presented here for data transmission have a peak emission of 450nm, however various other wavelengths across the visible spectrum can also be used.

Optical modulation bandwidths of over 400MHz have been achieved as well as error-free (defined as an error rate of <1x10-10) data transmission using on-off keying (OOK) non-return-to-zero (NRZ) modulation at data rates of over 500Mbit/s over free space. Also, as a step towards a more practical multi-emitter data transmitter, the frequency response of a micro-LED integrated with CMOS circuitry was measured and found to be up to 185MHz. Despite the reduction in bandwidth compared to the bare measurements using a high speed probe, a good compromise is achieved from the additional control available to select each pixel. It has been shown that modulating more than one pixel simultaneously can increase the overall data rate. For example, for one channel modulating at 500Mbit/s, it is possible to modulate four channels to get 2Gbit/s with the potential to increase the number of channels to optimise the data rate further.

In general terms, higher bandwidth values are achieved by using smaller pixels. This is due to their ability to operate at higher current densities than their larger counterparts. Micro-LEDs are suited to this work due to their size. Every pixel shares a common n-contact, and is connected by a metal track to separate p-contact pads of 100 x 100 μm2 in area. Commercial LEDs have a large surface area reducing their bandwidth, limiting their use in this area. Also, the use of

phosphor in such devices limits the bandwidth further. To the best of our knowledge, these modulation bandwidths, of over 400MHz using a 450nm micro-LED, exhibit the best results obtained for any blue LED fabricated in AlInGaN. As work continues in this area, the aim will be to further increase the data transmission rate by modulating more pixels on a single device to transmit multiple parallel data channels simultaneously.

References

[1] Jonathan J.D. McKendry, David Massoubre, Shuailong Zhang, Bruce R. Rae, Richard P. Green, Erdan Gu, Robert K. Henderson, A.E. Kelly and Martin D. Dawson, “Visible-Light Communications Using a CMOS-Controlled Micro-Light-Emitting-Diode Array”, Journal of Lightwave Technology, vol. 30, 2012, pp. 61-67

8540-16, Session 4

An overview of underwater free space communications developments

Henry J. White, BAE Systems (United Kingdom)

No Abstract Available

8540-17, Session 4

Extending the data rate of non-line-of-sight UV communication with polarization modulation

Hongwei Yin, Honghui Jia, Hailiang Zhang, Xiaofeng Wang, Shengli Chang, Juncai Yang, National Univ. of Defense Technology (China)

With low radiation background of solar-blind UV and strong scattering of UV photons by atmospheric particles, UV communication can be made use of to set up a non-line-of-sight (NLOS) free-space optical communication link. Although several modulation methods, including on-off keying (OOK), pulse position modulation (PPM) and differential pulse interval modulation (DPIM), have been made use of in the NLOS UV communication systems, the data rates of the UV communication systems that publicly reported can hardly meet the requirement of high data rate communication, and it is favorable to enhance the data rates. It is well known that light has two fundamental characteri stics－intensity and polarization, and the scattering matrix of atmospheric particles has unique characteristics, then polarization modulation, besides traditional intensity modulation, may also be made use of in the UV communication systems. The scattering processes of UV photons in atmosphere can be simulated with the NLOS polarized scattering model, the intensity and polarization of the photons are denoted by Stokes vector; theoretical simulation show that the polarization characteristics of the photons are maintained in a certain extent among the scattering processes, then the feasibility of polarization modulation is validated. Polarization modulation is accomplished by a time-dependent polarizer, and polarization demodulation by a time-independent analyzer array. By adding the polarizing devices and changing the coding procedures, the existing singly-modulated UV communication systems with intensity modulation are easily modified to be dually-modulated ones with polarization modulation and intensity modulation. Ideally speaking, the data rate of the dually-modulated UV communication system is the product of the data rate of the singly-modulated system and the number of polarization modulation. This paper describes the characteristics of the dually-modulated UV communication system based on the NLOS polarized propagation model, and discusses the influencing factors of polarization modulation. Although polarization modulation is more sensitive to communication environment than intensity modulation is, a dually-modulated UV communication system is still practicable and achievable under careful consideration.

8540-31, Session PS

A novel system with WiMax LDPC-coded OFDM for optical communication

Jing He, Hunan Univ. (China); Jinshu Su, National Univ. of Defense Technology (China); Yuan Huang, Hao Liu, Hunan Univ. (China)

Recently broadband wireless access technology, such as WiMax (IEEE 802.16) for Wireless Metropolitan Area Networks has become a strong candidate for the last mile wireless connectivity to provide flexible broadband services to end users. According to the IEEE 802.16 standard, the typical cell coverage can extend to 5 km in the atmosphere. However, when signal access inside a long tunnel and indoor, the WiMax signal distribution would be greatly hindered. The radio-over-fiber (ROF) technology at microwave/millimeter-wave bands is a promising solution to providing broadband service, wide coverage, and mobility. Using radio-over-fiber technology to carry WiMax signal could extend the cell coverage. Previous investigation reported that the transmission limitation and performance of the standard WiMax access in RoF link, but it focus on standard mobile WiMax for the applications in the high speed railway. And other research are based on integrate the 60-GHz optical-wireless system with the existing Wi-Fi and WiMax system. In the paper, we have proposed and investigated a novel ROF system transmitting 10-Gb/s WiMax LDPC-coded OFDM signal using 16-QAM format by simulation. The data with a pseudo random binary sequence of word length of 231-1 fed into WiMax LDPC (1153, 2304) Encoder with 1/2 code rate. The encoded LDPC data are then fed into 16-QAM OFDM baseband generator to obtain digital OFDM time-domain signal. The WiMax LDPC-coded OFDM signal with256 subcarrier is generated and each subcarrier is encoded with 16-QAM symbol, which is used as RF input of a MZM. After modulating the electrical field of the optical carrier, the output signal is mapped into the optical domain, and it can be transmitted over 200km SMF without any amplification. In order to evaluate the tolerance to fiber dispersion, WiMax LDPC-coded OFDM signal was injected in SMF characterized by an attenuation coefficient of 0.2dB/km and a dispersion coefficient of 17ps/ (nm.km). Based on the constellation diagrams of the received signal and the measured error vector magnitude after direct detection, simulation results show that the proposed system can successfully transmit a high capacity WiMax LDPC-coded OFDM signal over 200km SMF without any amplification, which is more cost-effective and simple.

8540-32, Session PS

Analytical model of non-line-of-sight multiple-scatter ultraviolet propagation

Hailiang Zhang, Hongwei Yin, Honghui Jia, Shengli Chang, Juncai Yang, National Univ. of Defense Technology (China)

Non-line-of-sight (NLOS) optical propagation works via the scattering of light by the atmospheric particles. The multiple-scatter irradiance always exists for NLOS optical propagation, only it is dominant among the whole scattered irradiance or not. There are already a plenty of works for the single-scatter and multiple-scatter propagations. For the single-scatter propagation, Luttegen developed the NLOS single-scatter propagation model based on the prolate-spheroidal coordinate system. This model is considered as the”standard”model of NLOS single scatter propagation, any other similar model shall be validated by it; Xu deduced some simplified equations on the assumption that FOV of transmitter and receiver were very small; Yin presented an analytical model which is can be applied for large FOV, and this model is in good agreement with Luttegen. For the multiple-scatter propagation, Yin presented the NLOS multiple-scatter propagation model based on Monte Carlo, this model can solve the problem of multiple scattering and gives exactly the same results as Luttegen. If only the single-scatter irradiance is considered; Ding did familiar work.

Two NLOS multiple-scatter propagation models have been set up based on Monte Carlo. Monte Carlo may be the only available method to solve the problem of multiple scattering with good accuracy, but it is a numerical method instead of an analytical one; both models are fit for the calculation on the condition that the influencing factors are given, rather than for the data analysis on the condition that one or some of the influencing factors are unknown. An analytical model of NLOS multiple-scatter propagation is favorable, and it is designed for the performance evaluation and the data analysis of the NLOS multiple-scatter link.

In this paper, based on the continuous wave transmitter and the isotropic scattering, an analytical model of non-line-of-sight (NLOS) multiple-scatter propagation is presented, which is validated by the available Monte Carlo model, with the consistent results in essence. Some characteristics of the multiple-scatter irradiance are disclosed by the analytical model, which are useful to distinguish the scattered irradiance with different total scattering time; the characteristics mentioned above remain true when the scattering is anisotropic. The following statements come into existence on the condition that the optical depth is small: the high-level-scatter (scattered more than

twice) irradiance is independent of the range, and the scattering links with the given elevation angles and the supplementary elevation angles have the same high-level-scatter irradiance. The impacts of the influencing factors on the multiple-scatter irradiance are clear from this analytical model. The analytical model can be used for the performance evaluation and the data analysis of a NLOS multiple-scatter link, for example, a NLOS UV communication link with the large optical depth or without the single-scatter volume.

8540-33, Session PS

Simulation of fog influence on laser beam distribution in atmosphere

Vladimir Vasinek, Jan Latal, Petr Koudelka, Jan Vitasek, Karel Witas, Stanislav Hejduk, Technical Univ. of Ostrava (Czech Republic)

Optical fibreless data networks P2P offer fast data transmissions with big transmittance from 1- 10 Gbps on a distance of 1- 6 km. Perfections of such networks are especially flexibility, rapid creation of communications. Sensitivity to atmospheric influences, necessity of light on sight belongs to disadvantages. Transmission through atmosphere be characterized by non-stationarity, inhomogeneity, the influences have random character. It means immediately that it is possible only with difficulty to project conclusions concerning to the measurement on one line upon fiberless line in another position. Contribution tackles a question of forming of the artificial hazy atmospheres, finding the statistical parameters of artificially created foggy atmospheres that could be reproduced to real environment. This work describes created laboratory apparatus powered with fog generator, heat source and ventilating fans, which allow in a controlled way to change the optical transmission inside the bounded space. Laser diode radiation at wavelength of 850 nm is transmitted into created space like this which is scanned with optical power meter after passing of artificially created turbulent vaporous environment. Changes in intensity of the passed lights are captured; the mean value and maximum deviation from the mean value are computed. In this way it is possible to change the reached specific attenuation in dB/km. Owing to turbulences it happens to deviations from the mean value, these abnormalities are characterized by the distribution function that describes the size of turbulences in time. By the help of ergodic theorem then it is possible to deduce that the distribution function of the foggy turbulences gained at continuous time evaluation has same history like the distribution function gained behind the same conditions in the setup in other times.

It holds as well that these distribution functions are the same for variety of points in experimental space, provided there are well - kept the same conditions of turbulence creations.

Contribution shows the experimental values, shapes of distribution functions, their influence on attenuation of fiberless communication lines and on achieved the transmission BER.

At the present time the verification of conclusions is performed from the experimental model on outdoor connecting link working upon the distance of 1,3 km at the transmission rate of 1,25 Gbps.

Fiberless line has been simulated in Optiwave sw that suitable for simulation of transmission properties. As a line attenuation (instead of optical fiber) the environment has been used described with mean attenuation value of artificial foggy atmosphere. At the same time with this value the largest deviation of attenuation has been evaluated as well and this maximum attenuation value has been considered as the most unfavorable state. Due to it was possible to use all sw tools that Optisystem sw makes possible. The detailed results will be also the content of contribution.

8540-18, Session 5

Morphological scene change detection (MSCD) for night-time security

Benjamin Jarvis, Andrew J. Tickle, Coventry Univ. (United Kingdom)

Morphological Scene Change Detection (MSCD) systems can be used to secure environments by sensing potential intruders and alerting security personnel to any security risks. To achieve this, the system compares the input from a camera to a reference image quantifying the level of change between the images, raising the alarm if this change is greater than a set triggering level. Morphological operators are then used to reduce the effect of any image change not related to a potential security risk; this includes noise and other minor changes thus decreasing the risk of false alarms. However in low light conditions MSCD systems can fail due to the reduced intensity differences between images containing security threats and reference images. This paper documents a proof-of-concept for a system that would use night vision images to address the problem. Here a low light scope camera attachment is used in place of a night vision camera and shows modifications to the previous MSCD system, which improves the performance when used with night vision images. The analysis of the modified system's performance in different low light environments, this includes the analysis of appropriate binary thresholds and alarm triggering levels for a range of environments. The latter include indoors at a distance, indoors at close range, outdoors at a distance and outdoors at close range. The results shown demonstrate that MSCD systems operating in low light conditions have the potential to be used as a useful tool in a security system and are compared to the original system to demonstrate the improvement.

8540-19, Session 5

Vector analysis for direction prediction on image strings

Andrew J. Tickle, Josef E. Grindley, Coventry Univ. (United Kingdom)

Vector analysis is a well-developed field that deals with details about line, surface and volume integrals which can be solved analytically to provide solutions to many problems. Using vector analysis, a curve can be divided up into many small arcs, each of which is a position vector. The summation of these position vectors can be used to represent the curve in detail; this is known as the total vector field. In this paper, there is shown a vector analysis methodology when applied to the wake immediately after a moving or stationary object, caused by the movement of the object through free space or the surrounding medium moving around the object respectively. The aim was to create a system that can determine the vectors between successive images in a video with the end result being able to establish an overall trajectory of the object. This could be implemented on a Field Programmable Gate Array (FPGA) or other device to be deployed in the field to track any type of object. If the device's orientation with magnetic north-south is known, the direction of the object is travelling in can be calculated and then relayed on. This could be useful as an easily deployable warning system for the armed forces or rescue services to inform personnel of potential incoming threats. This work builds upon the Morphological Scene Change Detection (MSCD) mechanism implemented in the DSP Builder environment and describes how the changes allow the system to track the wake and plot its trajectory. System simulations of real world data are shown and the resultant imagery is then discussed. Furthermore, tests are conducted on single objects and then multiple objects to investigate how the system responds as real world situations are likely to have more than a single object.

8540-20, Session 5

Integration of a digital watermarking system into a morphological scene change detector (MSCD) for tamper prevention and detection

Andrew J. Tickle, David Kamfwa, Coventry Univ. (United Kingdom)

Digital image watermarking is the process of embedding information into a digital image which may be used to verify its authenticity or the identity of its owners. This is the same as paper bearing a watermark for visible identification such as in money for example. In digital watermarking, if the signal is copied, then the information also is carried in the copy, proving that the data has been copied. In this paper, a digital watermarking approach is investigated using the DSP Builder methodology in order to provide the Morphological Scene Change Detector (MSCD) with a means by which if it detects an intruder, a watermarked copy of the triggering image is produced. This is so that if the image is required as proof in a court case; it can help show that the image has not been tampered with by means of the watermark. The system uses an 8-bit greyscale image and maps a binary watermark image onto the lowest bit level; this is then used

when the MSCD is triggered. For simplicity in this case, the watermark image is the same size and the target image to be watermarked, future variations with foresee a variable watermark image size. The result will be a watermarked image that if a section is copied and pasted into another file and that file is then analysed, the watermark will be visible. The process of integrating the watermarking process into the MSCD will also be discussed as this system originally used binary images to speed up the process. Finally, this watermark system can be used with any system designed as all that is required is to insert the sub-system into a larger system meaning that it is extremely interchangeable.

8540-21, Session 5

Examination of data fusion for personnel identification

Brian Maguire, Sachi V. Desai, U.S. Army Armament Research, Development and Engineering Ctr. (United States)

Interest in exploiting inexpensive sensing modalities to provide rich situational awareness for homeland defense and forward operating base applications has been growing. The power and cost limitations of these applications lead to a focus on non-imaging sensors. Such sensors lead to numerous challenges: low fidelity data, high false alarm rates, and widely varying granularity of classification amongst differing sensors. In order for these sensors to achieve acceptable performance in operational environments, a solution using data fusion is needed.

This paper proposes an approach for fusion of multi-modal sensor data for the purpose of personnel intrusion detection. The main challenge of fusing data from such sensors lies in the wide variation of information that they may provide. While some sensors may provide detailed characteristics of the motion in a scene and therefore a very fine classification, others may only provide simple alerts and little detail. In order to fuse data from a wide range of sensors that are often designed for disparate applications, an approach based on the Dempster-Shafer (DS) theory of evidence is used. The implicit handling of uncertainty and ambiguous propositions leads to a convenient hierarchical approach that can represent data from numerous sensor modalities.

Herein we examine application of the DS theory to data provided by a Passive Infrared Sensor (PIR) and an active ultrasonic micro-Doppler. The sensors are used to identify actors within a scene and the actors are defined as a human or an animal. A fusion approach reduces uncertainty and improves robustness in detecting the actor. Additionally, fusing data from the two disparate sensors enables classification of these actors as either a human or an animal. The results and analysis of the DS theory approach will be presented and the implications in improving situational awareness without the addition of an imager.

8540-22, Session 6

Wireless sensor networks in forest fire detection

Daniel E. Parra-Beratto, Silvia E. Restrepo, Jorge E. Pezoa Nunez, Univ. de Concepción (Chile)

Forest fires are unavoidable natural and man-made disasters which, unfortunately, keep increasing in number in spite of the efforts made to prevent these kind of fires. The negative consequences of forest fires affect not only the forest industry and the environment but also the human population living in areas surrounding the forests. Nowadays it is of great interest to develop novel solutions for both monitoring forests and accomplishing early detection of fires, thereby reducing the frequency of forest fires and amount of land that affected by such events.

This paper presents the initial steps towards the development of a forest fire detection system based on wireless sensor networks (WSNs). The idea is that each node in the WSN is capable of sensing information about the amount of carbon dioxide emissions and the surrounding temperature. This information is used by each sensor node to assess whether there is or not a forest fire in its surrounding environment. The assessment is carried out by computing, at each node, the Fine Fuel Moisture Code (FFMC). The FFMC is a figure of merit developed by the Canadian Forestry Service to assess the likelihood of ignition of a fire at a given point in space. To extend the lifetime of the WSN three approaches have been used. First, each sensor is equipped with both batteries and a solar cell. Second, a centralized power management scheme has been introduced to adapt the duty cycle of each node according to the FFMC and the historical data on the time occurrence of forest fires. Specifically, each sensor node uses its local estimate of the FFMC and a user-defined reference value to switch its state from sleep to active mode. Third, the sampling rate of the WSN has been bounded by the time taken by a forest fire to cover the maximum distance between sensing nodes, thereby ensuring that even if a sensor node is consumed by the fire while it is in sleep mode, the next sensor node should be active by the time the fire reaches it. In order to test the foregoing ideas, a laboratory prototype has been implemented and the sensors nodes have been characterized under different scenarios.

8540-23, Session 6

An open communication and sensor platform for urban search and rescue operations

Marko Korkalainen, Aki P. Mäyrä, Klaus M. Känsälä, VTT Technical Research Ctr. of Finland (Finland)

In this paper we present research results carried out in EU funded project SGL for USaR (Second Generation Locator for Urban Search and Rescue Operations). The aim of this project was to develop wireless standalone communication system with embedded sensor network which can be globally used in rescue operations after accidents or natural disasters.

The system is targeted to detect signs of life, locate victims in disaster areas and detect hazards threatening the rescue persons to enable more efficient and safe rescue operations. The main parts of the system are REDS (Remote Early Detection System) wireless sensor network and a portable first responder device (FIRST) integrating 5 different victim location methods.

During the development phase the main requirements for the sensor system was light weight so that it can be easily carried and installed at the accident site by the resque teams. The devices are autonomous and able to operate several days without external support. For communication, long range option is needed to enable sensor data transfer to operation command center that could be located kilometers apart from the disaster area.

REDS provides wireless CO and CO2 sensors for detection of life, a thermal camera for locating live bodies and objects, vibration sensors to detect possible signals of life and to give alarms in case of collapsing buildings or aftershocks (in case of a big earthquake) and a sound sensor to detect and indicate voice patters coming from different sources. The system provides a pointing device to locate objects on the search area. Victim positioning is possible outdoors with GPS and radio based methods. Radio based time of flight method provides also a possibility for indoor positioning. Currently a portable and custom developed IMS device is being integrated into REDS sensor network.

Portable and user operated FIRST device combines field chemical analysis, with audio and video analysis for early location of entrapped people, detection of buried people, air quality monitoring in confined spaces, safety and security monitoring and remote medical support to the located victims.

The system level communication is divided in two levels:
sensor network level uses short range local communication and communication hubs which use long range high level communication with operation command center. Local communication covers of few hundred meters with a high speed low power radio system. The same radio system is also used for local positioning of the sensors on the field. High level communication provides high speed communication over point to point links to the command post of the operation within one kilometer range.

In the beginning of the operation each rescue team defines the search area by placing four so called GPS anchor nodes to the four corners of the search area. After this the coordinates of the marked area will be sent to the command post and the search becomes active on digital map of the search operator. FIRST device can be operated in the disaster area independently or as a part of REDS sensor network. The rescue team can place the wireless sensor nodes on the desired spots on the search area. After a sensor is placed and activated it will be visible on the digital map as well and the sensor data also will be visualized and alarms given when necessary. All sensor data with positioning information and time stamps will be stored from each operation on a database for a further analysis of the operation.

The implemented REDS sensor network and FIRST device have been tested on field conditions and they have proven to be robust and reliable devices which can be used on demanding conditions. In the presentation new results from field tests will be shown together with the project progress and network implementation. The aim is to expand the application based approach by test results, user inteface development results and end-user feedback. One of the reported issues will be the results form integration of field operable and portable IMS device and REDS sensor system.

8540-24, Session 6

Embedded redundancy reduction guidance methodology for unmanned aircraft defense systems

George Dekoulis, Frederick Univ. (Cyprus)

This paper describes the design of a new state-of-the-art navigation system for unmanned aircraft defense systems. The project addresses the demands for more efficient autonomous navigation in a variety of aerospace altitudes. The proposed instrumentation is directly suitable for unmanned systems operation and testing of new airborne prototypes for defense applications. The system features a new sensor technology and significant improvements over existing solutions. Fluxgate type sensors have been traditionally used in unmanned defense systems such as target drones, guided missiles, rockets and satellites, however, the guidance sensors' configurations exhibit lower specifications than the presented solution. The current implementation is based on a recently developed material in a reengineered optimum sensor configuration for unprecedented low power consumption. The new sensor's performance characteristics qualify it for aerospace defense navigation applications. A major advantage of the system is the efficiency in redundancy reduction achieved in terms of both hardware and software requirements.

Attitude and heading control has been tested for various maneuvers. Data are presented from a test flight involving several maneuvers. Sample measurements of the pitch, roll and yaw values are presented. Minimum error compensation has been applied to show the limits of deviation. The heading accuracy error is up to 0.013 o/h in the 0-360o range. The pitch is 0.012 o/h for +/-45 o and 0.017 o/h for +/-90o. The roll is approximately 0.0011 o/h in the 0-360o range. The sensor has exceeded the specifications set at the beginning of this project. Further testing is necessary when updating the hardware and software components.

8540-25, Session 6

Reconfigurable SoC for the robust control of UGVs

George Dekoulis, Frederick Univ. (Cyprus)

This paper describes the latest results on the use of a new positioning system for unmanned ground vehicles. Emphasis has been given on the algorithmic processing, innovations and realization. A dynamic unmanned outdoor positioning example is presented, demonstrating the effectiveness of the overall instrumentation. There are many sectors of the security and defense industry that will benefit from the implementation of this new type of unmanned positioning technology. Improving the capabilities right at the sensing element enhances the virtues of robotic vehicles and broadens the range of applications. This was an essential advantage during the early stages of the project in order to achieve three-dimensional robust and accurate real-time operation.

Path planning and knowledge of the current geographical position are the foundation components in unmanned robotic vehicle navigation. The optimum path for an unmanned vehicle is based on the capabilities of the hardware and software to incorporate accurate vehicle dynamics. The efficiency of these algorithms is increased, when the algorithms have been tested in a variety of ground-based and airborne vehicles. Absolute positioning utilizes external references as the reference frame. For a known external frame, subsequent algorithms can derive the position typically with high accuracy. The major concern with these systems is that the environment needs to be appropriately modified before the commencement of the system's operation. Relative positioning does not require the processing of any external reference frame. Typical odometry applications are based on the usage of encoders. Inertial systems are typically based on sensors, such as accelerometers and gyros. Odometry and inertial sensor systems do not require alterations in the surrounding environment for robotic applications. Experimental results from a wide range of gyro-based implementations are also presented, identifying the main sources of errors expected from rate sensors. The significant drift errors over time and the complicated calibration techniques required to smoothen these errors inspired the creation of various gyroscope-free systems. Furthermore, the creation of new algorithms was inspired that reduce significantly the commonly observed computational redundancy.

Although geomagnetic positioning is an absolute positioning method, in reality it is also being used in relative measurements. It does not require any surrounding modifications, since it is based on the measurements of the planetary magnetic field. The solution presented in this paper is based on the implementation of a new algorithm based on the advantages of geomagnetic positioning.

The algorithmic implementation has been based on an outdoor commercial monster truck, which has been rebuilt and modified to a scientific research platform. The controller has previously been built. The system implements autonomous positioning based on the algorithm for geomagnetic positioning. Logic for implementing vision control exists. The resulting system-on-chip (SoC) has been implemented using the principles of reconfigurable computing and field programmable gate arrays (FPGAs). The FPGA has the capability to perform the positioning algorithms, to sample the various interfaces and to coordinate the DC motors. It can store data for up to 124 h using the on-board memory and when optimum data logging has been selected.

8540-26, Session 6

A formulation of bottom line requirements for next generation of unmanned sensor platforms and their networks

Andre Samberg, Sec-Control Finland Ltd. (Finland)

The unmanned sensor platforms can be divide into three main groups: Unmanned Airborne Vehicles (UAV), Unmanned Ground Vehicles (UGV), and Autonomous Underwater Vehicle (AUV). All together they can be called Remotely Operated Vehicles (ROV) and be connected by a centric network. Traditionally UAVs have been used by military for reconnaissance purposes. UGVs have been used by special forces bomb squads and anti-terrorist units as CBRNE robots for for EOD and IED detection and neutralization. AUVs have been used for inspection and transportation purposes under water. An overview of basic relations and formulation of the main network principles are given. The paper is divided into two main parts, the first treating ROV technology, and the second one referring to data collection and communication. A separate discussion is devoted to the definition of the requirements for next generation ROVs and and the factors influencing it. The trend is toward downsizing of the sensor's carrying platforms. The extensive research is carried out for artificial intelligent microbugs which can gather information without the disturbance of the environment. Such features as aerodynamic performances, guidance, obstacle avoidance, on-board data storage and micro-communication techniques have become of the high priority.

8540-27, Session 6

Land cover/use mapping using multi-band imageries captured by Cropcam Unmanned Aerial Vehicle Autopilot(UAV) over Penang Island, Malaysia

Mohd Zubir MatJafri, Lim Hwee San, Tan Fuyi, Khiruddin Abdullah, Norhaslinda Mohammad Tahrin, Beh Boon Chun, Univ. Sains Malaysia (Malaysia)

The problem of difficulty in obtaining cloud-free scene at the Equatorial region from satellite platforms can be overcome by using airborne imagery. Airborne digital imagery has proved to be an effective tool for land cover studies. Airborne digital camera imageries were selected in this present study because of the airborne digital image provides higher spatial resolution data for mapping a small study area. The main objective of this study is to classify the multi-bands imageries taken from a low-altitude Cropcam UAV for land cover∕use mapping over USM campus, penang Island, Malaysia. A conventional digital camera was used to capture images

from an elevation of 300 meter on board on an UAV autopilot. This technique was cheaper and economical compared with other airborne studies. The artificial neural network (NN) and frequency-based contextual classifier (FBC) were used to classify the digital imageries captured by using Cropcam UAV over USM campus, Penang Islands, Malaysia. The best supervised classifier was chosen based on the highest overall accuracy (>80%) and Kappa statistic (>0.8). The classified land cover map was geometrically corrected to provide a geocode map. The results produced by this study indicated that land cover features could be clearly identified and classified into a land cover map. This study indicates that the use of a conventional digital camera as a sensor on board on an UAV autopilot can provide useful information for planning and development of a small area of coverage.

8540-28, Session 7

Wireless acoustic modules for real-time data fusion using asynchronous sniper localization algorithms

Sébastien Hengy, Pascal Duffner, Sebastien De Mezzo, Pierre Naz, Institut Franco-Allemand de Recherches de Saint-Louis (France)

The presence of snipers in modern conflicts leads to high insecurity for the soldiers. In order to improve the soldier's protection against this threat, the French German Research Institute of Saint-Louis (ISL) has been conducting studies in the domain of acoustic localization of shots. Mobile antennas mounted on the soldier's helmet were initially used for real-time detection, classification and localization of sniper shots. It showed good performances in land scenarios, but also in urban scenarios if the array was in the shot corridor, meaning that the microphones first detect the direct wave and then the reflections of the Mach and muzzle waves (15% distance estimation error compared to the actual shooter array distance). Fusing data sent by multiple sensor nodes distributed on the field showed some of the limitations of the technologies that have been implemented in ISL's demonstrators. Among others, the determination of the arrays' orientation was not accurate enough, thereby degrading the performance of data fusion.

Some new solutions have been developed in the past year in order to obtain better performance for data fusion. Asynchronous localization algorithms have been developed and post-processed on data measured in both free-field and urban environments with acoustic modules on the line of sight of the shooter. These results are presented in the first part of the paper. The impact of GPS position estimation error is also discussed in the article in order to evaluate the possible use of those algorithms for real-time processing using mobile acoustic nodes. In the frame of ISL's transverse project IMOTEP (IMprovement Of optical and acoustical TEchnologies for the Protrection), some demonstrators are developed that will allow real-time asynchronous localization of sniper shots. An embedded detection and classification algorithm is implemented on wireless acoustic modules that send the relevant information to a central PC. Data fusion is then processed and the estimated position of the shooter is sent back to the users. A SWIR active imaging system is used for localization refinement. A built-in DSP is related to the detection/classification tasks for each acoustic module. A GPS module is used for time difference of arrival and module's position estimation. Wireless communication is supported using ZigBee technology. The first results of real-time asynchronous sniper localization using those modules are discussed in the article.

8540-29, Session 7

Time-domain hybrid model for small caliber ballistic shocks

Juan R Aguilar, Academia Politecnica Militar. Ejercito de Chile. (Chile); Sachi V. Desai, U.S. Army Armament Research, Development and Engineering Ctr. (United States)

Acoustics based sniper localization systems that uses shock wave information needs a ballistic model to obtain an estimate of the projectile trajectory. In these systems the accuracy of the employed ballistic model determines the exactness of the shock time of arrival (TOA) estimates and in turn of the sniper localization result. Examination of the ballistic model developed by Duckworth [1], which is employed in the Boomerang system, reveals this corresponds to "flat-fire" trajectory where notice that only aerodynamic drag force with constant drag coefficient acting upon the projectile has been considered. In this way, the model is applicable for trajectories restricted to be along x axis, and does not include the effects of gravity and wind forces upon the projectile. The Duckworth model for shock Time of Arrival exhibits some shortcomings. By definition, flat-fire trajectory approximation requires the trajectory angles of departure and of fall being less than 5.7 degrees [2], which could not be the case where gun elevation angles higher than this limit would be encountered. In the Duckworth model, flat-fire approximation is done by neglecting de effect of gravity force in the projectile equation of motion. However, at higher elevation angles the effects of gravity force would become more significant, indicating that a point-mass trajectory approach, rather than a flat-fire approximation, is required. Incorporation of gravity force in the ballistic model was done by Grasing and Ellwood [3]. According to the state of the art model introduced by Duckworth, the time of arrival tA is composed of two terms: the ballistic travel time, i.e., the time the projectile takes to reach point x along its trajectory which is derived from the ballistic model assumed. The second term in the Duckworth equation constitutes the acoustic travel time of the shock wave front, from the projectile at point x in trajectory, across the slant range, and up to the observation point r. Certainly, time of arrival estimates tA largely depends on the ballistic model employed, hence the importance of an accurate modeling of the different phenomena affecting the dynamics of the projectile in flight. On the other hand, current N-wave form models can predict shock duration and overpressure amplitude as function of propagation distance. An example is the Whitham approach for N-waves in the far field [5] which appropriately describes the nonlinear propagation of shock waves. Basically, the computer algorithm starts initializing a time sequence, at a given sampling frequency Fs, which begins at t = to, i.e., the time in which the weapon was fired. Then, for a given projectile trajectory and observation point r, it proceeds to calculate the time of arrival tA of the shock wave front, from its origin at the weapon muzzle up to observation point r. In this way a discrete time sequence containing the values of acoustic pressure versus time produced by the shock wave of a projectile at a given observation point r can be obtained. Our preliminary observations indicate this model could be suitable for estimating ballistic shock propagation up to distances between 25 a 50 m.

8540-30, Session 7

Substantial capability enhancement in small arms sensors using material improvements

Slobodan Rajic, Panos G. Datskos, John T. Simpson, Scott R. Hunter, Oak Ridge National Lab. (United States)

Material enhancements can substantially improve the capabilities of military weapons and sensor systems. Technologies such as low-cost high-strength titanium, hard and lubricious nickel-boron, ultra-high thermal conductivity carbon foam, and superhydrophobic materials are about to revolutionize system capabilities. We will primarily discuss our recent advances in superhydrophobic surface applications to various materials of interest such as glass, metal, and plastic. These surfaces are not only highly water repellant, but are also essentially self-cleaning. This can be particularly important to unattended systems.

Conference 8541: Electro-Optical and Infrared Systems: Technology and Applications

Tuesday - Thursday 25–27 September 2012 • Part of Proceedings of SPIE Vol. 8541
Electro-Optical and Infrared Systems: Technology and Applications IX

8541-1, Session 1

An investigation of material properties and performance for a selection of chalcogenide glasses for precision glass molding

William V. Moreshead, Alan Symmons, Ray J. Pini, LightPath Technologies, Inc. (United States)

The growing demand for lower cost infrared sensors and cameras has focused attention on the need for low cost optics for the long wave and Mid-wave infrared region. The combination of chalcogenide glasses and Precision Glass Molding (PGM) is the enabling technology for low cost infrared optics. The lack of detailed material properties data has limited its acceptance in the commercial market, but increased demand and recent cost reductions in infrared sensors has focused additional attention onto these materials as a cost driver for infrared systems.

This investigation reviews the material performance and repeatability for a number of different chalcogenide glasses. Material properties including material homogeneity, coefficient of thermal expansion, index of refraction, transmission and change in index over temperature are explored. Specific attention is given toward glasses that achieve high yields during precision glass molding and are candidates for commercial success.

This investigation reviews the accuracy and repeatability of material properties for a number of different chalcogenide glasses from different sources. Specific material properties that will be reviewed may include 1) transmission from visible to long wave IR wavelengths, 2) index of refraction at 10 microns, 3) change in index of refraction over a temperature range of -40°C to 80°C and a wavelength range of 1.5 to 14 microns, 4) coefficient of thermal expansion measured by dilatometry, 5) material homogeneity, 6) glass transition temperature measured by differential scanning calorimetry, 7) density, 8) microhardness, and 9) elemental analysis obtained by Proton Induced X-Ray Emission (PIXE). A brief discussion of moldability will also be included.

8541-2, Session 1

Recent advancements in EO/IR sensor windows

Shyam S. Bayya, Jasbinder S. Sanghera, Woohong Kim, Guillermo R. Villalobos, L. Brandon Shaw, U.S. Naval Research Lab. (United States); Ishwar Aggarwal, Sotera Defense Solutions, Inc. (United States)

This presentation will address the rugged passive optical window needs for various sensors operating in the visible, shortwave, midwave and longwave infrared regions. We are developing rugged optical materials for multiband applications covering the 0.2 - 12 μm wavelength region. These materials cover various parts of this multiband region and have mechanical properties that are superior to existing materials. A heavy metal oxide glass was developed to make very large and conformal windows with transmission in the 0.4-5.0 μm wavelength region. It is about 3x harder and >2x stronger than multispectral ZnS. A polycrystalline spinel ceramic was developed with transmission in the 0.2-5.0 μm region. Spinel is about 10x harder than multispectral ZnS and has ruggedness comparable to sapphire and AlON. Spinel has an advantage over sapphire and AlON with superior 4-5 μm transmission which becomes important for several applications. We are also developing a rugged ceramic with transmission in the 1-12 μm wavelength region. These materials can also be used to build multiband optics for imaging systems.

8541-3, Session 1

Multiscale optics for wide field-of-view thermal imaging

Gonzalo Muyo, Heriot-Watt Univ. (United Kingdom); Alistair Gorman, Univ. of Glasgow (United Kingdom); Nicholas K. Bustin, Andrew P. Wood, Qioptiq Ltd. (United Kingdom); Andrew R. Harvey, Univ. of Glasgow (United Kingdom)

Multiscale lens design is an attempt at severing the inherent connection between geometric aberrations and aperture size that plagues traditional lenses; that is, it is not possible, without excessive complexity, to simultaneously achieve long focal length, wide field of view and high numerical aperture. By taking advantage of the more ideal imaging capabilities of small-scale optics, a multiscale lens can effectively increase field-of-view and image size by simply arraying additional secondary optical elements, similar to a lens array, to locally correct image aberrations. The corollary of this is that the image formed at the detector consists of multiple overlapping sub images that must be digitally processed to create an image.

We report a new solution in multi-scale lens design that enables increased field of view using a single conventional detector array. We demonstrate this approach with a long-wave infrared imaging system that demonstrates high quality imaging across a field of view of 72 degrees with a total track length of only 21.8mm. This specification far exceeds what can be achieved using conventional approaches. A conventional front element is employed: since a conventional field-flattening element is able to provide aberration correction over only a modest field of view, a lenslet array is employed to locally correct for aberrations. Three distinct highly aspheric lenslet designs are arranged in an array of three concentric rings in an array totalling thirteen elements. Although the images formed at the detector array are then overlapping the aberration correction means that they are sharp and high quality image recovery is possible. Image formation for this system is described by a large system matrix which is fortunately highly sparse (only 0.1% of elements are non-zero) and the final high quality image is recovered using iterative back-propagation. The potential of this approach will be illustrated using representative detector array specification and noise levels.

8541-4, Session 1

Automated optical testing of LWIR objective lenses using focal plane array sensors

Daniel Winters, Patrik Erichsen, Christian Domagalski, Frank Peter, Josef Heinisch, Eugen Dumitrescu, TRIOPTICS GmbH (Germany)

The image quality of today's state-of-the-art IR objective lenses is constantly improving while at the same time the market for thermography and vision grows strongly. Because of increasing demands on the quality of IR optics and increasing production volumes, the standards for image quality testing increase and tests need to be performed in shorter time.

Most high-precision MTF testing equipment for the IR spectral bands in use today relies on the scanning slit method where the image of a test pattern as generated by a sample lens is scanned with a 1D detector and then reassembled for the image analysis. The disadvantages of this approach are that it is relatively slow, it requires highly trained operators for aligning the sample and the number of parameters that can be extracted is limited.

In this paper we present lesson learned from the R&D process on using focal plane array (FPA) sensors for testing of long-wave IR (8-12 μm) optics. Factors that need to be taken into account when switching from scanning slit to FPAs are e.g.: the thermal background from the environment, the low scene contrast in the LWIR, the need for advanced image processing algorithms to preprocess camera images for analysis and camera artifacts.

Finally, we discuss 2 measurement systems for LWIR lens characterization that we recently developed with different target applications:

1) A fully automated system suitable for production testing and metrology that uses uncooled microbolometer cameras to automatically measure MTF (on-axis and at several off-axis positions) and parameters like EFL, FFL, autofocus curves, image plane tilt, etc. for LWIR objectives with an EFL between 1 and 12 mm. The measurement cycle time for one sample is typically between 10 and 15s.

2) A high-precision research-grade system using again an uncooled LWIR camera as detector, that is very simple to align and operate. A wide range of lens parameters (MTF, EFL, FFL, distortion, etc.) can be easily and accurately measured with this system.

8541-61, Session 1

High resistant multispectral optical coatings for Infrared applications

Michael Degel, E. Gitter, T. Wagner, M. Serwazi, JENOPTIK Optical Systems GmbH (Germany); Peter Maushake, JENOPTIK Optical Systems, Inc. (United States)

Infrared optics which are built into optical systems for outdoor applications are required to transmit high-quality images and signals with long-time stability. It must do so despite harsh environmental conditions and process-induced impacts on optical components and their coatings. DLC – also referred to as “hard carbon“ IR coatings – represent the state-of-the-art in optical systems of thermo-sensor-based monitoring plants for industrial, civil and military applications. They can be manufactured on such materials as silicon or germanium. This can be achieved, in the simplest case, through adaptation of refractive indexes (single-layer coating). This coating is industry standard.

The newly developed Hybrid-DLC coating unites lasting resistance with the strongly improved transmittance of a dielectric coating (Fig.1). This enables the capability to selectively manufacture customized IR windows of highest durability and lowest residual spectral reflection. A sophisticated design and production process makes it possible to minimize internal coating tensions and, hence, warrant the durability and adhesive power in accordance with such established testing standards as TS 1888 (Windscreen-Wiper Test) or MIL.

In addition, these spectral properties can be achieved in two separate wavelength ranges (e.g. MWIR and LWIR). Multispectral coatings of this type provide users of coatings with new solutions in design and application. By way of example, Fig. 2 shows a multispectral Hybrid-DLC coating with optimized transmittance as a dual band coating with the properties of e.g. a transmission >85% for 3-5 µm a transmission of >90% for 8-11,5µm.

Therefore, an optical element that has been used to provide protection only with a narrow AR window is now a multifunctional tool including protection, a wide AR window and a dual-band filter coating which leads to less optical components in the lens system and therefore saving optical design space and weight.

The new approach in multifunctional and resistant optical elements requires much more a sophisticated coatings set-up. While the standard DLC coatings consists of one single layer is the stack of single layers for the Hybrid-DLC with up to 50 layers on each optical surface.

The state of the art of durable infrared coatings with coating designs and internal coating tension is described in this paper together with projections into the future.

8541-5, Session 2

IR detectors at AIM: status and roadmap *(Invited Paper)*

Johann Ziegler, Rainer Breiter, Detlef Eich, Joachim C. Wendler, Jan Wenisch, Richard Wollrab, AIM INFRAROT-MODULE GmbH (Germany)

Since 35 years, AIM INFRAROT-MODULE GmbH is developing and fabricating pc and pv infrared detectors for 1st, 2nd and 3rd Gen applications on the basis of HgCdTe (MCT) covering the spectral range from VIS-SWIR to VLWIR. Infrared systems with AIMs linear and 2-dim. FPAs are fielded in many national and international state of the art programs for surveillance and targeting, seeker head systems, and space borne applications.

The standard array processing is performed on LPE grown layers on CdZnTe substrates by n-on-p planar technique, Boron ion implantation, and intrinsic or extrinsic doping. To meet the requirements of 3rd Gen IR modules, such as higher resolution megapixel arrays or new functions like dual band capability, the MBE growth of MCT on GaAs is being established at AIM. This technology is capable of satisfying the rising demand for increasingly complex device structures and low cost detectors.

AIMs development accommodates new trends for IR systems by projects such as enhancement of the standard technology by extrinsic doping or novel p-on-n structures for HOT applications, on-chip ADC for digital data processing and low read out noise, SWIR detectors for hyperspectral detection, and avalanche SWIR photodiodes for low background and laser radar applications. This contribution will give an overview of the current IR-technology at AIM and the future progress according to AIMs technology roadmap. Results of the most important FPAs of the 2nd and 3rd Gen will be presented.

8541-6, Session 2

Status of IR detectors for high operating temperature produced by MOVPE growth of MCT on GaAs substrates *(Invited Paper)*

Peter Knowles, Les Hipwood, Nick Shorrocks, Ian M Baker, Luke Pillans, Paul Abbott, Richard M Ash, Jay Harji, SELEX Galileo Infrared Ltd. (United Kingdom)

Detector arrays using Metal-Organic Vapour Phase Epitaxy (MOVPE) grown HgCdTe on GaAs substrates have been in production at SELEX Galileo for over 10 years and are a mature technology for medium wave, long wave, and dual-band tactical applications. The mesa structure used in these arrays is optimised for MTF, quantum efficiency and dark currents. Further development of the technique has migrated to very long wave and short wave bands, mainly for space and astronomy applications.

This paper summarises the state of the art of MOVPE for this broad infrared spectrum and will report on the development of higher operating temperature (HOT) devices operating at up to 200K, very low dark current SWIR devices designed for astonomy application achieving sub 0.1 e/p/s at 80K, large format MWIR buttable arrays at a pixel pitch of 12 microns, and advances in two colour detection.

8541-7, Session 2

Last developments of MCT focal plane arrays in France *(Invited Paper)*

Michel Vuillermet, David Billon-Lanfrey, SOFRADIR (France); Gérard Destéfanis, CEA-LETI (France)

This paper describes the recent developments of Mercury Cadmium Telluride (MCT) infrared technologies in France at Sofradir and CEA-LETI made in the frame of the common laboratory named DEFIR.

Among these developments, one can find the crystal growth of high quality and large Cadmium Zinc Telluride (CZT) substrates which is one of the fundamental keys for high quality and affordable detectors. These last years, a great effort was done on this topic and also on MCT epilayer process from Short Waves (SW) to Very Long Waves (VLW).

These developments about the quality of the material are needed for the challenge of the High Operating Temperature (HOT). Over these lasts years, the operating temperature of n/p MCT detectors was increase of several tens of Kelvin. In addition the development of the p/n MCT technology that reduces dark current by a factor ~100 saves about twenty Kelvin more. The next step for the increase in operating temperature will be the complex photodiodes architectures using molecular beam epilayer.

The reduction of the pixel pitches is another challenge for infrared technologies for Small Weight and Power (SWAP) detectors. Moreover, this reduction allows the increase in the resolution and consequently in the detection range of the systems.

In addition, last results on 3rd generation detectors such as multicolor focal plan arrays, 2D, 3D, low noise and high images rate focal plane array using Avalanche Photodiose (APD) are described.

8541-8, Session 3

High-performance MCT and QWIP IR detectors at Sofradir

Yann Reibel, Laurent Rubaldo, Alexandre Kerlain, Alain Manissadjian, SOFRADIR (France); Rohtman Johan, Eric D. De Borniol, Gérard Destéfanis, CEA-LETI (France); Eric M. Costard, Thales Research & Technology (France)

Cooled IR technologies are challenged for answering new system needs like compactness and reduction of cryo-power which is key feature for the SWaP (Size, Weight and Power) requirements. This paper describes the status of MCT IR technology in France at Leti and Sofradir. A focus will be made on hot detector technology for SWAP applications. Sofradir has improved its HgCdTe technology to open the way for High Operating Temperature systems that release the Stirling cooler engine power consumption.

Solutions for high performance detectors such as dual bands, much smaller pixel pitch or megapixels will also be discussed. In the meantime, the development of avalanche photodiodes or TV format with digital interface is key to bringing customers cutting-edge functionalities.

Since 1997, Sofradir has been working with Thales & Research Technologies (TRT) to develop and produce Quantum Well Infrared Photodetectors (QWIP) as a complementary offer with MCT, to provide large LW staring arrays. A dual-band MW-LW QWIP detector (25µm pitch 384?288 IDDCA) is currently under development. We will present in this paper its latest results.

8541-9, Session 3

Uncooled 17 µm 1/4 VGA FPA development for compact and low power systems

Jean-Luc M. Tissot, Patrick Robert, David Pochic, Vincent Gravot, Fabien Bonnaire, Hervé Clerambault, Alain Durand, Sebastien Tinnes, ULIS (France)

The high level of accumulated expertise by ULIS and CEA/LETI on uncooled microbolometers made from amorphous silicon enables ULIS to develop ? VGA IRFPA formats with 17µm pixel-pitch to enable the development of small power, small weight (SWAP) and high performance IR systems. ROIC architecture will be described where innovations are widely on-chip implemented to enable an easier operation by the user. The detector configuration (integration time, windowing, gain, scanning direction...), is driven by a standard I?C link. Like most of the visible arrays, the detector adopts the HSYNC/ VSYNC free-run mode of operation driven with only one master clock (MC) supplied to the ROIC which feeds back pixel, line and frame synchronizations. On-chip PROM memory for customer operational condition storage is available for detector characteristics.

Low power consumption has been taken into account and less than 70 mW is possible in analog mode at 60 Hz and < 175 mW in digital mode (14 bits). A wide electrical dynamic range (2.4V) is maintained despite the use of advanced CMOS node. The specific appeal of this unit lies in the high uniformity and easy operation it provides. The reduction of the pixel-pitch turns this TEC-less ? VGA array into a product well adapted for high resolution and compact systems.

Electro-optical performances of this IRFPA will be presented. We will insist on NETD trade-off with wide thermal dynamic range, as well as the high characteristics uniformity and pixel operability, achieved thanks to the mastering of the amorphous silicon technology coupled with the ROIC design. This technology node associated with advanced packaging technique, paves the way to compact low power system.

8541-10, Session 4

Latest developments for pixel size reduction of uncooled IR-FPA at CEA, LETI

Sebastien Becker, Pierre Imperinetti, Jean-Jacques Yon, Jean-Louis Ouvrier-Buffet, Valérie Goudon, Antoine Hamelin, Claire Vialle, Agnes Arnaud, CEA, LETI (France)

Recent developments at the Laboratoire Infrarouge (LIR) of CEA-LETI have been concentrated on the pixel size reduction of uncooled infrared detectors. With ULIS support, we have successfully demonstrated the technological integration of 12µm pixels on a commercial ULIS PICO 640 x 480 ROIC. The 12 µm pixel has been designed, processed and characterized in CEA-LETI and first results showed exceptional performances. This paper presents the characterization results and the imagery associated.

8541-11, Session 4

320 x 240 uncooled IRFPA with pixel wise thin film vacuum packaging

Jean-Jacques Yon, Geoffroy Dumont, Wilfried Rabaud, Sebastien Becker, Laurent Carle, Valérie Goudon, CEA, LETI, Minatec (France); Claire Vialle, CEA,LETI, Minatec (France); Antoine Hamelin, Agnès Arnaud, CEA, LETI, Minatec (France)

Silicon based vacuum packaging is a key enabling technology for achieving affordable uncooled Infrared Focal Plane Arrays (IRFPA) as required by the promising mass market for very low cost IR applications, such as automotive driving assistance, energy loss monitoring in buildings, motion sensors...

Among the various approaches studied worldwide, the CEA-LETI is developing a unique technology where each bolometer pixel is sealed under vacuum at the wafer level, using an IR transparent thin film deposition. This technology referred to as PLP (Pixel Level Packaging), leads to an array of hermetic micro boxes each containing a single microbolometer.

Since the successful demonstration that the PLP technology, when applied on a single microbolometer pixel, can provide the required vacuum < 1e-3 mbar, the authors have pushed forward the development of the technology on fully operational QVGA readout circuits CMOS base wafers (320 x 240 pixels).

In this outlook, the article reports on the electro optical performance obtained from this preliminary PLP based QVGA demonstrator. Apart from the response, noise and NETD distributions, the paper also puts emphasis on its key features such as thermal time constant, image quality, residual fixed pattern noise, aging properties and pixel operability.

8541-12, Session 4

Metamaterials for infrared microbolometers

Dean P. Neikirk, Jong Yeon Park, Hoo Kim, The Univ. of Texas at Austin (United States); Joo-Yun Jung, Korea Institute of Machinery & Materials (Korea, Republic of)

This paper will discuss a wide range of metamaterial absorbers for use in mid-wave and long-wave infrared microbolometers. These structures range from wavelength selective dielectric coated Salisbury screen to patterned resistive sheets to stacked multi-spectral devices. For basic three color devices in the LWIR band we have designed and fabricated wavelength selective dielectric coated Salisbury screen (DSS) microbolometers. In order to produce wavelength selective narrowband absorption, the general design rules for DSS microbolometers show that the thickness of the air gap should be a half wavelength and the optical thickness of the dielectric support layer should be a quarter wavelength. This structure is also air gap tunable; i.e., by varying only air gap thickness, the center wavelength of the absorption curve is shifted. FTIR microscope measurements have been made on a number of the different devices demonstrating three color capability in the LWIR while maintain very high efficiency absorption. We have also shown that the use of patterned resistive sheet metamaterials consisting of a properly sized array of cross-shaped holes acts as a polarization independent frequency-selective absorber allowing a three-color system spanning the 7-14 micron band. For realistic metal layers the skin effect produces a complex surface impedance that can be quite large in the LWIR band. We have shown that metal layers of thickness between one and three skin depths can act as the absorber layer, and have shown that thick metal layers can still produce excellent absorption in the LWIR. Holes in the dielectric support layer also reduce the thermal mass in the system without compromising spectral selectivity. Broadband designs using rectangular holes that produce substantially reduced thermal mass (over 50%) while maintaining efficient spectral absorption have also been found. Finally, we have considered multispectral stacked structures, including Jaumann absorbers and stacked dipole/slot metamaterials. These structures promise either two band (MWIR/ LWIR) or two to three color LWIR in a multi-layer stacked pixel.

8541-13, Session 4

Short-wave infrared InGaAsSb photodiodes grown on GaAs substrates

Andrew R. J. Marshall, Lancaster Univ. (United Kingdom); Kalyan C. Nunna, California NanoSystems Institute (United States); Siew Li Tan, The Univ. of Sheffield (United Kingdom); Charles J. Reyner, Univ. of California, Los Angeles (United States); Baolai Liang, California NanoSystems Institute (United States); Anitha Jallipalli, Univ. of California, Los Angeles (United States); John P. R. David, The Univ. of Sheffield (United Kingdom); Diana L. Huffaker, Univ. of California, Los Angeles (United States) and California NanoSystems Institute (United States)

We report on the growth, fabrication and characterisation of InGaAsSb p-i-n photodiodes with a high sensitivity in the short-wave infrared. Uniquely these photodiodes have been grown on a GaAs substrate using the interfacial misfit array technique. This technique accommodates the lattice mismatch between GaAs and GaSb at an abrupt interface, supporting the subsequent growth of high quality epilayers without the need for a metamorphic buffer layer. Crucially this abrupt interface maintains short molecular beam epitaxy growth times and hence commercial viability. The conditions to grown a quaternary alloy composition of In0.18Ga0.82As0.16Sb0.84, matched to GaSb, have been established and a homo-junction photodiode structure grown. This alloy gives a cut-off wavelength of approximately 2.4μm at room temperature.

Conventional mesa photodiodes have been fabricated using BCl3 dry etch chemistry and characterised at room temperature. We report a zero bias resistance area product, R0A, of 260 Ωcm2 and a responsivity of up to 0.8AW-1 without an anti-reflection coating. Furthermore leakage current characteristics are found to be essentially independent of device area down to the smallest diodes investigated in this work, which had a diameter of 25μm. Importantly the use of a dry etch and the observation of minimal surface leakage will support high density focal plane arrays with small pixels. The D* at zero bias is estimated to be 4.5x1010 Hz1/2W-1 which is approaching the best results reported for InGaAsSb detectors grown lattice matched on GaSb substrates. This demonstrates that the interfacial misfit array technique can be used to realise high performance, cost effective, infrared detectors on GaAs substrates.

The photodiodes reported here represent an exciting alternative to comparable InGaAsSb detectors grown lattice matched on GaSb substrates, strained InGaAs detectors grown on InP substrates or HgCdTe detectors. The use of cheaper GaAs substrates, available in larger diameters, and dry etch based fabrication are particularly desirable to support the drive towards larger area, high density focal plane arrays approaching gigapixel resolution.

8541-15, Session 5

A novel snapshot polarimetric imager

Gerald J Wong, Ciaran McMaster, Robert Struthers, SELEX Galileo Ltd. (United Kingdom); Alistair Gorman, Univ. of Glasgow (United Kingdom); Peter Sinclair, Robert A. Lamb, SELEX Galileo Ltd. (United Kingdom); Andrew R. Harvey, Univ. of Glasgow (United Kingdom)

Polarimetric imaging (PI) is of increasing importance in determining additional scene information beyond that of conventional images. For very long range surveillance, image quality is degraded due to turbulence. Furthermore, the high magnification required to create images with sufficient spatial resolution suitable for target recognition and identification require long focal length optical systems. These are incompatible with the size and weight restrictions for aircraft. Techniques which allow detection and recognition of a target at the single pixel level are therefore likely to provide advance warning of approaching threats or long range target cueing.

PI is a technique that has the potential to detect target signatures at the pixel level. Early attempts to develop PI used rotating polarisers (and spectral filters) which recorded sequential polarised images from which the complete Stokes matrix could be derived. This approach has built-in latency between frames and requires accurate registration of consecutive frames to analyse real-time video of moving targets. Alternatively, multiple optical systems and cameras have been demonstrated to remove latency, but this approach increases cost and bulk of the imaging system.

In our investigation we present a simplified imaging system that divides an image into two orthogonal polarimetric components, which can be achieved using Feldman prisms. These images are them simultaneously projected onto a single array. Thus polarimetric data is recorded without latency on a single snapshot. We further show that, for sub-pixel targets, the data derived from only two orthogonal states (H and V) is sufficient to increase the probability of detection whilst reducing false alarms compared to conventional unpolarised imaging. This approach requires accurate sub-pixel registration of the two images on the array, however, once calibrated this registration is fixed for far field objects at extreme range.

A degree of polarisation (DoP) is defined and computed for all pixels based on the polarisation states. The DoP is then used as a material discriminant to highlight anomalies. Our analysis includes the limitations imposed by dynamic range, ambient solar background, the intrinsic polarisation of optical elements, non-uniformity of response and noise. This allows us to assess performance of the system against range. Experimental data from both laboratory and real-world scenes have been analysed.

The optical system is easily modified to detect orthogonal circularly polarised states, which given the reduced cost of CMOS and CCD arrays and the increasing array sizes, makes the technique versatile and low-cost. We also discuss the prospects for including 1D and 2D spectral filter masks and computational image mosaicing to derive multi-spectral, polarimetric images on a single frame.

8541-16, Session 5

Polarimetric imaging for air accident investigation

Mark D. Ashe, Grant J. Privett, Defence Science and Technology Lab. (United Kingdom); Dennis Holland, JARIC - The National Imagery Exploitation Ctr. (United Kingdom); Matthew Greaves, Cranfield Univ. (United Kingdom); Les Davidson, Defence Science and Technology Lab. (United Kingdom)

We report a trial wherein a simple 4 CCD visible-band Polarimetric Imaging (PI) camera was fielded against aircraft debris distributed across an arid terrain, a littoral region and a small number of maritime debris targets.

A debris field realistically simulating an aircrash and a debris grid of aircraft remains were observed from an air platform flying in dry and sunny conditions.

We present a range of visualisations and processing techniques that aim to give the investigator the ability to more easily pick out debris and map it in a shorter time frame.

We report PI utility in support of air accident investigation by an enhanced ability to successfully locate small targets within the scene via the use of colour enhanced and decorrelated intensity PI images. Our results indicate that handheld PI capability may represent an effective low cost, upgrade and augmentation option for existing and future imaging systems that would support air accident investigators and assist in the cueing of more sophisticated assets and/or analyst attention.

8541-17, Session 5

OTHELLO: a novel SWIR dual band detection system and its applications

Gil A. Tidhar, Elta Systems Ltd. (Israel)

A fourth generation of SWIR based optical detection and warning means is presented as the EL/O - 5220 OTHELLO passive Optical Threat Locator, which detects and precisely finds directions towards a source of battle tank gun fire and missile (e.g. Anti-Tank Guided Missiles (ATGMs) Rocket Propelled Grenades (RPGs)) launch events in the battlefield.

OTHELLO hardware is described followed by an explanation of some inherent advantages of SWIR imagers as building blocks for optical detection systems mounted on ground military vehicles at harsh and demanding operating conditions. Finally we describe possible application of OTHELLO with radar systems.

8541-18, Session 5

Archeological treasures protection based on early forest wildfire multi-band imaging detection system

Benedict Gouverneur, Xenics NV (Belgium); Steven Verstockt, IBBT (Belgium); Eric J. Pauwels, Jungong Han, Paul M. de Zeeuw, Ctr. voor Wiskunde en Informatica (Netherlands); Jan P. Vermeiren, Xenics NV (Belgium)

No Abstract Available.

8541-19, Session 5

Acoustic and optical multisensor threat detection system for border patrol against aerial threats

Motasem S. Alsawadi, Ahmad Ismail, Munir M. El-Desouki, Sultan Alghamdi, Mansour Alghamdi, Mansour Alghamdi, King Abdulaziz City for Science and Technology (Saudi Arabia); Badeea F. Al-Azem, Alfaisal Univ. (Saudi Arabia)

Saudi Arabia has borders covering over 4,300 km that are shared with seven countries. Such large borders pose many challenges for security and patrol. Thermal imagers are considered the most reliable means of threat detection, however, they are quite costly, which can prevent using them over large areas. This work discusses a multi-sensor acoustic and optical implementation for threat detection as an effort to reduce system cost. The acoustic sensor provides position and direction recognition by using a four microphone setup. The data analysis of field tests will be discussed in this work.

8541-20, Session 6

A compact 2048x1536 pixel infrared imager for long distance surveillance

Claude Chevalier, Nathalie Blanchard, Anne Martel, Marc Terroux, Carl Vachon, Luc Mercier, Lucie Gagnon, Bruno Tremblay, Linda Marchese, Alain Bergeron, INO (Canada)

The evolution of infrared imaging technology has always followed, from a distance, the evolution of the technology in the visible waveband with ever increasing resolutions and decreasing pixel pitch. With such evolution the cameras in the visible are smaller than ever and display high quality imaging. Nowadays the size of the pixels in the infrared is generally much larger than its counterpart in the visible. However, the ratio of the size of the pixel to the wavelength is much smaller in the infrared than in the visible with the consequence that the gain on the pixel size could be limited considering today's rules of design.

In the infrared the recent advent of large 1024 x 768 pixel focal plane array based on 17 um pixel for the 8 to 12 um waveband raises challenges in the infrared development. Nevertheless, it was recently shown that sampling a scene at a frequency higher than the one corresponding to the pixel pitch is an efficient way of increasing the resolution of an image for given pixel size and FPA dimensions. Following this strategy a 2048 x 1536 pixel imager with integrated microscan was developed based on an uncooled bolometer FPA.

Due to its very small 8.5 um efficient pixel pitch the imager offers very high resolution and large field-of-view (FOV) using a short 50 mm focal length. Furthermore, since the size of the FPA is maintained at a reasonable size and the pixel pitch is very small the optics is compact and lightweight and the level of aberrations at the larger angles of the FOV is kept to a minimum offering excellent imaging quality. Such a platform could thus be used for very compact surveillance system and remote sensing instrumentation. This paper reviews the optics developed to perform the microscanned acquisition, the acquisition electronics and presents various examples of high-resolution imaging in various indoors and outdoors conditions. Finally, comparison of imaging with and without microscan is provided illustrating the usefulness of the microscan system despite the fact that the efficient pixel pitch is very close to the lower limit of the 8 to 12 um infrared waveband.

8541-21, Session 6

Evaluation of appropriate sensor specifications for space based ballistic missile detection

Caroline Schweitzer, Fraunhofer-Institut für Optronik, Systemtechnik und Bildauswertung (Germany); Norbert Wendelstein, Karin Stein, Fraunhofer Institut für Optronik, Systemtechnik und Bildauswertung (Germany)

The detection and tracking of ballistic missiles (BMs) during launch or cloud break using satellite EO-sensors is a promising possibility for pre-instructing early warning and fire control radars. However, the successful detection of a BM is depending on the applied IR-channel, as emission and reflection of threat and background vary in different spectral (IR-) bands and for different observation scenarios. In addition, the spatial resolution of the satellite based system also conditions the signal-to-clutter-ratio (SCR) and therefore the predictability of the flight path.

Generally available satellite images provide data in spectral bands, which are suitable for remote sensing applications and earth surface observations. However, in the fields of BM early warning, these bands are not of interest making the simulation of background data essential.

The paper focuses on the analysis of IR-bands suitable for missile detection by trading off the suppression of background signature against threat signal strength. This comprises a radiometric overview of the background radiation in different spectral bands for different climates and seasons as well as for various cloud types and covers. A brief investigation of the BM signature and its trajectory within a threat scenario is presented. Moreover, the influence on the SCR caused by different observation scenarios and varying spatial resolution are pointed out. The paper also introduces the software used for simulating natural background spectral radiance images, MATISSE ("Advanced Modeling of the Earth for Environment and Scenes Simulation") by ONERA[1].

[1] L. Labarre, K. Caillault, S. Fauqueux, C. Malherbe, A. Roblin, B. Rosier and P. Simoneau , "An Overview of MATISSE-v2.0", Proc. SPIE, Vol. 782802, doi:10.1117/12.868183 (2010).

8541-22, Session 6

Infrared detection, recognition and identification of handheld objects

Uwe Adomeit, Fraunhofer-Institut für Optronik, Systemtechnik und Bildauswertung (Germany)

A main criterion for comparison and selection of thermal imagers for military applications is their nominal range performance. This nominal range performance is calculated for a defined task and standardized target and environmental conditions. The only standardization available to date is STANAG 4347. The target defined there is based on a main battle tank in front view. Because of modified military requirements, this target is no longer up-to-date. Of interest today are different topics, especially differentiation between friend and foe and identification of humans.

There is no direct way to differentiate between friend and foe in asymmetric scenarios, but one clue can be that someone is carrying a weapon. This clue can be transformed in the observer tasks detection: a person is or is not carrying an object, recognition: the object is a long / medium / short range weapon or civil equipment and identification: the object can be named (e. g. AK-47, M-4, G36, RPG7, Axe, Shovel etc.). These tasks can be assessed experimentally and from the results of such an assessment, a standard target for handheld objects may be derived.

For a first assessment, a human carrying 13 different handheld objects was recorded at four different ranges using an IR-dual-band camera. From the recorded longwave data, a perception experiment was prepared. It was conducted with 10 observers in a 13-alternative forced choice, unlimited observation time arrangement. Before the experiment, the observers were trained to 100 % identification of the objects using visible target data. The results of the test together with Minimum Temperature Difference Perceived measurements of the camera and temperature difference and critical dimension derived from the recorded imagery allowed calculating the number of cycles on target needed for the defined tasks. Practically these cycle, dimension, and temperature difference data is already usable as

standard target and allows calculating the nominal range performance against handheld objects, but it has to be checked and refined in the future.

8541-23, Session 6

Electro-optical sensor with automatic suppression of laser dazzling

Gunnar Ritt, Bernd Eberle, Fraunhofer-Institut für Optronik, Systemtechnik und Bildauswertung (Germany)

The progress in laser technology leads to very compact but nevertheless powerful laser sources. In the visible and near infrared spectral region, lasers of any wavelength can be purchased. Especially continuous wave laser sources pose a serious threat to the human eye and electro-optical sensors due to their high proliferation and easy availability. The manifold of wavelengths cannot be encountered by conventional safety measures like absorption or interference filters.

We present a protection concept for electro-optical sensors to encounter dazzling in the visible spectral region. The key element of the concept is the use of a digital micromirror device in combination with wavelength multiplexing. This approach allows selective spectral filtering in defined regions of interest in the scene. The system offers the possibility of automatic attenuation of dazzling laser radiation. The algorithm comprises the analysis of the laser wavelength and the subsequent activation of the appropriate micromirrors.

8541-24, Session 6

Development of 6w at 95k single stage coaxial and inline pulse tube crycooler for infrared focal plane array applications

Xiang K Yang, yinong yi wu, ankuo an zhang, chao chao xiong, Shanghai Institute of Technical Physics (China)

A 6.0W@95K single-stage coaxial pulse tube cryocooler(CPTC) with the same size of inline pulse tube crycooler (IPTC)have been developed in Shanghai Institute of Technical Physics, Chinese Academy of Sciences (SITP/CAS) to provide reliable low-vibration cooling for the space-borne infrared focal plane array. The coaxial configuration result in a compact system and the inertance tube together with a gas reservoir serves as the only phase-shifting to realize a highly reliable system. The inline configuration result in a high efficiency system and the inertance tube with gas reservoir is also used as the phase-shift system.All of these two crycoolers' inertance tubes consists of two parts with different inner diameter and length to obtain the desirable phase relationship.The design and optimization are based on the theoretical computation fluid dynamic (CFD)software model developed by the analyses of thermodynamic behaviors of gas parcels in the oscillating flow. The simulation results get different critical sizes for the CPTC and the IPTC,but the two cold fingers are kept with the same size except for the phase shifting system in order to find the relationship of the CPTC and the IPTC. Both cold tip and warm flange integrated with fine slit heat exchanges fabricated with electro discharge machining technology to enhance heat exchange of the liquid and solid performance,and the three-dimensional ditributions of the temperature,pressure and velocity in these hot exchangers are present by the CFD soft ware fluent. The same split Oxford-type linear compressor with dual-opposed piston configuration is used to connect the each cold finger with a 30 cm flexible metallic tube.Both of our 8.2cc and 6.6cc compressors can serve perfectly for the CPTC and the IPTC ,8.22cc compressor with linear variables differential transformer (LVDT) is chosen to display the higher performance of the cold finger at 95K.LVDT has been used to analyze the pressure-flow phase angle in the practical system, which then compare with the simulated one and give the direction of optimization. The status of both types of the coolers are outlined, including those currently undergoing performance optimization, qualification investigation, and characterization. The preliminary experiments show that the coxial pulse tube has a cooling power of 6 W at 95 K with 101 W of input power at 300K reject temperature. And a cooling power of 6W at 95K with 89W of input power at 300K rejet temperature has been achieved. Base on theoretical and experimental studies, the configuration of the inline type pulse tube crycooler is slected as the engerning model at last for its high efficency,reliability and simplicity which makes it very attractive for space applications,and the overall weight including cooler control electronics is controlled below 10 kg.

8541-25, Session 7

Intracavity, common resonator, Nd:YAG pumped KTP OPO

James D. Beedell, SELEX Galileo Ltd. (United Kingdom) and Heriot-Watt Univ. (United Kingdom); David Legge, Ian F. Elder, SELEX Galileo Ltd. (United Kingdom); Duncan P. Hand, Heriot-Watt Univ. (United Kingdom)

An intracavity KTP OPO was demonstrated, which used a common resonator for the Nd:YAG pump light and output light. This high energy laser containing an intracavity OPO could be electrically switched to operate at 1.064 µm or 1.573 µm. By using common folding optics, automatic co-boresighting of both outputs was ensured. This design reduces part count and complexity when compared to an extracavity OPO design. An extracavity OPO arrangement requires setting up of the co-boresight which is susceptible to variation during harsh environmental conditions. A typical extracavity OPO using KTP has a conversion efficiency of 30%.

Initially a Nd:YAG ring resonator pump source with a separate intracavity KTP OPO resonator (plane-plane resonator of length 210 mm) was set up to investigate the efficiency. This initial testing was carried out using an existing 1.064 µm ring resonator. Efficient, damage-free output coupling via wavelength conversion was demonstrated. A conversion efficiency of 50% from 1.064 µm to 1.573 µm was achieved while producing 39 mJ at 1.573 µm for 78 mJ of pump light at 1.064 µm. Dichroic mirrors were used to separate the OPO from the 1.064 µm resonator. Their insertion loss together with the OPO crystals resulted in a 15% drop in 1.064 µm output energy.

A common resonator intracavity OPO was then constructed with a length of approximately 750 mm. However, the OPO now shares all the same folding elements as the main 1.064 µm resonator and, since there is no walk-off in non-critically phase matched (NCPM) KTP, the 1.573 µm output is automatically co-boresighted. Wave plates were used to set hold-off and then the Q-switch voltage was used to control output reflectivity. An additional wave plate was used to optimise output coupling at 1.573 µm, while the 1.064 µm output coupling was maximised.

The Q-switch is AR coated for 1.064 µm only, with a measured loss of 6% at 1.573 µm and the loss through the zig-zag Nd:YAG slab, for p-pol incident light at 1573 nm wavelength was measured to be 9%. All other components are low loss at both wavelengths. Total round-trip loss at 1573 nm wavelength was estimated to be approximately 20%.

The maximum conversion efficiency for the common resonator geometry was 27% with a maximum output energy of 24 mJ at 1.573 µm. The co-boresight of the 1.064 µm and the 1.573 µm wavelength far field beam image centroids was 137 µRad in the horizontal axis and 16 µRad in the vertical axis. This represents 4% of the 1.064 µm beam divergence.

The intracavity OPO was therefore shown to produce superior conversion efficiency when compared with a typical extracavity OPO, when using a separate resonator. When using a common resonator the conversion dropped to 27%, which is comparable to an extracavity OPO. Full results of the OPO characterisation will be presented, including routes to full optimisation of the common resonator intracavity OPO design.

8541-26, Session 7

Athermal diode-pumped laser designator modules for targeting application

Bruno Crépy, Guillaume Closse, José Da Cruz, David Sabourdy, Luc Nguyen Duy, Jean E. Montagne, CILAS (France)

We report on the development and characteristics of athermal diode-pumped designator modules as Original Equipment Manufacturer (OEM) for targeting application. These modules are designed with the latest diode-pumped technology minimizing volume and power consumption.

The core technology allows to address multi-platforms requirements such as land or airborne. Products are composed of a Laser Transmitter Unit (LTU) and Laser Electronic Unit (LEU) for modular approach.

8541-30, Session 7

3D sensor for indirect ranging with pulsed laser source

Danilo Bronzi, Simone Bellisai, Federica A. Villa, Carmelo Scarcella, Andrea Bahgat Shehata, Alberto Tosi, Giorgio M. Padovini, Franco Zappa, Politecnico di Milano (Italy); Daniel Durini, Sascha Weyers, Werner Brockherde, Fraunhofer-Institut für Mikroelektronische Schaltungen und Systeme (Germany)

Over the last few years there has been a growing interest for fast, compact and cost-effective 3-D ranging imagers for security and safety applications, automotive, object tracking, face recognition and virtual reality. Techniques based on interferometry and triangulation require a precise optical setup preventing them to be portable and easily usable. Instead CMOS imagers that exploit phase-resolved techniques provide accurate 3D ranging, without complex optics, and are rugged and cost effective. Phase-resolved techniques indirectly measure the round-trip return of the light emitted by a laser and back-scattered from a distant target, computing the phase delay between the modulated light and the detected signal. The modulation can be either sinusoidal or pulsed, and the requirements of the light source and optical setup are more relaxed than for direct Time-of-Flight measurements. Single-photon detectors, with their high sensitivity, allow to employ a low power excitation (less than 10W with diffused daylight illumination) to actively illuminate the scene. We present a 4x4 array of CMOS SPAD (Single Photon Avalanche Diodes) fabricated in a high-voltage 0.35 μm technology, for pulsed-light modulation where each pixel computes the phase difference between the laser pulse and the reflected one. Each pixel (150 μm x 150 μm) comprises a high performances SPAD (30 μm diameter, noise of less than 15 counts/s, 50% efficiency at 410 nm), an analog circuit that rapidly quenches the avalanches and resets the detector, two 9 bit up-down counters, memories to store data during the readout, and output buffers. The first counter counts the photons detected by the SPAD in a time window synchronous with the laser pulse and integrates the whole echo signal. The second counter accumulates the number of photon detected in a window shifted with respect to the laser pulse, and acquires only a portion of the reflected signal. In order to extract the correct distance measurement, background light is subtracted from the two counters: to this purpose, both counters operated in down mode during a third window in which no laser pulse is emitted, just to collect background photons. External signals individually enable the two counters and control the counting direction (up or down). Pixels can achieve a counting rate of 20 Mcouts/s. Since the laser pulse duration is strictly dependent on the required range (i.e. pulse duration is set equal to the time necessary to a photon to cover the entire maximum round-trip), many frames must be acquired to obtain the depth information, with an adequate signal-to-noise ratio. The array is readout with a global shutter architecture (this is made possible by the in-pixel integration of latches to store counters data), with a 100 MHz clock the maximal frame rate is 3 Mframe/s. We presents the results of such a 3D CMOS SPAD camera in 3D ranging at medium distances (few tens of meters) in low light conditions.

8541-31, Session 7

Development of highly compact and low power consumption athermal military laser designators

Andrew Sijan, SELEX Galileo Ltd. (United Kingdom)

The utility of military lasers, particularly in the area of laser designation for laser-guided weapons, is well understood. Laser systems based on Nd:YAG have been fielded since the 1980's and over the last three decades have introduced incremental technology steps to improve performance and weight.

These include the four technology waves from the origin as (1) flash-lamp-pumped, liquid cooled, cylindrical rod to (2) introduction of the zig-zag slab to (3) introduction of diode pumping and (4) introduction of the athermal laser and multi-coloured and/or broad-band diode pumping

The most recent technology step has been the introduction of athermal lasers based on laser-diode pumping of Nd:YAG and products are now emerging for use on the battlefield. The technical performance, efficiency, size, weight and power for these lasers, has been key to driving the new production designs.

The athermal laser has allowed dramatic improvements in size, weight and in overall power consumption. For example, in the case of man-portable laser designators, from ~6 litres to ~2 litres in size, from ~5kg to 2kg in weight and from ~150W to ~65W in power consumption.

In this paper, we review the development of the laser designs and their introduction since the advent of laser designation. In particular, we compare the relative performance and characteristics over the evolution of fielded laser designators.

Moreover, we will review the key building blocks for the design of athermal lasers and describe some critical design issues for engineering and productionisation of a military laser system, including removal of thermal lensing, novel diode-pumping schemes and robustness over the environment.

A side-pumped zig-zag slab pumping scheme will be described, showing near elimination of thermal lens, consistent divergence performance over temperature (-40 to +60C) and PRF (up to 20Hz).

This will be exemplified using results from the development of the SELEX Galileo Type 162 and Type 163 Laser Target Designators. These will cover not only technical performance, power and efficiency, but also thermal management, mass, volume, cost and overall complexity for manufacture.

The key performance features of the Type 163 laser will be described, including laser performance parameters, such as energy, divergence and boresight performance over environment, and physical aspects such as size, weight and modular architecture.

8541-32, Session 7

IR thermography methods in detection of buried mines

Waldemar Swiderski, Pawel Hlosta, Maciej Miszczak, Military Institute of Armament Technology (Poland)

Thermography is one of many techniques used for nondestructive testing for which both passive and active approach could be taken. The passive approach is effective for materials and structures which are naturally at a different temperature than the environment. The active approach requires an external heating source to stimulate the materials or structures to be tested. These methods can be also applied to detect mines hidden in the ground. Passive approach is used when natural heating of soil by sun radiation is exploited. In the case of active approach it is used an external heating source for example a microwave source to provide thermal stimulation. In this paper the results of our experiments with both methods carried out in the laboratory set-up and in the outdoor measuring field are presented.

8541-33, Session 8

High dynamic range compression for visualization of IR images in maritime scenarios

Alessandro Rossi, Università di Pisa (Italy); Nicola Acito, Accademia Navale di Livorno (Italy); Marco Diani, Giovanni Corsini, Univ. di Pisa (Italy)

In modern infrared (IR) cameras low noise-equivalent temperature difference (NETD) combined to large differences of temperatures in typical surveillance scenarios, leads to store sensed images on a large number of bits (up to 16 bits). For this reason, IR images have a high dynamic range (HDR) with respect to both 8-bit displays and the human visual system. In this framework, the design of suitable techniques is required to display IR images on standard monitors, with the aim of improving the visibility of objects of interest.

The issue of HDR compression has already been studied in relation to images acquired in the visible light, while for IR only in recent years the problem of visualization has been handled by a few works which refer to modifications and improvements of the methods designed for the visible region. In this context, it is worth noting that most of the visualization techniques developed for IR images tightly depend on the operating scenario, on the properties of the imaging system and on the application of interest. Generally, the development of new techniques has to be carried out in regard of the specific application.

The methods proposed in the literature for the visualization of HDR images can be distinguished into two broad classes: contrast

enhancement (CE)-oriented techniques and dynamic range compression (DRC)-oriented techniques. The former operate on image contrast to improve the perceptibility of details and can be applied for HDR visualization by scaling the mapping function to match the number of digital levels of the output display. The latter reduce the signal dynamic by using different approaches to attenuate the large-scale intensity changes that do not contain relevant information. In the class of CE-oriented techniques, histogram equalization (HE)-based methods represent the most common approach used for contrast enhancement, due to good performance and small computational load. Techniques based on HE can be implemented in two different manners: global HE-based methods and adaptive HE-based methods. While global HE-based methods operate on the entire image, obtaining simple algorithms, but often not effective, adaptive HE-based methods locally adapt the equalization curve, typically using block-based approaches to compute the histogram.

In this work, CE approach based on HE is addressed and improved for HDR compression for the visualization of IR images sensed in a maritime scenario. A new method is presented that combines contrast enhancement and dynamic range compression. The proposed technique operates HE on the basis of clustering information assigning the output display levels in relation to the informative content of each cluster.

The performance of the proposed technique is analyzed using maritime IR images acquired in different case studies conditions. The comparison has been carried out using HE-based techniques previously proposed in the literature for the issue of HDR compression. Moreover, the evaluation is performed through subjective analysis too with a mean opinion score approach. The results show the effectiveness of the proposed technique in terms of details enhancement, robustness against the horizon effect and presence of very warm objects.

8541-34, Session 8

IR-videostream rendering based on high-level object information

Stefan Becker, Wolfgang Hübner, Michael Arens, Fraunhofer-Institut für Optronik, Systemtechnik und Bildauswertung (Germany)

IR-sensors are mainly utilized in video surveillance systems in order to provide vision during nighttime and in diffuse lighting conditions. The dynamic range of IR-sensors usually exceeds the dynamic range of conventional display devices. Hence, range compression associated with loss of information is always required. Range compression methods can be divided into global methods, which take the full intensity distribution into account, and local methods focused on smaller regions of interest. In contrast to local methods, global methods are computationally efficient. Nevertheless, global methods have the drawback that fine details are suppressed by intensity changes at image locations which are unrelated to the object of interest. For example, in surveillance tasks it may become difficult to decide whether a person is carrying equipment or not.

In order to overcome these restrictions, we propose a method to render IR images based on high level object information. The overall processing pipeline consists of a gradient based contrast enhancement method, followed by appearance based object detection, and a range compression method that takes the location of objects into account. Here, the representation of a specific object category relies on local feature and we choose pedestrians as an exemplary object category. The output of the person detector is a rectangular bounding box, centered at the person location.

Restricting the range compression to this person location, allows to display fine details on the person surface, e.g. carried objects, that most probably stay undetected using global range compression methods.

Without precise person segmentation local range compression is always affected by background information. Therefore the best possible result can be achieved by only considering intensities from foreground pixels. We compare the influence of background information, originating from the person detection method, on three different range compression methods. These are histogram equalization, linear quantization and a linear superposition of both methods, which has been shown to generate superior results. Comparison is done in two ways.

First, we compare the deviance between an ideal segmentation based quantization to quantization affected by background intensities. Furthermore the accuracy of the bounding box also depends on a temporal component. In compliance with this, we secondly evaluate the temporal stability of the quantization on a video sequence recorded with long-wave infrared sensors from a moving vehicle, reflecting a prototypical surveillance scenario.

The proposed combination of rendering with high level information is intended to be integrated in an advanced surveillance system to assist human operators. Towards this end, the paper provides several insights in the design of a visualization tool. By simply distinguishing regions in the overall image the method aims to help operators in improving their assessment of a situation without distracting them.

8541-35, Session 8

3D building structure generation from digital aerial images

Gaojin Wen, Beijing Institute of Space Mechanics and Electricity (China); Guijuan Zhang, Shenzhen Institute of Advanced Technology (China); Weiwei Zhang, Zhaorong Lin, Yigang Yao, Qian Zhang, Beijing Institute of Space Mechanics and Electricity (China)

Recently, the aerial triangulation has become a popular method for analyzing digital aerial images to calculate the 3-dimensional coordinates of object points. Many variants of aerial triangulation based on different features including linear, region and spectral properties, are proposed to improve the robustness of the method. Noise existed in the feature matching of adjacent images will affect the accuracy of the 3D reconstruction significantly. It is challenging to acquire the 3D building structure of high accuracy from digital aerial images, about which little literature is concerned.

This paper describes an automatic method of generating 3D building structure accurately from multispectral digital aerial images. First, scale-invariant feature transform (SIFT) is calculated for each digital aerial image, and is used to register the aerial images. Since the SIFT feature points are 2D and the height dimensional is missing, the resulting registration parameter will suffer from some obvious noise. Second, a specific layer for the building region in the multispectral images is obtained by classifying the spectral information. Line features are extracted from the resulting layer and divided into building structures according to their locations. Most of the 3D reconstruction lines from the lines features that belonging to one building are mutually perpendicular or parallel. Based on this assumption, the height of the building is estimated according to position and orientation of the camera, solar elevation angle and the shadow region besides the building, which will be used as initial value for optimization of the 3D building structure in the next step. Third, an iterated matching method is proposed to generate the accurate matching parameter between the aerial images and the 3D building structures through nonlinear optimization. The object function is a total weighted error of the approximate solution to an equation system, which is established by the projection equations for each building structure. This object is optimized by three steps during each iteration. First, the position and orientation of the camera for each image is refined according to the projection errors of all the building structures in this image. Second, the height dimensional of the building structure is calculated with the newly generated camera parameters. Third, the registration transform will be refined based on the corresponding matching feature points, which are assigned a weight depending on their fitness to the registration. Good fitness leads to large weight and accurate registration.

It is proved that the proposed method is convergent.

The implementation of our method is straightforward and the complexity of the computation is low. A data set acquired over the city of Dongying in R.P. China of autumn 2011 is used to testify the proposed method, which consists of 306 images flown in 5 strips. The along-track-overlap of this data set is 80%, and the across- track overlap is approximately 60%. The ground sampling distance (GSD) is around 6 cm. The performance and efficiency of our method is evaluated and analyzed. Results show that the presented method is highly efficient in generating 3D building structure accurately and automatically.

8541-36, Session 8

A hardware Kalman-based offset estimator for nonuniformity correction on IRFPA

Miguel E. Figueroa, Javier Contreras, Rodolfo Redlich, Sergio N. Torres, Univ. de Concepción (Chile)

Mismatch in the fabrication of the photodetectors of an Infrared Focal Plane Array (IRFPA) and its readout circuitry causes variations in the response of each detector to the same stimulus. Moreover, because the IRFPA operates in the IR spectral band, this non-uniformity (NU) in the spatial response of the photodetectors is accentuated by the random nature of the incident flow of photons and the low signal-to-noise ratio of the incident photons (with respect to the so-called dark-current noise). Consequently, an IRFPA is unable to respond in a uniform fashion when a spatially flat object is employed as a radiation source. The NU manifests itself as a spatially regular source of noise, typically modeled as a gain and offset for each detector, and is sufficiently strong to render the output of the IRFPA unusable unless it is properly corrected.

This paper presents the hardware implementation of a Kalman filter to estimate the NU noise and correct it in real time. Implementing the algorithm in hardware results in a fast, compact, low-power NUC system that can be embedded into an intelligent imager at a very low cost. Because it does not use an external reference, our nonuniformity correction (NUC) circuit works in real time during normal operation, and can track NU parameter drift over time.

Our NUC system models NU noise as a spatially regular source of additive noise, and assumes that the multiplicative effect is negligible. It uses a Kalman filter to estimate an offset for each detector in the array and applies an inverse model to recover the original information captured by the imager. Our experimental setup uses a CEDIP Jade UC33 IR camera, which delivers a 320x240-pixel image at 30 frames per second (fps). Because the digital output of the camera uses a proprietary USB protocol, we use a video acquisition circuit built around an Analog Devices ADV7183B chip, which delivers pixels to the NUC board using a 13.5MHz clock. Our NUC board is built around a low-cost Xilinx Spartan 3E XC3S500E FPGA. The architecture uses fixed-point arithmetic, with 16 bits (8-bits integer and 8-bits fractional) for most of the data and 19 bits (1-bit integer and 18-bits fractional) for the Kalman gains. The NUC circuit operates at 75MHz (currently limited by the pixel input rate), and consumes 17mW of dynamic power, while also accounting for 11mW of the static power of the chip. The circuit uses only about 10% of the logic resources of the FPGA, thus enabling the integration of NUC with other higher-level image processing tasks such as face recognition and tracking, temperature estimation, etc.

Despite ignoring the multiplicative effects of nonuniformity, our Kalman-based NUC circuit achieves a Peak Signal-to-Noise Ratio (PSNR) of 35dB in under 50 frames, referenced to two-point calibration using black bodies. This performance lies within 0.5dB of a double-precision Matlab implementation of the algorithm. Restricted only by the bandwidth of the external RAM that stores the offset estimations, our circuit can correct 320x240-pixel video at up to 1,250 fps.

8541-37, Session 8

Digital image processing techniques for uncooled LWIR thermal camera

Thiago Bittencourt, Centro Tecnologico do Exercito (Brazil); Adilson Gonzaga, Univ. de São Paulo (Brazil)

This paper aims to present the research and development of digital image processing algorithms for uncooled LWIR thermal camera in Brazil. The study of an infrared thermal camera is a strategic issue since that has more and more applications in military, judicature, rescue, industry, hospital and science areas. Infrared imaging systems often suffer from problems of low image quality that limit the overall performance of the system. This paper describes the design and implementation of all image-processing algorithms required to obtain high-performance images with low noise and high contrast, such as: functions for non-uniformity correction of sensor deficiencies, dead-pixel replacement algorithms, histogram generation, contrast enhancement methods and output pixel processing with frame rate of 30 frames per second based on 320 x 240 Uncooled Focal Plane Array (UFPA). Since that the implementation of algorithms in hardware is a difficult and time-consuming process, in this work all algorithms was implemented in software to get results quickly and to facilitate the validation of computer codes. The digital image processing of the prototype infrared camera is configured in three separate units: a signal acquiring unit, signal processing unit and electro-optical characterization. The last one presents some results of electro-optical characterization on the assembled system, indicating the main figures of merit that guide the study of this technology, such as: 3D noise components, noise equivalent power (NEP), signal transfer function (SiTF) and noise equivalent temperature difference (NETD). The results indicate that the proposed image-processing algorithms increase the quality of the corrected image, and the test results through the 16 bits digital video of the infrared camera show that all metrics are in accordance with its nominal value.

8541-29, Session PS

Speckle reduction of polarization image using CLEAN algorithm

Xuguo Zhang, Zhaorong Lin, Li Wang, Beijing Institute of Space Mechanics and Electricity (China)

Laser is utilized as the illumination equipment for laser polarization remote sensing. Because of its high coherence, black and white spots (speckle) will be produced when imaging targets whose surface is rough compared with optical wavelength. These speckles have no relation with target macro scattering characteristics. However, existence of speckles makes the image quality degrade and resolution decrease, which will form false targets and mistake judgments. Ability of target detection and recognition is greatly deteriorated due to the influences of the speckles. In this paper, CLEAN algorithm is applied to reduce and eliminate laser polarization image speckle. Imaging method is employed to calculate the system step response. Its point spread function (PSF) is derived through the derivative of step response, i.e., “dirty” pulse. The ideal PSF is fitted using Gaussian function, i.e., “clean” pulse. Anti-convolution is done on “dirty” image with “dirty” pulse to obtain the δ pulse distribution of target by using CLEAN algorithm. Finally, target δ pulse distribution convolutes with “clean” pulse to get the ideal image of target. In order to prove the availability of CLEAN algorithm on spectral reduction, equivalent number of looks (ENL) is defined, which describes the filter capability on speckle reduction. By compared images quality and ENL processed with CLEAN algorithm, Perona-Malik (P-M) nonlinear diffuse function, and super resolution method, we can conclude that CLEAN algorithm has the greatest effectiveness on polarization image speckle reduction.

8541-45, Session PS

Design and implementation of digital airborne multispectral camera system

Zhaorong Lin, Xuguo Zhang, Li Wang, Deai Pan, Beijing Institute of Space Mechanics and Electricity (China)

The multispectral imaging equipment is a kind of new generation remote sensor, which obtains the target image and spectra information simultaneously. A digital airborne multispectral camera system using discrete filter method has been designed and implemented for unmanned aerial vehicle (UAV) and manned aircraft platforms. It has the advantages of larger frame and higher resolution. It also has great potential applications in environmental and agricultural monitoring and target detection and discrimination areas. The system is composed of camera window, lens, filter components, CMOS imager, position and orientation system (POS), control and management circuit, temperature control unit, image acquisition and storage device, and ground image processing unit. The camera has the characteristics of panchromatic and multispectral imaging. The filter components contain ten filters for spectral division, one for panchromatic band and nine for multispectral band. Each filter on a filter wheel is inserted into the optical path successively driven by a motor. Camera is initialized (CMOS output mode, shutter speed for every band and filter wheel speed) before imaging. Exposure pulse is triggered when the center of the filter and CMOS is in a line. Image data is transmitted to image storage device through Camera Link interface. Data of image spectral band, aircraft attitude (pitch, roll, and yaw), position (longitude, latitude, and altitude), and time is transmitted to storage device through RS-232, which will be added at end of each image data to form a raw image file. And then, image and assistance information affixed at end of the images is stored in the high speed and mass

capacity storage device. The affixed data is utilized for image geometric correction and positioning.

In order to reduce the system dimension and weight, filters are installed before the CMOS sensor, where it could be made the system smallest size. Optical lens is designed as telecentric optical system so that spectral shift caused by the incident angle on filter could be reduced. Inertial sensor is installed near the rotation center of the camera to get accurate attitude data expressed in Euler angles, and the GPS antenna is placed outside of the aircraft to receive position, altitude and velocity data. Window frost and fog caused by temperature decrease with the height increase can be avoided by temperature control to enhance image quality. The filter speed is adjusted as the velocity to height ratio to guarantee the overlap ratio of same spectral band is larger than 30%. And the lateral overlap ratio is larger than 10% of the frame width, so that we could use these image data to make a large frame picture, do image fusion of different spectral bands.

Flying experiment was conducted to demonstrate the functionality and performance of the multispectral camera. Image processing was done to illustrate the capability of target detection and classification. The experimental results show that camera satisfy the design requirements.

8541-47, Session PS

Comparative analysis of high-performance infrared avalanche InxGa1-xAsyP1-y and Hg1-xCdxTe heterophotodiodes

Mikhail S. Nikitin, Alpha (Russian Federation); Viacheslav A. Kholodnov, Albina A. Drugova, Institute of Radio Engineering and Electronics (Russian Federation); Galina V. Chekanova, Alpha (Russian Federation)

Technology of infrared (IR) avalanche photodiodes (APDs) gradually moves from simple single element APD to 2D focal plane arrays (FPA). Spectral covering of APDs is expanded continuously from classic 1.3 μm to longer wavelengths due to using of narrow-gap semiconductor materials like Hg1-xCdxTe.APDs are of great interest to developers and manufacturers of different opticalcommunication, measuring and 3D thermal imaging systems. Major infrared detector materials for manufacturing of high-performance APDs became heteroepitaxial structures InxGa1-xAsyP1-y and Hg1-xCdxTe. Progress in IR APD technology was provided by serious improvement in material growing techniques. Today design of APD with separate absorption and multiplication regionsthat may provide the best performance and customer properties of APD can be realized both on InxGa1-xAsyP1-yand Hg1-xCdxTe multilayer heteroepitaxial structures.To create the best performance optimal design avalanche heterophotodiode (HAPD) it is necessary to carry out a detailed theoretical analysis of basic features of generation and multiplication of charge carriers in proper heterostructure.Optimization of HAPD properties requires comprehensive estimation of HAPD's pixel performance depending on pixel's multi-layer structure design, structure layers doping, distribution of electric field and operating temperature. Objective of the present work was to develop general approach for analytical description of basic processes in HAPDs and compare potential of HAPDs based on InxGa1-xAsyP1-y and Hg1-xCdxTe.

8541-48, Session PS

Design of large-field hyperspectral imaging system

ZhengHui Zhang, Beijing Institute of Space Mechanics and Electricity (China)

Based on the demand of SWIR hyperspectral sensor, a spectral imaging system is designed in this paper. Offner spectral imging system which can be divided into two types: prism and grating, is researched, for the large field and high spectral resolution of the sensor, and method to filter secondary spectrum is also discussed. The result shows, compared to Offner spectral imaging system with prisms, Offner spectral imaging system with gratings not only have high spectral resolution(8nm), large flat field(60mm), little spectral smile and keystone(1%), but also can satisfy the need of hyperspetral sensor that the system can be mounted on small or mini satellites.

8541-49, Session PS

The technology of non-uniformity correction for mid-infrared channel based on adjusting integration time to acquire imaging of single and uniform radiation field

Zhicheng Shi, Beijing Institute of Space Mechanics and Electricity (China)

According to the analysis of system noise for mid-infrared channel (including photon noise, dark current, temperature noise, amplifier noise and quantized noise), consider that non-uniformity correction of mid-infrared channel is achieved by adjusting integration time of detector to acquire imaging of single and uniform radiation field, after dark current and temperature noise of detector with circuitry being controlled on certain level. Specific method as follows, mid-infrared remote sensor photograph target which is a single and uniform radiation field. Numbers of images of uniform radiation field are acquired by adjusting integration time of detector. Non-uniformity correction parameters are computed in two methods which are two calibration algorithm and multi-point calibration algorithm. Non-uniformity correction of mid-infrared imaging is implemented from correction parameters. Residual image of non-uniformity correction imaging of uniform radiation field is used to evaluate correction effect. Comparing with previous method based on calibration of different radiance field, a difference of correction effect is less than 1%. Finally consider that adjusting integration time of detector to acquire imaging of single and uniform radiation field can be used to implement non-uniformity correction of mid-infrared channel.

8541-50, Session PS

Determination of range parameters of observation devices

Jaroslaw Barela, Mariusz Kastek, Krzysztof Firmanty, Piotr Trzaskawka, Rafal Dulski, Juliusz Kucharz, Military Univ. of Technology (Poland)

Range parameters of observation devices can be determined on the basis of numerical simulations (NVTherm) or on the basis of measured characteristics. Those measurements can be conducted in both laboratory and field conditions. It is, however, difficult to carry on reliable field measurements of range parameters because they are strongly depended on atmospheric conditions. Thus the laboratory measurements are more favorable option.

Analysis of literature and catalogue specifications reveal, that range parameters are given mainly on the basis of Johnson criteria or TTP model. The Johnson criteria has been used since the 50s and most of catalogue range specifications are determined according to it. There are also NATO standards, which describe the measurement procedures and methodology required to define the detection, recognition and identification ranges for standard NATO targets. For the determination of range parameters the following device characteristics must be known: minimal resolvable temperature for thermal imaging devices and minimal resolvable contrast for VIS devices.

The TTP model offers a new approach to the determination of range characteristics of observation devices. It has been developed by U.S. Army's Night Vision and Electronic Sensors Directorate since the year 2000. It was created because the modified Johnson criteria did not yield reliable results in case of modern systems with digital image processing. In order to determine the range parameters using TTP model, the modulation transfer function MTF, pre-sample MTF function, and 3D noise of a tested system must be known as well as its basic design data as optical magnification and display type.

The paper describes the measurement stand, measurement methodology and the procedure for the determination of range parameters. The results for thermal and VIS cameras are also presented, and they are analyzed and compared with the results obtained from current methods, including the measurement uncertainty figures. Some suggestions on the methodology of measurements are also given.

8541-51, Session PS

360° panoramic dynamic data acquisition system based on unmanned helicopter

Yigang Yao, Beijing Institute of Space Mechanics and Electricity (China); Shuguang Zhao, Tianjin Aurora UAV Technology Co., Ltd. (China); Zhaorong Lin, Gaojin Wen, Qing Zhang, Weiwei Zhang, Beijing Institute of Space Mechanics and Electricity (China)

In recent years, the archaeological tourism has rapidly been developed. However, the scope of the human activities has been restricted by complicated geographical terrain, and the popularization of archaeological tourism has been hampered. For the purpose of solving this problem, the 360°panoramic dynamic data acquisition system based on unmanned helicopter is proposed. The system consists of the unmanned helicopter module, the multi-modal monitoring module, data transmission module and vehicle real-time information processing module. The multi-modal monitoring module is composed of four interchangeable optical remote sensors, which include ultra-wide-angle visible light remote sensor, infrared wide-angle remote sensor, multi-spectral remote sensor and high-resolution remote sensor, and according to the different monitoring tasks, the different optical remote sensor will be replaced on the unmanned helicopter. In the data transmission module the image information can be decomposed to transmit in different channel by multi-channel data transmission technology, the image information will be combined after the data receiver getting them. The whole system is carried on the vehicle, and vehicle real-time information processing module can control the helicopter's flight according to the feedback information of the data processing, at the same time the information can be processed in real-time by the automatic image mosaic technology in order to monitor the surrounding environment, and the target localization and measure can be acquired at vehicle real-time information processing module.

The unmanned helicopter has the characteristics of the less vertical take-off and landing footprint, the low require of the topographical condition, the hovering in the air and the high-accuracy measurement, therefore the panoramic dynamic monitor employs the unmanned helicopter as the load platform, and the various optical remote sensors, the technique of the image processing and the image transmission are also exploited. So the images which are combined with mapping, information of the remote sensing and geography are acquired, and we can get the system with holism, real-time, dynamic monitor, analysis and application. During the archaeological tourism, the unmanned helicopter, optical remote sensor and the equipments of image processing and image transmission are placed in the vehicle, when we want to monitor the region where the vehicle and the people can not get, the unmanned helicopter equipped with optical sensor is imposed for panoramic real-time monitoring, and we can obtain the valid information by the image transmitted and processing. The application of the 360°panoramic dynamic data acquisition system based on unmanned helicopter may facilitate the development of the archaeological tourism.

Finally, this 360°panoramic dynamic data acquisition system based on unmanned helicopter has been applied in the archaeological tourism of the Chinese Ming Dynasty Great Wall, and the real-time 360°panoramic dynamic images are obtained, and this outcome indicates that our system can greatly increases the scope of the archeological tourism activities and contributes to the further development of human civilization.

8541-52, Session PS

Testing of hardware implementation of infrared image enhancing algorithm

Rafal Dulski, Tomasz Sosnowski, Piotr Trzaskawka, Mariusz Kastek, Taduesz Piatkowski, Juliusz Kucharz, Military Univ. of Technology (Poland)

The interpretation of IR images depends on radiative properties of observed objects and surrounding scenery. Skills and experience of an observer itself are also of great importance. The solution to improve the effectiveness of observation is utilization of algorithm of image enhancing capable to improve the image quality and the same effectiveness of object detection. The paper presents results of testing the hardware implementation of IR image enhancing algorithm based on histogram processing. Main issue in hardware implementation of complex procedures for image enhancing algorithms is high computational cost. As a result implementation of complex algorithms using general purpose processors and software usually does not bring satisfactory results. Because of high efficiency requirements and the need of parallel operation, the ALTERA's EP2C35F672 FPGA device was used. It provides sufficient processing speed combined with relatively low power consumption. A digital image processing and control module was designed and constructed around two main integrated circuits: a FPGA device and a microcontroller. Programmable FPGA device performs image data processing operations which requires considerable computing power. It also generates the control signals for array readout, performs NUC correction and bad pixel mapping, generates the control signals for display module and finally executes complex image processing algorithms. Implemented adaptive algorithm is based on plateau histogram equalization. Tests were performed on real IR images of different types of objects registered in different spectral bands. The simulations and laboratory experiments proved the correct operation of the designed system in executing the sophisticated image enhancement.

8541-53, Session PS

narcissus analysis of cooled IR optical system with multi-magnification in wide field of view

Jinsuk Hong, Youngsoo Kim, Samsung Thales Co., Ltd. (Korea, Republic of)

The cooled IR system with multiple-magnification including wide-field of view (WFOV) and narrow-field of view (NFOV) has some weakness in the point of inner reflection. First of all, this system uses one large objective lens as a common optical component in both WFOV and NFOV. However, WFOV mainly uses the center portion of the large objective lens, and the system feels the component almost flat. Direct inner reflection to the detector can occur at this component since the component lies perpendicular to the line of sight. Secondly, the system should be working in harsh condition, and consequently main objective lens needs to have a DLC (Diamond-Like Carbon) coating with relatively high reflectivity, which can work as a main source of stray light such as ghost images and narcissus.

This paper is focused on the stray light analysis for unwanted reflected bright source and its removal. To analyze the system's artifacts more effectively, we used mechanical structures constructed from IDEAs and Optical system from CODE V. We analyzed the system in ASAP and found some candidates for the image degradation and effectively identify the optical paths of these artifacts. Finally, we can confirm the stray light effect by experiment and suggest an effective way to remove the effect from the image.

8541-54, Session PS

High resolution and high frame rate three-dimensional LADAR architecture utilizing a large area detector

Bongki Mheen, Electronics and Telecommunications Research Institute (Korea, Republic of)

Tremendous applications based on three-dimensional (3D) laser detection and ranging (LADAR) sensors have been deploying such like autonomous car navigation, remote sensing, robot vision, surface mapping for buildings and scenes. Most LADAR architectures are largely divided into two groups, i.e., rotational motor based (Motor-based) and focal plane array based (FPA-based) structure to construct horizontal resolution. While the former constitutes horizontal resolution by simply rotating the mirror at a constant speed, the latter by utilizing horizontally spaced detectors in a narrow pitch, which makes this solution very expensive. Among various pros and cons of each architecture, the FPA-based architecture provide a unique solution at military applications such like target recognition and tracking on fast moving objects, thanks to the flash-type operation, but its expensive architecture prevents it being spread widely in the industry. The frame rate is also restricted by the repetition rate of the high power pulse laser, since normally it is not easy to implement higher repetition rate at higher peak energy than one joule. On the other hand, the performance of motor-based architecture is limited by the big rotating part of the sensor, resulting in relative less resolution (about 124x64

for the inspection angle of 11°) and low frame rate (normally less than 10 Hz), even though the architecture is simple and the fabrication cost can be lowered and have been widely commercialized.

To cope with better performance of 3D LADAR architecture in a cost-effective way over existing architectures, the 3D LADAR Group at Electronic Telecommunications and Research Institute, Korea, proposed a new eye-safe 3D LADAR architecture utilizing a high speed optical scanner and a large area detector. After the whole path optimization from the avalanche photodiode (APD) as a detector to the final 3D LADAR system based on high speed optical scanner, including the 3D display software to evaluate the captured 3D image and display the 3D scene, we have successfully implemented 3D LADAR system. The resolution of obtained 3D images from our system can be increased up to QVGA (320x240) for a given inspection angle, which is the highest resolution in 3D imager at a reasonable cost as far as author's knowledge.

For the successful implementation of the proposed architecture, two problems should be solved. The first problem is that the detector area should be increased since the reflected optical signal will be arrived at relatively large area due to dual-axis optical structure. The increased size of a detector normally makes the noise level increased and the bandwidth and detection range decreased However, such problems can be alleviated when a new scheme of APD is adopted with optimization. The required detector size for our system and the way to solve this problem will be presented in the conference presentation. Another problem is to control beam width at a long distance up to 200 meters. The design and achieved results of utilizing off-axis mirror to build such a beam will be also included. Additionally, since the mechanical part is problematic especially when vibration and module size issue are involved, we are also working on the elimination of the mechanical moving part, and some parts of this work also will be given. Meanwhile, it is not possible to capture high speed object due to rolling shutter effect, but it is also notable that such applications are quite restricted only on military applications involved with high speed missiles.

Consequently, the proposed architecture and the whole-level optimization based on a high speed scanner and large area detector gains a superior performance. Even though it cannot provide such features like flash image and no moving part as in the FPA-based architecture, it can provide the best resolution (QVGA) and higher frame rate (30 fps) at a reasonable implementation cost, which prove the competitive edge of the proposed 3D LADAR architecture over motor-based and FPA-based one in terms of cost and performance.

8541-55, Session PS

Research on sensor technology of Lamb-wave signal acquisition using optical low-coherence

Yongkai Zhu, Nanjing Univ. of Aeronautics and Astronautics (China)

Non-destructive testing of composite materials is a key technology issue in equipment testing. Among the emerging new testing methods, Lamb-wave based non-destructive testing is getting more and more attention. This paper proposes a sensing method to acquire the Lamb-wave signal in composite materials based on optical low-coherence principles. Methods to acquire Lamb-wave in composite materials using optical low-coherence technology were analyzed, and the technical path of non-contact, high-precision method was chosen. The sensor's technology to amplify optical distance based on low-coherence characteristics was proposed, to acquire weak scattering light. The technology to achieve precise location was proposed. Complete in-line experimental system and methods were designed and built up for testing. A sensor system based on Michelson low-coherence interferometer was set up. The distributed optical fiber sensors were arranged on the top of sample materials based on triangulation principle to detect damage signals. Mirrors to enhance reflection intensity were attached on the sample. The phase of sensing arm was modulated by the vibration excited by PZT. Then signals were detected and processed by Daubechies10 wavelet and Gabor wavelet. In-line testing of composite materials with features of high-precision and high signal-noise-ratio was realized, which is meaningful to dynamic sensing of large-scale structure.

8541-56, Session PS

Determining the responsivity of microbolometer FPA using variable optical aperture stop

Grzegorz Bieszczad, Slawomir Gogler, Tomasz Sosnowski, Henryk Madura, Juliusz Kucharz, Military Univ. of Technology (Poland); Alicja Zarzycka, Bumar Zolnierz S. A. (Poland)

In areas like military systems, surveillance systems, or industrial process control, more and more often there is a need to operate in limited visibility conditions or even in complete darkness. In such conditions vision systems can benefit by using thermal vision cameras. In thermal imaging an infrared radiation detector arrays are used. Contemporary infrared detector arrays suffers from technological imprecision which causes that the response to uniform radiation results in nonuniform image with superimposed fixed pattern noise (FPN). In order to compensate this noise there is a need to evaluate detectors characteristics like responsivity and offset of every detector in array.

Typically a reference based method is used to determinate the responsivity of detectors in array as a rise of voltage on detecotrs output due to difference in referene radiation exposed to detectors in array. Optical configuration of detector array and referance based measurement system is often neglected in evaluation of responsivity, but in some cases it can be significant and varry from one optical measurement system to other.

In article the method of determining the responsivity of detectors in a microbolometer array is described. In this method geometrical and optical parameters of the detector array and the measurement system are taken into account. A special test bench was constructed and is consisting of: two precise surface black bodies, aperture limiter, an electronic interface for data acquisition and software for measurement and correction of results with optical parameters of the measuring stand taken into account. Constructed aperture limiter enables evaluation of optical paths in measurement stand with equivalent relative aperture F# from 0.5 to 16.

In order to evaluate the impact of optical path to radiation distribution in the measurement system, special radiation model was elaborated and evaluated in Zemax software. A model of test bench consisting of: lambertian radiation sources, infrared sensor, aperture stops of a certain diameter and the distance from the detector array was simulated. Incident radiation intensity distribution on the detector surface was calculated using Monte-Carlo method for various parameters of the optical path in the measurement system. In the result a set of maps of radiation intensity on the detector array surface was calculated for optical paths of different parameters like equivalent relative aperture, size of detector array and distance to aperture limiter. Calculated maps were used to compensate radiation intensity nonuniformity of optical measurement system giving more precise responsivity evaluation of detector array parameters. In order to proove the method results of responsivity variation for different set of parameters of optical path were evaluated in real measurement compared with results from simulation.

The presented measuring system allows to perform precise measurements of the responsivity of detectors in the array. The obtained values of voltage responsivity of the detectors in the array, can be used in algorithms like nonuniformity correction and radiometric calibration of the infrared camera. In article results of responsivity evaluation is presented for microbolometer infrared arrays from ULIS company (France).

8541-57, Session PS

Model of an optical system's influence on sensitivity of microbolometric focal plane array

Slawomir Gogler, Grzegorz Bieszczad, Military Univ. of Technology (Poland); Alicja Zarzycka, Bumar Zolnierz S. A. (Poland); Magdalena Szymanska, Warsaw University of Technology, The Faculty of Electronics and Information Technology (Poland); Tomasz Sosnowski, Military Univ. of Technology (Poland)

Thermal imagers and used therein infrared array sensors are subject to calibration procedure and evaluation of their voltage sensitivity

on incident radiation during manufacturing process. The calibration procedure is especially important in so-called radiometric cameras, where accurate radiometric quantities, given in physical units, are of concern. Even though non-radiometric cameras are not expected to stand up to such elevated standards, it is still important, that the image faithfully represents temperature variations across the scene. During typical calibration procedure, detectors used in calibration set-up are illuminated by infrared radiation transmitted through a specialized, infrared radiation transmitting, optical system. To account for manufacturing differences in each single detector, all detectors are assumed to be linear in response and their voltage response is corrected, so that each detector yields the same voltage output when subject to the same temperature. However, each optical system used influences irradiation distribution across an array sensor. In order to assure, that the scene is faithfully imaged on the sensor (in terms of temperature variations), numerous physical phenomena have to be taken into account. One such phenomenon is the decrease of the radiant flux reaching off-axis image points, what might be perceived as a false decrease in temperature and makes interpretation of the image difficult. The said effect, is often referred to as “cosine to the fourth” law in classical textbooks. Derivation of the law is ill-conditioned with respect to assumptions regarding detector and source sizes, assumes small angles approximations and doesn’t take artificial apertures into account. Presented model makes no assumptions regarding angles’ sizes, takes simple artificial aperture into account and assumes infinite source size with respect to sensor size, which would be the case in real-life applications. It does however assume negligible optical absorption, which, in real life, would cause further decrease in irradiance distribution that would vary from optical system to optical system. Moreover it assumes Lambertian nature of the radiator (i.e. angular independence of luminance). From the analytical expression it is evident, that the irradiance distribution across image plane is dependent not only on the distance-to-diameter ratio (or focal ratio), but also on the distance itself. Furthermore, the decrease in irradiation is not as drastic as the “cosine to the fourth” law would predict. For validation purposes, a set of configurations comprising different aperture sizes and aperture-to-detector distances have been modeled in ray-tracing software (i.e. ZEMAX). By means of Monte-Carlo simulation, large number of rays has been traced to the sensor plane, what allowed to determine the irradiation distribution across the image plane for different aperture limiting configurations. Simulated results have been confronted with proposed analytical expression. The comparison shows, root mean square fit error to be less than 0.15%, compared to almost 10% roll-off in irradiance for maximum off-axis points. Presented radiometric model allows fast and accurate non-uniformity correction to be carried out. It is worth of mentioning, that presented model is by no means complete and cannot be used for carrying out full radiometric calibration. It is still a mere improvement to existing theoretical models.

8541-58, Session PS

Research on infrared small-target tracking technology under complex background

Lei Liu, Nanjing Univ. of Science & Technology (China); Xin Wang, Hohai Univ. (China); Jilu Chen, Tao Pan, Nanjing Univ. of Science & Technology (China)

Small target tracking in infrared (IR) image sequences has been an important part in many military or civil fields such as video supervision, precision guidance and human-computer interfaces. Nowadays, different algorithms have been proposed for infrared target tracking. However, under complex backgrounds, such as clutter, varying illumination, and occlusion, the traditional tracking method often loses the real infrared small target. To cope with these problems, in this paper we have researched on the traditional infrared small target tracking methods, summarized the advantages and disadvantages of these algorithms. On the basis of the analysis of these methods, according to the characteristics of the small target in infrared images, we propose an improved tracking algorithm to enhance the tracking performance. The experimental results show that, compared with the traditional algorithm, the presented method greatly improves the accuracy and effectiveness of infrared target tracking under complex scenes, and the results are satisfactory.

8541-59, Session PS

Solution based Al/PbS and Ti-Au/PbS Schottky Photodiodes for SWIR detection

Emre Heves, Yasar Gurbuz, Sabanci Univ. (Turkey)

Due to the low water absorption, sensing in SWIR is very attractive in applications such as; passive night vision, biomedical imaging and remote sensing. The integration of the optoelectronic detectors to the read-out circuits as closely as possible is desirable in many applications in order to increase density of detectors, reduce costs, system size and power consumption. Silicon photodiodes are fully integrable to integrated circuits, however, they are not suitable for SWIR range. Narrow bandgap semiconductors such as Ge, InSb, InGaAs, HgCdTe and PBs are commonly used for IR detectors, yet they require hybrid packaging that introduces parasitics and decreases yield, reliability and increases cost. Solution-processed semiconductors are a promising alternative to these since their production is low cost and easy, their bandgap can be tuned to UV, visible and IR region, depending on their sizes, and they can be easily integrated on any substrate. In this work, PbS colloidal quantum dot based photodiodes are realized that are compatible for the integration on ROICs.

PbS quantum dots are used in this work with the size of 5.3 nm that have the absorption peak around 1450 nm. Schottky photodiode architecture is selected for its fast response and moderate sensitivity. The device is formed from Indium tin oxide (ITO) anode, which is a transparent conductive layer used widely in optical devices, the photosensitive PbS layer and a schottky contact formed of titanium and gold.

Fabrication process carried out in class 1000 cleanroom. Special importance has been given to forming a pinhole-free uniform PbS quantum dots film on ITO coated glass substrate. Fabricated PbS quantum dots originally capped with long oleic acid ligands. These long ligands decrease the mobility of electrons and thus degrades photodetector performance. In order to remove these long ligands solid state ligand change procedure applied during film coating using 3-mercaptopropionic acid (3-MPA).In each layer PbS QDs spin coated then ligand exchange procedure is applied and then rinsed with methanol. These procedures are repeated 8-10 times to achieve ~150nm films. Following this step using sputter deposition first Ti layer and then immediately Au layer is deposited on top of PbS film.

The tests are carried out under DC probe station equipped with a dark box. I-V characteristics were measured with Agilent semiconductor parameter analyzer under dark and rectification ratios of 15 is observed at +/- 1V bias. The detector is illuminated from bottom with 16 uW 1530nm and I-V measurements are taken using Agilent semiconductor parameter analyzer. Preliminary tests shows a responsivity of 0.24 A/W. In addition to that, specific detectivity D* is calculated as 3,54*1010 that is limited due to high dark currents. These are better than similar work in literature and attributed to the our processing / deposition of Q-dots.

8541-38, Session 9

Long range staring and wide area assisted detection onboard land fighting vehicles

Douglas J. Macdonald, Thales Optronics Ltd. (United Kingdom)

This paper outlines a long range computer Assisted Detection (AD) capability using thermal imagery for use on future military land vehicles. Currently, in visual surveillance tasks, humans are unsurpassed in recognition and identification. In the realms of ‘computer vision’, fully automatic detection, recognition and identification with zero false alarms remains elusive. Still, there are visual surveillance tasks where human observational attentiveness falls rapidly, where an automatic vision system may assist. Given that the strengths and weaknesses are complimentary, a better solution may be for the human and the computer to work together - the user improving the computer’s discrimination performance and the computer improving the user’s attentiveness. A fully integrated AD concept that could be fitted to an armoured fighting vehicle is described. Development and testing with synthetic imagery, real-life trials imagery, Receiver Operator Characteristic (ROC) analysis and ‘expert’ assessment is explained. The examples in this paper demonstrate real-time ‘staring’ mode functionality and the results indicate that such a system is now ready for deployment in the military

land vehicle domain. Furthermore, prototype 'wide area search and detect' functionality is also demonstrated.

8541-39, Session 9

Single frame IR point target detection based on a Gaussian mixture model classification

Laure Genin, ONERA (France) and Astrium Satellites (France); Frédéric Champagnat, Guy Le Besnerais, ONERA (France)

Automatic point target detection from complex cluttered backgrounds is a subject of growing interest in many applications related to defense and security, such as in Infra-Red Search and Track systems.

We address a single frame detection problem and seek to take advantage at best of background spatial correlation to highlight targets. Such a method could of course be embedded in a more complex detection process using temporal information.

The detection algorithm proposed is a locally adaptive Matched Filter (MF) for which we propose to improve the estimation of the background statistics in each pixel. Whereas the so-called "background suppression" detection methods rely on a background mean estimation, our work is focused on the covariance matrix estimation.

A simple approach consists in estimating the covariance matrices from the whole image. However, the resulting estimate are often not well adapted to areas with strong background variations. Here we propose to classify the pixels of the image and to estimate one covariance matrix for each class.

To obtain a classification which brings together the pixels of similar covariance matrices, we propose a Classification Expectation-Maximization (CEM) algorithm based on a zero mean Gaussian mixture model. To deal with the presence of targets in the observed image, the CEM algorithm is applied on a observation vector made up of the intensity of the pixels included in a "square ring" (square window with an internal centered square hole) centered on the pixel to be classified. This simple scheme is very effective in assigning a target pixel to the surrounding background class, without resorting to more complex techniques like enforcing connected areas using Markov interactions. Moreover it has a very limited number of parameters, essentially the number of classes. The covariance matrices needed for the MF are estimated afterwards, from the classification obtained. The resulting GMMF (Gaussian-Mixture Matched Filter) detection algorithm has the advantage to handle second order non-stationary backgrounds.

The efficiency of the proposed GMMF approach is demonstrated on a large variety of cloudy sky backgrounds, by means of Receiver Operating Curves (ROC) probability of detection vs. probability of false alarm evaluation. The GMMF appears much more efficient than the MF on non-stationary backgrounds. It is able to deal with residual textures present after simple linear background suppression and to increase dramatically the performance.

Keeping in mind that tracking take place after detection, we propose to assess also the homogeneity of the spatial distribution of false alarms (FA) produced by a detection algorithm. Indeed, a consistent high rate of FA in difficult areas like cloud edges leads to temporally correlated FA and to potential false tracks. To reduce the number of false tracks, it is then better to have a spatial FA distribution as homogeneous as possible. We show that the proposed GMMF leads to a much more homogeneous FA distribution than the usual MF method.

8541-40, Session 9

Vehicle detection using multimodal imaging sensors from a moving platform

Christopher N Dickson, Thales UK (United Kingdom) and Heriot-Watt Univ. (United Kingdom); Matthew Kitchin, Thales UK (United Kingdom); Andrew M. Wallace, Heriot-Watt Univ. (United Kingdom); Barry Connor, Thales UK (United Kingdom)

The aim of this paper is to demonstrate the development of a mid-to-long range vehicle detection algorithm using multimodal sensors and the ego-motion of the host vehicle. The system has been designed to improve situational awareness capability on-board a potentially moving vehicle, while exploiting data from multiple sources and modalities.

Close range vehicle detection from a moving platform has received much attention due to the high volume of research into collision avoidance systems and driver assistance technologies; however, longer range vehicle detection, necessary for participants in a hostile environment, tends to rely strongly on the human operator, perhaps guided by some fairly basic algorithms limited by a number of constraints such as background subtraction for imagery collected from a stationary platform.

The presented system utilises a two-stage hypothesis generation (HG) and hypothesis verification (HV) approach. The HG stage parses the entire input field with a set of low-level algorithms (for example hotspot detection, optical flow, and texture segmentation) designed to return a set of possible vehicle locations. These detections are then passed to the more robust HV stage for final filtering in order to reduce the false positive rate, and further classify any detections.

The system is designed to be modular, such that additional modalities can be utilised where available, and as such the HG stage is built from interchangeable, user-selected algorithms which can be tailored to the current environment, and different properties of the available data. For the purposes of demonstration, the system has been set up to utilise Thales Optronics' high-resolution long wave infrared polarimeter and a four-band visible-near IR multispectral system. The HG stage currently combines cues from thermal intensity (vehicles tend to provide an intense hotspot), motion deviation from the global motion (to detect moving targets), and signatures from the polarimetric derived Q Stokes image (as explained in the paper) to determine hypothesis targets. These targets are then verified by a robust classifier (the HV stage) which can be trained on all, or a subset, of the available modalities. In addition, the motion of the host vehicle allows the system to exploit structure from motion type algorithms to calculate the distance to detected objects which can be provided directly to the user, to aid their decision on the correct course of action, or could be utilised by further distance-dependant processing stages.

The paper will present results using image sequences gathered from a moving vehicle featuring the above-mentioned sensors for various scenarios including mid-to-long range distance detection from a moving vehicle in a rural environment. The performance of the system will be assessed by Receiver Operator Characteristics, and other measures of success such as time to initial detection.

8541-41, Session 9

A research of the maritime moving target detection onboard processing techniques based on optical remote sensing

Yanhua Li, Beijing Institute of Space Mechanics and Electricity (China)

The traditional spaceborne optical remote sensing always transmits original data to ground station through data transfer channel and achieves imaging from original data by post-processing. With the rapid development of digital integrated circuit and digital signal processing technology, on-board image processing becomes possible in recent years, and it is also one of the new development trends of spaceborne remote sensor. It is necessary to realize the maritime moving target automatic real-time detection, localization and speed measurement. The processing technology of maritime moving target detection on-board base on optical remote sensing is researched. Firstly, the principle of photo-reconnaissance satellite and the characteristics of the maritime moving target are studied. In allusion to these characters, the image processing model for the maritime moving target is built. Eliminating image rotation, moving target detection, moving target tracking and speed measurement are the primary ingredients of the model. A simulated scenario was established by high fidelity satellite orbit data. The simulated images of maritime moving target were processed in MATLAB. The high target detection rate and speed accuracy of the processing model on-board are indicated by the simulation results.

8541-42, Session 9

Foreground/background separation methods for low SNR target tracking

John R. Maclean, SELEX Galileo Ltd. (United Kingdom)

The ability to track low Signal-To-Noise Ratio (SNR) targets in imagery is vital for effective directed countermeasure systems. High background spatial content, system noise, low target signature, and high dynamic motion all contribute to low contrast targets against backgrounds. This paper seeks to compare several methods of foreground / background separation techniques to allow low SNR targets of interest to be distinguished from spatially cluttered background in midwave-infrared (MWIR) imagery, both synthetic and real.

Synthetic imagery of a typical target of interest, both static and dynamic, created using predicted radiometric signatures using CameoSim is used as the test input. Varying levels of background scene clutter and simulated system noise is injected to produce test sequences with a range of controlled SNR values. Recorded imagery of live events from ground-based trials is also used as sample points for comparison, whose SNR value is computed, to compare directly to the results from simulated imagery. The use of real imagery also allows the algorithms to be grounded in reality.

Simple thresholding schemes are applied, across a region of interest in a MWIR scene, both statically and adaptively to create a binary image. Individual pixels in each frame with values above the threshold are labelled as foreground targets and are aggregated to create detections on which to form tracks. Frame-to-frame subtraction is the simplest method, but increasingly complex methods with rolling averages, temporal history and foreground / background selectivity are assessed. While most suited to moving targets against a static background, thresholding techniques are the easiest to implement in hardware and can be readily adapted to specific applications, which is why they have been proven to be reliable.

These thresholding schemes are then compared against more complex methods to model the background and then also both the background and target of interest in the scene, in order to again form a binary image, leading on to the same pixel aggregation and temporal tracking. Not being reliant on largely arbitrary thresholds to separate foreground targets from the background, these techniques effectively classify individual pixels as being either part of the foreground or background using direct and indirect characteristics of pixels and neighbouring pixels to create model groups. Pixels are then placed in one of each group based on similarity to the iteratively growing models of each group to form the required separation. As more computational steps are involved in each of these methods, typically involving multi-modal descriptions of the background, algorithm design must be carried out with hardware implementation in mind. However, they offer the possibility of low SNR target tracking for both static and dynamic targets (and backgrounds).

The metrics used for evaluation are track error and target acquisition time. Track error (the difference between the computed target location and the true target position in the image) is assessed for the varying levels of SNR. The time taken to robustly distinguish between foreground target and background is also recorded, as this is a critical parameter along with track error.

Track error as a function of SNR and target acquisition times are compared across all methods, leading to a robust low SNR target tracking solution that can be incorporated into future IR

countermeasure applications.

8541-43, Session 9

A continuous object tracking system with stationary and moving camera modes

Deniz Emeksiz, Alptekin Temizel, Middle East Technical Univ. (Turkey)

Automatic detection and tracking of objects get more important with the increasing number of surveillance cameras and mobile platforms having cameras. Tracking systems are either designed with stationary camera assumptions (such as systems using background subtraction) or designed to work in moving camera scenarios (such as mean shift or particle filter based systems). When the camera is stationary, correspondence based tracking with background subtraction has a number of benefits such as enabling automatic detection of new objects in the scene and better tracking accuracy. However these algorithms cease to function when the camera is moving or the background is affected by sudden light changes. On the other hand, mean shift is a histogram-based tracking method which is suitable for tracking objects under unconstrained scenarios like moving camera or lighting changes. However, with mean shift, the objects to be tracked cannot be detected automatically, only existing or manually selected objects can be tracked. Also, as it is a kernel based method, inclusion of background in its tracking kernel might cause accumulation of error resulting in inaccuracies and even failures in tracking after a while.

In this paper, we propose a dual-mode system which combines the advantages of correspondence based tracking and mean shift tracking. A reliability measure which is based on background update rate is calculated for each frame. Under normal operating conditions, when the background estimation reliability is high, correspondence based tracking is used. In this mode, object detection is performed automatically and the objects are tracked using the foreground information. When the reliability of background estimation decreases due to moving camera or sudden changes in the scene, the system automatically switches to mean shift tracking. Information about the objects is hand over between these trackers for seamless operation when there is a mode change. When the reliability of background estimation is detected as decreasing, a few frames might have already been processed with correspondence based tracking, potentially causing detection of false objects and inaccurate tracking of already tracked objects. To overcome this problem, a buffer that collects the information required for mean shift tracking is maintained for a predetermined time. Using this buffer, handover could be achieved by backtracking to the frames before the background information became unreliable and processing them by mean shift tracking.

The results show that the system can detect new objects and track them reliably using background subtraction. Even though the background subtraction based systems detect high number of false objects when the camera starts moving, the proposed system hands over the tracked objects to mean shift tracker and avoids detection of false objects and enables uninterrupted tracking. The results also show that by switching back to background subtraction based tracking when it is appropriate, objects can be tracked with higher precision and recall rates.

8541-44, Session 10

SR 5000N: a new IR spectroradiometer implementation

Dario Cabib, Amir Gil, Shmuel Shapira, Moshe Lavi, Uri Milman, CI Systems (Israel) Ltd. (Israel)

In a previous paper we have presented the design and the expected performance of the latest generation visible/infrared spectroradiometric system for field use, called SR 5000N. Examples of significantly advanced performance are in compactness, field of view response uniformity, measurement speed, and interchangeability of configuration modules, such as fields of view size, wavelength range and detectors. In this paper we present the actual system performance after being tested in real life.

8541-46, Session 10

Influence of area focal plane arrays on the deterioration of interference modulation for fourier transform spectral imaging

Xiarui Guo, Yan Li, Dongdong Fan, China Academy of Space Technology (China)

Due to the advantage of hyper-spectral measurements, temporally modulated Fourier transform spectrometer (TFTS) has developed as space detection and observations technology in orbit successfully. However, single-element detector used by TFTS can only detect radiation, therefore the application is restricted by its limited spatial resolution. Recently, with the advent of large area FPAs and high capacity electronics and microprocessors, imaging Fourier Transform Spectrometer (IFTS) would improve observations by providing a high temporal and spatial resolution. An IFTS is a Michelson interferometer in which a single-element detector is replaced by an area focal plane arrays (FPAs). For each pixel of detector arrays, the Fourier transform of such recording yields the spectrum of the observed area. Simultaneous, area focal plane arrays rise spatial resolution and expand area coverage. However, this technology is still young and many technical challenges have to be overcome.

In this paper, the unique challenges brought by area focal plane arrays are discussed. The simulations of Fourier transform spectral imaging are presented. The distortion of line shape function (ILS) and full width at half maximum (FWHM) caused by the off-axis effects is analyzed in detail. Furthermore, the deterioration of spectral resolution caused by expanding field of view (FOV) and extended radiation source is studied. In addition, the modulation changed as the extended of pixel are simulated and presented. As results shown, the optical path differences (OPDs) is the function of the off-axis angle. The off-axis pixels are sampled at slightly shorter OPDs. The spectrum line is broadened as the increasing of the FOV, and the peak of ILS as well as frequency of spectral is red-shift. The decreasing of modulation caused by area focal plane arrays has the direct proportion with the position of each pixel, maximum optical path difference, as well as FOV. In addition, the decreasing of interference modulation in visible waveband is more significant than that in infrared waveband.

Conference 8542A: Electro-Optical Remote Sensing

Tuesday - Wednesday 25–26 September 2012 • Part of Proceedings of SPIE Vol. 8542
Electro-Optical Remote Sensing, Photonic Technologies, and Applications VI

8542-2, Session 1

Range gated imaging with speckle-free and homogeneous laser illumination

Martin Laurenzis, Jean-Michel Poyet, Yves Lutz, Alexis Matwyschuk, Frank Christnacher, Institut Franco-Allemand de Recherches de Saint-Louis (France)

Range gated imaging has been investigated since the 1960s. It is based on an illumination with short laser pulses and a gated reception with a highly sensitive image sensor. Due to the photon time of flight only light which arrives at the sensor within the right timing window contributes to the imaging process. This method has two inherent effects: the reduction of the disturbing effects on the imaging process by scattered light and parasite light sources and the recording of information from a certain range gate.

Due to the improvements in sensor and laser technologies, range gated imaging is now discussed more for long-range observation, three-dimensional (3-D) imaging, target identification and remote sensing applications in military and security scenarios. Especially in the field of remote sensing, the analysis of the polarization of the reflected light enables laser range-gated imaging system for active polarimetry imaging to enhance the contrast between natural and man-made objects.

In contrast to the improvements in sensor technologies and the increase of the volume power of modern laser sources, most laser-based range-gated imaging systems suffer from poor illumination in terms of homogeneity and the appearance of speckle when using solid-state laser sources. This disproportion was figured out as the most important problem to be solved within future developments and applications of a laser range-gated imaging systems.

During the last decade, the French-German Research Institute of Saint-Louis (ISL) developed several laser illumination devices for laser range-gated imaging systems. These devices are based on a simple waveguide light homogenization technique that enables a homogeneous and speckle-free illumination of the scene. The purpose of this paper is to present these illumination devices with built-in speckle reduction using the spatial diversity approach. These waveguide homogenization devices have a high transmission efficiency of up to 95%. Even for single-laser pulse illumination from a solid-state laser source a reduction of the speckle contrast by a factor of better than 4.5 was demonstrated. In detail, two different illumination devices based on either a solid-state laser source or an array of semiconductor laser diodes are presented. These illumination devices are used for range-gated imaging and active polarimetry with speckle-free and homogeneous illumination.

The ability to reduce speckle effectively by the utilization of waveguide homogenization was studied in theoretical and experimental investigations. In detail, simulations were carried out using the ZEMAX ray tracing environment. These simulations were compared to the speckle theory and experimental results to give a guideline for the dimensional design of waveguides for laser illumination applications.

8542-3, Session 1

Coding of range-gates with ambiguous sequences for extended three-dimensional imaging

Martin Laurenzis, Emmanuel Bacher, Nicolas Metzger, Stéphane Schertzer, Frank Christnacher, Institut Franco-Allemand de Recherches de Saint-Louis (France)

During the past decades range-gated imaging has been rapidly developed due to enormous progress in the development of highly sensitive image sensors and the dramatic increase of the volume power of modern laser sources. The realization of compact and light-weight range-gated imaging systems have been demonstrated for different applications like long range observation, penetration of fog and camouflage nettings, target identification and 3D imaging.

Range-gated imaging is based on the synchronization of a pulsed illumination and a gated reception of the reflected light. Only light which arrives at the sensor within a defined timing window contributes to the imaging process. Therefore, reflectance information as well as range information are registered in a single range gated image.

In the past different methods were established for the restitution of the 3D information based on range-gated imaging. Typically, shorter laser pulses and shorter sensor gates are used to improve the performance of time-slicing, z-scanning or tomography techniques in means of depth accuracy by increasing the number of sampling points. Alternatively, coding techniques use the specific intensity profile of the range-gate to extract the depth information from a few images by an analysis of gray value variations due to defined changes of the range-gate conditions. With this method it is possible to achieve high depth resolution with high accuracy from a small number of sampling points.

By the application of multiple exposure of a single range-gated image it is possible to enhance the depth mapping range. By combination of different gate sequences, it is possible to realize a coding of range-gates. In the analysis of the images these range-gates can be identified from the combination of gray values and encoded to the determined ranges. For instance, it was show that for three images a number of twelve combinations of gray values can be uniquely identified.

In the present publication we show that it is possible to allow a certain kind of ambiguity in the coding sequences to enhance the depth mapping range and to enlarge the number of possible coding sequences. By a refinement of the encoding analysis of the coded range-gated images these ambiguity can be solved to a unique assignment to dedicated coding clock. Therefore, under certain conditions these coding sequence have a quasi-ambiguous structure. For instance, by the use of three images it is possible to determine fifteen different coding combinations. Thus, with this method it is possible to enlarge the depth mapping range. Nevertheless, this improvement of the depth mapping range was reached at the cost of a reduction of the depth accuracy by an increase of encoding errors. In this contribution we will presented a detail theoretical discussion and experimental investigation of this new method for the coding of range-gates.

8542-4, Session 1

Range accuracy of a Gated-Viewing system as a function of the number of averaged images

Benjamin Göhler, Peter Lutzmann, Fraunhofer-Institut für Optronik, Systemtechnik und Bildauswertung (Germany)

Primarily, a Gated-Viewing system provides range gated imagery. By increasing the camera delay time from frame to frame, a so-called sliding gates sequence is obtained from which 3-D reconstruction can be done. Scintillation caused by atmospheric turbulence degrades each Gated-Viewing image and thus, the range accuracy that can be achieved with the sliding gates method. By averaging a certain number of images, this degradation can be reduced.

In this paper we have studied the influence of the number of averaged images on the range gated imagery and the resulting range accuracy. Therefore, we have combined the Intevac Gated-Viewing detector M506 with a resolution of 640x480 pixels with a pulsed 1.57 μm laser source. The maximal laser pulse energy was 67 mJ. Two reflectance panels at a distance of 2 km were recorded. The plates were positioned diagonal to the line of sight with an angle of about 45 degrees from which the range accuracy was derived. The detector was equipped with a Cassegrain telescope with a focal length of 2032 mm, resulting in a small field of view of only 0.24°x0.18°.

8542-5, Session 1

Identification of handheld objects and human activities in active and passive imaging

Ove Steinvall, Swedish Defence Research Agency (Sweden); Magnus Elmqvist, Swedish Defense Research Agency (Sweden); Rolf T. I. Persson, Swedish Defence Research Agency (Sweden)

The identification of human targets including their activities and handheld objects at range is a prime military and security capability. We have investigated this capability using active and passive imaging for video cameras, and sensors operating in the NIR and SWIR regions. For a limited data set we also compare sensor imagery from visible, NIR and SWIR sensors with that from a thermal imaging camera.

The target recognition performance is studied vs. the gate position relative to the target, target range, turbulence conditions and target movement. A resolution chart is also included in the scene. The performance results from observer tests are compared with models and discussed from a system perspective.

8542-39, Session 1

A decade of experience from commercial laser range sensors for ground applications *(Invited Paper)*

Håkan Larsson, Swedish Defence Research Agency (Sweden)

For use in the development of synthetic environment models, the Swedish Defence Research Agency (FOI) bought two laser scanners in the beginning of this millennium, one from the Austrian company Riegl and one from the Canadian Optech. This was the start for over a decade of use of commercial laser range sensors at FOI. The laser scanners have so far been used for different applications such as point cloud algorithm development (detection, classification and reconnaissance of targets), phenomenology studies, reflectance measurements and environment and ground truth measurements. This paper presents different laser scanner technologies (pulsed Time of Flight, Continues Wave (CW), Flash and distributed light) and compare advantages and limitations of the technologies. The paper also include some examples of the use of laser scanning in applications and presents methods for laser range sensors performance evaluation used and developed at FOI.

8542-6, Session 2

Infrared focal plane detector modules for space applications at AIM *(Invited Paper)*

Dominique Hübner, Kai-Uwe Gassmann, Markus Haiml, Luis-Dieter Haas, Stefan Hanna, Andreas Weber, Johann Ziegler, Hans-Peter Nothaft, Richard Thöt, Wolfgang Fick, AIM INFRAROT-MODULE GmbH (Germany)

For more than 25 years, AIM has been offering high-performance first and second generation infrared Mercury Cadmium Telluride (MCT) detector modules and cameras for security, defence, and industrial applications.

In this presentation, some of the currently ongoing space projects at AIM covering the short-wavelength infrared (SWIR), the mid-wavelength infrared (MWIR), and the long-wavelength infrared (LWIR)/ very-long-wavelength infrared (VLWIR) spectral ranges will be presented in brief.

EnMap (Environmental Mapping and Analysis Program, http://www.enmap.de) is a joint effort of the Deutsches Zentrum für Luft- und Raumfahrt (DLR), German earth observation institutes, and the space industry in cooperation with international partners to gain quantitative information on the evolution of terrestrial ecosystems through hyperspectral imaging. AIM provides the integrated detector cooler assembly (IDCA) for EnMap's SWIR instrument (900-2500 nm wavelengths). The IDCA comprises a large-area Mercury Cadmium Telluride (MCT) focal plane detector array housed in an AIM dewar with an active long-life pulse-tube cooler.

For the German GLORIA (Gimballed Limb Observer for Radiance Imaging of the Atmosphere) mission as the "successor" of the MIPAS instrument, AIM has developed, manufactured, characterized, and delivered VLWIR MCT FPAs with a 13.3 μm cut-off wavelength at a 64 K operating temperature. GLORIA is a joint project of the Forschungszentrum Jülich and the Karlsruhe Institute of Technology (KIT). Its instrument is a limb sounder for 3-dimensional atmospheric spectros-copy of the upper troposphere/ lower stratosphere (UTLS). AIM has delivered a prototype IDCA (GLORIA I) for laboratory use and two improved units (GLORIA II/1, II/2) for remote sensing from high-altitude airplanes. With the GLORIA instrument, an unprecedented spatial resolution of 30 kilometers (horizontally)  200 meters (vertically) has been achieved.

The AIM MCT MWIR detector has been designed for a high resolution push-broom imaging satellite mission for the detection of forest fires and floods, the detection and supervision of pollution emissions, the detection and supervision of sewage disposal into rivers and seas, and the observation of volcanic activities.

8542-7, Session 2

A decision surface-based taxonomy of detection statistics

François Bouffard, Defence Research and Development Canada - Valcartier (Canada)

Current and past literature on the topic of detection statistics - in particular hyperspectral target detection statistics, which are widely used in remote sensing of atmospheric contaminants - can be intimidating for newcomers, especially given the huge number of existing detection tests. Detection tests for hyperspectral measurements, such as those generated by dispersive or Fourier-transform spectrometers used in remote sensing of atmospheric contaminants and other targets, are of paramount importance if any level of analysis automation is to be achieved. The detection statistics used in hyperspectral target detection are generally borrowed and adapted from other fields such as radar signal processing [1] or acoustics [2]. Consequently, although remarkable efforts have been made to clarify and categorize the vast number of available detection tests [3, 4], understanding their differences, similarities, limits and other intricacies is still an exacting journey. Reasons for this state of affairs include heterogeneous nomenclature and mathematical notation, probably due to the multiple origins of hyperspectral target detection formalisms. Attempts at sorting out detection statistics using ambiguously defined properties may also cause more harm than good.

Ultimately, a detection statistic is entirely characterized by its decision boundary. Thus, we propose to catalogue detection statistics according to the shape of their decision surfaces, which greatly simplifies this taxonomy exercise. We make a distinction between the topology resulting from the mathematical formulation of the statistic and mere parameters that adjust the boundary's precise shape, position and orientation. Using this simple approach, similarities between various common detection statistics are found, limit cases are reduced to simpler statistics, and a general understanding of the available detection tests and their properties becomes much easier to achieve.

We found that most popular detection statistics fall into one of two main categories. The first one includes detection statistics which possess a planar decision boundary. These statistics include abundance or energy estimators, and are generally not considered to possess the constant false alarm rate (CFAR) property. They can easily be transformed into target subspace detectors, whose decision boundaries are cylindrical, or into anomaly detectors, which have closed decision boundaries. The second category regroups detection statistics having a conical decision boundary. Those detectors can be thought of as SNR estimators and are in fact F-tests. They are most often associated with the CFAR property since the number of included clutter samples does not change after a radial swelling of the clutter distribution. Detection statistics with hyperbolic, parabolic, or hybrid decision surfaces are also explored, and natural extensions to common statistics are proposed.

REFERENCES

[1] Kelly, E. J., "An adaptive detection algorithm," IEEE Transactions on Aerospace and Electronics Systems 22-115, 1986

[2] Scharf, L. L. and B. Friedlander, "Matched subspace detectors," IEEE Transactions on Signal Processing, 42-2146, 1994

[3] Manolakis, D., D. Marden and G. A. Shaw, "Hyperspectral image processing for automatic target detection applications," Lincoln Laboratory Journal, 14-79, 2003

[4] Kraut, S., L. L. Scharf and L. T. McWorther, "Adaptive subspace detectors," IEEE Transactions on Signal Processing, 49-1, 2001

8542-8, Session 2

Signal processing for target detection

Yochay Danziger, Rafael Advanced Defense Systems Ltd. (Israel)

In order to detect a moving target the electro-optical system pre-filter the image by optics, than sample the image with a Focal Plane array (FPA) and finally reconstruct the image utilizing a numerical interpolation filter. The final step of reconstruction also includes warping and subtracting two images in order to detect changes in the images associated with motion of a target.

In this paper this process is optimized by incorporating signal processing methodologies. The pre-filter (optics) is optimized to suppress aliasing noise while the post-filter (interpolation filter) is designed as a Whitening Matched Filter (WMF) that incorporates target spatial distribution, target aliasing noise, clutter aliasing noise, detector noise and registration error as noise. It is shown that SNR and target positioning accuracy are improved substantially.

8542-10, Session 2

Implementation of a filters array on a VisSWIR InGaAs sensor for contrast enhancement

Jean-Luc Reverchon, Odile Huet, Jean Decobert, Mauricio Pires, Maxime Pozzi, Anne Rouvie, Jean-Patrick Truffer, Alcatel-Thales III-V Lab. (France); Bogdan Arion, Yang Ni, Vincent Noguier, New Imaging Technologies (France)

SWIR image sensors based on InGaAs p-i-n photodiodes arrays present a large interest in applications such as passive or active imagery. Some advantages from SWIR imagers lye in a larger transmission in the atmosphere and specific reflectivity contrasts in comparison to visible. InGaAs based FPA with visible extension are now available. They allow a large quantum efficiency from 400 nm to 1650 nm in order to maximize sensitivity in low light conditions. However with such wide spectral range, reflectivity contrasts are no more specific to the SWIR range, become sensitive to lighting conditions and can be affected by Rayleigh scattering in visible. This paper describes a single-chip InGaAs SWIR camera with a Bayer type filter array directly deposited on the backside of the FPA. The filters array is implemented on a visible extended InGaAs VGA format of 640 x 512 pixels with a pitch of 15 µm logarithmic single-chip camera. Combined with such a filter pattern, sensors will recover the advantage from the SWIR range so useful for specific contrast or deeper penetration in the haze. We will explain the process to align high pass filters and focal plane arrays and describe the optical crosstalk issues. This approach has been developed in the field of a FP7 European project called 2Wide_Sense dedicated to automotive safety. The Bayer type filters is based on one panchromatic and three high-pass filters pixel. The first one preserves the high quantum efficiency required for low light level. High-pass filters present a cutoff at 585 nm to discriminate car and traffic lights, and the two other ones at 730 nm and 1350 nm in order to determine road conditions.

8542-11, Session 2

Spectral reflectance of Kelantan Estuary with ALOS data to estimate turbidity and transparency

Saumi Syahreza, Univ. Sains Malaysia (Malaysia) and Syiah Kuala Univ. (Indonesia); Muhammad Z. Mat Jafri, Hwee-San Lim, Univ. Sains Malaysia (Malaysia)

The Kelantan estuary, located in the northeastern part of Peninsular Malaysia, is characterized by high levels of suspended sediments. Kuala Besar is the estuary of the river directly opposite South China Sea. Spectral reflectance (Rr) measurements, nephelometric turbidity and transparency (secchi disk depth) are carried out in the Kelantan estuary. The objective in this study is to establish empirical relationships between spectral remote sensing reflectance in ALOS satellite imagery and two parameters, i.e., turbidity and transparency through these numerous in situ measurement. We detected that remote sensing reflectance are exponential with turbidity and transparency. The result of this sampling show that the wavelengths range for 500-620 nm is the most suitable band for measuring transparency and turbidity. Reflectance in these bands was regressed against transparency and turbidity field data to derive two empirical equations for turbid water estimation and transparency. These equations were calculated using ALOS images data from 2009 and 2010. The result obtained indicated that reliable estimates of turbidity and transparency values for the Kelantan Estuary, Malaysia, could be retrieved using this method.

8542-12, Session 3

3D imaging flash lidar for space applications

Farzin Amzajerdian, Vincent Roback, Paul Brewster, NASA Langley Research Ctr. (United States); Alexander Bulyshev, Analytical Mechanics Associates, Inc. (United States); Carl S. Mills, NASA Langley Research Ctr. (United States); William Carrion, Coherent Applications, Inc. (United States); Anna M. Noe, Bruce W. Barnes, NASA Langley Research Ctr. (United States)

NASA has been pursuing Flash lidar technology for autonomous, safe landing on planetary bodies and for automated rendezvous and docking. During the final stages of the landing vehicle descent from about 1 km to 500 m above the ground, the Flash lidar can generate 3-Dimensional images of the terrain to identify hazardous features such as craters, rocks, and steep slopes. The onboard flight computer can then use the 3-D map of terrain to guide the vehicle to a safe site. During an earlier stage of the descent trajectory at an altitude of approximately 15 km, the flash lidar could provide updates to the navigation filter to reduce vehicle position uncertainty by performing the terrain-relative-navigation function in which surface contour maps of the terrain below the spacecraft are generated for on-board correlation to existing terrain databases for position fix determination. As an automated rendezvous and docking sensor, the Flash lidar can provide range and bearing from an approaching spacecraft to the docking port of the International Space Station or other spacecraft. NASA Langley Research Center has been advancing the Flash lidar technology under the Autonomous Landing and Hazard Avoidance (ALHAT) project for the past several years. This paper describes the component technologies that have recently been assembled into a prototype sensor system. The operation of this prototype lidar has been characterized through a series of static and dynamic (moving platform) tests. The prototype system will be integrated into a rocket-powered terrestrial free-flyer vehicle being built by NASA Johnson Space Center. Operating in a closed loop with the other ALHAT landing system components and vehicle guidance and control system, the viability of Flash lidar sensor for future landing missions will be demonstrated through a series of flight tests in 2012 aimed at autonomously flying to and landing in a simulated hazard field.

8542-13, Session 3

Multi-channel photon counting three-dimensional imaging laser radar system using fiber array coupled Geiger-mode avalanche photodiode

Rong Shu, Genghua Huang, Libing Hou, Zhiping He, Yihua Hu, Shanghai Institute of Technical Physics (China)

Photon counting laser radar is the most sensitive and efficiency detection method of direct-detection laser radars. With the use of Geiger-mode avalanche photodiode (APD) or other single photon detectors, every laser photon could be sufficiently used for ranging and three-dimensional imaging. The average energy of received laser signal could be as low as a single photon, or even less than one. This feature of photon counting laser radar enables ranging under conditions of long range, low laser pulse energy, and multi-pixel detection, while receiver size, mass, power, and complexity of laser radar are reduced.

In this paper, a latest multi-channel photon counting 3D imaging laser radar system using fiber array coupled Geiger-mode avalanche photodiode (APD) is introduced.A detection model based on Poisson statistics of a photon counting laser radar is discussed. Detection and false alarm probabilities as well as factors that influence them are

analyzed theoretically. Mean laser signal photon numbers, background light, and performance of a Geiger-mode avalanche photodiode are considered and discussed.A laser radar system has been designed and analyzed with the detection model and photon counting three-dimensional imaging theory. The system is designed to work under daylight condition with ultra-low signal level (less than single photon per pulse). A passively Q-switched microchip laser is used to transmit short sub-nanosecond laser pulses at 532nm. The output laser is divided into 1?8 laser spots by a diffractive optical element. A 1?8-pixel fiber array, which is connected to 8 Geiger-mode avalanche photodiodes, is used as the receiver at the focal plane of laser radar system. The use of multi-channel receiver makes the detection faster, while the detection probability improved. The Geiger-mode APDs with 50ns dead time are actively quenched and gated by a programmable range gate of 1μs, which enable laser radar system to work at a multi-hit model so that the detection probability could be improved effectively. A FPGA based time-to-digital converter (TDC), which is designed by delay line interpolation technology, is used for multi-hit signal acquisition. Two galvano scanner mirrors are used for two-axis scanning. Spacial, time, and spectral filter methods are used in the design to reduce false alarms caused by background noise, and to get better imaging performance. The algorithm of photon counting three-dimensional imaging is developed for signal photon events extraction and noise filter.

Outdoor experiments have been made to test the performance of laser radar system, and to demonstrate the design theory of photon counting laser radar working under daylight. Three-dimensional images under daylight and night conditions were acquired and analyzed. The results show that system could operate at strong solar background. The ranging accuracy of the system is 6.3cm (σ) while received laser pulse signal level is only 0.04 photoelectrons on average. In some experiments, the results show that the laser radar system has the ability to detect objects through obstacles like trees or nets. The advantages and feasibility of photon counting laser radar working at daylight have been demonstrated experimentally. High-accuracy and high-resolution three-dimensional imaging could be achieved by photon counting laser radar.

8542-14, Session 3

Kilometre range depth imaging at 1550nm wavelength using a superconducting nanowire single photon detector

Nathan R. Gemmell, Aongus McCarthy, Ximing Ren, Nils J. Krichel, Michael G. Tanner, Robert H. Hadfield, Gerald S. Buller, Heriot-Watt Univ. (United Kingdom)

Obtaining detailed three-dimensional surface information of targets at kilometre ranges has long been an objective in a number of application areas. The introduction of lasers and subsequently time-of-flight LiDAR systems have made this a reality. However, previous attempts at obtaining depth profile information at kilometre-scale stand-off distances have often necessitated the use of non-eyesafe laser output power levels and/or long acquisition times. We present a scanning time-of-flight depth imaging system which is based on the time correlated single photon counting (TCSPC) technique, and uses a femtosecond pulsed 1560 nm illumination source and a superconducting nanowire single photon detector (SNSPD). The high sensitivity and picosecond timing resolution of the TCSPC technique provides distinct advantages in the trade-offs between required illumination power, range, depth resolution and data acquisition durations. The high SNSPD efficiency at 1560 nm (~18% at kHz dark counts), the excellent timing resolution (<100 ps) of the system, and the flexibility of the TCSPC approach were used to construct a system that can acquire high precision depth information by illuminating the scene with eye-safe optical power levels (<250 μW average optical power). A custom-built transceiver unit housed a pair of galvanometer-actuated mirrors and relay optics which enabled the illumination beam to be steered in x and y across the target scene. The scattered return photons from the target that were collected by the transceiver were routed to a fibre-coupled single pixel detector and enabled a depth map to be constructed. The high efficiency of the SNSPD in the infra-red allows the system to take advantage of existing and well established telecommunication technology, while also operating in a spectral regime with reduced atmospheric attenuation and a much lower solar background level, this being the dominant source of noise in typical daylight conditions. Detailed depth profile images of humans and a life-sized mannequin were successfully acquired under bright daylight conditions at ranges of 325 metres and 910 metres using pixel dwell times in the millisecond regime. Depth precision was measured by scanning flat planes of cooperative target material, a least squares fit giving 1.1 mm depth residual at a range of 910 metres with a per pixel dwell time of 10 ms, and 1.5 mm depth residual at 4400 metres with a per pixel dwell time of 2 s. At a stand-off distance of 325 metres, a 0.8 mm depth residual was achieved with a per pixel dwell time of 1 ms which enabled a depth profile movie of a moving object to be recorded. This four-second movie had centimetre resolution in xyz and was captured at 10 frames per second, each frame having 10 ? 10 pixels.

8542-15, Session 3

Optical reflectance tomography using TCSPC laser radar

Markus Henriksson, Tomas Olofsson, Christina A. Grönwall, Carl Brännlund, Lars J. Sjöqvist, Swedish Defence Research Agency (Sweden)

In many cases the transmitted pulse energy is limited in laser radar systems. This limitation may be a result of size, weight and power consumption of the laser. At intermediate to long distances the returned signal from diffusely reflecting objects will be very low. If the returned laser photons are spread over multiple pixels in a focal plane array the signal may be too low to be detected. It may then be advantageous to use only a single pixel detector to record a range profile instead of a full image. Single pixel detectors may also be interesting because of limited availability of array detectors, or because the demand for supporting equipment as coolers and read-out electronics is too high for small platforms like UAVs. Also in very long range applications, e.g. imaging of satellites, the usability of array detectors is limited since large apertures are needed to spatially resolve the target.

If target data from different angles of incidence are available tomographic signal processing may be used to reconstruct an image of the target from range profiles measured with a single pixel detector. We present model experiments of optical reflectance tomography of rotating targets measured using a time-correlated single-photon counting (TCSPC) laser radar system. The system uses a mode-locked laser and single-photon avalanche diode (SPAD) with range bin histogramming electronics to generate high temporal resolution laser radar response signals with down to 50 ps FWHM instrument response function and 4 ps sampling bin size. Data from geometrical objects are used for performance estimation. Images of model targets are shown to illustrate the possibilities.

Scenarios include characterization of small objects on water from high altitude UAVs using 1.5 μm lasers, where the background reflection from the water is very low, and identification of airborne targets. The more difficult problem of targets in cluttered background, e.g. targets on the ground, is also investigated. The long ranges call for very high sensitivity of the laser radar system, making TCSPC a very interesting technology. The required integration time will demand that the relative motion of sensor and target is compensated to avoid blurring of the range profiles, and solutions for this will be discussed.

8542-16, Session 4

A new gain control and amplifying circuit for the 3D imaging lidar

Chunsheng Hu, Zongsheng Huang, Xingshu Wang, Ying Feng, National Univ. of Defense Technology (China)

The gain control and the amplifying circuit is a key part in the 3D imaging lidar. To the 3D imaging lidar, the range of laser echo amplitude is very large and mainly relative to the variation of the target distance. The laser echo amplitude is inversely proportional to the square of the target distance.

In the 3D imaging lidar, the common gain control method is some kind of a passive gain control method, which adjusts the current amplification in the amplifying circuit according to the last pulse signal peak-amplitude. This method requires a peak detector to measure the last peak amplitude, and can not effectively adjust the amplification when the last pulse signal is saturated. The passive gain control method generally needs several adjustments after saturation. The detection precision of the 3D imaging lidar will decrease significantly when the pulse signal is saturated.

In order to avoid the shortcoming of the passive gain control method and enhance the reliability of the 3D imaging lidar, we propose a new

gain control method, which adjusts the amplification of the amplifying circuit according to the target distance. This method complies with the principle that the laser echo amplitude is inversely proportional to the square of the target distance. This method does not need the information from the last pulse signal peak-amplitude or a peak detector.

Based on this method, a gain control and amplifying circuit is proposed, which is mainly composed of a variable gain amplifier (AD8330) and a gain control circuit. The amplifier is used to magnify the input signal with variable gain. The gain control circuit is used to realize the active gain control function. The circuit generates a gain control voltage and applied the voltage to the exponent gain control pin of the AD8330 amplifier. The theoretical waveform of the gain control is analyzed. In order to simplify the complexity of the gain control circuit, we propose a simple implement way based on the charging process of a capacitor. The gain control error is analyzed and simulated when the target distance ranges from 2 m to 20 m. When the gain ranges from 1 to 100, the maximum error of gain control is about 28%, the mean error of gain control is about 5%.

The gain control and the amplifying circuit is introduced in this paper. Some experiments are carried out to verify the entire circuit functions in a 3D imaging lidar. The result shows that the output signal amplitude basically keeps constant when the target distance is changing, and the circuit can amplify the pulse echo signal without distortion. The pass band of the circuit ranges from 0.33 MHz to 150 MHz and the maximum gain ranges 316 times. The input and output voltage is in the differential form and their voltage ranges are both 2 V. The gain control and the amplifying circuit is used and tested in a high-speed 3D imaging lidar. Besides the 3D imaging lidar, the detection circuit can be applied to the pulsed laser range finder and other amplifying circuit whose gain is proportional to the square of time interval.

8542-17, Session 4

SPAD imagers for remote sensing at the single-photon level

Federica A. Villa, Danilo Bronzi, Simone Bellisai, Gianluca Boso, Andrea Bahgat Shehata, Carmelo Scarcella, Alberto Tosi, Franco Zappa, Politecnico di Milano (Italy); Simone Tisa, Micro Photon Devices S.r.l. (Italy); Daniel Durini, Fraunhofer-Institut für Mikroelektronische Schaltungen und Systeme (Italy); Sascha Weyers, Werner Brockherde, Fraunhofer-Institut für Mikroelektronische Schaltungen und Systeme (Germany)

Combined 2D imaging and 3D ranging sensors provide useful information for both long (some kms) and short (few tens of m) distance, in security applications. To this aim, we designed two different monolithic imagers in a 0.35 µm cost-effective CMOS technology, based on Single Photon Avalanche Diodes (SPADs), for direct long-range time-of-flight (TOF) and indirect (phase-resolved) short-range depth-ranging. The single pixel (150 µm x 150 µm) consists of a SPAD (30 µm diameter, noise of less than 15 counts/s, 50% efficiency at 410 nm), an analog active quenching circuit, and an in-pixel digital processing circuitry. The latter being either a Time-to-Digital Converter (TDC) for TOF measurements or three up/down counters properly synchronized for phase-resolved depth measurements. In-pixel latches are added to parallelize data readout and provide no dead-time high frame-rate photon counting/timing.

Such smart pixels operate in two different modes: single photon counting for 2D intensity images; and either photon timing or phase-resolved photon counting for 3D depth images. In the 2D modality, each pixel has a counter that accumulated the number of photons detected by the corresponding SPAD, thus providing high-sensitivity (at the single-photon level) and high-frame-rate (100 kframe/s) “intensity” images. In the TOF 3D ranging imager, each pixel measures the reflected photon’s arrival time with a 312 ps resolution, thanks to a two-stage TDC that measures the delay between START (synchronous with the photon detection) and STOP (synchronous with the laser pulse) signals. The coarse stage is a 6 bit asynchronous counter (also used for 2D intensity imaging), that counts the pulses of the 200 MHz reference clock between START and STOP signal with a full scale range of 320 ns. The 4 bit fine interpolator divides the clock period in 16 intervals of the same duration, generated by a delay looked loop line. Therefore the resulting spatial resolution is 9 cm within a 50 m range, centered at an user-selectable distance (e.g. 100 m - 5 km). The TDC performances were characterized in terms of linearity (DNLrms=4.9% LSB, INLrms=11.7% LSB) and precision (175 ps). In the phase-resolved 3D ranging imager, the in-pixel electronics measures the phase difference between the modulated light emitted by a laser and the back-reflected light, by means of two 9 bit up-down counters. An additional 9 bit up counter (the same exploited for 2D image) is used for background suppression. The resolution of the camera and the maximum frame rate strongly depend on the illuminator power, ambient background and object reflectivity. We demonstrate that the sensor can be effectively used in indoor applications with a resolution better than 5 cm over a 20 m range, both with continuous-wave modulation and pulsed-light modulation techniques.

8542-18, Session 4

Real-time self-mixing sensor for vibration measurements

Michele Norgia, Alessandro Magnani, Alessandro Pesatori, Politecnico di Milano (Italy)

The presented work describes the development of an optical sensor for contactless measurement of vibrations and displacements. The principle of operation is based on the self-mixing interferometry, a simple optical setup that allows different contactless measurements. In the self-mixing configuration, the laser diode light is focussed on a remote target and the light back-scattered into the laser cavity is coherently mixed with the lasing field. This phenomenon induces a modulation of the emitted optical power which is detected by the monitor photodiode. The modulation is a periodic function of the target distance, with period equal to half wavelength (one fringe), and with amplitude and shape depending on the target surface reflectivity. In our prototype, the optical signal is read by a trans-impedance amplifier and acquired by a Digital Signal Processor (DSP) that also realizes the real-time reconstruction of the target displacement. Two separated algorithms were developed for the displacement reconstruction, applied for different optical conditions: the duty-cycle algorithm, for very weak target reflectivity, and the unwrap algorithm for weak-moderate target reflectivity. The first one calculates the target displacement by counting the single fringes of the interferometric signal with a resolution of half a wavelength. The information on the movement direction, positive or negative, is achieved by the intrinsic distortion of each fringe, evaluated by the real-time duty-cycle calculus. This algorithm allows robust reconstructions even in cases of very-low signal, with quasi-sinusoidal fringes. The main limitation is the resolution over the displacement measurement at exactly half wavelength that in our case is about 400 nm.

For higher values of reflections, the interferometric signal presents a good signal to noise ratio with sawtooth shape, and it is possible to achieve higher resolution exploiting the fringe linearity. In this condition, the second algorithm computes a sort of phase-unwrap on the sawtooth interferometric signal, and a continuous reconstruction is realized. In this case the spatial resolution is limited only by the signal-to-noise ratio of the signal and by the non-linearity of the fringes. Experimental results show that the vibrometer, under the ‘unwrap’ digital processing, reaches about 50 nm of resolution.

The hardware set-up was provided by an autofocus system; obtained by varying the position of the collimating lens in order to maximise the signal amplitude.

Many tests have been performed by frequencies ranging from 10 Hz to 10 kHz, with different vibration amplitudes. Tests on large displacements were also carried out by varying the target position of several centimeters. These experimental tests have shown a good working of the sensor, robust to various optical conditions of employment, without the need of a skilled operator. Globally, the system does not show limits in term of maximum range of displacement measurable inside of the focusing range of the optical beam.

8542-20, Session 4

Measurement and modeling of laser range profiling of small maritime targets

Ove Steinvall, Tomas R. Chevalier, Carl Brännlund, Swedish Defence Research Agency (Sweden)

The detection and classification of small surface targets at long ranges is a growing need for naval security. Laser range profiling offers a new capability for detecting and classifying such targets even if they appear as point (transversally unresolved) targets in radar or passive EO sensors.

Modifying a conventional laser range finder to have a higher range resolution can this increase it's value as a sensor. Laser range profiles will reveal basic reflecting structures on the ship. The best information is obtained for profiles along the ship. Several range profiles from different aspects will increase the classification performance. If many aspects angles are possible a tomographic reconstruction of the ship may be done.

We have used high resolution (sub cm) laser radar based on time correlated single photon counting (TCSPC) to acquire range profiles from different small model ships. The collected waveforms are compared with simulated wave forms based on 3 D models of the sips. A discussion of the classification accuracy based on the number of waveforms from different aspect angles is done as well as well as the influence of reflectivities from different part of the ship is made. The results are discussed with respect to the potential performance of modified laser range finder measuring on real ships and the combination with active imaging.

8542-21, Session 5

Practical issues in automatic 3D reconstruction and navigation applications using man-portable or vehicle-mounted sensors *(Invited Paper)*

Chris Harris, Carl Stennett, Estelle Tidey, Roke Manor Research Ltd. (United Kingdom)

This paper describes a number of 3D reconstruction and navigation systems developed by Roke Manor Research for different applications and using various man-portable and vehicle-mounted sensors. Building on this broad practical experience the paper identifies important issues relevant to sensors, scenarios and practical operation.

There is a well-established requirement across a range of applications and environments for automatic 3D reconstruction and navigation. 3D reconstruction can be exploited in simulation and modelling for many purposes including training, planning, familiarisation and awareness. In the military context there are two special requirements. Firstly there is the need for the methods to be based on self-contained, robust sensor systems, avoiding reliance on external infrastructures. Secondly there is the need for output based on up to date data and produced without adverse impact on operational logistics. In general there have been considerable advances in development of processing algorithms and their application in well-instrumented situations without operational constraints, but there remains much to be done with systems that are militarily practical. Much of the work in this field has been based on the development of SLAM or structure-from-motion algorithms - so reconstruction and navigation are inter-related capabilities - and the use of these algorithms applied to conventional machine-vision cameras. Recently alternative sensors have been developed, notably 360° viewing cameras such as the Point Grey's Ladybug 3 and RGB-Depth (RGB-D) cameras such as Microsoft's Kinect.

The paper begins with a brief discussion of military requirements and provides illustrated examples working with conventional cameras, Ladybug and Kinect data. The processing is largely based on structure-from-motion techniques and we discuss of some of the practical issues that need to be addressed in these applications. Our first main example is processing of vehicle-mounted sensor data to support enhanced street-level browsing services. The emphasis of the work has been on exploiting practical sensor fits, minimising human operator involvement and speed of delivery for familiarisation purposes. A second example of special interest is underground exploration where GPS is unavailable and the environmental constraints are challenging. Here Roke has completed a set of navigation experiments using RGB-D and conventional cameras fitted in a man-portable sensor pack so outputs can be compared. Data was collected in a complex of rooms and underground tunnels at a Victorian fort. The paper compares the navigational accuracies achieved using the different sensors (comparing processing of depth data from the RGB-D sensor and vision processing of conventional camera data) and shows some examples of the modelled scenes. We found that despite the many advantages of RGB-D sensing, the range-limitations of the RGB-D generally impaired navigation performance in these applications. (Other examples will be briefly presented depending on space limitations.) Finally we present some conclusions based on our overall experience to date with this range of sensors and applications.

8542-22, Session 5

Segmentation, classification, and pose estimation of maritime targets in flash-ladar imagery

Walter Armbruster, Marcus Hammer, Fraunhofer-Institut für Optronik, Systemtechnik und Bildauswertung (Germany)

Selecting a precise aim point on an erratically moving target such as an approaching speedboat is difficult even for the trained gunner. Automatic fire control is an important option. The paper shows that reliable automatic target acquisition, aim point selection and tracking is feasible if a flash-ladar sensor is used. Sensor data processing includes (i)elimination of water reflections, (ii) target detection and shape classification, and (iii) target pose estimation.

Two techniques of water segmentation are described, a "quick and dirty" routine for real time tracking applications and a slower but more accurate algorithm based on modeling surface waves, determining the expected water reflection signature and maximizing the image likelihood with respect to the water level hypothesis.

Shape classification is based on a generic hull model defined as a parametric surface representation. The ship hull is specified by 7 parameters, which can be extracted from the range image in order to decide whether a given connected component is in fact a maritime vessel and if yes, what kind.

Pose estimation determines the ship orientation by analyzing the visible contour of the hull projection into the horizontal plane. The ship position is found by associating contour corners with corners of the generic model. Generic aim points such as the tip of the bow at the water level can thus be automatically extracted and tracked. For maritime targets in flash laser imagery, precision targeting and tracking was demonstrated even for erratic sensor and target motions and highly agile target maneuvers.

8542-23, Session 5

Consistency in multimodal automated target detection using temporally filtered reporting

Toby P. Breckon, Ji W. Han, Cranfield Univ. (United Kingdom); Julia Richardson, Stellar Research Services (United Kingdom)

Autonomous target detection is an important goal in the wide-scale deployment of unattended sensors and sensor networks. Although current approaches offer a significant reduction in the required manual processing or review of sensor information they can equally suffer from false positive reporting and the subsequent trade-off required in detection sensitivity. Given the assumption of a sensitive yet "noisy" target detector - with high detection rates but (operationally) significant false positive detections - we look at how we can improve the consistency of the resulting global target/object reporting based on temporal filtering. Whilst widely considered in sensor processing for image stabilization, de-noising and compression, temporal filtering has received little attention within autonomous target detection outside of explicit object tracking approaches.

Firstly we assume, that for a given sensor imaging a true target, the number of "samples on target" (i.e. images containing the target) will be numerous and that they will be temporally consistent (and clustered) as the target transits the scene. Subsequently, for a sensitive detection approach we further assume true positives are detected over numerous samples as a target transits the sensor field-of-view. By contrast we also assume, that for such a "noisy" detector, false positives may be frequent but that their temporal distribution will be random. By treating the set of processed image samples as a temporally distributed ensemble classifier, and assuming that although "noisy" our automated detection approach is at least better than random for a true positive target, we introduce the use of temporally filtered detection reporting.

Over a given temporal window, detection of a given target must be statistically better better than random for a detection report to be generated by the temporal target detection filter. If the sample rate of the sensor and throughput is high in relation to target motion through the field of view (e.g. 25fps camera) then we can validly set the temporal window to a value above the background noise of spurious false positive detections. This can be further tuned to increase the robustness/confidence in reported detections by increasing the size of the temporal window. Furthermore if we consider multiple modalities

of sensor, each with a different likelihood characteristic for true/false automated detections, this concept can be extended to consider contributing detections from different sensors or even different detection algorithms applied to the same sensor.

Our filtered reporting approach is illustrated using a feature-driven automated detection algorithm for vehicle and people detection in visible (EO) and thermal (IR) imagery from an unattended dual-sensor pod. We use a sensitive target detection approach based on a cookbook of visual features processing targets extracted from the scene using an adaptive background model. The use of temporal filtering provides a consistent, fused onward information feed of targets detected from either or both sensors (EO and/or IR) whilst minimising the onward transmission of false positive detections and facilitating the use of a such sensitive detection approaches within a deployed sensor context.

8542-24, Session 5

Sensor fusion for improved indoor navigation

Erika Emilsson, Joakim Rydell, Swedish Defence Research Agency (Sweden)

A reliable positioning system providing high accuracy would increase the safety of first responders and military personnel significantly. Creating a positioning system that is accurate enough in GPS-denied environments, such as indoors, inside ships, and during harsh electromagnetic interference conditions, is a technical challenge. In many scenarios, it is not possible to use a priori information (e.g., magnetic field or image information, obtained through extensive pre-surveying, or building layouts) or pre-installed infrastructure (e.g., RFID units or WiFi base stations). Furthermore, the positioning system needs to be lightweight, small, inexpensive, and power efficient in order to be part of first responder or soldier equipment.

To enable navigation in a broad range of environments and get more accurate and robust indoor positioning results, we use a multi-sensor fusion approach. We describe and evaluate a positioning system, based on sensor fusion between a foot-mounted inertial measurement unit (IMU), and a head-mounted system for simultaneous localization and mapping (SLAM). The SLAM system uses both a stereo camera and an IMU. The complete system provides accurate navigation in relevant environments without depending on preinstalled infrastructure.

The camera-based part of the system uses both inertial measurements and visual data, thereby enabling navigation even in environments and scenarios where one of the sensors temporarily provides unreliable data. When sufficient light is available, the system provides good performance. In difficult light conditions, where the number of visible landmarks is very low, it navigates using only inertial measurements, which degrades performance noticeably after a few seconds. On the other hand, the camera-based system can handle a broader range of motion patterns (e.g., movement on escalators, where the foot-mounted system is not able to detect any distinct steps during movement). It also provides the ability to generate maps and 3D models of visited regions. The foot-mounted sensor in the navigation system can compensate for errors once every detected step. It can either be used by itself, or support the camera-based system in situations when camera-based navigation is difficult.

Combining the foot-mounted IMU and the camera-based system enables navigation in almost all kinds of environments and scenarios. To further improve the performance, these systems could also be complemented with, e.g., radio-based ranging, magnetometers, barometric altimeters or ultrasonic sensors.

8542-25, Session 5

Object tracking in the video sequence based on the automatic selection of the appropriate coordinate estimation method

Boris A. Alpatov, Pavel V. Babayan, Sergey Smirnov, Ryazan State Radio Engineering Univ. (Russian Federation)

The selection of the most effective coordinate estimation method to perform object tracking depends on the observation conditions. One of the effective approaches to track objects during the observation condition variations is to change a coordinate estimation method according to these variations. In this paper we propose such approach that includes the selection of an appropriate method from the set of source methods: cross-correlation, statistical segmentation, methods based on spatial and spatio-temporal filtering. Each of these possible methods has advantages in the specific conditions. Cross-correlation is more effective in the noisy imagery when the background is non-uniform, but the object doesn't change rapidly. Statistical segmentation is appropriate when the object changes rapidly, but it fails if the statistical difference between object and background is not essential. Spatial filtering approach is effective to track objects observed on the cloudy or other smooth background. Spatio-temporal method has good performance to detect and track moveable objects observed on the non-uniform slowly changing background.

It is hard to give accurate guidelines of usage of one or another method on the basis of the weather, time of day, object type or other prior knowledge. However, the tracking performance can be estimated with the help of the several parameters (performance features) that describe the reliability of tracking. Performance feature for cross-correlation is based on the comparison of the temporal object variance and its difference from the background. Such feature for the statistical segmentation is based on the entropy difference of the background and object probability distributions. Performance features for the spatial and spatio-temporal filtering approaches are based on the estimation of the signal-to-noise ratio using the background estimator calculated by the appropriate algorithm. The selected set of features is invariant to the changes of the mean brightness, contrast, scale and rotation.

The proposed features are not acceptable for direct comparison the performance of the different methods. To do this we suggest to use the binary characteristic that describe the tracking in the terms of work/not work. The binary characteristic has the value of "work" if the performance feature exceeds the specified threshold, otherwise it is "not work". The thresholds for the performance features are calculated experimentally based on the processing of large set of image sequences. If two or more methods have the binary characteristic of "work", the selection of the appropriate method is performed using the priority table.

The proposed object tracking algorithm is implemented in five steps carried out on each frame: the calculation of the performance feature for each coordinate estimation method, the calculation of the binary characteristic for each method, the selection of the appropriate method, the estimation of the object coordinates using the selected method, the correction of the tracking process performed by other methods.

The experimental research was performed on a set of image sequences obtained during observations of aerial and ground objects. The algorithm shows a good tracking performance during the variations of the observation conditions. In most cases it comprises the main advantages of each of the source methods. The approach has a good computational effectiveness for using in real-time object tracking systems.

8542-26, Session 6

An overview of turbulence compensation *(Invited Paper)*

Klamer Schutte, Adam van Eekeren, Judith Dijk, Piet B. W. Schwering, Miranda van Iersel, TNO Defence, Security and Safety (Netherlands); Niek Doelman, TNO (Netherlands)

In general, long range visual detection, recognition and identification are hampered by turbulence caused by atmospheric conditions. Much research has been devoted to the field of turbulence compensation. One of the main advantages of turbulence compensation is that it enables visual identification over larger distances. In many (military) scenarios this is of crucial importance. In this paper we give an overview of several software and hardware approaches to compensate for the visual artifacts caused by turbulence. These approaches are very diverse and range from the use of dedicated hardware, such as adaptive optics, to the use of software methods, such as deconvolution and lucky imaging. For each approach the pros and cons are given and it is indicated for which scenario this approach is useful. In more detail we describe the turbulence compensation methods TNO has developed in the last years and place them in the context of the different turbulence compensation approaches and TNO's turbulence compensation roadmap. Furthermore we look forward and indicate the upcoming challenges in the field of turbulence compensation.

8542-27, Session 6

Active range imaging via random gating

Grigorios Tsagkatakis, Foundation for Research and Technology-Hellas (Greece); Arnaud Woiselle, Sagem (France); George Tzagkarakis, Commissariat à l'Énergie Atomique (France); Marc Bousquet, Sagem (France); Jean-Luc Starck, Commissariat à l'Énergie Atomique (France); Panagiotis Tsakalides, Foundation for Research and Technology-Hellas (Greece)

The objective in range imaging (RI) is to generate images, where pixel values correspond to depth information. While passive RI, such as stereo and depth from defocus, can achieve this task, the resulting depth map is of low quality, it requires heavy-duty processing, and a specific hardware setup. In active RI on the other hand, methods such as time-of-flight (ToF) and structured light cameras employ a light source in addition to the camera sensor to generate the depth map. Generation of a depth map using classical ToF-RI gating techniques requires the acquisition of a large number of frames, which is proportional to the required depth resolution. In this work, we propose a system based on the premises of compressed sensing (CS) [1], which is able to achieve excellent depth map reconstruction from a significantly reduced number of frames.

CS is a novel approach in signal representation and sampling, which asserts that a signal can be recovered from a small number of random measurements, far below the Nyquist-Shannon limit. To achieve this goal, two major constraints have to be satisfied. First, the signal should be sparsely representable in a dictionary of exemplars and secondly, a critical number of measurements should be made by taking projections of the signal onto a set of random sampling vectors. By exploiting the incoherence between the measurement matrix and the representation dictionary, a property guaranteed by the random nature of the sampling matrix, recovery of the original signal from the random measurements is possible by solving an l1 minimization problem [2] or by greedy matching pursuit approaches [3].

The proposed system is able to reconstruct depth maps with minimum reduction in quality from significantly fewer measurements, when compared to a traditional system, by exploiting the CS framework. Formally, the depth map is constructed by acquiring a small number of frames, where each frame accumulates a large number of returning laser pulses. To achieve the incoherence property [4], the proposed system employs a random gating function where the shutter opens and closes at random intervals during each frame. This random gating function serves as the random projections process in the framework of CS. To recover the depth map, the method assumes that the received signals, that is, the returning laser pulses, are sparse with respect to a dictionary. This dictionary is constructed by taking orthogonal unit vectors, that span the space where the signal resides, multiplied by the random projections matrix.

To validate the theoretical motivation, software simulations were carried out. Our simulated results have shown that reconstruction of a depth map with 128 depth levels resolution is possible at sampling ratios equal to 12%, 15% and 20% of the original depth map dimension, with an RMSE of 17.43, 8.21 and 0.86, respectively. The following figures are examples of the original depth map and reconstructions using a sampling ratio of 12%, 15% and 20%, respectively. Our experimental results have also shown that the proposed method is robust to various types of noise and more realistic signal models.

8542-29, Session 6

Semi-automatic people counting in aerial images

of large crowds

Christian Herrmann, Juergen Metzler, Dieter N Willersinn, Fraunhofer Institute of Optronics, System Technologies and Image Exploitation IOSB (Germany)

Counting people in crowds is a common problem in visual surveillance. Many solutions are just designed to count less than one hundred people. Only few systems have been tested on large crowds of several hundred of people and no known counting system has been tested on crowds of several thousands of people. Furthermore, none of these large scale systems delivers people's positions, they just estimate the number. But having the position of people would be a large benefit, as the counting result gets reasonable. In addition, most approaches assume video data as input or a previously known scene. In order to generally solve the problem, these assumptions must not be made.

We propose a system that can count people on single aerial images of crowds. No assumptions about crowd density will be made, i.e. the system has to work from low to very high density. Also, there is no restriction of people size in the image, as long as an individual is still recognizable. The main challenge is the large variety of possible input data. Typical scenarios would be public events such as demonstrations or open air concerts. But it may also be a crowded pedestrian area. To solve this problem, we propose a system that detects individual humans in a model-based way. This includes the determination of their positions and the total number. In order to cope with the given challenges we divide our system into three steps: foreground segmentation, person size determination and person detection. For foreground segmentation and person size determination some computer-aided user input is necessary to complete these steps. The model-based person detection on the foreground mask is fully automated.

We evaluate our proposed system on a variety of aerial images showing large crowds with more than one thousand people. The counting results of our system are compared to the manually determined number of people. A comparison to pure manual counting is done as well. An evaluation of processing times shows the possible time saving.

With sufficient performance our system will open wide fields of application due to the few restrictions.

8542-30, Session 6

The design of image stabilization control system

Zhe Lin, Fei Yu, Beijing Institute of Space Mechanics and Electricity (China); Chunnan Wu, China Academy of Space Technology (China); Xiao-jun Kang, Beijing Institute of Space Mechanics and Electricity (China)

For high resolution satellite remote sensing cameras, the line of sight (LOS) moving during the image exposure period will cause the modulation transfer function (MTF) degradation and image blurring. Image stabilization component is used to improve image quality by actively removing the apparent motion induced by vibration, tracking error and attitude instability. In this paper, the image stabilization component is considered as a kind of closed loop servo control system, and image stabilization effect is converted into servo control performance to research. Firstly, the image stabilization servo loop scheme and transfer function model are constructed and the LOS jitter is considered as the output of a stochastic system derived by white-Gaussian noise. Based on the proposed model, the demand boundary of jitter rejection function is described, and the design criterion to be satisfied is obtained according to the requirement of image stabilization performance. And then, a discrete Kalman estimation algorithm is introduced into image stabilization servo loop to filter out the noise caused by PSS and compensate for the delay due to the PSS measurement. Based on the given design criterion, the control law is designed by using the output of Kalman filter. The computer simulation is achieved to show that the proposed control strategy can significantly improve the image stabilization performance.

8542-9, Session PS

Analysis of the application of mid-wave infrared HgCdTe FPAs on remote sensing systems

Xiaoman Li, Beijing Institute of Space Mechanics and Electricity (China)

With the development of science and technology, high spatial resolution, large field of view and high radiant resolution are required for Satellite infrared remote sensing imagery. IRFPA is one of the key components of the infrared remote sensing system. To meet the requirement, high responsivity and large format IRFPAs are needed. There are many kinds of IRFPAs with excellent performance in the world. 3-5μm infrared Spectral range is an important spectrum range

which is commonly used in IR imaging systems. In the article, one kind of MWIR HgCdTe IRFPA was utilized as a model.

Considering the total requirements of the radiant performance (for example, NETD ≤ 40mK @ 300K) of the Satellite infrared remote sensing system, performance of IR detectors was analyzed.

After analyzing the response model of the HgCdTe IRFPAs, the performance index of the IRFPA without imaging circuit was tested and the NETD with different integration time was analyzed. Besides, A low noise imaging circuit was developed for research. As the imaging circuit noise would affect the system performance by decreasing the specific detectivity of the system, the relationship between the specific detectivity and the circuit noise was obtained.

Integration time would obviously affect the performance of the system, by changing the responsivity,etc. Optimization of the integration time was introduced in the article.

A demo imaging system based on the MWIR HgCdTe was developed. The system contains a F/2 optics system. Based on the performance and imaging tests of the detector on the demo imaging system, performances of the MWIR IRFPA were introduced and influence factors of the specific detectivity of the detector were analyzed. images taken in the imaging experiments were reported in the article.

The contents of the article could be reference in the applications of the HgCdTe IRFPAs.

8542-31, Session PS

A wideband low-noise pulse laser detection circuit for the 3D imaging lidar

Chunsheng Hu, Zongsheng Huang, Xingshu Wang, Shiqiao Qin, National Univ. of Defense Technology (China)

The research of the 3D imaging lidar is a key area in the 3D information acquisition research. It has so many successful applications at present. The detection circuit of the pulsed laser is a key part in the 3D imaging lidar.

In order to enhance the measurement precision and detection range of the 3D imaging lidar, we propose a new broadband low-noise detection circuit for the pulsed laser, which is mainly composed of a high-speed APD detector and a broadband low-noise transimpedance amplifier. The APD detector is used to convert the pulsed laser into pulse current, and the C30737E500 APD detector is adopted. The transimpedance amplifier is used to amplify the output current of the APD detector, and then convert it into differential voltage. The adopted NE5210 has some advantages: low noise, wide band, and proper differential transresistance.

One of the advantages of the NE5210 amplifier is that it outputs differential voltage, which is beneficial to reduce the common mode noise of the detection circuit. The input current of the NE5210 amplifier ranges from -260 μA to 220 μA. It means that the negative current amplitude is 40 μA bigger than the positive current amplitude. In order to increase the input current range of the detection circuit, we apply a high negative bias voltage to the APD detector and set the static input current of the NE5210 amplifier to 200 μA with a proper bias method. By this bias method, the allowable input current range of NE5210 amplifier is enhanced about 1 time, increasing from 260 μA to 460 μA. This is very helpful improvement for the input laser power range of the detection circuit and the detection range of the 3D imaging lidar.

This paper introduces the main framework of the detection circuit and then investigates the characteristics of the detection circuit, such as the input equivalent noise current, the output voltage SNR, laser power detection range, bandwidth, and etc. Through the theoretical analysis of the noise and signal, the output noise voltage, output signal voltage and SNR of the detection circuit are calculated under the condition of the target distance ranging from 1 m to 100 m. The detection experiment has been carried out with the proposed circuit, showing that the circuit can detect a narrow pulsed laser with about 4 ns pulse width, with the output noise of about 0.6 mV.

Based on our experiments and analyses, the pass band of the detection circuit ranges from 0.56 MHz to 200MHz approximately, the allowable input current of the NE5210 amplifier varies from -460 μA to 0, and the effective output differential voltage ranges from -1.6 V to 1.4 V. As to the laser wavelength of 905 nm, the maximum peek laser power of the detection circuit could achieve 12 μW and the NEP of the detection circuit could reach 2.2 pW. The detection circuit is implemented and tested in a high-speed 3D imaging lidar here. Besides the 3D imaging lidar, the detection circuit can be applied to the pulsed laser range finder and other pulsed laser detection system.

8542-32, Session PS

Disturbance observer based control system design for inertially stabilized platform

Chunnan Wu, Zhe Lin, Beijing Institution of Space Mechanics and Electricity (China)

Airborne high-resolution imaging systems are essential for various military applications such as remote surveillance, target acquiring, tracking and pointing systems. An inertially stabilized platform (ISP) is indispensable for such systems to segregate the base angular movement and then achieve high Line-Of-Sight stability. Thus, the disturbance rejection ratio and command following performance of ISP are of primary concern. Currently, those high performances were achieved with various advanced control algorithms using, for example, state variable feedback, adaptive techniques and disturbance observer designs.

Based on disturbance observer, this paper demonstrates a composite control system design for the rate loop of a multi-gimbaled inertially stabilized platform. A quad gimbals platform is built with the two inner gimbals serve as an inertially stabilized platform with two degrees of freedom. Each inner gimbal is actuated by a brush type DC direct drive torque motor, a gyroscope is mounted on the platform to measure the inertial angular rate of the line-of-sight of the payload around the two axis orthogonal to it with respect to inertial space. The outer gimbals, on the other hand, tracks the inner gimbals on a real-time basis, making the inner gimbals coordinates constantly aligned. This paper is mainly focus on the inner inertial rate control loop. In the presence of inevitable cable spring torque, friction, mass imbalance and kinematic coupled disturbance imposed on the inner gimbals, the stabilization performance deteriorates significantly. In our controller design, a two-loop control structure is developed based on disturbance observer based (DOB) controller scheme to boost stabilization performance. The internal-loop compensator is constructed to make the system's behavior between control input and plant output, i.e., angular rate with respect to inertial coordinate, robust under the influence of external disturbance signals, modeling uncertainties and parameter variations. Also, the internal-loop compensator, which forces the actual plant to behave like an actively selected nominal model, is designed on an optimal basis to obtain both robust stability and optimized performance. The external-loop, which is designed based on the nominal model, serves as a feedback controller to attain a desired command following performance specification. The main contributions of this paper are to design the inertial stabilized platform on an optimal basis and to analyze the robust stability in the presence of variation of the platform inertia. Simulation and experimental results show the performance enhancement of our control structure in the presence of disturbance.

8542-33, Session PS

Circular Variable Filters (CVF) at CI: progress and new performance

Dario Cabib, CI Systems (Israel) Ltd. (Israel); Henry J. B. Orr, Nelson Consulting Partnership (United Kingdom)

As presented in September 2010 in Toulouse CI Systems has been developing a new technology for Circular Variable Filters (CVF) production. These filters are used as monochromators of medium spectral resolution in radiometric and spectroradiometric instrumentation for spectroscopic and remote sensing applications in the laboratory and in the field.

As mentioned then, OCLI, the original US company that developed the old CVF technology, stopped production in the '90's and CI started to reconstruct the technology in 2009. The first results of CVF performance following this new work were presented in the wavelength region of 1.3 to 2.5 microns in 2010. Since then we made progress and completed the development of segments up to 14.3 microns, with a spectral resolution up to 1.5% of the peak wavelength. The advantage of the new production method is that both the so called "tooling factor" and the peak wavelength profile along the circumference are controlled by software instead of by fixed hardware gear ratios, yielding higher design flexibility. A new high resolution CVF model in the 7.7 to 12.6 micron range with three times better resolution has also been developed.

8542-34, Session PS

A compact rangefinder based on self-mixing interferometry

Michele Norgia, Alessandro Magnani, E. Nastasi, Alessandro Pesatori, Politecnico di Milano (Italy)

Optical telemeters are commonly used for various industrial applications, thanks to the good accuracy and the possibility of non-contact measurement. The proposed instrument described in this contribution is based on a coherent technique for laser diode, known in literature as feedback interferometry or self-mixing. In the self-mixing optical configuration a small part of emitted light is reflected into the laser cavity by a target (cooperative, or also diffusive). This phenomenon induces a modulation of frequency and amplitude of the light emitted by the laser, easily measurable by the monitor photodiode. The interferometric signal is composed by a series of fringes whose amplitude and waveform depend on the characteristics of the target surface; in case of moderate back-injection (typical of reflecting, or white-diffusive surfaces) the fringes assume a sawtooth shape with high signal-to-noise ratio; for weak injection, instead, the interferometric fringes tend to become a noisy sinusoids. The interferometric signal is read from the monitor photodiode by a transimpedance amplifier and soon acquired by a Digital Signal Processor for managing the overall measurement procedure. Typically when the target moves, the variation of the absolute distance causes a series of fringes. However, with fixed target at a certain distance, it is possible to generate fringes simply by applying a variation to the pump current that induces a modulation of the laser wavelength. Theoretically, a small triangular current modulation generates a series of fringes with ideally constant period: the frequency of the induced fringes is proportional to the absolute distance of the target. To allow a class I safety working, the diode laser is kept below the threshold current and, periodically, the triangular modulation is applied for a short time. By doing this particular waveform the mean emitted power is equal to the mean power of a single triangular pulse reduced by the waveform duty cycle. The wavelength modulation in a laser diode is essentially due to thermal variation, induced by the pump current. The frequency behavior of this phenomenon is low-pass, with a series of zeros and poles. The choice of the frequency of the triangular modulation was made in order to meet a flat zone of characteristic, experimentally measured in order to keep a constant fringe period during the triangular modulation.

The target distance estimation is made possible by the evaluation of the main tone frequency, realized by an interpolated FFT applied on the ascent and the descent edges of the triangular modulation. The choice of making two calculations for each triangular pulse has the big advantage of minimizing the sensitivity to the movements of the target.

Globally, the realized rangefinder demonstrates very good working on diffusive surfaces, with low power emission, measurement range from 5 cm to 2 m, and less than 35 ms of measuring time. The standard deviation of a single measurement is about 100 μm and can reach 10 μm by averaging. Another feature of this sensor is its compact size and low cost, since it is composed only by a little electronic circuit mounted on a DSP board.

8542-35, Session PS

Innovative optical sensor for displacement measurement by precision laser applications

Dumitru Ulieru, SITEX 45 (Romania); Florian N. Pistritu, National Institute for Research and Development in Microtechnologies (Romania); Adrian Tantau, SITEX 45 (Romania)

An interferometric displacement sensor with useful properties has been built based on a laser with optical feedback. from light that is backlighted by a moving object. Information about the object motion is encoded in the phase and the amplitude the backscattered light which it turn influences the phase and the amplitude of the laser via injection looking physics. We derive the properties of the amplitude and phase modulation of the laser from standard injection looking relation augmented by a self augmented condition. These predictions are then confirmed by experimental results. An off the shell two mode frequency stabilized laser is used for displacement measurement as homodyne set-up. Second the phase modulation of the laser is used in a pseudoheterodyne interferometer. In both cases the backscattered light from the object could be injected into the laser cavity without the help of any focused optics. The injection locked sensor combine advantages of readily available equipment with straightforward optical setup without need for intricate alignment and thereby meets two important conditions for industrial applications.

Because there is a strong need in production industries to change the quality control from statistical sampling and off line inspection to continuous on line monitoring of parameters that quantify the quality of process. Laser fiber optic based sensing systems hold great potential for contributing towards this need. However the requirements for high precision alignment and a low signal to noise ratio are serious barriers to their use. In our paper we present an injection locked laser sensor that has developed as a component in a sensing system designed to meet the industrial environment. A special chapter will discuss the software approach for extraction of displacement informations of from laser sensor. Our proposed sensor will meet the requirements for a precise optical alignment necessary for industrial applications while simultaneously producing dynamic measurements with an adequate signalization ratio.

8542-37, Session PS

Water quality assessment in Kelantan delta using remote sensing technique

Mohd Rifhan Mustapha, Hwee-San Lim, Saumi Syahreza, Mohd Zubir M. Jafri, Univ. Sains Malaysia (Malaysia)

This paper presents the utilities of remote sensing technique for water quality assessment in Kelantan Delta. Remote sensing is very effective method for water quality monitoring trough analysis image over coverage of study area. The objective of this study is to examine potential of 10-m resolution images from the Advanced Land Observing Satellite (ALOS) on Japanese Earth Observing Satellite for assessing water quality in Kelantan Delta and to test the sensitivity of spectral signatures measured by a spectroradiometer from regions with different turbidity. There is a large correlation between turbidity and the in-situ reflectance at 500 - 620 nm (maximum spectra band between 300 and 1100 nm) that shown by exponential regression model (turbidity = 193.75e-111.2 x R (500-620), R? = 0.9582, n= 7), resulting from increasing of suspended concentrations, was developed and applied to ALOS band 1-band 3 (0.42-069 nm).An atmospheric correction, based on corrected satellite data using a radiative transfer code and in-situ reflectance measurements. The ALOS data provides accurate estimates of the mean water quality (r = 0.92 and RMSE = 1.89). The result acquired that reliable estimates of water quality values for the Kelantan Delta, Malaysia, and its future operation.

8542-38, Session PS

Improved Hough transform for curve detection based on directional control of connected regions

Shi Yu, Yuan Jie, Guoyou Wang, Li XiuHua, Huazhong Univ. of Science and Technology (China)

Accurate and efficient curve detection in images is a challenging computer vision problem. Hough transform is one of the most widely used techniques for curve detection. Existing HT-based methods have disadvantages of low accurancy and low speed. In this paper, a new and efficient Hough Transform for curve detection is presented. In view of kinematics, a curve can be regarded as movement locus of a given point, and point's velocity direction is the tangential direction of point on the smooth curve. Thus the main contributions are threefold. 1) We formulate the problem of curve detection as robustly fit curve in the connected region. 2) We propose the direction elements and directional control scheme to quickly discover the smooth curve. 3) We use a coarse-to-fine strategy to efficiently detect the final curve. We have tested our algorithm on simulated and natural image. Compared to other classical curve detection methods, experimental results indicated that our algorithm reduces the time cost and improves the detection accuracy greatly.

Conference 8542B: Emerging Technologies

Monday - Tuesday 24–25 September 2012 • Part of Proceedings of SPIE Vol. 8542
Electro-Optical Remote Sensing, Photonic Technologies, and Applications VI

8542-40, Session 7

Future directions in information sciences research: the role of sensors and networks *(Keynote Presentation)*

John Pellegrino, Barbara D. Broome, U.S. Army Research Lab. (United States)

The last decade has produced unprecedented advances in technologies to collect and manage data, text and imagery. The same decade has not produced the processing capabilities necessary to extract actionable intelligence from that information. One of the barriers to success is that we continue tackling this problem in a piecemeal manner. We improve our sensors and communications networks, processing and exploitation technologies, and human-computer interfaces, yet fail to account for the interdependencies of these information system components. Further, we fail to take advantage of critical between-component feedback loops that could improve the overall speed and accuracy of the decision processes these tools and technologies are established to support. In order to overcome these shortfalls, a trans-disciplinary research initiative is proposed, involving researchers in sensor processing, communications, information science and cognitive science, and focused on providing game-changing improvements to individual and collaborative decision making in military operations. Topics addressed will include the future role of sensors and sensor networks in providing context for decision making.

8542-41, Session 7

The other end of the scale: coded apertures in the near field for high resolution 3D gamma event localization in bulk scintillators *(Invited Paper)*

Klaus P. Ziock, Oak Ridge National Lab. (United States); Joshua B. Braverman, The Univ. of Tennessee (United States); Lorenzo Fabris, Mark J. Harrison, Oak Ridge National Lab. (United States)

Coded apertures were originally developed by the high-energy astrophysical community for use in imaging high-energy photons (x- and gamma-rays) for which focusing optics are ineffective. We are now taking what was developed as a tool for use in the extreme far field at high energies, to encode spatial information at optical wavelengths in the extreme near field to enhance the performance of position-sensitive x- and gamma-ray scintillator detectors. Spatial resolution for events within bulk scintillators is limited by the size of the light “spot” available at the sides of the scintillator, where phototransducers (PT) convert the light to an electrical signal. The ability to localize an event is determined by how well one can determine the centroid and the size of the spot. Generally, performance is limited to many millimeters in all three spatial dimensions, and one cannot resolve simultaneous events that are closer together than the width of the light spot (frequently of order 10 mm).

To improve on the spatial resolution of a bulk scintillator radiation detector, we are exploring the use of an optical coded-aperture shadow mask added to the light guide connecting the exit face of the scintillator crystal and a position-sensitive PT. The shadow mask encodes the location of a scintillation event as spatial changes in the light reaching the PT and the high frequency content in the pattern allows one to separate simultaneous events based on the size of the smallest mask element rather than the width of the overall light spot. Even further localization of individual events is possible by finding the centroid of the imaged event.

In principle, both of these properties could be achieved through the use of lenses to focus the light on a position-sensitive PT without paying the noise penalty of indirect imaging incurred by the coded-aperture approach. However the use of lenses is complicated by the need for a very fast optic to avoid loss of scintillation light and the inability of a lens-based approach to determine the depth of events within the crystal. In contrast, with a coded-aperture one can take advantage of their near-field property that the magnification of the pattern size at the PT is a function of event distance from the shadow mask. In the near field the magnification factor changes significantly with event distance and by reprocessing the observed shadow pattern with different magnification factors this provides a means of refocusing the system in software after the data is collected. Using this approach and looking for the sharpest spot, one can determine the event depth within the crystal. This provides the third dimension of the event location. Simulations indicate that spatial resolutions of order a cubic millimeter are possible at modest event energies (~ 200 keV) and a device to validate these simulations is under construction. Simulation and experimental results will be presented.

8542-42, Session 7

Enabling technologies for advanced imaging *(Keynote Presentation)*

Nibir K. Dhar, Defense Advanced Research Projects Agency (United States)

Advances in imaging technology have a huge impact on our daily lives. Innovations in optics, focal plane arrays (FPA), microelectronics and computation have revolutionized camera design. As a result, new approaches to camera design and low cost manufacturing are now possible. These advances are clearly evident in the visible wavelength band due to pixel scaling, improvements in silicon material and CMOS technology. CMOS cameras are available in cell phones and many other consumer products. Advances in infrared imaging technology have been slow to emerge due to market volume and many technological barriers in detector materials, optics and fundamental limits imposed by the scaling laws of optics. There is of course much room for improvements in both, visible and infrared imaging technology.

This presentation will describe the imaging vision of DARPA’s Microsystems Technology Office (MTO), the technology challenges and projects currently fielded. In particular, a description of new technology development under a portfolio program, “Advanced Wide Field of View Architectures for Image Reconstruction and Exploitation (AWARE)” will be described highlighting the following:

1. A modular and scalable camera architecture to overcome scaling limitations of conventional imaging system designs, and to demonstrate the feasibility of near-linear growth of optical information throughput with increasing imaging system scale in reasonably small and affordable form factors.

2. Advancement in pixel scaling and high density FPA technology.

3. Development of Focal Plane Arrays with broadband (0.5-5 m wavelength band), continuous (visible to MWIR) day/night FPA technology.

4. A day/night visible/NIR and LWIR room temperature FPA with improved optics and integrated processing.

8542-43, Session 8

Depth imaging using single-photon detection *(Keynote Presentation)*

Gerald S. Buller, Heriot-Watt Univ. (United Kingdom)

Active depth imaging approaches have been considered for an increasing number of potential applications in various emerging application scenarios, including environmental sensing, manufacturing, security and defence. Whilst time-correlated single photon counting cannot be considered a new approach - examples of single-photon time-of-flight measurements have been used for depth analysis over thirty years - the technique has undergone radical changes as a result of vast improvements in detector performance, acquisition hardware and signal processing algorithms and processing speeds. The high sensitivity and picosecond timing resolution of the time-correlated single photon counting can provide distinct advantages in the trade-offs between the required illumination power, range, depth resolution and data acquisition durations. Critically, these considerations must also address requirements for eye-safety, especially in applications requiring outdoor, kilometer range sensing. The shot noise limited detectivity of single-photon counting can provide the means for low

average power depth imaging from the low scatter returns expected from low signature, non-cooperative targets at ranges of greater than one kilometer.

We present experimental demonstrations of depth imaging from a scanning time-of-flight imager based on high repetition-rate (>MHz) pulsed illumination and various semiconductor-based single-photon detectors. In advanced photon-counting experiments, we have employed the system for unambiguous range resolution at several kilometers target distance, multiple-surface resolution based on adaptive algorithms, and a cumulative data acquisition method that facilitates detector characterisation and evaluation. Results illustrating the surface to surface resolution and potential for depth imaging through clutter will also be presented. We consider a range of optical design configurations and discuss the performance trade-offs in more detail. Much of this work has been performed at wavelengths around 850nm for convenient use with various Si-based single photon avalanche diode detectors. Also presented will be recent work at wavelengths near 1550nm which when compared to the shorter operational wavelength band, provide more relaxed eye safety requirements, reduced solar background levels and improvements in atmospheric transmission. This work illustrates kilometre range depth profiles with centimetre resolution, at sub-millisecond per pixel acquisition time, using average laser power levels of less than 1mW at one kilometer range in typical daylight conditions.

The Heriot-Watt work will be compared with that of the different approaches used by other laboratories, to examine the potential of single-photon time-of-flight imaging approach for long distance depth imaging.

8542-44, Session 8

An all-optronic synthetic aperture lidar

Simon Turbide, Linda Marchese, Marc Terroux, François Babin, Alain Bergeron, INO (Canada)

Synthetic Aperture Radar (SAR) is a mature technology that overcomes the diffraction limit of an imaging system's real aperture. This is done by taking advantage of the platform motion to coherently sample multiple sections of an aperture much larger than the physical one. A SAR system makes an image of the Earth's surface by pointing a radar beam approximately perpendicular to the sensor's motion vector, transmitting phase-encoded pulses, and recording the radar echoes as they reflect off the Earth's surface. This technology has permitted extensive observation of the Earth's surface from airborne and space borne platforms.

Synthetic Aperture Ladar (SAL) is the extension of SAR to much shorter wavelengths (1.5 μm vs 5 cm). This new technology can offer higher resolution images in day or night time as well as in certain adverse conditions. It could be a powerful tool for Earth monitoring (ship detection, frontier surveillance, ocean monitoring,...) from aircraft, unattended arieal vehicle (UAV) or spatial platforms. It is believed that this technology could also provide centimeter-class resolution with an aperture size no larger than a few meters on an observation range of thousand kilometers, ideal for the orbital observation of system solar objects.

A continuous flow of high-resolution images covering large areas would however produce a large amount of data involving a high cost in term of post-processing computational time. SAL image reconstruction may be performed either digitally or optronically. The digital processing relies on algorithms such as Range-Doppler or Chirp-Scaling. The optronic processing is based on digital holography. In this technique, the raw data are coherently illuminated and lenses are inserted into the beam's path focusing the raw data to form the image that is in turn captured by a digital camera or a film. The optronic processing mainly differ from the more traditional numerical approach by its real-time processing capability.

This paper presents a laboratory SAL image acquisition system that was designed and built. The system is based on a laser that can perform mode-hop free sweeps over its 1500-1630 nm tuning range with a maximum output power of 24 mW. The non-metallic diffusing target, made of paper, was mounted on a translation stage at a range above 3m. The same optical elements are use for transmission and reception. The data acquired by the SAL set-up was then processed using the optronic SAR processor designed for ENVISAT/ASAR data. No changes were made to the optronic processor; only a straightforward scaling was performed to change raw data focal lengths. Good agreement was found between the images processed numerically and optronically, both showing sub-millimeter spatial resolutions.

The results of the work presented in this paper demonstrate the feasibility of an all-optical SAL sensing-to-processing chain. An all optical SAL system would provide a compact, lightweight system that could provide both image acquisition and reconstruction on-board for immediate downlink of ultra-high resolution images.

8542-45, Session 8

A photon-counting optical communication system for underwater data transfer

Philip A. Hiskett, Robert Struthers, Roy Tatton, Robert A. Lamb, SELEX Galileo Ltd. (United Kingdom)

Communication to a submerged underwater vehicle is relevant to both civilian and military applications. These applications may include communication between a ship and a submerged remotely operated vehicle (ROV); from submarine to submarine or from an aircraft to a submarine. Optical communication schemes are widely used in free-space applications but less so in underwater applications. In an airborne to underwater system the surface characteristics of the ocean have to be considered which have the effect of varying the optical path length on a pulse to pulse basis. Waves therefore expand and compress the transmitted optical data pattern during transmission which at higher transmission rates can introduce error to the data because bits are assigned to incorrect clock periods. Also, an uneven sea surface distorts the wavefront of each individual optical pulse. Underwater to underwater transmission is more straightforward but the relative movement of the platforms has to be considered. Regardless of the transmitter location it is the often the significant attenuation of the optical signals when transmitted through water brought about by both absorption and scattering that limits the effectiveness of optical communication through sea water. This has prompted our investigation into the use of a single photon counting based communication system.

We will describe an optical communication system which was developed to investigate the transmission of an encoded data stream through water. This single photon-counting system used a fast semiconductor laser diode with a pulse width of ~100ps operating at a wavelength of 455nm which had a maximum transmission rate of 40Mb/s. Deep junction silicon single photon avalanche diode detectors were used to detect the transmitted optical signal. The aperture size of the optical receiver was only 50mm.

Results from a detailed investigation of the effects of attenuation and multi-path scatter on the transmitted data stream through water will be presented. In particular, the effect of scatter on the pulse duration and time of arrival of the optical pulses will be discussed. The bit error rate and the transmitted bit rate of the system were determined for several alternative particulates in a water tank. The length of the tank was restricted to ~1m with a cross section of 0.4m x 0.4m in these initial trials to minimise the amount of particulate necessary to achieve the required particulate density. For each particulate the bit error rate and bit rate were measured for a range of concentrations of particulate.

The practical design considerations for a system for use over large transmission distances in a non-laboratory environment will be presented. This will include clock recovery schemes for the scenarios where transmission occurs from one submerged platform to another submerged platform and transmission from airborne platform to a submerged platform. Operation at alternative wavelengths that minimise the solar background and error rate but optimise the signal-to-noise are also discussed.

8542-46, Session 8

Evaluation of image deblurring methods via a classification metric

Daniele Perrone, Heriot-Watt Univ. (United Kingdom); David Humphreys, Robert A. Lamb, SELEX Galileo Ltd. (United Kingdom); Paolo Favaro, Heriot-Watt Univ. (United Kingdom)

The performance of single image deblurring algorithms is typically evaluated via a certain discrepancy between the reconstructed image and the ideal sharp image. The choice of metric, however, has been a source of debate and has also led to alternative metrics based on human visual perception. While fixed metrics may fail to capture some small but visible artifacts, perception-based metrics may favor reconstructions with artifacts that are visually pleasant. To overcome these limitations, we propose to assess the quality

of reconstructed images via a task-driven metric. In this paper we consider object classification as the task and therefore use the rate of classification as the metric to measure deblurring performance. In our evaluation we use data with different amounts of noise and types of blur in two cases: Optical Character Recognition (OCR), where the goal is to recognize characters in a black and white image, and object categorization with no restrictions on pose, illumination and orientation.

For the first case we use the ISRI Fourth Annual Test of OCR Accuracy as training and test data and Tesseract OCR as the OCR engine.

In order to evaluate the accuracy of the OCR engine we use three standard classification metrics: character accuracy, that is the percentage of correctly recognized single characters; stop words accuracy, that is the percentage of correctly recognized “stop words” (notice that stop words are usually filtered out in systems that process natural language); non-stop words accuracy, that is the percentage of correctly recognized “non-stop words”.

For object categorization we use the Calltech 101 dataset and a one-vs-all SVM classifier for each category present in the dataset. We evaluate the accuracy of the classification using the receiver operating characteristic (ROC) curve, as commonly done for assessing object classification accuracy.

In both cases we evaluate different levels of noise in the image and different types of motion blur point spread functions (PSF). We consider both unimodal and multimodal PSFs for generality.

We test four different well-known deblurring approaches available in the literature and based on the following image priors: Gaussian prior on image gradients, sparse prior on image gradients, dictionary-based, non-local self-similarities.

Finally, we show how off-the-shelf classification algorithms benefit from working with deblurred images.

8542-47, Session 9

Controlling the localization and migration of optical excitation *(Keynote Presentation)*

David L Andrews, David S Bradshaw, Univ. of East Anglia Norwich (United Kingdom)

In the nanoscale structure of a wide variety of material systems, a close juxtaposition of optically responsive components can lead to the absorption of light by one species producing fluorescence that is clearly attributable to another. The effect is generally evident in systems comprising two or more light-absorbing components (molecules, chromophores or quantum dots) with well-characterized fluorescence bands at similar, differentiable wavelengths. This enables the fluorescence associated with transferred energy to be discriminated against fluorescence from an initially excited component. The fundamental mechanism at the heart of the phenomenon, molecular (resonance) energy transfer, also operates in systems where the product of optical absorption is optical frequency up-conversion.

In contrast to random media, structurally organised materials offer the possibility of pre-configured control over the delocalization of energy, through molecular energy transfer following optical excitation. The Förster mechanism that conveys energy between molecular-scale components is strongly sensitive to specific forms of correlation between the involved components, in terms of position, spectroscopic character, and orientation; one of the key factors is a spectroscopic gradient. Suitably designed materials offer a broad scope for the widespread exploitation of such features, in applications ranging from chemical and biological sensing to the detection of nanoscale motions or molecular conformations.

Recently, attention has turned to the prospect of actively controlling the process of energy migration, for example by changing the relative efficiencies of fluorescence and molecular energy transfer. On application of static electric fields or off-resonant laser light - just two of the possibilities - each represents a means for achieving active control with ultrafast response, in suitably configured systems. As the principles are established and the theory is developed, a range of new possibilities for technical application is emerging. For example, applications can be envisaged for new forms of all-optical switching and transistor action. There is also interest in engaging with the interplay of optical excitation and local nanoscale force, exploiting local responses to changes in London or Casimir forces, accompanying molecular energy transfer.

8542-48, Session 9

Mid-infrared photonics enabled by 3D laser writing chalcogenide glass

Airán Ródenas, John McCarthy, Heriot-Watt Univ. (United Kingdom); Nicholas D Psaila, Optoscribe Ltd. (United Kingdom); Graeme Brown, Henry T. Bookey, Robert R. Thomson, Ajoy K. Kar, Heriot-Watt Univ. (United Kingdom)

The mid infrared (MIR) range of the electromagnetic spectrum, between 3 μm to 25 μm (100-12 THz), is a key region for a large number of photonic applications such as: sensing in the medical, industrial and environmental fields, high resolution molecular spectroscopy, remote thermal imaging in modern satellites, space science, free-space communication, automotive and aerospace industries, and ground or spaceborne astronomy. MIR light suffers from less Rayleigh scattering than its near-IR or Visible counterparts, and it is also the region where the Earth’s atmosphere exhibits important transmission windows for either Earth or space observation. The MIR is the spectral region which covers the fingerprints of most molecular energy transitions, enabling a vast amount of applications to be developed such as for instance the direct detection of greenhouse gases like CO2 and CH4, or of pollutants such as HCN and CF4. Within astronomy, the MIR is also an exciting observing window. Regardless these important potential applications, MIR photonics are still in its infancy. Integrated optics (IO) technologies are now extremely well developed for the visible and near-infrared range; but the situation is quite different for the MIR spectral domain. Despite a number of two-dimensional (2D) MIR surface processing fabrication approaches have been recently demonstrated, these are all based on multiple-step surface processing and/or make use of thin-films for vertical confinement, therefore constraining the optical designs to strict in-plane propagations.

In this presentation we review our recent progress on the fabrication of waveguides (Wgs) for near future 3D MIR photonic technologies. The Wgs are fabricated by an ultrafast ultrashort-pulse laser-writing process which enables the incorporation of the optical circuits into any instrument device or substrate, as far as the material optical absorption band edge is below the laser wavelength, and without requiring any lithography or clean room facility.

Here we present recent results on the development of ultrafast laser microfabricated MIR chalcogenide photonics. Low loss single and multimode waveguide arrays were successfully laser fabricated, for the first time to our knowledge, for the whole NIR to MIR range (1 to 11 μm wavelengths). Using a fs optical parametric amplifier system, the optical nonlinearity of bulk gallium lanthanum sulphide (GLS) glass could be measured at 2.5 m. Upper limits for the nonlinear properties of the laser modified material could be estimated based upon the nonlinear spectral broadening of a 2.5 m fs pulse train coupled into single-mode waveguides. Further work showed the possibility of fabricating waveguides and on-chip 3D beam-combiners for the MIR (11 μm) for near future implementation in astronomical observatories. This work shows how ultrafast laser writing is an extremely powerful microfabrication tool for the development of mid infrared waveguides, and how it opens up the possibilities of directly integrating mid-IR photonics in present and future ground-based, airborne or space-based technologies.

8542-49, Session 9

Efficient, massively parallel exploration of networks by biological agents

Dan V. Nicolau, Univ. of Liverpool (United Kingdom); Dan V. Nicolau Jr., Molecular Sense Ltd. (United Kingdom)

The exploration of networks with a view to discovering certain of their global properties (such as the presence of a self-avoiding circuit) is a critically important problem in a multitude of defence applications, including cryptography, logistics and other planning tasks. In most cases of interest, the appropriate mathematical problem is combinatorial and “NP-hard” and therefore computing its solution is generally intractable using conventional computers. Biological systems, on the other hand, process information only in a massively parallel fashion (e.g. hundreds of metabolic processes proceed concurrently in each living cell). One can therefore hope to harness this property of living systems to efficiently solve combinatorial problems, as has been attempted with DNA computing. In this paper we describe the design of a device that uses molecular motors or

similarly sized, moving biological entities or “agents” to explore a given network or set of networks. We illustrate the potential of this purported device to solve one particularly relevant NP-hard problem in defence contexts: SUBSET SUM, which underlies many cryptography and limited-resource-allocation applications. Simulations of our design suggest that implementations of this device would perform well in comparison to conventional, electronic computers for any combinatorial task that can be encoded as a network architecture.

8542-50, Session 10

Plasmonics in nanophotonics and sensing *(Keynote Presentation)*

Anatoly V. Zayats, King’s College London (United Kingdom)

Recent advances in nanofabrication and subwavelength optical characterisation have led to the development of a new area of nanophotonics concerned with routing and conditioning of optical signals in scalable and integratable devices. In this context, plasmonics which is dealing with surface electromagnetic excitations in metallic structures, provides a great deal of flexibility in photonic integration in all-optical circuits since with surface plasmons the problem of light manipulation can be reduced from three to two dimensions. Surface plasmon polaritons, the electromagnetic excitations coupled to collective motion of conduction electrons near a metal surface, are emerging as a new optical information carrier that enables signal manipulation and processing on the subwavelength scale. Plasmonic nanostructures and metamaterials play crucial role in the development of novel paradigms for bio- and chemical sensing, both in optical and mid-IR regimes. In this talk we will discuss principles and applications of plasmonic components for applications in optical signal processing as well as for sensing applications including refractive index sensing, chemical sensing in mid-infrared spectral range, and Raman identification of explosive substances. This work has been supported by EPSRC (UK), EC FP7 IST project PLAISIR and EC FP7 SECURITY project BONAS.

8542-51, Session 10

Developments in MOVPE HgCdTe arrays for passive and active infrared imaging *(Keynote Presentation)*

Ian M Baker, Chris Maxey, Les Hipwood, Harald Weller, Peter Thorne, SELEX Galileo Ltd. (United Kingdom)

Modern infrared detectors have three key development aims: reducing the cost especially for large arrays, improving the operating temperature for lower power, size and weight cameras and increasing the functionality. Selex Galileo Infrared Ltd has developed a range of infrared detectors based on HgCdTe grown by Metal Organic Vapour Phase Epitaxy (MOVPE) on inexpensive 75mm GaAs substrates. The independent control of bandgap and doping levels (both N and P) over a wide range allows freedom to design complex device structures such as: two-colour detectors and avalanche photodiode arrays. MOVPE arrays use a mesa device structure with a small, weakly doped absorber, well suited to operation at higher temperatures. The HgCdTe is bump bonded onto a custom designed silicon readout IC which is becoming increasingly sophisticated. Using topomorphic design techniques these ICs can have multifunctional operation (active 3D and passive imaging in one focal plane array) so that many cameras can be combined into one. The state of the art for array size, pixel size, operating temperature and electro-optic performance is described in this paper together with projections into the future.

8542-52, Session 10

Linear photon-counting HgCdTe APDs

Gauthier Vojetta, Lydie Mathieu, Fabrice Guellec, CEA-LETI-Minatec (France); Philippe Feautrier, Institut de Planétologie et d’Astrophysique de Grenoble (France); Johan Rothman, CEA-LETI-Minatec (France)

HgCdTe APDs have been shown to exhibit single carrier multiplication (SCM) which gives desirable properties such as low multiplication excess noise (F<1.2) and gain independent response time up to multiplication gains exceeding 1000. Combined with quantum efficiencies (QE) which can approach 100 % in optimized detectors, theses detectors have the highest information conservation ratio QE/F of all amplified detectors, from ultra-violet wavelengths up to the infra-red cut-off of the APDs. Theses properties open new perspectives for photon-counting applications which can be achieved in a linear mode that enables proportional photon-counting, high photon detection efficiency (PDE), low after-pulsing, high count rates and low dark count rates (DCR).

In this communication we present the status of HgCdTe APD technology at CEA/Leti and show first results on linear photon-counting circuits made of HgCdTe APDs hybridized with specially designed read-out integrated circuits (ROICs). The ROICs are made using compact CMOS electronics that enables integration into large area-small pixel focal plane arrays. In particular, a specially designed low noise ROIC has been used to detect single photons at a record low APD gain of 60 and linear output signal for up to 50 simultaneous photons. The results will be discussed in terms of the impact of the HgCdTe APD gain and response time characteristics on the most common photon-counting figure of merits and which perspectives that can be expected from improved APD and ROIC design.

8542-53, Session 10

Fabrication of novel 3D stacked microbolometers for multispectral infrared detection

Jong Yeon Park, Dean P. Neikirk, The Univ. of Texas at Austin (United States)

In this paper, we will present the design and fabrication method of novel 3D stacked microbolometer with two infrared absorber/Germanium dielectric structural layers using self aligned process which is enabling to uncooled multispectral infrared detector. In recent years, multispectral (multicolor, multichannel) infrared systems, which have been extensively investigated for numerous critical applications such as chemical and biological sensing, environmental monitoring, astronomy, planetary and Earth remote sensing, thermal imaging, airborne surveillance, target acquisition and tracking and night vision system, etc. At present, multispectral infrared detectors fall into two approaches. First type is based on quantum well infrared photoconductors (QWIPs) and HgCdTe photodiodes present multicolor capability in the mid wave infrared (MWIR) and long wave infrared (LWIR) spectral range. However, these multispectral infrared detectors are required cryogenic cooling system. Second type is using single color focal plane arrays (FPAs) combined with general optical components such as grating, infrared band pass filters, lenses and prism to achieve the targeted infrared wavelength. Consequently, current platforms of multispectral infrared detectors are relatively complex and heavy components, more difficult device fabrication, high cost and large scale systems. Conventional Fabry-perot resonant cavity based uncooled microbolometers (2 to 2.5 μm Airgap) have limited design parameters due to multi color narrow band spectral response. Here, we will propose to promising novel design of multispectral uncooled infrared detector that can produce to achieve excellent tunable narrowband absorption in mid wave infrared (MWIR) and long wave infrared (LWIR) spectral range. In addition, we demonstrate novel fabrication methods of feasible direction to three dimensional multi stacked uncooled infrared detector for multispectral infrared detection. The fabricated 3D stacked microbolometers consist of two Germanium dielectric structural layers, two resistive sheets as infrared absorber layers above each Germanium dielectric structural layer, two space air gaps and reflective mirror layer for enhanced infrared absorption power efficiency. Germanium has been adopted as each structural layer above each polyimide sacrificial layer instead of silicon nitride as structural layer in conventional microbolometers. By using only germanium as both the interference layer for wavelength selectivity and the structural layer the problems associated with highly infrared absorbing and dispersive silicon nitride layers can be avoided. To the formation of thermally isolated uncooled microbolometers, most commonly used microfabrication method for free-standing device structure, use a high-temperature stable polyimide as the sacrificial layer with patterning process. We use a self-aligned process without a polyimide patterning process that helps eliminate deformation and stress in the two absorber/structural membranes and cost effective device fabrication due to reduced fabrication process flow. We demonstrated that the fabricated novel 3D stacked uncooled Germanium dielectric supported microbolometers have robust, flat absorber/structural membranes using self-alignment process which is enable to enhanced narrow band infrared power absorption and

experimentally show efficient multispectral infrared detection using stacked multi infrared absorber layers to produce excellent tunable narrowband absorption in the mid wave infrared (MWIR) and long wave infrared (LWIR) spectral region.

8542-54, Session 11

Advances in active and nonlinear metamaterials *(Keynote Presentation)*

Allan D Boardman, Rhiannon Mitchell-Thomas, Univ. of Salford (United Kingdom); Yuriy Rapoport, Kyiv National University (Ukraine)

Metamaterial research is an extremely important global activity that promises to change our lives in many different ways. These include making objects invisible and the dramatic impact of metamaterials upon the energy and medical sectors of society. Behind all of the applications, however, lies the business of creating metamaterials that are not going to be crippled by the kind of loss that is naturally heralded by use of resonant responses in their construction. This review sets out modern solutions to the management of loss and gain, coupled to controlled and nonlinear behavior, and discusses some critical consequences concerning stability. Under the general heading of active and tunable metamaterials, a set of solutions that addresses these issues in several directions will be reviewed. The range of such solutions is really fascinating. This presentation will provide an elegant route to the inclusion of nonlinearity and waveguide complexity through original forms of transformation dynamics. In addition, a lot of this will be framed within a magnetooptical environment that deploys externally applied magnetic field orientations. Light will be directed to achieve energy capture and be deployed for environmental and medical purposes. Quite apart from the fact that metamaterials are attracting such a lot of global, intrinsic, attention the ability to control light, for example, in these materials is immensely interesting and will lead to a new dawn of integrated circuits and computers. The latter will rely upon the ability of metamaterials to stop light and space-time cloaking. There has been a lot of talk, since general relativity burst upon the scientific scene in the early decades of the last century, of black holes and now, with the aid of metamaterials, it is possible to discuss optical black holes. More importantly, however, electromagnetic concentrators are set to have a great social, and economic, impact. If nonlinearity is added to the core of a concentrator it is possible to create dramatic optical hotspots, with many manufacturing and surgical applications. Indeed, a new form of nonlinear switching will be reviewed, and it will be illustrated in considerable detail. It is also becoming clear that activity with acoustic metamaterials is gaining strength and this can be viewed in terms of analogue electromagntic cases. In fact, the question of whether separate materials need to be analyzed, especially if transformation dynamics is used will be addressed in such a manner that optical, acoustic and even thermal outcomes can be addressed through a common analysis technique.

8542-55, Session 11

Latest developments in AlGaInN laser diode technology for defence applications

Stephen Najda, Piotr Perlin, TopGaN Ltd. (Poland); T Suski, L Marona, Institute of High Pressure Physics PAS (Poland); M M. Bockowski, M M. Leszczynski, P Wisniewski, R Czernecki, TopGaN Ltd. (Poland); R Kucharski, Ammono S.A. (Poland); G Targowski, TopGaN Ltd. (Poland)

The latest developments in AlGaInN laser diode technology is reviewed for defence applications such as underwater telecommunications, sensor systems etc. The AlGaInN material system allows for laser diodes to be fabricated over a very wide range of wavelengths from u.v., i.e, 380nm, to the visible, i.e., 530nm, by tuning the indium content of the laser GaInN quantum well. Advantages of using Plasma assisted MBE (PAMBE) compared to more conventional MOCVD epitaxy to grow AlGaInN laser structures are highlighted. Ridge waveguide laser diode structures are fabricated to achieve single mode operation with optical powers of >100mW in the 400-420nm wavelength range with high reliability. High power operation of AlGaInN laser diodes is also reviewed. We demonstrate the operation of a single chip, high power AlGaInN laser diode 'mini-array' consisting of a 3 stripe common p-contact configuration at powers up to 2.5W cw in the 408-412 nm wavelength range. Low defectivity and highly uniform TopGaN GaN substrates allow arrays and bars of nitride lasers to be fabricated. Packaging of nitride laser diodes is substantially different compared to GaAs laser technology and new processes & techniques are required to optimize the optical power from a nitride laser bar. Laser bars of up to 5mm with 20 emitters have shown optical powers up to 4W cw at ~410nm with a common contact configuration. An alternative package configuration for AlGaInN laser arrays allows for each individual laser to be individually addressable allowing complex free-space and/or fibre optic system integration within a very small form-factor. TopGaN are developing a new range of high power laser array technology over the u.v.- visible spectrum together with new packaging solutions for optical integration.

8542-56, Session 11

Emerging optical fibre technologies with potential defence applications

Wei H. Loh, Dan W. Hewak, Marco Petrovich, John R. Hayes, Will J. Stewart, W. Andrew Clarkson, Univ. of Southampton (United Kingdom)

Recent years have seen the development of a range of promising optical fibre technologies emerge, due to advances in materials and fabrication techniques. We describe 3 areas in optical fibre developments of interest to the defence community: nano-opto-mechanical fibres, microstructured hollow core fibres for high peak optical power and/or infrared transmission, and chalcogenide glasses for mid-IR lasers, fibres, and metamaterials.

With the concept of nano-opto-mechanical fibres, we introduce MEMS-type functionalities into optical fibres, and bring additional capabilities to sensing, and optical switching, as well as the development of continuously tunable optical delay lines, e.g. for rf photonics applications. We have recently succeeded in realising a unique dual core optical fibre, where both sub-micron sized cores are suspended in air inside the fibre by two 100nm thin glass membranes. With the cores located close to each other forming a waveguide coupler, small (nm-sized) displacements in the relative core positions relative to each otherinduced for example by gas pressure or electromagnetic fields can be detected optically. Conversely, mechanical actuation of the core displacement, e.g. by gas pressure or electrostatic forces, to bring the cores closer togetherthese displacements will change the effective index and the propagation constant of the light travelling through the fibre, resulting in continuously tunable optical delay lines. The small scales mean that these nanophotomechanical affects can be induced at MHz speeds.

Microstructured optical fibre technology allows for low loss transmission in a hollow core. These fibres, characterised by high damage thresholds, extremely low nonlinearity and extended transmission at infrared wavelengths, are of intense interest in diverse applications such as low latency (speed-of-light-in-air) communications, gas sensing and nonlinear spectroscopy, and high-peak power pulsed laser delivery. Light guidance is accomplished either through a bandgap effect (Photonic Bandgap Fibres) or through antiresonant guidance (Kagome-type fibres). We report the improvements in the fabrication of these challenging fibre waveguides; in particular the fabrication of low-loss (~few dB/km), wide bandwidth (>100nm) Photonic Bandgap Fibre geometries operating at 2um and beyond, and antiresonant hexagram fibres with broadband transmission for the delivery of extremely high peak optical powers.

Chalcogenide glasses provide a powerful material base for mid-IR photonic and electro-optical applications. These currently include optical fibre, active plasmonic waveguides, optically and electrically switchable thin films, metamaterials and solid state lasers, amongst others. Being in the core of rewritable DVDs and CDs, this robust technology is finding new applications provided by the combination of wide transmission band, high optical nonlinearity and the unique phase change switching functionality of advanced chalcogenide glasses. We describe our work with gallium and germanium sulphide based glasses and their potential for new solid state microsphere mid-IR lasers, improved low loss IR fibre for the 3-5 micron transmission window, and discuss their emerging role in plasmonic and metamaterials. The exploitation of chalcogenide materials has evolved from a simple infrared transmitting bulk glass into a multifunctional optoelectronic material for the future.

8542-57, Session PS

Test environment for image synthesis of a single pixel camera

Marcin Kowalski, Marek Piszczek, Mieczyslaw Szustakowski, Military Univ. of Technology (Poland)

The present trend of signal processing maintains that according to the Nyquist-Shannon theory a signal must be sampled at a rate at least twice its highest frequency in order to be represented without error. However, it is very common to compress the data just after sensing. This approach is very popular in the field of image acquisition. We compress images registered by a camera trading off signal representation complexity. Thus some of the information is simply thrown away.

Single pixel camera is an imaging device taking advantages of compressed sensing (CS) method. Over the past few years, a new theory known as compressed sensing has emerged. Compressed sensing is a signal processing method based on fact that a small group of non-adaptive linear projections of a compressible signal contains enough information for reconstruction and processing. The theory of compressed sensing allows to reconstruct a sparse or compressible image from a small set of linear, non-adaptive projections. Because most of images are sparse the theory of compressed sensing can be successfully applied to images. The compressive sensing method has led to the development of new signal acquisition hardware. This method is also an inspiration for research on new data processing techniques.

Sparse signal approximations have become a new tool in signal processing with wide range of applications. Recently, many algorithms for signal reconstruction have been developed, however, all of them need many parameters to be properly set before using. Setting proper parameters is crucial for preparing a real model of the single pixel camera as well as for fast and efficient image synthesis. Because of high complexity of image recovery algorithms based on compressed sensing method, image synthesis process needs to be optimized.

Optimization of signal acquisition and processing parameters can be achieved running various camera simulations. In the paper we present the integrated test environment for image synthesis of the single pixel camera and the test results of simulations run with various configurations and parameters values. We used two combined adaptive methods for image reconstruction - the Newton method and the conjugate gradient method. Test environment allows to run two kinds of tests. The first test type is simulation of various parameters of acquired signal e.g. bit resolution. Reduction of signal bit resolution and its impact to basic image quality parameters like MSE and PSNR as well as to image reconstruction time is an example. Image geometric transformation like rotation is the second type of tests. Simulation results include quality parameters values of MSE and PSNR and image reconstruction time. Integrated test environment can be used during the process of hardware selection as well as during camera tests with real signals. All of tests can be run with various number of iterations and for various image resolutions.

8542-58, Session PS

Determination of the density-of-states function in highly degenerate semiconductors in the existence of electric field strength

Subhamoy Singha Roy, JIS College of Engineering (India)

The eminent consequence of the density-of-states function for non-degenerate wide gap optical and optoelectronic materials with parabolic energy band has been obtained as special cases of our generalized theory under definite limiting background from our generalized term when electric field strength is zero.

Conference 8542C: Quantum-Physics-Based Information Security

Tuesday 25–25 September 2012 Part of Proceedings of SPIE Vol. 8542
Electro-Optical Remote Sensing, Photonic Technologies, and Applications VI

8542-60, Session 12

Information security: from classical to quantum *(Invited Paper)*

Stephen M. Barnett, Thomas Brougham, Univ. of Strathclyde (United Kingdom)

The problem of secure communications is as old as the desire to keep secrets. With the current explosion in communications and online information, hardly a week passes without a high-profile hacking story hitting the news. I shall review, briefly, the principles underlying secure communications including both private and public key cryptosystems. A more extended introduction to these topics may be found in.

Quantum cryptography was designed to provide a new approach to the problem of distributing keys for private key cryptography. The principal idea is that security can be ensured by the laws of quantum physics and, in particular, that any attempt to measure a quantum state will change it uncontrollably. This change can be detected by the legitimate users of the communication channel and so reveal the presence of an eavesdropper. I shall explain how quantum key distribution works and some of the progress that has been made towards making this a viable technology.

With the principals of quantum communication and of quantum key distribution firmly established, it is perhaps time to consider how efficient it can be made. It is interesting to ask, in particular, how many bist of information might reasonably be encoded on a single photon. I shall discuss this in terms of using the time of arrival of entangled photon pairs and show how shared information in excess of 10 bits per photon might be achieved. I shall also show how this systems might be adapted for use in high bit-rate quantum key distribution.

8542-61, Session 12

Direction in optical implementations of quantum key distribution *(Invited Paper)*

Norbert Lütkenhaus, Agnes Ferenczi, Razieh Annabestani, Univ. of Waterloo (Canada); Xiongfeng Ma, Tsinghua Univ. (China)

In practical QKD, we design point-to-point QKD devices and then connect these links to global or local trusted repeater networks. We will highlight two recent results in each of these steps.

Phase-encoding for the BB84 protocol has been practiced since very early on in optical implementations as this encoding is very robust for transmission over fiber optics cables. Effectively, this scheme corresponds to a Mach-Zehnder interferometer that prepares two light pulses of equal amplitude. The signals are then encoded in the relative optical phase of the pulses. These signal states are equivalent to the states used in polarization encoding. However, in practical implementations the amplitudes of the two pulses become asymmetric as the phase modulators that set the phase have about 3 dB insertion loss. In practice this does not lead to observed problems, as the losses of the phase modulator in the receiver re-establishes the symmetry in the interfering pulses. For the security analysis, though, it is crucial that the signal states have a relative structure that differs from the BB84 protocol. We analyze the new signal structure and give a security proof that covers for this deviation. Note that the resulting key rate is lower than the one for the BB84 protocol, so that this readjustment cannot be ignored for phase encoded BB84.

Trusted Repeater Networks have been implemented in several major QKD network demonstrations. They allow establishing a multi-user framework for QKD that addresses the distance and key rate performance of individual QKD links. The traditional paradigm is to establish secret keys between connected neighbors in these networks and then to propagate a secret key between two parties along a chain of nodes, using the respective nearest neighbor keys. We propose a different approach which reduces the amount of computational and communication resources that are required by the intermediate nodes. Intermediate nodes establish quantum correlated classical data with their neighbors. Instead of completing secret keys out of these classical data with their neighbors doing error correction and privacy amplification and then to propagate the final key, we propose that the nodes directly propagate the quantum correlated data using simple public announcements, thereby establishing quantum correlated classical data between the distant parties. Then only these distance parties need to complete the steps of error correction and privacy amplification to establish directly their secret key. We analyze the performance of this arrangement including implementations using weak coherent laser pulses. Note that our method not only reduces the work load for intermediate nodes, a reduction that scales with the number of intermediate nodes, but also offers additional protection of the final secret key against passive eavesdropping attacks by breach of trust in intermediate nodes, as the communication required to establish the secret key between the distant users no longer needs to pass through the intermediate (trusted) nodes.

8542-62, Session 12

Practical treatment of quantum bugs *(Invited Paper)*

Marco Lucamarini, Toshiba Research Europe Ltd. (United Kingdom); James F. Dynes, Zhiliang L. Yuan, Andrew J. Shields, Toshiba Research Europe Ltd. (United Kingdom) and Corporate Research & Development Center, Toshiba Corporation (Japan)

During years, several QKD protocols have been demonstrated theoretically to be unconditionally secure. However, any theory contains assumptions and these not always are met in practical realisations. One familiar example is the single-photon assumption: in practice, every light source produces sometimes more than a single photon. The extra photon constitutes a side channel that can be exploited by a malevolent party to hack the QKD system through the well known PNS attack. Other well known assumptions that are difficult to fulfil in practice are those about detectors' efficiencies, which are taken to be equal and independent of the receiver's basis choice.

Every time there is a gap between the theory and the practice of QKD, there is room for side channels, quantum hacking attacks and security loopholes. We group all these instances under the name of "quantum bugs", or "qbugs" for short. A "qbug" is then any fault of the QKD system, which can be due to an external attack, actively pursued by an eavesdropper, or to an inaccurate implementation by the users themselves. It is a priority of any QKD supplier to consider and possibly fix as many qbugs as possible.

One prominent qbug is related to the finite size fluctuations exhibited by the collected data samples, when this aspect is not taken into account in the security proof. In this respect, it is very important to use a suitable security proof and to be able to process rapidly blocks of at least 10^8 bits, in order to get close to the asymptotic limit. In other words, it is important to choose a protocol which is at the same time secure and efficient. But, as security and efficiency are two opposite requirements, this task is far from trivial.

An interesting protocol in this respect is the "biased BB84" [1] endowed with decoy states. To date, only a few security proofs exist for a finite-size version of this protocol [2-5]. Among these, the one described in [3] seems suitable for a practical implementation. In fact, besides providing quantifiable and composable security, it is also symmetric between the two QKD users and does not require the encryption of the error correction information nor a random permutation in the post-processing stage. The only problem is that it features quite a low resistance to the reduction of the sample size. Specifically, it provides a positive secure rate only for N>10^6, where N is the total number of events detected by Bob, while for other proofs N>10^4 suffices (see e.g. [5]).

We have found that this poor resistance to number fluctuations in small samples is due mainly to a non optimal estimation of the upper bounds to the single-photon gain and QBER of a QKD transmission. We have replaced the parameter estimation procedure in this proof by another one based on linear programming [6,7]; we have then adapted the resulting security to the new protocol; finally we have covered a few aspects which were not covered in the original proof. As a result, we have obtained an extremely secure protocol which also behaves

very well in efficiency and practicality.

[1] H.-K. Lo, H. F. Chau, and M. Ardehali, J. Crypt. 18, 133 (2005).

[2] J. Hasegawa et al., preprint arXiv:0707.3541 (2007).

[3] R. Y. Q. Cai and V. Scarani, New J. Phys. 11, 045024 (2009).

[4] T.-T. Song et al., Quant. Inf. Comput. 11, 0374 (2011).

[5] M. Tomamichel et al., Nat. Comm. 1631 (2012).

[6] J. W. Harrington et al., arXiv:quant-ph/0503002 (2005).

[7] P. Rice and J. Harrington, arXiv:0901.0013.

8542-63, Session 12

Towards long-distance continuous-variable quantum key distribution enforced by nonclassicality

Vladyslav C. Usenko, Palacky Univ. Olomouc (Czech Republic) and Bogolyubov Institute for Theoretical Physics (Ukraine); Radim Filip, Palacky Univ. Olomouc (Czech Republic)

Quantum key distribution (QKD) protocols use fundamental laws of quantum physics to allow two trusted parties to distribute a cryptographic key which they can further use for the unconditionally secure classical communication. During the last decades the field has grown mature with the commercial prototypes already being available. They mostly rely on the faint laser pulses implementing the protocols on the basis of single qubits (practically realized as single photons) and qubit pairs. Alternatively, the continuous-variable (CV) protocols based on the multi-photon states of light were developed recently and are aimed at the increase of the effectiveness and applicability of QKD. They are typically built using the modulation by phase-space displacement in the field amplitude and phase quadratures of the coherent or squeezed states of light and their subsequent homodyne detection. In the case of Gaussian modulation the security of the protocols is based on the extremality of Gaussian states, which allows estimating bounds on the eavesdropper knowledge on the raw key assuming the most general attacks strategies when the channel properties are known. The Gaussian CV QKD protocols were shown secure for any degree of channel attenuation upon reverse reconciliation, but are restricted by the untrusted noise present in the channel. Moreover, the applicability of Gaussian CV QKD protocols is limited by the effectiveness of classical post-processing algorithms, used by the trusted parties to process the measured data and distill the cryptographic key, as the efficiency scales down the classical mutual information between the trusted parties and consequently reduces the overall secure key rate. This limitation gets stricter upon strong channel loss, corresponding to long-distance channels. Under such realistic conditions of lossy channels and limited post-processing, the influence of the channel noise on the coherent-state CV QKD protocols becomes even more pronounced. On the other hand, the squeezed-state CV QKD protocols were previously considered ineffective under limited degrees of squeezing, while strong squeezing remains experimentally challenging. In the present work we use a generalized state preparation scheme to distinguish between the classical and quantum resources in the Gaussian CV QKD and address the role of nonclassicality in the Gaussian CV QKD protocols. We investigate the security properties of the generalized protocol in terms of the key rates and tolerable channel excess noise, which limits the security. We show that in the certain Gaussian modulation regime even moderate amount of nonclassicality is drastically improving the robustness of the protocol to channel noise in conditions of reduced post-processing efficiency. Moreover, upon strongly limited post-processing both direct and reverse reconciliation scenarios of CV QKD protocols are entering essentially nonclassical regime, when squeezing is required to provide the security of the schemes in the realistic channels. Further we demonstrate, that by properly combining squeezed resource and coherent modulation, trusted parties are able to decouple eavesdropper from the channel, thus being able to establish the secure key from any amount of the classical mutual information, practically regardless of the post-processing efficiency. Our result shows a very promising path towards the feasible long-distance CV QKD.

8542-64, Session 13

High bit rate quantum key distribution *(Invited Paper)*

Zhiliang Yuan, James Dynes, Andrew Sharpe, Alex R. Dixon, Andrew J. Shields, Toshiba Research Europe Ltd. (United Kingdom)

We report a recent advance in high bit rate quantum key distribution (QKD) designed for fibre optical network applications. We have developed compact control electronics based on field programmable gated arrays (FPGAs), robust stabilisation technique, and high count rate single photon detectors using self-differencing InGaAs avalanche photodiodes (APDs). Record key rates have been obtained both in laboratory and in field for continuous operation. An average key rate of 1 Mbit/s has been obtained over 50 km fibre spool (10 dB loss). Over the installed 45 km fibre with higher loss (14.5 dB), a secure bit rate of 304 kb/s was obtained in a continuous distribution session of 24 hours. Built on practical components only, the QKD system is suitable for deployment in the field environment to provide security for future communication infrastructures.

8542-65, Session 13

Report on proof-of-principle implementations of novel QKD schemes performed at INRIM

Alessio Avella, INRIM (Italy) and Dipartimento di Fisica - Università di torino (Italy); Giorgio Brida, INRIM (Italy); Andrea Cavanna, Max Planck Istitut fur die Physik des Lichts (Germany); Dino Carpentras, Ivo Pietro Degiovanni, Marco Genovese, Marco Gramegna, Paolo Traina, INRIM (Italy)

In recent years Quantum Key Distribution (QKD) has emerged as the most paradigmatic example of quantum technology allowing the realization of intrinsically secure communication links over hundreds of kilometers. Beyond its commercial interest QKD also has high conceptual relevance in the study of quantum information theory and the foundations of quantum mechanics. In particular, the discussion on the minimal resources needed in order to obtain absolutely secure quantum communication is yet to be concluded.

Here we present our last experimental implementations [1-2] concerning two novel quantum cryptographic schemes which do not require some of the most widely accepted conditions for realizing QKD.

In the first scheme, L. Goldberg and L. Vaidman [3] proposed a protocol in which, even if the data sharing is realized using two orthogonal states, any attempt to eavesdrop is detectable by the legal users. Usually, orthogonal states are not used in Quantum Cryptography schemes since they can be faithfully cloned without altering the transmitted data. Nevertheless, in the Goldberg-Vaidman scheme the orthogonal states are superpositions of two localized wave packets which travel along separate quantum channels, i.e. two different paths inside a balanced Mach-Zehnder interferometer. In our laboratories we have successfully implemented a reliable source of single photons, with a g(2)(0)=0.06±0.01, representing a good approximation of an ideal single-photon source to be used as carriers of information for the protocol, as well as the complete interferometric system. The quality of the transmission quantified by the QBER has been measured to be (7.0±1.6)% and proven to be stable for hundreds of seconds.

The second scheme is the Noh09 protocol [4] which, being based on the quantum counterfactual effect, does not even require any actual photon transmission in the quantum channel between the parties for the communication. In essence the scheme exploits a counterfactual measurement, also known as counterfactual QKD (CQKD), which relies on fundamental properties of quantum mechanics: it is a typical example of interaction-free measurement that detects the state of an object without an interaction occurring between it and the measuring device.

We report on the fully experimental implementation of the Noh09 scheme for CQKD, proving its unconditional security: the quality of our heralded single photon source was measured obtaining g(2)(0)=(7±5)?10–9, showing a negligible presence of multi-photon components. The mean QBER associated with our protocol measurements was QBER=(7±1)%, corrected for subtraction of background and accidental counts, and a full investigation over

possible photon-number-splitting attacks is reported.

Bibliography

[1] A. Avella et al., PRA 82, 062309 (2010)

[2] A. Avella et al., Laser Phys. Lett. 9, No. 3, 247-252 (2012)

[3] L. Goldenberg and L. Vaidman, PRL 75, 1239 (1995).

[4] T.-G. Noh, PRA 103, 230501 (2009).

8542-66, Session 13

Experimental demonstration of quantum digital signatures

Robert J. Collins, Patrick J. Clarke, Vedran Dunjko, Erika Andersson, Heriot-Watt Univ. (United Kingdom); John Jeffers, Univ. of Strathclyde (United Kingdom); Gerald S. Buller, Heriot-Watt Univ. (United Kingdom)

In the era of interconnected computer networks, authentication and privacy are important concerns. Computer data transfer commonly makes use of digital signatures based on classical public key encryption techniques. These provide a form of security which takes a sufficiently long time to break as to provide a significant deterrent to a potential attacker but do not posses mathematical proofs of long-term security. These systems typically rely on “trap-door one-way functions” where a result can be easily calculated from certain input parameters but the input parameters cannot be determined from the result without additional prior information. This prior information forms what is known as a “private key” and is used to decrypt information encrypted using the publicly distributed “public key”. It has been demonstrated that given sufficient computational resources these digital signature schemes can be rendered insecure using current technology. Future advances in computer or mathematical sciences may serve to make such attacks on the classical protocols less intensive.

Quantum digital signatures (QDS) offer a means of distributing a digital signature with security verified by information theoretical limits and quantum mechanics. We have designed, assembled and tested what is, to the best of our knowledge, the first QDS test-bed system to share a signature from one sender to two receivers. The receivers can verify that they have received the same signature from the sender and that it has not been altered by a malicious party. Comparing quantum systems is a non-trivial operation and can rely on a swap test or quantum comparison. A general swap test is difficult to implement as it relies on quantum computation resources whereas a quantum comparison of coherent states may be implemented using a beam splitter and has a higher success probability. If the two input states are identical they are not altered at the output and the measurement has non-demotion character.

The digital signature can be encoded as the phase of Glauber coherent states of pulses of photons. The receivers then compare these coherent states on a beam splitter to confirm the identical nature of the signatures. The phase encodings are chosen from the set 2πk/N, where N is the number of available phase encodings and k is an integer in the range 0 to N-1. The choice of N affects the mean number of photons per pulse used in transmission such that, within limits defined by information theory, larger N values permit a greater number of photons per pulse.

Our system utilizes fiber interferometers with active feedback loops to encode the signature on 850 nm wavelength photons, chosen to ensure compatibility with mature, low-dark-noise and high detection efficiency silicon single-photon detectors. We will present experimental results from this system for a variety of different numbers of non-orthogonal phase encodings with an honest sender distributing the same signature to both parties and a dishonest sender transmitting different phase encodings to each receiver.

8542-67, Session 14

Photon orbital angular momentum: generation and measurement and application to QKD *(Invited Paper)*

Miles J. Padgett, Daniele Giovannini, Martin P. J. Lavery, Univ. of Glasgow (United Kingdom); Jacqui Romero, Univ. of Glasgow (United Kingdom) and Univ. of Strathclyde (United Kingdom); Stephen M. Barnett, Fillipo Miatto, Univ. of Strathclyde (United Kingdom); Robert W. Boyd, Jonathan Leach, Univ. of Ottawa (Canada)

Secure Quantum Communication requires the ability to encode information onto a single photon in two or more complimentary basis. For this purpose, a basis set can be understood as a variable such that once a value for that variable is known, no information can ever be known for the value of the variable in the complimentary basis. Commonly, a variable of choice is polarization. Using linear polarization a single bit of information can be encoded as vertical or horizontally polarized light, representing a 1 or a 0. Alternatively the bit of information can be encoded as right circular or left circular, again corresponding to a 1 or 0. However, if the recipient chooses to measure in the linear basis then irrespective of the outcome of that measurement (i.e. 1 or 0) no similar measurement can be made of the circular states and visa versa.

But polarization is not the only basis in which the photon can be encoded. In principle any basis set along with its complementary set can be used to encode the information, the unifying feature is that the two corresponding variables are subject to an uncertainty relationship. It is immediately apparent that arrival time and measured frequency or arrival position and transverse momentum are also possible basis sets in which to encode information. The advantage of these basis sets is that whereas polarization is restricted to one bit per photon, continuous nature of time/frequency or position/momentum potentially gives an unlimited information capacity even on a single photon.

Central to our work has been another basis set, namely, orbital angular momentum (OAM). As identified by Allen et al. in 1992, OAM arises from the spatial phase structure of an optical beam [1]. Specifically helical phase fronts described by an cross-section carry an OAM corresponding to l hbar per photon. When described in terms of Laguerre Gaussian modes, these OAM states form a complete, orthonormal basis set. These orbital angular momentum states are a discrete yet unbounded basis with a complimentary variable of angular position that is continuous but periodic. This discrete/periodic nature raises fundamental questions as to whether the associated uncertainty relationship ensures the inherent security that one associates with quantum techniques. Our demonstration of an angular form of the Einstein Podolsky Rosen (EPR) paradox shows that orbital angular momentum has the potential to form a secure basis for a communication system [2]. One point to note is that to ensure the unbias nature of the OAM and angles states is, for example, each of the angle states must be obtained as a coherent addition of the range of OAM states [3]. For a finite number of OAM states this means the resulting angle states are complicated azimuthal functions with slightly overlapping intensity profiles. Alternatively, hard-edged and hence none overlapping angle states require an infinite range of OAM states.

Although OAM is potentially unbounded, in practice one only generates and measurable states over a finite range of values and one aspect of our work has been to both characterize and extend this range. For quantum applications it is possible to generate entangled OAM carrying photon pairs from parametric down-conversion [4]. By making small changes to the phase matching conditions we have now shown that it is practical to operate the orbital angular momentum variable over 50 values (c.f. 2 for polarization).

In principle all these different variables (polarization, time/frequency, position/momentum, angular momentum/angular position) can be combined in parallel to give massive amounts of information encoded on a single photon. Of course each of these basis sets creates technical challenges both in its generation and detection. Futhermore, decoherence, which leads to cross talk between states and a degradation both of information capacity and security, effects the various basis sets in different ways.

As an alternative to using OAM as a quantum variable it can simply be employed for the multiplexing of classical channels. Each classical channel can itself utilize a further variable to carry quantum secure information. Orbital angular momentum could therefore be used to give multiple classical channels, indeed we have shown an orbital angular momentum separator which routes different angular momentum states to different lateral positions [5]. Each of these classical channels could then be encoded with secure information. Despite being a subject of study for 20 years it is only our recent work that has shown a practical approach to the multistate rather than sequential measurement of orbital angular momentum.

The orbital angular momentum of light was only recognized as a macroscopic description of the light beam 20 years ago, and as a resource for quantum studies/applications within the last 10 [6]. In this work we have discussed both the generation and measurement of orbital angular momentum both in terms of understanding the nature of the quantum variable and its applications to communication and other systems.

[1] L. Allen, M. W. Beijersbergen, S. RJC, and J. P. Woerdman, “Orbital angular-momentum of light and the transformation of Laguerre-Gaussian laser modes,” Phys Rev A 45, 8185-8189 (1992).

[2] J. Leach, B. Jack, J. Romero, A. K. Jha, A. M. Yao, S. Franke-Arnold, D. G. Ireland, R. W. Boyd, S. M. Barnett, et al., “Quantum Correlations in Optical Angle-Orbital Angular Momentum Variables,” Science 329, 662-665 (2010).

[3] A. C. Dada, J. Leach, G. S. Buller, M. J. Padgett, and E. Andersson, “Experimental high-dimensional two-photon entanglement and violations of generalized Bell inequalities,” Nat Phys 7, 1-4, Nature Publishing Group (2011).

[4] A. Mair, A. Vaziri, G. Weihs, and A. Zeilinger, “Entanglement of the orbital angular momentum states of photons,” Nature 412, 313-316 (2001).

[5] M. P. J. Lavery, D. J. Robertson, G. C. G. Berkhout, G. D. Love, M. J. Padgett, and J. Courtial, “Refractive elements for the measurement of the orbital angular momentum of a single photon,” Opt Express 20, 2110-2115, Optical Society of America (2012).

[6] G. Molina-Terriza, J. P. Torres, and L. Torner, “Twisted photons,” Nat Phys 3, 305-310 (2007).

8542-68, Session 14

Projective quantum measurements on spatial modes of the photon

Mark T. Gruneisen, Air Force Research Lab. (United States); Raymond C. Dymale, James P. Black, Boeing-SVS, Inc. (United States); Kurt E. Stoltenberg, Boeing-SVS, Inc. (United States) and Air Force Research Lab. (United States)

Security in the BB84 quantum key distribution (QKD) protocol results from randomly changing the bases of polarization in which individual photons are prepared and measured. Theoretically, these measurements are described as projective quantum measurements in mutually unbiased bases (MUBs) having the properties that 1) the measurement of a photon prepared in a matched basis will result in a deterministic outcome and, 2) the measurement of a photon prepared in a dissimilar basis will result in a random outcome. In the latter case, the photon is considered to be in an equally weighted superposition of the measurement basis states and, upon measurement, the superposition collapses to one of the basis states with a uniformly (hence, without bias) random outcome. As a consequence, no information is revealed regarding the state or the basis in which the incident photon was prepared.

For applications involving free-space optical links, one can consider utilizing the spatial modes of the photon for multi-channel and multi-level encoding. Realizing such an approach requires the engineering of optical components capable of acting as spatial mode quantum projectors. While planar dielectric interfaces naturally lend themselves to the decomposition of polarization into orthogonal components, it is less clear that an analogous mechanism exists for spatial modes in arbitrarily large state spaces. This presentation reports the development and demonstration of transmission volume holograms as quantum projectors in a MUB system of spatial modes. Two- and four-dimensional state spaces are defined via mutually orthogonal spatial modes and the complex optical fields of the MUBs are calculated and generated with a spatial light modulator in order to record and subsequently illuminate the transmission volume holograms. Single-photon diffraction probabilities are measured experimentally and compared to the inner product relationships associated with projective quantum measurements in MUBs.

8542-69, Session 14

The efficient sorting of light’s orbital angular momentum for optical communications

Martin P. J. Lavery, Univ. of Glasgow (United Kingdom); David Roberston, Durham Univ. (United Kingdom); Mehul Malik, Brandon Robenburg, Univ. of Rochester (United States); Johannes Courtial, Univ. of Glasgow (United Kingdom); Robert W. Boyd, Univ. of Rochester (United States) and Univ. of Ottawa (Canada); Miles J. Padgett, Univ. of Glasgow (United Kingdom)

The desire to increase the amount of information that can be encoded onto a single photon has driven research into many areas of optics. One such area is optical orbital angular momentum (OAM) [1]. These beams have helical phasefronts and carry an orbital angular momentum of mbar per photon, where the integer m is unbounded, giving a large state space in which to encode information.

We recently developed a telescope system comprising two bespoke refractive optical elements to transform OAM states into transverse momentum states [2]. This is achieved by mapping the azimuthal position of the input plane to the lateral position in the output [3]. A mapping of this type transforms a set of concentric rings at the input plane into a set of parallel lines in the output plane. A lens can then separate the resulting transverse momentum states into specified lateral positions, allowing for the efficient measurement of multiple OAM states simultaneously.

Separating OAM states in this way presents an opportunity for this larger alphabet to improve the data capacity of a free space link and has potential application in both the classical and quantum regimes. In our system we generate these states through the use of spatial light modulator (SLM) and sort them using our bespoke optical elements.

The natural randomly time dependent variations in temperature and pressure of the atmosphere result in a change in density of the atmosphere give a spatial dependent change of the refractive index leading to a phase distortion across a transmitted beam. Such a phase distortion is a concern for any free space communications channel where the atmospheric turbulence may effect the cross-talk between channels. A phase distortion of this type can be approximated to a phase screen, and is commonly referred to as thin phase turbulence [4]. We introduce precisely simulated amounts of turbulence through the use of a phase only spatial light modulator. Once the turbulence is introduced, we can measure the resulting cross talk between OAM modes and relate this to atmospheric conditions.

We will present our latest design, increasing the bandwidth of measurable states to over 50 OAM modes. In such a system we study the crosstalk introduced by a thin phase turbulence, showing that turbulence similarly degrades the purity of all the modes within this range.

[1] L. Allen, M. W Beijersbergen, R. J. C. Spreuw, and J. P. Woerdman, Phys. Rev. A. 45, 8185 (1992).

[2] Martin P. J. Lavery, David J. Robertson, Gregorius C. G. Berkhout, Gordon D. Love, Miles J. Padgett, and Johannes Courtial, Optics Express, 20, 3, 2110-2115, 2012.

[3] Gregorius C. G. Berkhout, Martin P. J. Lavery, Johannes Courtial, Marco W. Beijersbergen, and Miles J. Padgett. 105, 15, 153601, 2010.

[4] D. L. Fried, J. Opt. Soc. Am. 55, 1427 (1965).

8542-70, Session 14

Increasing the orbital angular momentum bandwidth of entangled photons

Mary Jacquiline Romero, Univ. of Glasgow (United Kingdom) and Univ. of Strathclyde (United Kingdom); Daniele Giovannini, Sonja Franke-Arnold, Univ. of Glasgow (United Kingdom); Stephen M. Barnett, Univ. of Strathclyde (United Kingdom); Miles J. Padgett, Univ. of Glasgow (United Kingdom)

The bandwidth of any communication system, classical or quantum, is limited by the number of orthogonal states in which the information can be encoded. Quantum key distribution systems available commercially rely on the two-dimensional polarisation state of photons. Quantum computation has also been largely designed on the basis of qubits. However, a photon is endowed with other degrees of freedom. It has been shown that entangled photons generated via spontaneous parametric down-conversion (SPDC) are correlated in various other properties such as time and energy, and position and momentum, all of which reside in a higher-dimensional state space. This promises a higher information capacity per photon, more complex quantum computation protocols and more security and robustness for quantum cryptography. Most relevant to our work, entanglement of spatial modes has also been shown, one class of which are those associated with orbital angular momentum (OAM). OAM is an attractive basis to be used for quantum information because it is discrete and theoretically infinite-dimensional. However, any practical experiment utilising the innately high-dimensional entanglement of the orbital angular momentum (OAM) state space of photons is subject to the modal capacity of the detection system, only a finite subset of this space is accessible experimentally. Given such a constraint, we show that the number of measured, entangled OAM modes in photon

pairs generated by SPDC can be increased by tuning the phase-matching conditions in the SPDC process. We achieve this by tuning the orientation angle of the nonlinear crystal generating the entangled photons.

We use a beta barium borate (BBO) crystal cut for type 1 collinear SPDC. The BBO crystal is pumped by a 355 nm UV laser to generate two entangled 710 nm photons which are then incident on a beamsplitter. The output face of the crystal is imaged onto two separate spatial light modulators (SLM), and the SLMs are then imaged onto single mode fibres connected to avalanche photodiodes for single photon detection. We use the SLM to display holograms- either a forked diffraction grating to measure OAM, or an angular mask to measure in the conjugate variable, angular position. The coincidence count is recorded as a function of the hologram being displayed.

We demonstrate a factor of 2 increase on the half-width of the OAM-correlation spectrum, from 10 to 20, the latter implying ≈ 50 -dimensional two-photon OAM entanglement. We show the corresponding correlations in angular position, which can be derived from the Fourier relationship between OAM and angular position. We quantify the degree of entanglement by measuring concurrence values in the angular position qubits where we have obtained 0.96 and 0.90 for two phase-matching conditions, indicating bipartite, D-dimensional entanglement where D is tuneable.

8542-71, Session 14

High-dimensional spatial entanglement observed with an electron multiplying CCD camera

Daniel S. Tasca, Matthew P. Edgar, Univ. of Glasgow (United Kingdom); Frauke Izdebski, Ryan E. Warburton, Heriot-Watt Univ. (United Kingdom); Jonathan Leach, Megan Agnew, Univ. of Ottawa (Canada); Gerald S. Buller, Heriot-Watt Univ. (United Kingdom); Robert W. Boyd, Univ. of Ottawa (Canada); Miles J. Padgett, Univ. of Glasgow (United Kingdom)

Transverse spatial modes of paraxial photons have been shown to be useful in many quantum information and communications tasks. From quantum cryptography [1,2] and computation [3], as well as in fundamental tests of quantum mechanics [4,5], the spatial degrees of freedom (DOF) of single photons have been widely explored. Indeed, the high-dimensionality and large possibilities of manipulating the spatial DOF of photons offer an increased advantage in the use of spatial states.

Spontaneous parametric down-conversion (SPDC) is the most used technic to produce spatial entangled states of photons. The non-local properties of the spatial correlations from SPDC have been investigated in many experiments, either exploring the transverse linear position and momentum of the photons or by projections onto discrete modes such as the Laguerre-Gaussian modes.

In 2004, it was shown that the transverse position and momentum of thde photon pairs exihbit Einstein-Podolsky-Rosen (EPR) correlations. When working with transverse linear position and momentum, the quantum properties of the spatial correlations from SPDC are generally detected through measurements of intensity correlations in the near (image) and far-field of the down-converted field. Many others experiments have also explored these correlations to show entanglement properties of continuos variables quantum systems. Within this approach, the intensity correlations are generally measured by scanning a single-mode fibre in the detection plane and counting the coincidence detections as a function of transverse position in the detection planes.

In order to take full advantadges of the high-dimensionality of spatial states, it is desirable to have an efficient array of detectors. We report the joint detection of around 2500 spatial entanglend spatial states of photons pairs from SPDC, by employing an electron-multiplying CCD (EMCCD) camera in the detection system. The implementation of a bi-dimensional array of detectors enabled simultaneous access to both transverse spatial DOF of the photons. When using the camera in the image plane of the SPDC crystal, we observe a strong 2D correlation between the detected positions of the photons. To detect momentum correlations, we place the EMCCD in the far-field of the down-conversion source, observing a strong anti-correlation between the detection positions for both transverse DOF.

We also characterize the correlation introduced by noise events in the EMCCD by correlating the detected events for consecutive frames. This gives us a background correlation that we use as reference to subtract from the spatial correlation in both image and far-field measurements. We analyze the strength of the background subtracted correlations by applying EPR criterion, finding a strong violation that is in good agreement with the theoretical predictions.

References:

[1] S. P. Walborn et al. Phys. Rev. Lett. 96, 090501 (2006)

[2] M. P. Almeida et al. Phys. Rev. A 73, 040301(R) (2006)

[3] D. S. Tasca et al. Phys. Rev. A 83, 052325 (2011)

[4] J. C. Howell et al. Phys. Rev. Lett. 92, 210403 (2004)

[5] A. C. Dada et al. Nat. Phys. 7, 677-680 (2011)

8542-72, Session 15

Single-photon detectors for practical quantum cryptography *(Invited Paper)*

Alberto Tosi, Franco Zappa, Sergio Cova, Politecnico di Milano (Italy)

The implementation and commercialization of quantum cryptography technologies have to face some challenges related to the development of single-photon detectors operating at 1550 nm. The main requirements are: i) high detection efficiency; ii) low noise; iii) high count rate; iv) low timing jitter. Different technologies are currently available for single-photon detection in the short-wavelength infrared range (SWIR), including PhotoMultiplier Tubes (PMT), Superconducting Single-Photon Detectors (SSPD) and Single-Photon Avalanche Diodes (SPAD). Semiconductor devices (like SPAD) offer a photon detection efficiency that is inherently higher and more extended in the long-wavelength range than any photocathode employed in vacuum tube detectors. Additionally SPADs made in InGaAs/InP can detect single photons at 1550 nm with low noise when moderately cooled by means of thermo-electric coolers, while SSPD has to be cooled down to few degrees Kelvin, a temperature that strongly limits their exploitation in real-world quantum key distribution (QKD) systems. Consequently, InGaAs/InP SPAD can be the enabling technology of practical QKD systems, provided that the maximum count rate is increase above 1 Mcps. The main limit is the afterpulsing effect that usually sets an impractically too long (> 10 μs) hold-off time after each avalanche ignition.

We present the necessary development in InGaAs/InP SPAD device design, fabrication technology and front-end electronics in order to decrease the afterpulsing effect, while not impairing photon detection efficiency and timing jitter. We report a new InGaAs/InP SPAD designed with low noise and sharp temporal response, and new circuital solutions for operating such detectors at high speed with very fast avalanche quenching time. The new SPAD provides count rates higher than 1 Mcps and temporal response with 60 ps Full-Width at Half Maximum and very short tail (30 ps time constant). The new electronics includes a compact wide-band pulse generator able to gate the SPAD up to 133 MHz repetition rate. A fast avalanche-quenching scheme, working on both SPAD anode and cathode, minimizes quenching time to less than 1 ns, thus effectively reducing afterpulsing by decreasing the total charge flowing through the junction. A differential read-out electronics guarantees low time jitter. The joined exploitation of new InGaAs/InP SPADs and improved front-end electronics will pave the way to practical implementations of secure ICT systems.

8542-73, Session 15

Single photon detection and quantum cryptography *(Invited Paper)*

Gerald S. Buller, Patrick J. Clarke, Robert J. Collins, Heriot-Watt Univ. (United Kingdom)

Quantum key distribution (QKD) offers the prospect of verifiably secure communication between two parties with security determined by quantum theory. In QKD, the information is encoded on properties of photons that quantum theory tells us cannot be distinguished unambiguously. Unlike classical systems every photon represents a single bit of information and a single bit can only be encoded on a single photon. As QKD transitions from the experimental laboratory, a more detailed examination of system performance is required, with more attention drawn to the single-photon detectors used.

The evolution of experimental QKD has therefore led to an accelerated

development of single photon detectors. QKD is transitioning from the experimental laboratory to the installed system and new demonstrations should exhibit high data transmission rates and good long term stability to gain industrial acceptance.

We have developed a gigahertz clocked environmentally robust QKD test bed which operates using photons at a wavelength of 850 nm over a 9 μm core diameter standard telecommunications optical fiber channel and employs a novel depolarizing approach to reduce the effects of time varying birefringence in the fiber channel. The test bed has been operated using a number of different single photon detectors, including commercially available thick and thin (or shallow) junction silicon single photon avalanche diodes (Si-SPADs), experimental niobium nitride superconducting nanowires (NbN SSPDs) and an experimental resonant cavity Si-SPAD. The different detectors have been compared in terms of quantum bit error rate (QBER), and raw, sifted and secure bit rates. This test bed has experimentally demonstrated long term automatous operation with a secure key generation uptime of 89% for a thin junction Si-SPAD (mean QBER 6.2% and mean secure key rate 12 kbit/s) and 68% for the resonant cavity Si-SAPD (mean QBER 6.9% and mean secure key rate 60 kbit/s). We will present the experimental analysis of this test bed and briefly discuss the security of the implementation.

A theoretical model applicable to all QKD systems operating at any wavelength has been developed from these results and is used to highlight potential detector attributes that may be desirable for improved QKD systems. We will present an outline of this model and use it to highlight how detector performance parameters such as detection efficiency, timing jitter and dark noise may be better tuned to suit QKD and related applications.

Furthermore, a novel application of quantum information to the exchange and verification of digital signatures will be introduced and an experimental implementation will be outlined. This implementation represent what is, to the best of our knowledge, the first experimental demonstration of quantum digital signatures.

8542-74, Session 16

Device-independent security for quantum cryptography *(Invited Paper)*

Renato Renner, ETH Zurich (Switzerland)

No Abstract Available.

8542-75, Session 16

Measurement-device-independent quantum key distribution protocol with weak coherent sources *(Invited Paper)*

Hoi-Kwong Lo, Univ. of Toronto (Canada); Marcos Curty, Univ. de Vigo (Spain); Bing Qi, Univ. of Toronto (Canada)

Quantum key distribution (QKD) is a technology that can, in principle, provide cryptographic systems with an unprecedented level of security. Unfortunately, practical QKD schemes often suffer from imperfections in implementation and do not achieve the theoretical security. Indeed, quantum hacking against practical QKD systems, particularly via detector side channel attacks, has emerged as a hot topic. Existing counter-measures against this kind of attacks are either highly impractical or may not be fully effective.

Recently, we have proposed (H.-K. Lo, M. Curty and B. Qi, http://arxiv.org/abs/1109.1473) an entirely new approach, measurement-device-independent QKD (MDI-QKD), that can “short-circuit” all detector security loopholes. The key idea is to use a security proof based on a reversed EPR protocol and combine it with the decoy state method. Consequently, it can be implemented with practical weak coherent pulses (WCPs) generated by a laser.

A simple example of our method is as follows. Both Alice and Bob prepare phase randomized WCPs in the four possible BB84 polarization states and send them to an untrusted relay Charlie (or Eve), who performs a Bell state measurement that projects the incoming signals into a Bell state. Moreover, Alice and Bob apply decoy state techniques to estimate the gain (i.e., the probability that the relay outputs a successful result) and quantum bit error rate (QBER) (i.e., the error rate in quantum signals) for various input photon numbers. By post-selecting the events where they use the same basis and Charlie announces a success Bell measurement, Alice and Bob can establish a secure key given the QBER is below certain value. MDI-QKD can be implemented with current technologies, standard optical components, realistic detection efficiency, and highly lossy channels. Furthermore, its key generation rate is many orders of magnitude higher than that based on full device-independent QKD. Our simulation results based realistic devices show that long-distance quantum cryptography over 200km will remain secure even with seriously flawed detectors.

From the implementation point of view, one big concern in MDI-QKD is whether we can generate indistinguishable photons from two independent laser sources and observe stable Hong-Ou-Mandel (HOM) interference, since the physics behind this protocol is based on the photon bunching effect of two indistinguishable photons at a 50:50 beam splitter. We performed a simple proof of principle experiment to show that high-visibility HOM interference between two independent off-the-shelf lasers is actually feasible. More specifically, we measured the HOM interference between two phase-randomized WCPs at a photon level of 0.1 photon per pulse. The observed HOM dip is 0.53 ± 0.01 while the theoretical value is 0.50. This result confirms that a high-visibility HOM dip can be obtained with independent lasers, thus demonstrating the feasibility of the MDI-QKD protocol.

MDI-QKD has been further investigated in K. Tamaki, H.-K. Lo, C.-H. F. Fung and B. Qi, http://arxiv.org/abs/1111.3413, which considers issues such as basis-dependent flaw and phase encoding schemes.

8542-76, Session 16

Reference frame independence, device independence and limitless range quantum communications *(Invited Paper)*

John G. Rarity, Chengyong Hu, Univ. of Bristol (United Kingdom)

The secure exchanging of cryptographic keys over fibre [1] or free space [2] is now approaching a commercial reality through advanced quantum cryptography systems. One key limitation to all present quantum key distribution systems is the finite range of a single quantum link and the inability to amplify the fading signal by classical means. The quantum repeater [3] has been suggested as a possible solution to this exponential decrease of bit rate with distance. Ideal repeater schemes extend the distance using “entanglement swapping” and “teleportation” and by concatenating short entanglement swapping sub-sections it is in principle possible to generate entangled (correlated) bits over very long distances with bit rate only limited by the losses in one short section. If realised this would extend quantum key distribution out to distances of thousands of kilometres. Each sub-section is linked to the next by an optical circuit which performs a ‘Bell’ measurement between photons arriving from each direction. Proof of principle experiments [4] carried out to date have been limited to using quantum interference effects at a beamsplitter to perform a limited Bell measurement with 25% success rate when photons arrive simultaneously at the beamsplitter. These quantum ‘relays’ are extremely inefficient and cannot extend the range in practical system.

In this talk I will introduce the concept of a spin photon interface [5] where an incoming photon leaves its information in a spin memory until the next photon arrives whereupon the Bell measurement can be carried out with in principle 100% success probability thus making a near ideal quantum repeater [6]. This leads us to propose an all solid state quantum network where the sources of single photons and entangled photon pairs are realised by quantum dot emission into a microcavity while the repeater itself is a quantum dot strongly coupled to a cavity system.

I will go on to describe early experiments using high-Q micro-pillar cavitites containing single quantum dots where we are beginning to prove the feasibility of this concept [7]. I will also look at how such interfaces could be used in reference frame and device independent scenarios.

[1] N. Gisin, et al, Rev. Mod. Phys. 74, 145 (2002).

[2] R. Ursin, et al Nature Physics 3, 481 - 486, (2007).

[3] H.-J. Briegel et al, Phys. Rev. Lett. 81, 5932 (1998).

[4] H. de Riedmatten et al, Phys. Rev. Lett. 92, 047904 (2004).

[5] C.Y. Hu, et al., Phys. Rev. B 78, 085307 (2008).

[6] C.Y. Hu and J. G. Rarity, Phys. Rev. B 83, 115303 (2011).

[7] A. Young et al Phys. Rev. A 78, 125318 (2011).

Conference 8542D: Military Applications in Hyperspectral Imaging and High Spatial Resolution Sensing

Monday 24–24 September 2012 • Part of Proceedings of SPIE Vol. 8542
Electro-Optical Remote Sensing, Photonic Technologies, and Applications VI

8542-81, Session 17

A novel technique for adaptive anomalous change detection in airborne hyperspectral imagery

Marco Diani, Salvatore Resta, Nicola Acito, Giovanni Corsini, Univ. di Pisa (Italy); Sergio U. de Ceglie, CISAM (Italy)

Anomalous Change Detection (ACD) in Hyperspectral Imagery is a challenging task aimed at detecting a set of pixels that have undergone a relevant change with respect to a previous acquisition. The changes of interest are those due to the insertion, movement or removal of objects in the observed scene. When data are collected by airborne platforms, perfect registration between images is very difficult to achieve, and illumination and atmospheric conditions vary during the acquisitions. As a consequence, a residual mis-registration (RMR) error and a variation in the feature subspace spanning the spectral vectors of each hyperspectral image should be taken into account in developing ACD techniques. Recently, the Local Co-Registration Adjustment (LCRA) approach has been proposed to deal with the performance reduction due to those aspects, providing excellent performance in different ACD tasks.

In this work, we propose a novel technique based on the LCRA strategy that automatically estimates the first and second order statistics of the RMR noise by exploiting locally invariant spatial features extracted from the image pair. Afterwards, in the purpose of avoiding the detection of pervasive changes (i.e. changes due to variation in illumination and atmospheric conditions), the algorithm adaptively measures the spectral distance (SD) between the pixel under test (PUT) and the pixels belonging to a selected region containing the PUT. This is achieved by exploiting the local estimates of the random noise sources (i.e. thermal and photon contributions) obtained by the hyperspectral noise parameter estimator (HYNPE) algorithm. In particular, the noise and signal realizations are extracted from each pixel of the original image by resorting to the multiple-linear regression-based approach. Subsequently, the estimate of the signal to noise ratio (SNR) for each spectral component of the PUT is obtained using a maximum likelihood approach. Those estimates are employed to perform the comparison between the PUT and the pixel vectors included in the selected region by retaining only those components whose SNR is above a predetermined threshold. Different metrics have been adopted, based on Euclidean Distance (ED) and angular distance criteria, such as the spectral angle mapper (SAM), the personian correlation coefficient (PCC) and the spectral correlation mapper (SCM).

Experimental analysis has been conducted on a real hyperspectral dataset collected over an urban scenario. Two images strips have been recorded a few minutes apart with a SIMGA camera from SELEX GALILEO, a hyperspectral push-broom sensor covering the wavelength range 400 to 1000 nm with a spatial resolution of 1m at the flight altitude of 1000m. A ground truth map has been well documented with additional information provided by a high resolution panchromatic camera installed onboard. Working day activity in the city guaranteed numerous changes between the two images. Several targets have been evaluated spanning in size from two to five meters.

Performance evaluation highlighted the effectiveness of the proposed approach with respect to traditional methods, resulting in a consistent improvement of both the probability of detecting changes and the capability of suppressing the background.

8542-82, Session 17

People detection using fused hyperspectral and thermal imagery

Adrian Blagg, BAE Systems (United Kingdom)

No Abstract Available

8542-83, Session 17

A prior knowledge model for multidimensional striping noise compensation in hyperspectral imaging devices

Pablo F. Meza Narvaez, Jorge E. Pezoa Nunez, Francisca I. Parra, Sergio N. Torres, Univ. de Concepción (Chile)

The hyperspectral information acquired by a push-broom hyperspectral camera (PBHC) is degraded by imperfections on the devices, temperature fluctuations, non-uniform response in neighboring detectors, etc. As a result of these undesired effects, the acquired information is corrupted by the so-called striping noise, which is presented as a spatial and spectral structure. To tackle this problem, blind estimation using linear models is traditionally employed by striping noise compensation (SNC) algorithms due to its simplicity; however, their performance is limited because they disregard the information about hyperspectral acquisition process when linear models are assumed for the process. In this sense, a proper knowledge on the system is required to develop models aiming to recover the true hyperspectral data. Moreover, SNC algorithms rely on the spatial and temporal information available at the readout data; however, most of them disregard the large amount of spectral information also available. In particular, SNC algorithms can improve their performance by assuming a short-term stationary behavior on the spatial, spectral, and temporal information of the input radiance acquired by the PBHC. The results are promising but they are affected by the overuse of spectral information, reducing spectral detail as the number of bands included in estimation process increases.

In this work, a prior knowledge model is proposed in order to increase the effectiveness of a multidimensional SNC algorithm. This is accomplished by considering an optoelectronic approach, thereby generating a more accurate mathematical representation of the hyperspectral acquisition process. The proposed model includes knowledge on the system spectral response, which can be obtained by means of an input with known spectral radiation. Further, the model also considers the dependence of the noise structure on the analog-digital conversion process, that is, schemes such as active-pixel sensor (APS) and passive-pixel sensor (PPS) have been considered. Finally, the model takes advantage of the degree of crosstalk between consecutive bands in order to determinate how much of this spectral information is contributing to the read out data obtained in a particular band. All prior knowledge is obtained by a series of experimental analysis, and then integrated into the model.

After estimating the required parameters, the applicability of the multidimensional SNC is illustrated by compensating for stripping noise in hyperspectral images acquired using an experimental setup. A laboratory prototype, based on both a Photonfocus Hurricane hyperspectral camera and a Xeva Xenics NIR hyperspectral camera, has been implemented to acquire data in the range of 400-1000 [nm] and 900-1700 [nm], respectively. It is worth mentioning that both cameras present distinctive noise patterns in terms of its spectral structure. A mobile platform has been also used to simulate and synchronize the scanning procedure of the cameras and an uniform tungsten lamp has been installed to ensure an equal spectral radiance between the different bands for calibration purpose.

8542-84, Session 18

Advanced hyperspectral imaging solutions for near real-time target detection

Oliver Weatherbee, Justin Janaskie, SpecTIR, LLC (United States); Timo Hyvärinen, Specim Spectral Imaging Ltd. (Finland)

AISA hyperspectral imagers have been utilized in airborne applications for various defense related Intelligence, Surveillance and Reconnaissance (ISR) applications. In expanding the utility and capabilities of hyperspectral imagers for defense related applications, the implementation in a ground scanning configuration for check-point

and forensic purposes has been achieved. System specifications, design, and operational considerations for a fully automated, near real-time target detection capability are presented. The system utilizes modularized software architecture, combining C++ command, capture, calibration, and messaging functions with drop-in IDL exploitation module for detection algorithm and target set flexibility. Performance capability against known defense related targets of interest have been tested, verified, and are presented utilizing full 400-2450nm spectral range provided by combined AISA Eagle and Hawk hyperspectral imagers. Initial results are also described for a new extended InGaAs system, covering 585-1630nm to provide a similar capability for integrations which have size, weight, and power restrictions. Additionally, the potential of incorporating a new LWIR hyperspectral instrument into the presented architecture is discussed.

8542-85, Session 18

Compact snapshot birefringent imaging Fourier transform spectrometer

Michael W. Kudenov, Victoria C Chan, Eustace L. Dereniak, College of Optical Sciences, The Univ. of Arizona (United States)

The design and implementation of a Snapshot Hyperspectral Imaging Fourier Transform (SHIFT) spectrometer is presented. The sensor is based on a multiple-image Fourier transform spectrometer (FTS), originally developed by A. Hirai; however, the presented device offers significant advantages over her original implementation. Namely, its birefringent nature creates a common-path interferometer that is ultra-compact, insensitive to vibration, and offers greater radiometric throughput. The theory of the birefringent FTS is provided, followed by details of its specific embodiment and a description of our laboratory prototype. Spectral measurements of gas discharge lamps are provided and these spectra are subsequently verified against a calibrated Ocean Optics USB2000 spectrometer. Additional data were collected outdoors, demonstrating the sensor's ability to resolve spectral signatures in standard outdoor lighting and environmental conditions.

8542-86, Session 18

Compact medium-resolution hyperspectral imaging VIS/NIR sensors based on linearly variable filters for target identification and classification

Michele Dami, Gianluca Aroldi, SELEX Galileo S.p.A. (Italy)

It has been demonstrated that hyperspectral sensing has the potential to detect low contrast targets which are spectrally different to the background against which they are observed. The sensors here described are able to perform digital mapping of the target scene and to reveal, locate, identify and classify details based on their spectral reflectance features. Thanks to LVF technology, it is possible to realise hyperspectral imaging sensors more compact than the standard imaging spectrometers.

Linearly variable filters (LVF) are optical components based on thin-film depositions on glass or quartz substrates, integrated on matrix detectors in substitution of the standard closing windows. They are characterised by a 'spectral' direction along which the peak transmittance wavelength varies linearly with the displacement, and by the orthogonal 'uniform' direction along which the transmittance features remain constant. During integration, LVF is aligned with the detector rows parallel to the spectral gradient direction, and the detector assembly is integrated in a camera head equipped with standard objective. In order to make LVF working as an hyperspectral imager it is required a relative motion between optical head and object target, achieved by mounting the optical head on a rotating stage, performing angular scans along the spectral direction.

The proposed Fast Proximity Sensor (FPS) is a compact VIS-NIR/ panchromatic hyperspectral imager based on LVF, capable of continuous target acquisitions and automatic detection of warning/ alert conditions by means of image processing and analysis algorithms.

FPS is based on a custom designed LVF integrated in a CCD/APS detector covering a limited portion of its active surface, with the remaining part left uncoated and working as the focal plane of a panchromatic camera. The detector is provided with a cooling stage, fast readout electronics, a DSP for post-processing implemented at hardware level, a motorized optical zoom and a rotating platform supporting the optical head, allowing angular scanning of the target scene. The system is able to work both at finite and infinite distance from the target, and the matching between the field of view and the angular scan velocity of the rotating platform is automatically calculated via software. The real-time analysis of the differences among the continuously acquired images and reference images and spectral signatures, generates an alarm/warning event when exceeding a defined threshold. In this case FPS optical head is able to rotate and point toward the area where the alarm was generated, performing further acquisitions with higher spatial and spectral resolution by increasing its optical magnification.

The proposed concept of an LVF-based FPS follows from SELEX-Galileo experience on development of non-commercial linearly variable filters, designed, manufactured and characterised under ESA specifications with the ENEA Optical Coating Group contribution. Custom LVF components with high spectral gradient (60nm/mm), wide spectral range (with $\lambda max \lambda min > 2$) operating in VIS/NIR and SWIR, with high out-of-band rejection (less than 5%), were designed and manufactured, and a breadboard spectrometer was developed to validate the operating principle of LVF and the algorithms required to build hyperspectral images from the acquired frames.

8542-87, Session 18

Airborne infrared hyperspectral imager for intelligence, surveillance and reconnaissance applications

Philippe Lagueux, Vincent Farley, Martin Chamberland, Telops (Canada); Eldon Puckrin, Caroline S. Turcotte, Defence Research and Development Canada, Valcartier (Canada); John C. R. Bastedo, PV Labs (Canada)

Persistent surveillance and collection of airborne intelligence, surveillance and reconnaissance information is critical in today's warfare against terrorism. High resolution imagery in visible and infrared bands provides valuable detection capabilities based on target shapes and temperatures. However, the spectral resolution provided by a hyperspectral imager adds a spectral dimension to the measurements, leading to additional tools for the detection and identification of targets, based on their spectral signature.

The Telops Hyper-Cam sensor is an imaging spectrometer that enables the spatial and spectral analysis of targets using a single sensor. It is based on the Fourier-transform technology yielding high spectral resolution and enabling high accuracy spectroradiometric calibration.

The Hyper-Cam has been recently used for the first time in a gyrostabilized mount (gimbal). The gyrostabilized Hyper-Cam system is described in this paper, and successful results of the high-altitude detection and identification of a common chemical powder spill (ammonium sulphate) and Freon gas release (F-134a) are presented.

8542-88, Session 18

Remote sensing of gases by hyperspectral imaging: algorithms and results of field measurements

Samer Sabbah, Peter Rusch, Bruker Optik GmbH (Germany); Jens Eichmann, Technische Univ. Hamburg-Harburg (Germany); Joern-Hinnrich Gerhard, Roland Harig, Bruker Optik GmbH (Germany)

Remote gas detection and visualization provides vital information in scenarios involving chemical accidents, terrorist attacks or gas leaks. Imaging infrared spectroscopy can be used to assess the location, the dimensions, and the dispersion of a potentially hazardous cloud. In this work the latest developments of an infrared hyperspectral imager based on a Michelson interferometer in combination with a focal plane array detector are presented. An algorithm that combines the spectral and spatial information to enhance the detection and imaging of a gas cloud is presented. The performance of the system is evaluated by laboratory measurements. The hyperspectral imager was deployed in the field to identify industrial gas emissions. Excellent

results were obtained by successfully identifying released gases from long distances.

8542-89, Session 18

Evaluation of remote detection of explosives by multispectral and hyperspectral infrared detection techniques

Mariusz Kastek, Tadeusz Piatkowski, Tomasz Sosnowski, Rafal Dulski, Piotr Trzaskawka, Norbert Palka, Stanislaw Cudzilo, Military Univ. of Technology (Poland)

The recent global threats like terrorist attacks (for example Madrid, London and Minsk bombings) cause the problem of remote detection of explosives to become one of the most important tasks to cope with for the remote threat detection systems. The research on the remote detection of explosives in near, mid and far infrared ranges have been conducted for many years. The development of IR cameras and spectrometers makes it possible to detect explosive materials and precursors in various spectral bands using different signal processing techniques. During the research the multiband thermal cameras with optical filters were used as well as infrared imaging spectrometers. The measurement devices were operating in near, mid and far infrared spectrum. Evaluation of research results will show the influence of different factors (e.g. spectral bands of applied optical filters or spectral resolution of spectrometers) on the effectiveness of detection of several types of explosives. Additionally the measurement results obtained in terahertz range were included.

8542-90, Session 19

A comparative study of algorithms for target detection in hyperspectral images

Kailash C. Tiwari, Bharati Vidyapeeth's College of Engineering (India); Manoj K. Arora, Dharmendra P. Singh, Indian Institute of Technology Roorkee (India)

Recent advances in remote sensing technologies have made it possible to acquire remote sensing data in hundreds of narrow contiguous wavelength bands facilitating extraction of information which hitherto fore used to remain hidden in panchromatic and even in multispectral data. Hyperspectral data, due to narrow bandwidths has also made it possible to detect several small targets of military interest. A variety of spectral modeling based algorithms known as spectral matching algorithms such as Orthogonal Subspace Projection (OSP), Constrained Energy Minimisation (CEM), Spectral Angle Mapper (SAM) and Spectral Correlation Mapper (SCM) etc and anomaly detection algorithms such as, OSP anomaly detector (OSPAD), Reed-Xiaoli anomaly detector (RXD), Uniform Target Detector (UTD) and a combination of Reed-Xiaoli anomaly detector and Uniform Target Detector (RXD-UTD) etc have been commonly reprted in the literature. The application of hyperspectral data for military targets, however, has often been restricted due to a requirement of spectral modeling using a priori available target spectra, a condition difficult to meet in practice. It therefore necessitates algorithms which do not depend upon target spectra for target detection. Independent component analysis (ICA) is an evolving new technique that aims at finding out components which are statistically independent or as independent as possible. ICA has also been increasingly been extended for target detection as it does not have any requirement of availability a priori target spectra. The aim of this paper, therefore, is to compare ICA based algorithm with various other types of spectral matching algorithms for target detection in hyperspectral images. A set of synthetic and AVIRIS hyperspectral data containing aircrafts as targets were used for the experiments. A comparison of true positive and false positive rates of target detections obtained from ICA and other algorithms plotted on a receiver operating curves (ROC) space indicates superior performance of ICA over other algorithms.

8542-91, Session 19

Standoff aircraft IR characterization with ABB dual-band HSI

Florent M. Prel, Louis M. Moreau, Stephane Lantagne, ABB Analytical Measurement (Canada); Ritchie D. Bullis Jr., Naval Air Warfare Ctr. Aircraft Div. (United States) and PRISM (United States); Claude B. Roy, Christian A. Vallières, Luc E. Levesque, ABB Analytical Measurement (Canada)

Remote sensing infrared characterization of rapidly evolving events generally involves the combination of a spectro-radiometer and infrared camera(s) as separated instruments. Time synchronization, spatial coregistration, consistent radiometric calibration and managing several systems are important challenges to overcome; they complicate the target infrared characterization data processing and increase the sources of errors affecting the final radiometric accuracy.

MR-i is a dual-band Hyperspectal imaging spectro-radiometer, that combines two 256 x 256 pixels infrared cameras and an infrared spectro-radiometer into one single instrument. This field instrument generates spectral datacubes in the MWIR and LWIR. It is designed to acquire the spectral signatures of rapidly evolving events. The design is modular. The spectrometer has two output ports to either widen the spectral coverage or to increase the dynamic range of the measured amplitudes. Various telescope options are available for the input port.

Recent platform developments and field trial measurements performances will be presented for a system configuration dedicated to the characterization of airborne targets.

8542-92, Session 19

Multispectral and hyperspectral measurements of smoke candles and soldier's camouflage equipment

Philippe Lagueux, Telops (Canada); Mariusz Kastek, Tadeusz Piatkowski, Rafal Dulski, Military Univ. of Technology (Poland); Marc-André Gagnon, Telops (Canada); Piotr Trzaskawka2, Military Univ. of Technology (Poland)

The emergence of new infrared camouflage and countermeasure technologies in the context of military operations have paved the way to enhanced detection capabilities. Camouflage devices such as candles (or smoke bombs) and flares are developed to generate either large area or localized screens with very high absorption in the infrared. Similarly, soldier's camouflage devices such as clothing have evolved in design to dissolve their infrared characteristics with that of the background. In all cases, the analysis of the targets infrared images needs to be conducted in both multispectral and hyperspectral domains to assess their capability to efficiently provide visible and infrared camouflage.

The Military University of Technology has conducted several intensive field campaigns where various types of smoke candles and camouflage uniforms were deployed in different conditions and were measured both in the multispectral and hyperspectral domain. Cooled broadband infrared cameras were used for the multispectral analysis whereas the high spectral, spatial and temporal resolution acquisition of these thermodynamic events was recorded with the Telops Hyper-Cam.

This paper presents the test campaign concept and the analysis of the recorded measurements.

8542-93, Session 19

Chromotomosynthesis for high speed hyperspectral imagery

Randall L. Bostick, Glen P. Perram, Air Force Institute of Technology (United States)

A rotating direct vision prism, chromotomosynthetic imaging (CTI) system operating in the visible creates hyperspectral imagery by collecting a set of 2D images with each spectrally projected at a different rotation angle of the prism. Mathematical reconstruction techniques that have been well tested in the field of medical physics are used to reconstruct the data to produce the 3D hyperspectral image. The instrument operates with a 100 mm focusing lens in the spectral range of 400-900 nm with a field of view of 71.6 mrad and angular resolution of 0.8-1.6 μrad. The spectral resolution is 0.6 nm at the shortest wavelengths, degrading to over 10 nm at the longest wavelengths. Measurements using a point-like target show that performance is limited by chromatic aberration. We analyze the systematic instrumental error in collected projection data resulting from prism spectral dispersion, prism alignment, detector array

position and prism rotation angle. The shifting and broadening of both the spectral lineshape function and the spatial point spread function in the reconstructed hyperspectral imagery is compared with experimental results for monochromatic point sources. The shorter wavelength (λ<500nm) region where the prism has the highest spectral dispersion suffers mostly from degradation of spectral resolution in the presence of systematic error, while longer wavelengths (λ>600nm) suffer mostly from a shift of the spectral peaks. The quality of the reconstructed hyperspectral imagery is most sensitive to the misalignment of the prism rotation mount. The accuracy and utility of the instrument is assessed by comparing the CTI results to spatial data collected by a wideband image and hyperspectral data collected using a liquid crystal tunable filter (LCTF). The wide-band spatial content of the scene reconstructed from the CTI data is of same or better quality in terms of background noise and target intensities as a single frame collected by the undispersed imaging system with projections taken at every 1°. Performance is dependent on the number of projection used, with projections at 5° producing adequate results in terms of target characterization. The data collected by the CTI system can provide spatial information of equal quality as a comparable imaging system, provide high-frame rate slitless 1-D spectra, and generate 3-D hyperspectral imagery which can be exploited to provide the same results as a traditional multi-band spectral imaging system. While this prototype does not operate at high speeds, components exist which will allow for CTI systems to generate hyperspectral video imagery at rates greater than 100 Hz. The isngtrument has considerable potential for characterizing bomb detonations, muzzle flashes, and other battlefield combustion events.

8542-94, Session 19

Classification of parasite infected clams using hyperspectral images

María J. Parra, Silvia E. Restrepo, Pablo F. Meza Narvaez, Jorge E. Pezoa Nunez, Sergio N. Torres, Miguel E. Figueroa, Univ. de Concepción (Chile)

During some seasons of the year, the Chilean clam Mulinia Edulis is prone to be infected by the parasite Edotea magellanica. This parasite has a low frequency of appearance and it does not represent any harm to human health; however, finding a worm-like parasite hidden inside a commercial product is indeed a disgusting surprise, which may harm the reputation of the Chilean seafood industry. In order to comply with world-class health, production, and commercialization standards, clams must be thoroughly inspected to identify the infected ones and remove them from the production line.

In this paper, hyperspectral imagery will be used to devise classifiers aiming to identify which clams are infected by a parasite. A hyperspectral camera will be used to collect hyperspectral data cubes. The spatio-spectral images stored in the data cubes will be used as a priori information to devise analytical and machine-learning classifiers for the problem of parasite detection in clams. Classifiers will be devised by combining the spatial information in the images, with the spectral information supplied by the hyperspectral camera. Further, a priori information, such as the frequency of appearance of the parasite and/or the parasite size, will be also used to improve the accuracy of the classifiers. To evaluate the performance of the classifiers, standard metrics such as the analytical and the estimated classification probabilities, the false-positive probability, and the ROC curves will be obtained. Also, to assess the statistical validity of the devised classifiers, a repeated random subsampling cross-validation technique will be carried out.

With the purpose of generating a proper hyperspectral database for devising and testing the classifiers, a laboratory prototype based on a push-broom hyperspectral camera and a mobile platform will be used. The imaging system uses a Photonfocus Hurricane 40 V10E hyperspectral camera, which allows us to obtain 574 spectral images, of size 1024x400 pixels, in the band of 400 to 1000 [nm], at a spectral resolution of 1.04 [nm]. A mobile platform implements and synchronizes the scanning procedure of the camera. The set-up will be completed by a tungsten lamp used to obtain transillumination images. It must be commented that the imaging system imposes an additional constraint because, although the spectral resolution of the camera is high, the spatial resolution of the images is low.

8542-95, Session 19

Project “Peregrine: In-flight processing and streaming of hyperspectral imagery: an overview of the MOD funded proof-of-concept

David Burridge, Gareth Crisford, Exelis Visual Information Solutions (United Kingdom)

‘Peregrine is an innovation project for the UK MOD delivered in 2012, demonstrating real-time and near-real-time hyperspectral data processing (potentially in-flight) including target/feature detection and image streaming. To achieve the outcome it combined modular workflows for radiometric and geometric image processing with hardware accelerated JPEG2000 compression and streaming

Conference 8543: Technologies for Optical Countermeasures

Wednesday - Thursday 26–27 September 2012

Part of Proceedings of SPIE Vol. 8543 Technologies for Optical Countermeasures IX

8543-1, Session 1

Trends in electronic warfare *(Keynote Presentation)*

Carl R. Smith, Northrop Grumman Corp. (United States)

Protection of military aircraft from hostile threats is paramount to ensure the survivability of aircrews, platforms, and to ensure mission success. While the threat environment continues to become more complex the defense budgets are shrinking putting new challenges on the development of EW systems. This paper presents the latest trends in EW system development including designing in the following features: 1) affordability, 2) open architecture, 3) integrated avionics survivability equipment, 4) multi-functionality, and 5) enabling technologies for sensors, and optical sources. While these design features are not new, they have grown in importance in the design of EW systems. If treated correctly they can have a beneficial symbiotic relationship to each other and to the airframe they support. This paper presents the importance of these design features; provides guiding principles for implementation, and gives examples from current hardware.

8543-2, Session 1

Laser manufacturing: strategies for coping with the challenges *(Keynote Presentation)*

John R. M Barr, SELEX Galileo Ltd. (United Kingdom)

Volume manufacture of reasonably complex lasers, as distinct from the build of small numbers of units, provides a range of challenges for a manufacturing organisation. All aspects of the business play a role in ensuring that the shop floor output matches the customer and company expectations. This talk will explore some of the measures taken at Selex Galileo to ensure that the detailed laser design enables a smooth transition into production.

Selex Galileo started its involvement in laser products when, as Ferranti, the manufacture of a HeNe lasers was initiated in 1963. This strand of the business expanded into CO2 lasers and an early product line based around industrial machining lasers emerged in the early 70's. The start of solid state lasers began in 1968 with a technology swap (radars for lasers) with Westinghouse. The technology thus acquired was improved and developed into a series of solid state laser rangefinder and laser designator products which were built throughout the 70's, 80's and early 90's.

Towards the end of the 90's, development of laser diode pumped products for laser designation and for Optical Countermeasures was initiated. The technology developments lead to the award of the Joint Strike Fight (F-35) development contract in 2003. Full scale manufacturing was started in 2005 on a different product. Today, over 1100 laser diode pumped designators have been shipped on a variety of programmes.

While it is tempting to say this was a smooth activity, ramping laser production from a one per month to >35 per month has not been without its opportunities to learn. Some aspects of this will be shared.

An underlying theme in all cases is simplicity: a concept that is often easier to say than to achieve. Simplicity touches all aspects of the Selex Galileo laser design philosophy from the top level architecture down to the detailed design of a sub assembly. For example, the drive for simplicity has impacted the design for resonators which has markedly changed over the last 7 years. One result of this has been an improvement in resonator layout moving from a classical linear resonator (e.g. the "crossed Porro resonator" implemented in the 1970's) to ring lasers. The benefits have been noticeably with significant reduction in manufacturing cost and improved reliability.

A separate, but equally effective, trend has been a refocus on core business values, expressed in this case by focussing on detail: cost; root cause and corrective action; manufacturability; and reliability.

Finally, when discussing the performance of laser containing multiple components, the question of contamination control remains open and may ultimately limit the long term reliability of these product types. Our approach has led to a 10x improvement relative to previous generation products.

8543-3, Session 2

Quantum cascade lasers ready for IRCM applications *(Invited Paper)*

Manijeh Razeghi, Northwestern Univ. (United States)

After nearly two decades' development, the quantum cascade laser (QCL) has emerged from a cryogenically cooled micro-watt emitter to room temperature continuous wave laser source with watt-level output powers. The recent breakthroughs in the wall plug efficiency (WPE) of InP based mid-IR QCLs draws significant interest for IRCM applications toward lower cost, weight, and overall power consumption of the system. Recent research highlight of high power QCLs will be presented, including wavelength coverage, power levels, beam quality, and reliability.

8543-4, Session 2

New device development and 2 micron operation for IRCM *(Invited Paper)*

Erwan L. Normand, Cascade Technologies Ltd. (United Kingdom)

No Abstract Available

8543-5, Session 2

A hollow waveguide integrated optic QCL beam combiner

Ian F. Elder, Robert A. Lamb, SELEX Galileo Ltd. (United Kingdom); Richard M. Jenkins, HollowGuide Ltd. (United Kingdom)

Quantum cascade lasers (QCLs) provide efficient, direct emission of a wide range of wavelengths across the mid and far-IR wavebands. Since their first demonstration in the 1990s there have been rapid developments in power scaling, efficiency and wavelength coverage. QCLs are now used for research, medical diagnostics, environmental monitoring and defence. Defence applications include chemical & biological agent detection, covert optical comms and directed infrared countermeasures (DIRCM). All these applications can benefit from effective practical approaches to combining several QCL sources to achieve enhanced power scaling or multi-wavelength emission.

We describe the design and performance of a hollow waveguide (HWG) integrated optic circuit for combining the outputs of QCLs emitting in the mid-IR. The circuit is based on integrating dichroic beam combiner components in alignment slots in the surface of a dielectric substrate and then guiding the light between the components in hollow waveguides. The hollow waveguides take the form of square section channels milled in a Macor (machinable glass-ceramic) substrate in conjunction with a lid. The hollow waveguides have fundamentally different propagation properties to solid core waveguides leading to transmission characteristics close to those of the atmosphere while still providing light guidance. Compared to a solid core waveguide, the transmission bandwidth of a hollow core waveguide is very broad and much higher optical power densities can be supported. As there is no refractive index interface between free-space and the hollow core, coupling to the hollow guide circuit, and integrating discrete components in it, is straightforward.

The goal of the work has been a beam combiner for combining three QCLs emitting at 3.95 μm, 4.05 μm and 4.60 μm respectively, and a Ho:YAG laser emitting at 2.10 μm. The design work involved two main facets: (i) the definition of dichroic component reflection and transmission characteristics for use in an appropriate circuit configuration, (ii) the definition of physical parameters and tolerances for the hollow waveguide circuit and the associated component alignment slots. We opted for a circuit configuration based on three integrated dichroic components and used orthogonally polarised inputs for the 3.95 μm and 4.05 μm sources. The use of orthogonal

polarisations made the design of the dichroic coatings easier and meant that where the emission linewidths of the 3.95 µm and 4.05 µm QCLs overlapped the total combined power was not reduced as a result of interference effects.

The design of the hollow waveguide circuit involved assessing the impact of the choice of guide width and wall refractive index on the fundamental mode attenuation coefficients at the wavelengths of interest. The waveguide width also dictates the angular and lateral alignment tolerances necessary to ensure efficient propagation of the fundamental waveguide mode. We chose to work with a guide width of 1.0 mm. This was a compromise between minimising transmission losses and working with angular alignment tolerances of the order of 1.0 mrad. Details of the design, manufacture and performance of the beam combiner will be described in relation to maximising optical efficiency and providing a compact, rugged solution.

8543-6, Session 3

Efficient single-pass resonantly-pumped Ho:YAG laser *(Invited Paper)*

Ian F. Elder, SELEX Galileo Ltd. (United Kingdom); Timothy M. J. Kendall, Defence Science and Technology Lab. (United Kingdom)

Efficient solid-state lasers in the eye-safe two micron regime are required for a number of applications, including remote sensing, coherent LIDAR, and in medicine, and as a pump source for generating mid-IR laser light via nonlinear frequency conversion. Holmium lasers are commonly preferred over thulium lasers because of their longer laser wavelength, resulting in higher atmospheric transmission and lower absorption in certain nonlinear crystals (e.g. zinc germanium phosphide (ZGP)) for mid-IR light generation. Moreover, since the holmium upper level typically has a longer lifetime than that of thulium, in addition to a stronger emission cross section, holmium-doped laser materials have a saturation intensity that is typically an order of magnitude lower, allowing higher peak power generation when operating the laser in Q-switched mode.

Resonant (in-band) pumping of an end-pumped holmium laser using a thulium fibre laser is the most efficient solution. Published results to date have used a double-pass geometry for the holmium laser. The rationale behind this design choice is to allow efficient absorption of the pump light while using a low holmium doping concentration (typically ≤1%) in order to reduce the deleterious effects of energy transfer up-conversion. The long absorption path of the double-pass pump geometry places a tighter constraint on the mode-matching of the pump beam to the holmium resonator mode; furthermore, any unabsorbed pump light is directed back towards the thulium fibre laser, which can lead to feedback-induced instability in the fibre laser output, and ultimately to catastrophic damage of the fibre pump source, if the feedback level is sufficiently high. Feedback can be eliminated by use of an optical isolator; however this requires linearly polarised output from the fibre laser (at added complexity and cost), which is not required for pumping of Ho:YAG. Furthermore high power optical isolators based on the Verdet effect tend to be bulky compared with the other optical components, and have a temperature and wavelength -dependent performance, both of which issues limit their suitability for use in robust and reliable compact laser systems.

Here we present results of a thulium fibre laser pumped Ho:YAG laser using a simpler single-pass pump geometry, while maintaining the high optical conversion efficiency of the standard double-pass pump geometry. A compact L-shaped plano-concave resonator, incorporating a Brewster angle acousto-optic Q-switch, is used. The gain medium is a 25 mm length Ho:YAG laser rod with a nominal doping concentration of 1%. At a maximum absorbed pump power of 47.5 W the average output power in Q-switched mode is 31.7 W, an optical-to-optical conversion efficiency of 67%. Thermal roll-over occurs at high power, with a maximum conversion efficiency of 71% at 33 W of absorbed power. At a Q-switch PRF of 30 kHz the optical pulsewidth is 40 ns. The measured beam quality factor M2 is 1.4, with the centroid jitter in the far-field limited to 0.4% of the far-field beam divergence.

Full characterisation of the laser in cw and Q-switched mode, plus a comparison with the performance in a lower power configuration, will be presented.

8543-7, Session 3

Fiber laser pumped high energy cryogenically cooled Ho:YLF laser *(Invited Paper)*

Espen Lippert, Helge Fonnum, Knut Stenersen, Norwegian Defence Research Establishment (Norway)

High energy 2-µm-lasers are needed in both remote sensing applications and as pump sources for high energy mid-IR sources. We report on a high energy 2-µm-laser based on Ho:YLF. Holmium, especially in YLF, has a long upper level lifetime, 15 ms, which allows for efficient storage of energy. However, at room temperature it is difficult extract much of this energy due to the three-level nature of the laser material. To mitigate this problem we have cooled the laser crystal to liquid nitrogen temperature, at which Ho:YLF becomes an almost pure four-level system. The laser is pumped resonantly at 1940 nm using a thulium doped fiber laser. The fiber laser is an efficient and practical way of converting the power of laser diodes to high brightness radiation at the pump wavelength.

To avoid severe life-time quenching due to up-conversion from the excited state, we have chosen a doping level of 0.5 at. % Ho in the YLF host. The YLF crystal is a square rod with 30 mm length and 9 x 9 mm aperture. The rod is placed in a dewar with two CaF2 windows. The crystal is pumped with 58 W of un-polarized radiation from the fiber laser, with a 4.6 mm pump beam diameter (FWe-2M). The absorption at 1940 nm is strongly anisotropic; it is much stronger in the direction parallel to the optical axis (π) than in the orthogonal plane (σ), and in order to have good absorption, the polarization of the transmitted pump is rotated using a quarter-wave plate and reflected back for a second pass through the crystal. The crystal is pumped for 34 ms, after which >95 % of the pump energy has been absorbed by the crystal.

The laser resonator is a negative branch confocal unstable resonator with a graded reflection output coupling mirror, with a Gaussian profile with 5.2 mm spot-size (FWe-2M) and 50 % center reflectivity. The output coupler is convex with 3.6 m radius of curvature, and the HR-mirror is concave with 5 m curvature, which requires a 0.7 m resonator length in order to form a confocal resonator. The resonator also has two 45°-mirrors for pump input and output coupling, and an electro-optical Q-switch based on RTP.

When the laser was Q-switched it generated 346 mJ of output energy at 2.05 µm in a 14 ns long pulse. From near- and far-field measurements, using a pyro-electric camera, we determined the M2-value to be 1.25. The goal of this experiment was not to generate high pulse rates, and in order to avoid any thermal issues the laser was run at 1 Hz. Increasing this significantly should be possible due to the excellent thermo-optical properties of cryogenically cooled YLF, but this has not been attempted yet.

This concept has proven very efficient in converting the high average power of the fiber laser into high pulse energies. We have achieved a conversion factor of 6 J/kW from pump power to 2-µm-energy. The fiber laser still has available 42 W of pump power, which will be used in an amplifier stage in a future experiment. Based on the performance of the oscillator the complete system should be able to generate 600 mJ.

8543-8, Session 3

Operation improvement of side-pumped Er:Yb:glass lasers through optical compensation techniques

Marco Vitiello, Elisa Spinozzi, GEM elettronica (Italy)

In the last decades the development of high power all solid-state lasers emitting around 1.5um fed a great deal of research due to manifold reasons. Actually, such emission wavelength falls into the so-called “eyesafe” region of the light spectrum where the risk of human injury is greatly reduced; moreover it corresponds to a peak into the atmospheric transmission and suffers from a lower scattering by tiny particles, as haze and fog, with respect to the visible band thus being more effective when long distances have to be covered by the laser radiation without significant power losses. Efficient direct laser emission around 1.5um can be obtained by proper pumping of Erbium:Ytterbium co-doped phosphate glasses.

These systems, when passively q-switched, allow for rather simple and ruggedized cavity configurations but cannot be driven at high

repetition rates due to the poor thermal dissipation capability. Due to the high value of absorption coefficient of Yb ions, these doped phosphate glasses are usually exploited in end-pumped disk lasers or side-pumped slab/rod lasers. For high power applications, side-pumping configurations are the geometry of choice. Then, in order to design an efficient and cost-effective laser system, the number and geometry of pump diodes are chosen to optimize the amount of power need. This can lead to a lack of symmetry in the pumping configuration. In this paper we report the results of the research on a double side-pumped Er:Yb:glass slab laser. Due to the non-symmetric power distribution inside the slab a displacement of the laser beam is observed thus leading to cavity misalignment and consequently to extraction efficiency loss. At repetition rates of about 5Hz this allows just a burst operation with an increased thermal load inside the slab. Numerical-theoretical studies about time-dependent temperature distribution in the laser material with appropriate boundary conditions concerning the considered asymmetric geometry lead to a model for mode axis thermal bending and allow to evaluate the amount of cavity misalignment in order to restore the maximal extraction efficiency.

By turning or shifting the cavity mirrors is possible to improve the burst operation but the maximal overlap between the mode axis and the inverted region cannot be recovered. Then, an alternative optical configuration able to intrinsically account for the cavity misalignment has to be designed.

The matrix formalism was effectively employed to calculate the specifics of one or more optical compensators to be inserted in the cavity to realign the laser resonator. Several configurations were analyzed and the beneficial effects on both thermal lensing and bending were predicted.

Experimental measurements validated the model. In particular, an uninterrupted pulsed operation at the highest repetition rates was effectively recovered thus reducing the thermal load inside the laser slab and making such a laser system more effective in free-space laser applications.

8543-10, Session 4

High-energy laser research for infrared countermeasures *(Invited Paper)*

Cobus C. Jacobs, Hencharl J. Strauss, Wayne S. Koen, Dieter Preussler, Lourens R. Botha, Oliver J. P. Collett, Council for Scientific and Industrial Research (South Africa); Christoph Bollig, Carl von Ossietzky Univ. Oldenburg (Germany) and Council for Scientific and Industrial Research (South Africa); M. J. Daniel Esser, Council for Scientific and Industrial Research (South Africa)

Over the last few years we have developed high power and high energy solid-state lasers in the 2 µm range which are suitable for a number of applications, including Directed Infrared Countermeasures. The main technical focus of the solid-state laser research was to develop a system which can be used as high-energy pump source for an optically pumped molecular laser based on HBr, which produced output pulses in the 4 µm wavelength range. In this overview paper we will review the technologies that were developed by our group for this application, as well as other published work.

We have pushed the output power of continuous-wave Tm lasers, including Tm:GdVO and Tm:YLF, which are used as pump sources for high-energy Ho-doped 2 µm oscillators and amplifiers. Following a power scaling strategy, we have demonstrated the highest output power of 225 W from a diode-end-pumped Tm:YLF laser, operating at 1.91 µm. However, to be suitable as pump source for Ho:YLF or Ho:LuLF, we adjusted the output wavelength to 1.89 µm by controlling the laser losses and polarisation. More recently, we demonstrated that the high-power Tm:YLF slab laser can be wavelength-selected using a Volume Bragg Mirror. We believe that the power can still be scaled significantly prior to thermal fracture of the Tm:YLF laser crystal.

We have developed a 70 mJ narrow-bandwidth Ho:YLF oscillator-amplifier system, pumped by an 80 W Tm:Fibre laser, which was used as seed for a power amplifier. The power amplifier was pumped by the Tm:YLF slab laser and initially utilised both a Ho:YLF and a Ho:LuLF gain crystal to produce 200 mJ per pulse. After numerical simulations it was optimised and used a longer Ho:YLF slab gain medium, producing up to 330 mJ per pulse at 2.064 µm, which was stabilised to an absorption line of HBr.

Several HBr configurations were investigated to test the feasibility of this approach. The highest output energy was demonstrated in an oscillator-amplifier system which produced 9 mJ per pulse with simultaneous output at 4.20 µm and 4.34 µm. In an alternative arrangement, wavelength selection over 580 nm was demonstrated from 3.87 µm to 4.45 µm in an oscillator with an internal diffraction grating. Theoretical cascade lasing to the HBr ground-state could not be experimentally verified.

8543-11, Session 4

Ho:YAG (2.09µm) laser system pumped by cw Thulium fiber laser (1.9µm) with >120mJ pulse energy at 100Hz repetition rate

Karsten Schmidt, Christoph Reiter, Heike Voss, Frank Massmann, Martin D. Ostermeyer, IBL Innovative Berlin Laser GmbH (Germany)

Some methods of optical countermeasure are based on Ho:YAG lasers at 2.09 µm. E.g. Ho-lasers resonantly pumped by 1.9 µm Tm-Lasers are attractive candidates for pumping mid-infrared optical parametric oscillator and generator materials to emit coherent light in the 3 µm to 5 µm spectral range. At 1.908 µm there is a maximum in the absorption spectrum of the Ho3+ Ions and a minimum in the absorption spectrum of water. Pumping near the emission wavelength yields high quantum efficiency and small thermal load of the laser active material. The thulium fiber lasers used as pump sources were additionally equipped with beam profile homogenizers to realize appropriate excitation profiles in the 3-level Ho:YAG-laser rods similar to the pump scheme described in [1].

The layout of the Ho:YAG-MOPA double-pass-system is shown in figure 1. It is realized as master-oscillator power-amplifier system (MOPA) and is based on our earlier work reported in [2]. The oscillator rod is pumped by a 50 W cw thulium fiber laser. There is a 15 % loss of pump radiation due to the homogenizer. Pump power from the Tm-laser transmitted through the oscillator rod, is back reflected to the rod to increase the pump efficiency. The amplifier is pumped in a scheme analogous to the oscillator with a 70 W cw Tm-fiber laser. The amplifier is realized as a polarization coupled double pass ring. At a repetition rate of 100 Hz a maximum pulse energy of 125 mJ is realized. At this repetition rate the oscillator reaches a maximum output energy of 53 mJ with 20 ns pulse width. The output energies of the oscillator, single pass, and double pass of the amplifier as a function of repetition rate is depicted in Fig. 2. In the first amplifier stage the output energy increases to 97 mJ at 100 Hz. After the double pass the output energy reaches 125 mJ. At 1000 Hz repetition rate a final pulse energy of 22mJ results from approximately 100 W of pump power. The laser system operates in transversal fundamental mode regime. Employing this oscillator-amplifier scheme an efficient and compact Ho:YAG laser system is realized.

Scaling to higher pulse energies can be reached by additional amplifier stages as described in [3] for a Ho:YLF system.

References

[1] P.A. Budni, C.R. Ibach, S.D. Setzler, E. J. Gustafson, R.T. Castro, and E.P. Chicklis, “50-mJ, Q-switched, 2.09-µm holmium laser resonantly pumped by a diode-pumped 1.9-µm thulium laser”, OPTICS LETTERS, Vol. 28, No. 12, 1016-1018 (2003).

[2] G. Renz, M. Klose, C. Reiter, F. Massmann, and H. Voss, “A High Energy Tm:YLF-Fiber-Laser (1.9 µm) pumped Ho:YAG MOPA (2.09 µm) Laser System”, Advanced Solid State Photonics, Incline Village, USA 2006, WD3

[3] A. Dergachev, D. Armstrong, A. Smith, T.E. Drake, M. Dubois, “High power, high energy OPA pumped by a 2.05µm Ho :YLF-MOPA system”, Photonics West 2008

8543-12, Session 4

MILDA: Mid-infrared laser source for DIRCM application

Bruno Crépy, Guillaume Closse, Sandrine Cussat-Blanc, Marc Le Nevé, Jean E. Montagne, Pierre Morin, CILAS (France); Benoit Mellier, DGA-MI (France); Olivier Squaglia, CILAS (France)

We report on the development and characteristics of infrared solid state laser as compact and robust light sources for Directed Infrared Countermeasures (DIRCM). DIRCM against infrared missile seekers requires wavelength tunable laser sources. When adding an optical parametric oscillator (OPO) to a pump laser source, it is possible to

cover the 2-5 µm wavelength transmission windows.

After a risk reduction phase of five years, CILAS has designed a solid state laser source (SSLS) adapted for DIRCM jamming and has delivered a prototype to DGA-MI for testing and evaluation. The purpose of this paper is to recall the requirements of such a laser source, to present the main design trade-off and the testing experiments. This work is supported by the French MOD (DGA).

8543-13, Session 4

Demonstration of a wavelength selected optically pumped HBr laser

Wayne Koen, Cobus Jacobs, Christoph Bollig, Hencharl J. Strauss, Lourens R. Botha, M. J. Daniel Esser, Council for Scientific and Industrial Research (South Africa)

Mid-infrared optically pumped molecular lasers are attractive alternatives to non-linear crystals for generating high-energy pulses. One molecule that can be used to convert the output of a high-energy 2 µm Ho-laser to the mid-infrared is HBr [1, 2]. The highest reported output energy from an optically pumped HBr system was 9 mJ per pulse, operating at 4.20 µm and 4.34 µm [3]. In this paper we report for the first time, to our knowledge, an optically pumped HBr laser operating over a wavelength range including both the P and R molecular transitions.

As pump source for the HBr oscillator, we developed a single-frequency Ho:YLF ring laser and amplifier system which was wavelength-locked to the 2064 nm absorption line of HBr [4, 5]. The HBr oscillator was pumped in a double pass configuration with 50 mJ per pulse at a repetition rate of 50 Hz. The low-pressure HBr was contained in an absorption cell of length 510 mm at 73 mBar and 20 degrees Celsius. The folded HBr resonator cavity consisted of a flat output coupler mirror with a reflectivity of R=80% at 4 µm, and a high-reflection coating at 2 µm which enabled double-pass pumping. The dichroic pump mirror had a concave curvature of 5 m and was coated to be highly reflective at 4 µm and high transmission at 2 µm to allow pumping of the HBr. The pump mirror was slightly tilted to reflect light on to the diffraction grating which was blazed at 4.29 µm. The diffraction grating therefore acted as the end-mirror of the HBr resonator, and the wavelength could be selected by rotating the grating.

Laser oscillation was demonstrated on nineteen molecular transition lines including both the R-branch (from 3870 nm to 4014 nm) and the P-branch (from 4070 nm to 4453 nm). The highest output energy for the given input energy was 2.4 mJ at 4133 nm.

[1] H. C. Miller, D. T. Radzykewycz, and G. Hager, “Optically Pumped Mid-Infrared HBr Laser,” IEEE J. Quantum Electron. 30(10), 2395-2400 (1994).

[2] L. R. Botha, C. Bollig, M. J. D. Esser, R. N. Campbell, C. Jacobs and D. R. Preussler “Ho:YLF pumped HBr Laser,” Optics Express, 17 (22) 20615-20622 (Oct 2009).

[3] M. J. D. Esser, W. Koen, H. J. Strauss, C. Jacobs, L. R. Botha, and C. Bollig “An HBr Oscillator-amplifier Pumped by a High-energy Ho:YLF Laser System” in CLEO/Europe and EQEC 2011 Conference Digest, OSA Technical Digest (CD) (Optical Society of America, 2011), paper CA1_3 (2011).

[4] C. Bollig, M. J. D. Esser, C. Jacobs, W. Koen, D. Preussler, K. Nyangaza and M. Schellhorn, “70 mJ Single-Frequency Q Switched Ho:YLF Ring Laser - Amplifier System Pumped by a Single 82-W Tm Fibre Laser,” Middle-Infrared Coherent Sources, Trouville, France, 8-12 June 2009, Mo3 (invited) (2009).

[5] H. J. Strauss, D. Preussler, O.J. P. Collett, M. J. D. Esser, C. Jacobs, C. Bollig, W. Koen, and K. Nyangaza, “330 mJ, 2 µm, single frequency, Ho:YLF slab amplifier”, in ASSP 2011, Paper TuA4.

8543-9, Session PS

Single longitudinal mode and dual wavelength CW VBG lasers at 1342nm and 1064nm

Andrew L. White, Ian F. Elder, Gavin J. Hall, SELEX Galileo Ltd. (United Kingdom)

The use of Volume Bragg Gratings (VBGs) as high reflectivity mirrors within solid-state lasers is investigated. An end-pumped Nd:YVO4 laser was configured to operate at 1342nm and 1064nm using VBGs as the wavelength selective element. VBGs can offer very narrow spectral response, in the order of hundreds of picometers with high reflectivity, typically up to 99%. By using the VBGs as HR mirrors we can achieve both narrow line-width and high reflectivity without the need for intra-cavity components to narrow the line-width. The resultant line-narrowed source can be used to improve the efficiency of processes such as non-linear conversion, or allow operation on weaker emission lines. As a result, VBG lasers can be used to create a number of sources, each running on different emission lines to create a diverse wavelength source.

Initially, a single VBG configuration is demonstrated at both wavelengths separately, generating 6W and 4W at 1064nm and 1342nm respectively. The spectral narrowing effect reduces the line-width of the configurations by a factor of 25 to 60pm in both setups.

Thermal effects within the VBG are considered as a result of the performance observed in the single VBG configurations. Modelling of the VBGs in the FEA package Comsol is demonstrated and the reduction in factors such as reflectivity and line width are modelled, providing good agreement with the measured results.

A further line narrowed configuration was tested using a double VBG setup. In this configuration we use 2 VBGs in reflective operation to achieve single longitudinal mode operation. Temperature tuning of each VBG away from the other provides a convolved cavity spectral response that is narrower than the VBGs individual response. In this configuration we operated the Nd:YVO4 at 1342nm and achieve up to 2.3W in a single longitudinal mode. By temperature tuning the VBGs we can control the line width of the Laser from 60pm with 3 longitudinal modes down to 16pm for single longitudinal mode performance.

Finally, a dual wavelength Laser is investigated operating at both 1342nm and 1064nm simultaneously.

A doubly cavity is constructed using separate VBGs for both 1064nm and 1342nm operation. Broadband AR coatings allow for intra cavity VBGs to provide low loss for one wavelength whilst providing high reflectivity at the other. In order to maintain dual wavelength operation, attenuation of the higher emission cross-section is required. This is achieved by over coupling the 1064nm cavity compared to the 1342nm cavity. Other methods of achieving dual wavelength operation are discussed such matching the emission cross-sections by temperature tuning of the VBG and varying spot sizes for different emission lines.

We conclude with recommendations for optimal configurations for the various setups described and present modelling validated from the previous results on how such devices would behave.

8543-17, Session PS

The European air defence high energy laser weapon project

Karsten Diener, Institut Franco-Allemand de Recherches de Saint-Louis (France); Rudolf Protz, MBDA Germany (Germany)

In asymmetric warfare scenarios, a major threat is caused by hostile attacks using mortars and artillery rockets (RAM). To counter such a threat by an effective laser weapon, only a short time scale is available. We developed a laser-matter interaction simulation model to dimension the laser weapon. The main mechanisms of the laser neutralisation of explosive devices are the conversion of the laser source photonic energy into heat on the shell surface and the heat transfer to the explosive. The numerical model is a two-layer model that can handle the absorption of the laser beam on the shell surface as well as the heat interaction between the shell-explosive interface. The simulation model is able to manage the activation of the explosive by laser heating, the rotation velocity of the RAM targets and the airflow effects. The influence on the neutralisation times of geometric parameters like the shell thickness and the laser spot size on the target, was studied. The performed simulations were verified by means of experiments with an industrial laser and real RAM-targets. Different air flow conditions, rotation velocities, types of casing and types of explosives were tested. The calculated neutralisation times and the measurement results are in good agreement. Based on this model that allowed dimensioning the necessary laser power, a European consortium, composed of French, German, Polish and Portuguese specialists developed a layout of a complete air defence high energy laser weapon system. The lay out of the system contains different parts: the laser source, the cooling system, the tracking system with beam correction, the radar system and the vehicle which is capable to transport the complete system to its mission place.

8543-14, Session 5

Optics detection using a dual channel approach *(Invited Paper)*

Lars J. Sjöqvist, Lars Allard, Göran Bolander, Magnus Pettersson, Sten Edström, Swedish Defence Research Agency (Sweden)

Detection of optical assemblies is important in revealing threats arising from snipers or other weapons guided by optical means. Several approaches can be imagined using flood illumination or scanning laser techniques. Depending on target characteristics laser radiation is retro-reflected back to the interrogating system. Autonomous or operator controlled optics detection system can be devised. One challenging problem in optics detection applications in urban environments, particular if an autonomous approach is chosen, is to reduce the false alarm rate. False targets include e.g. traffic signs, reflectors from different lights, optical reflexes and glints from specular surfaces or windows.

In this work a dual channel approach for optics detection using a narrow scanning rectangular laser beam is described. One channel is used for locating targets in the vertical direction while a second channel simultaneously determines the distance to the targets. Utilising information from both channels the target discrimination capability can be improved and the number of false alarms reduced. An experimental system consisting of two channels (position and distance) operating at 0.8 micrometer wavelength was used to simultaneously study the characteristics of different targets and backgrounds. The rectangular beam profile was scanned in the horizontal plane to provide angular information. Different type of targets including traffic signs, optical reflexes, rifle sights and optical references were studied experimentally at different ranges and in different environments. In addition, turbulence effects were studied in a horizontal propagation path close to ground.

The experimental results show that information about target distance is important in order to discriminate false targets. In horizontal or weakly slant propagation paths close to ground the influence from atmospheric turbulence need to be considered. Turbulence effects may reduce the performance of an optics detection system. Schemes for improving the target discrimination and decreasing the false alarms are discussed and illustrated using experimental data. The performance of an optics detection system using a dual channel approach is discussed. The dual channel scheme is suggested to improve capabilities in optics detection using a scanning rectangular laser beam.

8543-16, Session 5

Non-lethal optical interruption (dazzling): technology, devices, and scenarios *(Invited Paper)*

David Shannon, B.E. Meyers & Co., Inc. (United States)

Bright lights have long been used to disorient individuals, but it has only been in the last decade that Non-Lethal Optical Interruption Lasers, or Dazzling Lasers, have been employed by the U.S. military in a variety of Escalation of Force scenarios. Dazzling Lasers achieve hail & warn, distraction, or suppression effects by directing high irradiance visible light into the eyes of targeted personnel. Green lasers are typically used for Dazzling sources due to their high directionality and the sensitivity of the human to green light.

This paper will discuss an overview of laser dazzling scenarios with an emphasis on effectiveness (hail & warn, distraction, or suppression) and the simultaneous goal of eye-safety. The primary focus will be hand-held visible Dazzlers, however a few UAV and airborne platforms will also be described.

Also discussed will be the basic guidelines & technology of hand-held military green laser systems that are; simple & intuitive, small, lightweight, inexpensive, very rugged & durable, and multi-use. Successful military small laser product designs require extensive systems engineering so that performance features and environmental constraints are aligned effectively.

A few counter-intuitive aspects of the use of lasers in the military will also be presented.

8543-26, Session 5

Coherent source transverse field profiles and far-field energy distribution

Ron K Meyer, Northrop Grumman Electronic Systems (United States)

Northrop Grumman presents analysis of near-field electrical field distributions of coherent sources and the resultant far-field energy distributions. This work comparatively analyzes the effect of coherent mode content, transverse phase modulation at the source, and apertures at the source. Gaussian, top-hat, and high order Hermite-Gaussian mode distributions are propagated to the far-field and the intensity distribution is compared. Both phase and aperture transformations are applied to the source distributions and the resultant far-field distributions are compared. Using the Fraunhofer approximation and Parseval's theorem it is possible to provide an accurate intensity profile at ranges wherein the approximation is valid. Using this method various phase transformations at the aperture are analyzed with regard to their resultant far-field distribution. For an arbitrary given source energy with a Gaussian profile, the coherent source energy required to achieve a minimum intensity over a given area is determined for phase distributions at the source aperture. Assuming a desired intensity distribution in the far-field and Gaussian source, an adaptive-additive algorithm is employed to synthesize a phase transformation at the source to achieve the desired distribution. The far-field intensity distribution of this synthesized phase distribution applied to a Gaussian source is compared to the far-field produced by a non-phase transformed Gaussian source.

8543-27, Session 5

Specifying and testing infra red threat warning systems

Les Youngman, Max R. Buttinger, Thales UK Ltd. (United Kingdom)

Thales UK are developing a Multi-Functional Infra Red Threat Warning System. Engagement with all the stakeholders at an early enough time is required to ensure IR systems are available for platform protection in a timely manner. Specifying an IRTWS similarities and/or differences to the more familiar UV Missile Warning Systems will be outlined. Possible growth capabilities made possible by the IR technology will be discussed. Planning, processes & techniques required to Test and Accept an IRTWS will be described. A Test, Verification and validation Strategy will be presented.

8543-18, Session 6

Modelling infrared signatures of ships and decoys for countermeasures effectiveness studies *(Invited Paper)*

Ric H. M. A. Schleijpen, Marianne A. Degache, Henny Veerman, Ronald van Sweeden, TNO Defence, Security and Safety (Netherlands); Bernadetta Devecchi, TNO (Netherlands)

Infrared guided missiles are a threat for modern naval forces. The vulnerability of ships can be reduced by applying countermeasures such as infrared decoys and infrared signature reduction.

This paper presents a recent improvements in a simulation toolset which can be used for assessing the effectiveness of these measures. The toolset consists of a chain of models which calculate the infrared signature of a ship (EOSM) and decoys, and generate infrared image sequences of the ship in a realistic sea and sky background (EOSTAR). A complete missile fly-out model (EWM) uses these images in closed loop simulations for the evaluation of countermeasure effectivenes. All model components will be discussed. Typical simulation results will be shown.

8543-19, Session 6

An open-source toolkit for infrared calculation and data processing *(Invited Paper)*

Cornelius J. Willers, Council for Scientific and Industrial Research (South Africa); Maria S. Willers, Petrus J van der Merwe, Denel Dynamics (South Africa); Johannes J. Calitz, Azwitamisi E. Mudau, Council for Scientific and Industrial Research (South Africa); Alta de Waal, Council for Scientific and Industrial Research (South Africa); Ricardo Augusto T. Santos, ITA (Brazil)

Electro-optical system design, data analysis and modelling involves a significant amount of calculation and processing. Many of these calculations are of a repetitive and general nature, suitable for adding to a generic toolkit. The availability of a toolkit facilitates and increase productivity during subsequent tool development. The concept of an extendible toolkit lends itself naturally to the open-source philosophy, where the toolkit user-base develops the capability cooperatively, for mutual benefit. This paper will cover the underlying philosophy to the toolkit development, brief descriptions and examples of the various tools used and an overview of the electro-optical toolkit.

The toolkit is an extendable, integrated and coherent collection of basic functions, code modules, documentation, example templates, unit tests and resources, that can be applied towards diverse calculations in the electro-optics domain. The toolkit covers (1) models of physical concepts (e.g. Planck's Law), (2) mathematical operations (e.g. spectral integrals, spatial integrals, convolution), (3) data manipulation (e.g. input/output, interpolation), (4) graphical depiction (2-D and 3-D graphs), (5) graphical user interfaces, and (6) all these in an interactive development environment.

Toolkits are commonly written in scriptable languages, such as Python and Matlab. This specific toolkit is implemented in Python and its associated modules Numpy, SciPy, Matlplotlib, Mayavi, and PyQt/PySide. In recent years these tools have been well tested, stabilised and matured sufficiently to support mainstream tool development. Collectively, these tools provide a very powerful capability, even beyond the confines of this toolkit alone. Furthermore, these tools are freely available.

Rudimentary radiometric theory is given in the paper to support the examples given. Examples of the use of the toolkit described in the paper include (1) spectral radiometric calculations of arbitrary source-medium-sensor configurations, (2) thermal camera calibration and analysis of measured countermeasure flare data, (3) sensor MTF performance analysis, (4) fourier transform data analysis and (5) analysis of missile performance simulation results.

The toolkit is developed as a co-operative effort between the CSIR (South Africa), Denel SOC (South Africa) and DCTA (Brazil). Details of the open source license and URL is described in the paper. Once released, the project will be managed in accordance with general practice in the open source community.

8543-20, Session 6

Modelling of self phase modulation for broadband DIRCM lasers

Robert A. Lamb, SELEX Galileo Ltd. (United Kingdom)

Efficient laser emission in the medium wave infrared (MWIR) is a long established requirement for directed infrared countermeasures (DIRCM). However, until the last decade, there has not been a viable technology for the direct generation of wavelengths in the 3-5m region and indirect methods using optical parametric conversion have been the subject of intense development. Several indirect methods have been developed using different pump wavelengths which represent mature laser technology. For example, 1.54 microns from Er:YAG or non-linear conversion from Nd:YAG (1.064 microns); 2.1 microns from Ho derived from Tm at 1.97 microns, or co-doped Ho:Tm in a fibre. These approaches produce the required pump wavelength for efficient 3-5 micron generation using either ZGP or OPGaAs, however, they are less efficient than direct generation by quantum cascade lasers (QCL). The direct conversion from electrical to optical energy in a QCL is very efficient; wall-plug efficiencies of >20%, depending on wavelength and operating temperature, are typical. High efficiency, together with the high average powers that are now commercially available suggest that the QCL is an attractive laser for DIRCM.

However, as protection measures and signal processing techniques advance, one can anticipate that the requirement for sophisticated laser emission in the MWIR becomes more refined. In particular, broadband emission covering a wider, continuous, spectral region will prove harder to counter than that from a few discrete wavelengths and a supercontinuum has been suggested as a possible mechanism for broadband emission. In most investigations into supercontinuum generation, the emphasis has been on producing a wide, flat spectrum covering several hundred nanometres in the visible, near and short wave infrared for stand-off spectroscopic sensing of chemical agents, atmospheric sensing or hyperspectral sensing. These supercontinua are characterised by a spectral bandwidth to pump wavelength ratio, R > 1 for a pump wavelength in the visible or near infrared. In most applications, the simultaneous generation of a wide spectrum is not required; instead a tuned output suffices. This has the added benefit of improving the efficiency of the laser sensor system since wavelengths which are not required, are not generated. The problem is to understand how a limited continuum might be generated. In the context of DIRCM, the spectral requirement is to produce a controlled spectral emission which matches the 3-5 micron atmospheric transmission window.

In this paper, a theoretical calculation is presented which shows that a continuous spectrum spanning a few hundred nanometres in the mid infrared (R ~ 0.2) can be generated in a simple pump geometry from a mode-locked, ultra-short pulse train using self phase modulation (SPM). Spectral broadening centred on the CO2 absorption band at 4.26 microns can be excited to produce all wavelengths for band IV DIRCM. The parameters which affect the spectral output such as pulse power, interaction length, pulse duration and pulse shape are considered for the case where the pump geometry is a collimated beam propagating through a mid infrared glass characterised by a non-linear refractive index n2. The prospects for developing a suitable pump laser are also discussed, in particular, the possibility of using a mode-locked QCL.

8543-21, Session 6

An intelligent tracking algorithm for an imaging infrared anti-ship missile

Greer J. Gray, Nabil Aouf, Mark A. Richardson, Cranfield Univ. (United Kingdom); Brian Butters, Meon Technology Ltd. (United Kingdom); Roy Walmsley, Chemring Countermeasures Ltd. (United Kingdom)

This paper describes the development of a target tracking algorithm for an anti-ship imaging infrared seeker. The tracking algorithm uses feature extraction and machine learning to discriminate between a desired target and decoys within the seeker field of view. The algorithm is developed within a high fidelity simulation architecture, used to simulate engagements of infrared missiles against ships, aircraft and land vehicles. The proposed seeker tracking algorithm will be evaluated in a naval engagement scenario, against a ship deploying countermeasures. The tracking algorithm performs the tasks of object detection, feature extraction and target selection. Object detection is achieved via image thresholding, and thereafter, shape and intensity based features are calculated for each object. These features are then used for target selection, to determine the seeker aim-point. Object features such as peak and average intensity, intensity moments, eccentricity, roundness, minimum, maximum and average radial perimeter distances are considered, to determine their discriminatory power. A selection of the most discriminatory features is then used as inputs to a neural network. The neural network is trained on images of various ships and decoys, generated by the front end of a seeker model within the simulation architecture. Examples of the performance of the tracking algorithm against targets and decoys will also be shown.

8543-22, Session 7

Simulating the DIRCM engagement: component and system level performance *(Invited Paper)*

Cornelius J. Willers, Council for Scientific and Industrial Research (South Africa); Maria S. Willers, Denel Dynamics

(South Africa)

Aircraft self protection against missiles requires increased sophistication as missile capabilities increase. Recent advances in self protection include the use of directed energy countermeasures (DIRCM), employing high power lamps or lasers as sources of infrared energy. The larger aircraft self-protection scenario, comprising the missile, aircraft and DIRCM hardware is a complex system. In this system, each component presents major technological challenges in itself, but the interaction and aggregate behaviour of the systems also presents design difficulties and performance constraints.

This paper presents a description of a simulation system, that provides the ability to model the individual components in detail, but also accurately models the interaction between the components, including the play out of the engagement scenario.

Objects such as aircraft, flares and missiles are modelled as three-dimensional objects with a physical body, radiometric signature properties and six-degrees-of-freedom kinematic behaviour. The object's physical body is modelled as a convex hull of polygons, each with radiometric properties. The radiometric properties cover the 1--5 micrometer spectral range (as is relevant to current technology missiles) and include reflection of sunlight as well thermal self-emission. The signature modelling includes accurate spectral descriptions as well as temporal behaviour of the object's signature. The object's kinematic behaviour is modelled in control system engineering modules, which are implemented using finite difference equations. The objects in the scenario are placed and appropriately orientated in a three-dimensional world, and the engagement is allowed to play out.

Low-power countermeasure techniques against the missile seekers include jamming (decoying by injecting false signals) and dazzling (blinding the sensor). Both approaches require knowledge of the seeker hardware and/or signal processing. Simulation of decoy operation is achieved by implementing the missile signal processing in the simulation (i.e. accurate white-box modelling of actual behaviour). Simulation of dazzling operation is more difficult and a parametric black-box approach is taken. The design and calibration of the black-box dazzling behaviour is based on heuristic modelling, to be subsequently verified by experimental laboratory and field work. The black-box behaviour can later be replaced, once information is available, with actual behaviour.

A description is given of the (1) respective object models in the simulation, including key performance parameters of the models and a brief description of how these are implemented, (2) the scenarios where the models are deployed and (3) results obtained from executing the simulations. The effect of various design decisions and performance parameters are investigated. The paper closes with recommendations for future research and simulation investigations.

8543-23, Session 7

Key considerations in infrared simulations of the missile-aircraft engagement *(Invited Paper)*

Maria S. Willers, Denel Dynamics (South Africa); Cornelius J. Willers, Council for Scientific and Industrial Research (South Africa)

The performance of modern imaging and non-imaging infrared missile systems strongly relies on the quality of the image and signal processing algorithms deployed. Likewise, the development of an effective countermeasure technique or system for aircraft self-protection requires accurate missile behaviour modelling. The development of these algorithms and protocols can be done most effectively in an accurate infrared imaging simulation. This paper investigates the requirements for, and the performance of, such a simulation system, supporting the evaluation of the missile behaviour in the missile-aircraft engagement scenario.

Missile performance depends on many factors, affecting the seeker, tracking and guidance behaviour. We investigate the necessity of the modelling and simulation of significant signature elements on the missile target detection and tracking performance, i.e. which signature elements are key to an accurate missile-aircraft engagement simulation?

The development and evaluation of missile detection and tracking algorithms, or countermeasure systems, requires a comprehensive simulation environment where thousands of missile flights can be simulated, covering a wide variety of scenarios and signature conditions. The missile seeker algorithms generally detect and classify targets based on intensity, spatial and dynamic characteristics.

The key considerations for such an imaging infrared simulation system are: 1) radiometric accuracy in all spectral bands, i.e. sunlight and thermal radiance to provide correct colour ratios; 2) accurate surface temperature behaviour, be it by aerodynamic or thermodynamic heating; 3) high fidelity geometrical and spatial texture modelling to provide shape of targets and countermeasures; 4) true dynamics and kinematic behaviour in six degrees of freedom; 5) detailed modelling of backgrounds; and 6) accurate atmospheric transmittance and path radiance models.

This paper briefly describes a physics accurate imaging simulation system, operating in the 0.4 to 14 micrometer spectral bands. The simulation system is evaluated with respect to the requirements for accurately simulating the missile-aircraft engagement scenario. A generic missile system, incorporating algorithms with simple target detection and countermeasure rejection principles, is defined for the study. It is shown how engagement is affected by target aircraft and countermeasure signature spectral colour ratio, spatial shape, kinematics, temporal behaviour, as well as the effect of the atmosphere and background. From this analysis the significance and relevance of the modelled signature elements are reviewed, thereby identifying the key requirements for simulating the missile-aircraft engagement.

8543-24, Session 7

Future-proofing an aircraft self-protection IR signature database

Mrwan Alayed, Munir M. El-Desoukia, Motasem S. Alsawadi, Khalid Alghamdi, King Abdulaziz City for Science and Technology (Saudi Arabia); Attiah A. Al-Ghamdi, King Abdulaziz Univ. (Saudi Arabia); Cornelius J. Willers, Council for Scientific and Industrial Research (South Africa); Johannes J. Calitz, Council for Scientific and Industrial Research (Saudi Arabia); Azwitamisi E. Mudau, Dirk F. Bezuidenhout, Council for Scientific and Industrial Research (South Africa)

Aircraft self-protection against heat seeking missile threats is an extremely important topic worldwide, recently even more so with the instability in the Middle East region due to, for example, the large number of man-portable air defense systems (MANPADS) that were stolen from army arsenals. A fundamental step in successfully achieving self-protection is the ability to capture and identify aircraft infrared signatures. This work discusses some of our efforts and results in creating an asset database for infrared signatures. The database was designed in a way that will feed an image processing engine to allow for automated feature and signature extraction. A common failing in the handling of target signature raw data is the fact that raw data files can become unreadable because of changes in technology, software applications or weak media archiving technology (e.g. corrupt DVD media). A second shortcoming is often the fact that large volumes of raw or processed data are stored in an unstructured manner, resulting in poor recall later. A third requirement is the portability of data between various processing software packages, legacy, current and future. This paper demonstrates how the challenge of future-proofing measured data is met with reference to the archiving and analysis of data from a recent measurement campaign. Recommendations for future work are given, based on the experience gained.

8543-25, Session 7

Aircraft plume infrared radiance inversion and subsequent simulation model

Stephanus J P Retief, Denel Dynamics (South Africa)

A radiance inversion technique, in which in-flight aircraft plume radiance recordings are exploited to construct a three dimensional (3D) radiance model of the plume, is presented. The recordings were done with a mid-wave infrared (3 - 6 micron) camera at different altitudes. The camera was integrated into an instrumentation pod of a 'carrier' aircraft and was directed towards a turbojet 'target' aircraft, viewed at aspect angles of 0 deg, 10 deg, 20 deg and 90 deg (side view of aircraft). The radiance inversion technique was applied to the recordings at the 90 deg aspect angle and a 3D radiance model could

be constructed from the extracted information. The recordings at the remaining aspect angles were used for verification of the correctness of the 3D radiance model.

The algebraic formulation of this inversion technique, also known as an emission-absorption technique, is stated for the ideal case of spectral radiance measurements of a high spatial sampling resolution over the plume area, as would be obtained from a hyperspectral imager. It is required of the plume to be representable by a series of concentric cylinders centred about the main (length) axis of the plume, divided into slices perpendicular to the plume's main axis, with homogeneous physical properties within each annular region within each slice. Each of the slices is being treated individually as an array of projected radiance values (pixel values in recorded image) at a 90 deg aspect angle during the radiance inversion process. The non-ideal case of having only broad-band (mid-wave) image measurements and only one spectral measurement of the plume, is then investigated. It is shown that from this incomplete information set, an effective spectral absorption coefficient can be calculated for which the associated plume spectral transmission and spectral emissivity calculations exhibit the correct qualitative behaviour. It is also shown that, by using this effective absorption coefficient, an optimization procedure can be used to determine the temperatures within each of the concentric cylinders within each slice of the plume. This optimization procedure consists of minimizing the difference between the observed line-of-sight (LOS) radiance in the image (i.e. a pixel radiance value in the image) and its theoretical projected radiance.

The observer LOS is then parameterized so that it can be described for an arbitrary angle with respect to the main axis of the plume. The intersections of the LOS with the boundaries of each annular region as well as the boundaries of the plume slices are then calculated in order to determine the traversed distances within each annular-slice region of plume. The above mentioned inferred temperatures, spectral transmissions and spectral emissivities are then used to calculate the expected spectral radiance at this arbitrary angle. The spectrally integrated/mid-wave broad-band radiances for aspect angles of 0 deg, 10 deg and 20 deg, and the intensities derived from it, are then calculated and compared with the actual measurements in order to determine the adequacy of this model for incorporation into existing infrared imaging system simulation software used in the training of infrared seekerhead missiles.

8543-28, Session 7

A novel system of equations for minimum resolvable contrast modelling and validation via measurements

Nicholas P. Smart, Thales Optronics Ltd. (United Kingdom)

A novel model for minimum resolvable contrast (MRC) modelling for visual band sensors is presented. Details of MRC measurement apparatus is provided and validation is shown for monochrome and colour CMOS and CCD as well as EMCCDs. Comparison is also made to the relevant products of the NVESD: SSCAM 2002 and SSCAM IP.

Conference 8544: Millimetre Wave and Terahertz Sensors and Technology

Wednesday - Thursday 26–27 September 2012 • Part of Proceedings of SPIE Vol. 8544
Millimetre Wave and Terahertz Sensors and Technology V

8544-1, Session 1

Development of passive submillimeter-wave video imaging systems for security applications *(Invited Paper)*

Erik Heinz, Torsten May, Detlef Born, Gabriel Zieger, Anika Brömel, Solveig Anders, Viatcheslav Zakosarenko, Torsten Krause, André Krüger, Marco Schulz, Frank Bauer, Hans-Georg Meyer, Institut für Photonische Technologien e.V. (Germany)

Passive submillimeter-wave imaging, i.e. thermal imaging in the submillimeter-wave range, is a concept that has been in the focus of interest as a promising technology for security applications for a number of years. It utilizes the unique optical properties of submillimeter waves and promises an alternative to millimeter-wave and X-ray backscattering portals for personal security screening in particular. Possible application scenarios demand sensitive, fast, and flexible high-quality imaging techniques. Considering the low radiometric contrast of indoor scenes in the submillimeter range, this objective calls for an extremely high detector sensitivity that can only be achieved using cooled detectors.

Our approach to this task is a series of passive standoff video cameras for the 350 GHz band that represent an evolving concept and a continuous development since 2007. Originally, it started out as an adaption of technology designed for submillimeter-wave astronomy. The cameras utilize arrays of up to 64 superconducting transition-edge sensors (TES), i.e. cryogenic microbolometers, as radiation detectors. The TES are operated at temperatures below 1 K, cooled by a closed-cycle cooling system based on pulse tube coolers and Helium evaporation coolers. The detectors are placed inside an optical cryostat while coupled to radiation by conical feed horn antennas and a set of cooled filters. Low-noise detector readout is done by superconducting readout electronics. By this means, background limited photometry (BLIP) mode is achieved, providing the maximum possible signal to noise ratio. The temperature resolution, being a figure of merit for a thermal imager, depends on the frame rate, the number of detectors, and the spatial resolution. At video rates, this leads to a pixel NETD well below 1 K.

The imaging system is completed by a reflector optics based on free-form mirrors. Two optical concepts have been developed so far, reflecting the need of different object distances and different fields of view for different application scenarios. For object distances of 3 to 10 m, a field of view up to 2 m height and a spatial resolution in the order of 1-2 cm is provided. The MTF (modulation transfer function) of the optics is diffraction-limited within significant parts of the image. Due to the limited number of detectors, an opto-mechanical scanner, integrated into the optical system, is used to construct the image. It is capable of a frame rate up to 25 frames per second.

Several electronic and software components are used for system control, signal amplification, data processing, and image generation. The current system generation is already close to a portable, application-ready, and user-friendly imaging system. The concept has been tested in the context of civil as well as military security scenarios, proving that ist is, in principle, capable of detecting hidden threats. Application in real world security screening scenarios will, however, require further work in the field of understanding, interpreting and automated processing of the submillimeter-wave thermal images, which are still in an early stage.

8544-2, Session 1

SUMIRAD: a near real-time mmw radiometer imaging system for threat detection in an urban environment

Stephan Dill, Markus Peichl, Daniel Rudolf, Deutsches Zentrum für Luft- und Raumfahrt e.V. (Germany)

The armed forces are nowadays confronted with a wide variety of types of operations. During peace keeping missions in an urban environment, where small units patrol the streets with armored vehicles, the team leader is confronted with a very complex threat situation. The asymmetric imminence arises in most cases from so called IEDs (Improvised explosive devices) which are found in a multitude of types and versions. In order to avoid risky situations the early detection of possible threats due to advanced reconnaissance and surveillance sensors will provide an important advantage.
A consortium consisting of the “Grupo Tecnològico e Industrial GMV S.A. (Spain)”, the “Royal Military Academy, RMA (Belgium)”, the “Deutsches Zentrum für Luft- und Raumfahrt, DLR” and the “Technische Universität München, TUM (Germany)” developed in the SUM project (Surveillance in an urban environment using mobile sensors) a low-cost multi-sensor vehicle based surveillance system in order to enhance situational awareness for moving security and military patrols. The project was funded by the European Defense Agency (EDA) in the Joint Investment Program on Force Protection (JIP-FP). In order to build a reliable system that can operate 24 hours a day in various conditions (e.g. dust, fog, smoke, rain), different types of sensors are applied, the complementarities of which are exploited through an advanced data fusion engine. The system is able to detect potential threats at large distances while driving at a normal cruising speed and is able to recognize and characterize threats in more detail at smaller distances and at slower speeds. The sensor suite includes an optical and an infrared camera, a millimeter-wave radar and a millimeter-wave imaging radiometer. The latter SUM Imaging Radiometer (SUMIRAD) has been developed by the DLR Microwaves and Radar Institute and is able to provide in near real-time quasi-optical microwave images. In combination with additional information (digital maps, imagery) from external sensors, like e.g. satellites or UAV (unmanned aerial vehicle), the SUM system shall support the patrol vehicle commander via a comprehensive MMI (Man Machine Interface) in order to recognize objects which could be a potential threat in due time.

The SUMIRAD system offers the advantage to detect and localize objects and persons under all atmospheric obstacles and also extents the surveillance capabilities behind non-metallic materials like clothing or thin walls and thin vegetation. The SUMIRAD innovative and light-weight fully mechanical scanning system with two MMW radiometer receivers (82-102 GHz) accomplish the demand to cover a large field-of-view with a high performance two dimensional imaging system for low cost. For the intended surveillance application SUMIRAD will be mounted on a suitable vehicle as part of the complete SUM system. SUMIRAD observes continuously the area of interest in front of the vehicle while the vehicle drives along the road. The minimum image acquisition time is one second.

This paper will present the principle and the development of the SUM imaging radiometer system and its key components. Furthermore the image processing of the final image product reconstructed from the data stream of each radiometer receiver will be described. Imaging results from several measurement campaigns will be presented. The overall SUM system and the individual subsystems are presented in more detail in separate papers.

8544-3, Session 1

IMAGINE project: a low cost, high performance, monolithic passive mm-wave imager front-end

Duncan Platt, Acreo AB (Sweden); Naomi E. Alexander, GATE S.A. (Spain); Peter Frijlink, OMMIC (France); John Hendricks, Rogers Corp. (Belgium); Ernesto Limiti, TECS - Technological Consulting Svcs S.R.L. (Italy); Sebastian Löffler, RHe Microsystems (Germany); Colin Macdonald, Rogers Corp. (United Kingdom); Hassan Maher, OMMIC (France); Lars Pettersson, Acreo AB (Sweden); Paul Rice, GATE S.A. (United Kingdom); Markus B. K. Riester, Daniel Schulze, Dyconex AG (Switzerland); Vessen Vassilev, Chalmers Univ. of Technology (Sweden)

There is an urgent need for security screening technology that can provide low cost, high performance, ‘walk-by’ screening at rapid flow

rates for security at airports and transportation hubs. Whilst mm-wave technology is a leading technology, cost is a barrier. The critical part of such systems is the detector module that can account for 60% of the overall system cost. At present this high cost is due to expensive components plus lengthy hand assembly and tuning.

The aim of the FP7 Research for SME IMAGINE project is to perform research and development of innovative solutions to increase integration, reduce size and costs, whilst maintaining high performance, for passive mm-wave camera front-end modules.

The standard radiometer equation, showing pixel temperature resolution, is shown in equation (1), (where Ts is the scene temperature, Tr is the receiver noise, B is the receiver bandwidth and b is the video noise bandwidth, with a limit defined by the integration time, b=1/2τ).

$$NETD=(Ts+Tr)\sqrt{(2b/B)} \quad (1)$$

To achieve low NETD then it is necessary to maximize B and minimize Tr. Receiver performance is dominated by antenna gain, LNA NF and gain, detector diode sensitivity, diode 1/f noise, impedance matching, and interconnection losses. The packaging should not degrade on performance.

The main innovation areas for the project are: development of a zero-biased detector diode; development of a LNA; MMIC integration of the diode and LNA; development of a broadband mm-wave antenna; integration of the front-end components into a compact, low cost module based on a high performance LCP carrier. The project targets a receiver NETD in the region of 0.5K using an integration time (τ) suitable for real time video.

Currently a zero biased RITD has been achieved by OMMIC that has been measured and characterized by Chalmers. Design improvements are on-going but the first results show tunnel diode behavior with a responsivity ~6000V/W.

An LNA design from OMMIC and TECS has been achieved with BW from 75-110GHz, gain 23±3dB and NF= ~2.8dB. Proof of concept to integrate the RITD with the LNA is on-going.

A broadband antenna design has been made by Acreo with expected performance: BW= 75-107GHz, RL < -25dB, gain = 21dBi, HPBW= 17.4°, side lobe < -36dB, back-lobe < -42dB, cross-polarization < -44dB.

Dyconex has manufactured a low-cost high frequency PCB using LCP materials from Rogers. The final demonstrator module has been assembled by RHe and is being tested by GATE using its passive mm-wave imaging system.

Test results from the final demonstrator module, together with the proof of concept MMIC integration will be presented at the conference.

8544-4, Session 1

Simulation and experiments to understand performance enhancements in aperture synthesis passive millimetre wave imagers

Neil A. Salmon, MMW Sensors Ltd. (United Kingdom)

Recent work demonstrated how the aperture synthesis technique can be used to generate images in the near-field by adapting far-field algorithms used in radio astronomy interferometry. This technique will lead to a compact planar format of passive millimetre wave imager that can be deployed on surfaces of aircraft to offer an all-weather capability and deployed unobtrusively in multitudes of scenarios for security screening of personnel. Through experimentation and simulation it became apparent that certain levels of clutter in the images were associated with sources in the scene that were outside the main beams of the antennas in the array. Through further work it became apparent that this clutter is a manifestation of aliasing associated with the periodicity of the antennas in the array. Simulation and experimentation has shown how randomising the array can reduce the effects of these, leading to performance enhancements in the form of a lower level of clutter.

8544-5, Session 2

3D millimetre-wave scanner for luggage and parcels *(Invited Paper)*

Helmut W. Essen, Ralph P. Zimmermann, Maxonic GmbH (Germany); Sebastian Hantscher, Fraunhofer FHR (Germany); Nils Pohl, Ruhr-Univ. Bochum (Germany)

Port security is an important topic for law enforcement against terroristic attack. While much effords have been undertaken to improve safety on airports, harbours by far not as much in the focus of such efforts. Taking this into account a research program has been launched dedicated to many aspects of port security. Within this approach, “VESPERplus”, one topic is the investigation of millimetre-wave based scanners for luggage and parcel control within the harbor environment.

New sensors used for security purposes have to cover the non invasive control of baggage and packages with the aim to detect weapons, explosives and chemical or biological threat material. Currently emphasis is put into system concepts and technology for this type of applications employing millimeter wave and terahertz sensors. This is based upon the capability of these frequency bands to look through dielectric material and the possibility to achieve a geometric resolution, which is sufficient to resolve critical items within the necessary range. To overcome the limitations of real aperture scanning systems synthetic aperture processing offers the advantage to achieve high lateral resolution using antennas with small aperture.

Due to other applications, civilian and military, radar sensors at W-band are technologically best developed. As well devices and components have been designed and built and exhibit a high degree of maturity. Key components are low noise and medium power HEMT amplifiers and multipliers. Considerable bandwidth can be achieved, which results in an extremely high range resolution. State of the art allows to use high performance SOC technology. For the application discussed here, the use of mmW-radar technology for a luggage scanner, not only the front-end hardware is a challenge, but also the adaption of SAR processing to the close range geometry. A fast two dimensional scan in combination with high resolution range processing offers the capability to assess the third dimension using the inherent ability to determine range and such to construct a three dimensional image of the content of a suitcase or parcel.

Radar front-ends have been developed, which based upon GeSi technology at 80 GHz offer a wide bandwidth of > 25 GHz resulting in a range resolution of about 7 mm. The system is based on a monostatic fully integrated SiGe transceiver chip, which is stabilized using conventional fractional-N PLL chips at a reference frequency of 100 MHz. The ultra-wide PLL-stabilization was achieved using a reverse frequency position mixer in the PLL (offset-PLL) resulting in a compensation of the variation of the oscillators tuning sensitivity with the variation of the N-divider in the PLL. The achieved flatness of output power is <. 3 dB.

The SAR signal processing relies on near field focusing avoiding the time consuming exact backprojection algorithm. Focusing is done under the assumption of nearly plane waves in the vicinity of a reference point. Deviations are handled by introducing a correction factor. As test method a nearest neighbour approach is used. For areas < 1m x 1m the resultant images are sufficiently sharp and exact. For larger areas a mosaicking method has to be applied.

8544-6, Session 2

Design and integration of ACTPol, a millimeter-wavelength, polarization-sensitive receiver for the Atacama Cosmology Telescope

Benjamin L. Schmitt, Univ. of Pennsylvania (United States); for the ACTPol Collaboration, Princeton Univ. (United States)

In this proceeding, we highlight considerations for the design and integration of ACTPol, a new receiver for the Atacama Cosmology Telescope (ACT), capable of making polarization-sensitive, millimeter-wavelength observations of the Cosmic Microwave Background (CMB) at arcminute angular scales. ACT is a six-meter telescope located in northern Chile, dedicated to enhancing our understanding of the structure and evolution of the universe by direct measurement of the CMB. We describe the design of the first ACTPol 150 GHz detector array package, which, along with a second 150 GHz array package and a multichroic array package with simultaneous 90 GHz and 150 GHz sensitivity, comprises the ACTPol focal plane. Each of these detector array packages reside behind a set of custom-designed, high-purity silicon reimaging optics with a novel anti-reflective coating geometry, the characteristics of which will be detailed. The 150 GHz array package consists of ~1000 transition-edge sensor (TES)

bolometers used to measure the response of ~500 feedhorn-coupled polarimeters, which enable characterization of the linear orthogonal polarization of incident CMB radiation. The polarimeters are arranged in three hexagonal and three semi-hexagonal silicon wafer stacks, mechanically coupled to an octakaidecagonal, monolithic corrugated silicon feedhorn array (~140 mm diameter). Readout of the TES polarimeters is achieved using time-division SQUID multiplexing. Each array package is cooled using a custom-designed dilution refrigerator providing a 100 mK bath temperature to the detectors, which have a target Tc of 150 mK. Given the unique cryomechanical constraints associated with this large-scale monolithic superconducting focal plane, we address the design considerations necessary for integration with the optical and cryogenic elements of the ACTPol receiver. Finally, specific consideration will be given to the context of these associated technologies and their synergistic application to support allied field applications, including interests in national security, counterterrorism, and nuclear nonproliferation.

8544-7, Session 2

Indoor portal security screening of personnel using a large aperture 35 GHz quasi-optical passive imaging system

Neil Anthony Salmon, Peter N. Wilkinson, The Univ. of Manchester (United Kingdom)

A large diffraction limited 1.6 m aperture 35 GHz passive millimetre wave quasi-optical imaging system is investigated for indoor personnel security screening. The system uses no artificial illumination and exploits signal processing and signal integration over periods of 1 to 10 seconds to generate images of subjects. The system uses mechanical scanning to generate images at a rate of 10 frames per second which are then processed and integrated to improve signal to noise ratio. The system uses an array of 58 receivers and a Schmidt corrector plate to minimise spherical aberration, enabling subjects to be imaged at a range of 1.6 from the imager. The system is characterised in terms of is point spread function and system noise temperature. Components of electronic pick-up are investigated and mitigating signal processing routines are applied prior to gain and off-set calibration to enable best quality images to be extracted.

8544-8, Session 2

Millimeter-wave measuring system for biomedical application

Yaroslav V. Savenko, Volodymyr I. Vodotovka, Fedir Repa, National Technical Univ. of Ukraine (Ukraine)

This paper reports results of the research work on development of techniques and devices for measuring of extra low radiation in mm-range. This radiation is widely used for investigation of environment and medical diagnostics of human physiological state. There are considered basic engineering aspects of measuring extra low mm-range radiation in the paper. It is also described an original measurer that helps researchers to get more clear understanding about environment physics and biomedical physiology, how low energy mm-range radiation interacts with human organism. Certain applications have been proposed for the measurer as for testing calibrating and diagnostic devices. This paper should be considered as a current completed step in the research process of a role of extra low mm-range radiation on environment and human being as well. At this step a previous mm-range extra low radiation measuring and medical experience had been analytically summarized. This analysis made possible to accept an assumption how we are able to measure (investigate) mm-wave influence on objects and human organism as well. It should be noticed that only extra low radiation was taking into account. There was the main problem, that it was required to measure radiation at the noise level. That is why the main task had been decided how these measurements must be provided. An original measurer was developed for investigations above mentioned. Proposed measuring system consists of subsystem of reflected or/ and self radiation scanning and subsystem of hardware-software processing scanned data from the object.

8544-9, Session 2

Millimeter-wave technology and system for milk quality inspection

Yaroslav V. Savenko, Fedir Repa, Volodymyr I. Vodotovka, National Technical Univ. of Ukraine (Ukraine)

It is considered mm-wave supersensitive measuring system for medical application in particular for medical diagnostics. There were investigated main subsystems of measuring system in particular a measurer-sensor, a measurer-amplifier and operating subsystems. It has been analyzed the main methods for measuring low-power mm-wave measuring; chosen mathematical models for measuring low-power mm-wave measuring; investigated a computer model, experiment setup and analysis results have been discussed as well. The development of extremely high frequency range led to the various measuring devices used in medical diagnostics. Self radiation of biological objects, in particular of the human body, in the mm-range gives important information on its functional state at the cell level. It could be used a self radiation registration for effective diagnostics of the functional state of the human body. Particularly it allows cancer diagnostics at the early stages of its occurrence. Urgent task is to create a measuring device to be able to register self radiation of the human body for purposes of medical diagnostics. As prototype it could be possible to use mm-wave sensitive power meters and sensors.

8544-21, Session PS

Perimeter surveillance using a miniaturized millimetre wave radar

Helmut W Essen, Maxonic GmbH (Germany); Stephan Stanko, Winfried Johannes, Fraunhofer FHR (Germany)

Modern society suffers from a massive threat at its neuralgic points by terroristic or criminal attack. An even higher threat is encountered at security check points of military installations, namely for camps in critical environment like Afghanistan.

This danger is countered by the introduction of extensive security checks, which increase security, but, on the other hand, significantly disturb the throughput of people. A special challenge is the detection of weapons and other dangerous material hidden under the clothes. Currently manual or semi manual checking techniques are used like the wellknown metal detector portals. These techniques are slow and not really able to allow for the necessary quality of operation, maintaining an acceptable false alarm ratio. Moreover there is a considerable danger for the security personal. It is obvious, that for a thorough check the human inspection is necessary, however a pre-selection of potential invaders has to take place at stand-off distance to allow to take precautions if a potential threat is detected.

In Europe and the USA considerable efforts have been put into the development of commercially available body scanners based upon millimetre wave technology, which allow to detect and localize threat items hidden under the clothes. Some are evaluated at different airports worldwide and also draw attention to camp protection applications. Most of the commercially available millimetre wave or Terahertz-scanners work on the basis of passive or active imaging and successive evaluation of the microwave images. The necessary technical effort is considerable, and the systems are quite expensive or suffer from sensitive technology, not necessarily suitable fort he rough environment typical for camp protection purposes.

A typical feature of radar sensors different from electro-optical sensors, is the ability to derive significant information from the backscattered signal without formation of an image. Range profiles, polarization and the RCS are typical features, which can be evaluated. Classification schemes can be constructed which are based on an evaluation of a feature map, characteristic for a specific target item. This method is used for ATR algorithms for seeker heads and can be adopted for threat detection using non-imaging millimetre wave radar sensors.

To demonstrate the capability of such an approach, a simple, miniaturized FM-CW radar operating at a centre frequency of 94 GHz has been equipped with a pair of antennas with high azimuthal gain and a broad beam in elevation and mounted on a rotating pedestal to cover an aspect angle range of 360°. For perimeter surveillance the radar covers a range width of 500 m. A change detection algorithm is used to discriminate invading persons or vehicles from the background. Tracking of non stationary target objects is maintained

by Kalman filtering. The RCS of detected objects is determined using a pre-calibration against a precision corner reflector at a defined range and employing the radar range equation. The measured RCS is compared with a threshold value to discriminate between dangerous and non-dangerous targets. Additional information from a video camera is necessary for a first discrimination between target classes.

8544-22, Session PS

Frequency multidimensional classification applied for reflection spectra of hexogen-based explosives

Radoslaw Ryniec, Norbert Palka, Marek Piszczek, Mieczyslaw Szustakowski, Military Univ. of Technology (Poland)

In recent decades, security has become a primary concern for all of the world's nations due to an increase in terrorist activities. One of primary causes for concern is the fact that as new weapon technology becomes available to revolutionaries, detecting threats will become more difficult. Current methods involve x-ray scanning are slow and lack the resolution so application of terahertz to research for security threats is promising development that could increase of ability. Terahertz waves (T-rays) are unique part of the electromagnetic spectrum that exhibit interesting characteristic. One of the most promising aspects of this technology is that terahertz radiation is very sensitive to interactions between molecules. This permits each different substance imaged by terahertz to produce its own unique signature that can be consistently identified. But, in real practice systems based on automated identification threats, small misclassification rates is difficult to achieve. One of the challenge is detection of weak signal in a noisy environment including atmospheric absorption which is often dynamic and limits the propagation distance of THz beam. This paper shows our approach to spectra classification problem of Hexogen-based explosives. The Principal Component Analysis (PCA) technique was applied to reduce dimension and construction of an informative data representation of different compounds. The use of Linear Discriminant Analysis(LDA),k-Nearest-Neighbor Method (kNN) and decision Trees to compare different techniques for estimation of classifier are discussed. We consider a data set containing about 1000 observations of 6 classes - RDX-based explosives and five others compounds. The samples under the test were prepared with different, controlled roughness, grain size and geometry of surface. For many THz applications, including security screening, it may be necessary to perform measurement in reflection configuration over a distance through the atmosphere. Thus, we carried out spectroscopic detection in reflection geometry using Time-Domain Spectroscopy system from Teraview Ltd under normal atmospheric conditions Distance to the samples was 30 cm with incident angle equal to 7o. THz impulses in time domain were apodized and next transformed to frequency domain by means of Fast Fourier Transform. The data set contained 591 dimensions (range limited to 0.3÷2 THz only in transmission windows of atmosphere). We obtained the eigenvectors, than we split the data set into training and test subsets to make possible to test classifier performance on signals unused when training the models for different number of largest eigenvalue. All computation were carried out in statistical R environment. The obtained results suggests that this method can be useful for data interpretation of a large number of collected parameters.

8544-23, Session PS

Hot electron bolometer for detection of fast terahertz impulses from optical parametric oscillator

Norbert Palka, Przemyslaw Zagrajek, Military Univ. of Technology (Poland); Adam Czerwinski, Warsaw University of Technology, Faculty of Physics (Poland); Tomasz Trzcinski, Elzbieta Rurka, Mieczyslaw Szustakowski, Military Univ. of Technology (Poland); Maciej Sypek, Warsaw University of Technology, Faculty of Physics (Poland)

We report on detection of nanosecond impulses by fast and sensitive Hot Electron Bolometer (HEB). Impulses were generated by an Optical Parametric Oscillator (OPO)-based source from M Squared Lasers Ltd. Pump light at 1064nm from a Q-switched Nd:YAG laser incident onto the nonlinear crystal (MgO:LiNbO3) in the OPO cavity and is converted into two OPO output beams - a THz 'signal' beam, and an 'idler' beam. The 'idler' beam varies between ~1060-1080nm according to the THz wavelength to which the laser is tuned. The nonlinear crystal is located at the intersection of the optical axis of the Nd:YAG laser cavity and the optical axis of the OPO idler wave cavity. THz radiation can be tuned by changing the angle between the pump and OPO cavity axes. The laser can be tuned in the range 0.7-2.5 THz; its repetition rate equals to 53 Hz, duration of the impulse is about 10-20ns, energy 10nJ and spectral width 50 GHz.

HEB from Scontel operates at temperature of about 8.5K in a cryogenic refrigeration system which is based on a closed-loop helium expansion cycle. A sensitive element is a bridge from a 4-mm thick NbN film integrated with a planar logarithmic spiral antenna on a high-resistive silicon. HEB works in 0.3-3THz range with NEP ~3x10-13 W/Hz1/2 and dynamic range 0.1 uW. Thanks to exploitation of hot electrons in superconducting state, the detector is very fast with minimum response time equals to 50ps. Cryogenically-cooled HEMT amplifier works in 1-3500 MHz range with gain of 25 dB. The THz radiation is focused with a silicon lens, and then is coupled to a sensitive bolometer using the planar antenna.

The THz radiation from the OPO, through a set of mirrors and attenuators (to avoid saturation of the HEB), was coupled to the detector. The distance between the source and detector was about 3m. Full Width at Half Maximum of the recorded impulses was about 15 ns, what agrees well with the manufacturer data. Moreover, we measured linearity of the detector rotating the polarizer axis in the range 0.7-2.0 THz. The impulses were averaged and integrated for better stability. We obtained a good similarity to the theoretical curve of the polarizer, where intensity of the radiation is proportional to cos2q, where q is the angle between the THz radiation polarization direction and the axis of the polarizer. We plan to test this system in spectroscopic applications.

8544-24, Session PS

Improvement of passive THz camera images

Marcin Kowalski, Marek Piszczek, Norbert Palka, Mieczyslaw Szustakowski, Military Univ. of Technology (Poland)

Detection and identification of hidden objects (e.g. explosive materials, drugs) is a very urgent and demanding problem at the present time. Finding objects hidden under clothes is getting more and more interesting especially for security society. Visual detection of hidden objects can be achieved using various imaging methods but not all of these methods can be applied for screening humans. Many methods utilize ionizing radiation which can be harmful for humans e.g. X-ray. Terahertz range of electromagnetic radiation seems to have a big potential in the field of hidden objects detection and some companies propose active or passive imaging systems.

All the passive systems working in the millimetre wave region can detect objects hidden under human clothing thanks to difference between naturally emitted radiation by human body and the objects. In most cases human skin emmits stronger radiation than any nonorganic objects because their temperature is usually smaller than the temperature of human body. Very important factor which should be particularly highlighted is emmisivity of human skin, which consists of 70% of water. Skin emissivity is ussually different than emmisivity of metalic or dielectric objects. Both features mentioned above connected with high transmission of THz radiation in ordinary clothes can enable a camera to look through clothes and find hidden objects like weapons, bombs etc. Such cameras are really promising solution for demanding security and defense applications.

The THz frequency band is specially suited for clothes penetration because this radiation does not point any harmful ionizing effects thus it is safe for human beings. Strong technology development in this band have sparked with few interesting devices. Even if the development of THz cameras is an emerging topic, commercially available passive cameras still offer images of poor quality mainly because of its low resolution and low detectors sensitivity. Therefore, THz image processing is very challenging and urgent topic. Digital THz image processing is a really promising and cost-effective way for demanding security and defense applications. In the article paper we demonstrate quality enhancement of images captured by a commercially available passive THz camera by means of various combined methods. Our research is focused on dangerous objects detection - guns, knives and bombs hidden under some popular types of clothing. A thermal phantom - a non-metallic model of human

placed on a four-wheel, wirelessly-controlled moving platform was applied to avoid many problems connected with humans carrying guns, bombs or knives during long-lasting measurements Processing techniques presented in the paper include adaptive image computing methods: segmentation, edge detection and denoising.

8544-10, Session 3

Unbiassed and biassed millimetre wave video detectors *(Invited Paper)*

Peter G. Huggard, Byron Alderman, Rutherford Appleton Lab. (United Kingdom); Jesús Grajal, Carlos G. Pérez-Moreno, Univ. Politécnica de Madrid (Spain)

Applications for sensitive, fast, room temperature, detectors for millimetre and submillimetre wave radiation are diverse. They range from imaging for Earth observation and for active and passive security scanning to plasma and particle beam diagnostics. Depending on the incoming signal strength, prior signal treatment via bandpass filtering and/or low noise amplification may be required. Thus detectors should be compact, and be capable of easy integration into planar antennas or microstrip circuits.

Modelling, design, build and test of a range of rectifying detectors targeting these requirements will be presented. The devices are made from planar GaAs and InGaAs airbridged Schottky diodes. These are fabricated in-house as discrete chips at the STFC Rutherford Appleton Laboratory from commercially grown wafers. The GaAs devices operate with a forward bias current, whereas the InGaAs detectors are designed to rectify at zero applied bias. We shall present measurements of the spectral responsivity and noise performance of the devices, and we will make a comparison of the speeds of response. In particular, the video bandwidth of the biased GaAs devices is limited by the preamplifier, whereas we expect the zero-bias InGaAs units to be governed by their intrinsic resistance and any external capacitance.

Our physics based modelling enables a comparison of the performance and characteristics of the devices with values expected from the semiconductor layer structures and Schottky contact areas. This enables us to focus on optimisation and to target areas for improvement, concentrating on the parameters to which performance is most sensitive.

For detector test purposes, the devices are fixed across the points of a 6 mm wide planar antennas that are defined in gold on either fused quartz or high resistivity silicon substrate. The type of antenna gives a broadband response to a single linear polarisation. Incoming radiation is focussed onto the antenna using a hyperhemispherical lens made of high resistivity silicon. The rectified signal then passes through a low noise preamplifier to either a lock-in amplifier or a high speed digital oscilloscope. Separate preamplifier designs deliver lowest noise or broadest post-detection bandwidth. The transmitter section of an ABmm vector network analyser is used as a widely tuneable test source for responsivity measurements. The source power is determined by a Absolute Power Meter from Thomas Keating. Speed of response measurements are made at 100 GHz frequencies using a 1.55 µm photomixer as a transmitter and with a 40 GHz bandwidth electro-optic amplitude modulator on the input light as a high speed on-off switch.

Currently, the responsivity and noise performance of the best zero-biased devices is comparable to the biased units. In the 250 - 400 GHz range, responsivities of circa 10 V/W are achieved, with noise equivalent powers of 300 nV/sqrt(Hz) at 10 Hz dropping to below 100 nV/sqrt(Hz) at 10 kHz. Response times of tens of nanoseconds have been observed from the GaAs detectors.

8544-11, Session 3

Components, concepts and technologies for useful video rate THz imaging

Linda Marchese, Marc Terroux, Ovidiu Pancrati, Martin Bolduc, Hubert Jerominek, Alain Bergeron, INO (Canada)

The recent arrival of TeraHertz large format focal plane arrays has opened the door for numerous applications not previously available for this exciting technology. Video-rate imaging is now a reality and no scanning is required. INO has a proven microbolometer based FPA that shows good sensitivity over a large THz bandwidth and videos have been successfully acquired of objects hidden behind barrier materials. While these videos successfully proved the real-time capabilities of the INO imager, the quality of the images required substantial system level improvement to be useful for detection and identification purposes in various applications. To this end, INO has designed and fabricated numerous optical components for its active imaging set-up that allows for superior quality real-time images.

This paper discusses the concepts and techniques used to create these components. A comparison of images taken using the same THz camera with and without these innovative techniques are presented and an analysis of the improvement and methods to further improve the THz active imaging system are discussed. Lastly, an analysis of the atmospheric attenuation over the THz wavelength region is presented.

8544-12, Session 3

Amorphous semiconducting Y-Ba-Cu-O: a silicon-compatible material for IR uncooled sensitive detection with microsecond response time

Alain J. Kreisler, Ecole Supérieure d'Electricité (France); Vishal S Jagtap, SUPELEC (France) and Univ Paris Diderot (France); Annick F Degardin, UPMC Univ Paris 06 (France)

The yttrium-barium-copper oxide cuprate (YBCO) is well-known to exhibit superconducting properties in its orthorhombic phase YBa2Cu3O(6+x) for x above 0.6. Oxygen depletion (x = 0.3-0.5) of this compound leads, however, to the tetragonal crystal structure of a semiconductor. An unusual although promising application of YBCO in this latter form can be sought in the field of uncooled thermal detectors of the bolometer type due to its large temperature coefficient of resistance (TCR = 1/R (dR/dT) = -3 to -4 %/K), a figure of merit that compares favorably with other bolometric sensing materials such as VOx or amorphous SiH. Besides, semiconducting YBCO films can be deposited without substrate heating in amorphous semiconducting form (a-YBCO), which makes the integration of this material compatible with already processed signal readout electronics (e.g. a CMOS chip). Finally, previous published work has shown encouraging IR detectivity values measured on semiconducting YBCO microbolometers, testifying the low noise potential of this material, with 1/f noise comparable to VOx and lower than amorphous SiH.

The aim of the present work was to examine two types of a-YBCO bolometric geometries, i.e. planar (PL) or tri-layer (TR), and compare their detection performance in terms of both responsivity and noise level, with reference to already reported semiconducting devices, mainly designed for room temperature operation. We also wish to show here that the pyroelectric behavior of a-YBCO specifically leads to high performance and fast devices that could pave the way to a new generation of imaging pixels ranging from the near-infrared to far-infrared / THz domains.

a-YBCO thin films were prepared by off-axis sputtering at low temperature (below 150°C) under an atmosphere of oxygen and argon. We used p-doped silicon substrates coated with a thermally grown 500 nm thick SiO2 layer. The surface roughness, measured by atomic force microscopy, was low (5 nm rms). For both PL and TR devices, the technological process started with a Ti/Au bottom contact level. An a-YBCO film of thickness 250 nm for device PL (360 nm for device TR) was then deposited and patterned using standard optical lithography to define the active area. Finally, for device TR, a Ti/Au top electrode was defined.

For both detector devices, the response was measured at 850 nm wavelength for experimental convenience. The PL response exhibited a low-frequency regular low-pass bolometric behavior (30 Hz cut-off frequency). Above 200 Hz, a high-pass behavior was observed (+6 dB/octave slope followed by 60 kHz cut-off / 3 µs time constant) that could be assigned to the pyroelectric state of a-YBCO. The TR response exhibited the high-pass behavior only. Detectivity values up to 3.5e8 cm rootHz/W have been measured. The high frequency sensitivity offers a promising solution for fast imaging applications, especially in the far IR / THz range where moderate cost systems should be considered. Improvements are under progress concerning both the input radiation coupling with THz micro-antennas and the back-end electric coupling of these high impedance devices to compensate for the low-frequency response attenuation.

8544-13, Session 3

Low cost satellite receivers for aperture synthesis passive millimetre wave imaging

Joel Radiven, The Univ. of Manchester (United Kingdom); Neil A. Salmon, MMW Sensors Ltd. (United Kingdom)

This paper investigates the use of low-cost Low-Noise Block Downconverter (LNB) satellite receivers to develop next generation passive centimetre and millimetre wave millimetre wave (PMMW) aperture synthesis imagers. Next generation demonstrators of this technology will require hundreds of receivers to achieve centimetre spatial resolution and a few hundred milli-Kelvin radiometric sensitivity over the full human body for personnel security screening. The widespread use of domestic satellite LNB receivers, sensitive over the band 10-12 GHz, offers a low cost route to procuring a packaged receiver comprising, dual polarisation waveguide probes, a low noise radio frequency amplifier, a heterodyne mixer and intermediate frequency amplifier. The paper will quantify the spectral noise and gain performance of a commercially available satellite receiver with respect to its adaption for use in an aperture synthesis imager. The performance of the LNB as a digital radiometer and two LNBs in an interferometric configuration will be evaluated. The LNBs are augmented with a second stage of heterodyning, further amplification, anti-alias filtering and digitisation using commercially available 8-bit ADCs sampling at a frequency of 100 MHz, employing phase locked local oscillators and sample clocks throughout.

8544-14, Session 3

Innovative monolithic detector for tri-spectral (THz, IR, Vis) imaging

Stephane Pocas, CEA, LETI-MINATEC (France); Matteo Perenzoni, Nicola Massari, Fondazione Bruno Kessler (Italy); François Simoens, Jérome Meilhan, Wilfried Rabaud, Sebastien Martin, Baptiste Delplanque, Pierre Imperinetti, Valérie Goudon, Claire Vialle, Agnès Arnaud, CEA, LETI-MINATEC (France)

Fusion of multispectral images has been explored for many years for security and used in a number of commercial products. CEA-Leti and FBK have developed an innovative sensor technology that gathers monolithically on a unique focal plane arrays, pixels sensitive to radiation in three spectral ranges that are terahertz (THz), infrared (IR) and visible. This technology benefits of many assets for volume market: compactness, full CMOS compatibility on 200mm wafers, advanced functions of the CMOS read-out integrated circuit (ROIC), and operation at room temperature. The ROIC houses visible APS diodes while IR and THz detections are carried out by microbolometers collectively processed above the CMOS substrate. Standard IR bolometric microbridges (160x160 pixels) are surrounding antenna-coupled bolometers (32X32 pixels) built on a resonant cavity customized to THz sensing. This paper presents the different technological challenges achieved in this development and first electrical and sensitivity experimental tests.

8544-15, Session 3

Micro-machined millimetre wave sensor array for FM radar application

Janez Trontelj, Aleksander Sesek, Univ. of Ljubljana (Slovenia)

The objective of this work is to create a low cost room temperature operating sensor array for millimetre wave applications to be used for FM radars and for various heterodyne receivers.

The selected technology is silicon wafer micromachining allowing to create microstructures on silicon membranes using different metal layers. The technology used allowed submicron dimensions for photolithography pattern and thin membranes down to few micrometers.

One of the most critical requirements for the sensor was to achieve high signal to noise ratio and high bandwidth of mixed frequency. The sensor is a titanium based micro-bolometer connected to the micro-antenna integrated with the bolometer. The frequency characteristics of the sensor is governed only by the antenna characteristic so a desired new frequency range and bandwidth can be manufactured with only one metal mask change in the fabrication process. Frequencies of 0.3THz, 0.65THz with bandwidth of +/-10% have been designed, fabricated and tested. Also a wideband antenna, covering frequency range from 0.3THz to 0.8THz, has been designed and tested. The achieved results are very promising showing a response to a femtosecond laser excitation for a single pulse with no overaging or using phase locked loop amplifiers.

The array of 4x1 and 16x1 has been designed, fabricated and characterised having a very good signal noise ratio, namely a NEP better than 10pW/√Hz and sensitivity close to 1000 Volts per Watt. Bolometer response time is defined by its thermal time constant which is lower than 1µsec. The resulting bandwidth 150 kHz is acceptable for any FM application or for heterodyne receivers.

In the paper the antenna - bolometer sensor microstructure is analysed in detail together with the fabrication procedure. Theoretical analysis and design guide lines for bolometer itself are discussed. Simulation results of sensitivity and NEP show very good matching to the measured results. Characterisation measurements are performed at DC and MHz range frequency as well as with THz test signal. For illumination source a solid state frequency modulated 25GHz synthetisator has been built, followed by a cascade of frequency multipliers by 4 and by 3 to provide approx 1mW at 0.3THz with +/-30GHz frequency sweep. Built FM radar using single illumination source and several receiving sites in the sensor array is described. The measurement results are presented for different targets. A combination of THz imager and FM radar is discussed.

The following topics are addressed in the paper:

- Theory of bolometer material, dimensions width, length and thickness influence to sensitivity and NEP. Simulation model based on finite elements software simulation tool combined with other simulators, measurements results and comparison to simulation and / or calculated results.

- FM millimetre wave radar system with description of building blocks with a special emphasis on front end electronics optimized to noise characteristic of the system and THz optics. Presentation of measured results and interpretation discussion.

- Possible improvement in the area of cost reduction and system compactness to be used in various field of interest.

8544-17, Session 4

Simulating the operation of millimeter-wave imaging systems *(Invited Paper)*

Roger Appleby, Stuart Ferguson, Queen's Univ. Belfast (United Kingdom)

This paper reports on a method of simulating the behaviour of millimeter wave imaging systems, such as a focal plane array or cooled Bolometers. The approach described uses a modified ray-tracing image renderer taken from an OpenSource 3D computer animation package OpenFX and replaces the visible spectrum illumination model with a model for surface reflectance in the 100GHz to 1THz range. The modified 'imaging' program is readily combined with the remaining modules in OpenFX to give an application program that has the capability to model highly complex scenes, with human figures etc. and to study the operation of the imaging systems in a dynamic environment, when animated human figure models are moving.

The simulation process consists of three main modeling stages. Firstly, a hybrid ray-tracing 'illumination' model that produces an output 'raster' image holding data for the scene. (For example the results of a basic radiometry calculation arising from multiple layers of clothing worn by a person.) Secondly, a model of the type of millimetre wave camera is used to simulate the output from the scene as it is imaged. This model includes features such as the inherent detector noise and scan patterns. Finally a model of the system interpolates the data from the camera and presents it to the system operator.

The data that describes the scene under examination is described by a network of interconnected planar triangular polygons, each polygon is assigned a material type that carries a number of attributes, emissivity, transmission, reflectivity, temperature, or refractive index etc.

The rendering engines is fast because it uses a software based scanline Z buffer hybrid approach where the first hit does not need to be determined by ray-tracing. Using a Phong smoothing approach allows for a good approximation to a real world surface to be obtained. Because the original OpenFX software also included a GPU

shader based real-time renderer driven using OpenGL, there is the potential to consider near real-time simulation.

The paper concludes with some examples and a discussion of how accurate such a modeling approach can be.

8544-18, Session 4

A millimetre-wave MIMO radar system for threat detection in urban environments

Andreas J. Kirschner, Johanna Guetlein, Sebastian Bertl, Juergen Detlefsen, Technische Univ. München (Germany)

More and more, the missions of European armed forces change from classical homeland defence to peace-keeping missions in conflict zones. Within a variety of tasks, there is the necessity of use of convoys or patrols for civil or military supply, for security purposes or for medical aid and transport. However, in asymmetric conflicts, such convoys are often the target of assaults with improvised explosive devices (IEDs), conventional land-mines or suicide bombing persons, which states a severe problem for all kind of personnel in such risk areas.

Therefore, the European Defence Agency (EDA) engages countermeasures by funding several scientific programs on threat awareness, countermeasures IEDs or land-mine detection, in which this work is only one of numerous projects. The program, denoted as Surveillance in an urban environment using mobile sensors (SUM), covers the idea of equipping one or more vehicles of a patrol or a convoy with a set of sensors exploiting different physical principles in order to gain detailed insights of the road situation ahead. In order to give an added value to a conventional visual camera system, measurement data from an infra-red (IR) camera, a visual camera, a radiometer and a millimetre-wave radar are fused and displayed on a human-machine-interface (HMI) which shall assist the vehicle's co-driver to identify suspect objects or persons on or next to the road without forcing the vehicle to stop its cruise.

In order to show the capabilities of fusing data from different sensor equipment, a European consortium of four partners with divided assignments was founded: Grupo Tecnologico e Industrial (GMV), Royal Military Academy (RMA), Deutsches Zentrum fuer Luft- und Raumfahrt (DLR) and Technische Universitaet Muenchen (TUM).

With the joint experiences, a low-cost demonstrator was not only designed but also implemented and tested on experimental and real targets. The system was then mounted on top of a truck and driven along different courses consisting of several false candidates or real threats hidden along the track.

This paper shall especially cover the role of the millimetre-wave radar sensor, its different operational modes and discuss measurement results. It is possible to alter the antenna mechanically which gives two choices for a field of view and angular resolution trade-off. Furthermore a synthetic aperture radar mode is possible and has been tested successfully.

The different data sets are then combined by a fuzzy logic and a threat level probability is determined for each suspect object. The results can be displayed with a handheld monitor or a tablet PC where the detected object is marked by a coloured bounding box in the visual image. The colour of the bounding box changes with the threat level from blue over green and yellow to red in order to give an intuitive support for operator while a cruise of the vehicle.

8544-20, Session 4

Real-time computer processing of image from the THz passive imaging device for the improving of images

Vyacheslav A. Trofimov, Vladislav A. Trofimov, Lomonosov Moscow State Univ. (Russian Federation)

We demonstrate real-time operating computer code improving the quality of images captured by the passive THz imaging system. The code does not attach to certain THz passive device: it can be applied for both any kind of such devices and active THz imaging system as well. The perfomance of current version of the computer code is greater than 1 treatment per second for the THz image having more than 5000 pixel for 24 bit number representation. Single THz image results in about 20 images corresponding to various spatial filters applied for the image treatment. The computer code allows changing the number of pixels for resulting image without noticeable reduction of image quality. Functionality of the computer code is illustrated by its application to the treatment of images from a real THz passive imaging system.

We develop spatial filters which allow to see the samples with sizes being less than 2 cm. The performance of the computer code can be increased many times.

Conference 8545: Optical Materials and Biomaterials in Security and Defence Systems Technology

Wednesday - Thursday 26–27 September 2012 • Part of Proceedings of SPIE Vol. 8545
Optical Materials and Biomaterials in Security and Defence Systems Technology IX

8545-1, Session 1

Enhancement of the second harmonic response with the aspect ratio of gold nanorods *(Keynote Presentation)*

Isabelle N. Ledoux-Rak, Anu Singh, Ecole Normale Supérieure de Cachan (France); Anais Lehoux, Lab. de Chimie Physique (France) and Univ. Paris Sud (France); Joseph Zyss, Ecole Normale Supérieure de Cachan (France); Hynd Remita, Institut d'Électronique Fondamentale (France) and Univ. Paris Sud (France)

Among gold nanoparticles (AuNPs) gold nanorods present two surface plasmon resonances (SPR) corresponding to the oscillation of the quasi-free electrons along (longitudinal SPR) and perpendicular (transverse SPR) to the rod long axis. The longitudinal resonance can be tuned from green to near infrared by modifying the nanorod aspect ratio (AR): the higher AR, the smaller the LSPR frequency.

We report here on the optical surface second harmonic response from gold nanorods with different AR. Gold nanopheres and nanorods were synthesized by one pot radiolytic synthesis. The average particle sizes and ARs were measured from at least 100 nanoparticles from TEM images.

Nanorods and nanospheres β values were measured in water solution as a function of their aspect ratio, using the hyper Rayleigh scattering (HRS). Large β values have been reported from gold nanospheres[1]. The fundamental wavelength being at 1.064 µm, its harmonic at 0.532 µm lies in the spectral resonance domain of AuNPs. Our reference sample is water (βH2O= 5 ? 10-32esu)

Hyper-Rayleigh scattering measurements clearly show that β values increase from 0.35 to 4.6 10-26 esu when the aspect ration increases from spheres (AR = 1) to AR = 3.2. Changing the shape from sphere to rod gives a direct way to enhance SPR sensitivity due to the longitudinal plasmon band. The SPR sensitivity correlatively increases with the shift of this band from visible to near infra-red. This confirms the work by Brevet et al, reporting that the HRS intensity collected from a solution of a mixture of gold nanorods and nanospheres shows that the HRS signal essentially arises from nanorods [2].

Brasselet and Zyss [3] introduced the concept of multipolar molecules, via the anisotropy ratio R = ||βJ=3||/||βJ=1||, where ||βJ=3|| (resp. ||βJ=1||) are the norms of the octupolar (resp. dipolar) contributions to the β tensor. This R factor was determined by carrying out variable incident polarization experiments in HRS for Au nanospheres and nanorods. We found that R decreases with the increase of nanorods AR, ranging from 2.25 for spheres to 0.92 for AR = 3.2. This evoluation appears to be related to the depart, for nanorods with increasing aspect ratio, from the spherical symmetry of nanospheres. Further studies will focus on the functionalization of Au NRs with different NLO dyes.

[1] I. Russier-Antoine, E. Benichou, G. Bachelier, C. Jonin, and P. F. Brevet, J. Phys. Chem. C, 111, 9044-9048 (2007).

[2] Nappa J., Revillod, G., Abid J.-P. , Russier-Antoine, I., Jonin C., Benichou E., G, H. H. and Brevet P. F., Faraday Discuss., 2004, 125, 145-156.

[3] S. Brasselet and J. Zyss, J. Nonlin. Phys. Mater. 5, 671 (1996).

We thank C'Nano Ile de France for financial support

8545-2, Session 1

Investigations of nanoparticles for optical power limiting *(Invited Paper)*

Bernd Eberle, Fraunhofer-Institut für Optronik, Systemtechnik und Bildauswertung (Germany); Olivier Muller, Institut Franco-Allemand de Recherches de Saint-Louis (France); Gunnar Ritt, Stefanie Dengler, Fraunhofer-Institut für Optronik, Systemtechnik und Bildauswertung (Germany)

The protection of the human eye and of electro-optical sensors against wavelength agile pulsed laser radiation is still a demanding problem, which has not been solved sufficiently during the past decades. The threshold of the protection measures is still too close to the damage level of the subjects to be protected.

A promising way is given by materials with a nonlinear optical behavior, known as optical power limiting. We investigated a number of different kinds of nanomaterials suspended in a solvent. Among them, we studied the nonlinear properties of homemade metallic nanoparticles of different shapes, and compared them with the well-known properties of carbon particles like multi walled carbon nanotubes (MWCNT), carbon black (CBS) and C60.

The nanoparticles were characterized regarding their geometry dependent linear optical properties by spectral transmission measurements. Their geometrical structure was analyzed by electron microscopy. The nonlinear behavior of the suspensions at the interaction with short and ultra-short laser pulses is discussed regarding their attenuation and angular dependent scattering characteristics.

8545-3, Session 1

Mid- to long-wavelength infrared surface plasmon properties in doped zinc oxides

Justin W. Cleary, Michael Snure, Kevin D. Leedy, Air Force Research Lab. (United States); David C. Look, Wyle Labs. (United States); Kurt G. Eyink, Air Force Research Lab. (United States); Ashutosh Tiwari, The Univ. of Utah (United States)

IR plasmonics is expected to play a key role in chip-scale nanophotonic system development due to lower propagation loss, improved chemical specificity in sensor applications, and the possibility of hybrid dielectric/plasmonic subsystems. In order to excite a surface plasmon, the optical frequency must be lower than the plasma frequency of the surface plasmon host. Noble metals satisfy this requirement but are known to either be lossy when the plasmon is tightly bound or suffer poor mode confinement when loss is low. This work investigates the excitation, propagation, and related losses of doped metal oxides and their use as plasmonic host materials in the mid- to long-wave (6-12 microns) infrared regime. A particular material may be useful for plasmonics when an acceptable tradeoff between loss and mode confinement is obtained. By varying the stoichiometry in pulse laser deposited Ga and Al doped ZnO, the plasmonic properties can be controlled via a fluctuating free carrier concentration. This deterministic approach enables us to investigate and develop the most appropriate stoichometry of ZnAlO and ZnGaO in regards to plasmonic applications for particular IR wavelengths. Presented are theoretical and experimental investigations pertaining to ZnAlO and ZnGaO as surface plasmon host materials. Samples are fabricated via pulsed laser deposition and characterized by infrared ellipsometry. Complex permittivity spectra are presented, as well as plasmon properties such as the field propagation lengths and penetration depths, in the infrared range of interest. Drude considerations are utilized to determine how the optical properties may change with doping. Finite element simulations verify these plasmonic properties. These materials not only offer potential use as IR plasmon hosts, but also offer new integrated device possibilities due to stoichiometric control of electrical and optical properties.

8545-4, Session 1

Proposal of a novel method for all optical switching with MMI coupler

Mehdi Tajaldini, Islamic Azad Univ. (Iran, Islamic Republic of) and Univ. Sains Malaysia (Malaysia); Mohd Zubir Mat Jafri, Univ. Sains Malaysia (Malaysia)

This paper, propose a novel approach to access to all optical switching performance usable in telecommunications and signal processing photonic circuits by one continuous MMI coupler under the nonelinear regime for achieving the switching at smaller length

of the Multimode interference waveguide, while the core layer is a polymer and clad is air. In past methods, there have been MMI switch with length about a few millimeters, but in this paper an MMI switch is simulated with a length which is less than 100μm. In this approach, the wave propagation is studied in base on MPA. The nonelinear wave equation in the presence of Kerr nonelinear effect is solved as a set of multiple coupled nonlinear equations so that any of equations are related to the one of guided modes of Multimode waveguide. After obtaining the Electric field throughout the central region, the electric fields at primordium of output waveguides is obtained with transversal and longitudinal overlap integral between central waveguide and any outputs whether we named them bar and cross. Intensity distribution is calculated inside Multimode waveguide, it shows different self-imaging property in the performance of Kerr nonlinear effect and also ability of change the position and type of interference throughout the region is demonstrated so that it make switching operation in user's brain. With the ability of calculating the field at the outputs for short MMI, the Multimode waveguide is optimized in terms of length, then the smallest length which shows the best switching is measured and it is 80μm, in fact switching in this status is performable with a variation of input intensity or electric field, thus the output fields have been measured with 〖10〗^5 Different amount of electric field at input and two input fields are chosen to switch the light into the cross and bar with low insertion loss as user's desirable, even turning on both or omitting them, two status of switching, are simulated by demonstrated the electeric fields throughout the coupler so that it shows switching into bar and cross wanguide.To the best of our knowledg, in input field equal to 5.101?〖10〗^8 N⁄C, the cross and bar wavguide are bright and dark, it mean by bright and dark are peak and valley of electromagnetic wave, respectively and in 6.006?〖10〗^8 N⁄C,situation will be converted. As the result, this switch is the outstanding proposal for new all optical digital signal processing in photonic because of its compact size and high speed and bandwidth. Also, it is ground of some complex devices such as all optical Flip-Flap and all types of Gates since they can be introduced by switching operation between outputs.

8545-5, Session 2

Semiconducting nanocrystals for photonic applications *(Keynote Presentation)*

Kwang-Sup Lee, Hannam Univ. (Korea, Republic of)

Our research focuses on the development of highly efficient semiconducting nanocrystals (quantum dots: QDs) for photonic applications. This involves the design, characterization and testing in devices of surface-engineered quantum dots (QDs), carbon nanotube (CNT)-QDs, and QDs-low band gap conjugated molecules. The hybrid materials can be combined to form polymeric nanocomposites for facilitating the charge separation and enhancing the charge carrier mobility, which can lead to highly efficient photonic devices. We are also working on various quantum dots with a photosensitive monolayer, rendering them solution-processable and photopatternable. Upon exposure to ultraviolet radiation, films composed of this material were found to polymerize, forming interconnected arrays with periodically spaced QDs. The photoluminescence properties of the nanocrystal films increased with photocuring. The pristine functionalized nanocrystals could easily be used for 2D patterning and was well doped into a photopolymerizable resin for fabricating 3D microstructures by two-photon stereolithography.

8545-6, Session 2

Effects of the liquid-crystalline order on the light-induced deformation of azobenzene elastomers *(Invited Paper)*

Vladimir P. Toshchevikov, Marina Saphiannikova Grenzer, Gert Heinrich, Leibniz-Institut für Polymerforschung Dresdene e.V. (Germany)

Azobenzene elastomers due to their ability to change the shape under light irradiation have a fascinating potential for technical applications serving as artificial muscles, sensors, microrobots, micropumps, actuators, etc. [1, 2]. Recently we proposed a microscopic theory [3] to describe light-induced deformation of azobenzene elastomers using an orientation approach [4], in which the preferable orientation of chromophores perpendicular to the polarization direction is described by an effective orientation potential. We showed that azobenzene elastomers can demonstrate either expansion or uniaxial contraction along the polarization direction depending on the orientation distribution of chromophores with respect to the main chains [3].

The present study deals with the effects of the orientational liquid-crystalline (LC) interactions between the chromophores on the light-induced deformation of azobenzene elastomers. The orientational LC-interactions between the chromophores are taken into account in the framework of the mean-field approximation, while interaction of the chromophores with the light is described, as in refs. 3 and 4, in the framework of the orientation approach. We show that photo-mechanical behaviour of azobenzene elastomers is determined by the strength of the LC-interactions which is proportional to the density of rod-like azobenzene chromophores, the proportionality coefficient being determined by the depth of the potential well for an effective pair interaction between rod-like azobenzene chromophores. At weak LC-interactions, the chromophores are oriented randomly in a plane perpendicular to the polarization direction and an azobenzene elastomer demonstrates a uniaxial deformation with respect to the polarization direction. The sign of deformation (expansion / contraction) is determined by the orientation distribution of chromophores with respect to the main chains. Elastomers with preferable orientation of chromophores perpendicular/parallel to the main chains demonstrate expansion/contraction along the polarization direction. At strong LC-interactions, the chromophores are able to form additionally a uniaxial order in the plane perpendicular to the polarization direction and an azobenzene elastomer demonstrates a biaxial deformation. This result is in a qualitative agreement with direct computer simulation study of the light-induced deformation of LC azobenzene polymers [5]. We calculate the components of the strain tensor for biaxial deformation of azobenzene elastomers depending on the light intensity, on the strength of the LC-interactions and on the orientation distribution of chromophores with respect to the main chains. We show that, depending on the structural parameters, LC azobenzene elastomers can demonstrate first or second order phase transitions under light illumination.

Acknowledgements: The financial support of the DFG grant GR 3725/2-1 is gratefully acknowledged.

References:

[1] M. Camacho-Lopez, H. Finkelmann, P. Palffy-Muhoray, M. Shelley. Nature Mater. 2004, 3, 307.

[2] Y. Yu, T. Ikeda. Macromol. Chem. Phys. 2005, 206, 1705.

[3] V. Toshchevikov, M. Saphiannikova, G. Heinrich. J. Phys. Chem. B 2012, 116, 913.

[4] V. Toshchevikov, M. Saphiannikova, G. Heinrich. J. Phys. Chem. B 2009, 113, 5032.

[5] J. Ilnytskyi, D. Neher, M. Saphiannikova. J. Chem. Phys. 2011, 135, 044901.

8545-26, Session 2

Two photon photosensitizers for PDT: molecular engineering towards understanding of their excited state photophysics *(Invited Paper)*

P.-H. Lanoë, Univ. de Nantes (France); Thibault Gallavardin, Ecole Normale Supérieure de Lyon (United States); Bastien Mettra, Lab. de Chimie Physique (France); Cyrille Monnereau, Chantal Andraud, Ecole Normale Supérieure de Lyon (France)

Photodynamic therapy (PDT) is a promising therapeutic approach, based on the light induced production of cytotoxic molecular singlet oxygen, that has been so far restricted to the treatment of superficial cancers and gliomas at their early stages because of inherently weak penetration of light into biological tissue. To extend its applicability to deep tissue and organ therapy, two-photon activation of the sensitizers, using lasers with wavelengths around 800-900 nm (which corresponds to the transparency domain of human tissues), is nowadays considered an appealing strategy. Typical photosensitizers for two photon PDT consist in long conjugated chromophores with a low-lying intramolecular charge transfer (ICT) excited state, featuring at least one moiety capable of promoting intersystem crossing (ISC) to a reactive triplet state, which will transfer its energy to molecular oxygen.[1]

In spite of all its promises, two-photons PDT is still in its infancy:

relatively few two-photon chromophoric structures that can efficiently sensitize singlet oxygen have so far been reported. Thus, we believe that molecular engineering has to be performed, with an accent put on the establishment of structure/ properties relationships. We have recently initiated a research project that aims at understanding how systematic variations of the number and positioning of a given ISC promoter (1,4-dibromophenyl) along the ICT axis of chromophores will affect the outcome of singlet oxygen production, and how this effect will be related to the nature of the ICT transition.[2]

In this presentation, this strategy will be discussed and our main findings will be summarized. We will see that a clear influence of the ISC promoter's position on the chromophore exists, but also that the extent of this effect is strongly dependent on the chromophore's symmetry.

[1] T. Gallavardin, M. Maurin, S. Marotte, T. Simon, A.-M. Gabudean, Y. Bretonnière, M. Lindgren, F. Lerouge, P. L. Baldeck, O. Stéphan, Y. Leverrier, J. Marvel, S. Parola, O. Maury, C. Andraud, Photochemical & Photobiological Sciences 2011, 10, 1216.

[2] a/ T. Gallavardin, C. Armagnat, O. Maury, P. L. Baldeck, M. Lindgren, C. Monnereau, C. Andraud, Chem. Comm. 2012, 48, 1689 b/ P-H Lanoë, T.Gallavardin, A.Dupin, O.Maury, P.L. Baldeck, M.Lindgren, C.Monnereau, C.Andraud,Org.Biomol.Chem. 2012, DOI : 10.1039/C2OB25536G

8545-7, Session PS

New side-chain azo-polymers for optical applications: Synthesis and characterization

Mitica Cezar Spiridon, Florica Adriana Jerca, Valentin Victor Jerca, Costin D. Nenitescu Institute of Organic Chemistry (Romania); Dan Sorin Vasilescu, Polytechnical Univ. of Bucharest (Romania); Dumitru Mircea Vuluga, Costin D. Nenitescu Institute of Organic Chemistry (Romania)

Azobenzene containing-polymers have drawn considerable research interest, due to their unusual photo-responsive behavior, as candidates in potential applications such as: optical switching [1], holographic memories [2], or optical storage data [3].

The incorporation strategy is critical to exploiting azobenzene unique behavior. One of the most attractive methods for incorporating azobenzene into functional materials is covalent attachment to polymers. Radical copolymerization is preferred for its simplicity and control upon the feed ratios (i.e. copolymer compositions), but on the other hand, this method implies the synthesis of reactive monomers bearing the azobenzene unit, needed to be incorporated into the final polymers. Nevertheless, the resulting materials will benefit from the inherent stability, rigidity, and processability of polymers, in addition to the unusual photo-responsive behavior of the azo moieties [4].

Herein, we describe the synthesis and characterization of new (co) polymers, obtained by radical polymerization, (left Figure illustrates their chemical structures). The copolymers were characterized by means of 1H-NMR, FT-IR, UV-Vis, DSC-TGA and SEC. The load in chromophore units were calculated from 1H-NMR, UV-Vis and elemental analysis.

Aknowledgements: The present work was partially supported by a grant of the Romanian National Authority for Scientific Research, CNCS-UEFISCDI, project number PN-II-RU-PD-2011-3-0063; and also funded by the Sectoral Operational Programme Human Resources Development 2007-2013 of the Romanian Ministry of Labour, Family and Social Protection through the Financial Agreement POSDRU/107/1.5/S/76903.

[1] T. Endo, H. K. Kim, X. S. Wang, Y. Fujita, A. Sudo, H. Nishida, M. Fujii, Macromol. Chem. Phys. 2005, 206, 2106.

[2] M. Hackel, L. Kador, D. Kropp, H. W. Schmidt, Adv. Mater. 2007, 19, 227-231.

[3] S. Kurihara, M. Z. Alam, T. Ohmachi, T. Ogata, T. Nonaka, Opt. Mater. 2006, 29, 365.

[4] F. A. Nicolescu, V. V. Jerca, D. M. Vuluga, D. S. Vasilescu, Polym. Bull. 2010, 65, 905.

8545-21, Session PS

Durability Evaluation of DLC coating through the Enhanced Environmental Tests

Joongkyu Choi, Sun Kyu Lee, Chang Jun Yoon, Seung Eun Oh, Samsung Thales Co., Ltd. (Korea, Republic of); Chang Hee Lee, Defense Agency for Technology and Quailty (Korea, Republic of)

DLC coating by a high transmittance in the infrared region is applied to the IR Optical System window. In General, we want to protect IR Optical system by using the IR window from external environment. DLC Coating durability evaluation follows the procedures for Mil spec. But DLC coating was came off and It is difficult to evaluate as the existing environment test. We have devised an enhanced environment tests, test results could be evaluated DLC coating durability. We analyzed the structure of the DLC coating by XPS and Raman spectroscopy and the results were able to find structural problems of the coating. Finally, We obtained a new evaluation of DLC coating durability.

8545-22, Session PS

Solid state isomerization kinetics and third harmonic generation study of 2,4-substituted azobenzenes containing-polymethacrylates

Florica Adriana Jerca, Ilie Murgulescu Institute of Physical Chemistry of the Roman Academy (Romania) and Costin D. Nenitescu Institute of Organic Chemistry (Romania); Valentin Victor Jerca, Costin D. Nenitescu Institute of Organic Chemistry (Romania); Ileana B. Rau, Francois Kajzar, Polytechnical Univ. of Bucharest (Romania); Dumitru Mircea Vuluga, Costin D. Nenitescu Institute of Organic Chemistry (Romania)

One of the most interesting and studied systems that can respond to changes in environmental conditions are those that contain the azobenzene chromophores. Their potential use in optics or optoelectronics, such as for optical switching devices [1], information storage [2], surface relief gratings [3], nonlinear optics, has motivated researchers over the years.

Despite of large number of publications devoted to the study of photo-responsive phenomena exhibited by the azobenzene derivatives, it is necessary to understand the relationship between particular molecular structures and photo-responsive behavior, in order to gain control over the response time, or displayed NLO properties. Compared to solution isomerization, very different behavior is expected in solid state due to low chain mobility and flexibility of the polymer backbone which does not favors the motion of the thermodynamically meta stable cis form, and when the azo dye is bonded to the polymer backbone than when it is just dissolved in the host polymer.

Herein, we describe the trans-cis-trans isomerization kinetics in thin films of four azo-poly(methyl methacrylate)s [4] (having the azobenzene moiety in the side-chain), carried out through UV-Vis spectroscopy. Further, the azo-polymer films are characterized by THG technique to establish the strength of the NLO response of each azo-moiety.

Aknowledgements: The present work was supported by a grant of the Romanian National Authority for Scientific Research, CNCS-UEFISCDI, project number PN-II-RU-PD-2011-3-0063.

References:

[1] F. J. Rodriguez, C. Sanchez, B. Villacampa, R. Alcala, R. Cases, M. Millaruelo, L. Oriol, Polymer 2004, 45, 2341.

[2] M. Hackel, L. Kador, D. Kropp, H. W. Schmidt, Adv. Mater. 2007, 19, 227-231.

[3] T. Endo, H. K. Kim, X. S. Wang, Y. Fujita, A. Sudo, H. Nishida, M. Fujii, Macromol. Chem. Phys. 2005, 206, 2106.

[4] F. A. Nicolescu, V. V. Jerca, D. M. Vuluga, D. S. Vasilescu, Polym. Bull. 2010, 65, 905.

8545-24, Session PS

Some technical methods to study the roughness of some surfaces, generated into metallic targets by laser micro piercing in determined conditions

Corina Bokor, Univ. Lucian Blaga in Sibiu (Romania); Ileana B. Rau, Polytechnical Univ. of Bucharest (Romania); Ilie V. Isarie, Claudiu Isarie, Univ. Lucian Blaga in Sibiu (Romania); Wilhelm Kappel, National Institute for Research and Development for Electrical Engineering (Romania); Doina Mortoiu, Aurel Vlaicu Univ. of Arad (Romania); Sorin Itu, Univ. Lucian Blaga in Sibiu (Romania)

Dimensional machining realized by laser beam and/or another concentrated energy sources in metallic targets, is based on melting, vaporisation and expulsion of some quantities of metal as a function of radiation parameters and material nature.

In some cases as: drawing plates used for the synthetic wires, fine fuel filters or fuel injectors, for the internal surface of the hole, is prefered more roughness in comparison of the holes, realized by classic piercing.

For instance, to realize some textures of simple synthetic fibres or in combination with natural fibres we want to have not a smooth surface, but a rough one because in this way, the texture will be more resistant in the places exposed at different efforts.

Concerning the fuel injectors we prefere the same: a rough surface, in order to ensure a better pulverized jet of the fuel. In the same time, when the hole is machined with a concentrated energy: L.B.M., E.B.M. a.s.o. the injector has a longer life.

It is not very easy to study the roughness resulted by L.B.M. in a hole with a cca 0,2 mm diameter.

To avoid errors of investigation, authors have experienced on pieces of carbide and alloyed steel which were drilled on separate adjacent plans, and in this way, the drilled surfaces were not affected by a cutting operation after boring, for such small diameters.

8545-25, Session PS

Optical third-harmonic generation measurements in biopolymer complexes

Ana Maria Manea, Alexandrina Tane, Roxana Zgarian, Polytechnical Univ. of Bucharest (Romania); James G. Grote, Air Force Research Lab. (United States); Francois Kajzar, Ileana B. Rau, Polytechnical Univ. of Bucharest (Romania)

Optical third- harmonic generation measurements on thin films of Rhodamine performed at 1064 nm fundamental wavelength in DNA and polymethyl methacrylate matrix will be presented. Influence of matrix as well as two photon resonant contributions will be described and discussed.

8545-9, Session 3

Spectroelectrochemistry as a strategy for improving selectivity of sensors for security and defense applications *(Keynote Presentation)*

William R. Heineman, Carl J. Seliskar, Laura K Morris, Univ. of Cincinnati (United States); Sam A. Bryan, Pacific Northwest National Lab. (United States)

Spectroelectrochemistry provides improved selectivity for sensors by electrochemically modulating the optical signal associated with the analyte [1-3]. The sensor consists of an optically transparent electrode (OTE) coated with a film that preconcentrates the target analyte. The OTE functions as an optical waveguide for attenuated total reflectance (ATR) spectroscopy, which detects the analyte by absorption. Alternatively, the OTE can serve as the excitation light for fluorescence detection, which is generally more sensitive than absorption. The analyte partitions into the film, undergoes an electrochemical redox reaction at the OTE surface, and absorbs or emits light in its oxidized or reduced state. The change in the optical response associated with electrochemical oxidation or reduction at the OTE is used to quantify the analyte. Absorption sensors for metal ion complexes such as [Fe(CN)6]4- and [Ru(bpy)3]2+ and fluorescence sensors for [Ru(bpy)3]2+ and the polycyclic aromatic hydrocarbon 1-hydroxypyrene have been developed [1-4]. The sensor concept has been extended to binding assays for a protein as demonstrated using avidin-biotin and 17β-estradiol-anti-estradiol antibodies [5]. The sensor has been demonstrated to measure metal complexes in complex samples such as nuclear waste [6] and water. This talk will focus primarily on potential applications of the sensor for the detection of target analytes in complex samples for security and defense applications.

[1] Y. Shi, A.F. Slaterbeck, C.J. Seliskar, W.R. Heineman, Anal. Chem. 69 (1997) 3679-3686.

[2] W.R. Heineman, C.J. Seliskar, J.N. Richardson, Aust. J. Chem. 56 (2003) 93-102.

[3] S.E. Andria, C.J. Seliskar, W.R. Heineman, Anal. Chem. 82 (2010) 1720-1726.

[4] T.S. Pinyayev, C.J. Seliskar, W.R. Heineman, Anal. Chem. 82 (2010) 9743-9748.

[5] H. Kuramitz, A. Piruska, H.B. Halsall, C.J. Seliskar, W.R. Heineman, Anal. Chem. 80 (2008) 9642-9648.

[6] M.L. Stegemiller, W.R. Heineman, C.J. Seliskar, T.H. Ridgway, S.M. Bryan, T. Hubler, R.L. Sell, Environ. Sci. Technol. 37 (2003) 123-130.

8545-10, Session 3

Direction sensing with a patterned bacteriorhodopsin film *(Invited Paper)*

Yoshiko Okada-Shudo, The Univ. of Electro-Communications (Japan)

Vectorial charge separation in the light-excited molecule of bacteriorhodopsin (bR) produces charge displacement photocurrents. The photocurrent is rectified and proportionate to light intensity. Such unique functions as a molecular diode have been applied to image sensors.

Direction sensing of an optical flow by bR films has been proposed utilizing differential responsivity. We have fabricated a simple direction sensor by choosing the pattern of underlying tin electrodes.

When a light sopt is scanned on the concentric array of pixels, each pixel outputs a plus or minus signal depending on the direction of optical flow. Our bR-based optical sensor can be made transparent by employing conductive glass ITO as electrodes. This enables design of a two patterned transparent electrodes. We demonstrated eight-motion detection of optical flow, up and down, from side to side and the opposite, from top right to bottom left, and the opposite, from top left to bottom right, and the opposite. We can assign these eight motions to eight commands of a controller.

8545-23, Session 3

Experimental design-based strategy for the simulation of complex gaseous mixture spectra to detect drug precursors

Marco Calderisi, Alessandro Ulrici, Laura Pigani, Univ. degli Studi di Modena e Reggio Emilia (Italy) and Consorzio INSTM (Italy); Alberto Secchi, SELEX Sistemi Integrati S.p.A. (Italy); Renato Seeber, Univ. degli Studi di Modena e Reggio Emilia (Italy) and Consorzio INSTM (Italy)

The EU FP7 project CUSTOM (Drugs and Precursor Sensing by Complementing Low Cost Multiple Techniques) aims at developing a new sensing system for the detection of drug precursors in gaseous samples, which includes an External Cavity-Quantum Cascade Laser Photo-Acoustic Sensor that is in the final step of realisation. Thus, a simulation based on FT-IR literature spectra must be accomplished, where the development of a proper strategy for the design of the composition of the environment, as much as possible realistic and representative of different scenarios, is of key importance. To this aim, an approach based on the combination of different experimental design techniques [1] has been developed.

The gaseous mixtures were built by adding the considered drug precursor (target) species to the gases typically found in atmosphere, taking also into account possible interfering species. The 4 chosen target gases are: 1-Phenil-2-Propanone, Acetic Anhydride, Ephedrine and Safrole. Interfering gases were selected considering typical custom environments, which led to the selection of 20 chemical species. Target concentrations ranged from 20ppb to 1000ppb, while interfering species concentrations ranged from 1ppb to different maximum concentration levels, inferred from literature data [2]. The concentration matrix for the target gases has been built by experimental design techniques, considering gas mixtures containing from 1 to 4 target species. In order to adopt a numerically balanced design, we used a 3 concentration levels Full Factorial Design (FFD) for mixtures with 3 and 4 targets, a 5 levels FFD for 2 targets mixtures and a 40 levels FFD for 1 target, leading to a total of 499 mixtures of targets. As for the interfering species, due to their high number and considering the simultaneous presence of a high number of them unrealistic, mixtures from 1 to 3 species were considered; FFDs with 13, 4 and 3 concentration levels were built for each combination of 1, 2 and 3 interfering species, respectively, leading to a total of 34080 mixtures. Both for targets and for interfering species, considering the large concentration ranges and in order to have a higher number of low-concentration mixtures, the FFDs with the lower number of levels (from 1 to 5) were built using a non-uniform spacing of the concentration values, based on the powers of 2. As for the air components, their mixtures were generated using, for each gas, random concentration values taken from the corresponding lognormal distribution based on real mean and maximum values derived from literature data. Finally, a global concentration matrix was obtained by randomly merging each mixture of target gases with a randomly selected mixture of interfering gases and with a randomly selected mixture of air components, in a way to generate 5000 gas mixtures to be used for further processing to tune the External Cavity-Quantum Cascade Laser Photo-Acoustic Sensor.

References

[1] G. Box, J. Hunter, W. Hunter. Statistics for Experimenters: Design, Innovation, and Discovery, Wiley, New Jersey, 2005

[2] I. Dunayevskiy, A. Tsekoun, M. Prasanna, R. Go, C.K.N. Patel, Appl. Optics, 2007, 46 (25), 6397-6404

8545-11, Session 4

Advances in surface plasmon resonance biosensors and their applications *(Keynote Presentation)*

Jiri Homola, Institute of Photonics and Electronics of the ASCR, v.v.i. (Czech Republic)

Optical biosensors based on surface plasmon resonance (SPR) present the most advanced optical label-free biosensor technology. Since their conception in early 1980s, SPR biosensors have received a great deal of attention and made significant advances both in terms of technology and applications. SPR biosensors have enabled direct observation of molecular interactions and have become an important research tool in molecular biology. Although the majority of SPR biosensors developed up to now have been designed for laboratory use, in recent years we have witnessed an increasing effort towards development of portable SPR sensing devices for use in the field.

This paper reviews selected recent advances in the field of SPR biosensing, focusing particularly on advances in the SPR method and instrumentation. These will include development of high-performance SPR biosensors for field use based on a recently developed approach to spectroscopy of surface plasmons and development of high-throughput SPR sensors based on SPR imaging in the polarization contrast. We also explore the potential of SPR sensors to detect a low number of molecules by dramatically reducing the sensor read-out area and show that by minimizing the read-out area, the number of binding molecules necessary to produce a measurable sensor output can be reduced by three orders of magnitude. Amplification methods that enhance the SPR sensor output by attaching a molecular tag with gold nanoparticles to the previously captured analyte are also discussed. It is demonstrated that this approach allows reducing the limits of detection for protein and nucleic acid targets by 2-3 orders of magnitude.

Finally, examples of bioanalytical applications of SPR biosensors will be given. Security applications to be covered include detection of foodborne pathogens (Salmonella, Listeria, E. coli, Campylobacter) and toxins (Tetrodotoxin, Staphylococcal enterotoxin B). Examples of applications of SPR biosensors for environmental monitoring (detection of environmental pollutants) and medical diagnostics (detection of disease biomarkers) will be also provided.

8545-13, Session 4

On electronic structure and optical properties of anthocyanidines extracted from grapes *(Invited Paper)*

Ileana B. Rau, Polytechnical Univ. of Bucharest (Romania); Ion Iosub, Univ. of Pitesti (Romania); Francois Kajzar, Polytechnical Univ. of Bucharest (Romania); Malgorzata Makowska-Janusik, J. Dlugosz Univ. de Czestochowa (Poland); Aurelia Meghea, Alexandrina Tane, Roxana Zgarian, Polytechnical Univ. of Bucharest (Romania)

The pallet of applications of natural dyes and pigments is continuously extending as a stringent need to meet the challenges arisen from sustainable development, particularly related to replacing synthetic chemicals by eco-friendly renewable raw materials. In this respect, the well known nutritive and therapeutic properties demonstrated by anthocyanine compounds present in selective plant extracts of numerous fruits, vegetables and flowers could be largely complemented by their characteristics as chromophores and fluorophores with high potential in promising applications in bio-imaging for diagnostic and therapy, but also in electronic and photonic devices, solar cells, etc. In this context, this paper proposes an improved protocol for extraction and HPLC detection of anthocyanidins from black grapes. In order to exploit their potential to be applied as chromatic and fluorescence molecular probes, the electronic properties have been studied by correlating spectral characteristics with trichromatic parameters and quantum chemistry computation.

8545-14, Session 4

Biomimetic DNA liquid crystals imaged by polarization sensitive two-photon microscopy *(Invited Paper)*

Katarzyna Matczyszyn, Joanna Olesiak-Banska, Marek J. Samoc, Wroclaw Univ. of Technology (Poland); Joseph Zyss, Ecole Normale Supérieure de Cachan (France)

The ability of DNA strains to organise in highly concentrated aqueous solutions in liquid crystal phases is an important feature of DNA. It has been found of high interest to investigate the mechanism of self organization of DNA chains into liquid crystalline phases as a biomimetic model of DNA packing in actual cell nuclei [1, 2]. This contribution reports on the investigation of the structure of DNA cholesteric and columnar phases by means of polarization sensitive two photon microscopy (PSTPM). This technique was successfully introduced by our group to resolve the 3D structure of ordered DNA stained with fluorescent dyes as well as to establish the relative orientation of the dye transition dipole with respect to the long axis of the DNA helix [3, 4]. We have also explored the doping of DNA in similar structures with luminescent nanorods so as to trace their organization in the DNA matrix.

The organization of liquid crystal phases formed in aqueous solutions of chromosomal DNA depend on the properties of solution (e.g. DNA concentration) and dopant molecules (i.e binding mode, charge) [5]. We discuss this influence based on one and two photon polarized light microscopy and local ellipsometric analysis of the two photon fluorescence emission. Interpretation of the results is performed by means of a theoretical model developed for PSTPM investigation of isolated nanoparticles [6]. We comment on the scope and limitations of the technique and on the optimization of measurement conditions towards specific DNA samples.

References

[1] Leforestier A. and Livolant F, Biophys. J. 65, 56 (1993).

[2] Livolant F, Levelut A M, Doucet J and Benoit J P, Nature 339, 724 (1989).

[3] Mojzisova H., Olesiak J, Zielinski M, Matczyszyn K, Chauvat D and Zyss J, Biophys. J. 97, 2348 (2009).

[4] Olesiak J, Matczyszyn K, Mojzisova H, Zielinski M, Chauvat D and Zyss J, Mat.Sci.-Poland 27, 813 (2009).

[5] Cherstvy A. G., J. Phys. Chem. B 112, 12585 (2008).

[6] Le Floc'h, V, Brasselet S, Roch J F, and Zyss J., J. Phys. Chem. B 107 12403 (2003).

8545-8, Session 5

Drug precursor vapor phase sensing by cantilever enhanced photoacoustic spectroscopy and quantum cascade laser

Juho Uotila, Gasera Ltd. (Finland); Jaakko Lehtinen, Tom Kuusela, Univ. of Turku (Finland); Sauli Sinisalo, Gasera Ltd. (Finland); Grégory Maisons, III-V lab. (France); Fabio Terzi, Univ. degli Studi di Modena e Reggio Emilia (Italy); Ilkka Tittonen, Aalto Univ. School of Science and Technology (Finland)

Chemical control is a crucial element for controlling the manufacturing and distribution of illegal narcotics and synthetic substances. This work is focusing on the vapor phase point detection methodology due to its applicability in custom, airport and harbor check point scenarios where inspection of trucks, cars, containers, as well as people and baggage is required. There are several techniques available that are able to screen and identify specific molecules even at very low concentration at laboratory or in controlled environment. However, a portable system which would be simple to use, sensitive, compact, and capable of providing screening over a large number of compounds and discriminate them with low probability of false alarms with short response time scale is still demanded.

Our solution is to combine cantilever enhanced photoacoustic spectroscopy with external cavity quantum cascade laser (EC-QCL), which is capable of measuring infrared gas phase spectra of the analyte substances. High sensitivity in a wide dynamic range is achieved with a silicon MEMS cantilever sensor coupled with an optical readout system and high power laser source, which is operating at the fundamental vibrational absorption wavelengths. High selectivity is achieved by measuring the infrared spectra of the sample gas utilizing widely tunable EC-QCL technology and novel signal processing methods.

Measurements with the initial prototype of the described system were performed to a selected drug precursor target molecules. The measurement results indicate low ppb-level gas phase sensitivity to selected drug precursor substances also in the presence of typical interfering molecules.

The research work, funded by the European Commission within the FP7 project called CUSTOM, has started in 2010. A brief project introduction is given in the presentation along with the description of the EC-QCL photoacoustic sensor technology. Also the results with example molecules and applicability to other drug precursors, drugs, and hazardous chemicals are discussed.

8545-16, Session 5

Optical sensing: recognition elements and devices *(Keynote Presentation)*

Guenter G Gauglitz, Eberhard Karls Univ. Tübingen (Germany)

Optical sensing at low limits of quantification and good selectivity requires highly optimized recogni-tion elements as biomolecules or molecular imprinted polymers as well as well advanced detection technologies. Optical detection principles can be classified according to monitoring labelled and non-labelled interaction partners, thus, applying fluorescence or direct optical detection techniques. The latter case can be further subdivided into evanescent field techniques (micro-refractometry) and micro-reflectometry based techniques. Principles of these methods are discussed and compared regarding advantages and disadvantages in various application fields.

The lecture will focus on Reflectometric Interference Spectroscopy (RIfS) as a powerful tool in direct optical detection and Total Internal Reflection Fluorescence (TIRF) as a detection principle for the low concentration range. Recent developments with respect to miniaturisation of measurement devices, simplification of optics and possibilities of detection are discussed.

In addition to typical antigen-antibody interaction as recognition structure during the last decade protein/protein-interaction and the monitoring of Viruses was successfully implemented. Further-more, molecular imprinted polymers (MIPs) have been developed to monitor at more harsh condi-tions.

There is certainly a huge amount of applications. For this reason the lecture will be focused to trace analysis in water and food as well as to an up-coming field of effect-based analytics. In detail results of measurements of Salmonella and Chlamydia are given. Furthermore possibilities of detection of viruses like H1N1 is discussed. Quantification of pesticides and endocrine disrupting compounds at sub-microgram per litre level are reviewed. Nuclear receptors are demonstrated as recognition elements which allow dose related detection of classes of e.g. endocrine disruptors. Recently nanoparticles are used for signal enhancement and also in food and environment. Their characterisation and detection is an additional topic for future control by advanced optical biosensing.

Acknowledgements:

The author thanks his many coworkers for supplied data. The authors group thanks for funding by EU project INSTANT (NMP.2011.1.3-1/280550), bmbf-project "Pepper and Salt" (16SV5049) and the BMWI/AiF-projects "Tierdiagnostik" (16061 N) and "Akutlab" (16696N)

Direct optical detection in bioanalysis: an update, G. Gauglitz, Anal Bioanal Chem (2010), 398(6), 2363-2372

Optical sensors with molecularly imprinted nanospheres: A promising approach for robust and label free detection of small molecules, F. Kolarov, K. Niedergall, M. Bach, G.E.M. Tovar, G. Gauglitz, Anal Bioanal Chem (2012), 402(10), 3245-3252

Reflectometric interference spectroscopy (RIfS) as a new tool to measure in the complex matrix milk at low analyte concentration, S. Rau, G. Gauglitz, Anal Bioanal Chem (2012), 402(1), 529-536

8545-17, Session 5

Drugs and precursor sensing by complementing low cost multiple techniques: overview of the European FP7 Project CUSTOM

Alberto Secchi, Anna Maria Fiorello, SELEX Sistemi Integrati S.p.A. (Italy); Sabato D'Auria, Antonio Varriale, Consiglio Nazionale delle Ricerche (Italy); Alessandro Ulrici, Renato Seeber, Univ. degli Studi di Modena e Reggio Emilia (Italy); Juho Uotila, Gasera Ltd. (Finland); Vincenzo Venditto, Univ. degli Studi di Salerno (Italy); Juan Carlos Antolin, Tecnalia (Spain); Francesco Colao, ENEA (Italy); Tom Kuusela, University of Turku (Finland); Ilkka Tittonen, Aalto University (Finland); Gregory Maisons, III-V Labs (France)

A large number of techniques for drug precursors chemical sensing has been developed in the latest decades. These techniques are able to screen and identify specific molecules even at very low concentration in lab environment.

Nevertheless the objective to build up a system which proves to be easy to use, compact, able to provide screening over a large number of compounds and discriminate them with low false alarm rate (FA) and high probability of detection (POD) is still an open issue.

The project CUSTOM, funded by the European Commission within the FP7, deals with stand alone portable sensing apparatus based on multiple techniques, integrated in a complex system with a complimentary approach. The objective of the project is to achieve an optimum trade-off between opposite requirements: compactness, simplicity, low cost, sensitivity, low false alarm rate and selectivity.

The final goal is the realization of an optical sensing platform able to detect traces of drug precursors compounds, such as ephedrine, safrole, acetic anhydride and the Benzyl Methyl Keton (BMK).

This is reached by implementing two main sensing techniques:

a) the fluorescence enhanced by the use of specially developed Organic macro-molecules, sensitive to the target compounds. The fluorescence analysis is based on different properly engineered fluorescent proteins able to bind the target analytes, as it happens in an 'immuno-type' reaction

b) a spectroscopic sensing technique in Mid-IR optical range, based on a Laser Photo-Acoustic Spectroscopy (LPAS), with a widely Tunable Quantum Cascade Laser. The post-processing algorithms implemented allows for a better selectivity and a lower Probability of False Alarm rate.

The sensing platform is equipped with an air sampling system

including a pre-concentrator module based on a sorption desorption cycles of a syndiotactic polystyrene (sPS) polimer.

8545-19, Session 5

Analysis and design of a multisensory array for explosive substances based on solid electrodes

Jose Gonzalez-Rodriguez, Mark G. Baron, Richard Barrett, Univ. of Lincoln (United Kingdom)

The aim of the work developed by our group was the electrochemical detection of explosives and related compounds in solution using a metal electrode array and differential pulse voltammetry. The multiple sets of voltammetric data were integrated using multivariate analysis and matched with known substances present in explosives. The electrodes consisted of multiple wires of the pure metal set into a plastic protection cover. The detection of explosives and explosive related compounds is a subject of importance in several areas including environmental health, de-mining efforts (land and sea) and security and defence against terrorist activity. In these areas, a method of analysis that will work effectively “in the field” is sometimes preferable to lab based methods. The use of electrochemical sensors is one of many methods that can be employed in the field to effectively detect explosives and related compounds, such as chemical taggants added to aid detection in some explosive formulations. Many common explosives contain suitable chemical groups to be detected using electrochemical methods. In these applications, there is particular interest in methods of detection that are deployable in the field, and so need to be portable, reliable, fast, sensitive and cheap. Electrochemical sensors fulfill these requirements and can be made suitable for use in hand held detectors.

Seven explosive substances: 2,4 dinitrotoluene, 2,6 dinitrotoluene, 3,4 dinitrotoluene, 2 nitrotoluene, octogen (HMX), Pentaerithrytol tetranitrate (PETN), trinitrotoluene (TNT) and cyclonite (RDX) and a taggant agent 2,3‐Dimethyl‐2,3‐dinitrobutane (DMNB) were subjected to analysis using four solid electrodes, namely glassy carbon, silver, gold and platinum in saline aqueous solutions to mimic an aquatic environment. The experiments were conducted in the cathodic section of the electrochemical range for each electrode. The reduction of the different explosives and taggant substance was studied and intensity versus potential curves recorded for different concentrations of the different analytes under study.

The results obtained in Differential Pulse Voltammetry (DPV) from the different experiments with each electrode were combined to produce a single voltammogram, which was subjected to chemometric analysis using Partial Least Squares (PLS) and Principle Component Analysis Non-Iterative Partial Least Squares (PCA-NIPALS).

A combination of the electrochemical signals obtained together with the use of chemiometric analysis made it possible to discriminate between explosives and their mixtures and also to quantitate their concentration in saline solutions.

Initial analyses demonstrated that some of the results clearly showed a different behaviour for each electrode and molecule studied, which could be used for identification purposes, however, in other cases the response obtained for other explosive molecules was very similar or even apparently inexistent when analysed using either different or the same electrode. In this case multivariate analysis (PLS and PCA-NIPALS) was used for both identification and quantification purposes with great success.

This separation was achieved by using a combination of the voltammograms obtained for all the electrodes. These combinations created a mathematical array, which clearly separates the explosives, even if the electrochemical information is buried or mixed with the electrode background noise.

8545-12, Session 6

Integrated luminescent chemical microsensors based on GaN LEDs for security applications using smartphones *(Keynote Presentation)*

Guillermo Orellana, Univ. Complutense de Madrid (Spain); Elias Muñoz, Univ. Politécnica de Madrid (Spain); Luz K. Gil-Herrera, Univ. Complutense de Madrid (Spain); Pablo Muñoz, Univ. Politécnica de Madrid (Spain); Juan Lopez-Gejo, Univ. Complutense de Madrid (Spain); Carlos Palacio, Univ. Autónoma de Madrid (Spain)

Development of PCB-integrateable microsensors for monitoring chemical species is a goal in areas such as lab-on-a-chip analytical devices, diagnostics medicine and electronics for hand-held instruments where the device size is a major issue. Cellular phones have pervaded the world inhabitants and their usefulness has dramatically increased with the introduction of smartphones due to a combination of amazing processing power in a confined space, geolocalization and manifold telecommunication features. Therefore, it is no surprise that the eyes of major manufacturers and service providers are on physical and chemical sensors that add value to their devices and offerings for easing the personal daily life. At the same time, the huge number of circulating cell phones provides a unique (bio)sensing network for monitoring airborne or waterborne hazardous chemicals or microorganisms for home, personal, industrial and national security applications. Micro- and nanotechnology are expected to play a pivotal role in the miniaturization required for integrateable sensors.1

Light-emitting devices (LEDs) are nowadays present in everyday’s life including domestic appliances, industrial instruments and illumination because of their long operational lifetime, output intensity and low cost. Their current emission wavelengths span from the uv to the near-infrared, but blue-violet LEDs are arguably the most attractive sources for fluorescence excitation of indicator dyes due to the absorption bands that most of them show in this region. GaN-based semiconductors are the cornerstone of blue LEDs because powerful chips have been developed (including laser diodes) and their emission wavelength can be tuned in a wide range if Al, In, or other metals are introduced in the GaN lattice.

Recently,2 we achieved for the first time (covalent) functionalization of semiconductor p- and n-GaN surfaces with tuneable luminescent indicator dyes of the Ru-polypyridyl family,3 as a key step in the development of innovative microsensors for smartphone applications. Chemical “sensoring” of LED chips with those indicators has also been achieved by plasma treatment of their surface, and the micrometer-sized devices have been tested to monitor O2 in the gas phase to show their full functionality.4 Novel strategies to increase the sensor sensitivity will be presented at the Conference.

Acknowledgements. This work is supported by the Spanish MICINN (CTQ2009-14565-C03-01) and UCM (GR35/10-A).

* orellana@quim.ucm.es; phone (+34)913944220

[1] Ryhänen, T., Uusitalo, M. A., Ikkala, O. and Kärkkäinen, A., Eds., [Nanotechnologies for Future Mobile Devices], Cambridge University Press, Cambridge (2010).

[2] López-Gejo, J., Arranz, A., Navarro, A., Palacio, C., Muñoz, E. and Orellana, G., J. Am. Chem. Soc. 132, 1746 (2010).

[3] Orellana, G. and García-Fresnadillo, D., in [Optical Sensors: Industrial, Environmental and Diagnostic Applications], Springer, Berlin-Heidelberg, 309-357 (2004).

[4] López-Gejo, J., Arranz, A., Navarro, A., Palacio, C., Muñoz, E. and Orellana, G., ACS Appl. Mater. Interf. 3, 3846 (2011).

8545-15, Session 6

Antioxidant and antimicrobial activities of Green Tea Extract loaded into solid lipid nanoparticles

Ana-Maria Manea, Nicoleta Badea, Ioana Lacatusu, Aurelia Meghea, Polytechnical Univ. of Bucharest (Romania)

Solid lipid nanoparticles (SLN) and nanostructured lipid carriers (NLC) are drug delivery systems based on solid lipids [1, 2]. Although both carrier types are based on solid lipids, the first type consists of pure solid lipids, while the second type is made of a solid matrix entrapping liquid oil [3]. The aim of this investigation was to develop solid lipid nanoparticles (SLNs) and nanostructured lipid carriers (NLC) loaded green tea extract by using a modified high shear homogenization technique and to evaluate their antioxidant and antimicrobial activities. SLN were prepared with cetyl palmitate and glyceryl stearate as solid lipids and for NLC, a mixture of the same solid lipids and grape seed oil has been used.

The developed lipid nanoparticles were characterized using particle size distribution (by dynamic light scattering-DLS), the physical stability has been evaluated by zeta potential measurements, the

morphology was examined by transmission electron microscopy (TEM), and the cristallinity behavior has been observed by differential scanning calorimetry (DSC).

GTE loaded solid lipid nanoparticles with average diameters of 172.4 ± 5.43 nm and good polydispersity index 0.201 ± 0.017 have been obtained by using Tween 20 as main non-ionic surfactant. Smaller main diameters have been obtained for GTE-NLC (125.6 ± 1.75 nm with a polydispersity index of 0.19 ± 0.01). The properties of GTE loaded SLN and NLC have been evaluated by appropriate in vitro analysis (chemiluminescence method for antioxidant measurements and diffusion disc method for antimicrobial test). The obtained results have shown enhanced antimicrobial properties (e.g. inhibition zone diameter of 3.5 cm for GTE-NLC as compared with 2.5 cm for native GTE) and significant antioxidant activities (GTE-NLC scavenging more then 95% the free radicals created in the simulated chemiluminescence system).

References

1. Rainer H. Muller, Karsten Mader, Sven Gohla, Solid lipid nanoparticles (SLN) for controlled drug delivery - a review of the state of the art, European Journal of Pharmaceutics and Biopharmaceutics 50 (2000), 161-167;

2. Tzu-Hui Wu, Feng-Lin Yen, Liang-Tzung Lin, Tong-Rong Tsai, Chun-Ching Lin, Thau-Ming Cham, Preparation, physicochemical characterization, and antioxidant effects of quercetin nanoparticles, International Journal of Pharmaceutics 346 (2008), 160-168;

3. Heike Bunjes, Structural properties of solid lipid based colloidal drug delivery systems, Current Opinion in Colloid & Interface Science 16 (2011), 405-411.

Acknowledgement: The work has been funded by the Sectoral Operational Programme Human Resources Development 2007-2013 of the Romanian Ministry of Labour, Family and Social Protection through the Financial Agreements POSDRU/107/1.5/S/76903.

8545-18, Session 6

A feature selection strategy for the analysis of spectra from a photoacoustic sensing system

Alessandro Ulrici, Renato Seeber, Marco Calderisi, Università di Modena e Reggio Emilia (Italy) and Consorzio INSTM (Italy); Giorgia Foca, Università di Modena e Reggio Emilia (Italy); Juho Uotila, Gasera Ltd. (Finland); Mathieu Carras, Alcatel-Thales III-V Lab. (France); Anna Maria Fiorello, SELEX Sistemi Integrati S.p.A. (Italy)

In the frame of the EU FP7 Collaborative Project (Theme: Security) CUSTOM, a new sensor system for the detection of drug precursors in gaseous samples is being developed, which also includes an External Cavity-Quantum Cascade Laser Photo Acoustic Sensor (EC-QCLPAS). For this sensor, the optimal wavenumbers within a 200 cm-1 range in the mid-infrared region must be identified, in order to lead to optimal detection of the drug precursor molecules in presence of interfering species and of variable composition of the surrounding atmosphere. To this aim, based on simulations made with FT-IR spectra taken from literature, a complex multivariate analysis strategy has been developed to select the optimal wavenumbers for the laser source. Firstly, algorithms to import spectral data with different file formats, wavenumber ranges, sampling rates and resolutions were developed, in order to obtain uniform datasets at constant 1 ppm concentration. Spectra were first denoised using a Wavelet Transform (WT) [1] based algorithm; subsequently, using WT and following previous literature suggestions [2], a thoughtful preselection of the spectral range was made, disregarding noisy regions ascribed to interfering small molecules. Concentration matrices were then built by using different combinations of experimental design techniques for the different types of gases, i.e. first considering the drug precursors, the air components and the interfering species as separate groups for the construction of sets of sub-mixtures, which were subsequently merged in order to simulate a wide variety of scenarios. Spectral data and concentration matrices were then merged, in order to build simulated spectra of gaseous mixtures; to this aim, a sigmoidal transfer function was implemented, in order to obtain as much realistic as possible spectral patterns. Then, instrumental noise was finally added, simulating the noise structure, evaluated from preliminary experimental measurements made with the EC-QCLPAS, by means of a WT-based algorithm developed ad-hoc. In this way, 5000 spectra were built, representing a wide variety of mixtures of 33 different gaseous species (including the 4 target molecules, 9 air components and 20 interfering species).The simulated mixtures were then used to select the optimal 200 cm-1 wavenumber range, by maximizing the classification efficiency estimated by Partial Least Squares - Discriminant Analysis [3] in cross-validation, on a moving window. Finally, the optimal wavenumber values were identified within the selected range using feature selection approach based on Genetic Algorithms [4] and on resampling. The work made will be relatively easily turned to the spectra actually recorded with the newly developed EC-QCLPAS instrument. Furthermore, the proposed approach allows to progressively adapt the spectral dataset to real situations, even accounting for specific, different environments.

[1] B. Walczak (ed.). Wavelets in Chemistry, Elsevier, Amsterdam, 2000

[2] I. Dunayevskiy, A. Tsekoun, M. Prasanna, R. Go, C.K.N. Patel, Appl. Optics, 2007, 46 (25), 6397-6404

[3] L. Pigani, A. Culetu, A. Ulrici, G. Foca, M. Vignali, R. Seeber, Food Chem., 2011, 129 (1), 226-233

[4] R. Leardi, A. Lupiáñez Gonzales, Chemom. Intell. Lab. Syst., 1998, 41, 195-207.

Conference 8546: Optics and Photonics for Counterterrorism, Crime Fighting and Defence

Monday - Wednesday 24–26 September 2012 • Part of Proceedings of SPIE Vol. 8546
Optics and Photonics for Counterterrorism, Crime Fighting, and Defence VIII

8546-1, Session 1

Trace detection of explosives by Surface Enhanced Raman Spectroscopy

Salvatore Almaviva, Antonio Palucci, Sabina Botti, ENEA (Italy); Francesco Saverio Romolo, Univ. degli Studi di Roma La Sapienza (Italy); Lars Landstrom, Serstech AB (Sweden); Alessandro Rufoloni, Luciano Cantarini, ENEA (Italy)

The detection of trace levels of explosives has become more important in the last decade as terrorists have increasingly targeted civilians and some type of explosives can be prepared from easily obtainable ingredients. Consequently, there is a need for explosives detection by both the military and homeland security organizations.

Several techniques have been applied for this purpose, including gas or liquid chromatography, capillary electrophoresis, mass spectrometry, ion mobility spectrometry, infrared absorption spectroscopy, optoacoustic spectroscopy and Raman spectroscopy (RS).

Among the detection technologies available, RS has recently gained a growing interest as potential tool for the detection of explosives because the Raman band frequencies relate to chemical bonding in the compound to be identified, so the detection by RS offers the distinct advantage of chemical specificity and benefits from the ability to generate valid reference Raman spectra under laboratory conditions, comparable with spectra obtained in the field.

However, the major drawback of Raman spectroscopy is the low cross-section of the Raman scattering, which affects the detection of substances at trace levels.

In 1977, Jeanmaire and Van Duyne demonstrated that the magnitude of the Raman scattering signal can be greatly enhanced when the scatterer is placed on a roughened noble-metal substrate. Strong electromagnetic fields are generated when the localized surface plasmon resonance of nanoscale roughness features on a silver, gold, or copper substrate is excited by visible light. This local field enhancement, combined with chemical effects, result in a process that nowadays is known as Surface-Enhanced Raman-Scattering (SERS).

In this work we report the results of SERS measurements of some common military explosives, including nitrate esters (ethylene glycol dinitrate, EGDN, pentaerythritol tetranitrate PETN), nitro-aromatic (trinitrotoluene TNT) and nitramine family (1,3,5-trinitroperhydro-1,3,5-triazine RDX), acquired with a table-top microraman system, integrated with a Serstech R785 minispectrometer.

Serstech R785 is an integrated miniaturised spectrometer (Size: 45 x 35 x 15 mm, weight 50 g) suitable for Raman and NIR measurements. For Raman measurements, it was attached via a fiber optic to a Raman probe, which in turn is attached to a suitable light source (laser).

The integration of R785 with a table-top Raman system aims to the realization of a portable SERS detector, able to perform in-situ measurements.

SERS spectra were obtained exciting the analyte with a focused diode-laser emitting at 785 nm, while each analyte was deposited onto a commercial SERS substrate with four different enhancing surfaces. Via investigation of the substrate area by SEM microscopy the sampled quantity was estimated to be 200 pg.

The main spectral features of each substance were clearly identified suggesting the possibility to create a database for data analysis/ pattern recognition and the spectral resolution was sufficiently high to clearly distinguish between substances belonging to the same and to different families.

8546-2, Session 1

Miniature multi-excitation wavelength raman spectrometers for handheld measurements of real-world samples

William Yang, BaySpec Inc. (United States)

We report on a variety of handheld Raman spectrometers combining multiple excitation wavelengths and detection ranges. In additional we report on the world's first dual-wavelength Near Infrared (NIR) and Shortwave NIR miniature spectral engine built with volume transmission gratings covering wavelength ranges from 800nm-1700nm. Other types of miniaturized Raman spectrometers have been realized, which are enabling handheld, portable, or at-line/ on-line applications for real-world sample measurements, such as threat determination of explosives, chemical and biological materials; quality assurance and contamination control for food safety; and forensics such as evidence gathering, narcotics, and anti-counterfeiting et al..

8546-3, Session 1

The detection limit of imaging Raman spectroscopy for 2,4,6-TNT, 2,4-DNT and RDX

Markus Nordberg, Henric Östmark, Swedish Defence Research Agency (Sweden)

When searching IED:s or other explosive threats, the explosive material itself will rarely be visible. Multi spectral imaging Raman spectroscopy is a novel detection method capable of detecting trace amounts of explosives at stand-off distances.

By illuminating a suspect surface by a laser and collecting high resolution multi-spectral imaging in the "Raman fingerprint" range, explosive particles at stand-of distances can be identified and displayed using color coding [Henric Östmark, Markus Nordberg, and Torgny E. Carlsson, "Stand-off detection of explosives particles by multi-spectral imaging Raman spectroscopy," Appl. Opt. 50, 5592-5599 (2011)].

We present the latest update on the limit of detection for the imaging Raman spectroscopy system for 2,4,6-trinitrotoulene (TNT), 2,4-dinitrotoulene (DNT), ammonium nitrate (AN) and cyclotrimethylenetrinitramine (RDX). The detection system is equipped with a green second harmonic Nd:YAG laser, an eight inch telescope, a liquid crystal tunable filter and an intensified CCD camera, in order to record high resolution narrow bandwidth images through the Raman spectrum. The target distance was 10 m and the field of view 28 mm ? 28 mm. The examined target was made of aluminum plates drilled with holes with decreasing widths and depths. The holes was then filled with eigther TNT, DNT, RDX or AN. The measured multi spectra data cubes were evaluated using least square fitting to determine the detection limit.

However in many civilian and military applications a detection system both eye- and skin-safe would be preferable. Therefore, in order to use an imaging Raman detection system in a real environment with people in the vicinity, the system has to use a non-dangerous laser. Here we presented an ultra violet imaging Raman system that uses an acousto optical tunable filter and a pulsed solid state laser at 355 nm with low pulse energy and high repetition rate in order to be skin-safe, eye-safe and invisible for the human eye.

8546-4, Session 2

Variable basis function least squares for chemical classification

Darren K. Emge, U.S. Army Edgewood Chemical Biological Ctr. (United States); Steven Kay, The Univ. of Rhode Island (United States); Jason A. Guicheteau, U.S. Army Edgewood Chemical Biological Ctr. (United States)

Raman spectroscopy is a valuable tool for detecting and classifying surface deposited chemicals. One difficulty, however, in utilizing its full capabilities is that the spectrum is highly dependent upon the chemical concentration. Spectral peaks can shift and even disappear as the concentration varies. A potential solution to this problem is to model the spectrum as a set of random basis functions, with each basis function depending upon a random unobserved parameter.

Relating these parameters to the concentration an expected least squares fitting procedure can be implemented. It is shown through computer simulation and some limited testing that the detection and classification performance can be improved over standard approaches that do not take into account this basis variation. The method proposed, however, is completely general. It is a viable alternative to standard least squares procedures whenever the goal is robustness of the procedure.

8546-5, Session 2

Lab-on-a-Bubble: direct and indirect assays with portable Raman instrumentation

Keith Carron, Snowy Range Instruments (United States); Aaron Strickland, iFyber, LLC (United States)

Lab-on-a-Bubble (LoB) is a new method for SERS assays that combines separation and concentration of the assay results. In addition, direct LoB techniques create much more stable SERS assay due to pre-aggregation of the nanoparticles on the ~30 micron silica bubbles. Direct assays will be demonstrated with a cyanide assay. An LOD of ~ 170 pptrillion was measured. We will describe the development and preparation of a new class of materials for surface enhanced Raman scattering (SERS) comprised of gold nanoparticles coated onto hollow, buoyant silica microspheres. LoB materials serve as a convenient platform for the detection of analytes in solution and offer several advantages over traditional colloidal gold and planar SERS substrates. An example assay is presented using the LoB method and cyanide detection. Cyanide binds to SERS-active, gold-coated LoBs and is detected directly from the corresponding SERS signal. Detection of cyanide on LoBs and in gold colloid is compared, and in both cases, a detection limit of ~170 part-per-trillion was determined. Prevention of aggregation common to colloidal nanoparticles is also discussed in relation to an assay for 5 μM 5,5'-dithiobis(2-nitrobenzoic acid) (DTNB).

Indirect assays couple a LoB and a SERS reporter together through the analyte. In this case, the method is similar to a paramagnetic pull-down assay, except the separation between the buoyant bubbles and the sinking SERS reporters is significantly improved. Paramagnetic methods can produce large blanks due to inclusion of the SERS reporters during the pull-down process. We will demonstrate the indirect assay principle with cholera. We describe a novel sandwich assay based on SERS comprised of buoyant silica microspheres coated with antibodies against the beta subunit of the cholera toxin (CT), and gold nanoparticles tagged with a Raman reporter, shelled with silica and coated with antibodies against the beta subunit of the CT. Together these components couple to form a sandwich which, after incubation, floats on the surface of the sample. LoB materials may provide a platform for rapid detection of antigen in solution and offers advantages over lateral flow or magnetic pull-down assays. The Raman reporter provides a unique and intense signal to indicate a positive analysis. Our limit of detection for the beta subunit of the CT in a buffer based system is 1100 ng.

In addition to these assay methods we will discuss the development of a robust miniature Raman reader for defense and security applications. The CBEx reader is designed to detect bulk materials and is adapted to reader SERS materials for trace detection. We will discuss trace detection of explosives with SERS and the CBEx system. The system has an intuitive touch screen interface, Bluetooth connectivity, and operates from 2-AA batteries. The CBEx is equipped with a unique orbital raster scan to average over heterogeneous bulk materials and SERS surfaces. The raster mechanism permits much higher laser powers to be used with sensitive SERS substrates. This effectively can increase the sensitive by 50x with the increase in laser power.

8546-6, Session 2

Time-resolved spectral characterization of a pulsed external-cavity quantum cascade laser

Jean-Michel Melkonian, Myriam Raybaut, Antoine Godard, Johan Petit, Michel Lefebvre, ONERA (France)

There is an increasing demand for compact sensors able to early detect hazardous chemicals, explosives, and their precursors. Optical spectrometry can be a real asset for situational awareness because it allows standoff detection and discrimination from the ambient environment, thanks to the characteristic absorbance patterns of the target molecules in the 8 12 μm region. In this context, there is a strong need for compact and spectrally tunable narrow-linewidth infrared sources.

Quantum cascade lasers (QCLs) are one of the few laser technologies that can currently provide efficient emission in the 8-12 μm range. However, it is still difficult to conciliate a high output power with single spatial mode and single-frequency operation. In the pulsed regime, a steady single-frequency emission is virtually impossible, because of strong transient thermal effects in the optical waveguide. The resulting linewidth broadening and increased noise are strongly detrimental to spectroscopic applications, and may also be a matter of concern for beam combining. Unfortunately, little information has been published on this subject because mid-infrared time-resolved spectrometers are extremely scarce.

In this work, we have measured the time-resolved spectrum of an external-cavity QCL by frequency up-conversion in a nonlinear crystal and analysis by a commercial near-infrared spectrometer.

Our setup is based on sum-frequency generation (SFG) in an AgGaS2 crystal, with type II phase matching according to: 1.064 μm (o) + 7.8 μm (e) -> 0.936 μm (e). The SFG bandwidth of 60 GHz is wider than the expected frequency excursion of the QCL. The pump laser is an injection-seeded Q-switched Nd:YAG laser emitting 18-ns-long pulses, with an optical spectrum of 90 MHz FWHM, and a frequency stability of 7 MHz rms over 30 s. With this setup any change in the QCL frequency is linearly transposed to the SFG frequency. A near infrared lambdameter (based on several Fizeau interfometers), is used to precisely follow the central wavelength of the SFG radiation with a resolution of 1 MHz. Besides, a diffraction grating monochromator with a 2 GHz resolution is used for analyzing complex spectrum shapes. The QCL trigger with respect to the pump trigger is finely delayed to select which part of the QCL pulse is to be probed.

The time-resolved spectrum of the QCL during a 500-ns-long pulse reveals 4 different zones: over [0-175 ns] a structured spectrum reveals that mode hops occur over 15 GHz; over [175-250 ns] the QCL emits a single-frequency radiation with a drift of 50 MHz/ns; over [250-350 ns] mode hops occur again spanning 11 GHz; over [350-500 ns] the emission is single-frequency with a drift of 30 MHz/ns. The continuous frequency drifts are the so-called frequency downchirps often reported in the literature. In addition, mode hops occur because of the combination of thermal effects and the relatively low selectivity of the diffraction grating in Littrow configuration. Complementary experiments made in CW operation and at different repetition rates helped to shed some more light on these phenomena. We also used the setup to estimate the central frequency stability of the QCL.

8546-7, Session 2

Ultra-high-brightness laser diode arrays for pumping of compact solid state lasers and direct applications

Andreas Kohl, Thierry Fillardet, Arnaud Laugustin, Olivier Rabot, Quantel Group (France)

High Power Laser Diodes (HPLD) have shown significant improvements of performances (especially in power and efficiency) over the last decade. Due to the drastically falling price per watt they are increasingly replacing flash lamps as pump sources. Furthermore their compact size and high efficiency makes diode laser arrays ideally suited as direct laser source for portable and even handheld devices.

The HPLD described here are based on so-called 'laser diode bars' having typically a width of up to 1 cm and consisting of up to 80 individual emitters. They are emitting mainly in the 808nm or 940nm wavelength window but bars at the "eye safe" wavelength of 1.5μm show steady progress. Several bars are assembled to form a stacked array. The peak power of such a stack is in the range of several kWatt.

Thanks to improvements in our assembly process mechanical tolerances are small enough to enable the collimation of the laser beam even with a bar to bar pitch of only 400μm. Low beam divergence together which a small pitch leads to highest brightness of diode laser arrays currently available. In order to further increase the power density of the stacks we have developed a technology to reduce the bar to bar pitch down to 150μm. Due to the increased power density and reduced emitting surface these stacks can be used for compact end pumping of solid state lasers with simple low cost optics. These stacks are therefore an enabling technology for the development of inexpensive, compact and highly efficient portable

solid state lasers for applications as telemeters and designators on small platforms such as UAVs and handheld devices.

For many direct applications of these diode arrays very short pulses in the range of 100ns are necessary. Examples are gated active imaging systems, luminescent spectroscopy or photo acoustic tomography. Available diode drivers for short pulses and high currents have very low efficiencies in the range of only 5%. We therefore have developed a new driver concept and integrated our diode array directly on the driver board. This results in a very compact laser source with up to 1mJ in a 100ns pulse. The overall efficiency of the driver plus diode is as high as 30%. No active cooling of diodes or driver is therefore necessary anymore. This enables the use of such a laser source for portable, even hand held devices.

In a further step we have also integrated the beam shaping optics on the driver board. These optics supply a homogenized beam of rectangular shape as it is required for example for laser illuminators in active imaging systems.

The compact size of this laser sources (< 0.08l) together with its high wall plug efficiency presents a disruptive improvement with respect to existing laser sources.

8546-8, Session 3

A first approach for digital representation and automated classification of toolmarks on locking cylinders using confocal 3D laser microscopy

Eric Clausing, Otto-von-Guericke Univ. Magdeburg (Germany) and Brandenburg University of Applied Sciences (Germany); Christian Kraetzer, Jana Dittmann, Otto-von-Guericke Univ. Magdeburg (Germany); Claus Vielhauer, Fachhochschule Brandenburg (Germany) and Otto-von-Guericke Univ. Magdeburg (Germany)

An important part of criminalistic forensic is the analysis of toolmarks. This field generally covers every kind of trace generated by some kind of tool - reaching from crowbar marks on window frames to the fine and subtle marks left on the components of illegally overridden locking cylinders. Such toolmarks often consist of plenty of single striations, scratches and dents which (in their entirety) can allow for a reliable conclusion in regards to the possible sequence of events or used tools. A forensic expert is capable of recognizing these single marks, putting them into context and by that drawing important conclusions. To receive a comparable result with an automated analysis of contactlessly acquired toolmarks, detailed digital representation of these and their connection to each other is needed. Whereas this representation e.g. for toolmarks of firearms can be a straight forward one-to-one mapping of the relevant marks to a simplified model, the representation of toolmarks on locking cylinders has to be of a more complex nature. The cause for that is the aim of such an analysis. For marks of firearms and tools the desired result of an analysis is a conclusion whether or not a mark has been generated by a tool in suspicion. Thus the challenge of the analysis is finding marks on both sample and reference that have identical (or almost identical) location and shape - actually a check on similarity of two images (or image like representations). For toolmark analysis on locking cylinders the whole thing changes with the specific aim. The aim here is not an identification of the used tool which is in most cases not possible anyways (because of the mostly filigree nature of used tools) but rather an identification of the opening method. The challenge of such an identification is that a one-to-one comparison of two images is not sufficient - although two marked objects look completely different in regards to the specific location and shape of found marks they still can represent a sample for the identical opening method. This paper provides the first approach on modelling toolmarks on lock pins and takes the several different requirements into consideration that are necessary to generate a detailed and interpretable digital representation. These requirements are “detail”, i.e. adequate features which allow for an detailed representation and interpretation of single marks, “meta detail”, i.e. adequate representation of the context and connection between all marks and “distinctiveness”, that is the possibility to reliably distinguish different sample types by the according model. The theoretical model implies an perfect pre-processing, i.e. no considerations in this direction are made within this paper although adequate approaches are referenced. The presented model is evaluated with a set of 15 physical samples (resulting in 675 digital scans) of lock pins from locking cylinders opened with three different opening methods, contactlessly scanned with a confocal laser microscope. First preliminary results suggest a high suitability for the aspired purpose although the experimental test set still has to be enlarged to hit statistical significance.

8546-9, Session 3

A first approach to the detection and equalization of distorted latent fingerprints and microtraces on non-planar surfaces with confocal laser microscopy

Stefan Kirst, Eric Clausing, Otto-von-Guericke Univ. Magdeburg (Germany) and Fachhochschule Brandenburg (Germany); Jana Dittmann, Otto-von-Guericke Univ. Magdeburg (Germany); Claus Vielhauer, Fachhochschule Brandenburg (Germany)

Fingerprints and microtraces play an important role as evidence within the field of criminalistics. Their conservative acquisition processes, are established, but are altering and impurifying the traces often. In case of microtraces even the integrity of the trace complex is affected. Using contactless methods, the acquisition process becomes non-invasiv and repeatable, but might be distorting on the other hand, when non-planar substrates are in use. Detecting and dealing with distortion in contactless aquired scans of non-planar surfaces is a novel field of research. Nowadays highly distorted fingerprints can only be used, if the substrate can be manually distorted by destroying or deforming it, which might not work for any surface, because of its consistence or value.

In this paper we suggest methods for detection and equalization of distortion for use in combination of types of traces, such as fingerprints and microtraces. Therefore we define different types of distortion in fingerprints and microtraces, as they occur on non-planar surfaces. A standardization of types is necessary to develop different solution for equalization. That includes distortions, that arise from dissimilar application of fingerprints. Since different types of distortion result, among other things, from different non-planar surfaces, this paper presents our approaches for detection and equalization of distortion on different non-planar surfaces. The equalization is meant to restore topology and distorted features, so operating errors can be eliminated, when analyzing highly distorted areas. Each method is evaluated via proper error rates and adaptively used to acquire fingerprints and microtraces under the perspective to use them in the field of forensic science. Both processes, the detection of distortion and the equalization, are automated and work without any intervention by the user.

Using the proposed methods, we are able to detect distortion and equalize fingerprints to support the investigators work, e.g. by visualize the distortion itself. Especially the detection can be used to discover areas containing false features due distortion. The equalization process, as a preprocessing step, ultimately makes it easier to work with distorted scans. In case of microtraces the presented techniques can even be used to equalize mircotraces themselves for better determination of their scale and topology.

For all scans the confocal 3D laser microscope “Keyence VK-X110” is used to gather color-, intensity- and topography information. The detection and equalization processes are evaluated separately, by analyzing the same testset of about 40 scans of different non-planar surfaces. To evaluate different levels of distortion, we modify the angle of the substrate to the microscope.

Despite our achievements in the field of distortion detection and equalization there are still challenges, like the non-isometric projection, that need to be focused on. Also the presented equalization methods may not completely remove any kind of distortion, such as added by deformation. Therefore we suggest and discuss future work for improving the distortion detection process by adding classification of sources of distortion to assure that the correct equalization method is used.

8546-10, Session 3

High-speed biometrics ultrasonic system for 3D fingerprint imaging

Roman G. Maev, Fedar Severin, Univ. of Windsor (Canada)

The objective of this research is to develop a new robust biometrics fingerprint identification technology based upon forming surface-

subsurface (under skin) ultrasonic 3D images of the finger pads. The presented work aims to create specialized ultrasonic scanning methods for biometrics purposes. Preliminary research has demonstrated the applicability of acoustic microscopy for fingerprint reading. The additional information from internal skin layers and dermis structures contained in the scan can essentially improve the confidence of person identification. Advantages of the described system include high resolution and short time of scanning. Operating in pulse-echo mode provides spatial resolution up to 0.05 mm. Technology advantages of the proposed device are the following:

• Full-range scanning of the fingerprint area “nail to nail” (2.5 x 2.5 cm) can be done in less than 5 sec with a resolution of up to 1000 dpi.

• Collection of information about the in-depth structure of the fingerprint realized by the set of spherically focused 50 MHz acoustic lens provide the resolution ~ 0.05 mm or better

• In addition to fingerprints pattern, this technology can identify sweat porous at the surface and under the skin

• No sensitivity to the contamination of the finger’s surface

• Detection of blood velocity using Doppler effect can be implemented to distinguish living specimens

• Utilization as polygraph device

• Simple connectivity to the databases of fingerprint images obtained with other techniques

• The digitally interpolated images can then be enhanced allowing for greater resolution

• Method can be applied to fingernails and underlying tissues, providing more information

A laboratory prototype of the biometrics system based on these described principles was designed, built and tested. It is the first step toward a practical implementation of this unique technique.

8546-12, Session 4

Combined optics and ultrasound for security screening

David A. Hutchins, Lee Davis, Aamer Saleem, The Univ. of Warwick (United Kingdom)

It has been shown that both optical and acoustic signals can be transmitted through clothing. This means that, in principle, both types of signal could be used for personal screening. In this paper, a description of how each of these signals interacts with clothing, and the information that can be obtained, will be presented. The wavelengths are very different - by three orders of magnitude. In fact, the wavelength of ultrasound is of a similar order of magnitude to that used by THz systems (≤ 1 mm), whereas the optical signals that could be used are typically in the micron or so range. This means that their use for screening relies on totally different mechanisms. Thus, both their interaction with the clothing and the hidden object will be different.

It is found that optical measurements can use the fact that imaging across a wide area is possible, using suitable optics. With the addition of spectroscopy, it is possible to identify certain chemicals that may be of interest. Spectroscopy can, in fact, take place without the need for imaging; it is possible to conceive of a situation where only a spectroscopic signature is sought from an individual. Conversely, ultrasound is unlikely to be able to provide spectroscopic information of interest. However, it is potentially possible for it to provide sub-clothing images.

In this paper, results will be shown for both types of measurements, where the location of hidden objects can be demonstrated. The imaging resolution that can be obtained will be described, together with a discussion of how both types of energy could be used for improved identification of objects hidden beneath layers of clothing. A combination of the two has some interesting properties, which will be discussed.

8546-13, Session 4

Criteria for the detection and identification of compound substances on the base of comparison of spectral lines dynamics

Vyacheslav A. Trofimov, Nikolay V. Peskov, Lomonosov Moscow State Univ. (Russian Federation); Norbert Palka, Mieczyslaw Szustakowski, Tomasz Trzcinski, Military Univ. of Technology (Poland)

We developed criteria for the detection and identification of substance in the mixture of substances. For this aim we detect the pure dynamics of spectral lines of substance of interest, which are distorted by action of ambient medium, in THz range of frequencies. We apply the developed method to both simulated signals and real THz signals transmitted through or reflected from explosive.

8546-14, Session 4

Detection of bottled liquid explosive by near infrared

Hideo Itozaki, Ryu Miyamura, Hideo Sato-Akaba, Osaka Univ. (Japan)

Terrorism has used liquid explosives in London and so on. Then bottled liquid was strictly limited to bring in airplane. Because it was difficult to detect bottled liquid explosive without opening bottles. Recently some methods are under developing using X-ray, electromagnetic, Raman scattering so on. They have some merits and demerits. Here we introduce a liquid detection method using near infrared. Water has poor absorption at visible light and large absorption at infrared. Many typical absorption peaks of content in water also located at infrared region. Therefore infrared spectroscopy is used for the detection of water solution. In this case, sample was usually very thin such as less than 1 mm, because of large optical absorption. Bottle scanning needs more than a few cm to evaluate inside the bottle. Therefore we tried to use near infrared instead of infrared or visible light.

Our device is adopted transmission method. Bottle is illuminated by the light source from one side of the bottle and transmitted light is detected by the spectrometer at the opposite side of the bottle. The infrared spectrum from 650 to 1100 nm was obtained at one time by a silicon linear sensor. This spectrum data is analyzed by compact PC. We collected various bottled liquid and obtained those near infrared spectrum. Multi valiance method has been applied to get judgment criteria to separate explosives from safety drinks. It worked very well at the trial test in Osaka international airport. Our device needs only less than a second to check bottled liquid. It needs space of less than a note PC and can be installed without extending existent space. It can detect not only explosives but also water solution of narcotics. We hope that our developed bottle scanner will be installed at security gate in airport as quickly as possible and we can bring our own bottles in the aircraft freely.

8546-15, Session 4

Identification and mapping of spilled liquids by passive hyperspectral imaging

Rene Braun, Roland Harig, Bruker Optik GmbH (Germany)

Previous studies showed that imaging infrared spectrometry allows remote detection and identification of traces of potentially hazardous liquid surface contaminants. In this work the identification of liquid surface contaminants by comparison of passive measurements of the spectra of contaminated samples to synthetic spectra is presented. Because the spectra depend on the liquid (composition and thickness), the background material, and on the radiation incident to the sample, a comprehensive radiative transfer model has been developed and applied to calculate the synthetic spectra for the specific sample surface irradiated by the surrounding hemisphere. The model requires spectra of the complex refractive indices of the liquids. These spectra were calculated by applying the Kramers-Kronig relations to spectra of the linear absorption coefficient. As the agreement between measured and modelled spectra of liquids is excellent and automatic identification of diverse liquid surface contaminants proves to be possible, the results confirm the validity of the model.

8546-16, Session 4

Increasing the quality of image of a commercially available passive THz camera due to computer processing of image

Vyacheslav A. Trofimov, Vladislav Trofimov, Lomonosov Moscow State Univ. (Russian Federation); Norbert Palka, Military Univ. of Technology (Russian Federation); Marcin Kowalski, Military Univ. of Technology (Poland)

We demonstrate the improvement of the quality of the image captured by TS4 - the commercially available THz passive camera manufactured by ThruVision Systems Ltd. The measurements range of this device reaches 10 meters. Our approach bases on application of novel spatial filters and algorithms, developed by us for computer processing of passive THz images produced by the camera. Using the computer processing of the image we can see the object with diameter of 25 mm at the distance of 10 meters, for example. We can also increase the number of pixels per image without losses the quality of image.

In the report there are demostration of the detection of bomb, knife, pistol, various small objects hidden under opaque clothes.

8546-17, Session 5

Active coherent laser spectrometer for remote detection and identification of chemicals

Neil A. MacLeod, Damien Weidmann, Rutherford Appleton Lab. (United Kingdom)

Currently, there exists a capability gap for the remote detection and identification of threat chemicals. The specified requirements are stringent: parts per billion (ppb) sensitivity with selectivity across a wide number of components, detection/identification range of 50 m or greater, response times in the range of seconds to minutes, eye-safe operation, compactness, ease of deployment, and cost effectiveness.

The sensitivity and response time requirements effectively rule out passive detection via thermal emission. Active instruments (including laser induced fluorescence and laser induced breakdown spectroscopy) in which a laser is transmitted into the open air can approach the required sensitivity levels but generally fail to meet the selectivity or eye-safe criteria.

We report here on the development and demonstration of an Active Coherent Laser Spectrometer (ACLaS) operating in the thermal infrared. Coherent (or heterodyne) detection in the mid-infrared spectral region (2-20 m) has a number of significant advantages over alternative remote sensing techniques. The absorption cross sections of chemicals are several orders of magnitude higher than in the near-IR, while the ultimate sensitivity limit is determined by the laser shot noise (< femto Watts) which allows operation at lower (eye-safe) levels of transmitted laser power. Chemical selectivity is provided by the combination of the narrow laser spectral bandwidth (typically 2 MHz or 10-4 cm-1) and frequency tunability that allows the recording of the full absorption spectrum of any species in the instrument line of sight. In addition, the coherent nature of the detection process provides a narrow field of view (< 0.5 mrad) ensuring a high spatial resolution (typically a few centimetres at 50 m). The spectroscopic sources used in the prototype demonstrator are Quantum Cascade Lasers (QCL's). The instrument has demonstrated high sensitivity and chemical selectivity in the stand-off detection and identification of vapour phase chemicals.

The ACLaS demonstrator is based on a single continuous wave distributed feedback QCL which provides both the active, transmitted beam and the local oscillator beam for coherent mixing. The transmitted radiation is directed towards a distant, diffusely reflective target mimicking topographic backscattering. The backscattered radiation is collected and analysed by the optical heterodyne receiver. As the QCL frequency is continuously tuned across absorption features of species within the line of sight, a full high resolution spectrum is obtained from which identification and quantitative information can be retrieved.

The instrument performance is optimised and assessed using a forward model which includes the scattering process, propagation through the atmosphere and absorption by chemical species of interest. For accurate, quantitative measurements, the model requires gas phase reference spectra of the chemicals of interest. We have developed a method based on permeation sources to generate this reference data to ~1% which was successfully applied to, for example, common energetic materials.

8546-18, Session 5

Real-time standoff gas detection and environmental monitoring with LWIR HSI

Florent M. Prel, Louis M. Moreau, ABB Analytical Measurement (Canada); Hugo Lavoie, Francois Bouffard, Jean-Marc Thériault, Defence Research and Development Canada, Valcartier (Canada); Christian A. Vallières, Claude B. Roy, ABB Analytical Measurement (Canada); Denis Dubé, Defence Research and Development Canada, Valcartier (Canada)

MR-i is a dual band Hyperspectral Imaging Spectro-radiometer. This field instrument generates spectral datacubes in the MWIR and LWIR. MR-i is modular and can be configured in different ways. One of its configurations is optimized for the standoff measurements of gases in differential mode. In this mode, the instrument is equipped with a dual-input telescope to perform optical background subtraction. The resulting signal is the differential between the spectral radiance entering each input port. With that method, the signal from the background is automatically removed from the signal of the target of interest. The spectral range of this configuration extends in the VLWIR (cut-off near 14 µm) to take full advantage of the LW atmospheric window.

8546-19, Session 5

LWIR hyperspectral imaging application and detection of chemical precursors

Hugo Lavoie, Francois Bouffard, Jean-Marc Thériault, Eldon Puckrin, Denis Dubé, Defence Research and Development Canada, Valcartier (Canada)

Detection and identification of Toxic industrial chemicals (TICs) represent a major challenge to protect and sustain first responder and public security. Passive Hyperspectral imaging (HSI) demonstrates promising standoff detection and identification of chemical vapors emanating from the venue under surveillance. To investigate this method, the Department of National Defense and Public Safety Canada have mandated Defense Research and Development Canada (DRDC) - Valcartier to develop and test Very Long Wave Infrared (VLWIR) HSI sensors for standoff detection. The initial effort was focused to address the standoff detection and identification of toxic industrial chemicals (TICs), surrogates and precursors. Sensors such as the Improved Compact ATmospheric Sounding Interferometer (iCATSI) were developed for this application.

Sensor developments and preliminary results of standoff detection and identification of TICs and precursors will be presented in this paper. The iCATSI sensors is based on the optical differential Fourier-transform infrared (FTIR) radiometric technology and are able to detect, spectrally resolve and identify small leak at ranges in excess of 1 km. Results from a series of trials in asymmetric threat type scenarios will be presented. These results will serve to establish the potential of HSI standoff detection of TICs, precursors and surrogates.

8546-20, Session 5

Infrared hyperspectral imaging for chemical vapour detection

Keith Ruxton, Gordon Robertson, William Miller, Graeme P. A. Malcolm, Gareth T. Maker, M Squared Lasers Ltd. (United Kingdom); Chris R. Howle, Defence Science and Technology Lab. (United Kingdom)

Active hyperspectral imaging is a valuable tool in a wide range of civilian and military applications. One example is the detection of chemical warfare agents (CWAs) through analysis of the infrared (IR) absorption spectrum. This work presents a selection of results from a prototype IR hyperspectral imaging instrument that has successfully been used for compound detection at a range of standoff distances.

Active hyperspectral imaging utilises a broadly tunable laser source to illuminate the scene with light at a range of wavelengths. While there are a number of potential illumination methods, this work illuminates the scene by raster scanning the laser beam using a pair of galvanometric mirrors. The resulting backscattered light from the scene is collected by the same mirrors, then directed and focussed onto a suitable single-point detector where the image is constructed pixel by pixel. The imaging instrument that was developed in this work is based around an optical parametric oscillator (OPO) source with broad tunability, operating in the 2.6 - 3.8 μm (midwave IR, MWIR) and 1.5 - 1.8 μm (short wave IR, SWIR) spectral regions. The MWIR beam was primarily used as it addressed the fundamental absorption features of the compounds under investigation compared to the overtone and higher order features in the SWIR region, which can be weaker by more than an order of magnitude.

8546-21, Session 5

Surveillance in an urban environment using mobile sensors

Wim Mees, Royal Belgian Military Academy (Belgium); Andreas J. Kirschner, Technische Univ. München (Belgium); Markus Peichl, Deutsches Zentrum für Luft- und Raumfahrt e.V. (Germany); Oscar Tejedor, GMV S.A. (Spain)

Improvised explosive devices (IEDs) are becoming an increasingly important threat in modern peace support operations. In order to assist a future vehicle commander in detecting IED threats, a consortium consisting of the Spanish “Grupo Tecnologico e Industrial” (GMV), the Belgian “Royal Military Academy” (RMA), and the German “Deutsches Zentrum fuer Luft- und Raumfahrt” (DLR) and “Technische Universitaet Muenchen” (TUM) has developed in the framework of the European Defense Agency (EDA) Joint Investment Programme Force Protection (JIP-FP) “Surveillance in an Urban environment using Mobile sensors” (SUM) project a prototype system that uses a combination of active and passive sensors to detect threats in the road surface and on the side of the road.

The system combines information from external sources, such as command & control networks and UAV or Satellite image processing, with information that is acquired locally through the on-board sensors. A visual and infrared camera ensure that anomalies on the road surface and on the side of the road are detected during both day and night operations; a radiometer and radar allow the system to distinguish innocent anomalies from potentially dangerous ones. Finally, the potential threats are shown in an intuitive graphical user interface that allows an operator, even in the difficult circumstances encountered inside a driving patrol vehicle, to get a quick overview of the threats that lie on the road ahead and examine them in more detail by looking at the images produced by the different sensors.

Because the sensors have different fields of view and acquire data asynchronously, a spatial and temporal fusion of the sensor data has been implemented. The fusion between the different channels is performed at feature level using a fuzzy expert system and the ordered weighted averaging aggregation operator. The fuzzy expert system makes it possible to implement expert domain knowledge about the way in which the different types of threats that are considered appear in the different channels.

The visual channel, or when it’s not available the infrared channel, is used for performing a coarse scene analysis in order to locate the road in the images. The next step consists in detecting anomalies in the road surface as well as on the side of the road in the visual and infrared images using a number of algorithms. These anomalies represent potential threats, for instance garbage bags, piles of dirt or cardboard boxes that might hide an improvised explosive device. It is obviously impossible to distinguish harmless bags or boxes from those containing an explosive device. This is why the supporting evidence provided by the radar and radiometer is essential to distinguish real threats from false alarms.

In order the evaluate the performance of the system, a test campaign was organized at a military site in Belgium. In this paper we present the overall architecture of the SUM system, explain the choice of the sensors, and present an overview of the experimental results. The individual subsystems are presented in more detail in separate papers.

8546-22, Session 6

A real-time processor for imaging through turbulence and other sub-optimal environments

John A. Cochrane, Melford Resolution Ltd. (United Kingdom); Steve Collier, Nigel Mitchell, Jon Shadforth, Amber Optix Ltd. (United Kingdom)

Melford Resolution Ltd (MRL) together with Amber Optix Ltd (AOL) have developed behind-the-focal-plane image processing techniques to improve the quality of images that have been degraded due to sub-optimal environmental conditions. Atmospheric turbulence can be a significant cause of spatial and temporal aberrations, along with the effects of camera shake and low light induced noise. The techniques are largely independent of the acquisition technology and require no a-priori knowledge of the sensor, optics or environment. These algorithms substantially reduce such undesirable artefacts to produce a real-time imaging system for use under extreme climatic conditions.

Variations in the refractive index of the air between the object and the camera caused by thermal fluctuations distort and aberrate the wave-fronts and lead to degraded images at the receiver resulting in the shimmering images that are familiar to many people. These effects are wavelength dependent; the effect is noticeable in the Visible, SWIR and MWIR bands, whilst the LWIR is largely unaffected.

Images captured from an unstable platform can suffer from excessive movement due to camera shake.

Images can also suffer from low signal to noise ratio for a variety of reasons such as low light, fast integration, small aperture or even sensor characteristics. High levels of noise in an image can hide features of interest within a captured scene.

The current version of the processor is a Windows® application that will run on most compatible desktops and laptops. Image input to the process can be from a sensor for live processing or from stored images or movie files for post-processing. An important feature is that almost any 2D imagery from any source can be processed without requiring any special knowledge of the environment, optics or hardware.

Images are initially stabilised to remove any camera shake, including rotation around an arbitrary origin. This is followed by scene analysis and detection of moving objects. Finally the effects of shimmer and noise are reduced, taking into account the overall nature of the scene and any moving objects within it.

The system is designed to operate in real-time utilising an automatic mode that requires little operator input. Achieving real-time processing is dependent on image format (e.g. image size) and computer hardware capabilities. Manual overrides are provided for unusual scenes or experimentation.

The presentation will review the following features:

1. Initial image stabilisation using software-based correction for X/Y translation and rotation.

2. Automatic scene analysis to control processing parameters automatically for ‘hands-off’ operation.

3. Manual parameter control for more involved operation.

4. Discrimination of moving objects vs shimmer by the use of multiple processing techniques and output image construction.

5. Local contrast enhancement (e.g. to see inside doorways or vehicle compartments).

6. Fixed Pattern Noise detection and correction.

7. Low light level benefits in terms of noise reduction to give better spatial and temporal resolution performance at night without any change in the processing modality.

8546-23, Session 6

Real-time Dictionary based Super-Resolution of Surveillance Video Streams and Targets

Timothy M. Hospedales, Shaogang Gong, Vision Semantics Ltd. (United Kingdom)

Real-time super-resolution within surveillance video streams would be a powerful tool for security and crime prevention allowing, for

example, faces, number-plates or other important features to be more accurately identified on the fly from a distance and under less-controlled conditions. However, many of the state-of-the-art approaches to super-resolution are computationally too expensive to be suitable for real-time applications to surveillance video. We consider one particular contemporary method using sparse coding (Yang et al, 2010) and show how, by relaxing some model constraints, it can be sped up by over three orders of magnitude compared to the reference implementation, and thus approach real-time performance with visually indistinct reduction in fidelity.

The principle of sparse coding for representing over-complete dictionaries has emerged in recent years as a powerful approach for many image processing tasks including super-resolution, de-noising and restoration. However, many such techniques require solving multiple computationally expensive constrained optimisation problems to process each incoming image, thereby limiting their applicability to surveillance. The sparse coding method of Yang et al. first trains a pair of corresponding low and high-resolution over-complete dictionaries. In the testing phase, for each input patch, a sparse representation is obtained by constrained optimisation and this representation is then used to index the high-resolution dictionary and reconstruct a synthesised high-resolution image patch corresponding to the low-resolution probe patch. However, this optimisation and its repeated application for all overlapping patches are computationally very expensive, with minutes being required to super-resolve a single image.

To overcome the problem, we consider and propose three modifications to the standard sparse coding approach. First, once good dictionaries have been learned, the subsequent indexing is performed without an explicit sparsity constraint. This achieves good high-resolution reconstruction whilst avoiding significant computational cost. Second, we observe that given the mentioned constraint relaxation, iteration over all overlapped patches optimising each independently is no longer necessary, and the entire the entire image can be super-resolved in four simple matrix operations using fast linear-algebra routines. Third, the resulting matrix procedure is simple to implement on a GPU for further speed increase. The whole computation is thus over 1000x faster than the reference implementation. Importantly, the margin of improvement is greater for larger output images (greater degrees of magnifications and/or larger input images). The quality of the output is maintained: PSNR of the super-resolved images compared to ground truth is not significantly different to the reference implementation, while maintaining a significant improvement over baseline bicubic-interpolation approach. For comparison, our matlab implementation achieves 20 frames per second for 4X super-resolution of a 64x64 pixel window whilst the reference implementation takes 2 minutes per frame for the same input and magnification factor.

8546-24, Session 6

Simulation of atmospheric turbulence effects and mitigation algorithms on stand-off automatic facial recognition

Kevin R. Leonard, U.S. Army Night Vision & Electronic Sensors Directorate (United States); Jonathan Howe, Defence Science and Technology Lab. (United Kingdom); David E. Oxford, Defence Science and Technology Lab. (United Kingdom) and U.S. Army Night Vision & Electronic Sensors Directorate (United States)

Stand-off base and force protection measures primarily rely on electro-optic and thermal imaging technology. Atmospheric turbulence causes blur, distortion and intensity fluctuations that can severely degrade the image quality of these systems. This work explores the effects of turbulence image degradation on the performance of automatic facial recognition software and also looks at the potential benefit of turbulence mitigation algorithms. The goal of this work is to understand the feasibility of long-range facial recognition in degraded imaging conditions. In order to create a large enough database to match against, simulated imagery of different ranges and turbulence conditions were created using a horizontal view turbulence simulator and a subset of the FERET database. The simulated turbulence degraded imagery was then processed with facial recognition software and the results are compared against those from the pristine image set. Finally, the performance of the facial recognition software with turbulence mitigated imagery is also presented.

8546-25, Session 7

A visual scene busyness measure through a region growing spatial segmentation

Gaurav Gupta, Alexandra Psarrou, Sophie Triantaphillidou, Jae-Young Park, Univ. of Westminster (United Kingdom)

Extracting and analysing meaningful components of an image is an important task in computational vision and imaging. The many approaches to image segmentation include those that work with histograms, graphs, edges, regions, compression and statistical clustering. While the state of the art, with respect to both quality and speed of segmentation, mainly revolves around the mean-shift, graph based and similar techniques, one of the most commonly applied family of techniques is region merging, where pixels are step-wise grouped into larger and larger segments.

In this paper we propose measures of visual scene busyness through spatial segmentations of static images. For this purpose we present a fast and effective region merging scheme using a semi-greedy merging criterion and an adaptive threshold (SGAT) to control segmentation resolution. The core of the framework is a hierarchical parallel merging model and region reduction techniques. The full segmentation consists of the following two phases: 1. algorithmic region merging, and 2. region reduction, which includes (a) weakness heuristic region reduction, (b) small segment reduction, and (c) enclosed region absorption.

The segmentation method favours the best merge over a fast merge, which while computationally slightly more expensive, produces better results. The best merge is defined as that merge that is optimal for both regions involved, rather than only a search for the optimal merge for a single region. Also, an adaptive distance threshold is applied as the segmentation progresses, using a technique known as dynamic merge relaxation. A large threshold allows incorrect merges to occur if two regions locally meet the merge criterion even if on a more global scale the merge in question would be suboptimal. This problem can be alleviated if the regions are given more time to move towards their respective cluster centers in feature space. Additionally, edge strengths established using an edge detector, such as the Canny detector, are incorporated into the region feature distance formulation to help restrict merges over strong boundary locations.

In quantitative analysis on standard benchmarks data, the proposed method performs the best, with respect to specific metrics as well as overall, compared to other segmentation methods. Several segmentation evaluation metrics are commonly used in the literature. Since we wish to compare segmentation performances based on values for different metrics, we propose a new performance summary indicator, the Relative Performance, as a function of multiple evaluation measures. This performance indicator uses the results for human segmentation as a baseline, and allows one to compare segmentation results using a single number. We take into account the fact that different metrics produce varying ranges of values and differences in some metrics may have less influence than others. We thus normalise each metric result by the relative importance of that metric with respect to the complete set of considered metrics.

Qualitative and quantitative evaluation of results points to semantic correlations between the segmented spatial regions and real world objects. We can thus quantify scene busyness in terms of global and local region properties. Busyness is then defined in terms of the number of spatial segments, statistical measures calculated on neighbouring pixel feature distances, region boundary statistics, and global and local pixel-level and segment-level pixel feature distributions.

8546-26, Session 7

Robust background subtraction for automated detection and tracking of targets in wide area motion imagery

Philip J Kent, QinetiQ Ltd. (United Kingdom); Simon Maskell, QinetiQ Ltd. (United Kingdom) and Imperial College London (United Kingdom); Oliver Payne, Sean Richardson, QinetiQ Ltd. (United Kingdom); Larry A. Scarff, Goodrich ISR Systems (United States)

It is becoming increasingly important to perform surveillance of large populations of targets, such that targets of interest can be identified on-the-fly as those that deviate from known patterns of benign

behaviour or those that exhibit known patterns of illicit behaviour. Persistent surveillance is therefore of increasing importance in both the defence and security domains. The use of existing Narrow Field-of-View (FoV) sensors onboard Unmanned Air Vehicles (UAVs) requires that other intelligence can inform the surveillance process and define targets that are of interest. Such existing NFoV sensors do not therefore meet the growing demand for persistent surveillance. In response to this, Wide Area Motion Imagery (WAMI) sensors with Wide FoVs are growing in popularity. Such WAMI sensors simultaneously provide high spatial and temporal resolutions, giving extreme pixel counts over large geographical areas. While it is feasible for a human analyst to maintain track on a very small number of targets (often just one) in Narrow FoV sensors, the scale of the WAMI sensors' data feeds is such that the scale of analysis either demands a very high capacity communications link coupled to a large number of human analysts or onboard automation. Here we focus on automated scene understanding. Specifically, we report on work that draws heavily on advances made as part of UK MoD's Persistent Wide Area Surveillance programme. We use an iterative quad-tree optical-flow algorithm to efficiently estimate the parameters of a perspective deformation of the background that aligns the previous background with the current frame. We then use a robust estimator to simultaneously classify each pixel as foreground or background and infer the parameters of a Gaussian distribution for the value of each background pixel in the current image. This process identifies foreground pixels, to which we apply morphological operators and connected component labelling. The resulting detections are referenced to the coordinates of the first frame (as a surrogate for geolocation that does not demand tight coupling into the navigation system) and passed to a multi-target tracker. The multi-target tracker is based on the use of a Kalman filter per target and a Global Nearest Neighbour approach to multi-target data association. The multi-target tracker thereby includes statistical models for missed detections (eg caused by targets that are obscured by tree cover) and false alarms (eg caused by errors in the registration process). We use spatial data structures to ensure that the multi-target tracker can scale to analysing large numbers of targets (ie thousands). We demonstrate that real-time processing (on modest hardware) is feasible on an unclassified WAMI infra-red dataset consisting of 4096 by 4096 pixels at 1Hz simulating data taken from a Wide FoV sensor on a UAV near to Rochester, NY. With low latency and despite intermittent obscuration and false alarms, we demonstrate persistent tracking of all but one of the vehicular targets that are present in the dataset considered, with no false tracks. The target that is not tracked is very low contrast indeed. The authors are unaware of alternative solutions that achieve similar performance.

8546-27, Session 7

Scaling up multi-camera tracking for real-world deployment

Yogesh Raja, Shaogang Gong, Vision Semantics Ltd. (United Kingdom)

A user-assisted multi-camera tracking system employing several key novel methodologies has previously been comprehensively shown to be highly effective in assisting human users in tracking targets of interest through challenging industry-standard i-LIDS multi-camera data (Raja et al 2011). A prototype system was developed in order to test and evaluate the effectiveness of this approach. In this paper, we develop this system further in order to improve tracking accuracy and to facilitate scalability to arbitrary numbers of camera inputs across much larger distributed spatial areas covering different locations with greater inter-camera distances. Specifically, we describe the following three areas of algorithm and system improvement: (1) dynamic learning mechanisms are deployed to apply user feedback in adapting internal models to improve performance over time; (2) modular design and hardware acceleration techniques are explored for real-time performance, extensive configurability to leverage available hardware and scalability to larger datasets; and (3) re-design of the user interface paradigm for greater effectiveness in user interaction and for working towards practical deployment as a secure asynchronous remote web-based service. We conduct an extensive evaluation of the system in terms of: (1) tracking performance; and (2) the speed of the system in computation and in usage over a network. We use a real-world dataset significantly more challenging than the UK Home Office i-LIDS multi-camera tracking benchmarking dataset. Our new dataset comprises six cameras covering two different London Underground stations. We show that: (1) dynamic learning is effective; (2) the user-assisted paradigm remains effective with this significantly more challenging dataset; (3) large-scale deployment and real-time computation is feasible due to linear scalability; (4) more considered user search strategies and external non-visual information can aid system performance; and (5) storage and querying of meta-data is a bottleneck to be overcome.

8546-28, Session 7

A methodology to evaluate the effect of video compression on the performance of analytics systems

Anastasia Tsifouti, Home Office (United Kingdom); Moustafa M Nasralla, Manzoor Razaak, James Cope, James Orwell, Maria G. Martini, Kingston Univ. (United Kingdom); Kingsley Sage, Home Office (United Kingdom)

The Image Library for Intelligent Detection Systems (i-LIDS) is a public set of video surveillance scenarios: a benchmark to measure the performance of analytics systems. This paper proposes a methodology to investigate the effect of compression and frame-rate reduction on this performance. Furthermore, the investigation makes recommendations for an appropriate suite of degraded datasets (compressed and with reduced frame-rate) to allow developers to test the performance of their systems.

The library consists of six scenarios: Sterile Zone (SZ), Parked Vehicle (PV), Abandoned Baggage (AB), Doorway Surveillance (DS), Multi-Camera tracking (MCT) , and 'New Technologies'. In a previous investigation[1], focused on the Sterile Zone scenario, the results indicate that the performance of an analytics system is significantly affected at 220kbps (with H.264 compression) by increasing missed detections and the alarm response time. The SZ and PV scenarios are investigated using two different compression algorithms (H.264 and JPEG) and a number of detection systems. PV has higher spatio-temporal complexity (e.g. frequent movement of cars) than the SZ. Compression performance is dependent on scene content [2-5], hence PV will require larger bit-streams in comparison with SZ, for any given distortion rate.

There is a wide range of encoding technologies available and the methodology must balance the various relevant factors, such as the extent of adoption in the surveillance industry, the trends and future prospects[6-8], the suitability for inclusion in this type of scientific experiment, the compression performance, and the ease with which interested parties can decode and use the output datasets. In the security industry, video data are compressed either to transmit, or to store. Compression algorithms that comply with industry standards (for transmission) and CCTV (Closed Circuit Television) recorders (for storage) are included in the study. CCTV recorders generally use proprietary formats: it is anticipated that these may significantly affect the visual information, as they perform further processes such as over-sharpening, cropping and resizing[2].

Encoding standards such as H.264 and JPEG use the Discrete Cosine Transform (DCT) technique, which introduces blocking artefacts that become more visible at low bit rates[9-11]. The H.264 compression algorithm follows a hybrid predictive coding approach to achieve high compression gains[12, 13]. In H.264, compression exploits both spatial and temporal redundancy[13], whereas in JPEG only spatial redundancy is exploited. The highly predictive approach of H.264 may introduce more artefacts resulting in a greater effect on the performance of analytics systems (e.g., increase the false alarm rate of analytics) than JPEG.

The paper describes the two main components of the proposed methodology to measure the effect of degradation on analytics performance. The first component is the execution of the standard tests, using the 'f-measure' to evaluate the performance, on a range of degraded video sets. The second component is the characterisation of the datasets, using quantification of scene features, defined using image processing techniques[2, 14, 15]. This characterization permits an analysis of the points of failure introduced by the degradation of the input video signal.

Reference:

1. Mahendrarajah, P. Investigation of the performance of video analytics systems with compressed video using the i-LIDS sterile zone dataset. in Optics and Photonics for Counterterrorism and Crime Fighting VII; Optical Materials in Defence Systems Technology VIII; and Quantum-Physics-based Information Security. 2011. Prague, Czech Republic: SPIE.

2. Tsifouti, A., Recommendations for acceptable compression levels of recording systems on London buses. 2011, Centre for Applied Science and Technology

3. Allen, E., S. Triantaphillidou, and R.E. Jacobson, Image Quality Comparison Between JPEG and JPEG2000. I. Psychophysical Investigation. Journal of Imaging Science and Technology, 2007. 51(3): p. 248-258.

4. Klima, M. and K. Fliegel. Image compression techniques in the field of security technology: examples and discussion. in Security Technology, 2004. 38th Annual 2004 International Carnahan Conference on. 2004.

5. Klima, M. and V. Kloucek. Some remarks on very high-rate image compression and its impact on security image data subjective evaluation. in Security Technology, 2002. Proceedings. 36th Annual 2002 International Carnahan Conference on. 2002.

6. Sira, Research project looking at CCTV imagery format structure Version 1 (documented for the Centre of Applied Science and Technology), Sira Defence and Security Ltd. 2011.

7. ONVIF, ONVIFTM Streaming Specification. 2011, ONVIF Streaming Spec. - Ver. 2.10.

8. MET, Personal Communications with Metropolitan Police. 2012.

9. Wallace, G.K., The JPEG still picture compression standard. Consumer Electronics, IEEE Transactions on, 1992. 38(1): p. xviii-xxxiv.

10. Wiegand, T., et al., Overview of the H.264/AVC video coding standard. Circuits and Systems for Video Technology, IEEE Transactions on, 2003. 13(7): p. 560-576.

11. Kalva, H., The H.264 Video Coding Standard. Multimedia, IEEE, 2006. 13(4): p. 86-90.

12. Sullivan, G.J. and T. Wiegand, Video Compression - From Concepts to the H.264/AVC Standard. Proceedings of the IEEE, 2005. 93(1): p. 18-31.

13. Ghanbari, M., Standard Codecs: Image compression to advanced video coding. 2003: IEE Telecommunications Series 49

14. Triantaphillidou, S., E. Allen, and R.E. Jacobson, Image Quality Comparison Between JPEG and JPEG2000. II. Scene Dependency, Scene Analysis, and Classification. Journal of Imaging Science and Technology, 2007. 51(3): p. 259-270.

15. ITU, Subjective video quality assessment methods for multimedia application, in ITU-R Recommendation P.910. 1999.

8546-29, Session 7

Multisensor data fusion for IED threat detection

Wim Mees, Royal Belgian Military Academy (Belgium); Roel Heremans, Royal Belgian Military Academy (Belgium) and AGT Group (R&D) (Germany)

Improvised explosive devices (IEDs) are becoming an increasingly important threat in modern peace support operations. In order to assist a future vehicle commander in detecting IED threats, a consortium consisting of the Spanish “Grupo Tecnologico e Industrial” (GMV), the Belgian “Royal Military Academy” (RMA), and the German “Deutsches Zentrum fuer Luft- und Raumfahrt” (DLR) and “Technische Universitaet Muenchen” (TUM) has developed in the framework of the European Defense Agency (EDA) Joint Investment Programme Force Protection (JIP-FP) “Surveillance in an Urban environment using Mobile sensors” (SUM) project a prototype system that uses a combination of active and passive sensors to detect threats in the road surface and on the side of the road.

The system combines information from external sources, such as command & control networks and UAV or Satellite image processing, with information that is acquired locally through the on-board sensors. A visual and infrared camera ensure that anomalies on the road surface and on the side of the road are detected during both day and night operations; a radiometer and radar allow the system to distinguish innocent anomalies from potentially dangerous ones.

The combination of slowly evolving external information sources with rapidly evolving on-board data sources requiring a near real-time reaction, was implemented through the use of threat-type specific a priori risk maps.

Because the images have different geometries and are acquired asynchronously and at different sampling frequencies on a moving vehicle, a temporal and spatial fusion between sensors, as well as between successive images from the same sensor, is required. This fusion is performed at the feature level. It requires an accurate registration between the sensors, which was implemented based on a perspective projection model and a local flat road hypothesis.

The fusion furthermore incorporates domain knowledge in the form of a fuzzy expert system. This allows an image interpretation expert to express for each of the considered threat types his knowledge about the expected values for the features that were extracted from the data in each channel using natural language terms. Finally an evidence aggregation mechanism was implemented that is based on the ordered weighted averaging operator and accumulates evidence in an incremental fashion as the information arrives at the fusion engine.

The human operator is an essential element in the decision process. The graphical user interface displays all threats above a certain user-controllable level and projects them on all sensor images so the operator can easily analyze them. As the evidence builds up, the color of the potential threats changes, allowing the operator to focus his attention on those threats for which the system found the most evidence in the data streams from the different sensors, combined with the auxiliary data from the external information sources.

In order to evaluate the performance of the system, a test campaign was organized at a military site in Belgium. In this paper we present the registration between the sensors, the fuzzy expert system and the evidence aggregation, and illustrate these using examples obtained during the measurement campaign.

8546-30, Session 7

Is automated conversion of video to text a reality?

Richard Bowden, Univ. of Surrey (United Kingdom); Stephen J. Cox, Richard W. Harvey, Yuxuan Lan, Univ. of East Anglia Norwich (United Kingdom); Eng-Jon Ong, Univ. of Surrey (United Kingdom); Gari Owen, Annwvyn Solutions (United Kingdom); Barry-John Theobald, Univ. of East Anglia Norwich (United Kingdom)

A recent trend in law enforcement has been the use of Forensic lip-readers. Criminal activities are often recorded on CCTV or other video gathering systems. So, knowledge of what suspects are saying enriches the evidence gathered. But lip-readers, by their own admission, are fallible so, based on long term studies of automated lip-reading, we are investigating the possibilities and limitations of applying this technique under realistic conditions. We have adopted a step-by-step approach and are developing a capability when prior video information is available for the suspect of interest. We use the terminology video-to-text (V2T) for this technique by analogy with speech-to-text (S2T) which also has applications in security and law-enforcement.

8546-31, Session PS

Mid-infrared hyperspectral imaging for the detection of explosive compounds

Keith Ruxton, Gordon Robertson, Bill Miller, Graeme P. A. Malcolm, Gareth T. Maker, M Squared Lasers Ltd. (United Kingdom)

Active hyperspectral imaging is a valuable tool in a wide range of applications. A developing market is the detection and identification of energetic compounds through analysis of the resulting absorption spectrum. This work presents a selection of results from a prototype mid-infrared (MIR) hyperspectral imagining instrument that has successfully been used to for compound detection at a range of standoff distances.

Active hyperspectral imaging utilises a broadly tunable laser source to illuminate the scene with light at a range of wavelengths. While there are a number of illumination methods, this work illuminates the scene by raster scanning the laser beam using a pair of galvanometric mirrors. The resulting backscattered light from the scene is collected by the same mirrors and directed and focussed onto a suitable single-point detector, where the image is constructed pixel by pixel. The imaging instrument that was developed in this work is based around a MIR optical parametric oscillator (OPO) source with broad tunability, operating in the 2.7 μm to 3.5 μm (MIR) and 1.5 μm to 1.7 μm (near IR; NIR) regions. The MIR beam was primarily used as it addressed the fundamental absorption features of the compounds under investigation compared to the 1st overtone features in the NIR region, which can be weaker by more than an order of magnitude. Absorption features are present due to stretch vibrations of the following bonds:

oxygen-hydrogen (O-H), carbon-hydrogen (C-H), nitrogen-hydrogen (N-H) and carbon-nitrogen (C-N).

Due to material handling procedures associated with explosive compounds, experimental work was undertaken initially using simulant compounds. A second set of compounds that was tested alongside the simulant compounds is a range of confusion compounds. By having the broad wavelength tunability of the OPO, extended absorption spectra of the compounds could be obtained to aid in compound identification. The prototype imager instrument has successful been used to record the absorption spectra for a range of compounds from the simulant and confusion sets and current work is now investigating actual explosive compounds. The instrument has a number of integrated data processing algorithms to aid in the enhancement of the constructed images, these include false colour and frame differencing. To aid in the successful construction of the images, the following operating parameters of the imager can be adjusted by the user: wavelength, brightness, contrast, zoom level, receiver gain and receiver gating. Gating of the receiver is an important control as the detector needs to be active only when the backscattered laser pulses are incident on the detector in order to maximise the signal to noise ratio.

The authors see a very promising outlook for the MWIR hyperspectral imager, with a range of improvements planned. From an applications point of view this format of imaging instrument could be used for a range of standoff: improvised explosive device (IED) detection applications and potential incident scene forensic investigation.

8546-32, Session PS

Stand-off detection of traces of explosives and precursors on fabrics by UV Raman spectroscopy

Roberto Chirico, Salvatore Almaviva, Sabina Botti, Luciano Cantarini, Francesco Colao, Luca Fiorani, Marcello Nuvoli, Antonio Palucci, ENEA (Italy)

In the wake of several terroristic attacks in various cities during the last years, there is a need to develop reliable and effective instrumentations able to detect explosives and precursors for homeland security applications. Explosives can be classified as primary or secondary and they can be organic or inorganic molecules. Some type of explosives can be prepared by terrorists from easily obtainable ingredients. Some common military explosives include the nitrate esters such as nitrocellulose (NC), nitroglycerin (NG), ethylene glycol dinitrate (EGDN), and pentaerythritol tetranitrate (PETN); nitroarenes such as trinitrotoluene (TNT), picric acid; and nitramines such as 1,3,5-trinitroperhydro-1,3,5-triazine (RDX). There are also various oxidizer salts that might be used as composite explosives when mixed with suitable fuels such as ammonium nitrate (AN), sodium chlorate [1]. Among the stand-off detection technologies available, Raman spectroscopy has recently gained consents as potential stand-off tool for the detection of explosives due to technical improvements [2]. The challenging requirements to face in the development of such technologies is the capability to have a high sensitivity in the detection of explosive materials at a certain distance and a high selectivity to uniquely identify the substance in a interfering background. Raman spectroscopy measurements have the limitation of a low Raman scattering cross sections and a low signal-to-noise ratio in presence of interfering fluorescence produced by the target sample. This happens because field Raman measurements are commonly performed with green, red, or near-infrared (IR) lasers. Ultraviolet (UV) excitation with a 266 nm laser brings to improvements in the detection of the Raman signal, because the background luminescence in this case is located in a different spectral region with respect to Raman signals that are used for the substance identification. Moreover, for shorter wavelengths in the UV region, the scattering cross section of substances increases [3]. A new instrumentation is under development at the Diagnostics and Metrology Laboratory (ENEA, Frascati) [4, 5], for the stand-off detection of explosives in the frame of the special NATO Science for Peace project STANDEX. The system, labeled RADEX (RAman Detection of EXplosives) due to the implementation of the UV Raman spectroscopy, will be presented. The system was built to detect residues of explosives on fibers taking in consideration of the constraint of a maximum permissible laser exposure (MPE) at the human cornea. The maximum permissible exposure at the human cornea for UV laser and pulse durations from 1 ns to 1 μs is about more than 3 orders of magnitude higher than that one of a laser emitting in the visible or near-infrared (400 nm - 1 μm). The RADEX system is mainly based on three main components as the UV laser transmitter, the sending/receiving optics and the detection electronics.

References

[1] Marshall, M and Oxley, J.C., Elsevier, ISBN:978-0-12-374533-0.

[2] Wallin, S., Pettersoon, A., Östmark, H., Hobro, A., Anal. Bioanal. Chem., 259-274, 395, 2009.

[3] Jander, P., Noll, R., Appl. Spectrosc., 559-563, 63, 2009.

[4] Botti, S., Cantarini, L., Palucci, A., J. Raman Spectrosc., 41, 866-869, 2010.

[5] Lazic, V., Palucci, A., Jovicevic, S., Poggi, C., Buono, E., Spectrochimica Acta Part B 64,1028-1039, 2009.

8546-33, Session PS

Stand-off spectroscopy for the detection of chemical warfare agents

Rhea Clewes, Chris R. Howle, Defence Science and Technology Lab. (United Kingdom); David J. M. Stothard, Malcolm H. Dunn, Univ. of St. Andrews (United Kingdom); Gordon Robertson, William Miller, Graeme P. A. Malcolm, Gareth T. Maker, M Squared Lasers Ltd. (United Kingdom); Rick Cox, Brad Williams, Matt Russell, DeltaNu, Inc. (United States)

The most desirable configuration for detection of toxic chemicals utilises the optimum distance between detector and hazard. This approach ensures that no contamination of equipment or personnel occurs. Where the target chemical is an involatile liquid, indirect detection of the liquid contamination is precluded by inherently low vapour pressure. Direct detection of the chemical hazard is the only viable approach. Recent technology developments have allowed spectroscopic systems to provide multiple options for the stand-off detection of involatile CWAs. Two different stand-off spectroscopic systems, based upon IR absorption and Raman spectroscopic techniques, which are able to detect liquid CWAs at distance are described here. The Negative Contrast Imager (NCI) from M Squared lasers is based on an optical parametric oscillator (OPO) source comprising a Q-switched intracavity MgO:PPLN crystal. This crystal has a fanned grating design and wavelength tuning is achieved by translating the PPLN crystal within the 1064nm pump beam. This approach enables the production of shortwave and midwave IR (1.5 - 1.8 μm and 2.6 up to 3.8 μm, respectively) radiation, which is scanned across the scene of interest. Target materials that have an absorption feature commensurate with the wavelength of incoming radiation reduce the intensity of returned signal, resulting in dark pixels in the acquired image. This method enables location and classification of the target material. Stand-off Raman spectroscopy allows target chemicals to be identified at range through comparison of the acquired signature relative to a spectral database. In this work, we used a Raman system based upon a 1047nm Nd:YLF laser source and a proprietary InGaAsP camera system. Utilisation of a longer excitation wavelength than most conventional stand-off detection systems (e.g. 532 nm) enables reduction of fluorescence from surface deposited chemicals, thereby revealing the Raman spectrum. NCI and Raman spectroscopy are able to detect CWA on surfaces at distances of 5 - 10 metres and have potential to detect over longer ranges.

8546-34, Session PS

TATP stand-off detection with open path: FTIR techniques

Christian Fischer, Tobias Pohl, Konradin Weber, Andreas Vogel, Günther van Haren, Fachhochschule Düsseldorf (Germany); Wenka Schweikert, Fraunhofer-Institut für Chemische Technologie (Germany)

TATP is a very easy to synthesize, sensitive and high volatile explosive with great absorption in the IR Spectra. In this project we detect TATP gas traces with open path FTIR - techniques. The poster shows some selected results of the continued research.

The first step was to construct and build a heatable multi-reflection cell with adjustable optical path length and a heatable intake to evaporate solid TATP samples. In this cell reference TATP - spectra were taken under controlled conditions with an OPAG 33 system.

The next step was to find out how the TATP gas will be diluted in the ambient air and validate some physical properties which are described inconsistently in literature e.g. evaporation rates.

In a further step of the project we constructed a special double - T shaped chamber with stabile air conditions. In this chamber the dispersion kinetics of the TATP vapour could be tested. It turned out that the TATP vapours has the tendency to sink down. Therefore the highest TATP - concentrations were measured below the TATP sample.

Successful measurements were taken in ambient air and will be continued with different system configurations of the OPAG 33 to lower the detection limit.

8546-35, Session PS

Exploiting high resolution Fourier Transform spectroscopy to inform the development of quantum cascade laser based explosives detection systems

Felicity Carlysle, Niamh Nic Daeid, Univ. of Strathclyde (United Kingdom); Erwan L. Normand, Michael T. McCulloch, Cascade Technologies Ltd. (United Kingdom)

The ongoing threat of terrorism around the world has resulted in the rapid development of systems capable of detecting concealed explosive devices. As the terrorist threat evolves, so must the systems designed to detect them. A successful detection system needs to fulfil several criteria, some dependent upon the situation where the system will be used, but all systems must be accurate and sensitive.

In order for a system to successfully detect explosive compounds and their precursors, these compounds must first be characterised in order to determine which identifying features of the compound can be targeted by the system.

One area of significant expansion within the explosives detection arena is that of laser based trace gas detection, particularly in the infrared region. Within that spectral range the use of high resolution Fourier Transform spectroscopy enables the fingerprint characterisation of materials that could be incorporated into improvised or home-made explosives devices and hence the development of suitable spectral databases to be used by laser based trace gas sensors. The range of wavelengths covered by a single scan allows a significant amount of information to be gathered about the interaction of a material with infrared radiation, and the variations in how different materials interact can then be used to identify individual characteristics. Similar approaches are already exploited in several other areas of forensic science such as the use of gas chromatographs or mass spectrometers for the identification of unknown compounds via established databases. Fourier transform spectroscopy can be carried out on all materials regardless of their phase, and this is significant as potential explosives and their precursors cover a wide range of compounds. The most significant feature of high resolution Fourier Transform spectroscopy is the resolving power. The ability to produce high resolution spectra allows for the minutiae of each spectrum to be examined. This is vital when selecting targets for laser detection as currently available lasers have a narrow wavenumber span and therefore the target must be a narrow absorption peak or feature rather than the more obvious broad peaks visible at lower resolution in order for detection with a quantum cascade laser to be successful. The information generated through this project directly supports the development of quantum cascade laser based airport security systems and also has implications for the wider explosives detection community as well as the potential to inform other forensic science disciplines.

In order to utilise Fourier Transform spectroscopy to its full potential the initial focus of this project has been the development of a suitable protocols for the analysis of liquid and solid samples, so as to produce suitable infrared spectra for a wide variety of compounds. In addition to this significant attention has been given to determining the best way to analysed the data produced. The data presented describes this development process, and discusses the results obtained from the initial analysis of several compounds of interest.

Conference 8547: High-Power Lasers: Technology and Systems

Monday - Wednesday 24–26 September 2012 • Part of Proceedings of SPIE Vol. 8547
High-Power Lasers 2012: Technology and Systems

8547-1, Session 1

Directed energy: a service perspective *(Keynote Presentation)*

David Robie, U.S. Air Force (United States)

No Abstract Available

8547-2, Session 1

HEL: Joint Technology Office *(Invited Paper)*

Mark W. Neice, High Energy Laser Joint Technology Office (United States)

No Abstract Available

8547-3, Session 2

Overview of the Laser activities at Rheinmetall Waffe Munition *(Invited Paper)*

Markus Jung, Klaus Ludewigt, Thomas Riesbeck, Rheinmetall Waffe Munition GmbH (Germany); Thomas Schreiber, Ramona Eberhardt, Andreas Tünnermann, Fraunhofer-Institut für Angewandte Optik und Feinmechanik (Germany)

The paper will give an overview over the laser weapon activities at Rheinmetall Waffe Munition over the last years. Starting from the actual scenarios for laser weapon applications as: CRAM (Counter Rocket Artillery Mortar), Air Defence and unexploded ordnance (UXO) clearing, the basic requirements for: beam diameter, beam quality, tracking capability, adaptive optics of a future laser weapon where deduced.

For the UXO scenario a mobile directed energy laser demonstrator for humanitarian mine and UXO clearing based on fiber lasers will be presented. Based on the parameters the system concept including the cooling system, power supply and the integration into the armoured vehicle TM 170 will be explained. The contribution will also show first experiments of UXO and IED clearing.

Different technical approaches to achieve laser power in the 100 kW range combined with very good beam quality to fulfil the requirements of the CRAM and Air Defence scenario the will be discussed. In detail the technology of spectral coupling and the beam superimposing both investigated by Rheinmetall Waffe Munition will be discussed.

At the spectral coupling the basic technology parameters for the fiber laser and the dielectric grating as the latest results were put into context with the power levels reached at other groups.

For the beam super imposing technology the basic experiments regarding the tracking capability and compensation of the atmosphere on the test range at Unterlüß will be explained.

After the introduction of the of the generic 10 kW Laser Weapon Demonstrator based on 2 Laser Weapon Modules from RWM each 5 kW fiber Laser with beam forming and tracking integrate by the RWM and RAD team into a Ground based Air Defend system from Rheinmetall Air Defence consisting of Skyguard the test setup of the Air Defence scenario will be presented.

The flight path of the UAV within the valley of the life firing range at Ochsenboden Switzerland will be shown. Selected results of the successful tests against UAV's, showing the capability of the generic 10 kW Laser Weapon Demonstrator from detection to tracking up to destroying the target will be demonstrated.

From these results the next steps of Rheinmetall Waffe Munition for a 100 kW class laser weapon will be explained.

8547-4, Session 2

US Navy LaWS System Overview, Historical Retrospective and Future Directions *(Invited Paper)*

Robert J. Pawlak, Naval Surface Warfare Ctr. Dahlgren Div. (United States)

The LaWS testbed has been a demonstrator of a number of High Energy Laser (HEL)-related technologies for the Navy. The LaWS system employs a shared aperture design with incoherent beam combining and makes extensive use of Commercial Off-The-Shelf (COTS) technologies in the areas of inertial sensing, fiber lasers, sensors and video trackers. Now that the system has demonstrated the art of the possible with COTS elements, it is useful to examine where performance can be increased with the greatest possible effect, as well as which modifications are necessary to support better integration with ship's systems. A review of past test events, architectures, and future plans will be given, along with an emphasis on how the LaWS system has evolved and will be evolving over this time, in line with the Navy's strategy for fielding a HEL weapon.

8547-5, Session 2

Robust Electric Laser Initiative *(Invited Paper)*

Robert S. Afzal, Lockheed Martin Aculight (United States)

No Abstract Available

8547-6, Session 2

US Army's high energy laser demonstrations for counter-rocket, artillery, mortar and missile and unmanned Ariel Systems defeat applications *(Invited Paper)*

Kip R. Kendrick, U.S. Army Space and Missile Defense Command (United States)

No Abstract Available

8547-7, Session 2

High-power beam combining - a step to a future laser weapon system *(Invited Paper)*

Rudolf Protz, Jürgen Zoz, Franz Geidek, Stephan Dietrich, MBDA Germany (Germany); Michael Fall, MBDA Germany (Germany) and MBDA Germany (Germany)

Due to the enormous progress in the field of high-power fiber lasers during the last years, commercial industrial fiber lasers are now available, which deliver a near-diffraction limited beam with power levels up to10kW. For the realization of a future laser weapon system, which can be used for Counter-RAM or similar air defense applications, a laser source possessing a beam power at the level of 100kW or more is required.

At MBDA/LFK, the concept for a high-energy laser weapon system is investigated, which is based on such existing industrial laser sources, as they are mentioned before. A number of individual high-power fiber laser beams are combined together, using one common beam director telescope. By this ‛geometric‛ beam coupling scheme, a total laser beam power sufficient for an operational laser weapon system can be achieved. The individual beams from the different lasers are steered by servo-loops, using fast tip-tilt mirrors.

This principle enables the concentration of the total laser beam

power at the common focal point on a distant target, also allowing fine tracking of target movements and first order compensation of turbulence effects on laser beam propagation. The proposed beam combination concept was demonstrated using several experimental set-ups. A number of experiments were performed to investigate laser beam target interaction and target fine tracking, also at large distances. Content and results of these investigations are reported. It can be concluded, that high-power beam combining may be an important step for the realization of a laser weapon system in the near future.

8547-8, Session 3

Diode-pumped alkali laser-bleached wave dynamics *(Invited Paper)*

Glen P Perram, Air Force Institute of Technology (United States)

A three level analytic model for optically pumped alkali metal vapor lasers is developed by considering the steady state rate equations for the longitudinally averaged number densities of the ground 2S 1/2 and first excited 2P3/2, and 2P1/2 states. The threshold pump intensity includes both the requirements to fully bleach the pump transition and exceed optical losses, typically about 200 Watts/cm2. Slope efficiency depends critically on the fraction of incident photons absorbed.. For efficient operation, the collisional relaxation between the two upper levels should be fast to prevent bottle-necking. By assuming a statistical distribution between the upper two levels, the limiting analytic solution for the quasi-two level system is achieved. For properly designed gain conditions, the quasi two level solution is usually achievable and represents ideal performance.

The model is anchored to several recent laser demonstrations. A rubidium laser pumped on the 5 2S1/2 - 5 2P3/2 D2 transition by a pulsed dye laser at pump intensities exceeding 3.5 MW/cm2 (> 1000 times threshold) has been demonstrated. Output energies as high as 12 μJ/pulse are limited by the rate for collision relaxation of the pumped 2P3/2 state to the upper laser 2P1/2 state. More than 250 photons are available for every rubidium atom in the pumped volume during each pulse. For modest alkali atom and ethane spin-orbit relaxer concentrations, the gain medium can only process about 50 photons/atom during the 2 - 8 ns pump pulse. At 110o C and 550 Torr of ethane, the system is bottlenecked in the 2P3/2 state and all of the incident photons cannot be absorbed. The output energy is linearly dependent on pump pulse duration for a given pump energy. The highly saturated pump limit of the recently developed three-level model for Diode Pumped Alkali Lasers (DPAL) is developed. The system efficiency based on absorbed photons approaches 36% even for these extreme pump conditions. Furthermore, at 320°C with 2500 torr of helium, a pulsed potassium laser with 1.15 MW/cm2 peak intensity and 9.3% slope efficiency has been demonstrated.

Localized heating in diode-pumped alkali lasers induces spatial variations in metal vapor density, leading to a reduction in laser power. A corresponding reduction in pump absorbance directly impacts output power. Here, we describe work showing that pump-beam heating induces a radial distribution of absorbance and establishes a significant temperature rise within the pumped volume.

8547-9, Session 3

Determination of low pressure broadening and shift rates for K, Rb, and Cs collisions with rare gases from Anderson Tallman theory

Gordon D. Hager, Matthew D Rotondaro, Glen P. Perram, Air Force Institute of Technology (United States)

In this paper we describe a mathematical method to determine the low pressure, impact limit, shift and broadening rates of the Alkali D1 and D2 transitions for collisions with the rare gases using theoretically computed interaction potentials. The method is based on the Anderson Tallman unified theory of pressure broadening, (1956), in which the line shape, (i.e. spectrum), is determined from the Fourier transform of the auto-correlation function. The auto-correlation function is computed from the interaction difference potential. The diatomic potential surface's that arise for collisions between the alkali metal in its ground state and first excited P states and a closed shell rare gas atom have the following designations. The ground state is designated X1/2 and correlates with the 2S1/2 atomic ground state of the Alkali atom. The A1/2 molecular state correlates with the excited 2P1/2 spin orbit state of the alkali atom. The A3/2 and B1/2 molecular states correlate with the four fold degenerate 2P3/2 spin orbit state of the alkali atom. In the short wavelength region these four potential surfaces give rise to three difference potentials that correlate to the zero pressure unperturbed free atom 2S - 2P D1 and D2 transitions. The procedure for finding the shift and broadening rates is to first fit the potential surfaces to power series. The constants c6 and c8 are determined from experimentally measured values of the dipole and quadrupole polarizability of the rare gas atom. These terms insure that the potential contains the theoretically predicted long range attractive behavior. For long correlation times, (corresponding to the impact limit), the real and imaginary parts of the correlation function are linear functions of the correlation time. The Fourier transform of these linear functions gives the familiar shifted Lorentzian line shape. If the line intercepts are not zero a dispersion like asymmetry at higher pressures is predicted. The slopes of these linear functions give the shift Δ and the width Γ FWHM.

8547-10, Session 4

High-power thin disk lasers *(Invited Paper)*

Adolf Giesen, Deutsches Zentrum für Luft- und Raumfahrt e.V. (Germany)

No Abstract Available

8547-11, Session 4

Recent disk laser developments at Trumpf *(Invited Paper)*

Tina Gottwald, Dominik Bauer, Alexander Killi, Jochen D. Kleinbauer, Vincent Kuhn, Sven Schad, Christian Stolzenburg, Dirk H. Sutter, TRUMPF Laser GmbH & Co. KG (Germany); Thomas Metzger, TRUMPF Scientific Lasers GmbH + Co. KG (Germany)

Recent developments towards power levels in the range of 10 kW infrared cw power per disk with optical-to-optical efficiencies of 65% are presented. The key development for the new product generation of Trumpf disk lasers, a cavity with 44-passes of the pump beam, is introduced.

In the disk laser resonator, a disk that is pumped at its endface and cooled from its back side is used as the active medium. The main advantage of this geometry is a nearly one-dimensional temperature gradient in the active medium. Therefore, effects of thermal lensing and phase distortions are minimized, allowing for high beam qualities. On the other hand, the absorption of the pump light is small. This disadvantage can be overcome by many passages of the pump beam through the active medium. High pump absorption is achieved by constructing a cavity consisting of a parabolic mirror and a number of prisms that image the pump beam multiple times to the disk.

Current state-of-the-art is a cavity with 24 passes of the pump light through the disk. In this contribution, a new cavity with 44 passes is presented. The purpose of the development is to increase the percentage of pump power absorbed in the crystal and with it the optical-to-optical efficiency of the laser. The cavity was designed employing extensive simulation and optimization studies which resulted in a non-telecentric imaging characteristic of the cavity. The 44-pass cavity is suitable for use in different resonator types with varying pump spot sizes and output beam quality.

By increasing the percentage of absorbed pump power from about 75% to 90%, the optical-to-optical efficiency of the laser can be increased by typically seven percentage points to values of above 65%. In this way, continuous wave power levels of 6kW per disk have been achieved in an industrial product. In an experimental setup with one disk, 10 kW, the highest power published for disk lasers, could be demonstrated.

Furthermore, the latest experimental results for disk lasers in pulsed operation are presented. More than 800W of nanosecond pulses have been achieved both at the fundamental wavelength of 1030nm as well as in frequency doubled operation at 515nm. Fundamental mode picoseconds disk lasers provide average power levels of 100W at 1030nm and 60W at 515nm. Mode locked disk oscillators provide by far the highest average power of any unamplified ultrafast lasers. Average power levels well above 100W have been achieved in

laboratory setups. Finally, perspectives for disk lasers in the field of extreme light, aiming for peak powers of petawatts and beyond, are discussed.

8547-12, Session 4

Thin disk laser work at Boeing *(Invited Paper)*

Michael Rinn, Matthew D. Nixon, Boeing-SVS, Inc. (United States)

No Abstract Available

8547-13, Session 4

Thin disk laser in the 2um wavelength range

Günther Renz, Jochen Speiser, Adolf Giesen, Deutsches Zentrum für Luft- und Raumfahrt e.V. (Germany)

The thin disk laser is a successful concept for high output power and/or high pulse energy, high efficiency and good beam quality in the 1 µm range. Holmium-doped materials are a promising approach to transform this success to the 2 ?m range. Ho:YAG is especially interesting for high pulse energies due to the long fluorescence lifetime (~ 8 ms) which provides good energy storage capabilities. We have realized a Ho:YAG thin-disk laser with a cw output power of 15 W at 2.09 ?m and a maximum optical-to-optical efficiency of 37%. The laser was pumped with a Tm-fiber laser. Numerical simulations of the Ho:YAG thin disk laser show the potential for further scaling. As broadly tunable alternative, also a Cr:ZnSe thin disk laser was investigated. A Tm-fiber laser and a fiber coupled diode stack were tested as pump sources. A laser power of 3.5 W was achieved with diode pumping.

8547-14, Session 5

Efficient broadband OPCPA *(Invited Paper)*

Czeslaw Radzewicz, Univ. of Warsaw (Poland)

No Abstract Available

8547-15, Session 5

Triggering and guiding electric discharge by a train of ultrashort UV pulses and a long UV pulse emitted by a hybrid Ti:Sapphire-KrF laser facility *(Invited Paper)*

Andrey A. Ionin, Sergej I. Kudryashov, Alexey O. Levchenko, Leonid V. Seleznev, Aleksey Shutov, Dmitry V. Sinitsyn, Igor V. Smetanin, Nikolai N. Ustinovskii, Vladimir D. Zvorykin, P.N. Lebedev Physical Institute (Russian Federation)

Non-self-sustained electric discharge and electric breakdown were triggered and guided by a train of ultrashort sub-TW UV pulses overlapped with a long (~100ns) free-running UV pulse of a hybrid Ti:Sapphire-KrF laser facility. Photocurrent sustained by this train is two orders of magnitude higher, and electric breakdown distance is twice longer than those for the discharge triggered by the long UV pulse only.

8547-16, Session 5

Experimental Component of the AFOSR-Supported MURI Program on Ultrafast Laser Filamentation in Transparent Dielectric Media *(Invited Paper)*

Pavel G Polynkin, College of Optical Sciences, The Univ. of Arizona (United States)

I will give an overview of the research under the US Air Force-supported Multi-University Research Initiative (MURI) on femtosecond laser filamentation in transparent media. This interdisciplinary program brings together established research teams from six US universities. The focus of the program is on the development of a fundamental understanding of all physical processes involved in the propagation of ultraintense femtosecond laser pulses through the atmosphere. The main on-going directions of the experimental component of this program include control of filamentation through laser beam and pulse shaping, studies of complex filament interactions, and the exploration of novel applications of laser filaments in air and other media. I will specifically discuss recent experiments on self-focusing dynamics and filamentation of ultraintense femtosecond optical vortex beams in air. These beams are of interest because they are good candidates for the generation of extended bottle-like distributions of plasma filaments in the atmosphere which can be used for guiding microwave radiation. Our results show that the azimuthal modulation instability breaks vortex intensity rings into filaments, the number of which grows with the input laser power. The entire filament pattern rotates on propagation at a rate consistent with the orbital momentum conservation.

8547-17, Session 5

Power Scaling of High-Power Optically-Pumped Semiconductor Lasers for Continuous Wave and Ultrashort Pulse Generation

Alexandre Laurain, Maik Scheller, Tsuei-Lian Wang, College of Optical Sciences, The Univ. of Arizona (United States); Jörg Hader, College of Optical Sciences, The Univ. of Arizona (United States) and Nonlinear Control Strategies, Inc. (United States); Jerome V. Moloney, College of Optical Sciences, The Univ. of Arizona (United States); Stephan W. Koch, Philipps-Univ. Marburg (Germany) and College of Optical Sciences, The Univ. of Arizona (United States) and Nonlinear Control Strategies, Inc. (United States); Bernd Heinen, Martin Koch, Bernardette Kunert, Wolfgang Stolz, Philipps-Univ. Marburg (Germany)

Despite many decades of research and development, high-power tens of Watt to kilowatt class semiconductor lasers manifest themselves as low brightness (incoherent) diode bars emitting highly divergent beams of very poor beam quality. Parallel developments in doped crystal high-power solid state lasers have shown much greater promise in delivering high-brightness beams. In the latter case, the above mentioned diode bars are typically utilized as optical pumps and require thermal control to confine the pump wavelength within a relatively narrow doped glass characteristic absorption peak. The more recent development of OPSLs, semiconductor disk lasers pumped by incoherent diode bars, has led to the promise of developing a whole new generation of high-power, high-brightness all-semiconductor laser sources that have the added advantage of versatility in operating wavelength. Furthermore there are no real constraints on the pump wavelength because of extremely broad barrier state absorption.

Thermal management plays a critical role in high-power optically-pumped VECSEL design and typically there are two approaches: 1) Conventional growth of a top emitter structure where the high reflectivity Bragg mirror is first grown on a GaAs substrate followed by the multiple quantum wells resonant-periodic gain 2) Upside down (bottom emitter) growth where the RPG active structure is grown first on the GaAs substrate followed by the DBR. The latter growth modality requires additional processing of the chip and may appear to be unnecessarily complicated. To date however, bottom emitters have far outperformed top emitters in terms of raw power. In both cases, heat extraction from the hot active region of the chip is critical and the thermal management strategy involves combining a high thermal conductivity diamond heats spreader with a Cu-based heat sink. In the top emitter geometry, the heat spreading is achieved by either capillary-bonding or directly contacting a single crystal diamond heat spreader to the active RPG structure. Logically this should offer the best heat extraction as the heat spreading element is in direct contact with the hottest region of the chip - however, all evidence points to relatively poor contacting and consequently a high thermal impedance pathway. Bottom emitters on the other hand are first bonded to a poorer quality nontransparent CVD diamond heat spreader and the latter is bonded directly to the heat sink. Consequently there is a

longer heat extraction pathway through the DBR but a large heat sinking volume.

We will report on our research in power scaling OPLs around 1μm to exceed 100W per chip by combining a rigorous quantum design of an optimized MQW epitaxial structure, highly accurate and reproducible wafer growth and an efficient thermal management strategy. Recently we have utilized these state-of-the-art optimized OPSL chips to achieve a new record for a mode-locked OPSL with an intra-cavity SESAM. The average output power of the laser in the optimum operation point of mode-locked operation was 3.4W while being pumped with 24W of net pump power. This corresponds to a pulse energy of 7.5nJ and a pulse peak power of 13.3kW. Both are record values for a semiconductor laser operation in the femtosecond regime.

8547-18, Session 6

All-solid photonic bandgap fibers for high power lasers *(Invited Paper)*

Liang Dong, Clemson Univ. Research Foundation (United States); Kunimasa Saitoh, Hokkaido Univ. (Japan); Fanting Kong, Paul Foy, Clemson Univ. Research Foundation (United States); Thomas Hawkins, Clemson Univ. (United States); Devon McClane, Guancheng Gu, Clemson Univ. Research Foundation (United States)

Despite the significant progress in high-power fiber lasers in recent years, there are still strong needs for further power scaling. In one hand, this is driven by industrial material processing, where high yields and ability to machine difficult materials are still much desired. On another hand, the significant needs in defense are still to be met. The fundamental solution for power scaling in fiber lasers is to scale mode areas in fibers to overcome their nonlinear limits while maintaining sufficient single-mode operation. Recently, there are strong evidences that mode instability at high powers can be initiated by very small amount of higher order modes. This requires fibers to have a very strong ability to suppress all higher order mode propagations. After many years of research, fibers with core diameters >40um, capable of single-mode operation and being deployed in coils, essential for high average power fiber lasers using long fiber lengths, are still not yet available.

We have been focusing our efforts on all-glass approaches which can be spliced in an all-fiber laser. We have recently demonstrated single-mode operation in all-solid photonic bandgap fibers with core diameter of ~50um for the first time. These fibers can be spliced and used as conventional fibers. They are compatible with double-clad designs, can be made into PM fibers and can be coiled. Overall, they satisfy all the requirements of a deployable solution in a tough environments and high average power applications in all-fiber configurations. Furthermore, our theoretical study shows it has the highest level of higher order mode suppressions of all known fiber solutions. In an all solid Photonic bandgap fiber, modes are guided due to anti-resonance of cladding photonic crystal lattice. This provides great potential for creating designs that support only the fundamental mode, i.e. selective mode guidance versus selective elimination of mode guidance as in some other approaches. The robust optical guidance and physical constructs of all-solid PBFs enable them to be made and used much like conventional fibers. Transmission can be made with strong wavelength-dependence in these fibers for use in SRS suppression, accomplished by introducing strong loss at the Raman Stoke wavelength, in FWM suppression by providing appropriate dispersion, and in lasers at wavelengths normally dominated by much stronger transitions.

In this paper, we will report for the first time our detailed theoretical study using finite element modeling, showing the extent of higher-order-mode suppression that are possible in these fibers. In some large-core designs, high order mode losses can be well over four orders of magnitudes over that of the fundamental mode. These theoretical studies have also shown the potentials for significant mode area scaling beyond 50um core diameter for coiled all-solid photonic bandgap fibers. We will also report our recent experimental results in fabrication and characterization of large-core all-solid photonic bandgap fibers with core diameter >50um, showing that these fibers can be manufactured with adequate levels of control to ensure the desired optical performance.

8547-19, Session 6

Single crystal fibers for high power lasers *(Invited Paper)*

Jasbinder S. Sanghera, Woohong Kim, U.S. Naval Research Lab. (United States); Catalin Florea, Sotera Defense Solutions, Inc. (United States); L. Brandon Shaw, Steven R. Bowman, Shawn P. O'Connor, Shyam S. Bayya, Guillermo R. Villalobos, Colin Baker, Daniel J. Gibson, U.S. Naval Research Lab. (United States); Ishwar Aggarwal, Sotera Defense Solutions, Inc. (United States)

In this paper, we present our recent results in developing cladded-single crystal fibers for high power single frequency fiber lasers significantly exceeding the capabilities of existing silica fiber based lasers. This fiber laser would not only exploit the advantages of crystals, namely their high temperature stability, high thermal conductivity, superior environmental ruggedness, high propensity for rare earth ion doping and low nonlinearity, but will also provide the benefits from an optical fiber geometry to enable better thermal management thereby enabling the potential for high laser power output in short lengths. Single crystal fiber cores with diameters as small as 35m have been drawn using high purity rare earth doped ceramic or single crystal feed rods by Laser Heated Pedestal Growth (LHPG) process. The mechanical, optical and morphological properties of these fibers have been characterized. The fibers are very flexible and show good overall uniformity. Spectral transmission through the doped crystal fibers has been measured for the first time. We also measured the optical loss as well as the non-radiative loss of the doped crystal fibers and the results show that the fibers have excellent optical and morphological quality. The gain coefficient of the crystal fiber matches the low quantum defect laser model and it is a good indication of the high quality of the fibers. We also discuss various approaches for applying a cladding to the fiber core.

8547-20, Session 6

High power all-fiber isolator *(Invited Paper)*

Shibin Jiang, AdValue Photonics, Inc. (United States)

High power fiber lasers have made significant progress in last several years. Ten kW of output power has been demonstrated, which enables a wide range of new applications from laser welding, laser cutting, and laser drilling to military defense. For the moment, free-space fiber pigtailed isolators have to be used, which is unsatisfactory because such systems require fiber termination, lens alignment, and re-coupling the laser to fiber.

We developed an all-fiber isolator using our proprietary highly Tb-doped optical fiber with high Verdet constant as Faraday rotator, which is fusion spliced together with fiber based polarizer. All-fiber isolator using Tb-doped Faraday rotating fiber was demonstrated, and a prototype was developed and tested. This presentation will describe the Tb-doped Faraday rotating fiber, fusion splicing, and test results of this all-fiber isolator.

8547-21, Session 6

Single-mode, high-power, narrow-linewidth, lightweight fiber amplifiers

John Edgecumbe, Kevin F. Farley, Josh Galipeau, David Björk, David Hosmer, Chih-Hao Wang, Kanxian Wei, Imtiaz Majid, Scott Christensen, Nufern (United States)

Nufern is currently producing custom kW-level fiber amplifiers for the military that deliver 1-2 kW output power with single mode beam quality and operate with narrow linewidths as required for the various beam combining schemes (coherent and spectral) currently under investigation in many DoD programs. These systems are designed for use in cases where near-perfect beam quality is needed, such as long propagation distances, or when a beam combination system is needed. Recent packaging improvements made possible through DARPA funding have achieved the low specific weight (5 kg/kW) and compact size needed to mount a ~25 kW system in a small airborne vehicle or a man-portable lower-power system. Coherently combinable single-mode fiber-based systems can provide overall laser efficiencies greater than 35 percent, while maintaining near-diffraction-

limited beam quality. Here we provide an overview of the systems in production.

8547-22, Session 7

Coherent combination of high-power fiber amplified femtosecond pulses *(Invited Paper)*

Jens Limpert, Friedrich-Schiller-Univ. Jena (Germany)

No Abstract Available

8547-23, Session 7

New design for passive coherent coupling of fiber lasers *(Invited Paper)*

David Sabourdy, CILAS (France); Jean E. Montagne, XLIM Institut de Recherche (France); François Jeux, XLIM Institut de Recherche (France) and Astrium (France); Agnes Desfarges-Berthelemot, Vincent Kermène, Alain Barthélémy, XLIM Institut de Recherche (France)

Passive techniques for coherent coupling of lasers offer an appealing way for the generation of high brightness laser beam because of their simplicity and their all-optical operation. Many configurations have been investigated which yield coherent summation of the optical power available from separate fiber amplifiers. An array of fiber amplifiers inserted in a common laser cavity and delivering an array of phase-locked beams appears most of time as the best suited to high power operation. It was quickly evidenced however that passive coherent coupling became less efficient as the size of the laser array increased. This is the reason why research in that field focused on some way to overcome the threshold size of about 10 lasers for an efficient coherent coupling. All the different published approaches (phase conjugation, coupled cavity) involved an optical nonlinearity. In that context we proposed and investigated a new cavity design featuring unidirectional ring geometry combined with a specific spatial filter. The nonlinearity considered here is due to the contribution of the population inversion (the gain) to the optical phase in the amplifiers. The gain-dependent refractive index change is significantly larger than the non resonant Kerr non linearity of silica in fiber amplifiers. It is usually assumed that the nonlinear phase shift evolves linearly with the gain (Kramers-Krönig relationships). We have carried out experiments using an Ytterbium doped fiber amplifier which confirm an almost linear relationship whatever the pump level. Then the basic idea behind our new cavity design is the following. Self-organization of the laser in standard design only relies on the selection of the lowest loss mode after iterative linear filtering. With a great number of lasers assumed to be of different length (with uncontrolled variations induced by the environment) longitudinal modes actually common to all the cavity arms no longer exist. The laser beams are no more perfectly in phase and phase deviations are observed in the array outputs. We suggested transforming the phase deviations into power deviations so that the gain can vary from one channel to another. Therefore a gain-dependent phase introduced during amplification can compensate for the linear phase delay between the different laser fields. In one implementation of that principle we proposed to use the set-up of phase-contrast microscopy due to Zernike. A simple phase plate inserted in the far field performs the phase to amplitude conversion. To assess the potential of the new scheme we have used numerical simulations of the laser operation. Our model takes into account the linear properties of the cavity as well as the gain bandwidth, saturation, and added phase in each amplifier. Starting from noise it reproduces the laser modes build-up until steady state giving the final laser frequencies and spatial pattern. Numerical results that will be reported at the conference show a gain in efficiency offered by the investigated configuration by comparison with previous schemes. Preliminary experiments are under way to confirm the theoretical expectations.

8547-24, Session 7

Monolithic eye-safer photonic crystal fiber lasers and amplifiers *(Invited Paper)*

Chad G. Carlson, Benjamin G. Ward, U.S. Air Force Academy (United States); Donald L. Sipes Jr., Jason D. Tafoya, Optical Engines, Inc. (United States)

We report on the performance of monolithic, polarization maintaining, Er-doped photonic crystal fibers (PCF) and amplifiers operating in the eye-safer wavelength regime from 1.55-1.6 um. Such eye-safer lasers are desirable for minimizing scatter related ocular injuries in directed energy applications due to their higher damage threshold in the eye relative to 1 um wavelengths. Photonic crystal fibers (PCFs) provide flexibility for fiber designs with very large mode areas, high cladding numerical aperture, bend insensitivity, mitigation of nonlinearities, and robust single mode operation. Recently, we have been developing Er-doped photonic crystal fibers with large mode areas for coherent beam combining applications. Coherently combined PCF laser arrays are a possible avenue of power scaling of eye-safer laser sources for tactical and remote sensing applications. State of the art finite element software has been developed at the US Air Force Academy for simulating the electromagnetic and acoustic modes in PCFs, and the effect of bending and induced stress on such modes. This work describes progress at the US Air Force Academy in simulating and fabricating very large mode area, erbium-doped PCFs and their related components for monolithic PCF lasers and amplifiers. In partner with NKT Photonics, we have developed a 40 um, 0.025 NA core, 200 um, 0.6 NA air-clad pump cladding Er-doped PCF which provides single transverse mode operation in the 1.5-1.6 um operating regime. The PCF has a 30 um mode field diameter at 1.55 um and a modest pump absorption of 0.6 dB/m at 1530 nm. As part of this effort, we have developed novel 6x1+1 pump/signal combiners for air-clad photonic crystal fibers with six 0.22 NA, 200/220 um pump input fibers and a 25/250 PM signal fiber that allow efficient pump and signal coupling to the air-clad Er-doped PCF. These etched air taper combiners have been demonstrated at the kilowatt level under 976 nm pumping and perform an efficient brightness transformation from 0.19 NA, 1532 nm fiber coupled diode pumps into the 0.6 NA air-clad Er-doped PCF with a measured pump throughput efficiency of 88-92% and a signal throughput of 65-70% with a PER of >18 dB. These novel combiners have been efficiently spliced to 40 um core, 200 um pump cladding Er-doped PCFs providing high efficiency resonantly pumped, monolithic, eye-safer PCF fiber lasers and amplifiers. Using grating stabilized 1532 nm pump diodes, our current experiments have demonstrated single transverse mode operation of both monolithic eye-safer PCF lasers and amplifiers at the multi-Watt level with slope efficiencies of over 55%. The power scaling of these devices and their use in coherently combined arrays will be discussed.

8547-25, Session 7

Spectral and coherent combining of fiber lasers by multiplexed volume Bragg gratings

Leonid B. Glebov, Apurva Jain, George B. Venus, Ivan B. Divliansky, Vadim Smirnov, CREOL, The College of Optics and Photonics, Univ. of Central Florida (United States)

The recent development of kW class fiber lasers makes the conception of laser systems operating at power levels from tens of kilowatts up to 100-kilowatt levels a reality. The use of volume Bragg gratings for spectral and coherent beam combining is one of the promising approaches to achieve that goal. To make such systems compact, lower the complexity and minimize the induced thermal distortions we propose and demonstrate the use of spectral beam combining by complex diffracting elements which have several volume Bragg gratings (VBGs) written inside.

Two types of multiplexed VBGs were recorded in photo-thermo refractive glass. The first one was designed for a combination of incoherent laser beams with wavelength offset of 1 nm. This optical element included two VBGs with different resonant wavelengths that had one of the Bragg angles overlapped. This type of VBGs was used for spectral beam combining. The other type included two or four VBGs with identical resonant wavelengths while one of the Bragg angles was overlapped for all of them (degenerated Bragg angle). These VBGs were used for coherent beam combining (phase locking of multichannel fiber lasers).

Two fiber lasers 150 W each with wavelength offset of 1 nm were successfully combined with efficiency of 98% and no significant beam quality degradation. Thermal experiments were also performed in order to investigate the detuning from Bragg condition and beam quality change at higher thermal loads resulted from absorption of high power laser radiation. The results demonstrated that the approach of using multiplexed volume Bragg gratings for spectral beam combining is excellent extension and alternative to the current state of the art

combining techniques. Especially valuable is the capability to reduce the number of optical elements in the system and still be able to manage the expected thermal load when kilowatt level sources are used for beam combining. The third laser beam transmitting through this VBG was added to a combined beam. Total 450 W with high beam quality were observed. Further scaling to larger number of channels and higher power is discussed.

Two beams coherent combining techniques by two VBGs recorded in the same glass plate have been recently presented. We report an important advance in the channel scaling of coherent beam combiners based on multiplexed volume Bragg gratings (M-VBGs), which are holographically recorded in a single photo-thermo-refractive (PTR) glass substrate, for radiation exchange between channels in a laser system. Experimental study of four-channel multiplexed Bragg grating combiners (M4-VBG) is presented. Using these M-VBG combiners, we present coherent beam combining of four single-mode fiber amplifiers in a passive architecture where the diffraction-limited combined beam is extracted from a single common output aperture. It is shown that the M-VBGs can be used as both broadband (100 pm - 10s of nm) and narrowband (< 10s of pm) combiners, and the system performance is compared in both regimes. Four fiber lasers are constructed using Yb-doped 6/125 PM fiber, core-pumped with a single-mode laser diode at 976 nm and 500 mW maximum power.

8547-26, Session 7

Beam combining concepts using Stimulated Brillouin Scattering

Andrew M. Scott, QinetiQ Ltd. (United Kingdom)

Stimulated Brillouin Scattering is seen as a deleterious effect in narrow-band high power fibre lasers. It can also be used to control and combine beams, although historically it has had limited success and limited efficiency. In this paper we describe a configuration that can lead to beam combining and amplification with high conversion efficiency and high gain. Some of the practical issues in implementing this will also be discussed.

8547-28, Session 7

Filled-aperture beam combining of high power Yb fiber amplifiers

Charles X. Yu, Steven J. Augst, Shawn M. Redmond, Oleg Shatrovoy, Daniel V. Murphy, Antonio Sanchez, Tso Yee Fan, Daniel J. Ripin, MIT Lincoln Lab. (United States)

Fiber lasers are attractive for many applications because of their high electrical efficiency, compact packaging and good beam quality. Currently kW-level fiber lasers are commercially available from multiple vendors. We present filled-aperture beam combining results using coherent and wavelength combining techniques with 500-W commercial fiber amplifiers. In the coherent case, five amplifiers are combined using a diffractive optical element and 2 kW combined output power has been achieved with ~80% efficiency. In the wavelength case, six amplifiers are combined using a multilayer diffraction grating and 2.5 kW combined output power has been achieved with ~92% efficiency. In both cases the combined beam is near diffraction limited.

8547-28, Session 8

Resonantly (in-band) pumped Er-doped eye-safe lasers: scaling power with high efficiency *(Invited Paper)*

Mark Dubinskii, U.S. Army Research Lab. (United States)

The design of high power eye-safe lasers based on Er3+ doped laser materials involves choosing the optimum host, pump source and its wavelength, gain medium geometry, Er concentration, etc. Solid-state laser power scaling with high beam quality is only achievable in laser designs with maximum possible reduction of heat generated by the absorbed pump along with efficient heat removal from the gain medium. The former can be achieved by minimization of the fundamental quantum defect (QD), χQD = 1–λP/λL (where λP and λL are the pump and laser wavelengths, respectively), while the latter is defined by the choice of the most thermally advanced host materials with thermal and thermo-optic properties superior to conventional (legacy) materials. This communication presents the most important and latest advances in resonantly (in-band) pumped eye-safe Er-doped laser development at ARL, based on new Er-doped laser materials - bulk and fibers. Reported are Er-laser optical-to-optical efficiencies of up to 85%, ultra-low quantum defect (QD) laser operation (QD ≈ 5%) and super-ultra-low QD (<1.5%) laser operation of Er-doped gain media, as it pertains to ultimate power scaling.

8547-29, Session 8

Coherent Polarization Locking of thermal sensitive Ho:YAG laser

Chern Fei Chua, Temasek Laboratories, Nanyang Technological University (Singapore) and School of Physical and Mathematical Sciences, Nanyang Technological University (Singapore); Lihao Tan, School of Physical and Mathematical Sciences, Nanyang Technological University (Singapore); Poh Boon Phua, Temasek Laboratories, Nanyang Technological University (Singapore) and School of Physical and Mathematical Sciences, Nanyang Technological University (Singapore)

We had demonstrated the advantage of using Coherent Polarization Locking (CPL) on thermal-sensitive Ho:YAG laser cavity. By using CPL in the Ho:YAG laser cavity, we passively coherent locked two orthogonal lasers, achieving 9.6W of output power with near perfect (>99%) combining efficiency. The resultant laser produced near diffraction-limited beam quality of M2 1.1 and excellent power stability.

The Ho:YAG crystal used was a 10mm length crystal with 0.75% doping concentration. It was pumped by a single Tm:Fiber laser, where the single pump laser was split into two separate pump beams. The two pump beams incident onto the gain medium at two spots, thus reducing the thermal load on the gain medium by half. The two orthogonal lasers were spatially overlapped using thin film polarizers placed at a common laser cavity arm. Coherent combining of the two lasers was performed by a wave plate and another thin film polarizer, where it served as a polarization selective element. If the two lasers were coherent, spatial overlapping of the beams will result in an elliptically polarized beam. The wave plate will rotate the elliptically polarized beam to horizontal polarization, allowing the beam to transmit through the thin film polarizer with no loss. In other words, the wave plate and the thin film polarizer passively coherent locked the phase of the two lasers, in order to survive and compete in the laser cavity.

Holmium laser is a quasi-three level laser system, where the ground state atoms will be thermally excited to the lower laser level under excessive heat load. This ground state thermal population will decrease the laser performance. Furthermore, the development of high power solid state laser is often accompanied by thermo-optic effects, such as thermally induced lensing and birefringence. These unwanted thermo-optic effects will lead to degradation of beam quality and laser efficiency. By using the CPL technique on the Ho:YAG laser system, the thermal effects were greatly reduced.

It is also well-known that highly doped Ho crystals will increase the upconversion loss. Thus to prevent upconversion loss, low Ho-doping concentrations are preferable. But this will limit the power scaling of such laser as ground state population depletion will occur with high pump power. CPL can coherently combine several low Ho-doped lasers, thus allowing power scaling of the laser with less issue of ground state population depletion.

Our result had shown the advantage of using CPL in the Ho:YAG laser system. By CPL of Ho:YAG, near diffraction limited beam was obtained, with output power of 9.6W. The output power was stable, with <1% power fluctuation. As compared, when the same full power was pumped into a single spot, the laser beam was greatly degraded by thermal effects which result in beam quality much inferior to the CPL case.

In conclusion, we had demonstrated the main advantages of using the CPL on Ho:YAG laser system. It reduces the thermal load on laser crystal hence improving the beam quality. Ground state population depletion was prevented. Lastly CPL has the potential in power scaling to develop high power laser system.

8547-30, Session 8

Recent advances in eye-safe Er3+:YAG solid-state heat-capacity technology *(Invited Paper)*

Marc Eichhorn, Stefano Bigotta, Thierry Ibach, Institut Franco-Allemand de Recherches de Saint-Louis (France)

In order to address the question of the possibility of a high energy laser with an emission in the “eye-safe” wavelength range, various architectures may be considered. To provide a truly scalable and efficient laser source, however, only bulk solid-state lasers using resonantly diode-pumped erbium show the necessary properties, when coupled with the solid-state heat-capacity (SSHCL) principle of operation. Although seen as nearly being impossible to realize, such a quasi-three-level laser medium can be used in heat-capacity operation. In this operation mode, the laser medium is not cooled during lasing in order to avoid the thermal lensing occurring in bulk lasers, which, in actively cooled operation, would result in a low beam quality, destabilize the laser cavity or would even cause crystal fracture. In heat-capacity mode, the laser medium will substantially heat up during operation, which will cause an increase in re-absorption for a quasi-three-level laser medium, resulting in a general drop in output power over time. However, theoretical and experimental investigations have proven that this effect is of no concern for an Er3+:YAG SSHCL. This paper presents an overview on the theoretical background of the Er3+:YAG SSHCL, experimental results including recent advances in output power and efficiency, an investigation on the laser scaling properties and recent results on intra-cavity adaptive optics for beam-quality enhancement. The effect of fluorescence re-absorption on the laser properties, especially on threshold and laser efficiency will also be discussed. Up to 4.65 kW and >440 J in less than 800 ms are achieved using optimized doping levels for upconversion reduction in this resonantly-diode-pumped Er3+:YAG SSHCL, representing the current world record in eye-safe diode-pumped solid-state laser technology. Optical-to-optical efficiencies of over 41% and slope efficiencies of over 51 % are obtained with respect to the incident pump power.

8547-31, Session 8

Transient analysis of thermal effects in non symmetrically pumped laser slabs

Elisa Spinozzi, Marco Vitiello, GEM elettronica (Italy)

The design of a laser cavity typically relies on a few steps: the definition of the pumping geometry, the modelling of the thermo-opto-mechanical properties of the active material, the definition of the resonator geometry. A fine modelling of the temperature distribution inside the active material is essential to evaluate the changes of its optical properties and, then, to tune the cavity geometry to maximize the resonator stability and the energy extraction efficiency.

In this paper the analytic solution to the problem of time dependent non-homogeneous heat equation is derived for a temporally pulsed and spatially non-homogeneous source term.

The problem of heat flow in a laser medium is typically studied within the approximation of time independent heat equation since the examined cases concern CW pumping or pulsed pumping with an inverse repetition rate much less than system thermal relaxation time. When the latter condition fails, due for instance to a short relaxation time (small rod/slab cross section, high thermal diffusivity) or to a low repetition rate, transient analysis of thermal effects becomes necessary.

Moreover, the pumping/cooling geometry typically reported in the literature lead to a symmetric, quadratic distribution of the heat load inside the active material. This is the framework of choice to effectively model the thermal behaviour of the active material as a thin lens and, then, to easily take into account its influence onto the resonator properties by means of the matrix formalism. However, asymmetric pumping/cooling schemes are often encountered especially for those active materials with a very short absorption length where a side pumping is required and a single or double pump scheme is chosen. In these cases, the time independent formalism fails in predicting both the focusing properties of the active material and any beam bending inside the resonator, while the time dependent formalism allows to finely predict the temperature distribution and to still apply, locally, the matrix formalism.

In the paper we apply the formalism to a double side pumped Er:Yb glass slab laser with a non symmetric cooling scheme at several repetition rates. By evaluating the temporal evolution of the local temperature in the slab cross section, the difference with the stationary spatial temperature distribution turns out to be not negligible at repetition rates below 10Hz.

In particular, we observe that the lack of symmetry in the temperature profile reduces thermal focusing effects, because the local curvature of temperature distribution is smoother than a symmetric case, but leads to a dynamic drift of mode laser axis which can make unstable the resonator cavity. We validated the model by comparing the theoretical values of slab focal length and of modal axis drift (which can be estimated only by the non-stationary model) with experimental measurements at several repetition rates, proving also that the thermal focusing becomes a secondary effect in comparison with modal axis drift at increasing repetition rates.

8547-32, Session 8

An overview on new diode lasers for defense applications

Joerg Neukum, DILAS Diodenlaser GmbH (Germany)

Diode lasers have a broad wavelength range from the visible to beyond 2.2µm. This allows a variety of applications in the defense sector, ranging from classic pumping of DPSSL in range finders or target designators, up to pumping directed energy weapons in the 50+kW range. Also, direct diode applications for illumination above 1.55µm, or direct IR countermeasures are of interest. Here, an overview is given on some new wavelengths and applications which are recently under discussion. In this overview, the following aspects are reviewed:

- High-power CW pumps at 808 / 880 / 940nm
- Pumps for DPAL - Diode-pumped alkaline lasers
- High-power diode lasers in the range > 1.0µm
- The scalable Mini-Bar concept for high-brightness, fiber-coupled modules
- The light-weight, fiber-coupled module based on the Mini-Bar concept

The programs for the development of DPSS lasers in the 50+ to 100kW range (based on disk, slab or zig-zag configurations) require very high-power pump modules based on the wavelength suitable for Nd3+ or Yb3+ pumping. Results are shown with up to 200W power levels per bar, respectively 5kW per stack.

To overcome the limitations of DPSS lasers at the 50+kW level in terms of thermal management, an alternative way is proposed, based on the diode pumping of alkaline vapor lasers (DPAL). These gaseous media do not suffer from the thermal management issues like DPSSL’s and may give a route beyond 100+ kW lasers for the use in missile defense applications. Results for the important wavelengths for pumping of Cesium (852nm), Rubidium (780nm), Potassium (766nm) and even Lithium (670nm) are presented.

In the range above 1µm, some important diode laser wavelengths are now available with high power. Results are shown for fiber-coupled modules in the range of 1470nm, 1532nm and 1910nm for pumping applications, as well as high-power QCW stacks at 1550nm for Illumination purposes.

In addition to the classic laser bar structures, we describe a new, scalable concept based on Mini-Bars. Such bars are designed to achieve high coupling efficiencies in fiber-coupled modules, together with the ability to manufacture such modules with a high degree of automation. These modules are used as pump sources for fiber lasers, hence offer high optical output powers at 976nm and 200µm fiber core diameter with electro-optical efficiencies of up to 50%.

Based on the Mini-Bar concept, we also introduce a very light-weight version, suitable for portable applications. With 300W in 200µm fiber core at a weight of ~300g and a volume of 87 x 65 x 45 mm?, such modules can be cooled with industrial water. This, together with its high electro-optical efficiency of up to 50%, makes this module a suitable tool for portable operations.

Overall, high-power diode lasers offer many ways to be used in new applications in the defense market.

References:

H.Kissel et. al. - “High-power diode laser pumps for alkali lasers (DPALs)”, Proc. SPIE 8241, 82410Q (2012).

B.Köhler et. al. - “Scalable high-power and high-brightness fiber coupled diode laser devices”, Proc. SPIE 8241, 824108 (2012).

8547-33, Session 8

High power high brightness volume Bragg semiconductor lasers *(Invited Paper)*

Leonid B. Glebov, George B. Venus, Ivan B. Divliansky, CREOL, The College of Optics and Photonics, Univ. of Central Florida (United States); K. Shavitranuruk, Vadim Smirnov, OptiGrate Corp. (United States)

While semiconductor lasers are the most efficient high power sources of optical radiation, their wide and unstable emission spectra and high divergence of radiation impede their utilization in a number of important industrial, medical, military, and scientific applications. One of the widely studied approaches to improve brightness of semiconductor lasers is the use of external resonators that provide spectral or angular mode selection. The most successful approach that was demonstrated during last ten years is the use of volume Bragg gratings (VBGs) recorded in photo-thermo-refractive (PTR) glass for spectral and angular selection in semiconductor laser resonators along with coherent and spectral beam combining. This paper describes increasing brightness of different types of single emitters and multichannel laser systems enabled by achievements in development of low absorption PTR glass and high optical quality of VBGs.

Spectral narrowing of laser diodes (LDs) is based on an important feature of semiconductors which is very wide homogeneous broadening of luminescence spectra. This feature allows locking of LDs by the use of narrow band feedback in external resonators with reflecting VBGs as output couplers. Spectral area of efficient locking can exceed several tens of nanometers. Proper combination of parameters of LD, VBG and collimating optics provides spectral narrowing of lasers by three orders of magnitude while keeping power and efficiency penalty within a few percent. The highest achieved results in spectral narrowing are: 25 W CW emission at 780 and 852 nm with spectral width below 20 pm from single edge emitters; 40 W QCW emission at 976 nm with spectral width of 50 pm from grating coupled surface emitting lasers (GCSELs); 250 W CW emission at 1532 nm with spectral width of 250 pm from 12 LD bars coupled to a fiber bundle; 750 W CW emission at 780 nm with spectral width of 22.5 pm from 21 LD bars coupled to a fiber bundle.

Beam quality improvement (decrease of divergence, transverse mode selection) was produced by the use of a transmitting VBG placed in a collimated beam between an emitter and an output coupler or a reflecting VBG placed in a convergent beam. For edge emitters with stripe widths ranged from 30 to 150 μm, both those approaches provided a single transverse mode regime up to ten thresholds that corresponded approximately 2 W CW emitting power with beam quality M2~1.7. GCSELs used for such experiments with a transmitting VBG in a collimated beam with a reflecting VBG as an output coupler. Single transverse mode regime was observed up to ten thresholds. Problems of stability of single transverse mode regime at high power are discussed.

Phase locking of two and three LDs mounted at different stages was observed by creation of a common resonator where a VBG was used for radiation exchange between channels. It was found that coherent radiation from both LDs was emitted if spectral width of the VBG was narrower than the distance between two longitudinal modes in the LD internal resonators.

8547-34, Session 9

Gain and lasing of optically pumped metastable rare gas atoms *(Invited Paper)*

Michael C. Heaven, Jiande Han, Emory Univ. (United States)

In recent years there have been concerted efforts to develop high energy diode-pumped alkali vapor lasers (DPAL). These hybrid gas phase / solid state laser systems offer possibilities for constructing high-powered lasers that have high beam quality. DPAL's utilize excitation of the alkali metal 2P3/2←2S1/2 transition, followed by collisional relaxation and lasing on the 2P1/2→2S1/2 line. Considerable progress has been made, but there are technical challenges associated with the reactivity of the metal atoms.

Rare gas atoms (Rg) excited to the np5(n+1)s 3P2 configuration are metastable and have spectral properties that are closely similar to those of the alkali metals. In principle, optically pumped lasers could be constructed using excitation of the np5(n+1)p ← np5(n+1) s transitions. We have recently demonstrated gain and lasing for optically pumped Ar*, Kr* and Xe*. Three-level lasing schemes were used, with He as the collisional energy transfer agent that established the population inversion. These laser systems have the advantage using inert reagents that are gases at room temperature, with excellent potential for closed-cycle operation.

8547-35, Session 9

Modeling of static and flowing-gas diode pumped alkali lasers

Boris D. Barmashenko, Salman Rosenwaks, Ben-Gurion Univ. of the Negev (Israel)

Diode pumped alkali lasers (DPALs) convert un-phased low beam quality radiation from diode laser arrays into coherent, high quality ~ 800 nm wavelength radiation of alkali (Cs, Rb) atoms. The diode laser pumping of the higher fine-structure level 2P3/2, via the D2(2S1/2 → 2P3/2) transition, is followed by rapid relaxation of 2P3/2 to the 2P1/2 fine-structure level and lasing on the D1(2P1/2 → 2S1/2) transition. For low power (< 30 W) CW DPALs there is no need to replenish the gas mixture. However, at higher powers, the heat release due to relaxation between the fine-structure levels of the alkali atoms results in an increase of the temperature T causing a decrease of the pump absorption in the active volume and fall of the slope and of the overall optical-to-optical efficiencies. The effects of the heat release become even more significant for scaling-up to high power, in the multi-kW range. To avoid the temperature rise in the laser and reach high (>50%) slope efficiencies there is a need to flow or at least transport the gas in a closed system so that waste heat can be removed outside of the laser cavity. For moderate powers (< 1 kW) the gas can flow in the optical axis direction, however operating at higher multi-kW power levels requires that the alkali vapor be flown transversely to the laser axis.

We report on a semi-analytical model of a gas flow DPAL with an end-pump geometry and flow direction either transverse or parallel to the optical axis of the resonator. The model is based on the analytical model of the DPAL with non-flowing gas suggested by Hager and Perram [1]. Unlike the model reported in [1] the present model takes into account the fact that T depends on the pump intensity I. T is found from the energy balance equation assuming that the heat release due to relaxation between the fine-structure levels is equal to the heat removal by both the gas flow and thermal conductivity to the walls. Narrow band optical pumping and fast relaxation between the fine-structure levels (relative to both the excited state lifetime and the absorption rate) are assumed. The dependence of T and the output power on the pump power is found for different flow velocities. It appears that the output power grows linearly with the pump power for low values of the latter; however, at higher values the output power rolls over deviating from the linear dependence and resulting in a decrease of the slope efficiency. The maximum values of the pump power for which the linear dependence still holds increases with increasing flow velocity. Using the model we estimate what values of the flow velocity are necessary to achieve several hundreds watts of the CW laser power. To prove the validity of the concept and to show that our approach is feasible we compare our results for the case of non-flowing gas with available experimental measurements [2] and model of the DPAL[1].

1.G. D. Hager and G. P. Perram, Applied Phys. B 45, 101(2010).

2.B.V. Zhdanov, J. Sell, R.J. Knize, Electron. Lett. 44, 582 (2008)

8547-36, Session 9

Advanced CO laser systems

Andrey A. Ionin, P.N. Lebedev Physical Institute (Russian Federation)

Different sorts of CO-laser systems developed at the Gas Lasers Lab of the Lebedev Physical Institute as an evolution of previous research are discussed. To increase a peak power of carbon monoxide laser emitting nanosecond pulses, a Master Oscillator-Power Amplifier (MOPA) laser system was developed. Amplification of nanosecond pulses in CO-laser amplifier was for the first time experimentally studied, gain and saturation intensity of amplifying media being measured. The MOPA CO-laser system emitted a train of nanosecond pulses with peak power up to ~0.1 MW on a single spectral line and up to ~0.4 MW with multiline spectrum.

Frequency doubling of mode-locked frequency-tunable fundamental

band CO-laser emission in ZnGeP2 nonlinear optical crystal was experimentally studied. The internal efficiency of frequency doubling exceeded 25% which was obtained by stabilization of mode-locking regime and increasing peak power of pump radiation produced by aforementioned MOPA CO-laser system.

Simultaneous second harmonic, sum and difference frequency generation of multiline CO laser radiation in a single nonlinear optical ZnGeP2 crystal was for the first time obtained. Home-made DC discharge pumped low-pressure cryogenic CO laser Q-switched by a rotating mirror and emitting radiation on ~80 spectral lines within the spectral range of 4.9-6.3 micron was used in the experiments. Second harmonic and sum frequency of fundamental band radiation contained ~110 spectral lines within 2.45 - 2.85 micron range. The internal efficiency of such frequency conversion was 3.6%. Difference frequency generation within spectral range of 4.3 -4.9 micron by nonlinear mixing of CO laser second harmonic and fundamental band spectral lines was for the first time observed. Internal efficiency of the difference frequency generation was ~0.5%. An enhancement of difference frequency conversion efficiency seems to be possible by application of aforementioned high-power MOPA CO-laser system.

A compact repetitively-pulsed cryogenically-cooled slab RF discharge overtone CO-laser with electrode length ~ 40 cm enlarged as compared to previous laser was developed. Its output power and efficiency came up to ~ 2.0 W and ~1.6%, respectively, spectral range being 2.95 - 3.45 micron

8547-37, Session PS

Analysis of a passively q-switched Nd:YAG slab laser oscillator/amplifier system

Ion I Lancranjan, CSA-INCAS -Advanced Study Center of National Institute for Aerospace Research Elie Carafoli (Romania); Dan M. Savastru, Sorin I. Miclos, Roxana S. Savastru, National Institute of Research and Development for Optoelectronics (Romania)

This paper presents the results obtained in analyzing a quasi-cw flash-lamp pumped high power Nd:YAG slab laser oscillator/two stages amplifier operated in passive optical Q-switching regime using LiF:F2- crystals with an improved design. A numerical simulation method based on laser rate equation is developed for theoretical analysis of a passively Q-switched Nd:YAG slab laser system. A comparison of simulation results with experimental data is also presented to certify the viability of the developed theoretical analysis method. Laser pulses output energy of 330 mJ at a FWHM time duration of 50-75 ns and at a repetition frequency of 10 - 25 kHz (pps) are reported and numerical simulation of these experimental results are presented pointing to the output parameters stability.

Plenary Lecture Information

Remote Sensing Plenary Session:

Maximizing the use of EO products: how to leverage the potential of open geospatial service architectures

Thomas Usländer, Head of the Information Management and Production Control Department, Fraunhofer IOSB, Germany

The demand for the rapid provision of EO products with well-defined characteristics in terms of temporal, spatial, image-specific and thematic criteria is increasing. Examples are products to support near real-time damage assessment after a natural disaster event, e.g. an earthquake. However, beyond the organizational and economic questions, there are technological and systemic barriers to enable a comfortable search, order, delivery or even combination of EO products. Most portals of space agencies and EO product providers require sophisticated satellite and product knowledge and, even worse, are all different and not interoperable.

This presentation will give an overview about the use cases and the architectural solutions that aim at an open and flexible EO mission infrastructure with application-oriented user interfaces and well-defined service interfaces based upon open standards. It presents corresponding international initiatives such as GEOSS (Global Earth Observation System of Systems) and HMA (Heterogeneous Missions Accessibility) and their associated infrastructure approaches. Furthermore, it highlights how such architectures are already successfully used in early warning systems for geo-hazards and research projects that investigate how EO products may be used to assess correlations between environmental situations and health impacts. Finally, the presentation mirrors these ideas with the vision of the Internet of Services and remaining challenges for future operational system-of-systems architectures.

Biography: Dr.-Ing. Thomas Usländer holds a degree in Computer Science from the University of Karlsruhe, Germany, and a PhD in Engineering of the Karlsruhe Institute of Technology (KIT), Germany. He is head of the department “Information Management and Production Control” and deputy speaker of the business unit “Energy, Water and Environment” at Fraunhofer IOSB. He was IOSB project leader in several international research projects and large environmental information system supply projects for German Environmental State Agencies. His research interests include the analysis and design of open geospatial service architectures where he has numerous publications. He is the representative of Fraunhofer in the architecture working group of the Open Geospatial Consortium (OGC). He was editor of the Reference Model for the ORCHESTRA Architecture (RM-OA) that has become OGC best practices document 07-097.

He was an invited expert of the European Commission in the Consultation Workshop “Towards a Single Information Space in Europe for the Environment (SISE)” and the final workshop of “Connectivity between Environment and Health Information Systems (CEHIS)”. He got the Object Management Group (OMG) Application Award 2000 in the category “Best Application utilizing reusable components leveraged from of for use in other projects” and the best-paper award of the European conference “Towards eEnvironment” in Prague, 2009.

The use of polar orbiting and geostationary satellite data for geospatial analyses in fisheries, environmental monitoring, ship routing and management decision making

Mitchell A. Roffer, President Roffer’s Ocean Fishing Forecasting Service, Inc., United States

The applications of new satellite visualization and data fusion products for 1) fisheries research with tuna, mackerel, squid, and marlin; 2) operational forecasting for fishing (commercial and recreational) and ship routing; and 3) mapping the oil - dispersant - water mixtures in the Gulf of Mexico during the Deepwater Horizon oil spill (April - August, 2010) will be presented. This will include a review of the benefits and limitations of the spectral, spatial, temporal resolution and geographic coverage on the polar orbiting (e.g. NOAA series, MetOpA, Terra, Aqua, Envisat, Jason, Topex, ERS-2, etc.) and geostationary satellites (e.g. GOES) related to their utility in environmental monitoring and fisheries research, as well as, decision making in fisheries (operations and management), maritime transportation and safety (i.e. search and rescue), and oil spill response.

Due to the differing spatial and temporal resolution of satellite derived infrared (AVHRR and MODIS), visible (MODIS and MERIS), synthetic aperture radar and altimetry, as well as, the type of information required under a variety of weather conditions (clouds, wind, etc.), it is often necessary to merge different data. Examples of data fusion efforts over a variety of spatial (e.g. 75 m – 6 km) and temporal (1 hour – 10 day) resolutions and geographic coverages will be presented. These will include the validation data derived from In situ data collection (visual observations and drifting buoy tracks). The ability and utility to identify water masses by their signature physical characteristics of sea surface temperature and ocean color, as well as, the water masses’ coherent Lagrangian structures using sequential image analysis will be demonstrated. This technique is especially valuable when working with cloud obstructed areas and where isothermal conditions exist, as well as for showing the motion of the currents. Examples from a wide variety of areas including the North Atlantic Ocean (including the Caribbean Sea and Gulf of Mexico), South Atlantic Ocean, and Pacific Indian Ocean will be shown.

Biography: Mitchell A. Roffer (Ph.D.) is founder and President of Roffer’s Ocean Fishing Forecasting Service, Inc. (ROFFS™ - www.roffs.com), a scientific consulting company based in West Melbourne, Florida. He received his Ph.D. from the University of Miami’s Rosenstiel School for Marine and Atmospheric Sciences in Biological Oceanography with an emphasis on satellite fisheries oceanography in 1987. Dr. Roffer has extensive experience in the use of satellite data, as well as, other oceanographic and meteorological data for producing applied operational and research products showing ocean currents and ocean frontal boundary dynamics. Roffer is best known for his research and operations related to tactical and strategic fisheries forecasts that are the result of the integration of satellite and other fisheries oceanographic data. He is intensively involved a broad range of projects from ship routing, oil and gas drilling operations, seismic and fish surveys, fisheries development, aquaculture, environmental monitoring, and applied scientific research.

Roffer remains active in both the scientific community and the fisheries resource management community locally, regionally, nationally and on an international basis. Roffer has a long history working on NASA research projects. He is currently the Principal Investigator in a four-year ($1.7M) project funded by the National Aeronautics and Space Administration (NASA), “Management and Conservation of Atlantic Bluefin Tuna (Thunnus thynnus) and Other Highly Migratory Fish in the Gulf of Mexico Under IPCC Climate Change Scenarios: A Study Using Regional Climate and Habitat Models” (10-BIOCLIM10-14). He is a member (eight years) of NASA’s internationally renowned Biodiversity & Ecological Forecasting Science Team. Dr. Roffer is an active participant in several regional and state Integrated Ocean Observing System (IOOS) associations and is currently serving as an Executive Board Member on the Southeast Coastal Ocean Observing System Regional Association (SECOORA), serves on the Products and Services Committee in Gulf of Mexico Coastal Ocean Observing System Regional Association (GCOOS), and is an Institutional Host of the Florida COOS Consortium.

Security + Defence Plenary Session:

The Promise of HEL Weapons

Mark W. Neice, Director, High Energy Laser Joint Technology Office, United States

The High Energy Laser Joint Technology Office (HEL-JTO) was established in 2000 for the purpose of developing and executing a comprehensive investment strategy for HEL science and technology that would underpin weapons development. The JTO is currently sponsoring 90 programs across industry, academia, and government agencies with a budget of approximately $70 million. The competitively awarded programs are chosen to advance the current state of the art in HEL technology and fill technology gaps, thus providing a broad capability that can be harvested in acquisition programs by the military services.

Electrically-driven lasers are attracting new science and technology funding because their magazine is limited only by the electrical prime power, and they are not encumbered by hazardous chemicals and chemical exhaust. The solid state laser has the special challenge that its waste heat is generated at fairly high energy density and rejected at relatively low temperature. The JTO, working with the Army SMDC and AF Research Laboratory (AFRL) recently completed the development and demonstration of a 100kW Joint High Power Solid State Laser (JHPSSL) project. The JHPSSL laser is currently being installed at the Solid State Laser Test Experiment site at HELSTF in New Mexico. Following the successful JHPSSL project, the JTO working with the Army SMDC and AFRL initiated the Robust Electric Laser Initiative (RELI) with a focus toward achieving size, weight and power (SWaP) limitations necessary to operate and field HEL technology on the battlefield.

The changing nature of the battlefield, particularly as it relates to the war on terrorism, provides strong motivation to assess HEL weaponry in the near term. Precision strikes measured in inches instead of meters, limited collateral damage, asymmetric threats, and rapid response to dynamic targets are all elements of warfare that are gaining in importance. The laser's ability to deliver modest energy to a precise spot from a safe distance is an ideal match to these requirements, if the right power levels, size, reliability, etc. can be attained. The JTO expects to play a key role in accelerating development of the capabilities underlying these next-generation weapons.

Biography: Mark Neice is the Director, High Energy Laser Joint Technology Office. He supervises the research and development of solid-state, free electron & gas laser devices, beam control technologies, lethality analysis, and the modeling & simulation tools that create military applications of laser energy for combat operations. He retired as a Colonel in the US Air Force in October 2004, after 25 years of active duty service.

Previously, Col Neice was the Chief of the Laser Division, Directed Energy Directorate, AF Research Lab. Past positions include director of space test operations, Det 12, AFSPC, and director of systems engineering & test operations for the Airborne Laser Program Office. A command pilot, Col Neice has time in the 4950th Test Wing, and as initial cadre of the Joint Stars test team. He has over 6000 flying hours, mainly in the C-135 and B-707 variants, and is a member of the Acquisition career force, certified in program management, test & evaluation, and systems planning, research, development & engineering.

Routes to Autonomy

Bill Bardo, Univ. College London, United Kingdom; Technical Director (retired), GEC, United Kingdom

The talk draws on the work undertaken for seven years by the Systems Engineering for Autonomous Systems Defence Technology Centre and will cover a number of research topics including decision making, sensor data interpretation, information management, communication, navigation, and power management. The goal of designing learning, adaptive systems to work with humans poses interesting problems for architectures.

Biography: Following PhD and postdoctoral theoretical and experimental investigations of the quantum mechanical behaviour of masers and lasers Bill Bardo worked at the Royal Signals and Radar Establishment, Malvern for nine years before joining GEC where he was for nineteen years the Technical Director of the GEC-Marconi group of companies followed by a period at BAE Systems. His current activities include Technical Director of the Systems Engineering for Autonomous Systems Defence Technology Centre (SEAS DTC) and educational activities on behalf of the Royal Academy of Engineering.

He is a Fellow of the Royal Academy of Engineering and recently President of the Institute of Measurement and Control [2009-2012]. In 2000 he received the Society Gold Medal of the Royal Aeronautical Society for contributions to systems engineering research.

He is Visiting Professor in Systems Engineering at University College London and was a founder member and President of the UK Chapter of the International Council of Systems Engineering.